
# Optimisation of Point of Connection and Effects of Power Electronic Distributed Energy Resources on Harmonic Levels in Low Voltage Power Distribution Networks

Graham Peter Gissing

Submitted in fulfilment of the requirements for the
Degree of Doctor of Philosophy (Ph.D.)

James Watt School of Engineering

College of Science and Engineering

University of Glasgow

August 2024

# Abstract

As of 2022, National Grid ESO stated that there were over one million electric vehicles (EVs) on United Kingdom (UK)'s roads, with an expectation that there will be approximately thirty-three million by 2050 under a 'falling short' scenario. Additionally, the Department for Energy Security and Net Zero (DESNZ) states that, as of November 2023, there were over 1.24 million 0 $\leqslant$ 4 kW photovoltaic (PV) generators connected to the low voltage electricity distribution network (LV EDN). Despite this, substantial physical upgrades to the LV EDN have not yet been carried out. In addition, within existing literature, consensus is that power-electronic loads such as electric vehicle chargers (EVCs) and distributed energy resources (DERs), such as PV generation and vehicle to grid (V2G), can lead to voltage, overloading, and power quality issues including harmonic distortion and flicker. Although each of these issues present significant engineering concerns, this thesis shall focus on harmonic distortion and aim to fulfil the identified research gaps.

The majority of supply points are connected to the LV EDN; therefore, changes in harmonics at this voltage level will directly affect these consumers. Harmonics can increase the risk of transformer, motor, and cable overheating, metering and computer errors, failure of electronic equipment, circuit breaker malfunction, and communication interferences. This thesis has two main purposes. Firstly, the effect that increased numbers of EVCs and PV generators have on the steady-state voltage total harmonic distortion (THDv) of a UK LV EDN under steady-state cable faults will be investigated using MATLAB simulations. In conjunction with the voltage harmonic limits stipulated within Engineering Recommendation G5/5, violation of harmonic limits, maximum penetration levels and the increase in individual limiting voltage harmonics after cable faults will be investigated. In addition, the impact of harmonics on infrastructure lifespan and voltage imbalances on risk of death to members of the public will be explored. Secondly, the optimal point of coupling for EVCs, PV generation and V2Gs to minimise the steady-state THDv on a radial LV EDN under a range of both normal and steady-state fault conditions will be ascertained using a combination of two algorithms, Elephant Herding Optimisation and Monarch Butterfly Optimisation, using simulations in MATLAB. This expansion of knowledge is critical for network operators. When implemented, this will ensure that voltage harmonic noncompliance under previously unconsidered fault scenarios can be identified, the design of LV EDNs can be optimised with respect of voltage harmonics, the risk of asset failure which leads to financial loss can be reduced and the risk of death can be mitigated.

# Table of Contents

# List of Tables

# List of Figures

# Acknowledgements

I would like to thank all of the people who have helped and supported me with this thesis. However, I would like to thank the following people in particular:

My Wife, Mrs Sarrah J. Gissing BSc PGCE PGCPSE (Open) NPQSL, for her support throughout the PhD programme and for taking on additional responsibilities to free up essential time which could be dedicated to this PhD.

My supervisor, Dr Jin Yang PhD SMIEEE CEng MIET, Glasgow University, for mentoring me throughout the PhD programme, and for providing research guidance on the subject of V2G and EVCs.

Dr Nagi R. Fahmi PhD CEng MIET, Aston University, for providing support and research guidance throughout the PhD programme.

Dr Nand K. Meena PhD SMIEEE MIET AMIET, NTT Data UK&I, for his guidance with algorithms, coding, and optimisation.

Dr Preye Ivry PhD MIEEE MIET, Nortech Management Ltd, for his guidance with V2G simulation.

Lastly, I would like to express my appreciation to my parents for their support.

# Declaration

With the exception of Chapters 1, 2 and 3, which contain introductory material, all work in this thesis was carried out by the author unless otherwise explicitly stated.

# Abbreviations and Nomenclature

Abbreviations

| | |
|---|---|
| ABC | Artificial Bee Colony |
| AC | Alternating Current |
| ACB | Air Circuit Breaker |
| ACO | Ant Colony Optimisation |
| ACSA | Adaptive Cuckoo Search Algorithm |
| AGA | Adaptive Genetic Algorithm |
| ALOA | Ant-Lion Optimisation Algorithm |
| BB | Busbar |
| BBO | Biogeography-Based Optimisation Algorithm |
| BEV | Battery Electric Vehicle |
| BFOA | Bacterial Foraging Optimisation Algorithm |
| BLSA | Binary Lightning Search Algorithm |
| BONMIN | Basic Open-source Nonlinear Mixed Integer programming |
| BPSO | Binary Particle Swarm Algorithm |
| CAS | Corrugated Aluminium Sheath |
| CB | Circuit Breaker |
| CIGRE | Conseil International des Grands Réseaux Electriques |
| COA | Coyote Optimisation Algorithm |
| DC | Direct Current |
| DCCBGA | Discrete-Continuous Chu & Beasley Genetic Algorithm |
| DCCSA | Discrete–Continuous Crow Search Algorithm |
| DCGNDO | Discrete-Continuous Generalized Normal Distribution Optimizer |
| DCPSO | Discrete-Continuous Particle Swarm Optimisation |
| DE | Differential Evolution |
| DESNZ | Department for Energy Security and Net Zero |
| DER | Distributed Energy Resource |
| DfT | Department for Transport |
| DG | Distributed Generation |
| DHPF | Decoupled Harmonic Power Flow |
| DNO | Distribution Network Operator |
| DVLA | Driver and Vehicle Licensing Agency |
| Dyn11 | Delta-Star with negative 30º phase displacement. |
| EDN | Electricity Distribution Network |
| EHO | Elephant Herding Optimisation |

| | |
|---|---|
| ENA | Energy Networks Association |
| EP | Evolutionary Programming |
| ESO | Electricity System Operator |
| ER | Engineering Recommendation |
| ESQCRs | The Electricity Safety, Quality and Continuity Regulations 2002 |
| EV | Electric Vehicle |
| EVC | Electric Vehicle Charger |
| FWA | Fireworks Algorithm |
| G2V | Grid to Vehicle |
| GA | Genetic Algorithm |
| GBO | Greedy Based Optimisation |
| GWO | Grey Wolf Optimisation |
| HHO | Harris Hawks Optimisation |
| HOP | Hamiltonian Optimisation |
| HSA | Harmony Search Algorithm |
| HSA-PABC | Harmony Search Algorithm and Particle Artificial Bee Colony hybrid algorithm |
| HV | High Voltage |
| HVAC | High Voltage Alternating Current |
| ICOA | Improved Chimp Optimisation Algorithm |
| IEEE | Institute of Electrical and Electronics Engineers |
| iV4G | Improved Vehicle for Grid |
| IWO | Invasive Weed Optimisation Algorithm |
| LSA | Lightning Search Algorithm |
| LV | Low Voltage |
| MBO | Monarch Butterfly Optimisation |
| MLSA | Modified Lightning Search Algorithm |
| MPGSA | Multi-paramedic Global Sensitivity Analysis |
| MV | Medium Voltage |
| OFGEM | Office of Gas and Electricity Markets |
| OHPF | Optimal Harmonic Power Flow |
| oLoC | Optimized Location Scheme for electric charging stations |
| ONS | Office for National Statistics |
| PCC | Point of Common Coupling |
| PFT | Pareto-Fuzzy Technique |
| PHEV | Plug-in Hybrid Electric Vehicle |
| PME | Protective Multiple Earthing |
| POC | Point of Connection |
| POT | Plug-Out Transient |
| PSO | Particle Swarm Optimisation |

| | |
|---|---|
| p.u. | Per Unit |
| PV | Photovoltaic |
| QBLSA | Quantum Binary Lightning Search Algorithm |
| QOT | Quadratic Optimisation Technique |
| QOTLBO | Multi-Objective Quasi-Oppositional Teaching Learning based Optimisation |
| RMS | Root Mean Square |
| SA | Simulated Annealing |
| SGA | Stud Genetic Algorithm |
| SI | Swarm Intelligence Algorithm |
| SNE | Separate Neutral Earth |
| SOS | Symbiotic Organism Search |
| SSA | Salp Swarm Algorithm |
| SSCP | Steady-State Charging Period |
| TDD | Total Demand Distortion |
| THD | Total Harmonic Distortion |
| THDi | Current Total Harmonic Distortion |
| THDv | Voltage Total Harmonic Distortion |
| TLBO | Teaching-Learning Based Optimisation |
| ULEV | Ultra-Low Emission Vehicle |
| ULEZ | Ultra-Low Emission Zone |
| UVDA | Uniform Voltage Distribution Based Constructive Algorithm |
| V2G | Vehicle to Grid |
| VSA | Vortex Search Algorithm |
| WOA | Whale Optimisation Algorithm |
| WPD | Western Power Distribution |
| XLPE | Cross Bonded Polyethylene |

Algorithm Nomenclature

| | |
|---|---|
| Max_EV_No | Maximum number of EVCs to be allowed to deploy at a single bus. |
| Max_PV_No | Maximum number of PV generators to be allowed to deploy at a single bus. |
| Min_EV_No | Minimum number of EVCs to be allowed to deploy at a single bus. |
| Min_PV_No | Minimum number of PV generators to be allowed to deploy at a single bus. |
| N_Bus | Number of busses in the system. |
| No_of_EV_Sites | Number of EVC sites/locations to be searched. |
| No_of_PV_Sites | Number of PV sites/locations to be searched. |

Conductor Heating and Loss of Life Equations Nomenclature

| | |
|---|---|
| $B$ | Blue phase conductor. |
| $B_c$ | Boltzmann constant (eV/ºK). |
| $d_c$ | Diameter of the conductor (m). |
| $E_a$ | Activation energy (eV) for thermo-oxidative ageing of the cable. |
| $f$ | Frequency (Hz). |
| $I_1$ | Fundamental current (50Hz). |
| $I_h$ | Harmonic current at the specified harmonic order (A). |
| $K_p$ | Variable which is 1 for a solid copper round conductor. |
| $K_s$ | Variable which is 1 for a solid round conductor. |
| $N$ | Neutral phase conductor. |
| $R$ | Red phase conductor. |
| $R_{ac}$ | AC cable resistance per harmonic order (Ω/m). |
| $R_{ac(1)}$ | Cable resistance at 50Hz (Ω). |
| $R_{ac(h)}$ | Cable resistance at the specified harmonic order (Ω). |
| $R_{dc}$ | DC cable resistance measured at 20°C (Ω/m). |
| $s$ | Distance between the centre of each conductor in m. |
| $t_a$ | Accelerated aging life of the cable in years when operating at $T_a$ |
| $T_a$ | Accelerated aging temperature of cable at in ºK (Temperature>90ºC) |
| $t_s$ | Aging life of the cable at service temperature $T_s$. $t_s$=40 years |
| $T_s$ | Service temperature of cable at 363.16ºK (90ºC) |
| $\theta_{NS}$ | Accelerated aging temperature of cable at in ºC (Temperature>90ºC) |
| $W_{NS}$ | Total power loss of the cable including harmonic losses (W). |
| $W_S$ | Total power loss of the cable excluding harmonic losses (W). |
| $Y$ | Yellow phase conductor. |
| $y_p$ | Proximity effect factor. |
| $y_S$ | Skin effect factor. |

Electrocution Equation Nomenclature

| | |
|---|---|
| $a$ | Constant of value 170 ($\Omega^{-1}$). |
| $b$ | Constant of value 67 ($V^{-1}\Omega^{-1}$). |
| $I$ | Current in amps (A) |
| $I_B$ | Steady state rms current in amps (A). |
| $K$ | electrocution constant ($As^{0.5}$) |
| $t$ | Exposure time in seconds (s) |
| $V$ | Voltage in volts (V) |

| | |
|---|---|
| $V_T$ | Steady state rms voltage in volts (V). |
| $Z_T$ | Total body impedance (Ω). |

Elephant Herding Optimisation Algorithm Nomenclature

| | |
|---|---|
| $\alpha$ | Scale factor determining influence of $x_{best,ci}$ and $x_{ci,j}$ (alpha within EHO Algorithm). |
| $\beta$ | Scale factor determining influence of $x_{center,ci}$ (beta within EHO Algorithm). |
| $ci$ | Elephant clan (*c* within EHO Algorithm). |
| $d$ | $d^{th}$ element. |
| $Fitness$ | THDv magnitude (elephant fitness). |
| $G_{\max}$ | Maximum number of iterations used within the EHO Algorithm. |
| $j$ | Elephant individual within a clan. |
| $max$ | Command within EHO Algorithm for returning he maximum value from an array. |
| $mean$ | Command within EHO Algorithm for mean average value. |
| $n_{ci}$ | Number of busses in the system (*nc* within EHO Algorithm). |
| $N$ | EHO Algorithm parameter which effects parameter *j*. |
| $r$ | Random number between zero and one (*rand* within EHO Algorithm). |
| $round$ | Command within EHO Algorithm for rounding a value to the nearest integer. |
| $x_{best,ci}$ | Bus producing lowest THDv (*pbest(c)* within EHO Algorithm). |
| $x_{center,ci}$ | Centre bus (*pp_center* within EHO Algorithm). |
| $x_{ci,j}$ | Bus of last iteration (*pp(j,c)* within EHO Algorithm). |
| $x_{ci,j,d}$ | $d^{th}$ of bus of last iteration (*pp(:,c)* within EHO Algorithm). |
| $x_{max}$ | Upper bound of bus position (upper bound of 'elephant position'). |
| $x_{min}$ | Lower bound of bus position (lower bound of 'elephant position'). |
| $x_{new,ci,j}$ | Bus of next iteration (*pp_new(j,c)* within EHO Algorithm). |
| $x_{worst,ci}$ | Bus producing highest THDv (*fworst* within EHO Algorithm). |

Exponential Distribution

| | |
|---|---|
| $a$ | Mean of the exponential distribution. |
| $Y$ | Single random number from the exponential distribution. |
| $\lambda$ | Inverse of the mean of the exponential distribution. |
| $ln$ | Natural logarithm. |
| $rand$ | A random value between zero and one. |

Fourier Nomenclature

| | |
|---|---|
| $f(t)$ | Waveform with period t. |
| $a_0$ | Fourier coefficient representing DC component of the waveform. |
| $a_n$ | Fourier coefficient representing even components of the waveform. |
| $b_n$ | Fourier coefficient representing odd components of the waveform. |
| $n$ | Harmonic Order. |

Harmonic Distortion

| | |
|---|---|
| $I_L$ | Magnitude of maximum demand current. |
| $I_1$ | Magnitude of fundamental current. |
| $I_n$ | Magnitude of specific harmonic order, orders range between $2 \leq n \leq \infty$. |
| $n$ | Harmonic Order. |
| $TDD$ | Total Demand Distortion. |
| $THD$ | Total Harmonic Distortion. |

Harmonic Level Calculations Nomenclature

| | |
|---|---|
| $\alpha$ | Summation exponent stated in Table 1.3.2.2. |
| $h$ | Harmonic order. |
| $I_h$ | Harmonic current per harmonic order (A). |
| $k$ | Worst-case reactance factor from Table 1.3.2.1. |
| $R_1$ | System resistance (Ω) at fundamental frequency. |
| $S_{equ\ 3ph}$ | Rating (VA) of the three-phase equipment to be connected. |
| $S_{equ\ 1ph}$ | Rating (VA) of the single-phase equipment to be connected. |
| $S_{SC\ 3ph}$ | Three-phase short-circuit level at the PCC (VA). |
| $S_{SC\ 1ph}$ | Single-phase short-circuit level at the PCC (VA). |
| $THD_I$ | Total current distortion of the equipment to be connected. |
| $THDV_p$ | Predicted voltage total harmonic distortion. |
| $\Delta V_h$ | Harmonic voltage drop of a single conductor (V). |
| $V_{h\,c}$ | Incremental increase in harmonic voltage distortion at the POC (V). |
| $V_{h\,i}$ | $i^{th}$ harmonic voltage including $V_{h\,c}$ and background harmonic values (V). |
| $V_{h\,p}$ | Predicted voltage harmonic distortion per harmonic order (V). |
| $V_{phase}$ | Rated phase-neutral voltage (V). |
| $X_1$ | System reactance at fundamental frequency (Ω). |
| $Z_{Ch}$ | Impedance per harmonic order of the cable (Ω). |
| $Z_h$ | Impedance per harmonic order (Ω). |

| | |
|---|---|
| $Z_{Sh}$ | Impedance per harmonic order of the grid (Ω). |
| $Z_{Th}$ | Impedance per harmonic order of the transformer (Ω). |

Monarch Butterfly Optimisation Algorithm Nomenclature

| | |
|---|---|
| $\alpha$ | Weighting Factor (*scale* within the MBO Algorithm). |
| $BAR$ | Butterfly adjusting rate. |
| $ceil$ | Command within the MBO Algorithm for rounding to nearest integer. |
| $dx$ | Walk step of the monarch butterfly ($deltaX$ within MBO Algorithm). |
| $exprnd(a,b,c)$ | Command within the MBO Algorithm to generate a random number or numbers from the exponential distribution with mean 'a' and matrix of 'b×c'. |
| $i$ | Monarch butterfly in *pop1*. |
| $j$ | Monarch butterfly in *pop2*. |
| $k$ | k[th] element ($ci$ within the MBO Algorithm). |
| *Levy* | Lévy flight performed by butterflies when migrating or moving (*LevyFlight* within the MBO Algorithm). |
| *Lnd1* | Flutter in region one. |
| *Lnd2* | Flutter in region two. |
| *Max_iter* | Maximum number of iterations. |
| *nFlutr* | Flutter length. |
| *nBF1* | Butterflies in region one. |
| *nBF2* | Butterflies in region two. |
| $p$ | Ratio of butterflies in *pop1* compared to *pop2*. |
| *peri* | Migration period (set to 1.2 within the MBO Algorithm). |
| *Pn* | Population size. |
| *pop1* | Population one. |
| *pop2* | Population two. |
| $r$ | Position of the monarch butterfly ($rr1$ within the MBO Algorithm). |
| $r_1$ | Position of the monarch butterfly selected from *pop1* ($rr2$ within the MBO Algorithm). |
| $r_2$ | Position of the monarch butterfly selected from *pop2* ($rr3$ within the MBO Algorithm). |
| *rand* | Random number drawn from uniform distribution. |
| $round$ | Command within the MBO Algorithm for rounding to the nearest integer. |
| $S_{Max}$ | Maximum step size per iteration (*stepmax* within the MBO Algorithm). |
| *stepsize* | Walk step size per iteration. |
| $x_{best,k}^{t}$ | Best iteration with respect to THDv in *pop1* or *pop2*. |
| $x_{i,k}^{t+1}$ | Next iteration step. ($Lnd1(j,ci)$ within the MBO Algorithm). |

| | |
|---|---|
| $x_j^t$ | Current iteration step of *pop2*. |
| $x_{j,k}^{t+1}$ | Next iteration step of *pop2* ($Lnd2(j, ci)$ within the MBO Algorithm). |
| $x_{r1,k}^t$ | Iteration step of *pop1*, newly generated position of the monarch butterfly $r_1$ ($pop1(rr2, ci)$ within the MBO Algorithm). |
| $x_{r2,k}^t$ | Iteration step of *pop2*, newly generated position of the monarch butterfly $r_2$ ($pop2(rr3, ci)$ within the MBO Algorithm). |
| $x_{r3,k}^t$ | Randomly selected solution from *pop2* ($pop2(rr4, ci)$ within the MBO Algorithm). |
| $t$ | Current generation or iteration (*iter* within the MBO Algorithm). |
| $t+1$ | Next generation or iteration. |

Transformer Heating and Loss of Life Equations Nomenclature

| | |
|---|---|
| $B$ | Constant, stated to be 15,000 for a transformer reference hot spot. temperature of 110ºC. |
| $F_{AA}$ | Relative aging factor of a transformer. |
| $h$ | Harmonic order. |
| $Hg_r$ | Temperature gradient of the hot spot temperature to the top oil temperature at rated current. |
| $I$ | Fundamental (50Hz) current (A). |
| $I_h$ | Harmonic current for the specific harmonic order (A). |
| $I_R$ | Rated (50Hz) current (A). |
| $L$ | Predicted insulation life of the transformer (years). |
| $L_s$ | insulation design life of the transformer (years). |
| $P_{EC-H}$ | Winding eddy current loss under harmonic current (W). |
| $P_{EC-R}$ | Rated winding eddy current loss (W). |
| $P_{I^2R-H}$ | Winding resistance loss under harmonic current (W). |
| $P_{I^2R-R}$ | Rated winding resistance loss (W). |
| $P_{LL-H}$ | Load loss under harmonic current (W). |
| $P_{LL-R}$ | Rated load loss, including no-load and load losses at rated load (W). |
| $P_{NL-H}$ | No-load loss under harmonic current (W). |
| $P_{NL-R}$ | Rated no-load loss (W). |
| $\theta_a$ | Ambient temperature (ºC). |
| $\theta_h$ | Hot spot temperature (ºC). |
| $\theta_{href}$ | Hot spot temperature reference value (ºC). |
| $\Delta\theta_{or}$ | Top oil temperature rise under rated total loss (ºC). |
| $U_1$ | Fundamental (50Hz) voltage (V). |
| $U_{(h)}$ | Harmonic voltage for the specified harmonic order (V). |

# Chapter 1 – Introduction

Within the United Kingdom (UK), National Grid ESO (Electricity System Operator, 2023) has produced four possible future energy scenarios. These are ‘consumer transformation,’ ‘falling short,’ ‘leading the way,’ and ‘system transformation.’ Under a ‘falling short’ scenario, there is an expectation that the number of EVs on UK roads will increase from over one million as of 2022 to approximately thirty-three million by 2050. Furthermore, the remaining energy scenarios would result in the peak number of EVs reaching thirty-two million by 2035-2040, dropping to between twenty and thirty million by 2050.

Furthermore, the Department for Energy Security and Net Zero (DESNZ, 2023) states that, as of November 2023, there were over 1.24 million $0 \leqslant 4$ kW photovoltaic (PV) generators connected to the low voltage electricity distribution network (LV EDN) within the UK with a capacity of 3,496.0 MW. Under a ‘consumer transformation’ or ‘leading the way’ scenario, National Grid ESO (2022) predicts that the capacity of domestic rooftop PV could increase to approximately forty-one thousand MW by 2050.

Despite these predicted increases, substantial physical upgrades to the LV EDN have not yet been carried out. Existing literature (Hu, et al. (2023), Alkahtani, et al. (2020) and Sivaraman and Sharmeela (2021)) states that power-electronic loads such as electric vehicle chargers (EVCs) and distributed energy resources (DERs) including PV generation and vehicle to grid (V2G) can lead to voltage, overloading, and power quality issues. Power quality issues include harmonic distortion and flicker. Although each of these issues present significant engineering concerns, this thesis shall focus on harmonic distortion and aims to fill the identified research gaps.

As of 2016, Gandolfi (2016) states that there were approximately 28 million electricity meters within Great Britain, each representing a domestic, commercial, or industrial customer. The vast majority of these meters are connected to the LV EDN. Therefore, changes in harmonics at this voltage level will directly affect these consumers.

Some consequences of increases in harmonics are as follows:

- Increased power losses within transformers leading to increased risk of failure.
- Increased power losses within conductors, leading to reduction in current carrying capacity and heating.
- Impact on the operation of and increased failure rate of electronic equipment.
- Reduced ability of circuit breakers (CBs) to disrupt current.
- Increased errors in measuring equipment such as meters or protection relays.
- Additional copper and iron losses, vibrations, noise, heat, and increased wear of rotating machines.
- Interference with telecoms equipment.

These consequences shall be elaborated upon in Section 1.4. However, it is in a Distribution Network Operator's (DNOs) interest to minimise harmonics on the electricity distribution network (EDN). To ensure that excessive harmonic levels are identified within the UK, the Energy Networks Association (ENA, 2020) has introduced Engineering Recommendation G5 Issue 5 (ER G5/5), which states planning levels of harmonic voltages. This recommendation is followed by the UK DNOs and forms the basis for identifying when harmonic levels may cause issues for the EDN and consumers.

Despite the knowledge presented, there are gaps within existing research. The aim of this thesis is to develop knowledge of the impact of power-electronic loads and DERs on the harmonic levels of the EDN under different network conditions and ascertain the best point of connection (POC) for these devices under a range of conditions to minimise harmonic levels within the EDN.

For context, the history of the National Grid, how it has evolved and why harmonics present such an issue will be discussed below in Section 1.1.

# 1.1 – Development of the EDN and Planning

Within the UK, the EDN has evolved over close to one-hundred and fifty years. The earliest example of legislation relating to the EDN is the Liverpool (Corporation) Electric Lighting Act 1879, which gave the Liverpool Corporation the legal power to excavate streets and lay electrical cable for the purposes of public lighting. These powers were then extended to 'every local authority, company, or person' authorised to supply electricity for 'lighting and other purposes in Great Britain and Ireland' by the Electric Lighting Act 1882. This led to the rise of independent corporations each covering a specific area and operating their own power generating station and electricity system. For example, The Electricity Council (1987) states that in 1882 the Edison Electric Light Station, London was opened which operated at 110V DC; in 1885 the Brighton Electric Light Company operated a 1.8kV single-phase alternating current (AC) system with individual house transformers transforming down to 100V AC, and in 1902 the Neptune Bank power station, Newcastle was opened which produced a 6.6kV three-phase AC system.

It was not until the Electricity (Supply) Act 1926 that the first national co-ordination of electricity generation was recognised in law which led to the creation of a 132kV grid system between select power stations completed in 1935. Much of this infrastructure, or continuations of these independent systems still exist today. Direct current (DC) concentric cables operating with AC current, single-phase high voltage alternating current (HVAC) networks, reverse rotation, networks which do not 'phase-in' and historic network faults can still be found throughout the EDN. Ideally engineers would be able to continuously replace or repair assets to ensure the network operates optimally and as flexibly as possible. However, the cost of replacing or repairing those assets, which are still considered serviceable, do not warrant the expense, since replacing or repairing the assets would come at the detriment of profit and costs will be passed onto customers. Therefore, the EDN has organically grown over this period. DNO network planning engineers must consider the constraints of the network they have inherited from their predecessors during their work.

Historically, the EDN was not designed for the magnitude of power electronic loads or DERs that are seen within the modern power system or for the mitigation of harmonics. In the past, due to lower numbers of power electronic loads or DERs, the EDN did not suffer from high levels of harmonics. As of 1989, Baker, Stoker and Simpson (2012) states that generation within the UK was historically spinning type such as coal, nuclear or oil and the use of non-linear loads was much lower. However, wind generation, PV generation, battery storage and non-linear loads have increased significantly in size and number in recent years as stated by Waters (2023), Ghorbani and Mokhtari (2015), Mexis and Todeschini (2020) and National Grid ESO (2023). Hu, et al. (2023) states that although spinning generation does create harmonics, they are not the main contributors. It is the power electronics and non-linear loads which are becoming more prevalent which are considered the main source of harmonic pollution. Although not intended for this purpose, delta windings of power transformers are able to remove and block triplen harmonic currents as per Abdullah, et al. (2011) and Kalair, et al. (2017).

There are two main components to the research carried out by this thesis. Firstly, the impact of EVCs and PV generation coupled with steady-state cable fault arrangements on the total harmonic distortion (THD) and equipment of the LV EDN will be understood. Using this information, it can be identified when numbers of EVCs and PV generation connected to LV EDNs should be restricted, or harmonic reducing technology implemented. This will assist with observing compliance with ER G5/5 or reduce negative impact on equipment. Secondly, identification of the optimum locations for EVCs, PV generation and V2G to be connected to the LV EDN under a range of different network conditions and parameters with regards to voltage total harmonic distortion (THDv) levels will be carried out.

Based on the research and data previously mentioned, requests for the connection of power-electronic loads and DERs will be higher than historic levels. This research will assist network planning engineers when considering the harmonic impact of those devices, understand the effect of abnormal network running arrangements on those harmonics, and identify the most advantageous POC for those devices. This will minimise voltage harmonics on the LV EDN and increase the likelihood that it will comply with ER G5/5.

# 1.2 – Harmonic Distortion

Before progressing further, some theoretical background of THD will be discussed. THD is calculated by dividing the square root of the sum of the harmonic waveforms ($\sum_{n=2}^{\infty} I_n^2$) by the magnitude of the fundamental waveform ($I_1$), as per Woodman, Bass and Donnelly (2018) shown in Equation 1.2.1. This is used to set harmonic limits within ER G5/5 published by Energy Networks Association (2020).

Equation 1.2.1 $$THD = \frac{\sqrt{\sum_{n=2}^{\infty} I_n^2}}{I_1}$$

Where:

$I_1$ is the magnitude of fundamental current.

$I_n$ is the magnitude of specific harmonic order, orders range between $2 \leqslant n \leqslant \infty$.

$n$ is the harmonic order.

$THD$ is the total harmonic distortion.

In contrast, Total Demand Distortion (TDD) is similar to THD. However, rather than dividing by ($I_1$), it is calculated by dividing the square root of the sum of the harmonic waveforms by the magnitude of the maximum demand current over a 15 minute window ($I_L$), as per Woodman, Bass and Donnelly (2018) shown in Equation 1.2.2. This is used to set harmonic limits within IEEE (Institute of Electrical and Electronics Engineers) Std 519-2014 (IEEE, 2014). For ease of comparison with other studies, and since this thesis will focus mostly on voltage distortion, THD will be used.

Equation 1.2.2 $$TDD = \frac{\sqrt{\sum_{n=2}^{\infty} I_n^2}}{I_L}$$

Where:

$I_L$ is the magnitude of maximum demand current.

$TDD$ is the total demand distortion.

The next point to be discussed is how the quantities of each of the harmonics are calculated. Illing (2008) states that complex periodic waveforms can be broken down into an infinite or series of simpler functions. This function f(t) can be seen in Equation 1.2.3.

Equation 1.2.3 $$f(t) = \frac{a_0}{2} + \sum_{n=1}^{\infty}[a_n cos(nt) + b_n sin(nt)]$$

Where:

*f(t)* is the waveform with period t.

$a_0$ is the Fourier coefficient representing DC component of the waveform.

$a_n$ is the Fourier coefficient representing even components of the waveform.

$b_n$ is the Fourier coefficient representing odd components of the waveform.

*n* is the harmonic order.

Within Equation 1.2.3, $a_0$, $a_n$ and $b_n$ are Fourier coefficients. 0 represents the DC component and n represents the harmonic number as a multiple of the fundamental frequency. Therefore, $a_0$, represents the DC component of the waveform, whereas $a_n$ and $b_n$ represent even and odd sinusoidal components of the waveform respectively. The Fourier coefficients mentioned can be illustrated separately in Equations 1.2.4-6.

Equation 1.2.4 $$a_0 = \frac{1}{\pi}\int_{-\pi}^{\pi} f(t)\, dt$$

Equation 1.2.5 $$a_n = \frac{1}{\pi}\int_{-\pi}^{\pi} f(t)\, cos(nt)\, dt$$

Equation 1.2.6 $$b_n = \frac{1}{\pi}\int_{-\pi}^{\pi} f(t)\, sin(nt)\, dt$$

By using this method, the percentage of each harmonic magnitude can be calculated. This can get relatively complicated for complex waveforms. Therefore, computers are usually used to calculate the harmonic waveforms.

## 1.2.1 – Voltage Harmonics

Voltage harmonics on a system, and specifically how they are generated, must now be addressed. Ghorbani and Mokhtari (2015) states that non-linear loads such as fluorescent lights and EVCs inject current harmonics into the EDN. L&T Electrical & Automation (2018) explains that voltage harmonics do not originate from these non-linear loads. It is the aforementioned current harmonics flowing through system impedances, which cause a harmonic voltage drop or rise across these impedances.

A simplistic model for this can be seen below in Figure 1.2.1.1 from L&T Electrical & Automation (2018). In Figure 1.2.1.1, harmonic current produced by the harmonic current source flows back to the voltage source. Using the principle of Ohms law, voltage across an impedance is proportional to the magnitude of the current and impedance. Equation 1.2.1.1 illustrates how the harmonic voltage rise is generated and the value of the harmonic voltage rise at the load, transformer, and grid, per harmonic order.

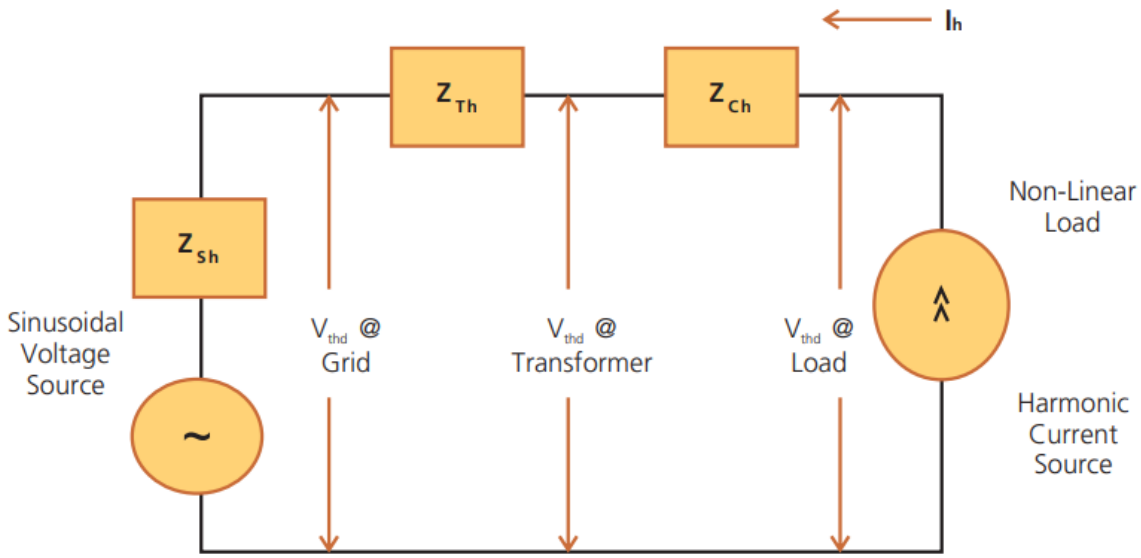


**Figure 1.2.1.1: Harmonic current flow in a system with impedance from L&T Electrical & Automation (2018).**

Equation 1.2.1.1, therefore states that the higher the impedance, or the higher the current, the higher the harmonic voltage drop or rise. Therefore, harmonic voltage drop or rise is likely to be higher when the system impedance is higher, for example, at lower voltages. Equation 1.2.1.1 is complex since there are real and imaginary components of impedance. For this reason, Equation 1.2.1.1 is only applicable for a single harmonic order, since capacitive and inductive reactance are based on the frequency of the current flowing. Taking this into account, the overall harmonic voltage drop for a single conductor, similar to Equation 1.2.1.1 can be written as Equation 1.2.1.2 below from Ghijselen, Ryckaert and Melkebeek (2003).

Equation 1.2.1.1 $$V_h = I_h(Z_{Sh} + Z_{Th} + Z_{Ch})$$

Where:

$V_h$ is the harmonic voltage drop of a single conductor per harmonic order (V).

$I_h$ is the harmonic current per harmonic order (A).

$Z_{Sh}$ is the impedance per harmonic order of the grid (Ω).

$Z_{Th}$ is the impedance per harmonic order of the transformer (Ω).

$Z_{Ch}$ is the impedance per harmonic order of the cable (Ω).

Equation 1.2.1.2 $$\Delta V_h = \sqrt{\sum_{h=2}^{\infty} |Z_h|^2 \, |I_h|^2}$$

Where:

$\Delta V_h$ is the harmonic voltage drop of a single conductor (V).

$I_h$ is the harmonic current per harmonic order (A).

$Z_h$ is the impedance per harmonic order (Ω).

## 1.3 – Engineering Recommendation G5/5

ER G5/5, published by Energy Networks Association (2020), as stated previously includes the planning and compatibility harmonic levels for EDNs within the UK and includes equations used for predicting harmonics on the EDN after the connection of equipment. Harmonics can lead to increases in network losses, interference with telecommunication circuits, overheating and failure of electronic equipment. This will be covered in more detail in Section 1.4. The following sections shall cover the harmonic levels and equations mentioned within ER G5/5.

## 1.3.1 – Harmonic Levels

The compatibility harmonic levels ⩽1kV, are set by the International Electrotechnical Commission (IEC) 61000-2-2:2018 (IEC, 2018a). The compatibility harmonic levels are assessed in relation to a flicker curve and to ensure that equipment immunity levels are not infringed. Above equipment immunity levels, damage to equipment may occur. The Electromagnetic Compatibility Regulations 2016 states that the disturbance generated by equipment must "not exceed the level above which radio and telecommunications equipment or other equipment cannot operate as intended." Additionally, equipment must be designed to have "a level of immunity to the electromagnetic disturbance to be expected in its intended use which allows it to operate without unacceptable degradation of its intended use."

To observe compliance with the compatibility harmonic levels, the planning harmonic levels are always equal to or lower than the compatibility harmonic level and should be used when designing and planning EDNs. Figure 1.3.1.1 shows the interaction of planning levels, compatibility levels and equipment immunity levels. It can be seen in this figure that there is distinct separation between the planning level and compatibility level. The compatibility level starts just before the bottom of the probability curve for the equipment immunity level. Therefore, compliance with the planning and compatibility levels will ensure that the equipment immunity level is not infringed. The equipment immunity level is the point at which equipment may become damaged as a consequence of the voltage harmonics.

The overall planning harmonic level, stated as THDv and the specific planning harmonic levels per harmonic order for ⩽0.4kV can be seen in Tables 1.3.1.1-2. The compatibility harmonic levels per harmonic order can be seen in Table 1.3.1.3. This thesis shall focus on the planning harmonic levels for ⩽0.4kV.

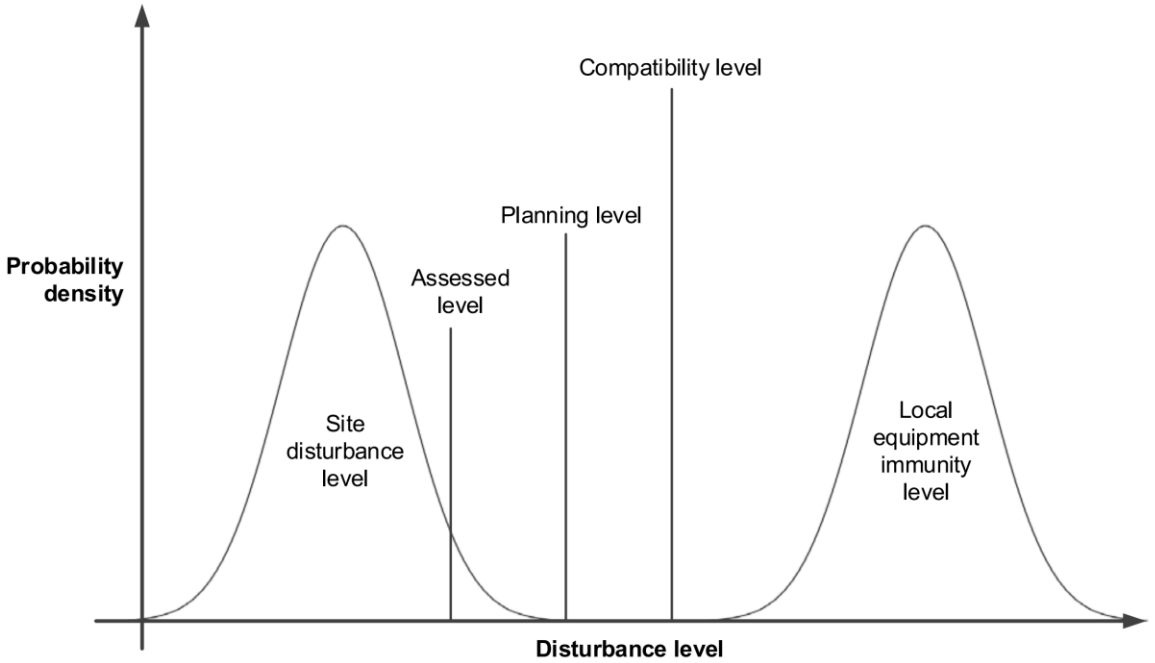


**Figure 1.3.1.1: An illustration of planning, compatibility, and immunity harmonic levels (Energy Networks Association, 2020).**

**Table 1.3.1.1: THDv planning levels at customer points of supply, separated by voltage level (Energy Networks Association, 2020).**

| Nominal voltage ($V$) kV | $THD_V$ % $h$ = 1 |
|---|---|
| $V \leq 0.4$ | 5 |
| $0.4 < V \leq 25$ | 4.5 |
| $25 < V \leq 66$ | 3.7 |
| $66 < V \leq 230$ | 3 |
| $V > 230$ | 3 |

**Table 1.3.1.2: Voltage harmonic planning levels at customer points of supply for ⩽0.4kV systems (Energy Networks Association, 2020).**

| Odd harmonics (non-multiple of 3) | | Odd harmonics (multiple of 3) | | Even harmonics | |
|---|---|---|---|---|---|
| Harmonic order ($h$) | Harmonic voltage % $h$ = 1 | Harmonic order ($h$) | Harmonic voltage % $h$ = 1 | Harmonic order ($h$) | Harmonic voltage % $h$ = 1 |
| 5 | 4.0 | 3 | 4.0 | 2 | 1.6 |
| 7 | 4.0 | 9 | 1.2 | 4 | 1.0 |
| 11 | 3.0 | 15 | 0.5 | 6 | 0.5 |
| 13 | 2.5 | ≥ 21 | 0.2 | 8 | 0.4 |
| 17 | 1.6 | — | — | 10 | 0.4 |
| 19 | 1.5 | — | — | ≥ 12 | 0.2 |
| 23 | 1.2 | — | — | — | — |
| ≥ 25 | 25/$h$ | — | — | — | — |

**Table 1.3.1.3: Voltage harmonic compatibility levels at customer points of supply for ⩽0.4kV systems (Energy Networks Association, 2020).**

| Odd harmonics (non-multiple of 3) | | Odd harmonics (multiple of 3) | | Even harmonics | |
|---|---|---|---|---|---|
| Harmonic order (*h*) | Harmonic voltage % *h* = 1 | Harmonic order (*h*) | Harmonic voltage % *h* = 1 | Harmonic order (*h*) | Harmonic voltage % *h* = 1 |
| 5 | 6.0 | 3 | 5.0 | 2 | 2.0 |
| 7 | 5.0 | 9 | 1.5 | 4 | 1.0 |
| 11 | 3.5 | 15 | 0.5 | 6 | 0.5 |
| 13 | 3.0 | 21 | 0.3 | 8 | 0.5 |
| 17 ≤ *h* ≤ 49 | 2.27(17/*h*) − 0.27 | ≥ 23 | 0.2 | ≥ 10 | 0.25(10/*h*) + 0.25 |
| 53 ≤ *h* ≤ 97 | 27/*h* | — | — | — | — |

## 1.3.2 – Harmonic Index Calculations

ER G5/5 from Energy Networks Association (2020) also contains equations for calculating the predicted LV EDN THDv levels at the point of common coupling (PCC) based on the worst case current harmonic levels of the equipment being connected and the existing background harmonic levels. Equation 1.3.2.1 states the incremental increase in harmonic voltage distortion per harmonic order for the connection of three-phase equipment and 1.3.2.2 for the connection of single-phase equipment. Worst-case reactance factor $k$ is identified by extrapolating the value from Table 1.3.2.1

**Table 1.3.2.1: Worst-case reactance factor, separated by voltage level (Energy Networks Association, 2020).**

| PCC voltage kV | Worst-case reactance factor (*k*) | | | |
|---|---|---|---|---|
| | *h* ≤ 7 | *h* ≤ 8 | *h* > 7 | *h* > 8 |
| 0.4 | 1 | | 0.5 | |
| 6.6, 11, 20, 22 | | 2 | | 1 |

Equation 1.3.2.1 $$V_{h\,c} = \frac{S_{equ\ 3ph} I_h \sqrt{h + k^2 h^2 \left(\frac{X_1}{R_1}\right)^2}}{S_{SC\ 3ph} \sqrt{1 + THD_I^2} \sqrt{1 + \left(\frac{X_1}{R_1}\right)^2}}$$

Equation 1.3.2.2 $$V_{h\,c} = \frac{S_{equ\ 1ph} I_h \sqrt{h + k^2 h^2 \left(\frac{X_1}{R_1}\right)^2}}{S_{SC\ 1ph} \sqrt{1 + THD_I^2} \sqrt{1 + \left(\frac{X_1}{R_1}\right)^2}}$$

Where:

$V_{h\,c}$ is the incremental increase in harmonic voltage distortion (% $V_{phase}$) at the PCC per harmonic order (V).

$V_{phase}$ is the rated phase-neutral voltage (V).

$S_{equ\ 3ph}$ is the rating (VA) of the three-phase equipment to be connected.

$S_{equ\ 1ph}$ is the rating (VA) of the single-phase equipment to be connected.

$S_{SC\ 3ph}$ is the three-phase short-circuit level at the PCC (VA).

$S_{SC\ 1ph}$ is the single-phase short-circuit level at the PCC (VA).

$I_h$ is the harmonic current per harmonic order (A).

$h$ is the harmonic order.

$k$ is the worst-case reactance factor from Table 1.3.2.1 above.

$X_1$ is the system reactance at fundamental frequency (Ω).

$R_1$ is the system resistance at fundamental frequency (Ω).

$THD_I$ is the per unit current total current distortion of the equipment to be connected.

To sum the harmonics from multiple sources in addition to the background harmonics, Energy Networks Association (2020) states that Equation 1.3.2.3 is used. The equation sums individual harmonic orders, therefore, producing a value of $V_h$ per harmonic order. This equation assumes operational and locational diversity between different equipment using the summation exponents shown in Table 1.3.2.2. For the 2nd, 3rd and 4th harmonic, an exponent of 1.0, or phase shift of 0° is assumed. For the 5th to 10th harmonic, an exponent of 1.4, or phase shift of 70° is assumed and for the 11th harmonic and greater, an exponent of 2.0, or phase shift of 90° is assumed. If this cannot be assumed, Energy Networks Association (2020) states that linear addition of harmonics should be used.

Equation 1.3.2.3 $$V_{h\,p} = \sqrt[\alpha]{\sum_i (V_{h\,i})^{\alpha}}$$

Where:

$V_{h\,i}$ is the $i^{th}$ harmonic voltage. This includes $V_{h\,c}$ and the background harmonic values (V).

$V_{h\,p}$ is the predicted voltage harmonic distortion per harmonic order (V).

$\alpha$ is the summation exponent stated in Table 1.3.2.2.

**Table 1.3.2.2: Aggregation exponents (Energy Networks Association, 2020).**

| Summation exponent (α) | Harmonic order (*h*) |
|---|---|
| 1.0 | $h < 5$ |
| 1.4 | $5 \leq h \leq 10$ |
| 2.0 | $h > 10$ |

Background harmonic measurements should be measured using a class A device applying 10-minute average characteristics and take place at the PCC prior to and during operation of the additional equipment. The 95$^{th}$ percentile value obtained over a seven-day period during the winter peak or summer minimum should be used for assessment. Additionally, although not used for these equations, for 33kV connections and above ER G5/5 requires background harmonic measurement at multiple remote nodes in addition to the PCC. The remote nodes could be at different voltages or within customer embedded networks. Lastly, the predicted THDv can be calculated by combining all the values of $V_h$, renamed $V_{h\,p}$ obtained in Equation 1.3.2.3 into Equation 1.3.2.4.

Equation 1.3.2.4 $$THDV_p = \sqrt{\sum_{h=2}^{h=100} {V_{h\,p}}^2}$$

Where:

$THDV_p$ is the predicted THDv.

Unfortunately, there are limitations with Equations 1.3.2.1-4. Firstly, the equations calculate the THDv at the PCC, not at all points on the EDN. An increase in current harmonics at the PCC may not cause the PCC to exceed harmonic limits, but may lead to harmonics exceeding compatibility limits at another location or voltage. Although not required for LV, this can be satisfied using a stage 3 assessment within ER G5/5.

Secondly, Equation 1.3.2.3 makes assumptions regarding the phase angle between harmonics from different sources. These are broad assumptions and may not be correct for all scenarios. However, Energy Networks Association (2020) does state that if operational and locational diversity cannot be assumed, linear addition of harmonics should be used.

Thirdly, the assessment does not take into account reconfiguration of the EDN, either as a permanent change due to a future network condition, or due to fault conditions which may lead to the EDN requiring rearrangement or becoming rearranged.

# 1.4 – The Effect of Harmonics on Power Networks

Harmonics have effects on various parts of the EDN. As previously mentioned, these include transformers, conductors, electronic equipment, CBs, rotating machines, telecommunication lines and induction meters. These will be explained in the following section. Therefore, explaining the reasons for minimising harmonics on the EDN.

## 1.4.1 – Transformers

Ceylan, et al. (2017) states that power system harmonics can lead to increases in power losses. These power losses are then converted into heat as stated by Balda, et al. (1993) which can lead to higher hot spot temperatures as highlighted by Gomez and Morcos (2003). Balda, et al. (1993) and Ceylan, et al. (2017) explain that this increased temperature can lead to increased insulation stress, which increases the risk of a winding fault and transformer failure. This therefore reduces the lifespan of the transformer. Typical distribution transformers are discussed in this section. Within the UK, a $\leqslant$2MVA delta connected 11kV high voltage (HV) winding and a star connected 400V (LV) winding with negative 30º phase displacement (Dyn11) transformer would be considered typical for the low voltage EDN.

Wan, et al. (2020) carried out experiments to ascertain the relationship between harmonic loading and hot spot temperature on a 10kVA 10kV:400V oil-insulated transformer at 60% rated load. The relationship between these factors, with both experimental and model results, can be seen within Wan, et al. (2020). The improved model used in Wan, et al. (2020) is based on improvements to the hot spot temperature model presented in IEEE Std C57.110-2018 (IEEE, 2018). The modification includes harmonic no-load loss, which was missing from the IEEE Std C57.110-2018 (IEEE, 2018) model. This model is much closer to the test results obtained during the experiments of Wan, et al. (2020). Limitations of this study include the size of the transformer used during experimentation and the omission of hysteresis and flux linkage losses. However, despite these shortcomings, the nature of the measured experimental results which have influenced the equations are thought to improve, rather than detract from their accuracy. Furthermore, since harmonic no-load loss, is a known missing component of the equations within IEEE Std C57.110-2018 (IEEE, 2018) it is thought that Wan, et al. (2020) is more reliable. Of course, without further datapoints this might not be the case.

The equations published by Wan, et al. (2020) and based on IEEE Std C57.110-2018 (IEEE, 2018) are explained and applied within Section 3.2.8 of this thesis. These equations shall be used to determine transformer hot spot temperature and loss of transformer life. As an example, using these equations for a transformer with a hot spot temperature reference value of 95ºC and predicted insulation life of 40 years, operating continuously at 105ºC, just 10ºC above its rated temperature, the transformer life would be reduced to 13.6 years. Therefore, it is critically important that harmonics within the power system are minimised where possible to ensure that assets can operate for their predicted life. It should be made clear that hot spot temperatures will be higher than the insulating oil temperature.

## 1.4.2 – Conductors

Gomez and Morcos (2003) states that harmonic current increases skin effect losses. Balda, et al. (1993) confirms this and explains that as current is forced into the outer layer of the cable, the effective resistance increases, leading to increased heating and power losses.

In addition, both Gomez and Morcos (2003) and Balda, et al. (1993) explain that harmonics can increase the impact of the proximity effect. The proximity effect states that if a current carrying conductor is positioned close to other current carrying conductors, eddy currents will be induced between the cables. This will concentrate current in areas furthest from the other cables, increasing the effective resistance of the cable, leading to heating and power losses.

It should also be noted that for a balanced, three-phase system, triplen harmonic currents e.g. $3^{rd}$, $6^{th}$, $9^{th}$ etc sum, rather than cancel on the neutral. Balda, et al. (1993) states that these neutral currents can be as "much as 1.7 times the phase current for converter loads." This could result in the neutral conductor becoming overloaded. Equations representing the effect of harmonics on the aging process of cables have been published by Patil and Gandhare (2012). These equations are explained and applied within Section 3.2.8 of this thesis.

Using these equations, Patil and Gandhare (2012) calculates the useful service life of a copper 1000mm$^2$ Cross Bonded Polyethylene (XLPE) cable, with an expected service life of 40 years at 90ºC and full rated fundamental load. For a full rated load with a current total harmonic distortion (THDi) of 20%, the temperature increases to 91ºC, dropping the expected useful life to 37 years. In contrast, for a full rated load with a THDi of 100%, the temperature increases to 124ºC, dropping the expected useful life to 8 years. Therefore, these findings highlight the importance of limiting harmonic current to prevent premature failure of cables. These calculations are based on the specific harmonic profile analysed within Patil and Gandhare (2012) and will differ between profiles.

### 1.4.3 – Electronic Equipment

Balda, et al. (1993) and Collombet, Lupin and Schonek (1999) state that electronic equipment can be impacted in a number of ways by harmonics. Firstly, many switched semiconductors and timing circuits are reliant on the zero-crossing point of the AC waveform. Multiple crossings caused by harmonics can result in timing circuits rapidly advancing and disruption to the operation of equipment reliant on switched semiconductors.

Secondly, disruption to the peak of the AC voltage waveform can result in power supply equipment reliant on this peak receiving an under or over voltage signal, even if the rms input voltage is within operating limits. If the peak distortion is large enough, this may impact on the equipment operation, even leading to equipment failure. Energy Networks Association (2020) writes that capacitors are particularly susceptible to damage from harmonics. Yukihira (2009) states that in 1994 the Japanese Ministry of International Trade and Industry prescribed current harmonic limits on large consumers supplied at a voltage equal to or greater than 6.6kV and small electrical appliances. Yukihira (2009) shows the reported equipment failures caused by harmonics within Japan per year between 1989-2006. This source shows that after 1993, the number of reported equipment failures dropped significantly from just over one-hundred and ten in 1993 to just over sixty in 1994.

### 1.4.4 – Circuit Breakers and Fuses

Balda, et al. (1993) explains that harmonics can reduce the ability of CBs to disrupt current. Therefore, this section shall investigate the effect of harmonics on three types of CBs. These are solid-state, magnetic-only, and thermal-magnetic types. The solid-state CB trip mechanism requires phase sensors, usually current transformers, a shunt trip coil, and a relay containing protection characteristic data, output contacts and a central processing unit.

It has been found by Estrada, Briggs and Khosla (1995) that temperature rise before tripping was not significant for LV solid-state type CBs and they operated within manufacturer trip times for 50-107% THDi. However, LV magnetic-only type CBs are adversely impacted by harmonic current. Between 50.5-68.4% THDi and 101.78-158.89% of trip setting, it was found that this type of CB failed to trip. Additionally, under a current of 158.89% of trip setting and 51.4% THDi, the magnetic-only type CB started smoking after 3,291s and CB temperature increased by 88.7ºC. Furthermore, for a 50A, 2-pole LV thermal-magnetic CB at 50% THDi and 150% of trip setting, the CB operated 20-30% slower than the manufacturer specified trip time and CB temperature increased by 22.6ºC.

The majority of CBs deployed by DNOs within the UK are of the type requiring a shunt trip coil and therefore may not be significantly negatively impacted by harmonics. However, there may be pockets of older DNO networks or private industrial customers still utilising magnetic-only or thermal-magnetic CBs.

Pinyol (2015) also explains that harmonics can increase the skin and proximity effect within fuses, similar to conductors previously mentioned. The additional heat generated by these harmonics can change the trip-time characteristic of the fuse or lead to premature operation. This could become a nuisance on DNO LV EDNs, since the majority of DNO LV EDNs outside of Central London use fuses. Central London uses air circuit breakers (ACBs) due to the operational requirements of running interconnected mesh networks.

### 1.4.5 – Meters and Relays

Current and voltage harmonics can lead to errors in induction disk equipment in meters or protection relays. For example, Collombet, Lupin and Schonek (1999) explains that for a class 2 induction meter, a $5^{th}$ order voltage and current harmonic of magnitude 5% of the fundamental will increase the error of the meter by 0.3%. Errors such as this will lead to inaccurate meter billing for customers and potential grading issues with protection relays. Morva, et al. (2017) explains that due to the design of induction type meters, the triplen harmonics (power of harmonics which are multiples of three, e.g., $3^{rd}$, $6^{th}$, $9^{th}$, $12^{th}$, $15^{th}$…) are ignored, but the meter is sensitive to other odd harmonics such as $5^{th}$, $7^{th}$, $11^{th}$, $13^{th}$, $17^{th}$…. Diahovchenko, et al. (2019) and Chou and Liu (1994) state the equations used to calculate the error of induction meters based on harmonic order and magnitude.

For smart meters and numerical protection relays, Diahovchenko, et al. (2019) states that errors caused by harmonics depend on the computing algorithms used. The algorithms can be divided into two groups, Fourier transforms and electrical methods of power determination. Fourier equations can be seen in Equations 1.2.3-4. Equations for these errors will not be covered, as errors will vary depending on the algorithm type and specific variations within the algorithms used. As an example, Shklyarskiy, Hanzelka and Skamyin (2020) found that if THDv did not exceed 14% and THDi did not exceed 40%, error within the electronic meter tested did not exceed 10%. Furthermore, if THDv did not exceed 3.5% and THDi did not exceed 33%, error within the electronic meter tested did not exceed 5%.

## 1.4.6 – Rotating Machines

Rotating machines are also affected by harmonics. Collombet, Lupin and Schonek (1999), Domeki, et al. (2004) and Wakileh (2003) explain that similar to transformers, rotating machines will experience additional copper and iron losses when harmonics are applied. A substantial proportion of these losses will be within the rotor. This is caused by the difference between the speed of the rotor and the magnetic fields induced by the harmonics. Additionally, these magnetic fields can cause pulsating mechanical torque, producing vibrations within the machine and audible noise, generating heat, and increasing wear. Wakileh (2003) has produced equations which can be used to quantify copper and iron losses due to fundamental and harmonic components.

## 1.4.7 – Telecoms Equipment

Lastly, Balda, et al. (1993) and Zubi and Khalifa (2017) explain that power system harmonics can lead to interference with telecoms equipment. Jacobson (2005) states that telecommunication systems are designed with interference in mind. Therefore, the majority of interference can be rejected by noise mitigation systems such as shielding, noise filtering devices or twisted pairs.

Despite this, small amounts of interference can still be induced in telecoms circuits, usually when power and telecoms circuits are electromagnetically coupled by being run in close proximity parallel over long distances. The interference could be induced by the fundamental waveform which could lead to damaged equipment, safety concerns and system disruption, especially from HV power circuits. Alternatively, the interference could be induced by the harmonics, which could lead to system disruption and additional noise on the telecommunication circuit. The voltage induced in an unshielded telecoms circuit from a power circuit can be calculated using the equations stated within IEEE Std 367-2012 (IEEE, 2012a).

A simplified approximation of Carson's equation for mutual impedance between a power and telecoms circuits can be seen in equation 35 from IEEE Std 367-2012 (IEEE, 2012a). IEEE Std 367-2012 (IEEE, 2012a) states that this equation and its supporting equations are accurate up to 5kHz and are valid for buried telecoms circuits if the natural logarithm term is removed and $h_2$ which represents the circuit height in metres is replaced with a negative number equal to the circuit depth. The burial depth must also be a small fraction of the skin depth of the earth. However, based on Ostheimer (2013) most cables will be within 2m of the surface, making equation 35 from IEEE Std 367-2012 (IEEE, 2012a) valid.

Eirgrid (2013) explains that the most problematic harmonic distortions are 500-1200Hz since these frequencies are primarily used to transmit speech for telephone communication. Jacobson (2005) states that a bandpass filter is used for these communication circuits. However, these filters allow approximately 300-3000Hz to pass, therefore large amounts of 500-1200Hz interference will cause a significant issue during communication. When determining the influence power harmonics will have on the telecoms circuits, telephone interference factor (TIF) is used. Each harmonic which could be induced is assigned a weighting. Ball and Poarch (1961) explain that this TIF weighting is based on:

- "The relative subjective effect of frequency $f$ in the message circuit, as heard in the telephone (message weighting)."
- "The coupling between the power and telephone circuits, assumed to be directly proportional to $f$."

# 1.5 – Abnormal Running Arrangements

For the purposes of this thesis, abnormal running arrangements shall mean an unrepaired network fault which has been left as a permanent running arrangement. Three specific network faults which can be left unrepaired and remain electrically sound include a two-phase fault, a three-phase fault (short circuit between phases but clear of neutral and earth) and a backfed open circuit fault on one, two or three phases plus neutral. Diagrams showing these arrangements can be seen below in Figures 1.5.1-4.

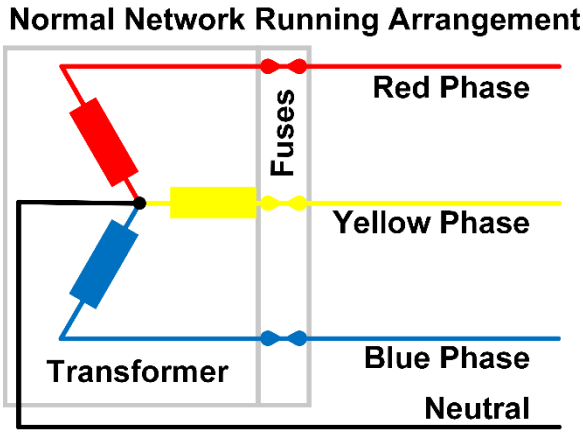


**Figure 1.5.1: Normal network running arrangements for a wye connected three-phase system.**

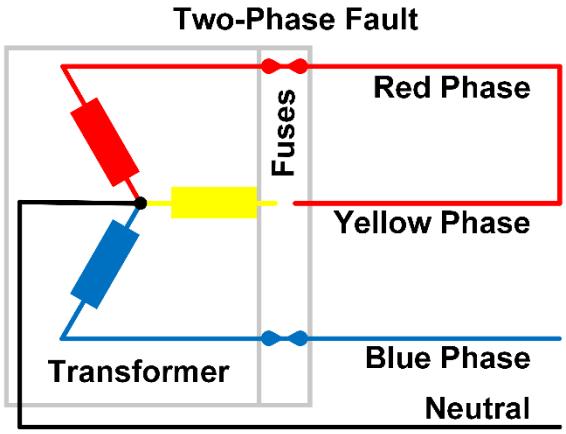


**Figure 1.5.2: Two-phase fault running arrangements for a wye connected three-phase system.**

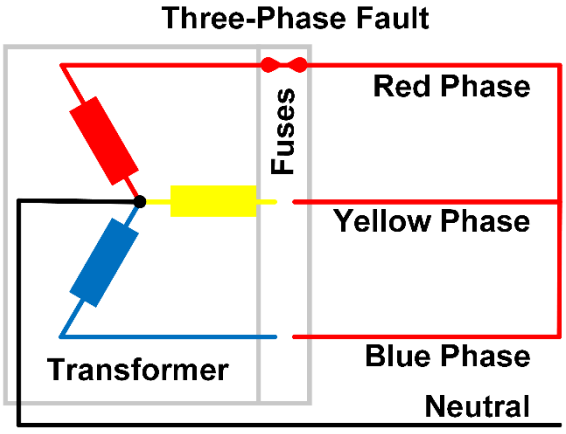


**Figure 1.5.3: Three-phase fault running arrangements for a wye connected three-phase system.**

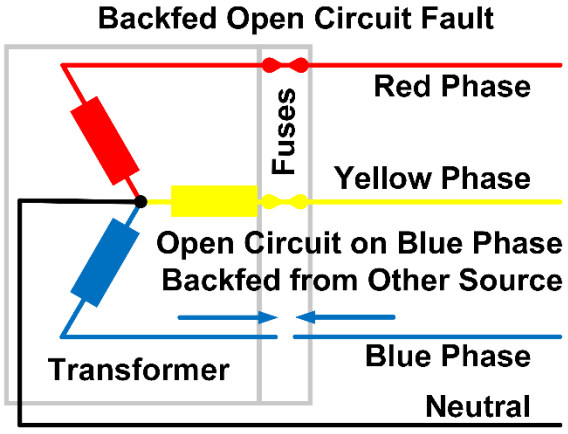


**Figure 1.5.4: Backfed open circuit fault running arrangements for a wye connected three-phase system.**

As long as all points of supply receive a voltage within the limits stated within the Electricity Safety, Quality and Continuity Regulations 2002 (ESQCRs) and earth loop impedance measurements remain within the limits stated by ER P23 Issue 2 2018 (Energy Networks Association, 2018), abnormal running arrangements can be left on the LV EDN and remain compliant.

A phase-to-phase fault represents a weld or short circuit between phases. One phase will support the load of the welded phase(s), whilst the remaining phase(s) fuse will blow at the LV pillar or downstream location supplying the cable. Therefore, in this case there is a short circuit between phases. However, the phases remain clear of earth and neutral. These faults can occur for a number of reasons, including cables or joints being manipulated by high energy flows during insulation breakdown or damage. Most suburban residential LV EDNs, excluding those with apartment complexes or shops will usually be comprised of single-phase points of supply. This type of fault will only remain compliant with the ESQCRs as long as only single-phase points of supply are connected to the LV EDN. A single-phase supply terminal can be seen in Figure 1.5.5. This would not be applicable in the event of three-phase points of supply, such as those found in apartment complexes, commercial or industrial properties as a phase-to-phase fault would result incorrect voltages being present at the supply terminals. Therefore, no longer being compliant with the ESQCRs. A three-phase supply terminal can be seen in Figure 1.5.6.

An open-circuit fault means that at least one phase conductor has isolated itself from the rest of the EDN at the fault location, therefore not allowing any current to flow. Open-circuit phase faults for single-phase points of supply can also remain compliant with the ESQCRs as long as supplies are back-fed from another source such as a linkbox. For three-phase points of supply, an additional condition that both the original and alternative supplies are in phase must be met to remain compliant. An example of a linkbox can be seen in Figure 1.5.7. In order to backfeed the open-circuit fault, fuses will be inserted into the linkbox. Fuses inserted into the linkbox must grade with fuses on the LV side of the transformer. Therefore, if the fault is not clear of earth or another phase, the fuse at the linkbox will blow rather than the fuse back at the transformer. However, in Figure 1.5.4 it is assumed that the open-circuit fault is clear of earth and the blue phase fuse was inserted without any issues.

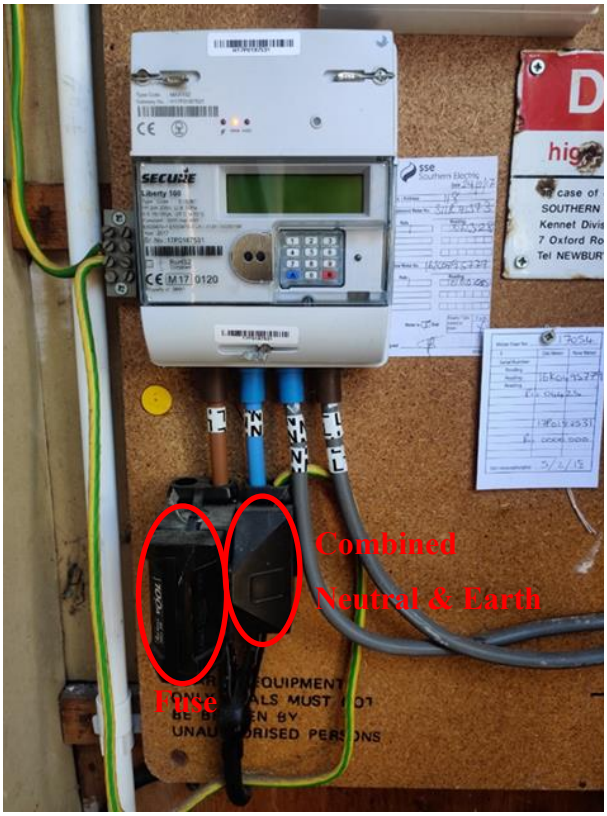


**Figure 1.5.5: Single-phase Protective Multiple Earthing supply terminal (PME, combined neutral earth) with a 100A fuse carrier on the left, neutral block on the right and meter on top in Slough area.**

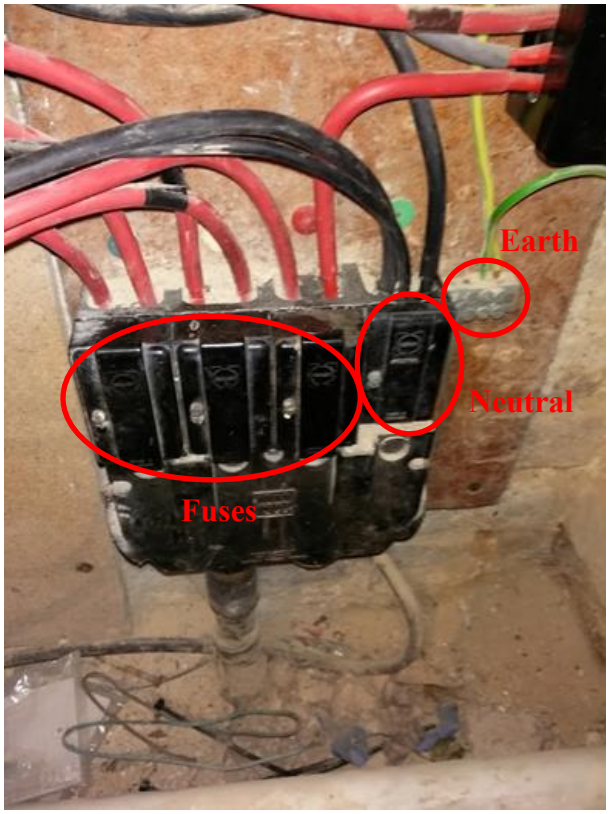


**Figure 1.5.6: Three-phase separate neutral earth (SNE) supply terminal with three 100A fuse carriers on the left, neutral block in the middle and earth block on the right.**

**Figure 1.5.7: Four-way LV linkbox showing two solid ways and two open ways in Hounslow, London.**

**Figure 1.5.8: 95mm Consac to 95mm Wavecon mains cable joint (Thorne & Derrick International, 2020).**

Two reasons for these types of faults are due to the cable being manipulated during a fault, or in the case of a phase-to-phase condition, could be due to the cable phases being combined at a jointing position due to an open circuit fault closer to the substation. As long as only single-phase supply terminals are connected to the cable, the configuration remains compliant with the ESQCRs and therefore no further work is required. The reason cables can be manipulated to this degree is due to the amount of power that flows under fault conditions. Electricity North West (2019) states that power flows during an LV fault could be up to a maximum of 19.4MVA. Even if the fault level is a fraction of this value, the total amount of energy is enormous, which results in conductors being melted, welded together, or blown apart. To help visualise how these complex faults occur, please see Figure 1.5.8. This shows how little clearance the cores have inside a joint. Therefore, the magnitude of power that flows could quite easily melt, weld, or blow apart conductors.

Although it remains good practice to repair a fault, this is not always practicable due to staffing constraints or digging permit requirements. Office of Gas and Electricity Markets (Ofgem, 2015) states that faults should be repaired within a 12-hour window. However, as long as the EDN maintains supplies whilst remaining compliant with the ESQCRs, no further work is required, and the fault may be left on the system. Additionally, if supplies are maintained, such as the faults mentioned earlier in this section, it may not be practicable to determine a fault is present due to the lack of any available point of testing such as an LV linkbox or pillar. Therefore, these faults may be left on the LV EDN indefinitely.

## 1.6 – Motivation and Research Aims

The research aims, objectives, motivation, problem formulation and further considerations will be covered in detail within Section 2.5. However, to ensure that the reader understands the purpose of this thesis, a summary of this information has been produced below.

Within Chapter 2 it will be identified that there are a lack of studies which have considered the impact of network faults on the harmonic levels of the EDN under high penetrations of EVCs and PV generation. Additionally, the maximum device penetration levels under various EDN fault conditions to remain compliant with ER G5/5 has not been investigated.

Furthermore, studies considering the optimum POC of EVCs and V2G with respect to reducing harmonic levels has not been carried out. A study looking at the optimum location of PV generation on a 15kV EDN with regards to THDv and THDi has been produced. However, LV EDNs, changes in phase angle, network parameters, base loads, and different running arrangements such as faults have not been considered.

Firstly, this thesis will aim to explore the impact that EVCs and PV generation have on the harmonic levels of LV EDNs under fault conditions, identify penetration limits, and determine the effects those levels have on EDN assets. Secondly, this thesis will aim to identify the optimal POC of EVCs, PV generation and V2G to reduce harmonic levels on the LV EDN under a range of network parameters, loads and characteristics.

## 1.7 – Organisation of the Thesis

The remaining parts of this thesis are organised as follows:

**Chapter 2 – Literature Review of EVCs, PV generation, and V2Gs**

This chapter shall examine existing literature pertaining to EVCs, PV generation and V2Gs. The size, current harmonic profile, cumulative effect of these devices on EDN voltage harmonics, and optimal location of each of these devices with respect to EDN voltage harmonics shall be researched. It is essential that this in-depth review of literature is carried out since this information will allow for research gaps to be identified and research objectives for this thesis to be determined.

### Chapter 3 – The Effect of EVCs and PV Generation on the Harmonic Levels of an LV EDN

This chapter shall produce accurate harmonic models for the EDN, EVCs and multiple PV generation profiles. The case-study EDN identified to be modelled shall be chosen based on the density of ultra-low emission vehicles (ULEVs) and PV generation. The EDN, EVC and PV generation models shall then be validated against existing research carried out in Chapter 2. At stated penetration levels of EVCs, PV generation and a combination of the two devices, phase and neutral current and voltage harmonics for these scenarios shall be determined for one EVC and three PV generation harmonic profiles. Harmonic limit breaches of phase voltage harmonics and maximum penetration levels in accordance with ER G5/5 shall be identified. Lastly, the effect these harmonics have on transformer and conductor lifespan shall be determined in addition to risk of injury to the public.

### Chapter 4 – The Effect of EVCs and PV Generation on the Harmonic Levels of an EDN Under Fault Conditions

Using the case-study EDN produced in Chapter 3, the effect of steady-state fault conditions on the harmonic levels of EDNs with high levels of EVCs, PV generation and a combination of the two devices shall be obtained.

The fault conditions investigated shall be three-phase, two-phase, open circuit, and complex faults. Similar to Chapter 3, phase and neutral current harmonics, phase voltage harmonics and neutral voltage levels for these scenarios shall be determined for one EVC and three PV generation harmonic profiles. Harmonic limit breaches of phase voltage harmonics and maximum penetration levels in accordance with ER G5/5 shall be identified. From this data, predictions shall be produced and used to identify when breaches of harmonic limits are likely under fault conditions across multiple feeders. Lastly, the effect these harmonics have on transformer and conductor lifespan shall be determined in addition to risk of injury to the public. From this data, predictions shall be produced used to identify the impact of faults on transformer and conductor asset life. This information can be used by network planning engineers to understand the impact of network faults on EDN harmonic levels, maximise asset life and reduce the risk of injury to the public.

**Chapter 5 – Advanced Learning Method Enabled Optimisation for THDv Minimisation**

This chapter shall produce two algorithms used to identify the optimum POC for EVCs, PV generation and V2G on the LV EDN with respect of THDv levels. A simplified version of the case-study network was produced to improve the reliability of conclusions drawn and a V2G harmonic model was produced. The algorithms were repeated for a range of network parameters, conditions and harmonic phase-shifts between the background EDN harmonics and the device under investigation. The results were then analysed to identify the optimum POC for the device and determine what parameters or conditions influence this optimum POC. This information can be used by network planning engineers when planning new connections of these devices on the EDN to minimise THDv levels.

**Chapter 6 – Conclusions and Future Work**

Descriptions of the primary research outcomes and contributions of the thesis are presented, as well as the conclusions and recommendations for future research.

# Chapter 2 – Literature Review of EVCs, PV Generation, and V2Gs

This chapter shall examine existing literature pertaining to EVCs, PV generation and V2Gs. The size, current harmonic profile, cumulative effect of these devices on EDN voltage harmonics, and optimal location of each of these devices with respect to EDN voltage harmonics shall be researched in Sections 2.1-4. This review of existing literature will allow for research gaps to be identified and research objectives for this thesis to be determined. The motivation, research aims, objectives, and further considerations shall be covered within Section 2.5.

For the purposes of this literature review, measured data, from reliable sources should be used for the collation of data. Simulated data, although potentially from a reliable author may not be as reliable as measured data. This is not an indictment of the scientific contribution of simulated data over measured data, however, simulated data is generally accepted as being more susceptible to results which contain a degree of error. Reasons for this could be variables which have not been accounted for within the simulation such as background harmonics, variations in model architecture between manufacturers not disclosed to the public, limitations within the simulation software itself or assumptions made. Using data obtained from reliable measured sources should improve the validity this research.

## 2.1 Electric Vehicle Chargers

In the period between December 2011 and September 2023, the Department for Transport (DfT) and Driver and Vehicle Licensing Agency (DVLA) (2023a) found that the number of ULEVs registered on UK roads increased from 8,695 to 1,443,791. Additionally, based on a ‘falling short’ scenario from National Grid ESO (2023) it is predicted that the number of EVs within the UK will increase to thirty-three million by 2050. This presents significant potential loading and harmonic issues.

Load issues relating to EVs on the LV EDN with existing infrastructure has largely been solved using demand side load control with smart meters explained by Silva and Mohammed (2013), where EVC charging could be limited or switched off remotely to prevent system overload or smooth out peak demand. However, there has been little research into using the same technology to limit harmonics. In fact, solving load issues by reducing the charging rate of every EVC on the network in comparison to switching off some EVCs could lead to increased THDi, since Watson, et al. (2015) and Gomez and Morcos (2003) found that, although current levels of EVCs are lower at reduced charging rates, THDi is higher.

Monteiro, Pinto and Afonso (2019) provides an insight into the architecture and control scheme of a single-phase EVC which uses a bridge of four IGBTs. These IGBT gates are used to convert the grids AC waveform into a pulsating DC wave. A dc-link capacitor then stores and discharges energy to produce a smooth DC waveform. A further two IGBTs are used to establish a buck or boost voltage which will either charge or discharge the battery. Due to the architecture, and the conversion of current from AC to DC, harmonic current will be drawn by the EVC.

### 2.1.1 – EVC Charging Rate

Regarding home charging rate, EVCs can charge up to 11.5kW from a wall box as per Tesla (2023). However, the rate at which EVs can be charged varies. Data published by the DfT and DVLA (2023a), shown in Table 2.1.1.1 illustrates the five most common EVs within the UK as of Q4 2022. Of these, two can charge up to a maximum rate of 11.5kW, and two are limited to 3.6kW when charged via a domestic wall box charger. The charging rates shown are the maximum, and therefore, limited by the property supply and the wall box fitted. Therefore, an EV rated to charge at 11.5kW may be reduced to 3.6kW due to these constraints. These charging rates can be corroborated by Dale (2018) and Dermot (2018).

**Table 2.1.1.1: Five most common EVs within the UK as of Q4 2022 and their maximum charging rate. DfT and DVLA (2023a), Tesla (2023), Nissan (2023), Mitsubishi Motors Europe B.V. (2017) and Bayerische Motoren Werke (2020).**

| Make | Generic model | Fuel | 2022 Q4 | Maximum home charging rate |
|---|---|---|---|---|
| TESLA | TESLA MODEL 3 | Battery electric | 83,401 | 11.5kW |
| NISSAN | NISSAN LEAF | Battery electric | 52,106 | 6.6kW |
| MITSUBISHI | MITSUBISHI OUTLANDER | Plug-in hybrid electric (petrol) | 47,681 | 3.6kW |
| BMW | BMW 3 SERIES | Plug-in hybrid electric (petrol) | 41,310 | 3.6kW |
| TESLA | TESLA MODEL Y | Battery electric | 35,300 | 11.5kW |

## 2.1.2 – EVC Harmonic Profile

Based on existing literature, such as the papers written by Dale (2018) and Paolo (2017), individual EVCs, when connected to an LV network produce harmonic distortions. There is also consensus between academic papers including Li, Wang and Deng (2018), Yuan, et al. (2017) and Zhao and Yue (2017) that the majority of harmonics produced by the EVCs are $5^{th}$, $7^{th}$, $11^{th}$, and $13^{th}$. The exact proportions of these harmonics depend on the type of EVC used and the number of pulses deployed.

For this thesis, a range of EVC profiles needed to be created. Unfortunately, "EV manufacturers are unwilling to share the specific data on EVs currently in circulation in the UK" (Dale, 2018). Sources such as Pinto, et al. (2017), Ceylan, et al. (2017), Deilami, et al. (2010), Lucas, et al. (2015), Watson, et al. (2015), Moses, et al. (2010) and Gomez and Morcos (2003), quote values of THDi for EVCs ranging from 2.5% to 47%. This is a very large range of values for THDi. The higher THDi values tend to be from simulated, rather than measured results such as in Deilami, et al. (2010), Ceylan, et al. (2017), Moses, et al. (2010) and Gomez and Morcos (2003).

Lucas, et al. (2015) uses measured results, however, this is for fast chargers, which are not currently common in residential housing estates as corroborated by Table 2.1.1.1. Pinto, et al. (2017) uses the measured data for an EVC. However, this is for an unknown single charger on an unknown LV network. An isolating transformer was also installed between the grid and the house to convert 220V split-phase to 220V single-phase. Therefore, this will have increased the impedance of the EVC connection, rendering the results unreliable.

Dale (2018) produced a <16A median current harmonic profile measured for EVCs on Western Power Distributions (WPDs) 'Electric Vehicle Emissions Testing' project. This profile contains the median of the harmonic profiles of the makes and models used within Dale (2018) which were the most popular battery electric vehicles (BEVs) and plug-in hybrid electric vehicles (PHEVs) in the UK at the time of the study. The median THDi of the EVCs are 3.54%. By comparing Dale (2018) and Dermot (2018), it can be seen that these studies share the majority of vehicles. Additionally, Table 2.1.1.1 contains three of the EVs used within Dale (2018) and Dermot (2018). The discrepancy occurs with the Tesla models S and X, which are replaced by the later models 3 and Y within Table 2.1.1.1. Distortion rate could have arguably been reduced, however, all of these Tesla models share the same charging rate. Therefore, the median current harmonic profile appears to be representative of EVCs in the UK. Furthermore, the background harmonic distortion within Dale (2018) is stated to be 1.36%, giving a baseline for comparing to other studies.

Watson, et al. (2015) measured the THDi for a Nissan Leaf (11%), MiEV (8.78%) and Mitsubishi Outlander (2.5%). This was measured for vehicle charging from a household socket with an in-line charger (portable AC-DC converter with three-pin plug), rather than a dedicated external charger. However, the results for a JuicePoint dedicated external charger did not vary far from the in-line values at 10.6%, 7.1% and 1.8% respectively. A Tesla Model S was also measured at 4.8% for a 16A charger and 6.1% for a 32A charger. It can be seen that the values from Watson, et al. (2015) operate around the median value stated in Dale (2018) of 3.54%. Unfortunately, this study looks at a very limited number of vehicles not representative of the UK as a whole and does not state the background harmonic distortion, making the results hard to verify or accurately use. Therefore, this data could not be used for this simulation study, however, it does, to a degree, verify the THDi value from Dale (2018).

Foskolos (2021) also measured THDi from four different EVCs. The harmonic current measurement was taken using a Yokogawa WT3004E, which is compliant with IEC 61000-4-7:2008 (IEC, 2008). All four of the EVCs measured were single-phase, mode 3 chargers. The grid connection was via an 800kVA, 10kV to 400V transformer. The mean charging rate for each of the EVCs are as follows, EV1, 20.9A, EV2, 16.7A, EV3, 13.3A and EV4, 14.5A. This results in mean measured THDi values of EV1, 5.4%, EV2, 4.7%, EV3, 4.2% and EV4, 4.0%. Foskolos (2021) shows the harmonic spectrums of theses EVCs against IEC61000-3-12 (IEC, 2011) and IEC61000-3-2 (IEC, 2018b) harmonic limits. It can be seen that EV3 and EV4 exceed the limits of IEC61000-3-2 (IEC, 2018b) for the 23$^{rd}$, 25$^{th}$, 35$^{th}$, and 37$^{th}$ harmonic orders and limits are reached for the 13$^{th}$, 31$^{st}$ and 33$^{rd}$ harmonic orders. EV1 and EV2 are only shown up until the 13$^{th}$ harmonic order but do not exceed or meet the limits of IEC61000-3-12 (IEC, 2011). The THDi values measured for EVs 1-4 are of a similar magnitude to the 16A median current harmonic profile measured within Dale (2018).

A summary of the mean/steady state THDi, charging rate and vehicle model for the EVCs measured by Dale (2018), Watson, et al. (2015) and Foskolos (2021) can be seen in Table 2.1.2.1.

**Table 2.1.2.1: Summary of measured THDi for EVCs captured within this literature review.**

| Paper/Author(s) | Mean/Steady State THDi | Charging rate | Vehicle Model |
|---|---|---|---|
| Dale (2018) | 3.54% | <16A (3.6kW) | <16A median current harmonic profile measured for EVCs within the study. |
| Watson, et al. (2015) | 11.0% | 10.9A (2.3kW) | Nissan Leaf |
| | 10.6% | 16.2A (3.7kW) | |
| | 8.78% | 9.25A (2.1kW) | Mitsubishi MiEV |
| | 7.1% | 13.2A (3.0kW) | |
| | 2.5% | 9.48A (2.2kW) | Mitsubishi Outlander |
| | 1.8% | 14.4A (3.3kW) | |
| | 4.8% | 16A (3.7kW) | Tesla Model S |
| | 6.1% | 32A (7.4kW) | |
| Foskolos (2021) | 5.4% | 20.9A (4.8kW) | Unknown |
| | 4.7% | 16.7A (3.8kW) | Unknown |
| | 4.2% | 13.3A (3.1kW) | Unknown |
| | 4.0% | 14.5A (3.3kW) | Unknown |

It should also be noted that the harmonic current transients drawn and THDi at the start and end of an EV charging cycle differs from the steady state period. Watson, et al. (2015) shows that in the first twenty seconds of the charging cycle, the harmonic current magnitude is low and the THDi is high when compared to the steady state charging current. Due to the short duration of this transient period, this will not be simulated during the study. Additionally, the magnitude of the harmonic current is lower. Therefore, it is assumed that the effect on the network will not be as great as the steady state period and therefore the steady state period should be simulated as a worst case.

Watson, et al. (2015) shows that towards the end of the charging cycle the same effect occurs, the current drops off and the THDi increases. Despite an increase in THDi, the relatively lower fundamental current means that the magnitude of the harmonic current is lower than the steady state charging current. Therefore, similar to the first twenty seconds of the charging cycle, it is assumed that the effect on the network will not be as great as the steady state period and therefore the steady state period should be simulated as a worst case. However, as mentioned previously, reducing the charging rate of every EVC on the network in comparison to switching off some EVCs to cope with load restrictions could lead to increased THDi.

### 2.1.3 – EVC Cumulative Effect

Research by Dale (2018), Deilami, et al. (2010), Moses, et al. (2010), Staats, et al. (1998), Watson and Watson (2017a), and Xu, et al. (2014) include residential base load and found that increases in the numbers of EVCs increase the THDv on the LV system under steady state conditions. It was also found that the rate of increase of THDv decreases as shown within Deilami, et al. (2010) and Xu, et al. (2014). However, it should be noted that background THDv has not been taken into account in these studies. In a system with a level of background harmonics, even linear loads will draw harmonic current. Therefore, the harmonic current contribution from the EVC itself is lower than the total harmonic current drawn. Within these two studies, the EVC THDi was set at somewhere between 2-5.3% for Xu, et al. (2014) and 31.9% for Deilami, et al. (2010).

The findings of Deilami, et al. (2010) and Xu, et al. (2014) are corroborated by Bentley, et al. (2010), Ceylan, et al. (2017), Gomez and Morcos (2003), Li, Wang and Deng (2018), Lucas, et al. (2015), Orr, Emanuel and Pileggi (1984), and Yuan, et al. (2017), which show that when multiple EVCs are connected to the EDN, the current harmonics from these EVCs will start to cancel. The magnitude of the cancellation will vary depending on the variety of EVCs connected and EDN construction. A degree of cancellation can be assumed for LV grids with separate services and driveways for each dwelling as per Energy Networks Association (2020). However, this might not be assumed for multiple chargers coupled to a single bus such as blocks of flats with communal EVC areas.

Ceylan, et al. (2017) found that both THDi and THDv dropped below that of the base load THDi and THDv after 20:30 in the evening. Although the simulation contains both PV and EV, it is assumed that PV will not produce any current after this time. Ceylan, et al. (2017) and Dale (2018) are the only two papers studied which do not assume the base load has a negligible THDi. The base load THDi of Ceylan, et al. (2017) is assumed to be 8.24% as per the findings of Cherian, Bindu and Chandramohanan Nair (2016) and verified by Ruwaida, Holmberg and Bollen (2015), which found that for 95% of the measured network points, the THDi value was 11% or lower. THDv dropping below that of the base load suggests that the magnitude of the harmonic current drops, not just the THDi. This suggests a significant level of harmonic cancellation between the base load and EVCs. However, this level of harmonic cancellation has not been corroborated by other studies.

Some limitations of the studies mentioned should now be considered. It was found that methodology was inconsistent between sources. For example, Li, Wang and Deng (2018) and Yuan, et al. (2017) used three-phase EVCs, Xu, et al. (2014) simulated up to five single-phase EVCs, Yuan, et al. (2017) simulated up to sixteen EVCs and Ceylan, et al. (2017) investigated the extent of penetration of PV generation and EVCs concurrently, rather than exact numbers. However, despite methodology being inconsistent between sources, with the exception of Ceylan, et al (2017), it can be ascertained that THDv increases as EVC penetration increases and THDi, or the rate of increase of THDv decreases as EVC penetration increases.

The studies mentioned produced results for multiple numbers of EVCs using simulation software as opposed to data collected from networks with EVCs. Therefore, the results of these studies are dependent on the assumptions made and the methods used. Unfortunately, the results of these studies have not been verified using real data obtained from monitored networks. Lastly, the majority of studies which have looked at the effect of multiple chargers such as Ceylan, et al. (2017), Deilami, et al. (2010) and Orr, Emanuel and Pileggi (1984) assume that all of the EVCs used on the EDN produce the same harmonic current profile. However, it is likely that a proportion of the EVCs chosen by each household will be different. Watson and Watson (2017a) applied a different methodology to their simulation and randomly assigned different EVCs using a lookup table. However, in line with other studies, increases in EVCs connected to the network within Watson and Watson (2017a) leads to increases in THDv.

In conclusion, research shows that by considering base load and phase shift, the general trend is that THDv on a pre-existing three-phase LV AC network increases and THDi, or the rate of increase of THDv decreases with increased numbers of EVCs. Future simulation studies of pre-existing three-phase LV AC networks should take into account phase shift, different EV manufacturers, base load THD, minimum loading and abnormal network running arrangements.

### 2.1.4 – EVC Optimal Location

In this section, existing literature regarding the optimal connection location of EVCs on EDNs is reviewed. Firstly, the majority of existing literature such as Jamatia, Bhattacharjee and Sharma (2022), Golla, Sudabattula and Suresh (2022), Pal, Bhattacharya and Chakraborty (2020), Awasthi, et al. (2017), Bilal, et al. (2021), which considers the optimum connection location of EVCs, consider only voltage drop and power losses. This falls outside of the focus of this thesis.

In contrast, Mehar and Senouci (2013) carries out optimisation of EVC location with regard to cost of charging stations' location. Additionally, Islam, Shareef and Mohamed (2018) carried out optimisation of EVC location with regard to EV transportation energy loss, station build-up cost and substation energy loss. Again, this falls outside of the focus of this thesis.

Lastly, Nasir, Jamian and Mustafa (2018) carried out optimisation of variable passive filter location to mitigate harmonic distortion and network losses. This does fall within the focus of this thesis. The algorithm deployed 22 filters across the network to improve maximum THDv by 39.14%, maximum THDi by 52.5%, and apparent power loss by 2.96%. Although the focus of this paper was 132 EVCs connected to a 449 bus 23kV system, the methodology could be applied to any voltage or configuration. Therefore, the optimum connection of filters to minimise harmonics should be discounted from future work as has already been carried out by other researchers.

These papers cover a range of algorithms which may be of use for network optimisation regarding harmonics and should be considered for future work. These are Binary Lightning Search Algorithm (BLSA), Genetic Algorithm (GA), Grey Wolf Optimisation (GWO), Harris Hawks Optimisation (HHO), Modified Lightning Search Algorithm (MLSA), Pareto-Fuzzy Technique (PFT), Particle Swarm Optimisation (PSO), Symbiotic Organism Search (SOS) and Whale Optimisation Algorithm (WOA).

Table 2.1.4.1 provides a summary of the papers which have been researched for this section. However, by investigating these papers it can be seen that only 132-11kV networks are considered, therefore considering the impact on the wider grid. The impact on LV networks to which consumers are directly connected is not considered.

**Table 2.1.4.1: Overview of the literature review of EVC optimal location.**

| Paper/ Author(s) | Overview | Optimum Solution | Test System | Algorithm |
|---|---|---|---|---|
| Awasthi, et al. (2017) | Identified the optimum connection location of EVCs with respect of power losses, initial cost and voltage drop. This study uses the Allahabad 220/132/33kV distribution system for comparison. Therefore it is hard to compare to the IEEE 33 bus system which is a lower voltage system. | The best location of EVCs were 2.4, 3.1, 4.3, 4.5, 5.1, 5.2, 5.3, 5.4, 5.5, 5.6, 5.7, 5.8, 6.1 and 6.5 in varying numbers of EVCs at each bus. | Allahabad 220/132/ 33kV distributio n system. | Swarm Intelligence Algorithm (PSO) and Genetic Algorithm (GA). |
| Bilal, et al. (2021) | Identified the optimum connection location of EVCs with respect of power losses and voltage drop. | Regarding the IEEE 33 bus network, the best busses are bus 2 and 19 for 2 EVCs or bus 2 for 1 EVC. Both are around 210kW. Regarding the IEEE 69 bus network, the best busses are bus 8 and 28 for 2 225kW EVCs or bus 28 for 1 255kW EVC. | IEEE 33 and IEEE 69 bus systems. | Swarm Intelligence Algorithms (PSO and GWO). |
| Mehar and Senouci (2013) | Uses optimised location scheme for electric charging stations to identify the optimum connection location of EVCs with respect of cost of charging stations' location. Considered the best location and number of 22kVA EVCs across 11 locations. | The algorithm determined the best placement of EVCs in each of the 11 locations and determined that between 12-17 EVCs should be deployed at each of the locations. | City of Cologne distributio n system. | Optimised Location Scheme. |
| Golla, Sudabattula and Suresh (2022) | Identified the optimum connection location of EVCs with respect of power losses and voltage drop. | The best busses for a single bus to have an EVC connected were 7, 12, 17 and 31. | IEEE 33 bus system. | Swarm Intelligence Algorithms (PSO and HHO). |
| Jamatia, Bhattacharjee and Sharma (2022) | Identified the optimum connection location of EVCs with respect of power loss and voltage drop. It was found that SOS performs better than PSO. The paper considered the best location of EVCs across three busses for two scenarios, each with 10, 20 and 30 EVCs connected. | For scenario 1, bus 2, 19 and 20 were optimal. For scenario 2, bus 2, 21 and 30 were optimal considering different areas. | IEEE 33 bus system. | Swarm Intelligence Algorithms (PSO and SOS). |

| | | | | |
|---|---|---|---|---|
| Islam, Shareef and Mohamed (2018) | Identified the optimum connection location of EVCs with respect of EV transportation energy loss, station build-up cost and sub-station energy loss. The first case considers EV transportation energy loss, station build-up cost and sub-station energy loss. The second case considers station build-up cost and sub-station energy loss. | For the first case it was found that locations 3, 4, 5, 7, 12, 14, 17 and 19 with station capacities of 288, 288, 96, 192, 288, 288, 384 and 288 kW, respectively were the best locations and sizes. For the second case it was found that locations 1 and 6 with station capacities of 672 kW, respectively were the best locations and sizes. | Bangi City, Malaysia. 32/33/ 11kV distributio n system. | Lightning Search Algorithm (BLSA), Swarm Intelligence Algorithm (PSO) and Genetic Algorithm (GA). |
| Nasir, Jamian and Mustafa (2018) | Identified the optimum connection location of variable passive filters to mitigate harmonic distortion and network losses from 132 EVCs on a 449 bus 23kV system. | The algorithm deploys 22 filters across the network to improve maximum THDv by 39.14%, maximum THDi by 52.5%, and apparent power loss by 2.96%. | 23kV 449 bus system. | Lightning Search Algorithm (MLSA) and Pareto-Fuzzy Technique (PFT). |
| Pal, Bhattacharya and Chakraborty (2020) | Identified the optimum connection location of EVCs with respect of power losses and voltage drop. Considered the best location of EVCs across three busses for two scenarios, each with 10, 20 and 30 EVCs connected. | For scenario 1, bus 2, 19 and 20 were optimal. For scenario 2, bus 2, 21 and 30 were optimal considering different areas. | IEEE 33 bus system. | Swarm Intelligence Algorithms (GWO and WOA). |

## 2.1.5 – EVC Research Gaps

From Sections 2.1.3-4, it can be concluded that there is lack of in-depth research addressing the reduction of harmonics on EDNs with high penetrations of EVCs. Nasir, Jamian and Mustafa (2018) considered the connection of variable passive filters to minimise harmonics. The other papers reviewed in Section 2.1.4 considers optimal connection of EVCs to improve power losses, voltage drop, costs of charging stations' location, EV transportation energy loss, station build-up cost and sub-station energy loss. However, the optimum location of EVCs on the EDN with regard to reducing harmonics has yet to be studied and therefore, it is identified as the potential research gap to be addressed.

One limitation of all papers studied in Sections 2.1.3-4 is that they assume that the network is under normal running arrangements with zero faults on the system. In practice, this is not always the case as mentioned in Section 1.5. Therefore, the cumulative harmonic effect of multiple EVCs interacting with these fault conditions on THDv levels and equipment lifespan is unknown. It is critical that this effect is known, since over the lifetime of a network, the probability of these faults developing is extremely high. Additionally, parameters or loads of the network were not varied to identify how those parameters might affect the optimum connection location of EVCs. Therefore, changes in network parameters on the overall results should be considered.

There are a lack of studies which use measured data from a live electricity network to show the effect of increased numbers of EVCs on the electricity network. This is identified in Section 2.1.3. Additionally, Watson and Watson (2017a) is the only study which looks into the effect of increasing the numbers of EVCs from different manufacturers on the network. Therefore, this is something that should be considered in future studies.

Lastly, Ceylan, et al. (2017) and Dale (2018) are the only studies to take into account base load, excluding EVCs with pre-existing THD. The base load THD selected, harmonic distribution and the effect this has on a network with increased number of EVCs must be investigated. Additionally, within the studies mentioned, variations in harmonic phase angle are not considered.

## 2.2 Photovoltaic Generation

DESNZ (2023) states that as of November 2023, there were over 1.24 million $0 \leqslant 4$ kW photovoltaic (PV) inverters within the UK, with a further 133,481 $4 \leqslant 10$ kW PV inverters. As of January 2010, there were 4,460 $0 \leqslant 4$ kW PV inverters and 472 $4 \leqslant 10$ kW PV inverters. This presents a very large potential UK generation capacity and a very extensive increase in the numbers of small-scale PV generation connected to the UK grid. Therefore, it is important that the effect of PV generation on EDN harmonics is understood.

Nduka and Pal (2017) provides an insight into the architecture and control equations of PV generation. The single-phase PV generation model within this paper uses a bridge of four IGBTs to convert the DC output of the PV cells into an AC waveform. A filter capacitor and inductor are then used to filter out or reduce harmonic currents prior to exporting to the grid.

### 2.2.1 – PV Generation Power Ratings

The typical size of domestic PV microgeneration within the UK is approximately 2kW or below as explained by De Boar, et al. (2020) and Western Power Distribution (2016 and 2013). This is corroborated by the DESNZ (2023) which states that as of November 2023, there were over 1.24 million 0 $\leqslant$ 4 kW photovoltaic (PV) inverters within the UK, the most of any category and significantly higher than 4 $\leqslant$ 10 kW PV at 133,481. Lastly, Calais, et al. (2002) further validates a value of 2kW as shows that available single-phase inverters vary in size between 0-6kW, however, the majority fall between 0-3kW.

### 2.2.2 – PV System Harmonics Profile

Research papers which contained profiles of PV inverters were investigated. However, out of those studies, many used simulated data and were not taken forward. These studies include, Aprilia (2012), Anurangi, Rodrigo and Jayatunga (2017), Armstrong, et al. (2005), Busatto, Bollen and Rönnberg (2018), Niitsoo, et al. (2015) and Phannil, Jettanasen and Ngaopitakkul (2017).

However, there are many papers which have published measured data of existing PV inverters available on the market from 1989 to 2015. The range of THDi values were between 1.444% to 10% at values at or above 80% of maximum PV inverter output as stated by Chicco, Schlabbach and Spertino (2008), Chidurala, Saha and Mithulananthan (2015), Cyganski, et al. (1989), Du, et al. (2013), Kontogiannis, et al. (2013), Papaioannou, et al. (2011), Schlabbach (2008), and Schlabbach and Gross (2007).

The worst-case value of 10% shown in Kontogiannis, et al. (2013) was taken at 83% of maximum PV inverter output and was an outlier among the results of the papers previously discussed. The worst-case values of 20% and 25% from Langella, et al. (2016), seem to be outliers. Following the curves provided in Langella, et al. (2016), the THDi increases to between 150-250% at 10% output, therefore raising doubt over these values and how they were collected, since they do not align with any other results. At 10% output, the maximum THDi within Papaioannou, et al. (2011) is 14% and within Fekete, Klaic and Majdandzic (2011) is 30%. The remaining results at 80% of maximum PV inverter output were between 1.444% and 6%. By removing peaks or troughs, observed for a short time, the majority of the results appear to be between 2% and 5% THDi. This data can be observed in Table 2.2.2.1 below. Chicco, Schlabbach and Spertino (2008) and Papaioannou, et al. (2011) displayed peaks as high as 6% whereas Cyganski, et al. (1989) and Du, et al. (2013) measured THDi below 2%. In addition, Schlabbach (2008) also showed a maximum THDi of 5% at 100% inverter output which would normally be observed much closer to 80% of maximum inverter output.

Langella, et al. (2016) measurements shown in Table 2.2.1.1 suggests that increases in source impedance will have a marginal effect on the THDi output of the inverters. However, higher background harmonics will have a much more profound increase on the THDi output of inverters.

Schlabbach (2008), Kontogiannis, et al. (2013), and Papaioannou, et al. (2011) also show that as the PV inverter output decreases, the THDi increases. However, in the case of lower output, the magnitude of the harmonic currents would either be equal to or lower than the current magnitude when exporting at maximum output. Therefore, for worst case analysis, it shall be assumed that the inverters are exporting at maximum output.

This relationship can be seen clearly over the course of a day within Fekete, Klaic and Majdandzic (2011) where THDi is higher, at the beginning and end of the day when less solar irradiance is available and minimises towards the middle of the day when more solar irradiance is available.

**Table 2.2.2.1: Overview of the literature review of the THDi output from PV Inverters connected to an LV EDN.**

| Paper/Author(s) | Overview | THDi | Inverter Rating |
|---|---|---|---|
| Schlabbach and Gross (2007) | The harmonics of a 3kW PV inverter was measured for 1 week. | 2-5% above 80% of rated output | 3kW |
| Cyganski, et al. (1989) | The harmonics of three 1.8kW PV inverters were measured for 1 week | 1.444-2.108% | 1.8kW |
| Kontogiannis, et al. (2013) | The harmonics of seven 8-10kW PV inverters were measured for 8 hours. | Inverters 1,2,4,5,6 and 7 were between 3-5% above 80% of rated output. Inverter 3 had a THDi output of 10% up to 83% of rated output. | 8-10kW |
| Du, et al. (2013) | The harmonics of nine 1-1.5kW PV inverters were measured at the CSIRO Energy Centre, Newcastle, Australia. | 2.11-4.77% above 80% of rated output. Some inverters did not exceed 70% of rated output and measured 1.85-2.59%. | 1-1.5kW |
| Chicco, Schlabbach and Spertino (2008) | Harmonics of a 850W, 1.5kW and 3kW PV inverters were measured. | 2.03% | 850W |
| | | 4-6% above 80% of rated output. | 1.5kW |
| | | 3.5-4% above 80% of rated output. | 3kW |
| Chidurala, Saha and Mithulananthan (2015) | Harmonics of a 12kW inverter were measured at the University of Queensland PV site with FLUKE 434 series-II and 1735 power quality analysers. | 2-4% measured between 8am and 12pm when excluding the choppy waveform which is assumed to be due to intermittent cloud cover. | 12kW |
| Schlabbach (2008) | Harmonics of a 5kW PV inverter measured at multiple times from 4 days to 1 week. | 2-5% above 80% of rated output. | 5kW |
| Papaioannou, et al. (2011) | Harmonics of a 5kW PV inverter was measured over one day. | 2% with a few instances of peaks at 6% above 80% of rated output. | 5kW |
| Langella, et al. (2016) | Source impedance of 0Ω and no background harmonics. | 2% at 100% inverter output. | 4.6kW (1) |
| | | 2% at 100% inverter output. | 10kW |
| | | 1.5% at 100% inverter output. | 4.6kW (2) |
| | Source impedance of 0.4+j0.25Ω and no background harmonics. | 2.5% at 100% inverter output. | 4.6kW (1) |
| | | 2% at 100% inverter output. | 10kW |
| | | 1.5% at 100% inverter output. | 4.6kW (2) |
| | Source impedance of 0.4+j0.25Ω and background harmonics typical of residential customers with two-pulse rectifiers. | 3.5% at 100% inverter output. | 4.6kW (1) |
| | | 25% at 100% inverter output. | 10kW |
| | | 4% at 100% inverter output. | 4.6kW (2) |
| | Source impedance of 0.4 + j0.25 Ω and background harmonics typical of industrial customers with six-pulse rectifiers. | 3.5% at 100% inverter output. | 4.6kW (1) |
| | | 20% at 100% inverter output. | 10kW |
| | | 3% at 100% inverter output. | 4.6kW (2) |

### 2.2.3 – PV Cumulative Effect

Busatto, Bollen and Rönnberg (2018) found that twenty-eight 2.5kW PV inverters producing 3.13% THDi resulted in an increase of 0.05-0.1% THDv in the worst case if spread across three phases and 0.1-0.2% in the worst case if connected to a single phase. This simulated study was based off measured PV inverter and customer data for a single supply. The network impedance at the LV bus bar of the transformer from Busatto, Bollen and Rönnberg (2018) was roughly 0.42 + j10.60 Ω at 10kV or j0.017 Ω at 400V. The longest LV feeder measures 377m from B1 to CB24, presenting an impedance of 0.57 + j0.03 Ω. Therefore, the cable provides most of the network impedance. The twenty-eight PVs are spread across four feeders, which may have an impact on the measured THDv, compared to a network with a singular feeder. This is due to the harmonic current being split across four feeders rather than forced along a single conductor. The simulation also models other non-linear loads such as microwaves, leading to a base THDv of around 1.9% within Busatto, Bollen and Rönnberg (2018). Because of this, this may lead to harmonic cancellation. Additionally, Busatto, Bollen and Rönnberg (2018) mentions that the PV had little effect on the THDv and one possible reason for this is due to the resonant impedance being within the 0-2 kHz range.

Vasanasong and Spooner (2000) produced results showing the effect of 50 1kW PV inverters on the THDv of a single-phase LV EDN at the remote end. The study uses measured data of single-phase PV Inverters and background harmonics to produce a simulation which looks at the effect of multiple numbers of PV inverters. The results of the simulation from Vasanasong and Spooner (2000) produced a THDv on the network of 1.5-1.9% at the end of the feeder. This was based on a HV network impedance of roughly 12.2 Ohms and background harmonic levels are considered in this study.

De Silva, Jayamaha and Lidula (2019) produced results for a network with 50% harmonic load. This produced a base THDv of 0.8%-1.0% for low loading (below 30% load) along the length of the network and 1.3-1.7% for high loading (above 90% load) along the length of the network. Although not presented as a normal base THDv, it at least produces a base voltage harmonic which may cancel or sum up with the PV Inverter, rather than allowing the THDv to continually sum as would be the case in a simulated system with no base voltage harmonics. The study considers the addition of 50kW of PV generation connected across three phases. Based on the data produced by this study, the increase in THDv is approximately 0.2-0.3% for the low loading scenario and 0.3-0.4% for the high loading scenario. The simulation considers a 250kVA transformer. Assuming an impedance of 4.9%, obtained from Busatto, Bollen and Rönnberg (2018) the network impedance is approximately j24 Ω at 11kV, or j0.03 Ω at LV. This is around double the impedance presented in the previous two studies discussed. If the LV conductor impedance is considered at a length of 400m, the impedance becomes 0.18 + j0.06 Ω. Therefore, the cable provides most of the network impedance.

Busatto, Bollen and Rönnberg (2018), split the PV generation across four feeders, therefore splitting harmonic current across feeders. Dividing the cable impedance by four, to represent the impedance of four equal feeders gives us 0.14 + j0.01 Ω. Summing together the transformer and cable impedance for Busatto, Bollen and Rönnberg (2018) presents a value of 0.14 + j0.03 Ω and De Silva, Jayamaha and Lidula (2019) a value of 0.18 + j0.06 Ω at LV. Therefore, these networks are reasonably comparable. Therefore, for comparable networks, with PV penetration of between 50-70kW, we would expect a THDv rise of between 0.05-0.3% for low loaded networks. It should also be noted at this point that De Silva, Jayamaha and Lidula (2019) has a much lower base THDv of 0.8-1.0%, compared to the base THDv of 1.9-4.3% provided by Busatto, Bollen and Rönnberg (2018). A higher THDv may possibly allow for a greater proportion of harmonic cancellation.

### 2.2.4 – PV Optimal Location

The following section shall consider existing literature regarding the optimal connection location of PV generation on EDNs. Firstly, the majority of existing literature such as Moupuri and Kamakshy (2020), Nguyen-Phuoc, Vo-Ngoc and Tran-The (2017), Tran-The, Nguyen-Quoc and Vo-Ngoc (2020), Fu, et al. (2023), Quan-Duong, et al. (2019) and Doan, Duong and Mussetta (2021) which considers the optimum connection location of PV generation, considers voltage drop and power losses. This falls outside of the focus of this thesis. Cortés-Caicedo, et al. (2022) uses the Discrete–Continuous Crow Search Algorithm (DCCSA) to identify the optimum connection location of PV generation to reduce cost of purchase, investment in PV generation, and operation/maintenance costs. Again, this falls outside of the scope of this thesis.

Alame, Azzouz and Kar (2020) focusses on using PV generation to provide harmonic compensation, similar to an active filter. This paper assumes fixed locations of PV generation and EVCs and then provides the optimum harmonic compensation to produce a minimum THDi, with a THDv below 5%. Similarly, Liao, Milanović and Hashempour (2021) uses an algorithm to identify the optimum location of filters on a network containing renewable generation to reduce harmonics. This falls within a similar scope to Nasir, Jamian and Mustafa (2018) mentioned in Section 2.1.4. Both Alame, Azzouz and Kar (2020) and Liao, Milanović and Hashempour (2021) fall within the focus of this thesis. Therefore, the optimum connection of filters or harmonic compensation via PV generation to minimise harmonics should be discounted from future work as has already been carried out by other researchers.

Lastly, Sharew, Kefale and Werkie (2021) and Parihar and Malik (2022), use PSO Algorithms to identify the optimum connection location of PV generation with regards to power losses, THDv and THDi. Additionally, Sharew, Kefale and Werkie (2021) identifies the maximum PV penetration to comply with harmonic limits. It should be noted that both of these studies consider THDv rather than individual harmonic constraints as stated in ER G5/5 and use a 12.66kV and 15kV EDN with an optimal PV generation size of 2588.4kW and 744kVA respectively. The majority of PV microgeneration within the UK is approximately 2kW and will be connected to the LV EDN. Therefore, the results of these studies will likely be very different when considering an LV EDN due to the differences in network structure and impedance between HV and LV EDNs.

It should be mentioned that within the references stated, depending on the algorithm used, different optimum results were found. Although this was used to illustrate that the chosen algorithm produced a better solution, it brings into question whether the optimum solution published is optimum, or whether there is a better solution which can be obtained. This applies to Doan, Duong and Mussetta (2021), Cortés-Caicedo, et al. (2022), Parihar and Malik (2022), Quan-Duong, et al. (2019), Fu, et al. (2023), Nguyen-Phuoc, Vo-Ngoc and Tran-The (2017), and Tran-The, Nguyen-Quoc and Vo-Ngoc (2020). Additionally, despite many of the papers attempting to solve the same problem, using the same network, they come to different solutions, therefore again bringing into question whether the optimum solution published is optimum. For example, Quan-Duong, et al. (2019) and Nguyen-Phuoc, Vo-Ngoc and Tran-The (2017) present different best solutions when optimising power losses on both the IEEE 33 and 69 bus networks as seen in Table 2.2.4.1 below. It should be noted that Doan, Duong and Mussetta (2021) and Quan-Duong, et al. (2019) produce very similar solutions for the IEEE 69 bus network when optimising power losses, therefore increasing reliability of these two papers.

These papers cover a range of algorithms which may be of use for network optimisation regarding harmonics and should be considered for future work. Some of these algorithms are shared with those identified by Section 2.1.4. These are Ant Colony Optimisation (ACO), Adaptive Cuckoo Search Algorithm (ACSA), Biogeography-Based Optimisation (BBO), Coyote Optimisation Algorithm (COA), Decoupled Harmonic Power Flow (DHPF), Discrete–Continuous Crow Search (DCCSA), Fireworks Algorithm (FWA), GA, Greedy Based Optimisation (GBO), GWO, Harmony Search Algorithm (HAs), Multi-paramedic Global Sensitivity Analysis (MPGSA), Optimal Harmonic Power Flow (OHPF), PSO, SOS, Teaching-Learning Based Optimisation (TLBO) and Uniform Voltage Distribution Based Constructive Algorithm (UVDA)

Table 2.2.4.1 provides a summary of the papers which have been researched for this section.

**Table 2.2.4.1: Overview of the literature review regarding PV generation optimal location.**

| Paper/ Author(s) | Overview | Optimum Solution | Test System | Algorithm |
|---|---|---|---|---|
| Alame, Azzouz and Kar (2020) | Identified the optimum harmonic compensation injection of PV at busses 14, 20 and 25 and EVCs connected to busses 15, 16 and 24. | The optimum quantity was minimum injected THDi, with a THDv below 5%. | IEEE 33 bus system. | Decoupled Harmonic Power Flow (DHPF). |
| Moupuri and Kamakshy (2020) | Identified the optimum connection location of PV with an EV connected to an unbalanced network on bus 2 with respect of power losses and voltage drop. | It was found that be best bus for a single PV to be connected was bus 19. | IEEE 25 bus system. | Swarm Intelligence Algorithm (PSO). |
| Nguyen-Phuoc, Vo-Ngoc and Tran-The (2017) | Identifies the optimum size, location, and number of distributed generation (DG) on an EDN. The objective of this paper is to minimise power losses. | For the 33 bus system, the best location and size are busses 6 (2.2066 MW), 28 (0.2 MW) and 29 (0.7167 MW). For the 69 bus system, the best location and size are busses 57 (0.2588 MW), 58 (0.2 MW) and 61 (1.5247 MW). For the 118 bus system the best location and size are busses 70 (2.5018 MW), 104 (0.6784 MW), 68 (0.2 MW), 106 (0.7226 MW), 108 (2.2610 MW), 69 (0.2 MW) and 67 (0.8759 MW). | IEEE 33, IEEE 69, and IEEE 118 bus systems. | Swarm Intelligence Algorithm (SOS and ABC), Genetic Algorithm (GA) and TLBO. |
| Tran-The, Nguyen-Quoc and Vo-Ngoc (2020) | Identifies the optimum DG to minimise power losses. Seven scenarios were tested for each of the test systems. | The results of this study will not be mentioned here due to the number of and complexity of these results. | IEEE 33, IEEE 69, IEEE 84, and IEEE 119 bus systems. | Swarm Intelligence Algorithm (SOS, ACSA and GWO with PSO), FWA, MPGSA and UVDA. |
| Fu, et al. (2023) | Identifies the optimum connection location of DG with regards to power losses, whilst harmonic and voltage limits are constraints. The study considers THDv rather than individual harmonic constraints. | The model reduces line losses by 108.26 kW considering harmonic constraints by placing a single DG at node 832. | IEEE 34 bus system. | Swarm Intelligence Algorithm (PSO and ALOA) and Genetic Algorithm (GA). |

| | | | | |
|---|---|---|---|---|
| Liao, Milanović and Hashempour (2021), | Identifies the optimum connection location of filters for networks with renewable generation connected with respect of harmonics. | It was found that the best bus for a single filter to be connected was bus 24. | IEEE 68 bus system. | Greedy Based Optimisation (GBO). |
| Quan-Duong, et al. (2019) | Identifies the optimum connection location and size of PV generation with regards to power losses, whilst voltage harmonic and voltage profile limits are constraints. | The best busses and sizes for the 33 bus system are 14 (0.7539 MW), 24 (1.0994 MW) and 30 (1.0714 MW). The best busses and sizes for the 69 bus system are 11 (0.5388 MW), 18 (0.3669 MW) and 61 (1.7184 MW). | IEEE 33 and IEEE 69 bus systems. | Swarm Intelligence Algorithm (ABC and PSO), Genetic Algorithm (GA) and BBO. |
| Sharew, Kefale and Werkie (2021) | Identifies the optimum connection location of PV generation with regards to THDv and THDi. The study does not consider individual harmonic constraints. | The model states that the best location for PV generation is bus 34. The maximum PV penetration is 48%. At this level THDv is 4.97% and THDi is 14.98%. | 34 bus 15kV system from Bahir Dar. | Swarm Intelligence Algorithm (PSO). |
| Parihar and Malik (2022) | Identifies the optimum connection location of PV generation to improve THDv and reduce network losses. This study models the PV generation as a harmonic current source for the purposes of simulation. | The optimal location of PV generation with respect of THDv and network losses is bus 6. THDv was also found to reduce by 25.29% and 6.2% for the 33 and 34 bus systems respectively after PV generation was applied. | IEEE 33 12.66kV and IEEE 34 11kV bus systems. | Swarm Intelligence Algorithm (PSO). |
| Cortés-Caicedo, et al. (2022) | Identifies the optimum connection location of PV generation to reduce cost of purchase, investment in PV generation, and operation/maintenance costs. | For the 33 bus system, the best location and size are busses 10 (1.0092 MW), 16 (0.9137 MW) and 31 (1.7246 MW). For the 69 bus system, the best location and size are busses 21 (0.4890 MW), 61 (2.4 MW) and 64 (0.9254 MW). Costs were reduced by 27.0449% and 27.1589% for the 33 and 69 bus systems respectively. | IEEE 33 and IEEE 69 bus systems. | Swarm Intelligence Algorithm (DCCSA). |
| Doan, Duong and Mussetta (2021) | Identifies the optimum connection location of PV generation to reduce network losses. | The best locations and sizes are busses 11 (0.4883 MW), 17 (0.3863 MW) and 61 (1.733MW). The optimal result reduces power loss significantly from 0.2253 MW to 0.0704 MW. In addition, THDv and THDi also decreased positively from 5.5179% and 3.5665% to 3.3260% and 2.1488%, respectively. | IEEE 69 bus system. | Swarm Intelligence Algorithm (COA). |

### 2.2.5 – PV Research Gaps

The following section shall heavily reference Sharew, Kefale and Werkie (2021) and Parihar and Malik (2022), since these papers contain the most similarities with the proposed research of this thesis. Sharew, Kefale and Werkie (2021) uses PSO algorithm to identify the optimum POC of PV generation with regards to THDv and THDi. Parihar and Malik (2022) uses PSO algorithm to identify the optimum POC of PV generation with regards to power losses and THDv.

In addition, the maximum penetration of PV generation has been determined by Sharew, Kefale and Werkie (2021) based on overall THDv. However, there are some limitations of this study. The maximum possible THDv for this study with regards to identifying maximum penetration was taken to be 5%, however, ER G5/5 also provides additional limits on individual harmonics. Therefore, if harmonic levels were exceeded for a particular harmonic order, either due to network resonance, or PV generation producing a large contribution of one particular harmonic order, this should cause the individual orders planning limit to be exceeded before the overall planning limit is exceeded. In addition to this, the impact of these individual harmonics on equipment lifespan and operation has not been mentioned.

Sharew, Kefale and Werkie (2021) and Parihar and Malik (2022) investigated the optimum POC for PV generation on an EDN. However, the optimum busses identified are specific to the EDN investigated. Parameters, running arrangements or loads were not varied to identify how they might affect the optimum connection location of PV generation. Therefore, changes in network parameters should be considered. Additionally, Sharew, Kefale and Werkie (2021) considers a 15kV EDN with an optimal PV generation size of 744kVA. Parihar and Malik (2022) considers a 12.66kV EDN with an optimal PV generation size of 2588.4kW. These are vastly different problems to solve compared to considering the optimum location of 2kW PV microgeneration on an LV EDN. For example, network impedance will be considerably different, and the placement of delta windings of transformers connected to the 12.66kV or 15kV EDN will be different for an LV EDN. These can absorb specific harmonic orders, leading to lower harmonic magnitudes at the 12.66kV or 15kV voltage level.

Although Sharew, Kefale and Werkie (2021) and Parihar and Malik (2022) consider background harmonics with a THDv of 0.75% and 0.1141-0.3674% respectively as a base case, variations in harmonic phase angle are not considered. Changes in the phase angle of harmonics produced may lead to differences in the optimum PV generation location.

Lastly, abnormal running arrangements as mentioned in Section 1.5 are not considered in any of the papers mentioned in Sections 2.2.3-4. It is important these running arrangements are investigated. As long as these running arrangements remain compliant with the ESQCRs, they could be left on the system for extended periods of time.

## 2.3 Combined Effect of PV Generation and EVCs

The next chapter of this thesis will consider the impact of EVCs & PV generation in combination with each other on LV EDNs. The findings of the papers which have researched the combined effect of PV generation and EVCs state a range of potential results from an increase in THDv, to a decrease in THDv, to no discernible effect on the THDv at all when compared to EVCs or PVs on their own.

Busatto, Rönnberg and Bollen (2020) is one of the papers which stated that overall, there was very little increase in the THDv of the network when EVCs and PV generation are combined. This paper based the EVC and PV generation harmonics on real world measured data. The EVC harmonics were measured in the Pehr Högström laboratory with Luleå University of Technology in Skellefteå and the PV generation harmonics were measured at TU Dresden laboratories with more detail given by Langella, et al. (2016). Based on this measured data, and the network data of an LV EDN in Sweden, Monte Carlo simulations were produced. It showed no real increase in THDv, however, there were specific harmonics which increased and decreased by small amounts along the spectrum. Evans and MacLeman (2013), a paper written by Scottish and Southern Power Distribution, a DNO within the UK also stated that the effect of EVCs and PV generation on the THDv of the LV network was not distinguishable from base load conditions. However, it is stated that this may have been due to the PV generation being small compared to the load of the feeder and there only being one EVC on charge at a time.

Foyer and Maruszak (2020) considers the effect of PV generation, EVCs and battery storage on the power quality of the Conseil International des Grands Réseaux Electriques (CIGRE) European LV benchmark distribution grid provided by CIGRE (2014). The source then implemented a background harmonic distortion stated in National Grid (201?) and produced ideal simulated harmonic models for PV generation and EVCs. Based on this model, at a maximum of 270kW of PV generation, the THDv of the network at the 8$^{th}$ node, furthest from the source, increased from 1.087% background harmonic distortion to 1.52%, an increase of 0.43%. Once 200kVA of EVCs were connected to the network in conjunction with the PV generation this then fell to 1.36%, a reduction of 0.16%. Therefore, in this case, connection of the EVCs reduced the increase in THDv of the network by 37%.

In comparison, Müller, et al. (2014) suggests the opposite result and uses measured EVC and PV generation data to form a basis of a lab conducted study. The laboratory used a programmable three-phase supply and therefore is more reliable than other simulated studies used for this literature review. Unfortunately, this study is very small in size and produces four devices, 2 EVCs and 2 PV generation inverters. The harmonic current from a single EVC can be calculated to be approximately 1.0A, 0.8A and 1.1A for WF1, WF2 and WF3 respectively. These represented different background THDv levels of 0.03% for WF1, 3.07% for WF2 and 3.61% for WF3. Once a single PV generation inverter was added, this increased the harmonic current to approximately 1.4A, 1.2A and 1.5A for WF1, WF2 and WF3 respectively. When harmonic current was measured separately, the PV generation inverter was measured at 0.3A, 0.6A and 0.6A for WF1, WF2 and WF3 respectively. This would suggest that in the case of WF1, the harmonics have summed linearly, whereas in the case of WF2 and WF3 there has been some degree of cancellation. The same pattern as previously mentioned for WF1-3 can be seen by observing the 3$^{rd}$ harmonic specifically, and it was found that PV generation when added to WF2 and WF3 with EVCs already present increased the harmonic magnitude by approximately 60-70% of the harmonic magnitude observed when the PV generation was measured separately. Therefore, it is unlikely that all harmonics for PV generation inverters and EVCs will sum linearly, since it is dependent on the PV generation inverters and EVCs connected, background harmonics and likely several other factors. However, this might be a consideration when planning a network for possible worst case harmonic levels.

Tovilović and Rajaković (2015) simulated a 10kV and LV distribution network with both EVCs and PV generators based on measured harmonic profiles published in Fekete, Klaic and Majdandzic (2011) and Collin, et al. (2012). Interestingly this paper shows both increases and decreases in THDv, depending on the node measured. One of the more interesting results was produced when the grid and EVC harmonics were randomised. This always resulted in the combination of EVCs and PV generation reducing THDv within Tovilović and Rajaković (2015). However, as we have already found based on other research which uses actual measured harmonic data, EVCs and PV generation in combination can lead to an increase, decrease or no change in THDv. Based on EVC and PV generation models with measured phase angles, increases of up to 20% for specific harmonics were experienced in a winter scenario and decreases of up to 18% for specific harmonics in a summer scenario. This data was based on a network simulation of 150kW of PV generators and sixty-six single-phase 3.3kW EVCs spread evenly across three 10kV:400V transformers.

Furthermore, Watson and Watson (2017a) shows reinforcement or cancellation depending on the specific harmonic measured. The EVC harmonic profile is based on measurements taken from a 3.6kW public EV charging station and the PV generation harmonic profile is based on measured results from a 5kW inverter shown in Watson and Watson (2017b). Background harmonic data was obtained by measuring three suburban houses for 2 to 3 weeks. This data was then programmed into MATLAB. At a penetration of 40% for PV generation and 50% for EVCs it was found that the 3$^{rd}$ and 5$^{th}$ harmonics reduced whereas the 7$^{th}$ and 9$^{th}$ harmonics increased with the addition of PV generation to a system with EVCs already connected. Using the results within Watson and Watson (2017a), the magnitude to which cancellation of PV generation harmonics occurs with the background and EVC harmonics can be calculated. The 3$^{rd}$ harmonic decreased by 75% of its independent PV generation harmonic magnitude and 5$^{th}$ harmonic decreased by 30% of its independent PV generation harmonic magnitude whilst rounding to the nearest 5% due to potential errors. The 7$^{th}$ harmonic increased by 25% of its independent PV generation harmonic magnitude and 9$^{th}$ harmonic increased by 35% of its independent PV generation harmonic magnitude. Since the PV generation and EVC THDv in these studies increased and decreased linearly, even during the test which included EVCs and PV generators, for the purposes of simulation, it will be assumed that these percentages also apply to current harmonics, which will increase somewhat linearly as penetration increases.

Table 2.3.1 summarises the research conclusions of each study.

**Table 2.3.1: Overview of the literature review of the combined effect of EVCs and PV generation on LV EDN harmonics.**

| Paper/Author(s) | Overview of Results |
|---|---|
| Busatto, Rönnberg and Bollen (2020) | No significant increase in THDv after the introduction of PV generation to an EDN containing EVCs. Considers background harmonics. |
| Evans and MacLeman (2013) | Effect of adding EVCs and PV generators to the EDN harmonics are indistinguishable from the base load harmonics. |
| Foyer and Maruszak (2020) | THDv dropped from 1.52% for the EDN with 270kW of PV generation, down to 1.36% when four 50kVA EVCs were connected. The background harmonic distortion level was 1.087%. This data may not be reliable for 3.6kVA EVCs due to the use of 50kVA charging stations in the study. The study considers background harmonics. |
| Müller, et al. (2014) | Depending on the background harmonic levels, PV generation and EVC harmonic currents can either sum arithmetically or cancel slightly. Cancelling will still provide an increase in overall harmonic current on the network of around 65% of the PV generation harmonic current when measured separately. |
| Tovilović and Rajaković (2015) | When EVCs are introduced to an EDN with PV generation, increases of up to 20% for specific harmonics were experienced in a winter scenario and decreases of up to 18% for specific harmonics were experienced in a summer scenario. Based on a network simulation of 150kW of PV generation and sixty-six single-phase 3.3kW EVCs. Considers background harmonics. |
| Watson and Watson (2017a) | When PV generation is introduced to an EDN with EVCs, the 3$^{rd}$ and 5$^{th}$ harmonics decreased by 75% and 30% respectively of its independently measured PV generation harmonic magnitude. The 7$^{th}$ and 9$^{th}$ harmonics increased by 25% and 35% respectively of its independently measured PV generation harmonic magnitude. Increase and decrease in THDv is linear. The data is based on a 3.6kW EVC and 5kW PV inverter. Considers background harmonics. |

Combined effects of PV generation and EVCs on network harmonics are still a research challenge in academia and industry. Based on the data shown in Table 2.3.1, there is a very large range in which PV and EVC harmonics can cancel and sum up to form a complete THDv profile of the network. This ranges from summing arithmetically as shown in Müller, et al. (2014) (e.g. 1 p.u. from EVC + 1 p.u. from PV = 2 p.u.) to cancelling by up to 75% of its original PV harmonic magnitude when EVCs are added as shown in Watson and Watson (2017a) (e.g. 1 p.u. from EVC + 1 p.u. from PV = 0.25 p.u.). For each of these cases, the maximum summation or cancellation is for specific harmonic current or voltage orders only. There are also examples of variations in between these values given by Busatto, Rönnberg and Bollen (2020), Evans and MacLeman (2013), Foyer and Maruszak (2020) and Tovilović and Rajaković (2015). However, from a planning perspective, simulating worst case scenarios can be used to ascertain a point where it may be necessary for further investigation of harmonic levels to be carried out by a DNO.

### 2.3.1 – Combined Effect of PV Generation and EVCs Research Gaps

Based on the findings of Section 2.3, several research gaps have been identified. Firstly, all the papers mentioned in Section 2.3 assume that the network is under normal running arrangements with zero faults on the system. As mentioned in Section 2.1.5, this is not always the case and should be considered.

Secondly, none of the studies mentioned cover the optimal location of either EVCs or PV generation on an EDN which currently has either EVCs or PV generation previously connected with respect to THDv. This research would be essential when deciding the POC for new equipment requests from members of the public. Existing networks are very likely to have either EVCs or PV generation connected, and it would be beneficial to understand how existing equipment may alter the optimum POC.

Thirdly, the papers mentioned in Section 2.3 do not consider the maximum penetration levels of EVCs and PV generation that can concurrently be connected whilst remaining compliant with the harmonic standards set by ER G5/5. This information would benefit DNOs, which needs to ascertain the maximum penetration levels to remain compliant with ER G5/5.

Lastly, there are no studies which have considered individual harmonics, or their limits past the $15^{th}$ harmonic order. The limits imposed by ER G5/5 are much lower at higher harmonic orders, therefore there may be a strong likelihood of breaching limits at higher harmonic orders. Additionally, the impact of these harmonics on equipment lifespan and operation under the scenarios mentioned have not been investigated.

## 2.4 Vehicle to Grid

As part of research conducted by Ofgem (2021), three-hundred and thirty V2G capable EVCs were installed across the UK. The V2G chargers were optimised to charge EV batteries when there was an excess of generation on the grid and discharge when load is increased. This is supported by Banks (2021). Therefore, V2G can assist with network constraints that are amplified by too much load or generation, by smoothing out peaks in both. Additionally, V2G can be used as a backup power source for vulnerable households or critical infrastructure during power outages. Ofgem (2021) explains that EV owners which volunteered in the research earned up to £725 a year by allowing their vehicle to utilize the V2G functionality. Additionally, the flexibility offered by V2G could save £3.5 billion per year in grid reinforcement, storage, and generation. Banks (2021) explains that the use of tariffs could be used at specific times and in specific areas with too much load or generation to incentivise customers making their EV available for V2G.

Therefore, there is a strong case for V2G compatible chargers to be installed across the UK and it is likely that these will become more common across the UK power grid. Therefore, it would be beneficial to understand the influence V2G chargers have on the harmonics of the EDN.

### 2.4.1 – V2G Harmonic Profile

Research papers which contained profiles of V2G inverters were investigated. Unfortunately, a considerable number of papers use simulated results including, Cai, et al. (2022), Wu, et al. (2018) and Li, et al (2014). Therefore, these papers were not taken forward. Papers considered for this literature review which contain measured data are Tan, Chen, Zhou and Zhang (2019), Magnum Cap (2018), Pinto, et al. (2017), Grasel, Baptista and Tragner (2022), Monteiro, Pinto and Alfonso (2019), Ekström and Leijon (2014), and Casaleiro, et al. (2021). The range of measured THDi produced by V2G inverters was between 2.06% and 48.4%.

This is a very large range so the papers containing these values will be analysed below. Starting with Magnum Cap (2018), which is a manufacturer specification sheet, states that for this three-phase, 400V, Mode 4, CHAdeMO, Nissan compatible V2G charger, during discharging mode, the THDi at rated power will be <3%. This provides a basis from which to work from, however, the value given should not be taken as fact, since these figures are generally not obtainable outside of lab conditions.

Firstly, at rated power, Monteiro, Pinto and Alfonso (2019) states that V2G will produce a higher THDi magnitude than grid to vehicle (G2V). This is corroborated by Grasel, Baptista and Tragner (2022) which shows this relationship for a 10kW V2G charger. Therefore, the expectation is that THDi will be higher than many of the THDi values identified in Section 2.1.2.

Monteiro, Pinto and Alfonso (2019) used a single-phase, 230V, 16A, 50Hz bi-directional EVC prototype to analyse the THDi on an LV EDN with base load under discharging situations. The first base algorithm gave a THDi reading of 1.1% for the V2G only and 65.5% including the base load harmonic current of the LV EDN. The second denominated improved vehicle–for–grid (iV4G) algorithm gave a THDi reading of 28.9% for the V2G only and 2.1% including the base load harmonic current of the LV EDN. This is due to harmonic cancellation from the V2G compensating for the base harmonic load. Therefore, only the base algorithm should be considered for this paper, since the iV4G algorithm was used to implement harmonic filtering using V2G, which falls outside the scope of this thesis.

Similar to Monteiro, Pinto and Alfonso (2019), Ekström and Leijon (2014) compares two algorithms used within an 11kW three-phase bi-directional inverter under discharging situations. At maximum output, THDi under zero-crossing detection (ZCD) algorithm results in a THDi of 7-8% and under phase-locked loop (PLL) algorithm results in a THDi of 6-7%.

Casaleiro, et al. (2021), measured the THDi output of a Nissan Leaf connected to a 10kW CHAdeMO bi-directional inverter. At a capacity of 85%, the THDi output was around 5%. Grasel, Baptista and Tragner (2022) found a similar range for a 10kW bi-directional inverter controlled via open charge point protocol. At 100% output the THDi was 3.8% and at 75% output was 5.4%. Pinto, et al. (2017) found similar results, at a THDi of 4.0% for approximately 70% of rated output of a 40kW three-phase bi-directional inverter. Unfortunately, for each of these papers, the background harmonic distortion during measurement is unknown, therefore making the results hard to compare.

Lastly, Tan, Chen, Zhou and Zhang (2019) carried out an investigation into the effect that a plug-in repetitive controller has on the THDi of a single-phase 220V, 10kW four-leg bi-directional inverter. By comparing the measured results, it can be seen that without a plug-in repetitive controller (RC) the THDi is 7.82% at rated output. With a plug-in RC, THDi is 2.06%. The background voltage harmonic distortion is 2.96%.

A summary of the literature mentioned in this section can be seen below in Table 2.4.1.1.

It should be mentioned, that THDi is linked to the utilisation of the bi-directional inverter when discharging. Ekström and Leijon (2014) shows that as the inverter utilisation reduces, the THDi increases, forming a relationship not dissimilar to an $X^2$ curve. This relationship is corroborated by Grasel, Baptista and Tragner (2022) who found that as bi-directional inverter utilisation was reduced during discharging, the THDi followed the same relationship. For example, at 100% output, THDi was 3.8%, 75% was 5.4%, 50% was 8.5%, 25% was 17.1%, 10% was 34.7%, and 5% was 48.4%.

**Table 2.4.1.1: Overview of the literature review of the THDi output from V2G.**

| Paper/ Author(s) | Overview | THDi | Inverter Rating |
|---|---|---|---|
| Tan, Chen, Zhou and Zhang (2019) | Obtained experimental harmonic measurements for a single-phase 220V, 10kW four-leg inverter used to represent V2G. The background voltage harmonic distortion is 2.96%. | 7.82% at rated output without a plug-in repetitive controller.<br>2.06% at rated output with a plug-in repetitive controller. | 10kW (Single-Phase) |
| Magnum Cap (2018) | States the discharging output for a 9.5kW 400V AC V2G compatible charger. Unsure of this source's reliability as unsure if the THDi value is measured or assumed. | < 3% | 9.5kW (Three-Phase) |
| Pinto, et al. (2017) | The EV connected consists of an 82kWh battery. During V2G mode, the charger discharges at a rate of 27.8 kW and 4.38 kVAr. The paper states that the 3rd, 9th, and 15th harmonics did not present significant magnitude, however, the charger is three-phase rather than single-phase. | The current harmonics measured are 2nd, 1.98%, 4th, 1.15% and 5th, 3.3%, presenting a THDi of 4.0%. | 40kW (Three-Phase) |
| Grasel, Baptista and Tragner (2022) | Measured the THDi of a 10kW V2G at different output power levels. Output power was controlled via Open Charge Point Protocol. | At 100% output, THDi was 3.8%<br>At 75% output THDi was 5.4%<br>At 50% output THDi was 8.5%<br>At 25% output THDi was 17.1%<br>At 10% output THDi was 34.7%<br>At 5% output THDi was 48.4% | 10kW (Three-Phase) |
| Monteiro, Pinto and Alfonso (2019) | A bi-directional EVC prototype was connected to a single-phase, 230V, 16A, 50Hz network. A new algorithm called iV4G was implemented and the harmonics of the system were measured. There is significant background harmonic distortion and the V2G is used to perform harmonic compensation. | V2G THDi measured is 1.1% without iV4G algorithm implemented and 28.9% with the algorithm implemented. Total current to appliances and EV are 65.5% and 2.1% without and with the algorithm implemented. The waveforms were measured with a FLUKE 435 Analyzer and Yokogawa DL708E. | <1kW (Single-Phase) |
| Ekström and Leijon (2014) | Compares two methods of generating AC waveforms for an inverter. The two methods are zero-crossing detection (ZCD) and phase-locked loop (PLL). The 11kW three phase inverter is connected to an 80kVA 345V:11kV transformer. | PLL method produces better THDi results. Interestingly, lowest measured THDi values are found at 6kW, contrary to the model. At maximum output, THDi of PLL is around 6-7% and ZCD is 7-8%. | 11kW (Three-Phase) |
| Casaleiro, et al. (2021) | This paper studied a Nissan Leaf connected to a 10kW CHAdeMO V2G charger. | Harmonics were measured using a Chauvin Arnoux PEL 103 data logger. At 85% capacity, the THDi level of the V2G charger was around 5%. | 10kW (Three-Phase) |

## 2.4.2 – V2G Optimal Location

The following section shall consider existing literature regarding the optimal connection location of V2G on EDNs. A much larger pool of literature exists for EVCs used in charging mode, than V2G in discharging mode. Therefore, the number of studies which can be used are limited.

Firstly, Tahir (2017), Xu and Huang (2020) and Yang, et al. (2020) use algorithms to determine the optimum charging techniques to minimise cost of charging, minimise battery degradation and reduce fluctuations of load on the grid. This falls outside the focus of this thesis.

Aljanad, et al. (2018) and Ahmad, et al. (2022) use algorithms to determine the optimum location of V2G capable EVCs in discharge mode with respect of line loading, voltage deviation, circuit power loss, installation cost and power loss cost. Due to using two different IEEE networks, it is hard to compare these networks. However, the best locations, assuming more than one V2G is connected seems to be spread across multiple positions at the start, middle and end of the EDN.

These papers cover a range of algorithms which may be of use for network optimisation regarding harmonics and should be considered for future work. Some of these algorithms are shared with those identified by Section 2.1.4 and 2.2.4. These are GWO, PSO, Quadratic Optimisation Technique (QOT) and Quantum Binary Lightning Search Algorithm (QBLSA).

Table 2.4.2.1 provides a summary of the papers which have been researched for this section.

**Table 2.4.2.1: Overview of the literature review of V2G optimisation regarding EDN harmonics**.

| Paper/ Author(s) | Overview | Optimal Solution | Test System | Algorithm |
|---|---|---|---|---|
| Aljanad, et al. (2018) | Identifies the optimum connection location of V2G capable charging stations during discharge mode with respect of line loading, voltage deviation, and circuit power loss. | The optimal connection busses are 709, 701, 703, 736 and 718 for this algorithm, however, by using different comparison algorithms, the best busses change. | IEEE 37 bus system. | Lightning Search Algorithm (QBLS). |
| Ahmad, et al. (2022) | Identifies the optimum connection location of V2G with respect of voltage, power loss, installation cost and power loss cost only. | The optimal connection busses for C-2 which considers EVCs capable of V2G are 2, 3, 14, 15 for this algorithm. For comparison, when considering EVCs without the capability of V2G mode the best busses are 2, 13, 14, 29. | IEEE 34 bus system. | Swarm Intelligence Algorithm (GWO). |
| Tahir (2017) | This thesis optimises the cost of charging for both electric utilities and EV owners. This works by using EVs to provide energy during peak hours and charge during off-peak hours. | The thesis designs a fast-charging station which can provide utility owners with reactive and active power, in addition to speeding up charging times. | N/A | Quadratic Optimisation Technique (QOT). |
| Xu and Huang (2020) | Identifies the optimal charging strategy for V2G capable EVCs. The study uses 1000 EVCs within a Stackelberg Game Model Solution. | The study identifies the optimal charging strategy which can reduce vehicle charging costs and reduce fluctuations of load on the grid. | N/A | Swarm Intelligence Algorithm (Multi-Objective PSO). |
| Yang, et al. (2020) | Identifies the optimal strategy for V2G capable EVCs to satisfy EV requirements whilst minimising battery degradation. | The study identifies the optimal charging strategy which can reduce vehicle charging costs, minimise battery degradation and reduce fluctuations of load on the grid. | N/A | Swarm Intelligence Algorithm (PSO). |

### 2.4.3 – V2G Research Gaps

Based on the papers and thesis referenced in Section 2.4.2, there is currently no research into the optimal connection location of V2G with regards to minimising harmonics. In addition, Ahmad, et al. (2022) and Aljanad, et al. (2018) consider networks with no EVCs connected at all. In reality, loading and voltage issues are likely to come about due to increases in EVCs on a network. Therefore, it would be far more beneficial to consider the best connection location or conversion location of an EVC to V2G on a network with high penetrations of EVCs. That way, V2G could be used to combat the voltage and loading issues presented by the existing EVCs.

Additionally, Ahmad, et al. (2022) and Aljanad, et al. (2018) do not consider changes in network parameters. Changes in network parameters may lead to differences in optimum connection location. This is an aspect which should be considered. Ahmad, et al. (2022) and Aljanad, et al. (2018), carry out their studies under normal running arrangements, therefore failing to consider abnormal running arrangements such as network imbalances or faults.

## 2.5 – Research Objectives and Contents

Based on the research gaps identified, the following section details the motivation behind the research, the research aims and objectives, and further aspects that should be considered.

### 2.5.1 – Motivation and Problem Formulation

Based on the research gaps identified in Sections, 2.1.5, 2.2.5, 2.3.1 and 2.4.3, a summary of the findings can be produced below:

There are a lack of studies which have considered the impact of network faults on the harmonic levels of the EDN under high penetrations of EVCs and PV generation. Additionally, the maximum device penetration levels under various EDN fault conditions to remain compliant with ER G5/5 has not been investigated. Furthermore, when evaluating maximum penetration based on harmonic levels, existing research does not consider individual harmonics or their limits beyond the $15^{th}$ harmonic. Lastly, existing research using measured harmonic data, rather than simulated harmonic data, from a range of different models or manufacturers and EDN base load harmonics is limited. A study may include one of these research gaps, but never all four. Lastly, the impact of harmonics produced under EDN fault conditions on network assets and their lifespan has not been explored.

Furthermore, studies considering the optimum POC of EVCs and V2G with respect to reducing harmonic levels have not been carried out. A study looking at the optimum location of PV generation on a 15kV EDN with regards to THDv and THDi has been produced. However, LV EDNs, changes in phase angle, network parameters, base loads, and different running arrangements such as faults have not been considered. Furthermore, this study considers three-phase converters, where-as LV EDNs will have a greater proportion of single-phase converters connected. The way three and single-phase converters will present themselves with respect to harmonics on an LV and 15kV network will produce very different outcomes. Lastly, when considering the optimum POC of V2G, it would be far more beneficial and cost effective to consider EDNs which already have high penetrations of EVCs. Additionally, it would be beneficial to cover the optimal POC of either EVCs, or PV generation on an EDN which currently has either EVCs or PV generation previously connected.

It is essential that harmonic levels at multiple supply terminals and phase-shifts between multiple devices or background harmonics is accounted for where this is appropriate. It was identified within Section 1.2.1 that ER G5/5 has limitations relating to only calculating THDv at the POC and assuming harmonic phase angles between different harmonic sources which may not be appropriate for all scenarios.

Carrying out studies on multiple live networks would require large amounts of funding due to the infrastructure required, and the support from a DNO to experiment on a live system. Due to a DNOs licencing obligations under the ESQCRs, this is very unlikely. Additionally, using live networks present limitations, such as variations of parameters, connection of equipment and the ability to produce fault situations which could lead to loss of supplies or present dangerous situations to members of the public.

Experimenting on a physical EDN model within a laboratory is a possible solution to some of these issues. However, this presents many of the same constraints including funding requirements and lack of possible variations in parameters. Additionally, producing a scale model adds further doubt regarding its reliability, since a scale model may not accurately model a full-scale EDN. For example, a lower capacity 10kVA transformer will have vastly different impedance than a 1MVA transformer with the same percentage impedance, thus altering the results. Furthermore, grid impedance in a laboratory, generally fed at LV will be much greater than at the 11kV bus, due to the addition of 11kV cable, distribution transformer and LV cable. Therefore, current harmonics will have a much greater impact on voltage harmonics, considering the explanation stated in Section 1.2.1.

Because of these physical limitations, it was ascertained that simulation software was the best compromise. A simulation of the EDN provides full flexibility in terms of modelling faults, varying network parameters and correctly modelling the component magnitudes. Accuracy of simulations can be disputed, however, with careful calibration this issue can be mitigated.

Following the completion of this thesis, the results can be validated, and research gaps which could not be fulfilled via simulation software can be tested using live networks or physical EDN models.

## 2.5.2 – Research Aims and Objectives

Based on the research gaps identified, this thesis will have the following two main research aims:

- Explore the impact of EVCs and PV generation on the harmonic levels of LV EDNs under EDN fault conditions, identify penetration limits and determine the effects those levels have on EDN assets.
- Identify the optimal POC of EVCs, PV generation and V2G to reduce harmonic levels on the LV EDN under a range of network parameters, loads and characteristics.

To address these aims the following research goals will be achieved:

- Using simulation software, create accurate models for EVCs, PV generation and V2G which use measured harmonic data, ideally from a range of different models or manufacturers.
- Using simulation software, create an accurate model of an LV three-phase EDN with at least two feeders which can account for background harmonics, base load, and a range of network faults. THDv must be measured at multiple supply terminals.
- Using simulation software, identify the impact that EVCs and PV generation have on individual harmonic orders up to the $50^{th}$ harmonic for LV EDNs under fault conditions.
- Using simulation software, identify the number of EVCs and PV generation, when distributed evenly throughout the network, at which the voltage harmonics, either THDv or individual harmonic orders up to the $50^{th}$ harmonic exceed ER G5/5. This should be determined under both normal and fault conditions. Identify the limiting harmonics and produce data which can be used to determine potential penetration limits across other networks.
- Identify the impact that harmonic levels under fault conditions have on the lifespan of network assets. Quantify the impact each successive fault across both feeders may have on asset life which can be used to assign a financial value to faults.
- Using simulation software, identify the optimum POC of EVCs, V2G and PV generation on the LV EDN under a range of different network conditions and parameters, including network faults whilst considering phase-shift. V2G POC is to be assessed on a network with 100% EVC penetration.

## 2.5.3 – Further Considerations of Research

The specific three-phase LV EDN which is focused on within these research goals will be a network with separate services and driveways for each dwelling. The reason for this is that the electrical load and generation of these established networks can evolve over time with less red tape and from DNOs. Conversely, blocks of flats with communal EVC or PV generation areas exceeding their authorised capacity will likely need to apply to the DNO for a load increase, since an existing whole current metering landlord supply would not likely be able to support a large number of EVCs. Therefore, it is assumed that issues with regards to loading and harmonics would be identified by the DNO at the design stage.

It has been identified in Sections 2.1.4, 2.2.4 and 2.4.2 that the best way of identifying the optimum POC is by using an algorithm. In Sections 2.1.4, 2.2.4 and 2.4.2 many algorithms have been discussed. The best algorithms should be identified and implemented for use when identifying the optimum POC of EVCs and DERs.

Measured rather than simulated harmonic data for EVCs, PV generation, V2G and background harmonics must be used to produce reliable results. Simulated data can be unreliable, which will lead to disputable conclusions.

Where possible, harmonic data for EVCs, PV generation and V2G should be obtained from a range of different manufacturers or models. This will ensure diversity of harmonic profiles and ensure that conclusions are not drawn based on one model of equipment.

# Chapter 3 – The Effect of EVCs and PV Generation on the Harmonic Levels of an LV EDN

This chapter shall produce accurate models for the EDN, EVCs and multiple PV generation profiles. The case-study EDN, EVC and PV generator models are covered within Sections 3.1, 3.2 and 3.3 respectively and shall be validated against the existing research studied in Chapter 2. Within Sections 3.2-4, at stated penetration levels of EVCs, PV generation and a combination of the two devices, harmonic limit breaches of phase voltage harmonics and maximum penetration levels in accordance with ER G5/5 shall be identified. Lastly, the effect these harmonics have on transformer and conductor lifespan shall be determined in addition to risk of injury to the public.

## 3.1 – Case Study

The following section contains details and data regarding the case study EDN chosen for the research in this thesis.

### 3.1.1 – Network Chosen for Simulation

The network which has been chosen for this simulation is the three-phase network feeding the mid-1980's development at the end of Road A, Slough area, shown in Figure 3.1.1.1. The network is typical for a suburban housing estate of this age within Slough. Due to the Ultra-Low Emission Zone (ULEZ) imposed by Transport for London (2023), expanding to cover the whole of Greater London, the lack of practical public transport outside of London and the range of more affordable EVs, it is likely that the uptake of ULEVs will be higher here than most other areas. This is supported by data from the DfT and DVLA shown in Table 3.1.1.1 which showed that as of September 2023, Slough had the highest density of ULEVs within the UK. Furthermore, the PV generation density within Slough is much higher than most other areas within the UK, beaten only by Portsmouth and Ealing as shown in Table 3.1.1.2. Therefore, Slough is likely to experience the highest combined impact of EVCs and PV generation within the UK. Considering this data, this makes EDNs within Slough area the most logical location to carry out this study.

**Figure 3.1.1.1: Satellite view showing the 1980s addition to Road A highlighted in yellow (Google, 2020).**

**Table 3.1.1.1: Top eleven regions/local authorities with the highest density of registered ULEVs from DfT and DVLA (2023b) and Office for National Statistics (ONS, 2021).**

| Region/Local Authority | Total number of ULEVs registered as of September 2023 | Size of Region/Local Authority in km$^2$ | ULEV Density (ULEVs/km$^2$) |
|---|---|---|---|
| Slough | 47,969 | 33 | 1453.6 |
| Stockport | 114,400 | 126 | 907.9 |
| Westminster | 18,331 | 21 | 872.9 |
| Portsmouth | 15,312 | 40 | 382.8 |
| Swindon | 55,982 | 230 | 243.4 |
| Windsor and Maidenhead | 43,435 | 197 | 220.5 |
| Milton Keynes | 52,759 | 309 | 170.7 |
| Ealing | 8,233 | 56 | 147.0 |
| Hillingdon | 13,459 | 116 | 116.0 |
| Peterborough | 39,202 | 343 | 114.3 |
| Barnet | 9,303 | 87 | 106.9 |

Many of the papers evaluated during the Sections 2.1.4, 2.2.4 and 2.4.2 such as Alame, Azzouz and Kar (2020) and Nguyen-Phuoc, Vo-Ngoc and Tran-The (2017) used variations of the IEEE network, such as the 25, 33, 69 and 118 bus IEEE networks. This aids comparison between studies. However, it was decided that these generic IEEE networks would not be used, in favour of a real-world example network as they could lead to misleading results. The aim of this was to produce results reflective of the networks which would be most affected by EVCs, as identified above.

**Table 3.1.1.2: PV generation density and capacity of the regions/local authorities selected within Table 3.1.1.1 from DESNZ (2023) and ONS (2021).**

| Region/Local Authority | Installed capacity (MW) | Total number of PVs registered as of November 2023 | Size of Region/Local Authority in km$^2$ | PV Density (PVs/km$^2$) |
|---|---|---|---|---|
| Portsmouth | 7.9 | 2,153 | 40 | 53.8 |
| Ealing | 7.4 | 2,121 | 56 | 37.9 |
| Slough | 3.3 | 1,018 | 33 | 30.8 |
| Westminster | 2.5 | 492 | 21 | 23.4 |
| Peterborough | 21.5 | 6,921 | 343 | 20.2 |
| Swindon | 15.6 | 4,463 | 230 | 19.4 |
| Hillingdon | 7.4 | 2,071 | 116 | 17.9 |
| Milton Keynes | 19.3 | 5,473 | 309 | 17.7 |
| Windsor and Maidenhead | 12.2 | 3,353 | 197 | 17.0 |
| Stockport | 4.9 | 1,824 | 126 | 14.5 |
| Barnet | 4.3 | 1,202 | 87 | 13.8 |

LV EDNs of this age and location were usually constructed of Consac cable, run radial, and not interconnected. Due to the lack of interconnection, the cable sizes installed were usually the minimum size required for the radial load and therefore, large amounts of 95mm$^2$ Consac was used. Therefore, it is likely that these networks will reach their thermal capacity earlier than other networks. A few of these networks may have had a single point of interconnection with the grid installed at LV to allow for maintenance of the HV switchgear whilst maintaining supplies or for the restoration of supplies following an HV fault. However, the lack of interconnection and large number of pot ends, means that open circuit faults towards a pot end cannot be restored and supplies remain off for the duration of the repair. Although not originally designed for this network, during a fault repair, a linkbox was installed outside number eighty-two. Although this has been installed mid-way along the network, rather than at the pot ends, it can allow the restoration of supplies if an open circuit fault occurs between the linkbox and the substation. The network can be seen in Figure 3.1.1.2.

The lack of interconnectivity of these networks and smaller cable sizes means that these networks are more susceptible to the effects caused by increases in load, less adaptable should load need to be shifted between transformers and in the majority of instances unable to restore supplies to open circuit faults. Additionally, a higher cable impedance with the same harmonic current flowing will produce a higher harmonic voltage drop than a cable with a lower impedance as shown in Equation 1.2.1.2. Therefore, this EDN is likely to reach harmonic limits set out by ER G5/5 sooner, making it a good benchmark. This, along with the widespread use of this network design philosophy is the reason that this network was chosen for this study.

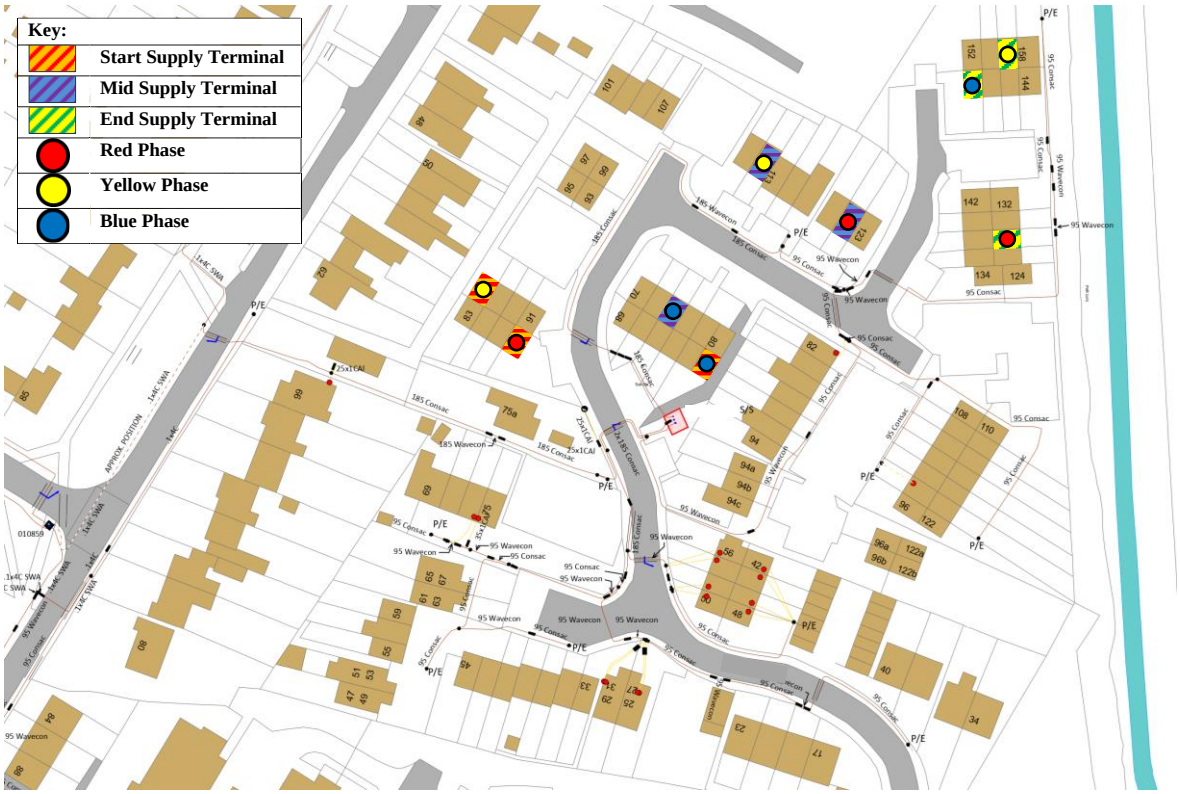


**Figure 3.1.1.2: Geographic diagram of the LV cable and substation for the 1980s addition to Road A, with phase allocation, 'start,' 'mid' and 'end' supply terminals highlighted (Scottish and Southern Energy Power Distribution Ltd, 2020).**

The LV EDN as shown in Figure 3.1.1.2 is constructed of two radial LV feeders with one-hundred and twenty-five single-phase supplies, split fifty-five on feeder one and seventy on feeder two. Therefore, 100% penetration represents one-hundred and twenty-five EVCs or DERs connected to the network, one per single-phase service. The LV EDN is connected to the National Grid via a 500kVA 11kV:400V Dyn11 local transformer with impedance of 4.74%. Three-core Wavecon and Consac mains cable sized between 95mm$^2$-185mm$^2$ are used. Each of the single-phase services are connected to the mains cable via 25mm$^2$ concentric service cable. The 11kV cable, which connects the primary substation (or 11kV source) to the local transformer, is 5.8km long and is constructed of three-core cable sized between 65mm$^2$-300mm$^2$. A simplified schematic diagram of this EDN can be seen in Figure 3.1.1.3 to provide greater context regarding how the 11kV source, 11kV cable, transformer and LV mains cable and LV single-phase services are connected. The 'start,' 'mid' and 'end' supply terminals within the key on Figure 3.1.1.2 applies to Sections 3.2-4 and Chapter 4. These are the supply terminals, where the voltage harmonics are measured for investigative purposes within the sections and chapters mentioned. These were selected by dividing the feeder one of the LV EDN into thirds and randomly selecting properties from the first, second and third section of feeder one.

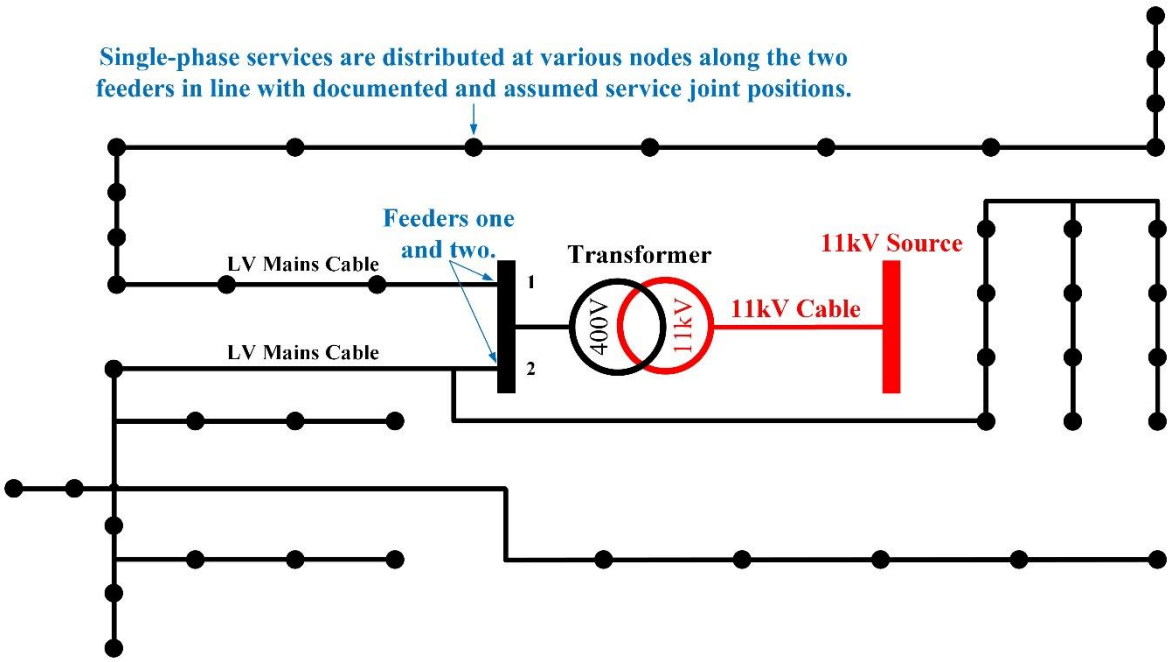


**Figure 3.1.1.3: Simplified schematic diagram of the LV cable, transformer, 11kV cable and 11kV source for the 1980s addition to Road A.**

## 3.1.2 – Consac Mains Cable

Another reason for choosing this LV EDN over others is that it is far more susceptible to faults than other networks. This is because Consac mains cable is very susceptible to faulting. Michalowski (2006) explains that this is due to poor backfill materials, third party damages and the jointing techniques used at the time, which allowed moisture into the joints through the seals. Consac cores and extruded sheath are aluminium. Mak (2014) states that aluminium forms a protective, non-conductive aluminium oxide film on exposure to air which prevents the aluminium reacting further. However, if damaged, the aluminium reforms a new oxide layer. Therefore, moisture within the joint, which allows arcing to ground can damage this layer, restarting the process and corroding the conductor further. In addition, Department of the Army U.S. Army Corps of Engineers (1995) states that aluminium's "contact with clay soils should be minimized unless special corrosion treatment measures are instituted," as these soils tend to be corrosive to aluminium. Lastly, concentric services continued to be made from copper and were jointed onto the aluminium Consac. Mak (2014) states that "Galvanic corrosion occurs when two metals of different potentials come into direct contact with one another while immersed in an electrolyte." The electrolyte in this instance is water with dissolved elements from the soil, which can get to the aluminium through the poor joint seals or damaged cable sheath.

Each of the processes mentioned in the previous paragraph can lead to the Consac cable failing. The makeup of the cable including the extruded aluminium sheath and aluminium conductors which causes so many issues can be seen in Figure 3.1.2.1.

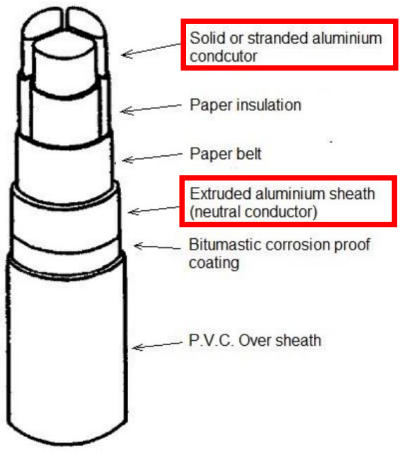


**Figure 3.1.2.1: Annotated diagram of an LV 3-phase Consac cable (Hall, 2015).**

A number of fault repairs can be seen on the cable shown in Figure 3.1.1.2 and are shown as Wavecon, which is a newer cable type installed from 1989 as explained by Michalowski (2006). Phase-to-phase, open circuit and neutral faults are common and will be explored as part of this study.

## 3.1.3 – Simulation of the Network and Assumptions Made

The network simulation of the identified EDN will be carried out using MATLAB Simulink software. There are several reasons for using this software over other packages available. These include:

- The software can simulate each conductor of a 3-phase, 4-wire system separately via a graphical interface.
- Each service cable can be connected onto whichever phase is desired and the load of each service can be altered as required to simulate complex loads.
- The impedance of the National Grid can be accurately modelled at the 11kV bus.
- Background, EVC, and DER harmonics can be modelled.
- The conductors can be manipulated as required to simulate different steady-state network conditions such as network faults.

MATLAB allows for algorithms to interface with the graphical interface making it easier to alter network parameters, correct errors, and verify results via manual assessment of the graphical interface.

The network simulation includes a grid connection at a 132kV-11kV substation, 11kV cable, 11kV:400V transformer, LV mains and service cable, off-peak domestic load, and background harmonics. In order to produce the simulation, network data and assumptions are required. These will be covered in Sections 3.1.4-9.

## 3.1.4 – Grid impedance measured at the 11kV Busbar

Grid impedance data was obtained at the 11kV bus bar of the primary substation. The values were given as R: 0.0469 p.u. and X: 0.4162 p.u. on a 100 MVA base as stated by Scottish and Southern Electricity Networks (2019). This is where the 11kV busbar feeding the 11kV circuit for Road A substation is situated. From this 11kV CB, 11kV cable transports the electricity for Road A substation and many other substations several miles until it reaches its desired location. The simulated grid connection can be seen in Figure 3.1.4.1 below.

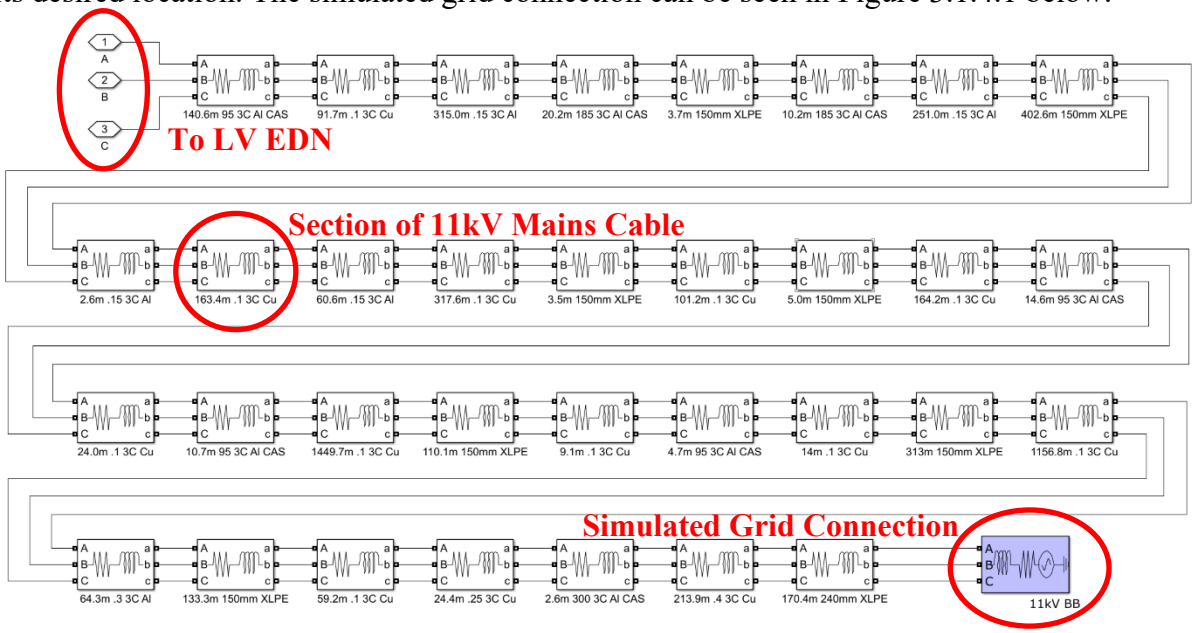


**Figure 3.1.4.1: Overview of the simulated 11kV EDN and grid connection using Simulink. (The Mathworks, Inc., 2021).**

The grid connection simulation contains several abbreviations. These include the metal conductor within the cable, such as copper (Cu) and aluminium (Al), type of cable such as Cross Bonded Polyethylene (XLPE), Corrugated Aluminium Sheath (CAS) or conventional (unmarked) and 11kV Busbar (11kV BB) at the primary substation. XLPE cable should be considered to have Al conductors for the purposes of this simulation. Further details of the cable sections and types used shall be covered in the next section.

## 3.1.5 – Cable impedance of HV and LV cable

The 11kV cable between the 11kV busbar at the primary substation, Road A substation, and the LV cable feeding properties within Road A needed to be accurately modelled. Therefore, the simulation of the lengths of cable sections and various types of cable within Figures 3.1.4.1 and 3.1.5.1 was built from scratch to accurately model the real world measured lengths and types of cable sections from the case study network identified in section 3.1.1. The resistance and inductance data for each type of cable was obtained from Baker (2017). This includes the 11kV three-core cable, made up of conventional, CAS and XLPE, the LV three-phase cable made up of Consac and Wavecon, and the single-phase services made up of 25mm$^2$ concentric cable. The simulated cables which make up the network can be seen in Figure 3.1.4.1 and 3.1.5.1. The values given for cable impedance within Baker (2017) include the inductance and resistance, however, do not include resistance to other cable conductors and earth, in addition to capacitance values.

In reality, to accurately simulate cable, an infinite number of capacitors, inductors and resistors should be modelled along its length. In addition to resistance and inductance being modelled in series, capacitance and resistance should be modelled in parallel between all cable conductors and earth as shown within Turan and Kalenderli (2009). Despite the parallel resistance and capacitance data for the cables used within the simulation not being easily available, this would also have complicated the EDN model, slowing down the simulation. Additionally, for the voltages used within the simulation, which is 400V and 11kV, a requirement for cables during commissioning is that the parallel DC resistance between all conductors and all conductors and earth is greater than 1MΩ, therefore making the impact of this resistance minimal.

For the reasons mentioned, to simplify the simulation, cable shall be modelled as several resistors and inductors in series. This simplification shown within Liang, et al. (2020) is considered acceptable for voltage deviation studies as stated by Liang, et al. (2020).

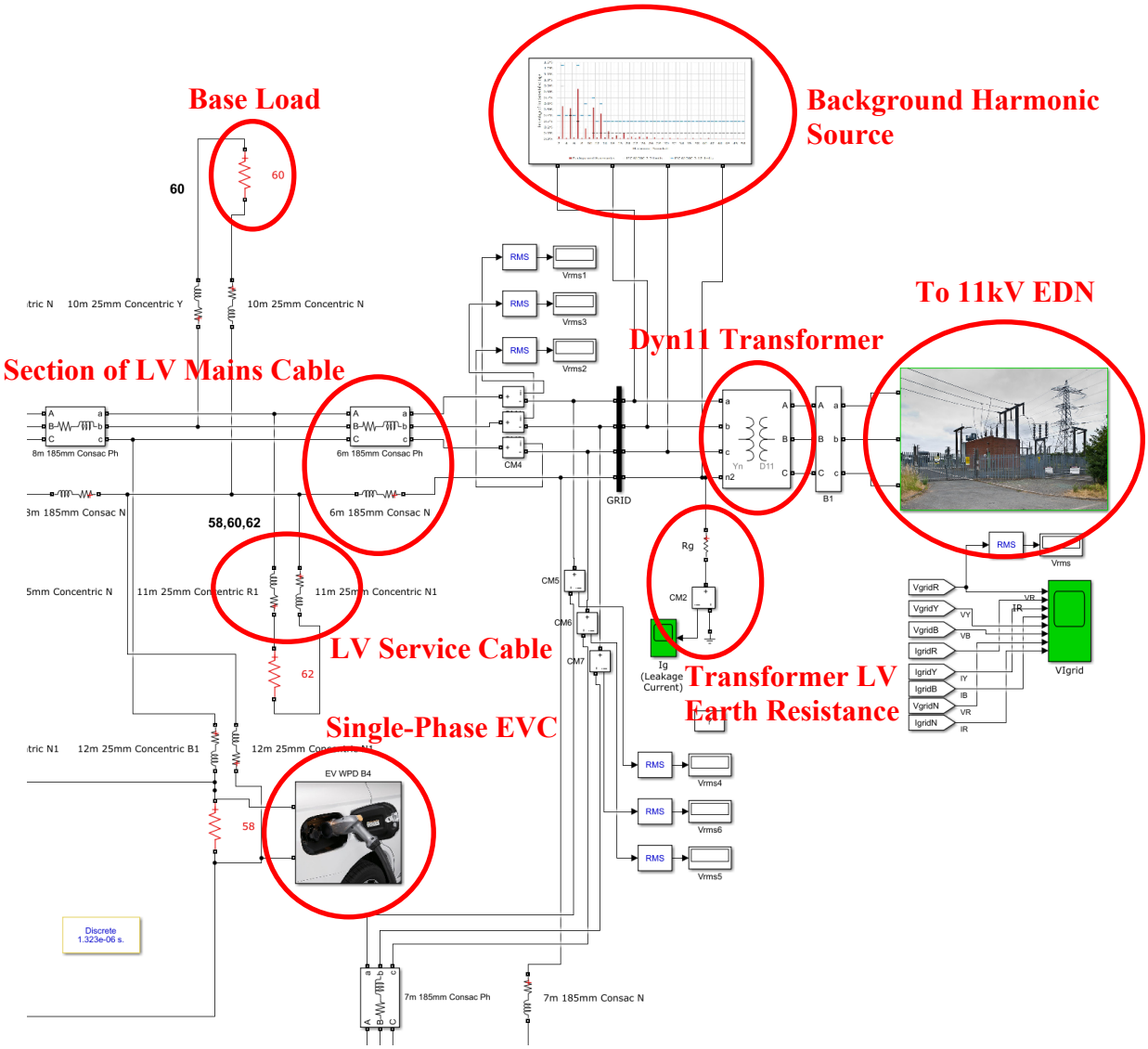


**Figure 3.1.5.1: Portion of the simulated LV EDN, Dyn11 transformer, base load, single-phase EVC and background harmonics (The Mathworks, Inc., 2021). Embedded images from, Capper (2013), Dale (2018) and Hickory Mitsubishi (2018).**

## 3.1.6 – Transformer Rating and Impedance

Once the 11kV cable distributes the electricity from the grid substation to the secondary substation at Road A, it travels through an 11kV switchboard, and is then transformed from 11kV to 400V through the transformer, and finally is configured to flow into the LV cables via the fuses in the LV cabinet.

Now that the structure of a secondary substation is understood, the specifics of the transformer will be explored. The 11kV:400V Dyn11 transformer at Road A substation has a capacity of 500kVA with an impedance at 75˚C of 4.59-4.74% based on the transformer rating plate. For worst case impedance, it will be assumed that the transformer is at the upper limit impedance of 4.74%. Equations 1.2.1.1-2 state that as impedance increases, voltage harmonic distortion increases. Therefore, based on this information, using this impedance should simulate the worst-case scenario with regards to voltage harmonics. The simulated transformer can be seen in Figure 3.1.5.1.

Research by Najar, et al. (2015) looks at the effect of temperature on an 800kVA distribution transformer. Fig 10-11 within Najar, et al. (2015) shows that transformer resistance increases with temperature, whereas inductance remains constant. At 75˚C the resistance of the transformer in question is approximately 3.2mΩ and reactance 13.2mΩ, presenting a total impedance of 13.6mΩ with an angle of 76.4°. This value represents a P.U. impedance value of 6.2% at 75˚C, which is comparable to the transformer used in this study at 4.74% at 75˚C. This ratio of resistance and reactance shall be applied to this simulation. By calculation this produces a resistance of 3.6mΩ and reactance 14.7mΩ, presenting a total impedance of 15.2mΩ with an angle of 76.4°. A lower ratio of resistance and reactance, applicable at lower temperatures was considered, however, a higher resistance scenario of 75˚C was chosen, since this will have a higher impact on the voltage harmonics.

Additionally, the HV steelwork earthing resistance has been assumed to be 0.1Ω and earth potential rise at the secondary substation is assumed to be below 466V for a maximum three-phase to earth HV fault. Therefore, in this case the HV and LV earths at the substation have been assumed to be combined in line with Tucker (2023) resulting in the earth resistance of the transformer also being 0.1Ω. This is due to the interconnected nature of the area being studied. Butter, Batten and Paalman (2020) state that for an area interconnected with at least three primary substations and one-hundred and fifty secondary substations, the Network Contribution Minimum Earth Resistance can be assumed to be 0.1Ω. This is corroborated by Tucker (2023) which states that without a known source substation earth resistance it can be assumed to be 0.1Ω.

## 3.1.7 – Background Harmonics

The harmonic current drawn by EVCs and DERs is dependent on the unique profile of the EVC or DER itself in addition to the background harmonic distortion of the network. Therefore, to accurately model the harmonic profile of the EVC or DER, the background harmonics of that network needed to be simulated. The background harmonics for this study were obtained from within Dale (2018). This is a reliable source of background voltage harmonic information and was obtained by a UK DNO measuring the background harmonics of a UK LV distribution network with no EVCs connected. To measure the background harmonics, a PM7000 Power Quality Analyser was connected to the bus bars of the LV feeder pillar used for the study. Outram Research Ltd (2012) states that the PM7000 is capable of measuring the phase-neutral and neutral-earth harmonic values. Therefore, the background voltage harmonics shown in Table 3.1.7.1 shows the phase-neutral values. These values represent a THDv of 1.36%. For this study, it will be assumed that the voltage harmonics are equal to their respective fundamental voltage phase shift across all three phases.

**Table 3.1.7.1: Table of the background voltage harmonics across the red phase LV terminal of the transformer against the limits set out in ER G5/5 (Energy Networks Association, 2020).**

| Harmonic Number | Harmonic Magnitude (%) | ER G5/5 Limits (%) | Harmonic Number | Harmonic Magnitude (%) | ER G5/5 Limits (%) |
|---|---|---|---|---|---|
| 2nd | 0.04 | 1.60 | 22nd | 0.02 | 0.20 |
| 3rd | 0.55 | 4.00 | 23rd | 0.04 | 1.20 |
| 4th | 0.02 | 1.00 | 24th | 0.01 | 0.20 |
| 5th | 0.52 | 4.00 | 25th | 0.04 | 1.00 |
| 6th | 0.03 | 0.50 | 26th | 0.01 | 0.20 |
| 7th | 0.85 | 4.00 | 27th | 0.03 | 0.20 |
| 8th | 0.02 | 0.40 | 28th | 0.01 | 0.20 |
| 9th | 0.18 | 1.20 | 29th | 0.02 | 0.86 |
| 10th | 0.03 | 0.40 | 30th | 0.00 | 0.20 |
| 11th | 0.53 | 3.00 | 31st | 0.03 | 0.81 |
| 12th | 0.03 | 0.20 | 33rd | 0.02 | 0.20 |
| 13th | 0.43 | 2.50 | 35th | 0.02 | 0.71 |
| 14th | 0.03 | 0.20 | 37th | 0.02 | 0.68 |
| 15th | 0.12 | 0.50 | 39th | 0.02 | 0.20 |
| 16th | 0.03 | 0.20 | 41st | 0.01 | 0.61 |
| 17th | 0.07 | 1.60 | 43rd | 0.01 | 0.58 |
| 18th | 0.02 | 0.20 | 45th | 0.01 | 0.20 |
| 19th | 0.10 | 1.50 | 47th | 0.01 | 0.53 |
| 20th | 0.02 | 0.20 | 49th | 0.01 | 0.51 |
| 21st | 0.05 | 0.20 | | | |

The background harmonics published by Dale (2018) were measured between the 1st of February to the 23rd of July 2017. The DfT and DVLA (2023a) states that there were 113,766 EVs registered within the UK of Q2 2017. As of September 2023, this number increased to 1,443,791 EVs, a twelve-fold increase. Additionally, National Grid ESO (2023) predicts that this may increase to thirty-three million by 2050 under a 'falling short' scenario. Therefore, it has been considered that this might affect the background harmonic level of the network. Several papers have been published regarding THD trends over long periods of time. Iglesias, et, al. (2002) shows an increase in both the LV and 11kV THDv on a residential transformer within the UK, measured by the UK Electricity Council. The LV THDv increases from 2.3% in 1979 to 4.5% in 1999 and 11kV THDv increases from 3.1% in 1980 to 4.4% in 1995.

In contrast, Issouribehere, et, al. (2010), Elphick, et, al. (2010) and Yukihira (2009) shows no change in the THDv levels of their respective networks. Firstly, Issouribehere, et, al. (2010) shows an average THDv level of around 1.8-1.9% between 1997 to 2006. The data is from an average of three different Argentinian utility providers, measured on the LV side of a distribution transformer.

Elphick, et, al. (2010) shows the 95th percentile THDv measured across 292 LV sites and 248 medium voltage (MV) sites, measured by 10 electricity distributors in Australia between 2004-2009. Within this period across both LV and MV points of measurement, it can be seen that the 95th percentile of THDv reduces slightly over the measured period. For LV shown within Elphick, et, al. (2010) this reduces from around 70% to 65% of the maximum harmonic limit, and for MV this reduces from around 70% to 55% of the maximum harmonic limit.

Lastly, Yukihira (2009) shows the average THDv measured at 6.6kV at two different substations in Japan between 1994 and 2007. Over this period, the average seems to be reasonably constant, however, there are periods of limited increasing and decreasing of THDv. The average THDv for the residential substation was between 2-2.5% and for the business substation was between 1.5-2%.

By comparing Iglesias, et, al. (2002), Issouribehere, et, al. (2010), Elphick, et, al. (2010) and Yukihira (2009), it would appear that THDv levels rose until 1999, as shown in Iglesias, et, al. (2002) and Yukihira (2009). However, from 2000, THDv seems to have dropped or stayed at a constant level as shown in Issouribehere, et, al. (2010), Elphick, et, al. (2010) and Yukihira (2009).

The DfT and DVLA (2023a) states that as of Q4 2009, there were only 7,897 EVs on UK roads. If the countries considered in Iglesias, et, al. (2002), Issouribehere, et, al. (2010), Elphick, et, al. (2010) and Yukihira (2009), which are the UK, Argentina, Australia and Japan respectively, have a similar uptake of EVs to the UK, the harmonic data would not include the rapid increase of EVCs, which may lead to more harmonic distortion. Therefore, the long-term impact of EVCs on the THDv across multiple voltage levels is not known. Therefore, it has been opted to leave the background harmonics at the level identified in Dale (2018) for this simulation, and not increase the figures based on predicted increases in background THDv in the future.

The background harmonics will be simulated as a harmonic current source on the LV side of the distribution transformer, similar to the methodology used by Parihar and Malik (2022). The current produces a harmonic voltage, which when calibrated, accurately reproduces the harmonic profile shown in Table 3.1.7.1. Additionally, the harmonic current can be varied depending on the transformer and network impedance to keep a constant background voltage harmonic level across a variety of potential tests.

The background harmonics were produced by accurately modelling the grid impedance at the primary substation on the 11kV bus, the 11kV cable and 11kV:400V transformer at the distribution substation. Harmonic current was then injected back into the grid from the LV bus of the 11kV:400V transformer via a harmonic current source. This can be seen in Figure 3.1.5.1. A portion of the harmonic current source can be seen in Figure 3.1.7.1. Due to the impedance of this network, the injected harmonic current produced voltage harmonics. The voltage harmonic profile of the substations LV bus produced through this method can be seen in Table 3.1.7.1, which accurately matched the harmonic profile shown within Dale (2018). This represents a THDv of 1.36%. Therefore, this method accurately produces the background harmonics of the network, enabling the accurate simulation of EVC and DER harmonic profiles.

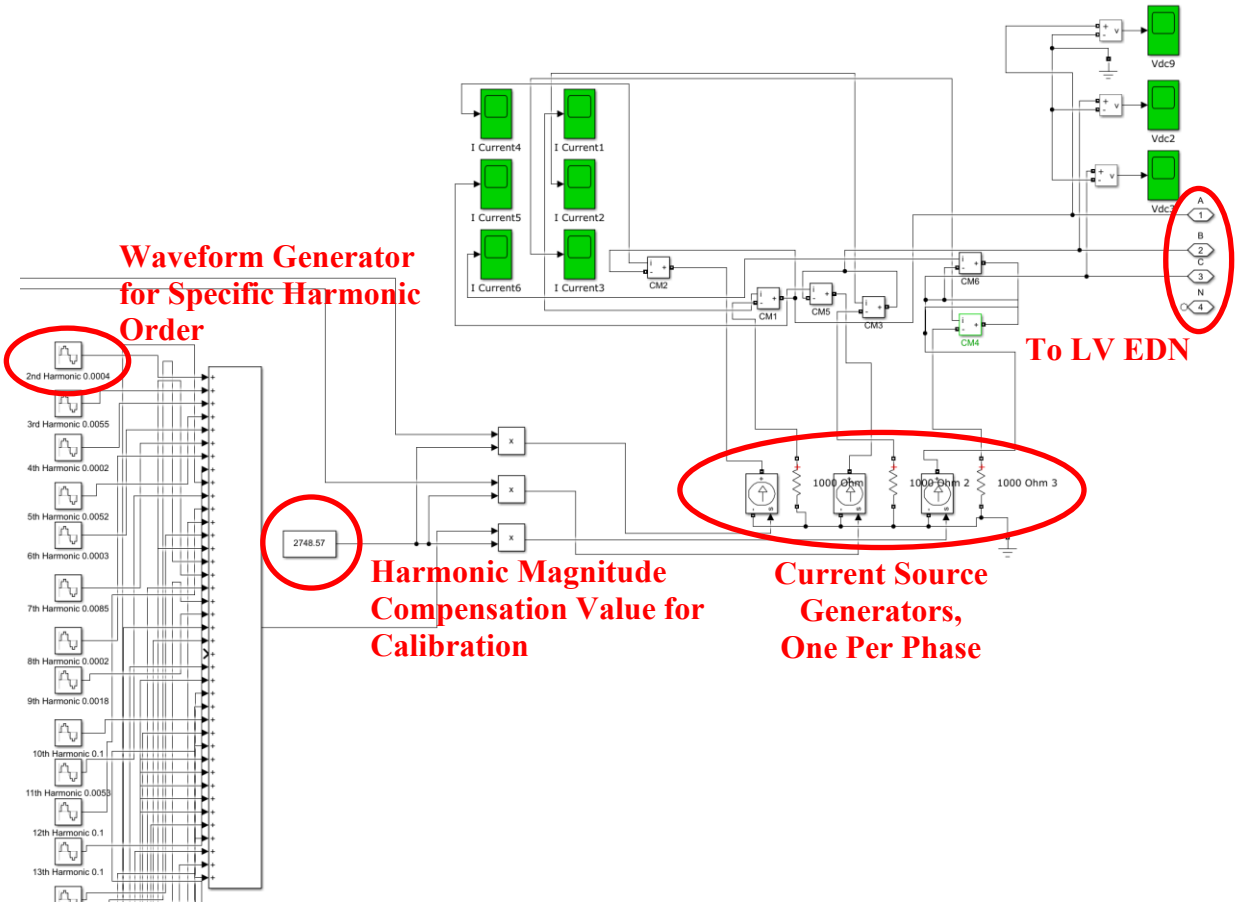


**Figure 3.1.7.1: Portion of the simulated background harmonic current source (The Mathworks, Inc., 2021).**

Another variable which should be mentioned is that the voltage harmonic profile simulated in Table 3.1.7.1 had a constant phase angle for all harmonics. The phase angle of background harmonics in relation to the phase angle of EVC harmonics were not published in Dale (2018). In reality, background voltage harmonics will have an infinite number of phase angles. Measured voltage harmonics from an industrial customer in West London via a PM7000 previously mentioned are shown in Table 3.1.7.2. The reason for simulating the harmonics as having a constant phase angle was to better control phase-shift within the simulation.

**Table 3.1.7.2: Table of the background voltage harmonics across the red phase LV terminal of the transformer measured using a PM7000 power quality meter for an industrial customer in West London.**

| Harmonic Number | Harmonic Magnitude (%) | Phase Angle (º) | Harmonic Number | Harmonic Magnitude (%) | Phase Angle (º) |
|---|---|---|---|---|---|
| 2nd | 0.3 | 52.8 | 22nd | 0.0 | 108.3 |
| 3rd | 0.1 | -126.8 | 23rd | 0.1 | -37.5 |
| 4th | 0.1 | 54.7 | 24th | 0.0 | 88.0 |
| 5th | 2.4 | -123.8 | 25th | 0.0 | -99.4 |
| 6th | 0.1 | -47.0 | 26th | 0.0 | 100.3 |
| 7th | 3.4 | 126.9 | 27th | 0.0 | -66.2 |
| 8th | 0.1 | 113.0 | 28th | 0.0 | 92.0 |
| 9th | 0.1 | 20.9 | 29th | 0.0 | -130.1 |
| 10th | 0.1 | 75.1 | 30th | 0.0 | 134.2 |
| 11th | 0.5 | -127.6 | 31st | 0.0 | 44.6 |
| 12th | 0.0 | 96.2 | 33rd | 0.0 | -61.8 |
| 13th | 0.4 | 167.9 | 35th | 0.0 | -39.9 |
| 14th | 0.0 | 118.1 | 37th | 0.0 | -124.7 |
| 15th | 0.1 | -122.7 | 39th | 0.0 | -54.3 |
| 16th | 0.0 | 106.4 | 41st | 0.0 | -158.8 |
| 17th | 0.1 | -106.0 | 43rd | 0.0 | 8.7 |
| 18th | 0.0 | 112.6 | 45th | 0.0 | 2.9 |
| 19th | 0.0 | -82.2 | 47th | 0.0 | -73.6 |
| 20th | 0.0 | 105.8 | 49th | 0.0 | -61.4 |
| 21st | 0.0 | -109.4 | | | |

## 3.1.8 – Off-peak Load value

In order to allow the maximum number of EVCs on the network before network capacity is reached, the base load of the network will be simulated at its minimum. Staats, et al. (1998) states that the lower the network load and the higher the EVC or DER penetration, the higher the network harmonics. The minimum load for economy seven customers is 500W as shown in Figure 3.1.8.1. Since the estate is only served by electricity, it will be assumed that this load profile is correct. Assuming this load is for heating, this will be assumed to be fully resistive load as will predominantly be of a traditional resistive type. Heat pumps are not yet common within the UK and uptake is far lower than government targets as per Harrington (2023).

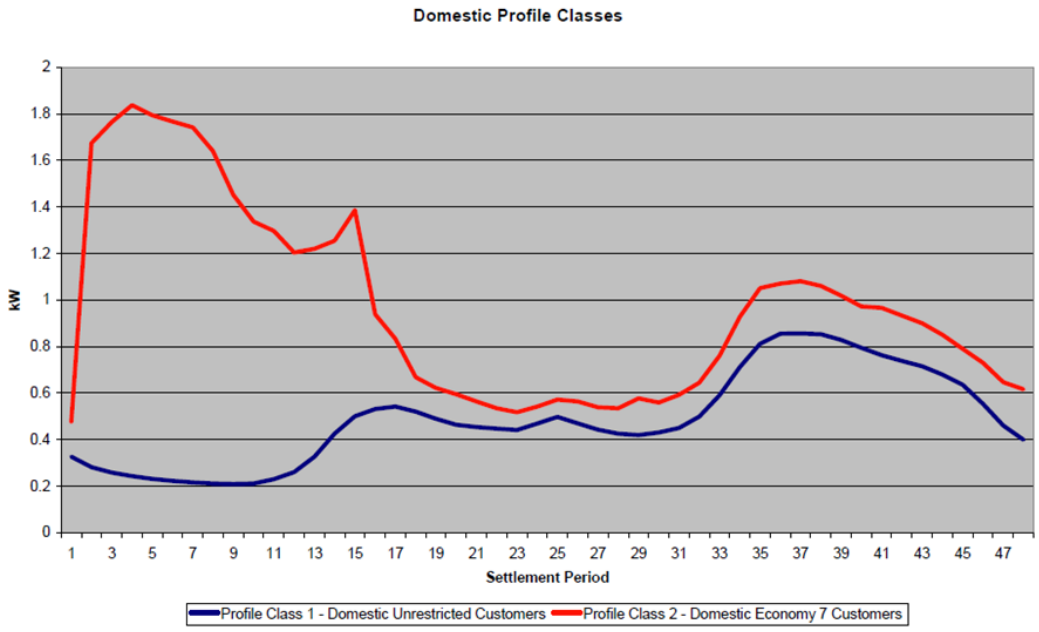


**Figure 3.1.8.1: Load profile of both domestic unrestricted customers and domestic economy seven customers (Elexon Ltd, 1997).**

However, due partly to the introduction of modern electronics in homes, this base load will likely contain harmonics. This is confirmed by Yamini, et al. (2019). Examples of the currents drawn by multiple devices including a laptop charger, mobile charger and LED lightbulb can be seen within Yamini, et al. (2019). Lachaume, Deflandre and Meunier (2002) has produced equations for predicting the harmonic current produced per harmonic order and per N number of customers for an LV domestic network, with less than 100 customers per phase and can be seen in the table within Section 3.2 of Lachaume, Deflandre and Meunier (2002). Macedo, Resende and Samesima (2003) measured low voltage (LV) harmonic current across multiple transformer feeders and found the typical harmonic currents are I3, 1.83%, I5, 3.25% and I7, 0.98%.

Additionally, there are current distortion limits stated by IEEE Std 519-2014 (IEEE, 2014) which users connected to the network should comply with. Current harmonics should be complied with except for 3s and 10-minute intervals which could be up to 2x or 1.5x the values stated within IEEE Std 519-2014 (IEEE, 2014) respectively. IEEE Std 519-2014 (IEEE, 2014) states the values for odd harmonics. Even harmonics within the ranges stated are limited to 25% of these values.

To model harmonics within the base load using MATLAB, each load would need to be modelled as several harmonic current sources alongside a resistive and inductive load as shown in Figure 3.1.8.2. This will add additional complexity to the model, which will lead to longer computation times and will increase the background voltage harmonic level. The effect that this will have on the background harmonics will depend on the network impedance, therefore, this is not conducive to keeping a consistent background harmonic level for test purposes, when varying transformer size or network impedance. Additionally, the current harmonics produced by multiple loads could increase or decrease the voltage harmonic level, leading to a harmonic feedback loop, since the resistive and inductive load will draw current harmonics based on the voltage harmonic level. This is of course dependent on the phase angle of the harmonic currents produced by the loads in relation to the background harmonic distortion.

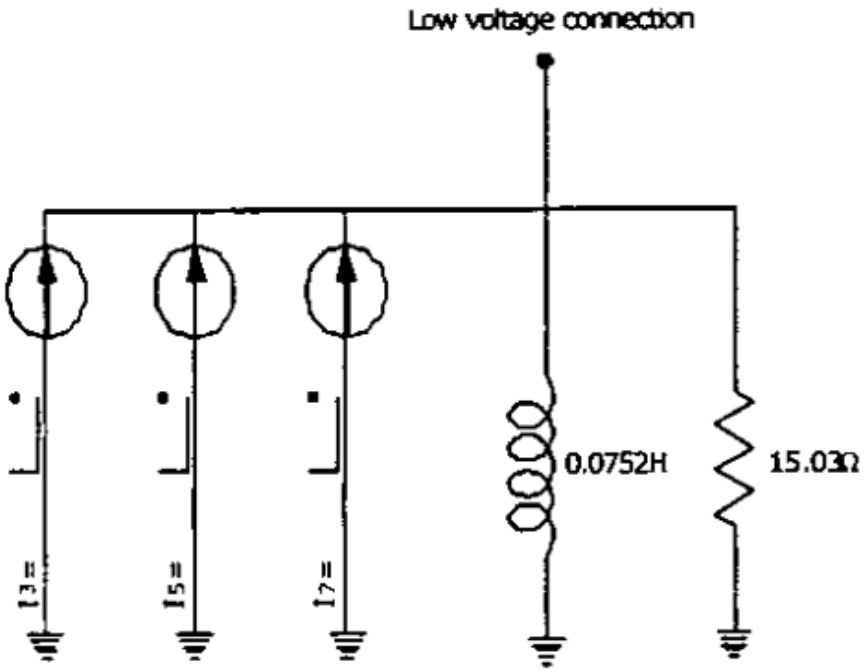


**Figure 3.1.8.2: Model of an LV consumer, containing harmonic load. (Macedo, Resende and Samesima, 2003).**

Therefore, for simplicity, the base load will be assumed to be for heating only and will be simulated as a resistive load with no power electronics or non-linear loads. These simulated resistive loads can be seen as resistors in Figure 3.1.5.1. The background voltage harmonics generated in Section 3.1.7 will also lead to the resistive loads drawing harmonic current, proportional to the background voltage harmonic level. Therefore, this solution should, depending on the phase angle of harmonic currents lead to similar simulation results, whilst reducing simulation complexity, speeding up computation times and improving control.

### 3.1.9 – Further Assumptions

The simulated LV EDN shown in Figure 3.1.5.1 has been modelled under normal conditions. Under these conditions, there are no network faults and the linkbox outside number eighty-two (see Figure 3.1.1.2 and accompanying explanation) is an open point.

Assumptions made for this simulated network are as follows:

- The fault impedance during abnormal running arrangements is assumed to be negligible.
- Linkbox and connections present negligible impedance
- The EVC and DER penetration is balanced evenly across all three phases.
- Services are balanced across all phases and each subsequent property will be connected to a different phase.
- The neutral is earthed at Road A's local transformer only. It should be mentioned that there may be token earths connected to the neutral and laid next to joints to try and lower voltage extremes following an open circuit neutral. The location of these are unknown and therefore it will be assumed that there are none.

## 3.2 – Electric Vehicle Chargers

### 3.2.1 – EV Harmonics

By considering the results of Table 2.1.2.1, the THDi output of EVCs could vary between 1.8-11.0%. Although the harmonic profiles differ between manufacturers, it can be seen that odd harmonics dominate within Watson, et al. (2015), Lucas, et al. (2015) and Gomez and Morcos (2003). Unfortunately, a single reliable study which includes the harmonic profiles for background harmonics and multiple EVCs is not currently available. Harmonic profiles for different EVCs from a range of studies are not compatible as the results are dependent on several factors including the background harmonic distortion and source impedance.

Therefore, Dale (2018) was used as the best compromise available at the time. This study produced the <16A median current harmonic profile measured for EVCs on WPDs 'Electric Vehicle Emissions Testing' project. This median profile is shown in Figure 3.2.1.1 and contains the median of the harmonic profiles of the makes and models used within the study conducted by Dale (2018).

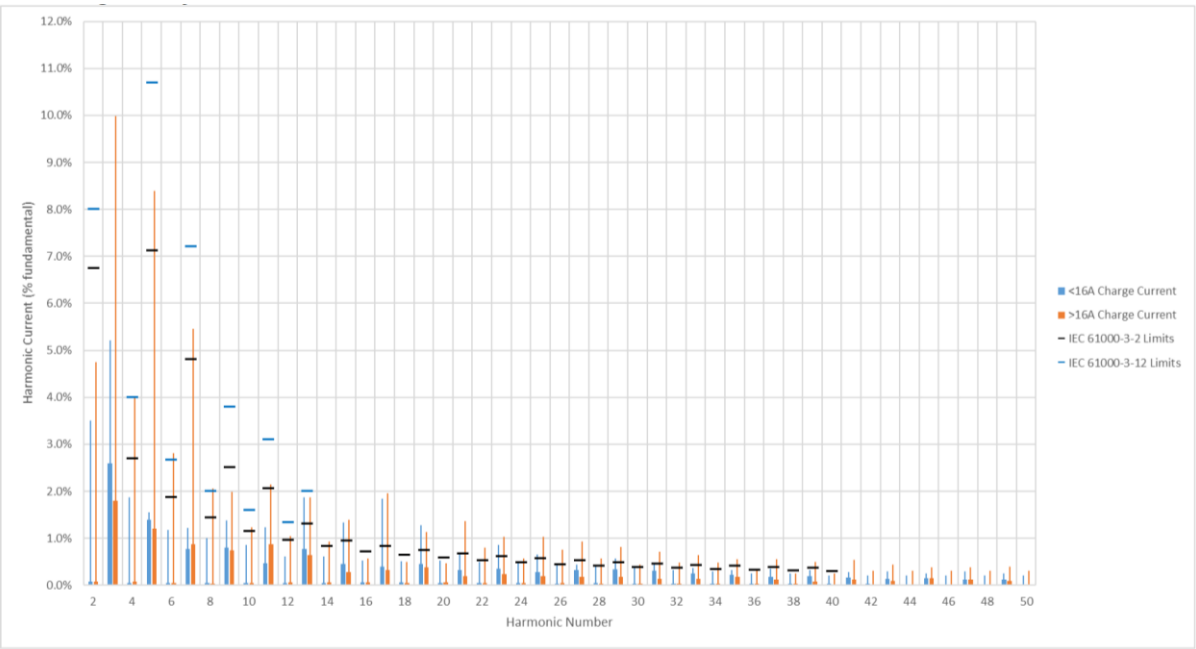


**Figure 3.2.1.1: Median current harmonics measured for EVCs during WPDs 'Electric Vehicle Emissions Testing' project compared to IEC 61000-3-2:2018 (IEC, 2018b) and IEC 61000-3-12:2011 (IEC, 2011) limits (Dale, 2018).**

The median THDi of the <16A EVCs within Figure 3.2.1.1 is 3.54%. As mentioned in Section 2.1.2, by comparing Dale (2018) and Dermot (2018), it can be seen that these sources share the majority of vehicles. Additionally, except for the Tesla Model S and X, Table 2.1.1.1 contains three of the EVs used within Dale (2018). Therefore, the median current harmonic profile appears to be representative of EVCs in the UK. This does not consider the transients experienced at the start and end of a charging cycle as explained in Section 2.1.2 since these transients are only experienced for a short time and produce a lower magnitude of harmonic current.

The harmonic profile produced by Dale (2018), falls within the lower end of the measured values stated by Watson, et al. (2015), but is lower than the values stated by Foskolos (2021). The reason for the THDi of Dale (2018) being at the lower end of the expected levels may be due to each of the individual harmonic magnitudes being a median of the individual harmonic magnitudes of the EVs used within Dale (2018), as opposed to individually measured examples stated in Watson, et al. (2015) and Foskolos (2021). Additionally, Dale (2018) includes background harmonic data, gathered from the same LV EDN as the EVC study and measurements. Where possible it is important that the EVC harmonic profiles and background harmonic profile are measured from the same network since variations in background harmonics will lead to variations in the EVC harmonics. Therefore, Dale (2018) is the most reliable source available which has published both background and EVC harmonic profiles, the background harmonic profile of which has been used in the model as stated in Section 3.1.7.

As identified in Section 2.1.1, there are many EVs available which are limited to a charging rate of 3.6kW. Additionally, an EV capable of charging at a higher rate may be limited by the EVC wall box. Therefore, for the purposes of this thesis, the maximum charging rate of EVCs will be assumed to be 3.6kW. Further to this, although the peak harmonic level is higher, the harmonic level of the >16A median profile shown in Figure 3.2.1.1 is lower than the <16A median profile. Therefore, by using <16A median profile, this produces a worst-case harmonic scenario.

## 3.2.2 – Simulation of the EVC

Using the background voltage harmonic profile discussed in 3.1.7, the harmonic profile for the EVC was calibrated against the <16A median profile shown in Figure 3.2.1.1. This was produced by creating a load of 3.05kW and 3.28kVA as per Pinto, et al. (2017) and injecting harmonic current at the same node. This is based off the methodology by Macedo, Resende and Samesima (2003) and shown in Figure 3.1.8.2. An image of the simulation of the EVC can be seen in Figure 3.2.2.1. The profile produced using this method can be seen in Table 3.2.2.1 and is identical to the <16A profile shown in Figure 3.2.1.1

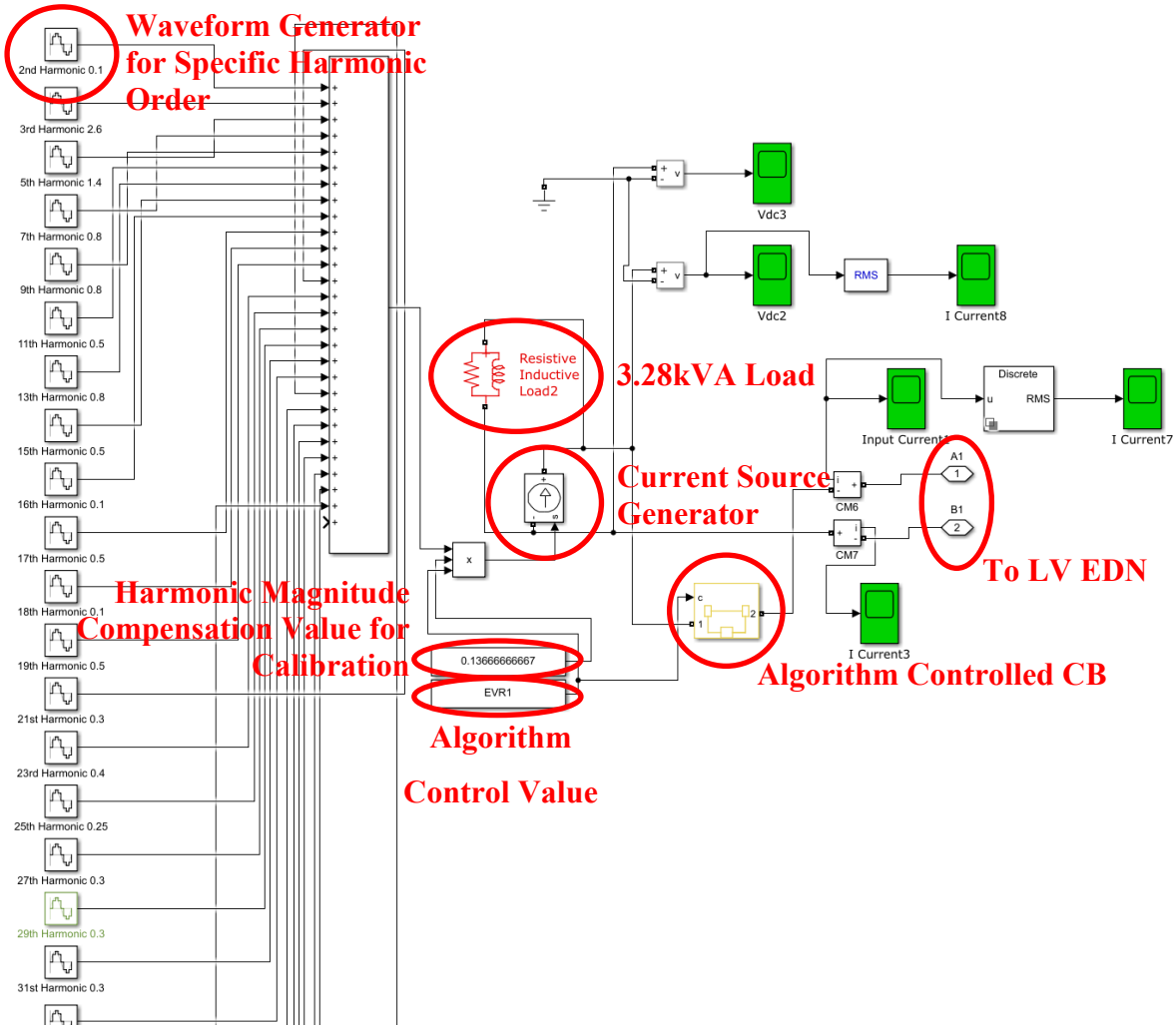


**Figure 3.2.2.1: Overview of the simulated single-phase EVC with CB control using Simulink (The Mathworks, Inc., 2021).**

**Table 3.2.2.1: The current harmonic profile for the EVC, calibrated against the <16A median profile shown in Figure 3.2.1.1, data from Dale (2018).**

| Harmonic Number | Percentage of Fundamental (%) | Harmonic Number | Percentage of Fundamental (%) | Harmonic Number | Percentage of Fundamental (%) |
|---|---|---|---|---|---|
| 2nd | 0.10 | 15th | 0.50 | 28th | 0.00 |
| 3rd | 2.60 | 16th | 0.10 | 29th | 0.30 |
| 4th | 0.00 | 17th | 0.50 | 30th | 0.00 |
| 5th | 1.40 | 18th | 0.10 | 31st | 0.30 |
| 6th | 0.00 | 19th | 0.50 | 33rd | 0.25 |
| 7th | 0.80 | 20th | 0.00 | 35th | 0.25 |
| 8th | 0.00 | 21st | 0.30 | 37th | 0.20 |
| 9th | 0.80 | 22nd | 0.00 | 39th | 0.20 |
| 10th | 0.00 | 23rd | 0.40 | 41st | 0.15 |
| 11th | 0.50 | 24th | 0.00 | 43rd | 0.15 |
| 12th | 0.00 | 25th | 0.25 | 45th | 0.15 |
| 13th | 0.80 | 26th | 0.00 | 47th | 0.10 |
| 14th | 0.00 | 27th | 0.30 | 49th | 0.10 |
| THDv: 3.54% | | | | | |

However, it should be noted that the current harmonic profile shown in Table 3.2.2.1 was calibrated at number fifty-eight Road A. To ensure that the profile remains valid for the rest of the properties on this road, the simulated EVC was trialled at several other locations. These are numbers thirty-three, thirty-four, forty-nine, one-hundred and twenty-two b and one-hundred and fifty-two visible within Figure 3.1.1.2. one-hundred and fifty-two deviated the most, drawing 98.9% of the total current and 98.9% of the THDi when compared to fifty-eight. If the results or correlation is marginal, then this error should be considered when drawing conclusions.

Within the EVC model, the phase angle of harmonic currents are assumed to be in phase with the harmonic currents producing the background harmonic distortion. However, the impedance between each EVC will lead to differences in the phase angle of the harmonic voltage generated. The effect will be greater for higher order harmonics since reactance is proportional to frequency and will result in a higher degree of cancellation similar to the summation exponent used in Table 1.3.2.2. By using cable impedance as a means of introducing harmonic phase shift, the model will be applicable for dwellings, with separate driveways and LV service cables, as well as blocks of flats or communal EVC charging areas which will have multiple EVCs connected to a single POC.

## 3.2.3 – Limitations of the EVC Model

One limitation of the <16A median profile is that the profile provides median values for multiple EVCs, rather than the measured profile of individual chargers. Therefore, the simulation may not capture the impact of low numbers of EVCs. This will be explained in Section 3.2.4. In addition, most studies available at the time of this thesis look at low numbers of EVCs including Xu, et al. (2014) and Deilami, et al. 2010. Therefore, it is hard to verify the results of this simulation when this simulation is not applicable for low numbers of EVCs. When reliable harmonic profile data for multiple individual EVCs, with a base background harmonic profile is available, future simulations should include multiple harmonic charger profiles and charging rates from a range of different EVCs representative of the most popular UK BEVs and PHEVs shown in Table 2.1.1.1.

Additionally, this thesis has focussed on single-phase, 3.6kW in-line EVCs which can be plugged into a 3-pin socket. This is most relevant to residential properties which have access to private parking outside their homes as per the network shown Figure 3.1.1.2. However, many new EVCs which would be applicable to these residential streets now charge at 7.2kW. In addition, many homes do not have access to be able to charge their vehicle from their home and are reliant on dedicated three-phase EVC points and charge points from streetlights. The differences in charge rate, harmonic profile, and charger location, such as dedicated three-phase EVC charging points may change the dynamic of the simulation and lead to different results. These should be considered in future simulations.

### 3.2.4 – Validation of the Simulation

To validate the EVC model, the simulated LV EDN shown in Figure 3.1.5.1 had varying numbers of EVCs on both feeders ranging from 0% EVC penetration to 98.4% penetration in increments of approximately 10%. 0% penetration represents a network with zero EVCs connected, 100% penetration represents a network with one EVC connected per single-phase service. There are one-hundred and twenty-five single-phase services on this LV EDN and therefore 100% EVC penetration represents one-hundred and twenty-five EVCs.

For this simulation, the EVCs were connected evenly across all three phases, however, the geographical location of the EVCs were random, resulting in slight deviations in the results as the EVC numbers increase. 98.4% EVC penetration corresponds to one-hundred and twenty-three EVCs and is the maximum number of EVCs which can be connected to ensure that all three phases are balanced. This equates to forty-one EVCs per phase.

The results of this validation simulation can be seen in Figure 3.2.4.1. The phase-neutral harmonic values were assessed. The reason for this rather than the phase-earth values are firstly, the data is only valid for phase-neutral values, since the PM7000, which measured voltage harmonics on the network for Dale (2018), measured phase-neutral, rather than phase-earth harmonics. Secondly, the phase-neutral voltage is what is experienced by the consumer since the LV EDN uses a PME system, therefore combining the neutral and earth. Therefore it is the power quality of this voltage which has an impact on equipment within a home. The two points on the network which were measured for this study are the LV bus of the 11kV:400V transformer at Road A substation (red, yellow, and blue bus) and supplies at the end of feeder one defined in Figure 3.1.1.2 (red, yellow and blue terminal).

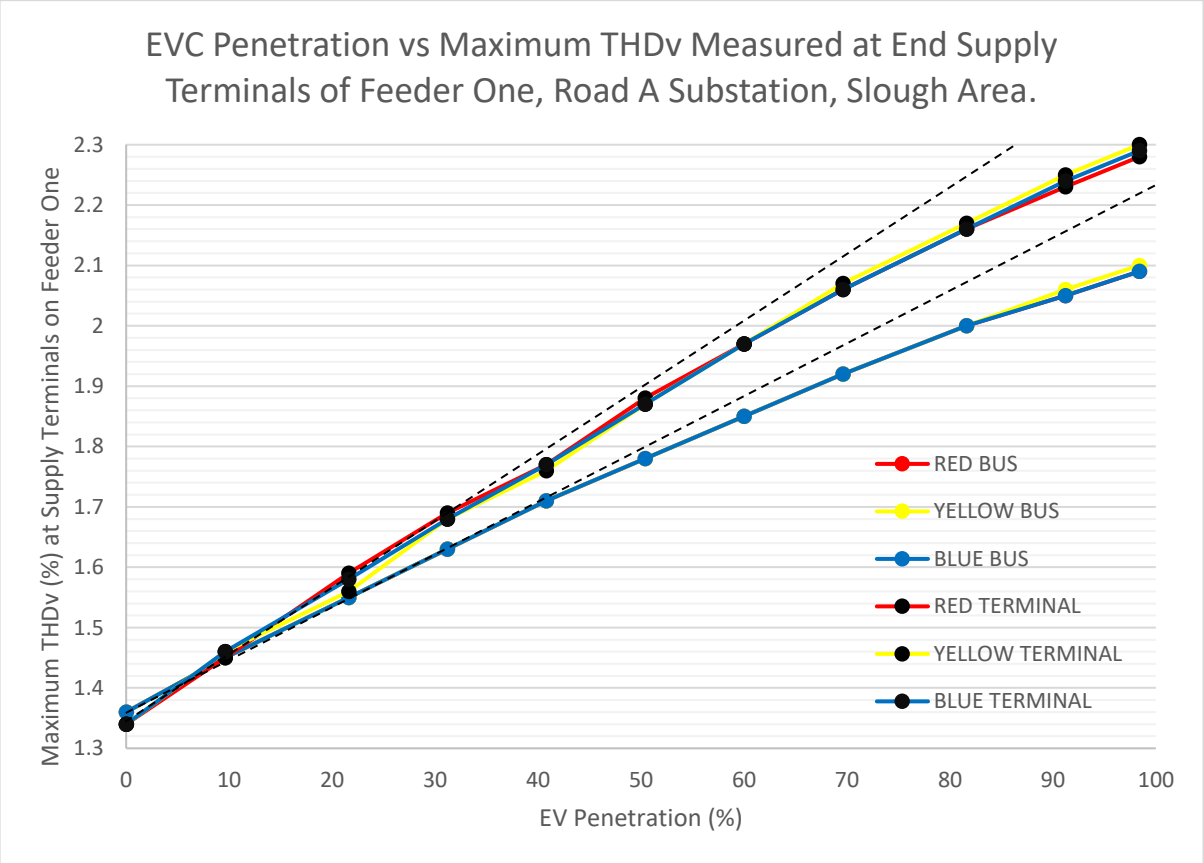


**Figure 3.2.4.1: Maximum THDv vs EVC penetration for feeder one, Road A substation, measured at the LV bus of the 11kV:400V transformer and supply terminals at the end of the feeder.**

As mentioned in Section 3.2.3, the EVC harmonic model used is the median value for <16A chargers measured as part Dale (2018). Therefore, it is likely that this study is only representative for networks with multiple EVCs. For a network with lower numbers of EVCs, research has shown that the effect each EVC has on the power quality of the EDN is more pronounced as shown in Li, Wang and Deng (2018).

To validate the study, the results were compared to Deilami, et al. (2010) and Xu, et al. (2014) which consider base load in their studies. Most studies investigating the effect of EVCs on THDv do not consider base load. By considering base load it can be seen that as EVC penetration increases, the rate of increase of THDv decreases. However, it should be noted that background voltage harmonic distortion has not been considered in these studies. In a system with a level of background harmonics, even linear loads will draw harmonic current. Therefore, the harmonic current contribution from the EVC itself is lower than the total harmonic current drawn. Within these two studies the EVC THDi was set at somewhere between 2-5.3% for Xu, et al. (2014) and 31.9% for Deilami, et al. (2010). The THDi drawn in this thesis' simulation is 3.54% as per Table 3.2.2.1, putting the THDi closer to the values used by Xu, et al. (2014). Therefore, the work of Xu, et al. (2014) is likely to produce THDv results closer to the values expected within this thesis.

In each of the studies shown in Deilami, et al. (2010) and Xu, et al. (2014), the network impedance is unknown which makes comparison difficult. However, it can be seen in Xu, et al. (2014) that under a steady-state charging period (SSCP) that there is a noticeable drop off in the increase of THDv at node 800, increasing by 0.2%, 0.16%, 0.13%, 0.12% and 0.12% with each subsequent EVC added, up to a maximum of five chargers and value of 0.73%. At node 890 there is a similar pattern, increasing by 0.53%, 0.31%, 0.16%, 0.2% and 0.2% with each subsequent EVC added, up to the maximum of five chargers and value of 1.4%. A similar characteristic can be seen in Deilami, et al. (2010), where for un-coordinated EV charging between 5pm-12pm, the THDv increases from 12.0450% (six EVs), to 19.1976% (eleven EVs) and lastly 23.2272% (eighteen EVs). A clear reduction in rate of increase of THDv can be seen with penetration. These relationships are useful for understanding the behaviour of multiple chargers, however, it does not produce comparable results due to the lack of known network impedance and the use of <16A median current harmonic profile within this thesis' study.

Moving on to the results of this thesis, by drawing a straight line through the first four THDv data points in Figure 3.2.4.1, it can be seen that the rate of increase of voltage harmonic distortion decreases as more EVCs are added. This occurs at approximately 40% (fifty-one EVCs) for the terminals, and 50% (sixty-three EVCs) for the LV bus of the 11kV:400V transformer at Road A substation. However, the drop off effect is not as instantaneous or dramatic as the effect seen in Deilami, et al. (2010) or Xu, et al. (2014). This may be explained by a lower network impedance than the other studies. Although the exact impedance of the network for Deilami, et al. (2010) is unknown, a 100kVA transformer is used, which would indicate a higher impedance.

The THDv of the network shown in Figure 3.2.4.1 can be seen to be significantly lower than in Deilami, et al. (2010) for similar numbers of EVCs. There are up to eighteen EVCs in Deilami, et al. (2010). Whereas there are up to one-hundred and twenty-three EVCs simulated at 98.4% EVC penetration for the Road A EDN. The lower THDv can be explained by a lower harmonic current contribution from the EVCs of 3.54% as stated previously. However, in the case of Deilami, et al. (2010), this may also be explained by a lower network impedance within the Road A network, which reduces the impact harmonic current will have on harmonic voltage as per Section 1.2.1.

Xu, et al. (2014) simulates up to five EVCs. At five EVCs, the THDv value of 1.4% at node 890 is not dissimilar from the value which can be extrapolated from Figure 3.2.4.1. However, it should be repeated that Xu, et al. (2014) does not consider background harmonics which will have an impact on the THDv results. In addition, the THDv value almost doubles between node 800 and node 890, at 0.73% and 1.4% respectively indicating a much higher LV EDN impedance than the Road A EDN used for this thesis' study. The THDv values measured at node 800 are much lower than other studies and considering a higher network impedance do not seem far from what might be expected from the Road A network assuming background harmonics were not considered. As mentioned previously, Xu, et al. (2014) uses much more comparable values of EVC THDi with a range of 2-5.3%.

Therefore, based on the available comparable studies, the results of this thesis' study appear to be plausible, although there are clear differences when compared to the studies Deilami, et al. (2010) and Xu, et al. (2014). It must be reiterated that in contrast to the study produced for this thesis, Deilami, et al. (2010) and Xu, et al. (2014) do not take into account background harmonics. In addition, there are a number of other differences including base load, EVC harmonics and network parameters. Unfortunately, the data used to produce these simulations has not been published so accurate replication and validation is not possible.

Despite this, the measured data from Dale (2018) used for this thesis' study has been produced by WPD, a DNO regulated by Ofgem and is part of a group of DNOs who work with the ENA on research and development. The THDv rate of increase, decreases as more EVCs are added to the network, albeit, at a much later stage when compared to Deilami, et al. (2010) and Xu, et al. (2014). In addition, the EVC and background harmonic profiles used in the simulation match the measured values from Dale (2018) very closely. Not being able to verify the model must be taken into account when conclusions are drawn. However, the reliability of the data and the curves shown in Figure 3.2.4.1 suggests that the simulation produces reliable results. Further work could be carried out by a DNO to verify the results of this simulation in a live measured network.

## 3.2.5 – THDv at the Transformer and Remote End

Tables 3.2.5.1-2 shows the harmonic spectrum of the voltage measured between phase and neutral at supply terminals at the end of feeder one and at the LV terminals of Road A substations distribution transformer on the yellow phase at an EVC penetration of 98.4%. The terminals at the end of feeder one were the points with the highest measured THDv as per Figure 3.2.4.1. This penetration value represents an EVC quantity of one-hundred and twenty-three evenly distributed amongst the three phases, fifty-four on feeder one and sixty-nine on feeder two. By comparing these results with the standards in ER G5/5, shown in Tables 3.2.5.1-2, it can be seen that there are several points when the harmonic levels of the network exceed the limits set out by this standard. These are the 21$^{st}$, 27$^{th}$ and 33$^{rd}$ harmonics for Table 3.2.5.1 and the 21$^{st}$ and 27$^{th}$ harmonics for Table 3.2.5.2.

**Table 3.2.5.1: Table of the voltage harmonics across the yellow phase supply terminal at the end of feeder one with an EVC penetration of 98.4% against the limits set out in ER G5/5 (Energy Networks Association, 2020).**

| Harmonic Number | Harmonic Magnitude (%) | ER G5/5 Limits (%) | Harmonic Number | Harmonic Magnitude (%) | ER G5/5 Limits (%) | Harmonic Number | Harmonic Magnitude (%) | ER G5/5 Limits (%) |
|---|---|---|---|---|---|---|---|---|
| 2nd | 0.05 | 1.60 | 15th | 0.40 | 0.50 | 28th | 0.01 | 0.20 |
| 3rd | 0.94 | 4.00 | 16th | 0.09 | 0.20 | 29th | 0.26 | 0.86 |
| 4th | 0.02 | 1.00 | 17th | 0.38 | 1.60 | 30th | 0.00 | 0.20 |
| 5th | 0.85 | 4.00 | 18th | 0.08 | 0.20 | 31st | 0.27 | 0.81 |
| 6th | 0.03 | 0.50 | 19th | 0.42 | 1.50 | 33rd | 0.22 | 0.20 |
| 7th | 1.07 | 4.00 | 20th | 0.01 | 0.20 | 35th | 0.23 | 0.71 |
| 8th | 0.02 | 0.40 | 21st | 0.25 | 0.20 | 37th | 0.19 | 0.68 |
| 9th | 0.49 | 1.20 | 22nd | 0.01 | 0.20 | 39th | 0.19 | 0.20 |
| 10th | 0.03 | 0.40 | 23rd | 0.33 | 1.20 | 41st | 0.14 | 0.61 |
| 11th | 0.71 | 3.00 | 24th | 0.01 | 0.20 | 43rd | 0.14 | 0.58 |
| 12th | 0.03 | 0.20 | 25th | 0.22 | 1.00 | 45th | 0.14 | 0.20 |
| 13th | 0.80 | 2.50 | 26th | 0.01 | 0.20 | 47th | 0.10 | 0.53 |
| 14th | 0.02 | 0.20 | 27th | 0.26 | 0.20 | 49th | 0.10 | 0.51 |
| Harmonics higher than the limits set by ER G5/5 | | | | | | | | |
| THDv: 2.30%. ER G5/5 Limit 5.0% | | | | | | | | |
| Number of EVCs on Feeder 1: 54 Number of EVCs on Feeder 2: 69 | | | | | | | | |

**Table 3.2.5.2: Table of the voltage harmonics measured on the yellow phase at the LV terminals of Road A substations distribution transformer with an EVC penetration of 98.4% against the limits set out in ER G5/5 (Energy Networks Association, 2020).**

| Harmonic Number | Harmonic Magnitude (%) | ER G5/5 Limits (%) | Harmonic Number | Harmonic Magnitude (%) | ER G5/5 Limits (%) | Harmonic Number | Harmonic Magnitude (%) | ER G5/5 Limits (%) |
|---|---|---|---|---|---|---|---|---|
| 2nd | 0.05 | 1.60 | 15th | 0.34 | 0.50 | 28th | 0.01 | 0.20 |
| 3rd | 0.86 | 4.00 | 16th | 0.07 | 0.20 | 29th | 0.21 | 0.86 |
| 4th | 0.02 | 1.00 | 17th | 0.32 | 1.60 | 30th | 0.00 | 0.20 |
| 5th | 0.78 | 4.00 | 18th | 0.07 | 0.20 | 31st | 0.22 | 0.81 |
| 6th | 0.03 | 0.50 | 19th | 0.36 | 1.50 | 33rd | 0.19 | 0.20 |
| 7th | 1.02 | 4.00 | 20th | 0.01 | 0.20 | 35th | 0.19 | 0.71 |
| 8th | 0.02 | 0.40 | 21st | 0.21 | 0.20 | 37th | 0.15 | 0.68 |
| 9th | 0.43 | 1.20 | 22nd | 0.01 | 0.20 | 39th | 0.16 | 0.20 |
| 10th | 0.03 | 0.40 | 23rd | 0.27 | 1.20 | 41st | 0.12 | 0.61 |
| 11th | 0.67 | 3.00 | 24th | 0.01 | 0.20 | 43rd | 0.12 | 0.58 |
| 12th | 0.03 | 0.20 | 25th | 0.19 | 1.00 | 45th | 0.12 | 0.20 |
| 13th | 0.72 | 2.50 | 26th | 0.01 | 0.20 | 47th | 0.08 | 0.53 |
| 14th | 0.02 | 0.20 | 27th | 0.22 | 0.20 | 49th | 0.08 | 0.51 |
| Harmonics higher than the limits set by ER G5/5 | | | | | | | | |
| THDv: 2.10%. ER G5/5 Limit 5.0% | | | | | | | | |
| Number of EVCs on Feeder 1: 54 Number of EVCs on Feeder 2: 69 | | | | | | | | |

In addition to the effect of maximum penetration shown in Figure 3.2.4.1 and Tables 3.2.5.1-2, the tipping point for feeder one to no longer remain compliant with ER G5/5 was identified. It was found that a penetration of 60% was the tipping point for this feeder. This penetration value represents an EVC number of seventy-five evenly distributed amongst the three phases, thirty-three on feeder one and forty-two on feeder two. Table 3.2.5.3 shows the harmonic spectrum of the voltage measured between phase and neutral at a customer's supply terminal at the end of feeder one on the yellow phase at this EVC penetration. At this penetration, the 21st and 27th harmonic is at 0.20%, which is the maximum harmonic percentage allowed under ER G5/5 to remain within limits. It is interesting to note that the maximum harmonic penetration allowed occurs at only 60% and a low THD of 1.97%, just 0.61% higher than the background harmonic value and 0.33% lower than at 98.4% penetration. This shows just how few EVCs can be accepted on the network before ER G5/5 is breached and how little tolerance there is between the network remaining compliant or exceeding the limits.

**Table 3.2.5.3: Table of the voltage harmonics across the yellow phase supply terminal at the end of feeder one with an EVC penetration of 60% against the limits set out in ER G5/5 (Energy Networks Association, 2005)**

| Harmonic Number | Harmonic Magnitude (%) | ER G5/5 Limits (%) | Harmonic Number | Harmonic Magnitude (%) | ER G5/5 Limits (%) | Harmonic Number | Harmonic Magnitude (%) | ER G5/5 Limits (%) |
|---|---|---|---|---|---|---|---|---|
| 2nd | 0.05 | 1.60 | 15th | 0.31 | 0.50 | 28th | 0.01 | 0.20 |
| 3rd | 0.79 | 4.00 | 16th | 0.07 | 0.20 | 29th | 0.20 | 0.86 |
| 4th | 0.02 | 1.00 | 17th | 0.28 | 1.60 | 30th | 0.00 | 0.20 |
| 5th | 0.72 | 4.00 | 18th | 0.06 | 0.20 | 31st | 0.21 | 0.81 |
| 6th | 0.03 | 0.50 | 19th | 0.31 | 1.50 | 33rd | 0.18 | 0.20 |
| 7th | 0.99 | 4.00 | 20th | 0.02 | 0.20 | 35th | 0.18 | 0.71 |
| 8th | 0.02 | 0.40 | 21st | 0.20 | 0.20 | 37th | 0.15 | 0.68 |
| 9th | 0.38 | 1.20 | 22nd | 0.02 | 0.20 | 39th | 0.15 | 0.20 |
| 10th | 0.03 | 0.40 | 23rd | 0.25 | 1.20 | 41st | 0.11 | 0.61 |
| 11th | 0.65 | 3.00 | 24th | 0.01 | 0.20 | 43rd | 0.12 | 0.58 |
| 12th | 0.03 | 0.20 | 25th | 0.17 | 1.00 | 45th | 0.12 | 0.20 |
| 13th | 0.68 | 2.50 | 26th | 0.01 | 0.20 | 47th | 0.08 | 0.53 |
| 14th | 0.03 | 0.20 | 27th | 0.20 | 0.20 | 49th | 0.08 | 0.51 |
| Harmonics on the boundary of the limits set by ER G5/5 | | | | | | | | |
| THDv: 1.97%. ER G5/5 Limit 5.0% | | | | | | | | |
| Number of EVCs on Feeder 1: 33 Number of EVCs on Feeder 2: 42 | | | | | | | | |

## 3.2.6 – Current Harmonics Drawn

At 98.4% EVC penetration, the current harmonics drawn should also be inspected. By considering Table 3.2.6.1, which shows the red phase harmonic current at the LV bus of the transformer. The magnitudes of the harmonic currents have been broken down into their constituent values. It can be seen that lower odd harmonics have significant magnitude, the values decreasing in magnitude as the harmonic number increases in line with the results of Watson, et al. (2015).

**Table 3.2.6.1: Table of the current harmonics measured on the yellow phase of the LV terminals of Road A substations distribution transformer with an EVC penetration of 98.4%.**

| Harmonic Number | Harmonic Magnitude (A) | Harmonic Number | Harmonic Magnitude (A) | Harmonic Number | Harmonic Magnitude (A) |
|---|---|---|---|---|---|
| 2nd | 0.51 | 15th | 2.18 | 28th | 0.06 |
| 3rd | 13.31 | 16th | 0.45 | 29th | 0.90 |
| 4th | 0.13 | 17th | 2.05 | 30th | 0.00 |
| 5th | 7.42 | 18th | 0.38 | 31st | 0.90 |
| 6th | 0.19 | 19th | 1.98 | 33rd | 0.70 |
| 7th | 6.02 | 20th | 0.06 | 35th | 0.70 |
| 8th | 0.12 | 21st | 1.15 | 37th | 0.51 |
| 9th | 3.97 | 22nd | 0.06 | 39th | 0.51 |
| 10th | 0.12 | 23rd | 1.41 | 41st | 0.38 |
| 11th | 3.58 | 24th | 0.06 | 43rd | 0.32 |
| 12th | 0.12 | 25th | 0.83 | 45th | 0.33 |
| 13th | 4.10 | 26th | 0.06 | 47th | 0.19 |
| 14th | 0.12 | 27th | 0.96 | 49th | 0.19 |
| THDi: 2.87% | | | | | |
| Number of EVCs on Feeder 1: 54 Number of EVCs on Feeder 2: 69 | | | | | |

## 3.2.7 – Voltage and Current Harmonics of Neutral

Interestingly, despite the loads being balanced, at 98.4% EVC penetration, harmonics in the neutral other than multiples of the third harmonic, which would be expected due to the third harmonic each being 120° out of phase with each of the other phases, and are therefore in phase, are present on feeder one. This includes harmonic voltages in the neutral at the remote end of feeder one, in addition to harmonic currents flowing in the neutral of the LV side of the distribution transformer at Road A substation. This information can be seen in Tables 3.2.7.1-2.

This is a Consac network and is therefore a PME system. This means that the neutral and earth are the same conductor as shown in Figure 3.1.2.1. Therefore, the neutral is used to bond all metalwork in the home. Voltages present on the neutral could lead to members of the public receiving electric shocks off bonded metalwork, especially if they are stood outside of the property. For example, using an outdoor tap. This issue is far more dangerous during a neutral fault, where the neutral becomes disconnected from the star point of the transformer and is allowed to float, sometimes reaching several hundred volts.

**Table 3.2.7.1: Table of the voltage harmonics measured on the neutral at the end of feeder one with an EVC penetration of 98.4%.**

| Harmonic Number | Harmonic Magnitude (V) | Harmonic Number | Harmonic Magnitude (V) | Harmonic Number | Harmonic Magnitude (V) |
|---|---|---|---|---|---|
| 2nd | 0.02 | 15th | 0.01 | 28th | 0.00 |
| 3rd | 0.14 | 16th | 0.00 | 29th | 0.00 |
| 4th | 0.01 | 17th | 0.01 | 30th | 0.00 |
| 5th | 0.08 | 18th | 0.00 | 31st | 0.00 |
| 6th | 0.01 | 19th | 0.01 | 33rd | 0.00 |
| 7th | 0.09 | 20th | 0.00 | 35th | 0.00 |
| 8th | 0.00 | 21st | 0.00 | 37th | 0.00 |
| 9th | 0.02 | 22nd | 0.00 | 39th | 0.00 |
| 10th | 0.00 | 23rd | 0.00 | 41st | 0.00 |
| 11th | 0.04 | 24th | 0.00 | 43rd | 0.00 |
| 12th | 0.00 | 25th | 0.00 | 45th | 0.00 |
| 13th | 0.03 | 26th | 0.00 | 47th | 0.00 |
| 14th | 0.00 | 27th | 0.00 | 49th | 0.00 |
| Number of EVCs on Feeder 1: 54 Number of EVCs on Feeder 2: 69 Voltage on Neutral: 1.218V | | | | | |

**Table 3.2.7.2: Table of the current harmonics measured on the neutral of feeder one at the LV terminals of Road A substations distribution transformer with an EVC penetration of 98.4%.**

| Harmonic Number | Harmonic Magnitude (A) | Harmonic Number | Harmonic Magnitude (A) | Harmonic Number | Harmonic Magnitude (A) |
|---|---|---|---|---|---|
| 2nd | 0.04 | 15th | 0.01 | 28th | 0.00 |
| 3rd | 0.05 | 16th | 0.00 | 29th | 0.01 |
| 4th | 0.02 | 17th | 0.01 | 30th | 0.00 |
| 5th | 0.03 | 18th | 0.00 | 31st | 0.00 |
| 6th | 0.01 | 19th | 0.01 | 33rd | 0.00 |
| 7th | 0.02 | 20th | 0.00 | 35th | 0.00 |
| 8th | 0.01 | 21st | 0.01 | 37th | 0.00 |
| 9th | 0.01 | 22nd | 0.00 | 39th | 0.00 |
| 10th | 0.01 | 23rd | 0.01 | 41st | 0.00 |
| 11th | 0.01 | 24th | 0.00 | 43rd | 0.00 |
| 12th | 0.01 | 25th | 0.01 | 45th | 0.00 |
| 13th | 0.01 | 26th | 0.00 | 47th | 0.00 |
| 14th | 0.01 | 27th | 0.01 | 49th | 0.00 |
| Number of EVCs on Feeder 1: 54 Number of EVCs on Feeder 2: 69 | | | | | |

It should be stated that the simulation assumes that the neutral is earthed at Road A substations local transformer only as stated in 3.1.6. It is likely that there are token earths connected to the neutral and laid next to joints to try and lower voltage extremes following an open circuit neutral. Unfortunately, the location of these are unknown and therefore, it has been assumed that there are none. If there are token earths, it is likely that these will reduce both fundamental and harmonic voltages on the neutral.

Gomatom, Dorr and Sutherland (2005) states that current required to produce fibrillation of the heart in humans is related to time exposure as stated in the electrocution equation, Equation 3.2.7.1.

Equation 3.2.7.1 $$I = \frac{K}{t^{0.5}}$$

Where:
$I$ is current in amps (A).
$K$ is the electrocution constant (As).
$t$ is the exposure time in seconds (s).

Using the above equation, Dalziel and Lee (1969) states that to cause ventricular fibrillation, for a three second exposure, 67-107mA is required for 50kg adults and 30-40mA for 18kg children. For a minimum exposure of 5 cycles, 403-642mA is required for 50kg adults and 180-240mA for 18kg children. These results are based on 60Hz, rather than 50Hz so may differ at lower frequencies.

The amount of voltage required to lead to these currents will also vary. Gomatom, Dorr and Sutherland (2005) states that the electrical impedance of the human body is non-linear with respect to voltage. Additionally, DC skin resistance is higher than AC skin impedance due to skin capacitance being in parallel with DC skin resistance, therefore reducing the overall impedance. The reason for non-linearity is due to skin impedance, which changes depending on voltage and exposure time. From experimental results, non-linearity occurs above 2-4V. Short-term voltage-current relationship can be expressed using the leakage current equation shown in Equation 3.2.7.2 from Stevens (1963).

Equation 3.2.7.2 $$I = aV + bV^2$$

Where:

$I$ is current in amps (A).

$V$ is voltage in volts (V).

$a$ is a constant of value 170 ($\Omega^{-1}$).

$b$ is a constant of value 67 ($V^{-1}\Omega^{-1}$).

Total body impedance varies with skin impedance, contact area with the live equipment and wetness. This can be expressed using Equation 3.2.7.3 from Reilly (1998) which assumes the subject is bare foot.

Equation 3.2.7.3 $$Z_T = \frac{V_T}{I_B}$$

Where:

$Z_T$ is total body impedance ($\Omega$).

$V_T$ is steady state rms voltage in volts (V).

$I_B$ is steady state rms current in amps (A).

Using these equations produces hand-hand impedance shown in Reilly (1998), Biegelmeier (1985) and Table 3.2.7.3 below. This produces a value of 1750Ω at 25V at the lower wet limit. There is also an assumption that hand-foot impedance is 70% of hand-hand impedance, therefore sitting at 1225Ω.

**Table 3.2.7.3: Table of hand-hand and hand-foot impedance depending on voltage from IEC TS 60479-1:1994 (IEC, 1994).**

| Touch Voltage | 5th percentile | | 50th percentile | | 95th percentile | |
|---|---|---|---|---|---|---|
| | *Hand -hand* | *Hand -foot* | *Hand -hand* | *Hand -foot* | *Hand -hand* | *Hand -foot* |
| **25** | 1750 | 1225 | 3250 | 2275 | 6100 | 4270 |
| **50** | 1450 | 1015 | 2625 | 1838 | 4375 | 3063 |
| **75** | 1250 | 875 | 2200 | 1540 | 3500 | 2450 |
| **100** | 1200 | 840 | 1875 | 1313 | 3200 | 2240 |
| **125** | 1125 | 788 | 1625 | 1138 | 3875 | 2713 |
| **220** | 1000 | 700 | 1350 | 945 | 2125 | 1488 |
| **700** | 750 | 525 | 1100 | 770 | 1550 | 1085 |
| **1000** | 700 | 490 | 1050 | 735 | 1500 | 1050 |
| **Asymptotic** | 650 | 455 | 750 | 525 | 850 | 595 |

Based on a hand-foot impedance of 1225Ω, and 30mA over a three second exposure, which can cause ventricular fibrillation in an 18kg child, a voltage of 36.75V is the voltage threshold which may prove fatal. In addition to this, respiratory tetanus (breathing difficulty) and startle threshold voltages should be calculated. Currents to cause respiratory tetanus stated by Gomatom, Dorr and Sutherland (2005) are 15mA for women and 23mA for men. A value for children is not stated. Current to startle is stated at 2.2-3.2mA for women. The value for men and children is not stated. Based on these currents and the hand-foot impedance of 1225Ω, a voltage threshold of 18.38V may cause respiratory tetanus and 2.70V may cause startling. Respiratory tetanus may lead to hospital admission and startling may lead to complaints from residents. The voltage presented in Table 3.2.7.1 is 1.218V and therefore not of concern. The neutral voltage in future scenarios should be checked to determine if they pose a threat to human life. Table 3.2.7.4 below states the relevant voltage thresholds for future reference. Of course, values may be different for animals, however, the focus of this section is for the preservation of human life.

**Table 3.2.7.4: Table of voltage thresholds to cause potential conditions.**

| | |
|---|---|
| Voltage to cause ventricular fibrillation | 36.75V |
| Voltage to cause respiratory tetanus | 18.38V |
| Voltage to cause startling | 2.70V |

## 3.2.8 – Asset Lifespan

It is important to ascertain whether the harmonic currents are sufficient in magnitude to lead to a noticeable loss of transformer or conductor life as explained in Sections 1.4.1-2. Equation 3.2.8.1 below shows the improved and experimentally validated model from Wan, et al. (2020), previously mentioned in Section 1.4.1 for calculating the hot spot temperature of transformers. The improvements include harmonic no-load loss, which was missing from the IEEE Std C57.110-2018 (IEEE, 2018) model. This model is much closer to the test results obtained during the experiments of Wan, et al. (2020). This is supplemented by Equations 3.2.8.2-8, which are used to calculate the parameters required for Equation 3.2.8.1. The equations shall use the current and voltage harmonic data from Tables 3.2.5.2 and 3.2.6.1 for these calculations.

The hot spot temperature reference value for these calculations will be 110ºC, the top oil temperature rise under rated total loss will be 65ºC and ambient temperature will be taken to be 30ºC. Due to unit cancellation within the equations, the rated load loss shall be taken to be 1 p.u. The transformer shall be assumed to be running at rated load of 722A per phase for a 500kVA transformer. Therefore, the loss of life calculation assumes that the transformer hot spot temperature is currently at 110ºC due to fundamental current. Any additional harmonics will lead to additional heating.

Equation 3.2.8.1 $$\theta_h = \theta_a + \Delta\theta_{or}\left(\frac{P_{NL-H}+P_{LL-H}}{P_{NL-R}+P_{LL-R}}\right)^{0.8} + Hg_r\left(\frac{P_{I^2R-H}+P_{EC-H}}{P_{I^2R-R}+P_{EC-R}}\right)^{0.8}$$

Where:

$\theta_h$ is the hot spot temperature (ºC).

$\theta_a$ is the ambient temperature (ºC).

$\Delta\theta_{or}$ is the top oil temperature rise under rated total loss (ºC).

$P_{NL-H}$ is the no-load loss under harmonic current (W).

$P_{LL-H}$ is the load loss under harmonic current (W).

$P_{NL-R}$ is the rated no-load loss (W).

$P_{LL-R}$ is the rated load loss, including no-load and load losses at rated load (W).

$Hg_r$ is the temperature gradient of the hot spot temperature to the top oil temperature at rated current.

$P_{I^2R-H}$ is the winding resistance loss under harmonic current (W).

$P_{EC-H}$ is the winding eddy current loss under harmonic current (W).

$P_{I^2R-R}$ is the rated winding resistance loss (W).

$P_{EC-R}$ is the rated winding eddy current loss (W).

Equation 3.2.8.2 $$P_{I^2R-R} = 0.8P_{LL-R}$$

Equation 3.2.8.3 $$P_{EC-R} = 0.05P_{LL-R}$$

Equation 3.2.8.4 $$P_{NL-R} = 0.15P_{LL-R}$$

Equation 3.2.8.5
$$P_{I^2R-H} = \left(\frac{I}{I_R}\right)^2 \left[\frac{\sum_{h=1}^{h=h_{max}} \left[\frac{I_h}{I}\right]^2 h^{0.5}}{\sum_{h=1}^{h=h_{max}} \left[\frac{I_h}{I}\right]^2} P_{I^2R-R}\right]$$

Equation 3.2.8.6
$$P_{EC-H} = \left(\frac{I}{I_R}\right)^2 \left[\frac{\sum_{h=1}^{h=h_{max}} \left[\frac{I_h}{I}\right]^2 h^2}{\sum_{h=1}^{h=h_{max}} \left[\frac{I_h}{I}\right]^2} P_{EC-R}\right]$$

Equation 3.2.8.7
$$P_{LL-H} = \left(\frac{I}{I_R}\right)^2 \left[\frac{\sum_{h=1}^{h=h_{max}} \left[\frac{I_h}{I}\right]^2 h^2}{\sum_{h=1}^{h=h_{max}} \left[\frac{I_h}{I}\right]^2} P_{EC-R} + \frac{\sum_{h=1}^{h=h_{max}} \left[\frac{I_h}{I}\right]^2 h^{0.5}}{\sum_{h=1}^{h=h_{max}} \left[\frac{I_h}{I}\right]^2} P_{I^2R-R}\right]$$

Equation 3.2.8.8
$$P_{NL-H} = P_{NL-R}\left[\frac{\sum_{h=1}^{\infty}\left(h\left(\frac{U_{(h)}}{U_1}\right)^{1.6} + h^2\left(\frac{U_{(h)}}{U_1}\right)^2\right)}{2}\right]$$

Where:

$h$ is the harmonic order.

$U_{(h)}$ is the harmonic voltage for the specified harmonic order (V).

$U_1$ is the fundamental (50Hz) voltage (V).

$I_h$ is the harmonic current for the specific harmonic order (A).

$I$ is the fundamental (50Hz) current (A).

$I_R$ is the rated (50Hz) current (A).

After executing Equations 3.2.8.1-8, using the data from Tables 3.2.5.2 and 3.2.6.1, the transformer hot spot temperature was found to be 110.6520ºC. This can then be used to ascertain the relative aging factor of the transformer. This is shown in Equation 3.2.8.9 from IEEE Std C57.91-2011 (IEEE, 2012b) below. The rated hot spot rise over ambient temperature is 80ºC, the ambient temperature is 30ºC, and the hot spot temperature reference value $\theta_{href}$ will be 110ºC.

Equation 3.2.8.9 $$F_{AA} = exp^{\left(\frac{B}{\theta_{href}+273} - \frac{B}{\theta_h+273}\right)}$$

Where:

$F_{AA}$ is the relative aging factor of a transformer.

$\theta_{href}$ is the hot spot temperature reference value (ºC).

$\theta_h$ is the hot spot temperature (ºC).

$B$ is a constant, stated to be 15,000 for a transformer reference hot spot temperature of 110ºC.

The value of $F_{AA}$ can then be applied to Equation 3.2.8.10 from Wan, et al. (2020).

Equation 3.2.8.10 $$L = \frac{L_S}{F_{AA}}$$

Where:

$L$ is the predicted insulation life of the transformer (years).

$L_s$ is the insulation design life of the transformer (years).

By substituting the transformer hot spot temperature of 110.6520ºC into Equations 3.2.8.9-10, the life of the transformer would be reduced by 2.58 years, assuming a forty-year transformer lifespan, resulting in a remaining life of 37.42 years. This assumes that the ambient temperature remains at 30ºC all year and the transformer is situated at sea level. Within the UK, ambient temperature can exceed or remain below 30ºC for long periods.

Equations 3.2.8.9-10 have been validated by transformer functional life testing of distribution transformers carried out by Acker (1976), McNutt and Kaufmann (1983), Electric Power Research Institute (1982a) and Electric Power Research Institute (1982b). Therefore, these equations are considered reliable for the calculation transformer life loss.

Explanation regarding the assumed forty-year transformer lifespan will now be provided. Based on functional tests and service experience stated within IEEE Std C57.91-2011 (IEEE, 2012b), a transformer with a top oil temperature rise under rated total loss of 65ºC, running at hot spot temperature of 110ºC shall have a normal lifespan of 180,000 hours or twenty years. This assumes the transformer remains at exactly full load 24 hours a day, 365 days a year. However, the expectation from DNOs is that a distribution transformer will be subject to some sort of cyclic load and therefore have 'a service life in excess of 40 years' as per Dyer (2023). Since this thesis is written to be read by and advance the knowledge of network planning engineers, a forty-year lifespan has been applied to provide a familiar context which is comparable to a DNOs expectations. The figures applied have been used for comparison, but compensation factors can be applied to account for lower ambient temperatures, higher altitudes, various load profiles, or other expected transformer insulation design lives.

Next, the effect of the harmonics on conductor lifespan should be considered. It should be identified whether the harmonics in question will lead to a noticeable loss of conductor life. For the calculation, the conductor in question will be assumed to be the LV three-core cable between the LV winding of the local transformer and the LV cabinet. In order to be able to supply the required load for the transformer, it shall be assumed that two 300mm$^2$ Al Wavecon cables are connected, each rated at 435A summer sustained as per Baker (2019).

Using Equations 3.2.8.11-19, the loss of cable life shall be calculated. For comparison, the loading of the cable shall be assumed to be 870A per phase and 0A on the neutral conductor. The reason for this is to produce a worst-case temperature under fundamental conditions of 90ºC, to understand what effect the harmonics produced have on the cable temperature and life.

As previously mentioned within Section 1.4.2, the skin and proximity effect must be taken into account, since these effect $R_{ac(h)}$which, therefore effects Equations 3.2.8.16-19. Riba (2015), referencing IEC 60287-1-1:2006 (IEC, 2006) produces Equations 3.2.8.11-15 which considers skin and proximity effects on the $R_{ac(h)}$ of three-phase cables. Equations 3.2.8.12-13 represent the skin effect and Equations 3.2.8.14-15 represent the proximity effect. Equations 3.2.8.12-15 from Riba (2015) and IEC 60287-1-1:2006 (IEC, 2006) are based on sound scientific knowledge and have been verified by experimentation and testing.

Equation 3.2.8.11 $$R_{ac} = R_{dc}[1 + y_s + y_p]$$

Where:

$R_{ac}$ is the AC cable resistance per harmonic order measured in (Ω/m).

$R_{dc}$ is the DC cable resistance measured at 20°C measured in (Ω/m).

$y_S$ is the skin effect factor.

$y_p$ is the proximity effect factor.

Equation 3.2.8.12 $$y_s = \frac{x_s^4}{192+0.8x_s^4}$$

Equation 3.2.8.13 $$x_s^4 = \left[\frac{8\pi f K_s}{R_{dc}10^7}\right]^2$$

Where:

$f$ is the frequency (Hz).

$K_s$ is a constant, stated to be 1 for a solid round conductor.

Equation 3.2.8.14 $$y_p = \frac{x_p^4}{192+0.8x_p^4} \cdot \left[\frac{d_c}{s}\right]^2 \cdot \left[0.312\left[\frac{d_c}{s}\right]^2 + \frac{1.18}{\left(\frac{x_p^4}{192+0.8x_p^4}\right)+0.27}\right]$$

Equation 3.2.8.15 $$x_p^4 = \left[\frac{8\pi f K_p}{R_{dc}10^7}\right]^2$$

Where:

$d_c$ is the diameter of the conductor (m).

$s$ is the distance between the centre of each conductor (m).

$f$ is the frequency (Hz).

$K_p$ is a constant, stated to be 1 for a solid copper round conductor, however, IEC 60287-1-1:2006 (IEC, 2006) states this can be presumed applicable for aluminium conductors due to lack of research in this area.

Alternative values of $K_s$ and $K_p$ for various conductors such as a hollow or four segment structure can be obtained from IEC 60287-1-1:2006 (IEC, 2006).

The calculations for $R_{ac}$, $y_S$ and $y_p$ within Equations 3.2.8.11-15 must be repeated multiple times from the fundamental to the 49th harmonic. Therefore, these calculations have not been shown. These can be calculated by the reader if required and the use of a spreadsheet is recommended. However, the following values used within the calculations shall be given:

- $R_{dc}$ shall be taken as 0.100Ω/km for the phase and neutral conductors of 300mm$^2$ Al Wavecon at 20ºC as stated in Baker (2017) and Thorne & Derrick International (2023). The cables of which there are two shall be assumed to be 10m long.
- $d_c$ shall be assumed to be 0.0195m for the phase and neutral conductors at 300mm$^2$.
- $s$ shall be assumed to be 0.0231m between the centres of the phase and neutral conductors, assuming 1.8mm of insulation around each core, therefore 3.6mm of insulation between conductors as per Thorne & Derrick International (2023).
- $K_s$ $and$ $K_p$ shall be assumed to be 1 as per Equations 3.2.8.13 and 3.2.8.15.

Following from this, the additional losses and temperature rise can be calculated as follows using Equations 3.2.8.16-19 from Patil and Gandhare (2012) below and current harmonic data from Tables 3.2.6.1 and 3.2.7.2. Equation 3.2.8.16 represents the power loss of a balanced cable with only 50Hz being transmitted and Equation 3.2.8.17 represents the power loss of a balanced cable including harmonic losses. Equation 3.2.8.18 represents the operating temperature of the cable and Equation 3.2.8.19 represents the Arrhenius equation, used for determining the accelerated thermal aging of the cable.

Equation 3.2.8.16 $$W_s = \left[I_1^2 R_{ac(1)}\right]_R + \left[I_1^2 R_{ac(1)}\right]_Y + \left[I_1^2 R_{ac(1)}\right]_B$$

Where:

$W_S$ is the total power loss of the cable excluding harmonic losses (W).

$I_1$ is the fundamental current (50Hz).

$R_{ac(1)}$ is the cable resistance at 50Hz (Ω).

$R$ represents red phase conductor.

$Y$ represents yellow phase conductor.

$B$ represents blue phase conductor.

Equation 3.2.8.17 $$W_{NS} = \left[I_1^2 R_{ac(1)} + \sum_{h=3}^{49} I_h^2 R_{ac(h)}\right]_R + \left[I_1^2 R_{ac(1)} + \sum_{h=3}^{49} I_h^2 R_{ac(h)}\right]_Y + \left[I_1^2 R_{ac(1)} + \sum_{h=3}^{49} I_h^2 R_{ac(h)}\right]_B + \left[I_1^2 R_{ac(1)} + \sum_{h=3}^{49} I_h^2 R_{ac(h)}\right]_N$$

Where:

$W_{NS}$ is the total power loss of the cable including harmonic losses (W).

$I_h$ is the harmonic current at the specified harmonic order (A).

$R_{ac(h)}$ is the cable resistance at the specified harmonic order (Ω).

$N$ represents neutral phase conductor.

Equation 3.2.8.18 $$\theta_{NS} = 90\left(\frac{W_{NS}}{W_S}\right)°C$$

Where:

$\theta_{NS}$ is the accelerated aging temperature of cable at in ºC (Temperature>90ºC)

Equation 3.2.8.19 $$t_a = t_s \cdot e^{\left[\frac{E_a}{B}\left(\frac{1}{T_a} - \frac{1}{T_S}\right)\right]}$$

Where:

$T_s$ is the service temperature of cable at 363.16ºK (90ºC).

$T_a$ is the accelerated aging temperature of cable at in ºK (Temperature>90ºC).

$t_a$ is the accelerated aging life of the cable in years when operating at $T_a$ (years).

$t_s$ is the aging life of the cable at service temperature $T_s$. $t_s$=40 years.

$E_a$ is the activation energy of the cable at 160 kJ/mol for thermo-oxidative ageing as per Hongkun, et al. (2020).

$B_c$ is the Boltzmann constant of 0.00831446261815324 kJ/mol·ºK from National Institute of Standards (2023).

Based on Equations 3.2.8.11-19 and current harmonic data from Tables 3.2.6.1 and 3.2.7.2, the temperature of the cable was found to be 90.0610ºC, reducing the life of the cable by 0.35 years. This assumes a forty-year cable lifespan as per Patil and Gandhare (2012), resulting in a remaining life of 39.65 years. This assumes that the cables remain at exactly full load 24 hours a day, 365 days a year. The loading of cables could exceed or remain below full loading over the life of the cable. These numbers have been used for comparison, to illustrate the effect that harmonics may have on the life of cables, but compensation factors can be applied to account for cyclic load profiles.

Equations 3.2.8.16-19 from Patil and Gandhare (2012) are based on the model developed by Demoulias, et al. (2007) which was verified by validating the equations against Meliopoulos and Martin (1992), IEEE (1993) and experimental test measurements. The activation energy of thermally aged XLPE was obtained by Hongkun, et al. (2020) which verified the value via testing and experimentation.

## 3.3 – Photovoltaic Generation

### 3.3.1 – PV Generation Harmonics

By considering the information collated in Sections 2.2.1-2, a generation rate and harmonic profile for PV generation will be identified.

A PV generation rate of 2kW will be implemented as per the finding of Section 2.2.1. Of course, it is likely that many of the homes will have larger PV systems, and many homes will have smaller PV systems. This however is the typical sized domestic PV system used within the UK.

Using Table 2.2.2.1, and removing outliers from Langella, et al. (2016), it was identified that at 80% of maximum PV inverter output, the THDi was between 1.444% and 6%. By removing peaks or troughs observed for a short time, the majority of the results appear to be between 2% and 5% THDi.

Based on these findings, data from measured PV inverters which successfully measured high order harmonics needed to be found. To provide a range of PV inverters for the simulation, six PV inverters harmonic profiles measured by Bosman (2006) were used. The six PV inverter harmonic profiles used were of a similar magnitude to the papers mentioned in Table 2.2.2.1. PV inverter harmonic profiles from Bosman (2006), which were not of a similar magnitude to the papers mentioned in Table 2.2.2.1 were excluded from this study.

Due to the data from Bosman (2006) not containing even harmonics and harmonics past the 25$^{th}$ harmonic, data from Latheef (2006) was used to supplement Bosman (2006). This harmonic data was produced by averaging the data from three sources. This includes data from Haeberlin, et al. (1995), Haeberlin, Liebi and Beutler (1997) and Comfort, et al. (2001). Haeberlin, et al. (1995) and Haeberlin, Liebi and Beutler (1997) contain measured harmonic data from seven different inverter manufacturers. The THDi produced from this averaged data was 4.63%, which is above mid-way between the range of reliable papers discussed previously in Table 2.2.2.1, therefore producing a pessimistic data set. This data can be seen in the Table 3.3.1.1 below.

**Table 3.3.1.1: Table of current harmonics which represent a PV inverter from Latheef (2006) produced by averaging data from Haeberlin, et al. (1995), Haeberlin, Liebi and Beutler (1997) and Comfort, et al. (2001).**

| Harmonic Order | THDi | 2 | 3 | 4 | 5 | 6 | 7 | 8 | 9 | 10 |
|---|---|---|---|---|---|---|---|---|---|---|
| Percentage of Fundamental (%) | 4.63 | 0.76 | 2.89 | 0.44 | 2.46 | 0.10 | 1.54 | 0.15 | 1.06 | 0.07 |
| Harmonic Order | 11 | 12 | 13 | 14 | 15 | 16 | 17 | 18 | 19 | 20 |
| Percentage of Fundamental (%) | 0.82 | 0.07 | 0.90 | 0.07 | 0.48 | 0.06 | 0.53 | 0.07 | 0.30 | 0.07 |
| Harmonic Order | 21 | 22 | 23 | 24 | 25 | 26 | 27 | 28 | 29 | 30 |
| Percentage of Fundamental (%) | 0.38 | 0.03 | 0.24 | 0.08 | 0.26 | 0.03 | 0.24 | 0.07 | 0.28 | 0.11 |
| Harmonic Order | 31 | 32 | 33 | 34 | 35 | 36 | 37 | 38 | 39 | 40 |
| Percentage of Fundamental (%) | 0.28 | 0.11 | 0.22 | 0.07 | 0.07 | 0.06 | 0.09 | 0.02 | 0.08 | 0.08 |

The resultant of data from Bosman (2006) and Latheef (2006) produced six PV inverter harmonic profiles ranging between 5.59% and 1.71% at maximum inverter output. Data showing the harmonics of these profiles can be seen below in Tables 3.3.1.2-7. A PV inverter model representing each of these profiles was built in Simulink.

**Table 3.3.1.2: Table of current harmonics for a G&H Powertrap 1500 inverter operating at 940W, based on data from Bosman (2006) and supplemented by Latheef (2006).**

| Harmonic Order | THDi | 2 | 3 | 4 | 5 | 6 | 7 | 8 | 9 | 10 |
|---|---|---|---|---|---|---|---|---|---|---|
| Percentage of Fundamental (%) | 2.94 | 0.8 | 1.7 | 0.4 | 1.6 | 0.1 | 0.8 | 0.1 | 0.4 | 0.1 |
| Harmonic Order | 11 | 12 | 13 | 14 | 15 | 16 | 17 | 18 | 19 | 20 |
| Percentage of Fundamental (%) | 0.4 | 0.1 | 0.4 | 0.1 | 0.4 | 0.1 | 0.4 | 0.1 | 0.4 | 0.1 |
| Harmonic Order | 21 | 22 | 23 | 24 | 25 | 26 | 27 | 28 | 29 | 30 |
| Percentage of Fundamental (%) | 0.3 | 0.0 | 0.3 | 0.1 | 0.3 | 0.0 | 0.2 | 0.1 | 0.3 | 0.1 |
| Harmonic Order | 31 | 32 | 33 | 34 | 35 | 36 | 37 | 38 | 39 | 40 |
| Percentage of Fundamental (%) | 0.3 | 0.1 | 0.2 | 0.1 | 0.1 | 0.1 | 0.1 | 0.0 | 0.1 | 0.1 |

**Table 3.3.1.3: Table of current harmonics for a Mastervolt Sunmaster 1200QS operating at 400W, based on data from Bosman (2006) and supplemented by Latheef (2006).**

| Harmonic Order | THDi | 2 | 3 | 4 | 5 | 6 | 7 | 8 | 9 | 10 |
|---|---|---|---|---|---|---|---|---|---|---|
| Percentage of Fundamental (%) | 3.02 | 0.8 | 1.8 | 0.4 | 0.9 | 0.1 | 0.8 | 0.1 | 0.8 | 0.1 |
| Harmonic Order | 11 | 12 | 13 | 14 | 15 | 16 | 17 | 18 | 19 | 20 |
| Percentage of Fundamental (%) | 0.5 | 0.1 | 0.5 | 0.1 | 0.9 | 0.1 | 0.6 | 0.1 | 0.7 | 0.1 |
| Harmonic Order | 21 | 22 | 23 | 24 | 25 | 26 | 27 | 28 | 29 | 30 |
| Percentage of Fundamental (%) | 0.4 | 0.0 | 0.1 | 0.1 | 0.2 | 0.0 | 0.2 | 0.1 | 0.3 | 0.1 |
| Harmonic Order | 31 | 32 | 33 | 34 | 35 | 36 | 37 | 38 | 39 | 40 |
| Percentage of Fundamental (%) | 0.3 | 0.1 | 0.2 | 0.1 | 0.1 | 0.1 | 0.1 | 0.0 | 0.1 | 0.1 |

**Table 3.3.1.4: Table of current harmonics for a Mastervolt Sunmaster 1200QS operating at 850W, based on data from Bosman (2006) and supplemented by Latheef (2006).**

| Harmonic Order | THDi | 2 | 3 | 4 | 5 | 6 | 7 | 8 | 9 | 10 |
|---|---|---|---|---|---|---|---|---|---|---|
| Percentage of Fundamental (%) | 1.69 | 0.8 | 0.9 | 0.0 | 0.6 | 0.1 | 0.4 | 0.1 | 0.3 | 0.1 |
| Harmonic Order | 11 | 12 | 13 | 14 | 15 | 16 | 17 | 18 | 19 | 20 |
| Percentage of Fundamental (%) | 0.3 | 0.1 | 0.1 | 0.1 | 0.1 | 0.1 | 0.3 | 0.1 | 0.1 | 0.1 |
| Harmonic Order | 21 | 22 | 23 | 24 | 25 | 26 | 27 | 28 | 29 | 30 |
| Percentage of Fundamental (%) | 0.1 | 0.0 | 0.3 | 0.1 | 0.2 | 0.0 | 0.2 | 0.1 | 0.3 | 0.1 |
| Harmonic Order | 31 | 32 | 33 | 34 | 35 | 36 | 37 | 38 | 39 | 40 |
| Percentage of Fundamental (%) | 0.3 | 0.1 | 0.2 | 0.1 | 0.1 | 0.1 | 0.1 | 0.0 | 0.1 | 0.1 |

**Table 3.3.1.5: Table of current harmonics for a second Mastervolt Sunmaster 1200QS operating at 850W, based on data from Bosman (2006) and supplemented by Latheef (2006).**

| Harmonic Order | THDi | 2 | 3 | 4 | 5 | 6 | 7 | 8 | 9 | 10 |
|---|---|---|---|---|---|---|---|---|---|---|
| Percentage of Fundamental (%) | 1.71 | 0.8 | 0.9 | 0.1 | 0.6 | 0.1 | 0.3 | 0.1 | 0.4 | 0.1 |
| Harmonic Order | 11 | 12 | 13 | 14 | 15 | 16 | 17 | 18 | 19 | 20 |
| Percentage of Fundamental (%) | 0.2 | 0.1 | 0.2 | 0.1 | 0.2 | 0.1 | 0.1 | 0.1 | 0.3 | 0.1 |
| Harmonic Order | 21 | 22 | 23 | 24 | 25 | 26 | 27 | 28 | 29 | 30 |
| Percentage of Fundamental (%) | 0.2 | 0.0 | 0.3 | 0.1 | 0.2 | 0.0 | 0.2 | 0.1 | 0.3 | 0.1 |
| Harmonic Order | 31 | 32 | 33 | 34 | 35 | 36 | 37 | 38 | 39 | 40 |
| Percentage of Fundamental (%) | 0.3 | 0.1 | 0.2 | 0.1 | 0.1 | 0.1 | 0.1 | 0.0 | 0.1 | 0.1 |

**Table 3.3.1.6: Table of current harmonics for two Mastervolt Sunmaster 1200QS operating at 800W, based on data from Bosman (2006) and supplemented by Latheef (2006).**

| Harmonic Order | THDi | 2 | 3 | 4 | 5 | 6 | 7 | 8 | 9 | 10 |
|---|---|---|---|---|---|---|---|---|---|---|
| Percentage of Fundamental (%) | 1.88 | 0.8 | 1.0 | 0.1 | 0.7 | 0.1 | 0.4 | 0.1 | 0.4 | 0.1 |
| Harmonic Order | 11 | 12 | 13 | 14 | 15 | 16 | 17 | 18 | 19 | 20 |
| Percentage of Fundamental (%) | 0.2 | 0.1 | 0.4 | 0.1 | 0.1 | 0.1 | 0.2 | 0.1 | 0.4 | 0.1 |
| Harmonic Order | 21 | 22 | 23 | 24 | 25 | 26 | 27 | 28 | 29 | 30 |
| Percentage of Fundamental (%) | 0.1 | 0.0 | 0.3 | 0.1 | 0.3 | 0.0 | 0.2 | 0.1 | 0.3 | 0.1 |
| Harmonic Order | 31 | 32 | 33 | 34 | 35 | 36 | 37 | 38 | 39 | 40 |
| Percentage of Fundamental (%) | 0.3 | 0.1 | 0.2 | 0.1 | 0.1 | 0.1 | 0.1 | 0.0 | 0.1 | 0.1 |

**Table 3.3.1.7: Table of current harmonics for two Mastervolt Sunmaster 130S operating at 90W, based on data from Bosman (2006) and supplemented by Latheef (2006).**

| Harmonic Order | THDi | 2 | 3 | 4 | 5 | 6 | 7 | 8 | 9 | 10 |
|---|---|---|---|---|---|---|---|---|---|---|
| Percentage of Fundamental (%) | 5.59 | 0.8 | 4.5 | 0.1 | 1.6 | 0.0 | 1.4 | 0.1 | 1.2 | 0.1 |
| Harmonic Order | 11 | 12 | 13 | 14 | 15 | 16 | 17 | 18 | 19 | 20 |
| Percentage of Fundamental (%) | 1.0 | 0.1 | 0.9 | 0.1 | 0.7 | 0.1 | 0.6 | 0.1 | 0.6 | 0.1 |
| Harmonic Order | 21 | 22 | 23 | 24 | 25 | 26 | 27 | 28 | 29 | 30 |
| Percentage of Fundamental (%) | 0.6 | 0.0 | 0.5 | 0.1 | 0.4 | 0.0 | 0.2 | 0.1 | 0.3 | 0.1 |
| Harmonic Order | 31 | 32 | 33 | 34 | 35 | 36 | 37 | 38 | 39 | 40 |
| Percentage of Fundamental (%) | 0.3 | 0.1 | 0.2 | 0.1 | 0.1 | 0.1 | 0.1 | 0.0 | 0.1 | 0.1 |

## 3.3.2 – Simulation of the PV Generation

Using the harmonic profiles in Tables 3.3.1.1-7, Simulink PV models were created. These were produced by creating a harmonic current source generator. This is similar to the methodology used for the EVC model, based off Macedo, Resende and Samesima (2003) and shown in Figure 3.1.8.2, however, rather than placing a resistive and inductive load, a current source injecting at fundamental frequency was installed. An image of the simulation of the PV generation can be seen in Figure 3.3.2.1. The profiles produced using this method match the data shown in Tables 3.3.1.1-7. Furthermore, the power factor of the fundamental waveform for the PV generation must be determined. Cyganski, et al. (1989) states that the phase angle of PV generation was measured between 172-176°, representing a power factor of between 0.99-1. Figure 4(b) within Bouchakour, et al. (2012) shows that for an average solar irradiance day, the power factor of the power generated was greater than 0.99. Lastly, Elisabeta, Piroi and Piroi, (2020) found that for illumination levels above 20 lux, the power factor of the power generated was 1. Therefore, within this study, the power factor of the PV generation fundamental waveform model shall be assumed to be 1.

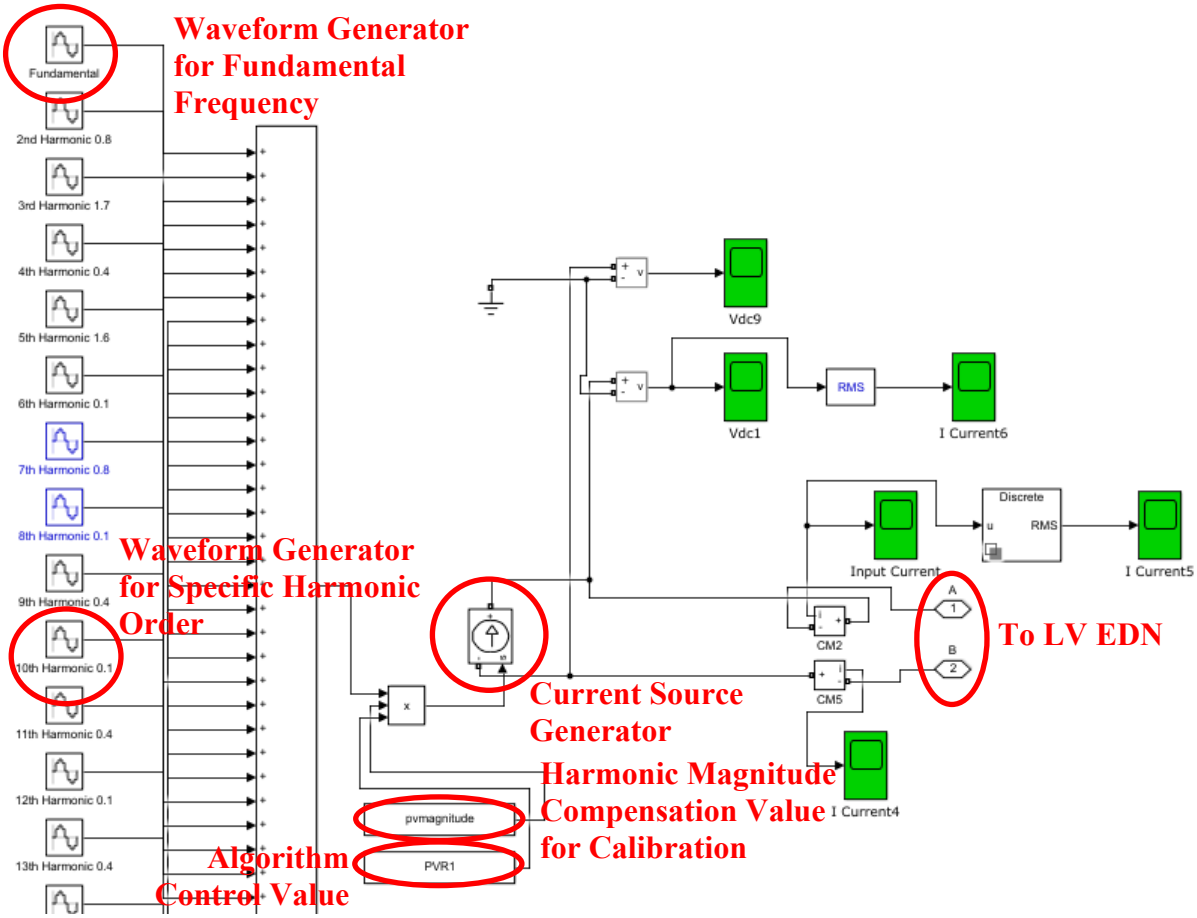


**Figure 3.3.2.1: Overview of the simulated single-phase PV generator using Simulink (The Mathworks, Inc., 2021).**

## 3.3.3 – Limitations of the PV Generation Model

One limitation of these simulations is that each simulation assumes that the PV generation profile used for each run of the simulation is the same with no diversity between profiles. Diversity of harmonic profiles would lead to averaging and potentially reduce the effect of extremes, where specific harmonics may exceed harmonic limits set out in ER G5/5, due to a specific harmonic current of higher magnitude compounding with other similarly high harmonic currents of the same harmonic order. The reason for not doing this, however, is to limit the number of variables and reduce randomised placement of different harmonic profiles which would be hard to reproduce. Using randomised placement of different harmonic profiles based on probability distribution could be considered for future work.

The simulation model assumes maximum output of all 2kW PV generation connected to the grid. The reason for this as previously discussed is because this results in the highest magnitude of harmonic current, but not necessarily the highest THDi which can be found at lower output levels. In reality, PV generation will be connected to different roof faces, since not all properties are aligned in the same direction. This will introduce a degree of diversity. Therefore, it is unlikely that all PV generation will be outputting at maximum rate at the same time. However, the degree of diversity is a level of detail that could not be assumed as a generic case but would have to be assessed on an EDN-by-EDN basis.

The simulation assumes that all PV generation systems connected to the LV EDN are 2kW as this is the typical sized domestic PV generation system used within the UK. Of course, many properties may have larger or smaller systems. However, this has not been taken into account since placing different size PV generation systems at different locations would add an additional variable, producing an additional factor to consider when drawing conclusions, and randomising placement would be hard to reproduce. Using randomised placement of different size PV generation systems based on probability distribution could be considered for future work.

## 3.3.4 – Validation of the Simulation

Using the same methodology used in Section 3.2.4, the Simulink PV generation model created in Section 3.3.2 was input into the LV EDN model produced in Section 3.1. As with Section 3.2.4, the maximum penetration was 98.4% and PV generation was connected evenly across all three phases.

In comparison to the validation study shown in Section 3.2.4 which looked at the effect of EVC penetration on the THDv of the LV EDN, the effect of PV generation on the THDv of the EDN is comparatively lower except for the PV generation harmonic profile from Table 3.3.1.7, however, this is expected due to the capacity of the apparatus at 2kW for PV generation and 3.28kVA for EVCs. The THDi of these two harmonic sources are comparative, ranging from 5.59% to 1.71% for PV and 3.54% for EV. This can be seen by comparing Figures 3.2.4.1 and 3.3.4.1. Like Section 3.2.4, the phase-neutral harmonic values were assessed, the reasons for which are identical.

The highest THDv measurement at the end supply terminals of feeder one for the LV EDN defined by Figure 3.1.1.2, PV generation harmonic profiles defined by Tables 3.3.1.1-7 and the PV generation penetration specified between 0%-98.4% is shown in Figure 3.3.4.1.

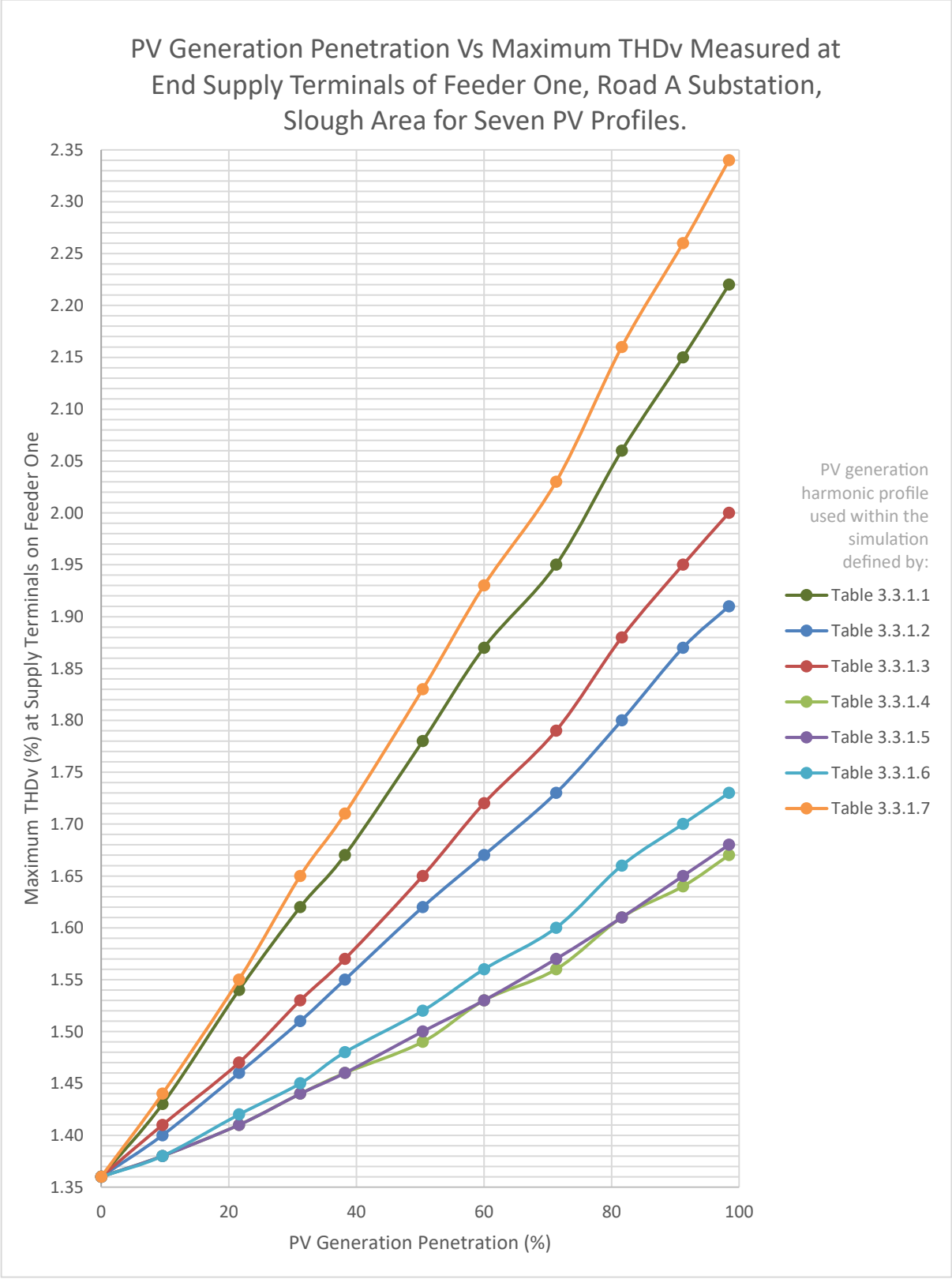


**Figure 3.3.4.1: Maximum THDv vs PV generation penetration for feeder one of the simulated LV EDN, measured at the end customer supply positions for the PV profile defined in the legend.**

Based on these results, it was important that the validity of the model was confirmed. The LV EDN model was already verified during the previous EVC scenario discussed in Section 3.2.4. Therefore, only the PV generation model needed to be verified by comparing the results with existing research. Busatto, Bollen and Rönnberg (2018) found that twenty-eight 2.5kW PV inverters (at 3.13% THDi) resulted in an increase of 0.05-0.1% THDv in the worst case if spread across three phases. Comparing this to Figure 3.3.4.1 above, thirty-five 2kW inverters (at 2.99% THDi in Table 3.3.1.3) resulted in an increase of 0.14-0.15% THDv if spread across three phases. The network impedance at the LV bus bar of the transformer from Busatto, Bollen and Rönnberg (2018) was j0.017 Ω at 400V. The network impedance at the LV bus bar of the transformer used within the EDN used in Sections 3.1.3-6 was j0.017 Ω at 400V. Based on the THDi of Table 3.3.1.3 being 4.5% lower, at 3.02% opposed to 3.13% and the network impedance being identical when measured on a 400V base, it would be expected that the results be comparable. However, there is around a 40%-50% increase in maximum THDv when comparing Busatto, Bollen and Rönnberg (2018) and Figure 3.3.4.1. This might be explained by Busatto, Bollen and Rönnberg (2018) splitting the PV generation evenly across four feeders as opposed to two, therefore reducing the harmonic current per feeder, and reducing the harmonic voltage drop. It may also be the case during simulation that a higher degree of harmonic cancellation occurs within Busatto, Bollen and Rönnberg (2018), since the background THDv level was measured between 1.9-4.3%, significantly higher than 1.36% used within Figure 3.3.4.1. Additionally, Busatto, Bollen and Rönnberg (2018) states that PV generation caused no significant increase in THDv due to the networks resonance impedance which sits within the 0-2 kHz range.

Vasanasong and Spooner (2000) produced results showing the effect of fifty 1kW PV inverters on the THDv of an LV EDN measured at the remote end when connected to a single phase. The results of the simulation produced a THDv of 1.5-1.9% at the end of the feeder shown in Vasanasong and Spooner (2000). This was based on an 11kV network impedance of roughly 12.2 Ω, comparable to Sections 3.1.3-6 which used an 11kV network impedance of 12.6 Ω. To compare these results with that of the Simulink simulation, a penetration of 60% was used as this represents 50kW of PV inverter export per phase. Within Figure 3.3.4.1, the THDv is between 1.53-1.93%, almost exactly following the range of 1.5-1.9% shown within the study by Vasanasong and Spooner (2000). The study includes background harmonics, thus increasing reliability.

De Silva, Jayamaha and Lidula (2019), presented two scenarios, a low loading scenario with a base harmonic level of 0.8-1.0% and a high loading scenario with a base harmonic level of 1.3-1.7%. The study considers the addition of 50kW of PV generation with a THDi of 3% connected across three phases. Based on the data produced by this study, the increase in THDv is approximately 0.2-0.3% for the low loading scenario and 0.3-0.4% for the high loading scenario. However, this data is based on a grid impedance of j24 Ω at 11kV, approximately double, when compared to the simulation in Sections 3.1.3-6 measured at j12.6 Ω at 11kV. By adjusting this data for a similar grid impedance, based on the oversimplification that an increase in grid impedance leads to a linear increase in THDv, the theory for which is mentioned in Section 1.2.1, the THDv range would be 0.1-0.15% for the low loading scenario and 0.15-0.2% for the high loading scenario. By comparing these results to Table 3.3.1.3 with a comparable THDi of 3.02%, the THDv increase for twenty-seven 2kW PV inverters is 0.11%. This result falls within the comparable result for the low loading scenario. Since Figure 3.3.4.1 takes place during a minimum loading situation, this result seems to concur with De Silva, Jayamaha and Lidula (2019).

Based on these papers, the results of Figure 3.3.4.1 is very comparable to De Silva, Jayamaha and Lidula (2019) and Vasanasong and Spooner (2000). However, the results were 40-50% higher than Busatto, Bollen and Rönnberg (2018). This might be explained by a higher degree of cancellation, since the background harmonic level was much higher at 1.9-4.3% and lower impedance since the harmonic current was split across four LV feeders.

All these papers were simulated but based off measured data. There are not currently any comparable studies of the magnitude required which use measured data and control all variables to ensure that external influences do not skew the results. Due to the variety of results produced by other studies, they suggest that this thesis' study is of the right magnitude, however, does not verify that the results are correct. It should however be repeated that the EDN model used was verified as part of the verification used for the EVC modelling and the PV generation models have been based on measured data as stated earlier in this thesis.

## 3.3.5 – THDv at the Transformer and Remote End

Tables 3.3.5.1-2 shows the harmonic spectrum of the voltage measured between phase and neutral at a customer's supply terminals at the end of feeder one and at the LV terminals of Road A substations distribution transformer on the red phase with a PV penetration of 98.4%. These are across three of the harmonic profiles shown in Section 3.3.1, these are Tables 3.3.1.1, 3.3.1.4 and 3.3.1.7. The reason for selecting the red phase supply terminal at the end of feeder one was because this resulted in the highest measured THDv against all measurement points. 98.4% penetration represents a PV generation number of one-hundred and twenty-three evenly distributed amongst the three phases, fifty-four on feeder one and sixty-nine on feeder two. By comparing these results with the standards in ER G5/5 shown in Tables 3.3.5.1-2, there are several points when the 21$^{st}$ harmonic exceeds the limit set out by this standard. It is unknown if these harmonics will cause issues to customers equipment, however, the effect of these harmonics on transformer and cable lifespan will be calculated. Further research should be carried out to determine if exceeding the limits set out in this standard, by the amounts shown in Tables 3.3.5.1-2 will cause issues with customer equipment.

The data from Table 3.3.1.1 was selected to be taken forward due to it being the only complete dataset as explained in Section 3.3.1. The other two datasets from Table 3.3.1.4 and 3.3.1.7 were selected as they formed the upper and lower dataset within Figure 3.3.4.1.

In addition to the effect of maximum penetration shown in Tables 3.3.5.1-2, the tipping point for feeder one to no longer remain compliant with ER G5/5 was identified. It was found that a penetration of 60% was the tipping point on this feeder for the profile shown in Table 3.3.1.1 and 38.4% was the tipping point on this feeder for the profile shown in Table 3.3.1.7 This penetration value represents a PV generation number of seventy-five and forty-eight respectively. Thirty-three and twenty-one respectively on feeder one and forty-two and twenty-seven respectively on feeder two. Table 3.3.5.3 shows the harmonic spectrum of the voltage measured between phase and neutral at a customer's supply terminal at the end of feeder one on the red phase at the PV penetrations mentioned above. At these penetrations, the 21$^{st}$ harmonic dropped sufficiently to 0.2% or below. This is the maximum harmonic percentage allowed under ER G5/5 to remain within limits. The harmonic profile seen in Table 3.3.1.4 did not exceed limits under ER G5/5 at 98.4% as shown in Tables 3.3.5.1-2 and therefore did not require reducing further.

**Table 3.3.5.1: Table of the voltage harmonics measured across the red phase supply terminal at the end of feeder one with a PV generation penetration of 98.4%, PV generation profile defined in the table, against the limits set out in ER G5/5 (Energy Networks Association, 2020).**

| Harmonic Number | Harmonic Magnitude (%) (PV Generation Harmonic Profile from Table 3.3.1.1) | Harmonic Magnitude (%) (PV Generation Harmonic Profile from Table 3.3.1.4) | Harmonic Magnitude (%) (PV Generation Harmonic Profile from Table 3.3.1.7) | ER G5/5 Limits (%) |
|---|---|---|---|---|
| 2nd | 0.09 | 0.09 | 0.09 | 1.6 |
| 3rd | 0.80 | 0.62 | 0.94 | 4.0 |
| 4th | 0.07 | 0.02 | 0.03 | 1.0 |
| 5th | 0.87 | 0.59 | 0.74 | 4.0 |
| 6th | 0.05 | 0.05 | 0.05 | 0.5 |
| 7th | 1.13 | 0.91 | 1.11 | 4.0 |
| 8th | 0.04 | 0.04 | 0.04 | 0.4 |
| 9th | 0.46 | 0.25 | 0.49 | 1.2 |
| 10th | 0.06 | 0.06 | 0.06 | 0.4 |
| 11th | 0.77 | 0.61 | 0.83 | 3.0 |
| 12th | 0.06 | 0.06 | 0.06 | 0.2 |
| 13th | 0.76 | 0.46 | 0.76 | 2.5 |
| 14th | 0.03 | 0.03 | 0.03 | 0.2 |
| 15th | 0.37 | 0.20 | 0.46 | 0.5 |
| 16th | 0.08 | 0.08 | 0.08 | 0.2 |
| 17th | 0.31 | 0.21 | 0.36 | 1.6 |
| 18th | 0.07 | 0.07 | 0.07 | 0.2 |
| 19th | 0.26 | 0.15 | 0.42 | 1.5 |
| 20th | 0.08 | 0.08 | 0.08 | 0.2 |
| 21st | 0.29 | 0.11 | 0.41 | 0.2 |
| 22nd | 0.02 | 0.02 | 0.02 | 0.2 |
| 23rd | 0.17 | 0.24 | 0.37 | 1.2 |
| 24th | 0.08 | 0.08 | 0.08 | 0.2 |
| 25th | 0.25 | 0.18 | 0.32 | 1.0 |
| 26th | 0.01 | 0.01 | 0.01 | 0.2 |
| 27th | 0.18 | 0.18 | 0.18 | 0.2 |
| 28th | 0.09 | 0.09 | 0.09 | 0.2 |
| 29th | 0.26 | 0.26 | 0.26 | 0.86 |
| 30th | 0.08 | 0.08 | 0.08 | 0.2 |
| 31st | 0.29 | 0.29 | 0.29 | 0.81 |
| 32nd | 0.09 | 0.09 | 0.09 | 0.2 |
| 33rd | 0.20 | 0.20 | 0.20 | 0.2 |
| 34th | 0.09 | 0.10 | 0.09 | 0.2 |
| 35th | 0.12 | 0.12 | 0.12 | 0.71 |
| 36th | 0.10 | 0.10 | 0.10 | 0.2 |
| 37th | 0.12 | 0.12 | 0.12 | 0.68 |
| 38th | 0.00 | 0.00 | 0.00 | 0.2 |
| 39th | 0.13 | 0.13 | 0.13 | 0.2 |
| 40th | 0.11 | 0.11 | 0.11 | 0.2 |
| Harmonics higher than the limits set by ER G5/5 | | | | |
| Harmonics on the boundary of the limits set by ER G5/5 | | | | |
| Number of PVs on Feeder 1: 54 Number of PVs on Feeder 2: 69 | | | | |

**Table 3.3.5.2: Table of the voltage harmonics measured on the red phase on the LV terminals of Road A substations distribution transformer with an PV generation penetration of 98.4%, PV generation profile defined in the table, against the limits set out in ER G5/5 (Energy Networks Association, 2020).**

| Harmonic Number | Harmonic Magnitude (%) (PV Generation Harmonic Profile from Table 3.3.1.1) | Harmonic Magnitude (%) (PV Generation Harmonic Profile from Table 3.3.1.4) | Harmonic Magnitude (%) (PV Generation Harmonic Profile from Table 3.3.1.7) | ER G5/5 Limits (%) |
|---|---|---|---|---|
| 2nd | 0.08 | 0.08 | 0.08 | 1.6 |
| 3rd | 0.76 | 0.61 | 0.88 | 4.0 |
| 4th | 0.06 | 0.02 | 0.03 | 1.0 |
| 5th | 0.83 | 0.59 | 0.71 | 4.0 |
| 6th | 0.04 | 0.04 | 0.05 | 0.5 |
| 7th | 1.10 | 0.91 | 1.09 | 4.0 |
| 8th | 0.04 | 0.04 | 0.04 | 0.4 |
| 9th | 0.42 | 0.24 | 0.45 | 1.2 |
| 10th | 0.05 | 0.05 | 0.05 | 0.4 |
| 11th | 0.74 | 0.61 | 0.80 | 3.0 |
| 12th | 0.06 | 0.06 | 0.06 | 0.2 |
| 13th | 0.72 | 0.46 | 0.72 | 2.5 |
| 14th | 0.03 | 0.03 | 0.03 | 0.2 |
| 15th | 0.34 | 0.19 | 0.42 | 0.5 |
| 16th | 0.07 | 0.07 | 0.07 | 0.2 |
| 17th | 0.28 | 0.19 | 0.32 | 1.6 |
| 18th | 0.06 | 0.06 | 0.06 | 0.2 |
| 19th | 0.24 | 0.14 | 0.38 | 1.5 |
| 20th | 0.07 | 0.07 | 0.07 | 0.2 |
| 21st | 0.26 | 0.10 | 0.36 | 0.2 |
| 22nd | 0.02 | 0.02 | 0.02 | 0.2 |
| 23rd | 0.15 | 0.20 | 0.32 | 1.2 |
| 24th | 0.07 | 0.07 | 0.07 | 0.2 |
| 25th | 0.22 | 0.16 | 0.28 | 1.0 |
| 26th | 0.01 | 0.01 | 0.01 | 0.2 |
| 27th | 0.16 | 0.16 | 0.16 | 0.2 |
| 28th | 0.08 | 0.08 | 0.08 | 0.2 |
| 29th | 0.23 | 0.23 | 0.23 | 0.86 |
| 30th | 0.07 | 0.07 | 0.07 | 0.2 |
| 31st | 0.25 | 0.25 | 0.25 | 0.81 |
| 32nd | 0.08 | 0.08 | 0.08 | 0.2 |
| 33rd | 0.18 | 0.18 | 0.18 | 0.2 |
| 34th | 0.08 | 0.08 | 0.08 | 0.2 |
| 35th | 0.10 | 0.10 | 0.10 | 0.71 |
| 36th | 0.09 | 0.08 | 0.09 | 0.2 |
| 37th | 0.11 | 0.11 | 0.11 | 0.68 |
| 38th | 0.00 | 0.00 | 0.00 | 0.2 |
| 39th | 0.11 | 0.11 | 0.11 | 0.2 |
| 40th | 0.10 | 0.09 | 0.10 | 0.2 |
| Harmonics higher than the limits set by ER G5/5 | | | | |
| Number of PVs on Feeder 1: 54 Number of PVs on Feeder 2: 69 | | | | |

**Table 3.3.5.3: Table of the voltage harmonics measured across the red phase supply terminal at the end of feeder one with a PV generation penetration and PV generation profile defined in the table, against the limits set out in ER G5/5 (Energy Networks Association, 2020).**

| Harmonic Number | Harmonic Magnitude (%) (PV Generation Harmonic Profile from Table 3.3.1.1 & penetration 60%) | Harmonic Magnitude (%) (PV Generation Harmonic Profile from Table 3.3.1.4 & penetration 98.4%) | Harmonic Magnitude (%) (PV Generation Harmonic Profile from Table 3.3.1.7 & penetration 38.4%) | ER G5/5 Limits (%) |
|---|---|---|---|---|
| 2nd | 0.07 | 0.09 | 0.06 | 1.6 |
| 3rd | 0.70 | 0.62 | 0.71 | 4.0 |
| 4th | 0.05 | 0.02 | 0.02 | 1.0 |
| 5th | 0.73 | 0.59 | 0.61 | 4.0 |
| 6th | 0.04 | 0.05 | 0.04 | 0.5 |
| 7th | 1.02 | 0.91 | 0.95 | 4.0 |
| 8th | 0.03 | 0.04 | 0.03 | 0.4 |
| 9th | 0.35 | 0.25 | 0.30 | 1.2 |
| 10th | 0.05 | 0.06 | 0.04 | 0.4 |
| 11th | 0.68 | 0.61 | 0.65 | 3.0 |
| 12th | 0.05 | 0.06 | 0.04 | 0.2 |
| 13th | 0.63 | 0.46 | 0.56 | 2.5 |
| 14th | 0.03 | 0.03 | 0.03 | 0.2 |
| 15th | 0.28 | 0.20 | 0.25 | 0.5 |
| 16th | 0.06 | 0.08 | 0.05 | 0.2 |
| 17th | 0.22 | 0.21 | 0.18 | 1.6 |
| 18th | 0.05 | 0.07 | 0.04 | 0.2 |
| 19th | 0.20 | 0.15 | 0.23 | 1.5 |
| 20th | 0.05 | 0.08 | 0.04 | 0.2 |
| 21st | 0.20 | 0.11 | 0.19 | 0.2 |
| 22nd | 0.02 | 0.02 | 0.02 | 0.2 |
| 23rd | 0.12 | 0.24 | 0.17 | 1.2 |
| 24th | 0.05 | 0.08 | 0.04 | 0.2 |
| 25th | 0.17 | 0.18 | 0.15 | 1.0 |
| 26th | 0.01 | 0.01 | 0.01 | 0.2 |
| 27th | 0.12 | 0.18 | 0.09 | 0.2 |
| 28th | 0.06 | 0.09 | 0.04 | 0.2 |
| 29th | 0.17 | 0.26 | 0.12 | 0.86 |
| 30th | 0.05 | 0.08 | 0.03 | 0.2 |
| 31st | 0.19 | 0.29 | 0.13 | 0.81 |
| 32nd | 0.06 | 0.09 | 0.04 | 0.2 |
| 33rd | 0.13 | 0.20 | 0.09 | 0.2 |
| 34th | 0.06 | 0.10 | 0.04 | 0.2 |
| 35th | 0.08 | 0.12 | 0.06 | 0.71 |
| 36th | 0.06 | 0.10 | 0.04 | 0.2 |
| 37th | 0.08 | 0.12 | 0.06 | 0.68 |
| 38th | 0.00 | 0.00 | 0.00 | 0.2 |
| 39th | 0.09 | 0.13 | 0.06 | 0.2 |
| 40th | 0.07 | 0.11 | 0.04 | 0.2 |
| Harmonics on the boundary of the limits set by ER G5/5 | | | | |

Similar to the EVC analysis in the previous section, the harmonic penetration allowed was much lower than 100% penetration, except for the harmonic profile from Table 3.3.1.4. In addition, a low THDv of 1.87% for the harmonic profile from Table 3.3.1.1 at 60% PV penetration and 1.71% for the harmonic profile from Table 3.3.1.7 at 38.4% PV penetration is only 0.51% and 0.35% higher than the background harmonic value respectively. These THDv values can be seen in Figure 3.3.4.1. Therefore, depending on the harmonic spectrum of the load or generation, harmonic limits can be exceeded even at low harmonic levels.

## 3.3.6 – Current Harmonics Drawn

At 98.4% PV penetration, the current harmonics drawn should also be inspected. By considering Figure 3.3.6.1, the red phase harmonic current at the LV bus of the transformer for the harmonic profile shown in Table 3.3.1.1 can be seen. The magnitude of the red phase harmonic current at the LV bus for Tables 3.3.1.1, 3.3.1.4 and 3.3.1.7 have been broken down into their constituent values in Table 3.3.6.1. Lower odd harmonics have significant magnitude, the values decreasing in magnitude as the harmonic number increases in line with the results of Section 3.2.6 shown in Figure 3.3.6.1.

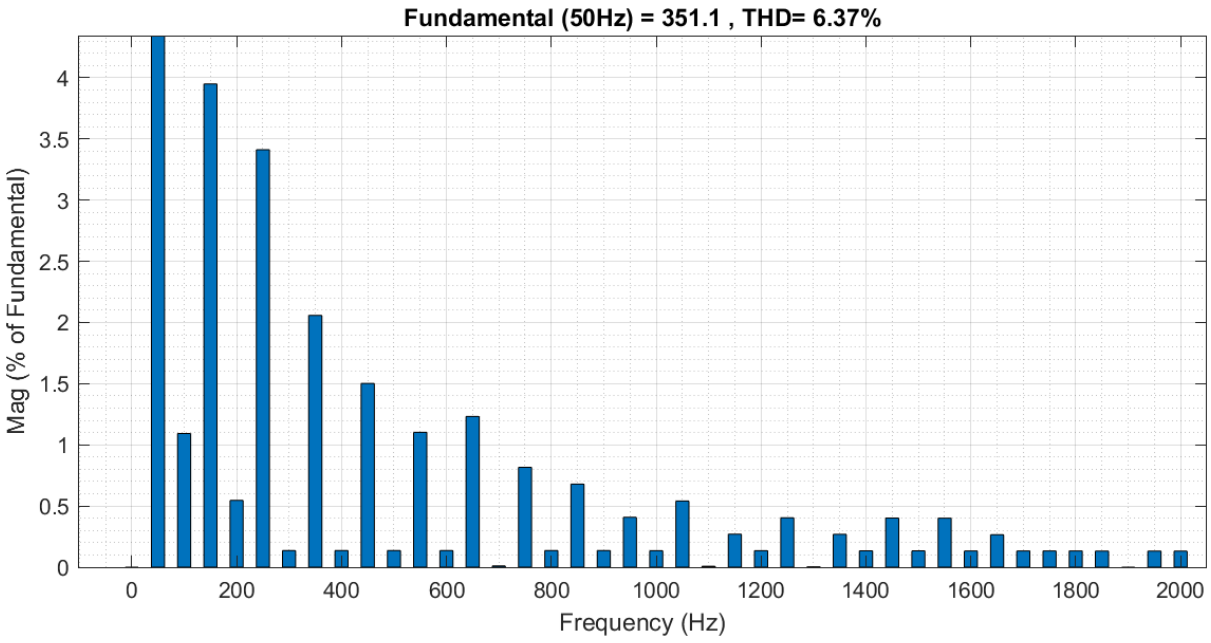


**Figure 3.3.6.1: Graphical representation of the current harmonics measured on the red phase at the LV terminals of Road A substations distribution transformer with a PV generation penetration of 98.4% and PV generation profile of Table 3.3.1.1 (generated in MATLAB/Simulink, The Mathworks, Inc. (2021)).**

**Table 3.3.6.1: Table of the current harmonics measured on the red phase at the LV terminals of Road A substations distribution transformer with a PV generation penetration of 98.4% and PV generation profile defined in the table.**

| Harmonic Number | Harmonic Magnitude (A) (PV Generation Harmonic Profile from Table 3.3.1.1) | Harmonic Magnitude (A) (PV Generation Harmonic Profile from Table 3.3.1.4) | Harmonic Magnitude (A) (PV Generation Harmonic Profile from Table 3.3.1.7) |
|---|---|---|---|
| Fundamental Current | 248.3 | 248.3 | 248.3 |
| 2nd | 2.72 | 2.72 | 2.72 |
| 3rd | 9.81 | 3.04 | 15.24 |
| 4th | 1.36 | 0.02 | 0.34 |
| 5th | 8.47 | 2.06 | 5.42 |
| 6th | 0.34 | 0.34 | 0.34 |
| 7th | 5.11 | 1.53 | 4.77 |
| 8th | 0.34 | 0.34 | 0.34 |
| 9th | 3.73 | 1.03 | 4.07 |
| 10th | 0.34 | 0.34 | 0.34 |
| 11th | 2.74 | 1.11 | 3.41 |
| 12th | 0.34 | 0.34 | 0.34 |
| 13th | 3.06 | 0.51 | 3.06 |
| 14th | 0.03 | 0.03 | 0.03 |
| 15th | 2.03 | 0.68 | 2.70 |
| 16th | 0.34 | 0.34 | 0.34 |
| 17th | 1.68 | 1.01 | 2.02 |
| 18th | 0.34 | 0.34 | 0.34 |
| 19th | 1.01 | 0.35 | 2.02 |
| 20th | 0.34 | 0.34 | 0.34 |
| 21st | 1.34 | 0.34 | 2.02 |
| 22nd | 0.02 | 0.02 | 0.02 |
| 23rd | 0.67 | 1.00 | 1.67 |
| 24th | 0.33 | 0.33 | 0.33 |
| 25th | 1.00 | 0.67 | 1.34 |
| 26th | 0.01 | 0.01 | 0.01 |
| 27th | 0.66 | 0.66 | 0.66 |
| 28th | 0.33 | 0.33 | 0.33 |
| 29th | 1.00 | 1.00 | 1.00 |
| 30th | 0.33 | 0.33 | 0.33 |
| 31st | 1.00 | 1.00 | 1.00 |
| 32nd | 0.33 | 0.33 | 0.33 |
| 33rd | 0.66 | 0.66 | 0.66 |
| 34th | 0.33 | 0.33 | 0.33 |
| 35th | 0.33 | 0.33 | 0.33 |
| 36th | 0.33 | 0.33 | 0.33 |
| 37th | 0.33 | 0.33 | 0.33 |
| 38th | 0.00 | 0.00 | 0.00 |
| 39th | 0.33 | 0.33 | 0.33 |
| 40th | 0.33 | 0.33 | 0.33 |
| THDi (%) | 6.37% | 2.34% | 7.62% |
| Number of PVs on Feeder 1: 54 Number of PVs on Feeder 2: 69 | | | |

## 3.3.7 – Voltage and Current Harmonics of Neutral

In contrast to the findings of Section 3.2.7, the harmonics measured in the neutral are much lower and the only predominant harmonic is the 3rd order, which is of minimal magnitude of 0.06A on the neutral of the LV side of the transformer and 0.02V on the neutral at the remote end of feeder one. The results of this for the PV harmonic profile shown in Table 3.3.1.7 can be seen in Figure 3.3.7.1 and the results for the PV harmonic profile shown in Tables 3.3.1.1, 3.3.1.4 and 3.3.1.7 are shown in Table 3.3.7.1. The magnitude of these harmonics is minimal and therefore should not present any issues in terms of conductor heating or safety concerns.

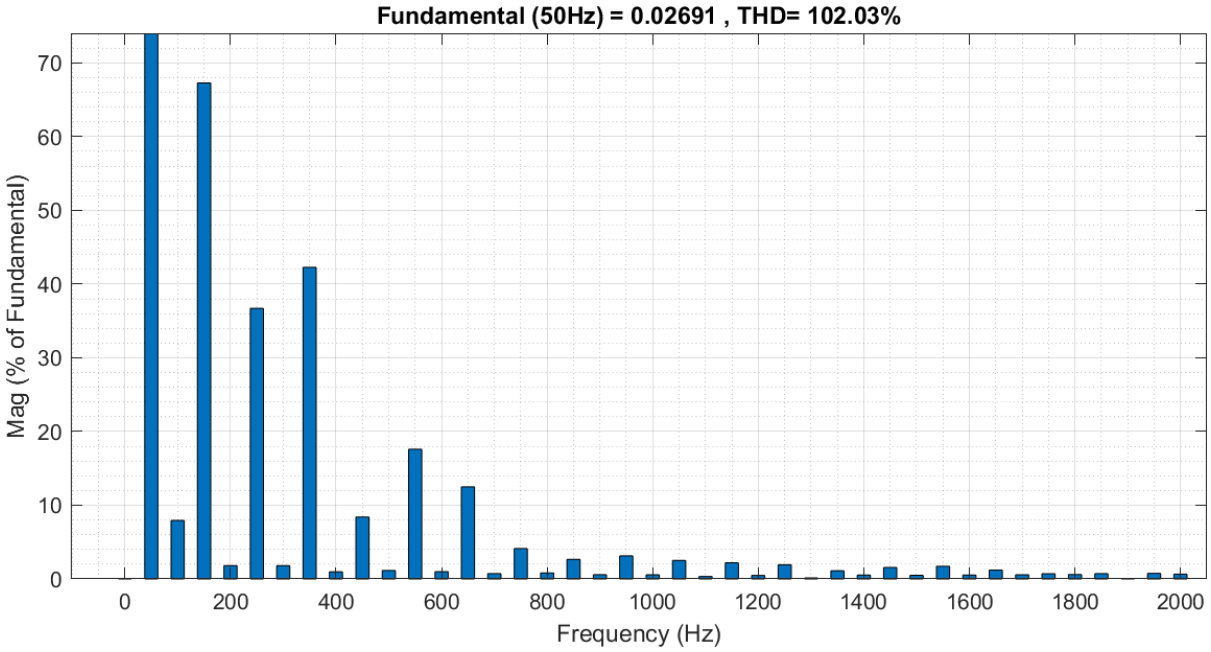


**Figure 3.3.7.1: Graphical representation of the voltage harmonics measured on the neutral at the end of feeder one with a PV generation penetration of 98.4% under a PV generation profile of Table 3.3.1.7 (generated in MATLAB/Simulink, The Mathworks, Inc. (2021)).**

**Table 3.3.7.1: Table of the voltage harmonics measured on the neutral at the end of feeder one and current harmonics measured on the neutral at the LV terminals of Road A substations distribution transformer with a PV generation penetration of 98.4% under the PV generation profile defined in the table.**

| Harmonic Number | Harmonic Magnitude (PV Generation Harmonic Profile from Table 3.3.1.1) | | Harmonic Magnitude (PV Generation Harmonic Profile from Table 3.3.1.4) | | Harmonic Magnitude (PV Generation Harmonic Profile from Table 3.3.1.7) | |
|---|---|---|---|---|---|---|
| | V | A | V | A | V | A |
| 2nd | 0.00 | 0.01 | 0.00 | 0.01 | 0.00 | 0.01 |
| 3rd | 0.01 | 0.03 | 0.01 | 0.00 | 0.02 | 0.06 |
| 4th | 0.00 | 0.00 | 0.00 | 0.00 | 0.00 | 0.00 |
| 5th | 0.01 | 0.02 | 0.01 | 0.00 | 0.01 | 0.01 |
| 6th | 0.00 | 0.00 | 0.00 | 0.00 | 0.00 | 0.00 |
| 7th | 0.01 | 0.00 | 0.01 | 0.01 | 0.01 | 0.01 |
| 8th | 0.00 | 0.00 | 0.00 | 0.00 | 0.00 | 0.00 |
| 9th | 0.00 | 0.01 | 0.00 | 0.01 | 0.00 | 0.01 |
| 10th | 0.00 | 0.00 | 0.00 | 0.00 | 0.00 | 0.00 |
| 11th | 0.00 | 0.01 | 0.00 | 0.01 | 0.00 | 0.01 |
| 12th | 0.00 | 0.00 | 0.00 | 0.00 | 0.00 | 0.00 |
| 13th | 0.00 | 0.00 | 0.00 | 0.01 | 0.00 | 0.01 |
| 14th | 0.00 | 0.00 | 0.00 | 0.00 | 0.00 | 0.00 |
| 15th | 0.00 | 0.00 | 0.00 | 0.00 | 0.00 | 0.00 |
| 16th | 0.00 | 0.00 | 0.00 | 0.00 | 0.00 | 0.00 |
| 17th | 0.00 | 0.00 | 0.00 | 0.00 | 0.00 | 0.00 |
| 18th | 0.00 | 0.00 | 0.00 | 0.00 | 0.00 | 0.00 |
| 19th | 0.00 | 0.00 | 0.00 | 0.00 | 0.00 | 0.00 |
| 20th | 0.00 | 0.00 | 0.00 | 0.00 | 0.00 | 0.00 |
| 21st | 0.00 | 0.00 | 0.00 | 0.00 | 0.00 | 0.00 |
| 22nd | 0.00 | 0.00 | 0.00 | 0.00 | 0.00 | 0.00 |
| 23rd | 0.00 | 0.00 | 0.00 | 0.00 | 0.00 | 0.00 |
| 24th | 0.00 | 0.00 | 0.00 | 0.00 | 0.00 | 0.00 |
| 25th | 0.00 | 0.00 | 0.00 | 0.00 | 0.00 | 0.00 |
| 26th | 0.00 | 0.00 | 0.00 | 0.00 | 0.00 | 0.00 |
| 27th | 0.00 | 0.00 | 0.00 | 0.00 | 0.00 | 0.00 |
| 28th | 0.00 | 0.00 | 0.00 | 0.00 | 0.00 | 0.00 |
| 29th | 0.00 | 0.00 | 0.00 | 0.00 | 0.00 | 0.00 |
| 30th | 0.00 | 0.00 | 0.00 | 0.00 | 0.00 | 0.00 |
| 31st | 0.00 | 0.00 | 0.00 | 0.00 | 0.00 | 0.00 |
| 32nd | 0.00 | 0.00 | 0.00 | 0.00 | 0.00 | 0.00 |
| 33rd | 0.00 | 0.00 | 0.00 | 0.00 | 0.00 | 0.00 |
| 34th | 0.00 | 0.00 | 0.00 | 0.00 | 0.00 | 0.00 |
| 35th | 0.00 | 0.00 | 0.00 | 0.00 | 0.00 | 0.00 |
| 36th | 0.00 | 0.00 | 0.00 | 0.00 | 0.00 | 0.00 |
| 37th | 0.00 | 0.00 | 0.00 | 0.00 | 0.00 | 0.00 |
| 38th | 0.00 | 0.00 | 0.00 | 0.00 | 0.00 | 0.00 |
| 39th | 0.00 | 0.00 | 0.00 | 0.00 | 0.00 | 0.00 |
| 40th | 0.00 | 0.00 | 0.00 | 0.00 | 0.00 | 0.00 |
| Number of PVs on Feeder 1: 54 Number of PVs on Feeder 2: 69 | | | | | | |

## 3.3.8 – Asset Lifespan

Similar to Section 3.2.8, it is important to ascertain whether the harmonic currents are sufficient in magnitude to lead to a noticeable loss of transformer or conductor life. This will be calculated using Equations 3.2.8.1-19 and Tables 3.3.5.2, 3.3.6.1 and 3.3.7.1. The same assumptions and values such as reference hottest-spot temperature, ambient temperature and conductor impedance will be made as per Section 3.2.8 to carry out these calculations.

Based on these calculations, at a reference hottest-spot temperature of 110ºC, the PV generation harmonic profiles from Tables 3.3.1.1, 3.3.1.4 and 3.3.1.7 resulted in an increase in the transformer hot spot temperature of 0.5356ºC, 0.0458ºC and 0.6625ºC respectively. Therefore, this would result in a loss of transformer life of 2.13 years, 1.33 years, and 2.62 years respectively. Comparing this to loss of asset lifespan, considering EVCs in Section 3.2.8, there was a transformer temperature increase of 0.6520ºC and loss of transformer life of 2.58 years. The THDi generated by the EVCs is 3.54% and PV harmonic profile shown in Table 3.3.1.7 is 5.59%. The EVC draws a load of 3.28kVA, whereas the PV generation produces 2kW. Adjusting the EVC output to 2kW, whist keeping the harmonic magnitude constant produces an EVC THDi of 5.81%, which is comparable to Table 3.3.1.7 at 5.59%. Based on this, the loss of transformer life is comparable at 2.62 years for the PV generation harmonic profile stated in Table 3.3.1.7 and 2.58 years for the EVC harmonic profile.

Using the calculations for conductor lifespan, at a reference conductor temperature of 90ºC, the PV generation harmonic profiles from Tables 3.3.1.1, 3.3.1.4 and 3.3.1.7 resulted in an increase in temperature of 0.0458ºC, 0.0067ºC and 0.0625ºC, respectively. Therefore, this would result in a loss of conductor life of 0.27 years, 0.04 years, and 0.36 years respectively. Comparing this to loss of asset lifespan considering EVCs in Section 3.2.8, there was a conductor temperature increase of 0.0610ºC and loss of conductor life of 0.35 years. Again, the harmonic magnitude of the EVC profile is comparable to the PV harmonic profile from Table 3.3.1.7 which produces a comparable outcome.

# 3.4 – Combined Effect of PV Generation and EVCs

Further to the research carried out in Section 2.3, the impact of EVCs & PV generation in combination with each other on LV EDNs was researched. The findings of the papers mentioned in Section 2.3, state this ranges from summing arithmetically to cancelling by up to 75% of its original PV harmonic magnitude when EVCs are added. For each of these cases, the maximum summation or cancellation is for specific harmonic currents or voltages only. However, simulating worst case scenarios can be used to ascertain a point where it may be necessary for investigation of harmonic levels to be carried out by a DNO.

## 3.4.1 – Effect of Harmonic Phase Shift

The next step is to identify a probability distribution for the range of harmonic interactions mentioned in Section 2.3.

Using the same simulations covered in Sections 3.1-3, the effect of varying the phase angle between the EVCs and PV generation with respect to maximum THDv measured across feeder one supply terminals was explored under three-phase fault conditions at the end of feeder one via the pot end joint outside one-hundred and fifty-eight fed via red phase. A diagram of the connections for this fault can be seen in Figure 1.5.3. It is assumed that the impedance of the fault is zero and all supplies have been restored via the fault. Further details can be obtained by reading Section 4.1. The network consisted of one-hundred and twenty-three PV generators using the PV generation harmonic profile from Latheef (2006), shown in Table 3.3.1.1 and one-hundred and eight EVCs across feeders one and two. This represents the maximum numbers of PV generators and EVCs the network can support for normal running arrangements. The angle of EVCs is varied with respect to the network and PV generation under three-phase fault conditions on feeder one. Depending on the phase angle between the PV generation and EVCs, the level of cancellation and therefore THDv varies significantly as shown in Figure 3.4.1.1 from a maximum of 4.48% to a minimum of 1.26%. This is to be expected since opposing harmonics should cancel. The cancellation of harmonics reduces the measured THDv below that of the background level, therefore proving the concept of using EVCs as active harmonic filters. If they were to be used for this purpose, the THDv could be reduced below the background harmonic level.

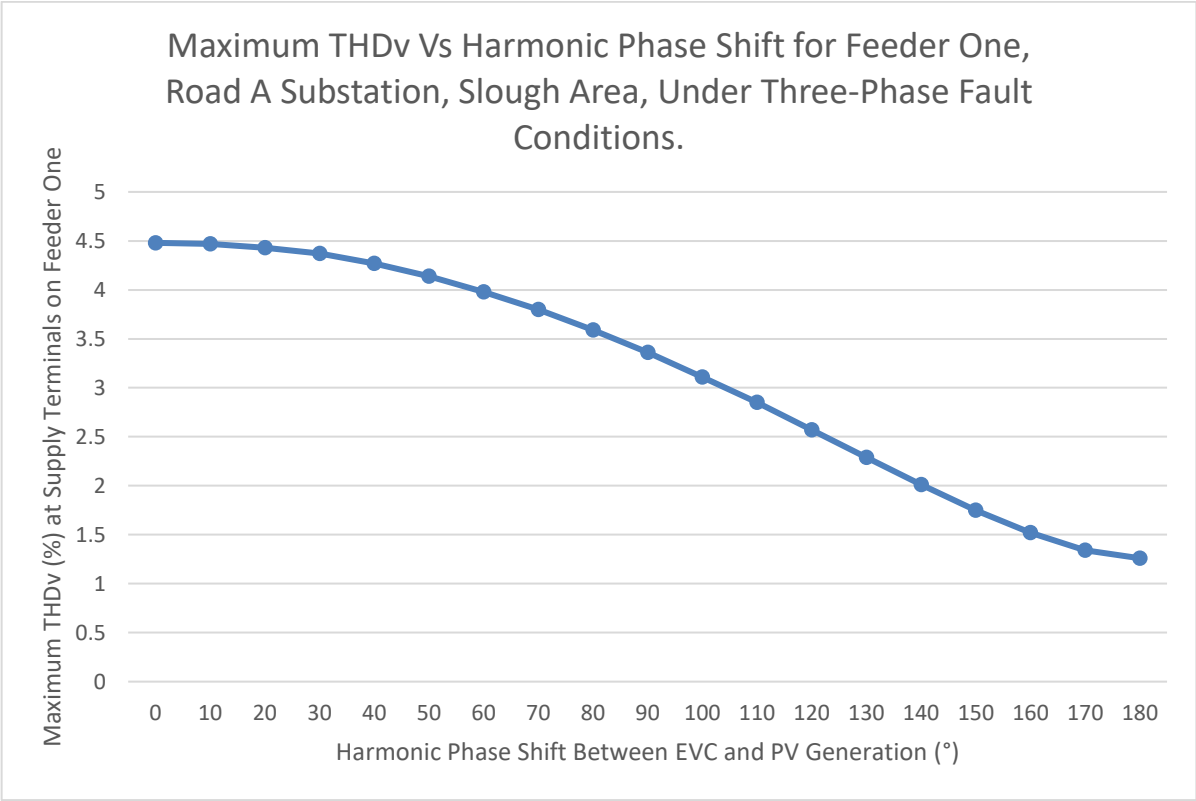


**Figure 3.4.1.1: Effect of EVC phase angle on maximum THDv for feeder one under three-phase fault conditions with fifty-four PV generators / forty-eight EVCs on feeder one and sixty-nine PV generators / sixty EVCs on feeder two. Data from Latheef (2006) and Dale (2018).**

It can be seen above in Figure 3.4.1.1 above that as phase shift increases, the maximum THDv measured reduces. However, the drop between 0º and 30º is 0.11%. Over the same period from 110º and 140º the drop is 0.84%, an eight-fold increase. Therefore, a range of phase angles, between 0º and 30º results in a close to linear summation of the harmonics. Since this study is interested in specific harmonic breaches under ER G5/5, rather than the total THDv, and Energy Networks Association (2020), states that harmonic phase shift cannot always be assumed, simulations will assume a 0° phase shift. This will cover the worst-case scenario for specific harmonics.

Similar to previous sections, the maximum harmonic levels at maximum penetration will be identified and recommendations for the maximum combined numbers of PV generation and EVCs to observe compliance of ER G5/5 will be made.

## 3.4.2 – THDv at the Transformer and Remote End

Table 3.4.2.1 shows the highest THDv measured between phase and neutral at a customer's supply terminal at the end of feeder one on the yellow phase, location defined within Figure 3.1.1.2, with a PV generation penetration of 98.4%, EVC penetration of 86.4% and phase shift of 0°. These are across the three PV harmonic profiles shown in Tables 3.3.1.1, 3.3.1.4 and 3.3.1.7. This penetration value represents a PV generator number of one-hundred and twenty-three and EVC number of one-hundred and eight evenly distributed amongst the three phases, fifty-four PV generators and forty-eight EVCs on feeder one and sixty-nine PV generators and sixty EVCs on feeder two. By comparing these results with the standards in ER G5/5 shown in Table 3.4.2.1, it can be seen that the 15$^{th}$, 21$^{st}$, 27$^{th}$, 33$^{rd}$, and 39$^{th}$ harmonics exceeded limits. The only exception is the 15$^{th}$ harmonic which was not exceeded for the PV harmonic profile from Table 3.3.1.4. Table 3.4.2.2 shows the highest THDv measured between phase and neutral at the LV terminals of the transformer on the red phase with a PV generation penetration of 98.4%, EVC penetration of 86.4% and phase shift of 0°.

In addition to the effect of maximum penetration shown in Tables 3.4.2.1-2, the tipping point for feeder one to no longer remain compliant with ER G5/5 was identified. It was found that a penetration of 26.4%, 33.6% and 21.6% was the tipping point on this feeder for the harmonic profiles from Tables 3.3.1.1, 3.3.1.4 and 3.3.1.7 respectively. This penetration value represents an EVC and PV generation number of thirty-three, forty-two and twenty-seven respectively. Fifteen, eighteen and twelve respectively on feeder one and eighteen, twenty-four and fifteen respectively on feeder two. Table 3.4.2.3 shows the harmonic spectrum of the voltage measured between phase and neutral at a customer's supply terminal at the end of feeder one on the red phase, location shown within Figure 3.1.1.2, at the EVC and PV penetration mentioned above. The tabulated values of these penetrations can be seen in Table 3.4.2.3. At these penetrations, the 15$^{th}$, 21$^{st}$, 27$^{th}$ and 33$^{rd}$ harmonic dropped sufficiently to below their harmonic limits allowed under ER G5/5.

Due to the combination of EVCs and PV generation in this chapter, the maximum penetration of EVCs and PV generation combined is much lower than the previous two chapters. Based on the modelling technique used, which sums the harmonic currents, this is expected.

**Table 3.4.2.1: Table of the voltage harmonics across the yellow phase supply terminal at the end of feeder one with a PV generation penetration of 98.4%, PV generation profile defined in the table and EVC penetration of 86.4% against the limits set out in ER G5/5 (Energy Networks Association, 2020).**

| Harmonic Number | Harmonic Magnitude (%) (PV Generation Harmonic Profile from Table 3.3.1.1) | Harmonic Magnitude (%) (PV Generation Harmonic Profile from Table 3.3.1.4) | Harmonic Magnitude (%) (PV Generation Harmonic Profile from Table 3.3.1.7) | ER G5/5 Limits (%) |
|---|---|---|---|---|
| THDv | 2.99 | 2.48 | 3.10 | 5.0 |
| 2nd | 0.10 | 0.10 | 0.10 | 1.6 |
| 3rd | 1.13 | 0.95 | 1.28 | 4.0 |
| 4th | 0.07 | 0.02 | 0.03 | 1.0 |
| 5th | 1.15 | 0.87 | 1.02 | 4.0 |
| 6th | 0.05 | 0.05 | 0.05 | 0.5 |
| 7th | 1.31 | 1.10 | 1.29 | 4.0 |
| 8th | 0.04 | 0.04 | 0.04 | 0.4 |
| 9th | 0.72 | 0.52 | 0.74 | 1.2 |
| 10th | 0.05 | 0.05 | 0.05 | 0.4 |
| 11th | 0.91 | 0.76 | 0.96 | 3.0 |
| 12th | 0.06 | 0.06 | 0.06 | 0.2 |
| 13th | 1.04 | 0.78 | 1.04 | 2.5 |
| 14th | 0.03 | 0.03 | 0.03 | 0.2 |
| 15th | 0.58 | 0.44 | 0.65 | 0.5 |
| 16th | 0.12 | 0.12 | 0.12 | 0.2 |
| 17th | 0.54 | 0.46 | 0.58 | 1.6 |
| 18th | 0.12 | 0.12 | 0.12 | 0.2 |
| 19th | 0.51 | 0.43 | 0.64 | 1.5 |
| 20th | 0.06 | 0.06 | 0.06 | 0.2 |
| 21st | 0.41 | 0.28 | 0.50 | 0.2 |
| 22nd | 0.01 | 0.01 | 0.01 | 0.2 |
| 23rd | 0.39 | 0.44 | 0.54 | 1.2 |
| 24th | 0.05 | 0.05 | 0.05 | 0.2 |
| 25th | 0.35 | 0.30 | 0.40 | 1.0 |
| 26th | 0.01 | 0.01 | 0.01 | 0.2 |
| 27th | 0.34 | 0.34 | 0.34 | 0.2 |
| 28th | 0.06 | 0.06 | 0.06 | 0.2 |
| 29th | 0.39 | 0.39 | 0.39 | 0.86 |
| 30th | 0.05 | 0.05 | 0.05 | 0.2 |
| 31st | 0.41 | 0.41 | 0.41 | 0.81 |
| 32nd | 0.05 | 0.05 | 0.05 | 0.2 |
| 33rd | 0.32 | 0.32 | 0.32 | 0.2 |
| 34th | 0.06 | 0.06 | 0.06 | 0.2 |
| 35th | 0.27 | 0.27 | 0.27 | 0.71 |
| 36th | 0.06 | 0.06 | 0.06 | 0.2 |
| 37th | 0.23 | 0.23 | 0.23 | 0.68 |
| 38th | 0.00 | 0.00 | 0.00 | 0.2 |
| 39th | 0.23 | 0.23 | 0.23 | 0.2 |
| 40th | 0.06 | 0.06 | 0.06 | 0.2 |
| 41st | 0.13 | 0.13 | 0.13 | 0.61 |
| 43rd | 0.13 | 0.13 | 0.13 | 0.58 |
| 45th | 0.13 | 0.13 | 0.13 | 0.2 |
| 47th | 0.09 | 0.09 | 0.09 | 0.53 |
| 49th | 0.09 | 0.09 | 0.09 | 0.51 |
| Harmonics higher than the limits set by ER G5/5 | | | | |
| EVCs & PVs on Feeder 1: 48 & 54 respectively. EVCs & PVs on Feeder 2: 60 & 69 respectively. | | | | |

**Table 3.4.2.2: Table of the voltage harmonics measured on the red phase of feeder one at the LV terminals of Road A substations distribution transformer with a PV generation penetration of 98.4%, PV generation profile defined within the table and EVC penetration of 86.4% against the limits set out in ER G5/5 (Energy Networks Association, 2020).**

| Harmonic Number | Harmonic Magnitude (%) (PV Generation Harmonic Profile from Table 3.3.1.1) | Harmonic Magnitude (%) (PV Generation Harmonic Profile from Table 3.3.1.4) | Harmonic Magnitude (%) (PV Generation Harmonic Profile from Table 3.3.1.7) | ER G5/5 Limits (%) |
|---|---|---|---|---|
| THDv | 2.70 | 2.27 | 2.79 | 5.0 |
| 2nd | 0.09 | 0.09 | 0.09 | 1.6 |
| 3rd | 1.03 | 0.88 | 1.15 | 4.0 |
| 4th | 0.06 | 0.02 | 0.03 | 1.0 |
| 5th | 1.05 | 0.82 | 0.94 | 4.0 |
| 6th | 0.04 | 0.04 | 0.04 | 0.5 |
| 7th | 1.24 | 1.06 | 1.22 | 4.0 |
| 8th | 0.04 | 0.04 | 0.04 | 0.4 |
| 9th | 0.63 | 0.46 | 0.65 | 1.2 |
| 10th | 0.05 | 0.05 | 0.05 | 0.4 |
| 11th | 0.84 | 0.72 | 0.89 | 3.0 |
| 12th | 0.05 | 0.05 | 0.05 | 0.2 |
| 13th | 0.94 | 0.72 | 0.94 | 2.5 |
| 14th | 0.02 | 0.03 | 0.03 | 0.2 |
| 15th | 0.50 | 0.38 | 0.56 | 0.5 |
| 16th | 0.10 | 0.10 | 0.10 | 0.2 |
| 17th | 0.46 | 0.40 | 0.50 | 1.6 |
| 18th | 0.10 | 0.10 | 0.10 | 0.2 |
| 19th | 0.44 | 0.37 | 0.55 | 1.5 |
| 20th | 0.05 | 0.05 | 0.05 | 0.2 |
| 21st | 0.35 | 0.24 | 0.43 | 0.2 |
| 22nd | 0.02 | 0.01 | 0.01 | 0.2 |
| 23rd | 0.34 | 0.37 | 0.45 | 1.2 |
| 24th | 0.05 | 0.05 | 0.05 | 0.2 |
| 25th | 0.30 | 0.26 | 0.34 | 1.0 |
| 26th | 0.01 | 0.01 | 0.01 | 0.2 |
| 27th | 0.29 | 0.29 | 0.29 | 0.2 |
| 28th | 0.05 | 0.05 | 0.05 | 0.2 |
| 29th | 0.33 | 0.33 | 0.33 | 0.86 |
| 30th | 0.04 | 0.04 | 0.04 | 0.2 |
| 31st | 0.34 | 0.35 | 0.35 | 0.81 |
| 32nd | 0.04 | 0.05 | 0.05 | 0.2 |
| 33rd | 0.27 | 0.27 | 0.27 | 0.2 |
| 34th | 0.04 | 0.04 | 0.04 | 0.2 |
| 35th | 0.23 | 0.23 | 0.23 | 0.71 |
| 36th | 0.05 | 0.05 | 0.05 | 0.2 |
| 37th | 0.19 | 0.19 | 0.19 | 0.68 |
| 38th | 0.00 | 0.00 | 0.00 | 0.2 |
| 39th | 0.20 | 0.20 | 0.20 | 0.2 |
| 40th | 0.05 | 0.05 | 0.05 | 0.2 |
| 41st | 0.11 | 0.11 | 0.11 | 0.61 |
| 43rd | 0.11 | 0.11 | 0.11 | 0.58 |
| 45th | 0.11 | 0.11 | 0.11 | 0.2 |
| 47th | 0.08 | 0.08 | 0.08 | 0.53 |
| 49th | 0.08 | 0.08 | 0.08 | 0.51 |
| Harmonics higher than the limits set by ER G5/5 | | Harmonics on the boundary of the limits set by ER G5/5 | | |
| EVCs & PVs on Feeder 1: 48 & 54 respectively. EVCs & PVs on Feeder 2: 60 & 69 respectively. | | | | |

**Table 3.4.2.3: Table of the voltage harmonics across the yellow phase supply terminal at the end of feeder one with an EVC penetration, PV generation penetration and PV generation profile defined in the table, against the limits set out in ER G5/5 (Energy Networks Association, 2020).**

| Harmonic Number | Harmonic Magnitude (%) (PV Generation Harmonic Profile from Table 3.3.1.1 & penetration 26.4%) | Harmonic Magnitude (%) (PV Generation Harmonic Profile from Table 3.3.1.4 & penetration 33.6%) | Harmonic Magnitude (%) (PV Generation Harmonic Profile from Table 3.3.1.7 & penetration 21.6%) | ER G5/5 Limits (%) |
|---|---|---|---|---|
| THDv | 1.88 | 1.82 | 1.78 | 5.0 |
| 2nd | 0.06 | 0.06 | 0.05 | 1.6 |
| 3rd | 0.73 | 0.71 | 0.72 | 4.0 |
| 4th | 0.03 | 0.02 | 0.02 | 1.0 |
| 5th | 0.71 | 0.66 | 0.64 | 4.0 |
| 6th | 0.03 | 0.04 | 0.03 | 0.5 |
| 7th | 1.00 | 0.95 | 0.96 | 4.0 |
| 8th | 0.03 | 0.02 | 0.02 | 0.4 |
| 9th | 0.35 | 0.32 | 0.32 | 1.2 |
| 10th | 0.04 | 0.04 | 0.04 | 0.4 |
| 11th | 0.66 | 0.63 | 0.64 | 3.0 |
| 12th | 0.04 | 0.04 | 0.04 | 0.2 |
| 13th | 0.64 | 0.59 | 0.60 | 2.5 |
| 14th | 0.03 | 0.03 | 0.03 | 0.2 |
| 15th | 0.28 | 0.26 | 0.27 | 0.5 |
| 16th | 0.06 | 0.07 | 0.06 | 0.2 |
| 17th | 0.24 | 0.25 | 0.22 | 1.6 |
| 18th | 0.06 | 0.06 | 0.05 | 0.2 |
| 19th | 0.26 | 0.26 | 0.26 | 1.5 |
| 20th | 0.03 | 0.04 | 0.03 | 0.2 |
| 21st | 0.19 | 0.16 | 0.19 | 0.2 |
| 22nd | 0.02 | 0.02 | 0.02 | 0.2 |
| 23rd | 0.19 | 0.24 | 0.20 | 1.2 |
| 24th | 0.03 | 0.03 | 0.02 | 0.2 |
| 25th | 0.17 | 0.22 | 0.16 | 1.0 |
| 26th | 0.01 | 0.01 | 0.01 | 0.2 |
| 27th | 0.16 | 0.19 | 0.14 | 0.2 |
| 28th | 0.03 | 0.03 | 0.03 | 0.2 |
| 29th | 0.18 | 0.22 | 0.15 | 0.86 |
| 30th | 0.02 | 0.03 | 0.02 | 0.2 |
| 31st | 0.20 | 0.33 | 0.17 | 0.81 |
| 32nd | 0.02 | 0.03 | 0.02 | 0.2 |
| 33rd | 0.16 | 0.18 | 0.13 | 0.2 |
| 34th | 0.02 | 0.03 | 0.02 | 0.2 |
| 35th | 0.14 | 0.16 | 0.12 | 0.71 |
| 36th | 0.02 | 0.03 | 0.02 | 0.2 |
| 37th | 0.12 | 0.14 | 0.10 | 0.68 |
| 38th | 0.00 | 0.00 | 0.00 | 0.2 |
| 39th | 0.13 | 0.15 | 0.11 | 0.2 |
| 40th | 0.03 | 0.03 | 0.02 | 0.2 |
| 41st | 0.07 | 0.08 | 0.06 | 0.61 |
| 43rd | 0.08 | 0.09 | 0.07 | 0.58 |
| 45th | 0.08 | 0.09 | 0.05 | 0.2 |
| 47th | 0.05 | 0.06 | 0.05 | 0.53 |
| 49th | 0.06 | 0.06 | 0.05 | 0.51 |

### 3.4.3 – Current Harmonics Drawn

At 98.4% PV generation penetration, the current harmonics drawn should also be inspected. By considering Table 3.4.3.1 which shows the red phase harmonic current at the LV bus of the transformer for the harmonic profiles shown in Tables 3.3.1.1, 3.3.1.4, and 3.3.1.7 and Figure 3.4.3.1 which shows the same for only the harmonic profile shown in Table 3.3.1.1. The magnitudes of the harmonic currents have been broken down into their constituent values in Table 3.4.3.1. It can be seen that lower odd harmonics have significant magnitude, the values decreasing in magnitude as the harmonic number increases in line with the results of Sections 3.2.6 and 3.3.6.

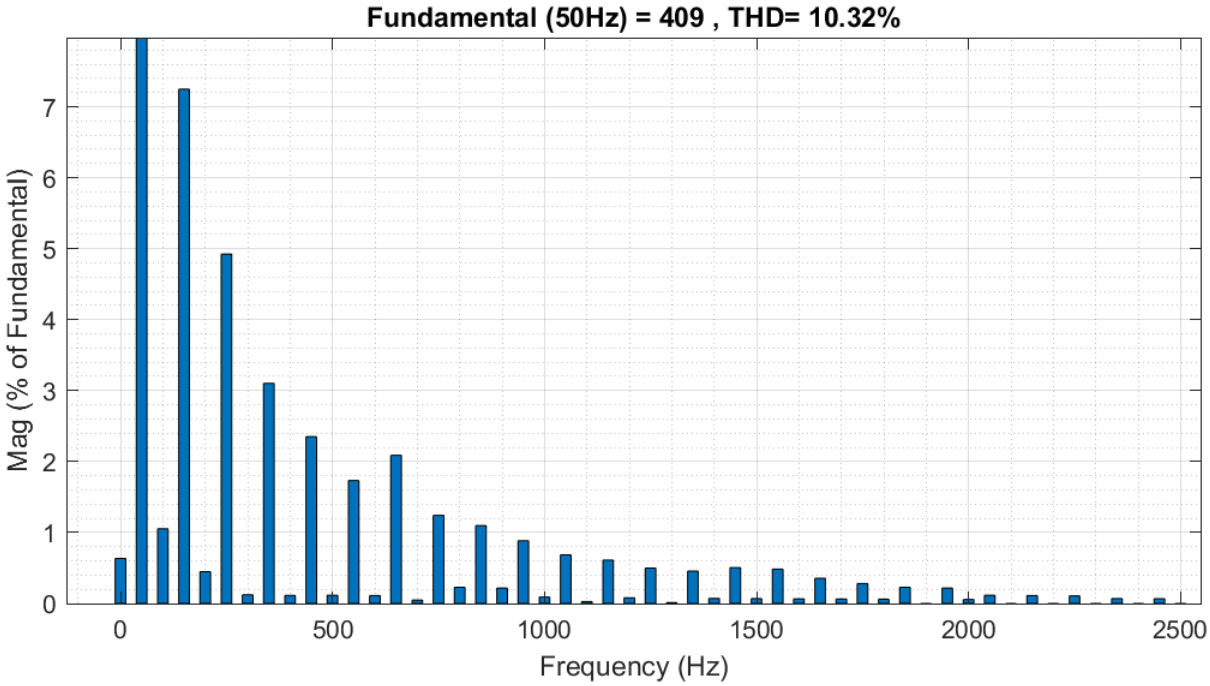


**Figure 3.4.3.1: Graphical representation of the current harmonics measured on the red phase of feeder one at the LV terminals of Road A substations distribution transformer with a PV generation penetration of 98.4%, PV generation profile of Table 3.3.1.1 and EVC penetration of 86.4% (generated in MATLAB/Simulink, The Mathworks, Inc. (2021)).**

**Table 3.4.3.1: Table of the current harmonics measured on the red phase of the LV terminals of Road A substations distribution transformer with a PV generation penetration of 98.4%, PV generation profile defined in the table, and EVC penetration of 86.4%.**

| Harmonic Number | Harmonic Magnitude (A) (PV Generation Harmonic Profile from Table 3.3.1.1) | Harmonic Magnitude (A) (PV Generation Harmonic Profile from Table 3.3.1.4) | Harmonic Magnitude (A) (PV Generation Harmonic Profile from Table 3.3.1.7) |
|---|---|---|---|
| Fundamental Current | 289.2 | 289.2 | 289.2 |
| 2nd | 3.05 | 3.05 | 3.05 |
| 3rd | 20.97 | 14.58 | 26.10 |
| 4th | 1.30 | 0.12 | 0.35 |
| 5th | 14.25 | 8.39 | 11.44 |
| 6th | 0.36 | 0.36 | 0.36 |
| 7th | 8.97 | 6.22 | 8.70 |
| 8th | 0.33 | 0.33 | 0.33 |
| 9th | 6.80 | 4.41 | 7.10 |
| 10th | 0.34 | 0.34 | 0.34 |
| 11th | 5.01 | 3.84 | 5.52 |
| 12th | 0.32 | 0.32 | 0.32 |
| 13th | 6.04 | 3.98 | 6.04 |
| 14th | 0.14 | 0.14 | 0.14 |
| 15th | 3.60 | 2.53 | 4.13 |
| 16th | 0.66 | 0.66 | 0.66 |
| 17th | 3.17 | 2.66 | 3.43 |
| 18th | 0.63 | 0.63 | 0.63 |
| 19th | 2.56 | 2.07 | 3.30 |
| 20th | 0.26 | 0.26 | 0.26 |
| 21st | 1.98 | 1.27 | 2.45 |
| 22nd | 0.08 | 0.08 | 0.08 |
| 23rd | 1.77 | 2.00 | 2.45 |
| 24th | 0.23 | 0.23 | 0.23 |
| 25th | 1.44 | 1.23 | 1.66 |
| 26th | 0.04 | 0.04 | 0.04 |
| 27th | 1.32 | 1.32 | 1.32 |
| 28th | 0.21 | 0.21 | 0.21 |
| 29th | 1.46 | 1.46 | 1.46 |
| 30th | 0.20 | 0.20 | 0.20 |
| 31st | 1.40 | 1.40 | 1.40 |
| 32nd | 0.19 | 0.19 | 0.19 |
| 33rd | 1.03 | 1.03 | 1.03 |
| 34th | 0.18 | 0.18 | 0.18 |
| 35th | 0.81 | 0.81 | 0.81 |
| 36th | 0.18 | 0.18 | 0.18 |
| 37th | 0.66 | 0.66 | 0.66 |
| 38th | 0.00 | 0.00 | 0.00 |
| 39th | 0.63 | 0.63 | 0.63 |
| 40th | 0.16 | 0.16 | 0.16 |
| 41st | 0.34 | 0.34 | 0.34 |
| 43rd | 0.33 | 0.33 | 0.33 |
| 45th | 0.31 | 0.31 | 0.31 |
| 47th | 0.20 | 0.20 | 0.20 |
| 49th | 0.20 | 0.20 | 0.20 |
| THDi (%) | 10.32% | 7.06% | 11.36% |

## 3.4.4 – Voltage and Current Harmonics of Neutral

In contrast to the findings of Section 3.2.7, but comparable with Section 3.3.7, the voltage harmonics measured on the neutral are minimal in magnitude as shown in Figure 3.4.4.1 and Table 3.4.4.1. Additionally, the current harmonics measured on the LV side of the transformer are low in magnitude as shown in Table 3.4.4.1. The highest magnitude harmonic is the 2$^{nd}$ at 0.22A across all three PV harmonic profiles and the harmonics following this reduce in magnitude to 0.01A at the 30$^{th}$ harmonic. Therefore, the effect of these harmonics is minimal in terms of conductor heating or safety concerns.

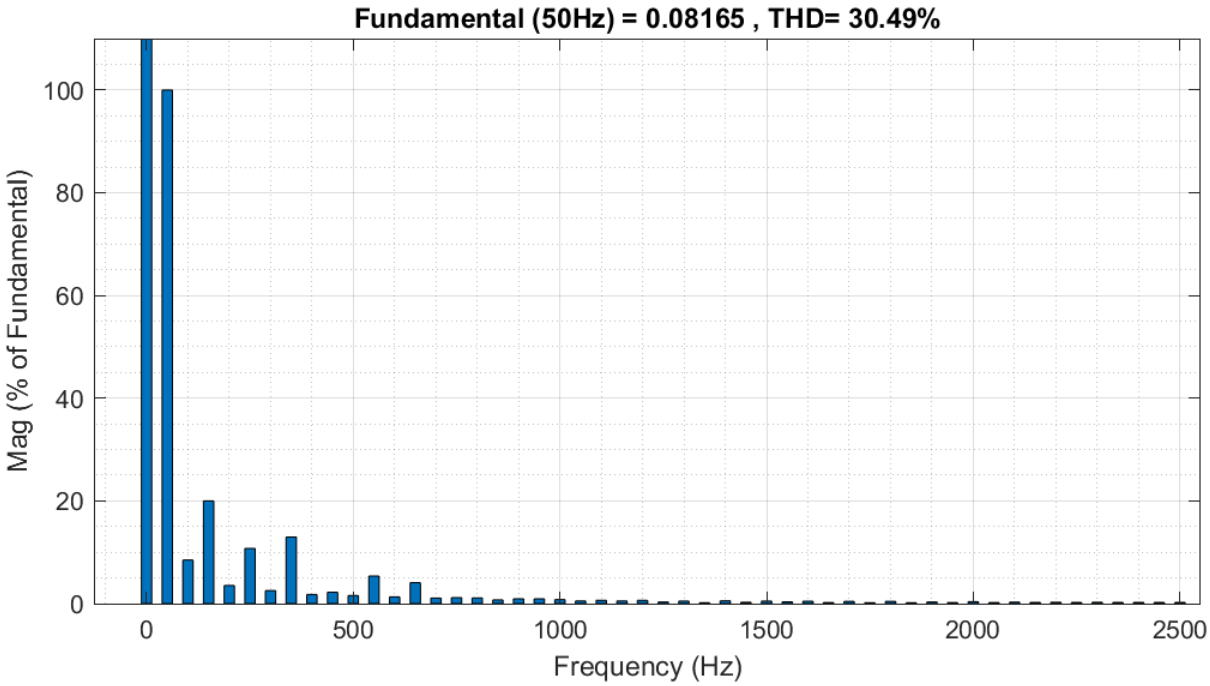


**Figure 3.4.4.1: Graphical representation of the voltage harmonics measured on the neutral at the end of feeder one with a PV generation penetration of 98.4%, PV generation profile of Table 3.3.1.7 and EVC penetration of 86.4% (generated in MATLAB/Simulink, The Mathworks, Inc. (2021)).**

**Table 3.4.4.1: Table of the voltage harmonics measured on the neutral at the end of feeder one and current harmonics measured on the neutral at the LV terminals of Road A substations distribution transformer with a PV generation penetration of 98.4%, PV generation profile defined in the table and EVC penetration of 86.4%.**

| Harmonic Number | Harmonic Magnitude (PV Generation Harmonic Profile from Table 3.3.1.1) | | Harmonic Magnitude (PV Generation Harmonic Profile from Table 3.3.1.4) | | Harmonic Magnitude (PV Generation Harmonic Profile from Table 3.3.1.7) | |
|---|---|---|---|---|---|---|
| | V | A | V | A | V | A |
| 2nd | 0.00 | 0.22 | 0.00 | 0.22 | 0.00 | 0.22 |
| 3rd | 0.01 | 0.19 | 0.01 | 0.17 | 0.01 | 0.20 |
| 4th | 0.00 | 0.11 | 0.00 | 0.11 | 0.00 | 0.11 |
| 5th | 0.01 | 0.11 | 0.01 | 0.10 | 0.01 | 0.10 |
| 6th | 0.00 | 0.08 | 0.00 | 0.08 | 0.00 | 0.08 |
| 7th | 0.01 | 0.06 | 0.01 | 0.06 | 0.01 | 0.06 |
| 8th | 0.00 | 0.06 | 0.00 | 0.06 | 0.00 | 0.06 |
| 9th | 0.00 | 0.05 | 0.00 | 0.05 | 0.00 | 0.05 |
| 10th | 0.00 | 0.05 | 0.00 | 0.05 | 0.00 | 0.05 |
| 11th | 0.00 | 0.04 | 0.00 | 0.04 | 0.00 | 0.04 |
| 12th | 0.00 | 0.04 | 0.00 | 0.04 | 0.00 | 0.04 |
| 13th | 0.00 | 0.03 | 0.00 | 0.03 | 0.00 | 0.03 |
| 14th | 0.00 | 0.03 | 0.00 | 0.03 | 0.00 | 0.03 |
| 15th | 0.00 | 0.03 | 0.00 | 0.03 | 0.00 | 0.03 |
| 16th | 0.00 | 0.03 | 0.00 | 0.03 | 0.00 | 0.03 |
| 17th | 0.00 | 0.03 | 0.00 | 0.03 | 0.00 | 0.03 |
| 18th | 0.00 | 0.03 | 0.00 | 0.03 | 0.00 | 0.03 |
| 19th | 0.00 | 0.02 | 0.00 | 0.02 | 0.00 | 0.03 |
| 20th | 0.00 | 0.02 | 0.00 | 0.02 | 0.00 | 0.02 |
| 21st | 0.00 | 0.02 | 0.00 | 0.02 | 0.00 | 0.02 |
| 22nd | 0.00 | 0.02 | 0.00 | 0.02 | 0.00 | 0.02 |
| 23rd | 0.00 | 0.02 | 0.00 | 0.02 | 0.00 | 0.02 |
| 24th | 0.00 | 0.02 | 0.00 | 0.02 | 0.00 | 0.02 |
| 25th | 0.00 | 0.02 | 0.00 | 0.02 | 0.00 | 0.02 |
| 26th | 0.00 | 0.02 | 0.00 | 0.02 | 0.00 | 0.02 |
| 27th | 0.00 | 0.02 | 0.00 | 0.02 | 0.00 | 0.02 |
| 28th | 0.00 | 0.02 | 0.00 | 0.02 | 0.00 | 0.02 |
| 29th | 0.00 | 0.02 | 0.00 | 0.02 | 0.00 | 0.02 |
| 30th | 0.00 | 0.01 | 0.00 | 0.01 | 0.00 | 0.01 |
| 31st | 0.00 | 0.02 | 0.00 | 0.02 | 0.00 | 0.02 |
| 32nd | 0.00 | 0.01 | 0.00 | 0.01 | 0.00 | 0.01 |
| 33rd | 0.00 | 0.02 | 0.00 | 0.02 | 0.00 | 0.02 |
| 34th | 0.00 | 0.01 | 0.00 | 0.01 | 0.00 | 0.01 |
| 35th | 0.00 | 0.01 | 0.00 | 0.01 | 0.00 | 0.01 |
| 36th | 0.00 | 0.01 | 0.00 | 0.01 | 0.00 | 0.01 |
| 37th | 0.00 | 0.01 | 0.00 | 0.01 | 0.00 | 0.01 |
| 38th | 0.00 | 0.01 | 0.00 | 0.01 | 0.00 | 0.01 |
| 39th | 0.00 | 0.01 | 0.00 | 0.01 | 0.00 | 0.01 |
| 40th | 0.00 | 0.01 | 0.00 | 0.01 | 0.00 | 0.01 |
| 41st | 0.00 | 0.01 | 0.00 | 0.01 | 0.00 | 0.01 |
| 43rd | 0.00 | 0.01 | 0.00 | 0.01 | 0.00 | 0.01 |
| 45th | 0.00 | 0.01 | 0.00 | 0.01 | 0.00 | 0.01 |
| 47th | 0.00 | 0.01 | 0.00 | 0.01 | 0.00 | 0.01 |
| 49th | 0.00 | 0.01 | 0.00 | 0.01 | 0.00 | 0.01 |

### 3.4.5 – Asset Lifespan

Similar to Sections 3.2.8 and 3.3.8, it is important to ascertain whether the harmonic currents are sufficient in magnitude to lead to a noticeable loss of transformer or conductor life. This will be calculated using Equations 3.2.8.1-19 and Tables 3.4.2.2, 3.4.3.1 and 3.4.4.1. The same assumptions and values such as reference hottest-spot temperature, ambient temperature and conductor impedance will be made as per Section 3.2.8 to carry out these calculations. The PV generation penetration was 98.4% and EVC penetration was 86.4%.

At a reference hottest-spot temperature of 110ºC, the PV generation harmonic profiles from Tables 3.3.1.1, 3.3.1.4 and 3.3.1.7 resulted in an increase in transformer hot-spot temperature of 1.2074ºC, 0.9087ºC and 1.3535ºC respectively. Therefore, this would result in a loss of transformer life of 4.63 years, 3.54 years, and 5.15 years respectively. As expected, a combination of EVCs and PV generation, which leads to higher current and voltage harmonics also leads to a higher loss in transformer life. However, for example, when comparing the combination of EVCs and PV generation using data from Table 3.3.1.7, to just EVCs in Section 3.2.8, the THDv at the transformer increased from 2.10% to 2.79% and the current harmonic magnitude increased from 18.37A to 32.85A. This represents an increase of 33% THDv and 79% harmonic current when extrapolating data from Figures 3.2.6.1 and 3.4.3.3. The EVC scenario transformer temperature increase was 0.6520ºC and loss of transformer life of 2.58 years. This increase in harmonics led to an increase in transformer hot-spot temperature of 108% and transformer life loss of 100%. There is a degree of weighting to different harmonic orders, which means that comparatively, higher order harmonics will have a higher effect on transformer life lost or increase in hot-spot temperature.

Using the calculations for conductor lifespan, at a reference conductor temperature of 90ºC, the PV generation harmonic profiles from from Tables 3.3.1.1, 3.3.1.4 and 3.3.1.7 results in an increase in temperature of 0.1595ºC, 0.0758ºC and 0.1874ºC, respectively. Therefore, this would result in a loss of conductor life of 0.92 years, 0.44 years, and 1.08 years respectively. Comparing this to loss of asset lifespan, considering EVCs in Section 3.2.8, there was a conductor temperature increase of 0.0610ºC and loss of conductor life of 0.35 years. Like the transformer calculations, an increase in harmonic current magnitude of 79% has led to an increase in temperature of 207% and an increase in loss of cable life of 209%. Therefore, as harmonic current magnitude increases so does its proportional effect on the cable lifespan.

# Chapter 4 – The Effect of EVCs and PV Generation on the Harmonic Levels of an EDN Under Fault Conditions

This chapter shall use the case-study EDN and harmonic models produced in Chapter 3 to study the effect of steady-state fault conditions on the harmonic levels of EDNs with high levels of EVCs, PV generation and a combination of the two devices in Sections 4.2, 4.3 and 4.4 respectively. Similar to Chapter 3, phase and neutral current harmonics, phase voltage harmonics and neutral voltage levels for these scenarios shall be determined for one EVC and three PV generation harmonic profiles. Harmonic limit breaches of phase voltage harmonics and maximum penetration levels in accordance with ER G5/5 shall be identified. From this data, predictions shall be produced and used to identify when breaches of harmonic limits are likely under fault conditions across multiple feeders. The fault conditions investigated shall be explained in Section 4.1.

Lastly, the effect these harmonics have on transformer and conductor lifespan shall be determined in addition to risk of injury to the public. From this data, predictions shall be produced which can be applied to identify the impact of faults on transformer and conductor asset life. This information can be used by network planning engineers to understand the impact of network faults on EDN harmonic levels, maximise asset life and reduce the risk of injury to the public.

## 4.1 – Faults

As stated in Section 2.5 one of the main aims of this thesis is to look at the effect that sustained faults have on the power quality of networks with significant amounts of EVC and DER penetration. In order for these faults to be left on the system, these faults must still be able to supply customers within acceptable limits according to the ESQCRs (2002). Further detail has been given in Section 1.5. As identified within Chapter 2, the effect of faults on EDN harmonics is a limitation of existing research and answering this research gap will advance existing knowledge.

The phase-to-phase scenario on feeder one to be looked at is a fault on the pot end joint outside one-hundred and fifty-eight Road A. Since a pot end is used to terminate the EDN, there are no link boxes upstream of this. Therefore, an open circuit fault will not be applicable in this scenario. However, two-phase or three-phase faults, as explained in Figures 1.5.2-3, will be applicable. In each case it will be assumed that the red phase feeds into the fault. In the case of the two-phase fault, the yellow, and in the case of the three-phase fault, the yellow and blue will be fed by the fault and feed back to an empty or blown LV fuse way at Road A substation.

The phase-to-phase scenario on feeder two to be looked at is a fault on the pot end joint outside one-hundred and twenty-two Road A. Like the phase-to-phase fault on feeder one, it will be assumed that the red phase feeds into the fault. In the case of the two-phase fault, the yellow, and in the case of the three-phase fault, the yellow and blue will be fed by the fault and feed back to an empty or blown LV fuse way at Road A substation. Therefore, both the faults on feeders one and two are assumed to be fed via the red phase. It is important to note this, since if the faults on feeders one and two are fed from different phases this will lead to different, likely lower, voltage harmonic values.

The open-circuit scenario to be looked at is a three-phase open-circuit fault at the beginning of feeder one on the cable termination within the LV cabinet. The open-circuit fault will be back-fed via the linkbox outside number eighty-two to restore supplies. This arrangement results in all of the harmonic current from feeder one being redirected along each of the three phase conductors of feeder two. 200A fuses will be inserted into the linkbox, in order to grade with the 315A fuses at the LV cabinet feeding feeder two.

# 4.2 – EVCs

In order to analyse the effect that these faults have on the LV EDN, the EVC penetration was set at 31.2%. This penetration value represents thirty-nine single-phase 3.28kVA EVCs each connected to separate properties on the LV EDN and evenly distributed amongst the three phases, eighteen on feeder one and twenty-one on feeder two. This is the maximum load penetration which can be sustained in the event of a three-phase fault on feeder one without blowing the LV fuse at the substation and allows for a whole number of EVCs to be applied to the network. At this penetration, the current drawn by the phase feeding the fault under three-phase conditions is 338.9A. The maximum LV fuse size which can be installed for 185mm$^2$ Al Consac cable is 315A as per Baker (2015). Although this is 1.08 times the fuse rating, current drawn at fifteen EVCs on feeder one is 300.9A and therefore is below the fuse rating. As long as 338.9A is not sustained permanently, and the current drops lower than 315A, the fuse could potentially last for several days or months before blowing as supported by Beama (2022).

## 4.2.1 – Results of Phase-to-Phase Faults

The supply terminals (metering positions) to be measured will be on all three phases at the start, middle and end of feeder one between phase and neutral. The reason for measuring between phase and neutral was discussed in Section 3.2.4 and the location of these supply terminals has been defined within Figure 3.1.1.2.

Moving on to the results of the simulation, within Figure 4.2.1.1, under normal running arrangements, the further the supply terminal is from the 11kV:400V transformer and therefore, the larger the network impedance, the higher the harmonic voltage drop measured as per Section 1.2.1. However, the increase in THDv between the beginning and end of the LV EDN is only around 0.05-0.06%.The individual harmonic levels can be seen in Table 4.2.1.1, and it can be seen that although there are no breaches of harmonic limits under ER G5/5, a few voltage harmonics, namely the 14$^{th}$, 20$^{th}$ and 22$^{nd}$ increased in magnitude when compared to the results of 98.6% penetration in Section 3.2.5. The increase however was 0.01V and therefore is negligible.

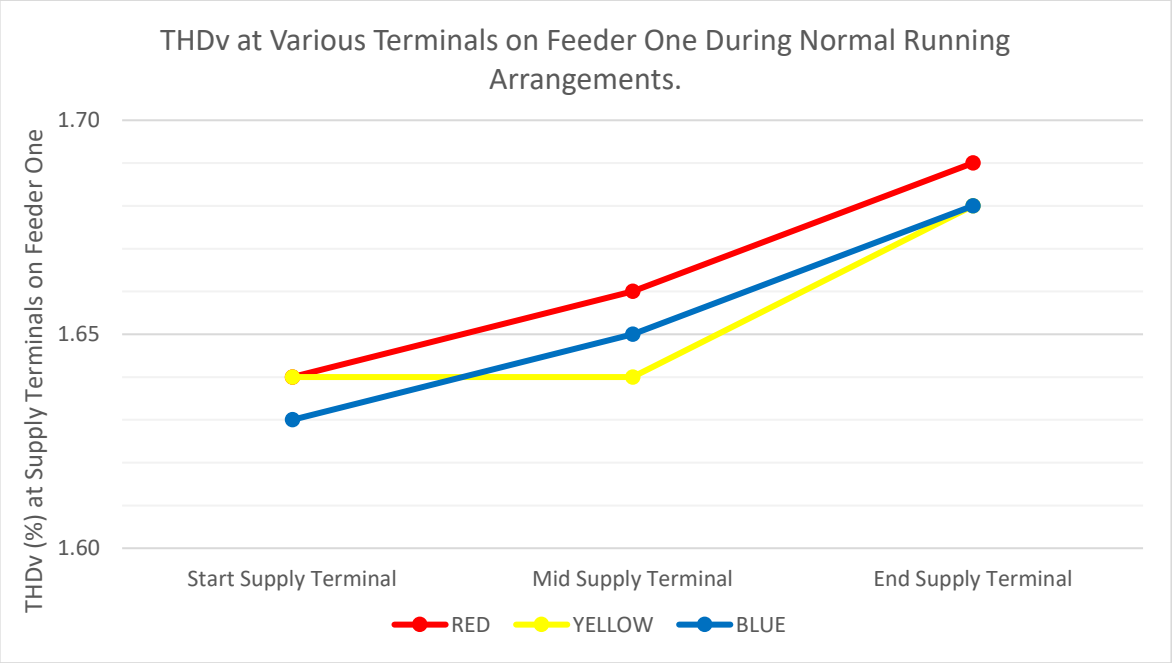


**Figure 4.2.1.1: Graphical representation of the THDv measured on each phase at supply terminals at the start, middle and end of feeder one under normal running arrangements at 31.2% EVC penetration.**

As stated in Table 3.2.5.3 the tipping point for this particular scenario with normal running arrangements on feeder one to remain compliant with ER G5/5 was identified. It was found that a penetration of 60% allowed the EDN to remain compliant. This relates to seventy-five EVCs evenly distributed amongst three phases, thirty-three on feeder one and forty-two on feeder two. This level of penetration was required to keep the 21$^{st}$ and 27$^{th}$ harmonics to or below the 0.2% harmonic limit.

The data stated in Table 4.2.1.1 and subsequent tables is as follows unless otherwise stated.

- The worst-case voltage harmonic magnitude data at the supply terminals was measured at the end of feeder one on red phase between phase and neutral as per Figure 4.2.1.1.
- The worst-case voltage harmonic magnitude data at the transformer was measured on the red phase at the LV terminals of the 11kV:400V transformer.
- the worst-case phase current harmonic magnitude data at the transformer was measured on the red phase at the LV terminals of the 11kV:400V transformer.
- The neutral harmonic current magnitude data at the transformer was measured at the neutral of the LV terminals of the 11kV:400V transformer.

**Table 4.2.1.1: Table of harmonics on feeder one for normal running arrangements with an EVC penetration of 31.2% against the limits set out in ER G5/5 (Energy Networks Association, 2020).**

| Harmonic Number | Worst Case Voltage Harmonic Magnitude at Supply Terminals (%) | Worst Case Voltage Harmonic Magnitude at Transformer (%) | ER G5/5 Limits (%) | Worst Case Phase Current Harmonic Magnitude at Transformer (A) | Neutral Harmonic Current Magnitude at Transformer (A) |
|---|---|---|---|---|---|
| 2nd | 0.04 | 0.04 | 1.60 | 0.18 | 0.01 |
| 3rd | 0.68 | 0.65 | 4.00 | 4.44 | 0.02 |
| 4th | 0.02 | 0.02 | 1.00 | 0.05 | 0.01 |
| 5th | 0.63 | 0.61 | 4.00 | 2.62 | 0.01 |
| 6th | 0.03 | 0.03 | 0.50 | 0.08 | 0.00 |
| 7th | 0.93 | 0.91 | 4.00 | 2.48 | 0.02 |
| 8th | 0.02 | 0.02 | 0.40 | 0.05 | 0.00 |
| 9th | 0.29 | 0.27 | 1.20 | 1.41 | 0.01 |
| 10th | 0.03 | 0.03 | 0.40 | 0.08 | 0.00 |
| 11th | 0.60 | 0.59 | 3.00 | 1.55 | 0.01 |
| 12th | 0.03 | 0.03 | 0.20 | 0.08 | 0.00 |
| 13th | 0.57 | 0.55 | 2.50 | 1.68 | 0.01 |
| 14th | 0.03 | 0.03 | 0.20 | 0.08 | 0.00 |
| 15th | 0.23 | 0.21 | 0.50 | 0.87 | 0.01 |
| 16th | 0.05 | 0.05 | 0.20 | 0.18 | 0.00 |
| 17th | 0.19 | 0.17 | 1.60 | 0.83 | 0.00 |
| 18th | 0.05 | 0.04 | 0.20 | 0.17 | 0.00 |
| 19th | 0.23 | 0.21 | 1.50 | 0.84 | 0.01 |
| 20th | 0.02 | 0.02 | 0.20 | 0.05 | 0.00 |
| 21st | 0.14 | 0.12 | 0.20 | 0.49 | 0.00 |
| 22nd | 0.02 | 0.02 | 0.20 | 0.05 | 0.00 |
| 23rd | 0.17 | 0.14 | 1.20 | 0.63 | 0.00 |
| 24th | 0.01 | 0.01 | 0.20 | 0.02 | 0.00 |
| 25th | 0.12 | 0.11 | 1.00 | 0.39 | 0.00 |
| 26th | 0.01 | 0.01 | 0.20 | 0.02 | 0.00 |
| 27th | 0.14 | 0.12 | 0.20 | 0.46 | 0.00 |
| 28th | 0.01 | 0.01 | 0.20 | 0.02 | 0.00 |
| 29th | 0.13 | 0.11 | 0.86 | 0.45 | 0.00 |
| 30th | 0.00 | 0.00 | 0.20 | 0.00 | 0.00 |
| 31st | 0.15 | 0.13 | 0.81 | 0.44 | 0.00 |
| 33rd | 0.12 | 0.10 | 0.20 | 0.36 | 0.00 |
| 35th | 0.13 | 0.11 | 0.71 | 0.35 | 0.00 |
| 37th | 0.11 | 0.09 | 0.68 | 0.28 | 0.00 |
| 39th | 0.11 | 0.09 | 0.20 | 0.27 | 0.00 |
| 41st | 0.08 | 0.07 | 0.61 | 0.20 | 0.00 |
| 43rd | 0.08 | 0.07 | 0.58 | 0.19 | 0.00 |
| 45th | 0.06 | 0.07 | 0.20 | 0.19 | 0.00 |
| 47th | 0.06 | 0.05 | 0.53 | 0.12 | 0.00 |
| 49th | 0.06 | 0.05 | 0.51 | 0.12 | 0.00 |
| Harmonics higher than the limits set by ER G5/5 | | | | | |
| Harmonics on the boundary of the limits set by ER G5/5 | | | | | |
| Harmonics higher than the result from 98.4% EVC penetration | | | | | |
| Number of PVs on Feeder 1: 18 Number of PVs on Feeder 2: 21 Voltage on Neutral 0.540V | | | | | |

By introducing a two-phase fault, between red and yellow phases, with red phase feeding the fault as seen in Figure 4.2.1.2, it has been found that the THDv increases significantly along the length of the network on red phase, with the THDv also increasing slightly on yellow phase as the current travels from the pot end outside one-hundred and fifty-eight back towards the transformer. The worst-case harmonic distortion was measured between phase and neutral on the yellow phase supply terminal at the start of feeder one as shown in Figure 4.2.1.2. This leads to the THDv measured on the yellow phase supply terminal at the start of the network rising from 1.64% to 2.00%, an increase of 0.36% at 31.2% EVC penetration. There is no noticeable effect on the blue phase THDv which is excluded from the faulted phases. By comparing the results in Table 4.2.1.1 to the results seen in Table 4.2.1.2 generally, under the two-phase fault condition, the maximum measured magnitude of individual harmonics on the EDN measured at the yellow phase supply terminal at the start of feeder one increase, for example, the 15$^{th}$ harmonic increased from 0.23% to 0.31%, the 21$^{st}$ from 0.14% to 0.20% and the 27$^{th}$ from 0.14% to 0.20%. Most notably, the harmonics and voltage on the neutral increase significantly as would be expected during a network imbalance.

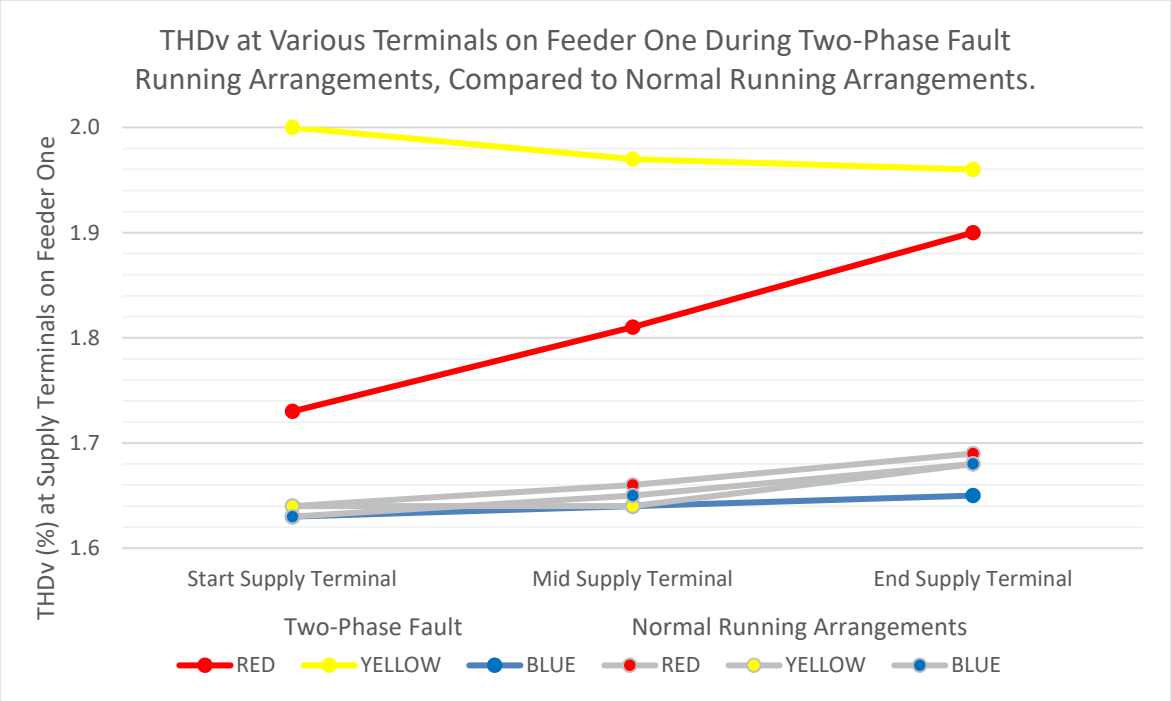


**Figure 4.2.1.2: Graphical representation of the THDv measured on each phase at supply terminals at the start, middle and end of feeder one during a two-phase fault at 31.2% EVC penetration compared to normal running arrangements.**

**Table 4.2.1.2: Table of harmonics on feeder one for a two-phase fault with an EVC penetration of 31.2% against the limits set out in ER G5/5 (Energy Networks Association, 2020).**

| Harmonic Number | Worst Case Voltage Harmonic Magnitude at Supply Terminals (%) | Worst Case Voltage Harmonic Magnitude at Transformer (%) | ER G5/5 Limits (%) | Worst Case Phase Current Harmonic Magnitude at Transformer (A) | Neutral Harmonic Current Magnitude at Transformer (A) |
|---|---|---|---|---|---|
| 2nd | 0.05 | 0.04 | 1.60 | 0.25 | 0.14 |
| 3rd | 0.81 | 0.81 | 4.00 | 6.27 | 3.23 |
| 4th | 0.02 | 0.02 | 1.00 | 0.08 | 0.04 |
| 5th | 0.74 | 0.64 | 4.00 | 3.67 | 1.85 |
| 6th | 0.03 | 0.03 | 0.50 | 0.11 | 0.06 |
| 7th | 1.00 | 0.93 | 4.00 | 3.44 | 1.69 |
| 8th | 0.02 | 0.02 | 0.40 | 0.07 | 0.04 |
| 9th | 0.39 | 0.30 | 1.20 | 1.94 | 0.94 |
| 10th | 0.03 | 0.03 | 0.40 | 0.11 | 0.05 |
| 11th | 0.66 | 0.59 | 3.00 | 2.10 | 0.99 |
| 12th | 0.03 | 0.03 | 0.20 | 0.10 | 0.05 |
| 13th | 0.69 | 0.57 | 2.50 | 2.25 | 1.04 |
| 14th | 0.03 | 0.03 | 0.20 | 0.10 | 0.05 |
| 15th | 0.31 | 0.23 | 0.50 | 1.15 | 0.52 |
| 16th | 0.07 | 0.05 | 0.20 | 0.23 | 0.11 |
| 17th | 0.29 | 0.20 | 1.60 | 1.08 | 0.48 |
| 18th | 0.08 | 0.05 | 0.20 | 0.22 | 0.10 |
| 19th | 0.33 | 0.23 | 1.50 | 1.07 | 0.46 |
| 20th | 0.02 | 0.02 | 0.20 | 0.06 | 0.03 |
| 21st | 0.20 | 0.13 | 0.20 | 0.61 | 0.26 |
| 22nd | 0.02 | 0.02 | 0.20 | 0.06 | 0.03 |
| 23rd | 0.25 | 0.16 | 1.20 | 0.78 | 0.32 |
| 24th | 0.01 | 0.01 | 0.20 | 0.03 | 0.01 |
| 25th | 0.18 | 0.12 | 1.00 | 0.48 | 0.19 |
| 26th | 0.01 | 0.01 | 0.20 | 0.03 | 0.01 |
| 27th | 0.20 | 0.13 | 0.20 | 0.55 | 0.22 |
| 28th | 0.01 | 0.01 | 0.20 | 0.03 | 0.01 |
| 29th | 0.20 | 0.13 | 0.86 | 0.53 | 0.20 |
| 30th | 0.00 | 0.00 | 0.20 | 0.00 | 0.00 |
| 31st | 0.22 | 0.14 | 0.81 | 0.51 | 0.20 |
| 33rd | 0.18 | 0.11 | 0.20 | 0.41 | 0.15 |
| 35th | 0.18 | 0.12 | 0.71 | 0.40 | 0.15 |
| 37th | 0.15 | 0.10 | 0.68 | 0.31 | 0.11 |
| 39th | 0.15 | 0.10 | 0.20 | 0.30 | 0.11 |
| 41st | 0.11 | 0.07 | 0.61 | 0.22 | 0.08 |
| 43rd | 0.12 | 0.07 | 0.58 | 0.21 | 0.07 |
| 45th | 0.12 | 0.07 | 0.20 | 0.20 | 0.07 |
| 47th | 0.08 | 0.05 | 0.53 | 0.13 | 0.04 |
| 49th | 0.08 | 0.05 | 0.51 | 0.13 | 0.04 |
| Harmonics higher than the limits set by ER G5/5 | | | | | |
| Harmonics on the boundary of the limits set by ER G5/5 | | | | | |
| Harmonics higher than the result from 98.4% EVC penetration | | | | | |
| Number of PVs on Feeder 1: 18 Number of PVs on Feeder 2: 21 Voltage on Neutral 4.075V | | | | | |

A two-phase fault results in the 21st and 27th harmonic reaching the boundary of limits set out by ER G5/5. Above this limit would result in a non-compliance. Therefore, this presents the limit for the EVC penetration to remain compliant with ER G5/5 under a two-phase fault scenario.

During a three-phase fault, fed by red, as seen in Figure 4.2.1.3, the THDv increased further at the start, middle and end of the network on the red phase. Interestingly, the THDv does not seem to increase significantly along the length of the network on the yellow and blue phases as the current travels from the pot end back towards the transformer. The worst-case harmonic distortion of 2.17% was measured between phase and neutral on the yellow phase supply terminal at the start of feeder one as shown in Figure 4.2.2.3. Therefore, this presents an overall increase of 0.53% when compared to normal running arrangements or 0.17% when compared to a two-phase fault. Therefore, although a three-phase fault presents the highest impact, the impact is not linear between normal running arrangements, a two-phase fault, and a three-phase fault.

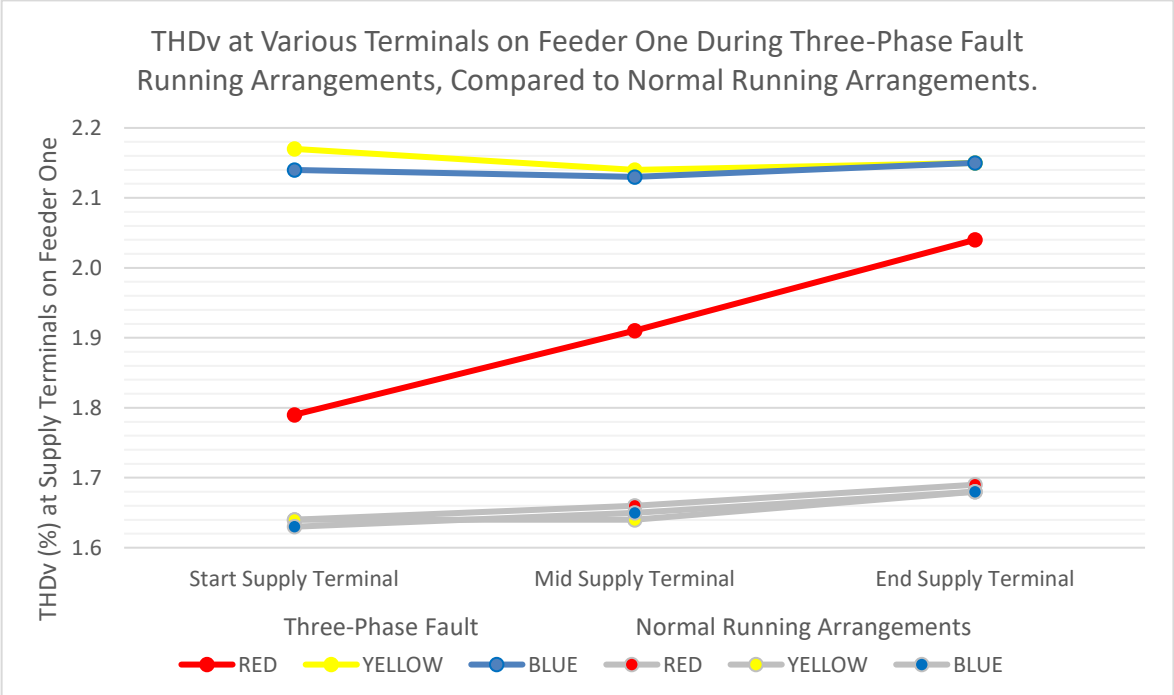


**Figure 4.2.1.3: Graphical representation of the THDv measured on each phase at supply terminals at the start, middle and end of feeder one during a three-phase fault at 31.2% EVC penetration compared to normal running arrangements.**

By comparing the results in Table 4.2.1.3, to the results seen in Table 4.2.1.2, it can be seen that under a three-phase fault condition, the magnitude of individual harmonics at the yellow phase supply terminal at the start of feeder one increase. For example, the 15$^{th}$ harmonic increased from 0.31% to 0.36%, the 21$^{st}$ from 0.20% to 0.22% and the 27$^{th}$ from 0.20% to 0.22%. The harmonic currents on the neutral increase significantly, however, similar to the phase voltage harmonics, not to the same magnitude seen from normal to two-phase fault arrangements. A three-phase fault results in the 21$^{st}$ and 27$^{th}$ harmonic exceeding the boundary of limits set out by ER G5/5. The 33$^{rd}$ harmonic sits on the boundary of these limits. Therefore, if this network was to be left with a three-phase fault, as would be compliant with the ESQCRs, this would result in a non-compliance with ER G5/5.

By analysing the reasoning for this, it can be determined that a degree of cancellation between current harmonics takes place. For example, between normal and two-phase fault conditions, the 3$^{rd}$, 5$^{th}$, and 7$^{th}$ harmonics increased by 1.83A, 1.05A and 0.96A respectively on the red phase at the terminals of the transformer. Between a two-phase and three-phase fault the 3$^{rd}$, 5$^{th}$ and 7$^{th}$ harmonics increased by 1.66A, 0.93A and 0.82A respectively on the red phase at the terminals of the transformer. In each case, the same amount of additional load, one phase of feeder one is added, which should, assuming zero cancellation lead to the harmonic current increasing at the same rate, however, due to harmonic cancellation this is not the case.

In addition to the effect of a three-phase fault under 31.2% EVC penetration shown in Figure 4.2.1.3 and Table 4.2.1.3, the tipping point for this particular three-phase fault to remain compliant with ER G5/5 was identified. It was found that a penetration of 26.4% allowed the network to remain compliant. This penetration value represents an EVC number of thirty-three evenly distributed amongst the three phases, fifteen on feeder one and eighteen on feeder two. This level of penetration was required to reduce the 21$^{st}$ and 27$^{th}$ harmonics to or below the 0.2% harmonic limit.

**Table 4.2.1.3: Table of harmonics on feeder one for a three-phase fault with an EVC penetration of 31.2% against the limits set out in ER G5/5 (Energy Networks Association, 2020).**

| Harmonic Number | Worst Case Voltage Harmonic Magnitude at Supply Terminals (%) | Worst Case Voltage Harmonic Magnitude at Transformer (%) | ER G5/5 Limits (%) | Worst Case Phase Current Harmonic Magnitude at Transformer (A) | Neutral Harmonic Current Magnitude at Transformer (A) |
|---|---|---|---|---|---|
| 2nd | 0.05 | 0.05 | 1.60 | 0.32 | 0.23 |
| 3rd | 0.91 | 0.73 | 4.00 | 7.93 | 5.52 |
| 4th | 0.02 | 0.02 | 1.00 | 0.09 | 0.07 |
| 5th | 0.81 | 0.67 | 4.00 | 4.60 | 3.19 |
| 6th | 0.03 | 0.03 | 0.50 | 0.14 | 0.09 |
| 7th | 1.04 | 0.94 | 4.00 | 4.26 | 2.93 |
| 8th | 0.02 | 0.02 | 0.40 | 0.09 | 0.06 |
| 9th | 0.45 | 0.32 | 1.20 | 2.38 | 1.64 |
| 10th | 0.03 | 0.03 | 0.40 | 0.13 | 0.09 |
| 11th | 0.68 | 0.59 | 3.00 | 2.53 | 1.73 |
| 12th | 0.03 | 0.03 | 0.20 | 0.12 | 0.08 |
| 13th | 0.74 | 0.58 | 2.50 | 2.67 | 1.82 |
| 14th | 0.02 | 0.03 | 0.20 | 0.12 | 0.08 |
| 15th | 0.36 | 0.24 | 0.50 | 1.34 | 0.91 |
| 16th | 0.08 | 0.05 | 0.20 | 0.27 | 0.18 |
| 17th | 0.33 | 0.21 | 1.60 | 1.24 | 0.83 |
| 18th | 0.07 | 0.05 | 0.20 | 0.25 | 0.17 |
| 19th | 0.37 | 0.24 | 1.50 | 1.21 | 0.81 |
| 20th | 0.01 | 0.02 | 0.20 | 0.07 | 0.04 |
| 21st | 0.22 | 0.14 | 0.20 | 0.68 | 0.45 |
| 22nd | 0.01 | 0.02 | 0.20 | 0.07 | 0.04 |
| 23rd | 0.29 | 0.17 | 1.20 | 0.86 | 0.56 |
| 24th | 0.01 | 0.01 | 0.20 | 0.03 | 0.02 |
| 25th | 0.20 | 0.12 | 1.00 | 0.52 | 0.34 |
| 26th | 0.01 | 0.01 | 0.20 | 0.03 | 0.02 |
| 27th | 0.23 | 0.14 | 0.20 | 0.59 | 0.38 |
| 28th | 0.01 | 0.01 | 0.20 | 0.03 | 0.02 |
| 29th | 0.23 | 0.13 | 0.86 | 0.56 | 0.35 |
| 30th | 0.00 | 0.00 | 0.20 | 0.00 | 0.00 |
| 31st | 0.24 | 0.14 | 0.81 | 0.54 | 0.34 |
| 33rd | 0.20 | 0.12 | 0.20 | 0.43 | 0.27 |
| 35th | 0.20 | 0.12 | 0.71 | 0.41 | 0.25 |
| 37th | 0.16 | 0.10 | 0.68 | 0.32 | 0.19 |
| 39th | 0.16 | 0.10 | 0.20 | 0.30 | 0.18 |
| 41st | 0.12 | 0.07 | 0.61 | 0.22 | 0.13 |
| 43rd | 0.12 | 0.07 | 0.58 | 0.21 | 0.12 |
| 45th | 0.12 | 0.07 | 0.20 | 0.20 | 0.12 |
| 47th | 0.08 | 0.05 | 0.53 | 0.13 | 0.07 |
| 49th | 0.08 | 0.05 | 0.51 | 0.13 | 0.07 |
| Harmonics higher than the limits set by ER G5/5 | | | | | |
| Harmonics on the boundary of the limits set by ER G5/5 | | | | | |
| Harmonics higher than the result from 98.4% EVC penetration | | | | | |
| Number of PVs on Feeder 1: 18 Number of PVs on Feeder 2: 21 Voltage on Neutral 6.971V | | | | | |

In addition to ER G5/5 being violated between phase and neutral under three-phase fault conditions, it was found that the neutral voltage present at the end of feeder one increased to 4.075V under two-phase fault conditions shown in Table 4.2.1.2 and 6.971V under three-phase fault conditions shown in Table 4.2.1.3. This is 3.535V or 6.431V higher than normal running conditions respectively. The increase in voltage is caused by the LV EDN no longer being balanced, and therefore, the neutral currents from different phases no longer cancel. Based on Table 3.2.7.4, these voltages could lead to residents perceiving shocks off exposed bonded metal work, potentially leading to complaints. However, it does not seem high enough to cause ventricular fibrillation or respiratory tetanus.

## 4.2.2 – Results of Phase-to-Phase Faults, with a Two-Phase Fault on Feeder Two

Further to Section 4.2.1, the effect of faults on feeder one will be explored whilst a second two-phase fault on feeder two is present. Firstly, it can be seen in Figure 4.2.2.1 that there is a marked drop in THDv on the yellow phase and marked increase in THDv on the red phase when compared to Figure 4.2.1.1. This is for normal arrangements on feeder one and a two-phase fault on feeder two. This is due to load being removed from the yellow phase and added to the red phase via a two-phase fault on feeder two. Considering the reasons for harmonic voltage drop explained in Section 1.2.1, the difference in THDv can be explained. Due to the current being drawn on feeder one remaining the same, the increase in THDv between the beginning and the end of feeder one remains at 0.04-0.06%, similar to Figure 4.2.1.1. The individual harmonic levels can be seen in Table 4.2.2.1 and it can be seen that there are no breaches of harmonic limits under ER G5/5. Despite the two-phase fault on feeder two leading to the neutral voltage increasing from 0.540V to 1.741V, the voltage does not exceed 2.70V on feeder one and therefore should not be high enough to cause perceived shocks to residents. However, based on the results of Table 4.2.1.2, it is likely that residents will receive shocks off of feeder two.

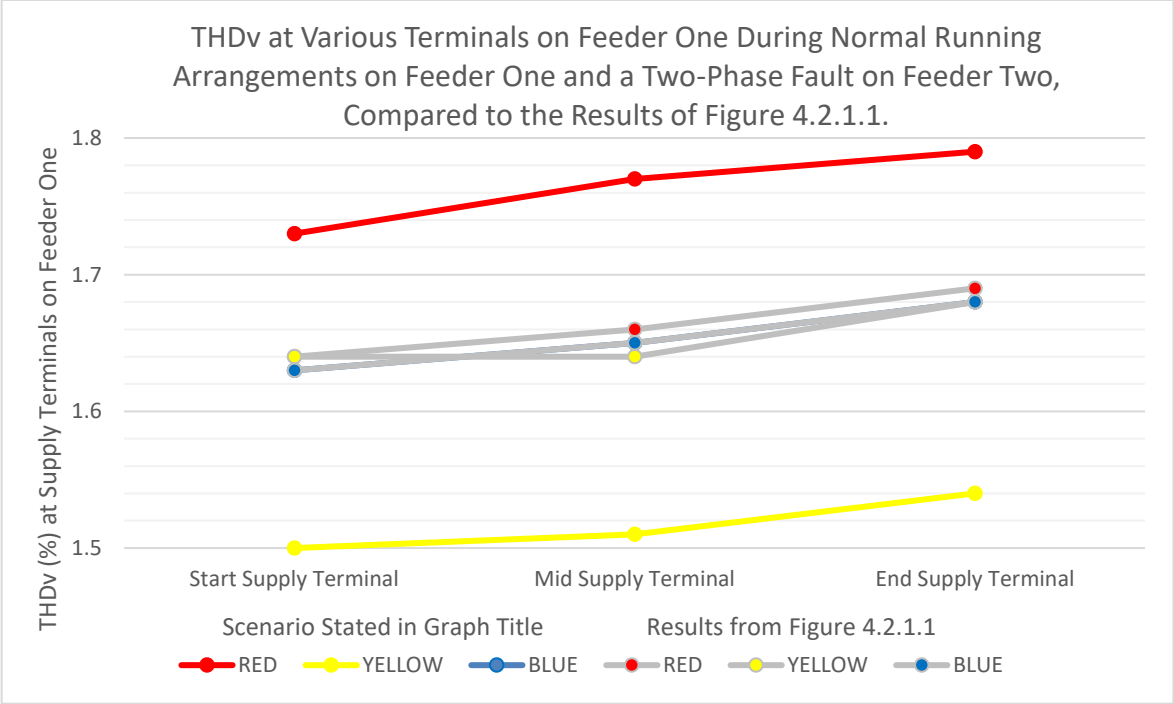


**Figure 4.2.2.1: Graphical representation of the THDv measured on each phase at supply terminals at the start, middle and end of feeder one under normal running arrangements at 31.2% EVC penetration whilst a two-phase fault is present on feeder two, compared to normal running arrangements on feeders one and two (Figure 4.2.1.1).**

The tipping point for this particular scenario with normal running arrangements on feeder one to remain compliant with ER G5/5 was identified. It was found that a penetration of 50.4% allowed the EDN to remain compliant. This relates to an EVC number of sixty-three evenly distributed amongst three phases, twenty-seven on feeder one and thirty-six on feeder two. This level of penetration was required to keep the 21$^{st}$ and 27$^{th}$ harmonics at or below the 0.2% harmonic limit. This is lower than normal arrangements under Section 4.2.1, which allowed an EVC penetration of 60%. Therefore, the two-phase fault on feeder two reduced the number of EVCs which can be connected to the LV EDN by twelve. It should be stated that this reduction in penetration ensures that feeder one is compliant, however, it is likely that due to the two-phase fault on feeder two, harmonic voltages exceed the limits stated in ER G5/5 and therefore isn't compliant.

**Table 4.2.2.1: Table of harmonics on feeder one for normal running arrangements with an EVC penetration of 31.2% whilst a two-phase fault is present on feeder two against the limits set out in ER G5/5 (Energy Networks Association, 2020).**

| Harmonic Number | Worst Case Voltage Harmonic Magnitude at Supply Terminals (%) | Worst Case Voltage Harmonic Magnitude at Transformer (%) | ER G5/5 Limits (%) | Worst Case Phase Current Harmonic Magnitude at Transformer (A) | Neutral Harmonic Current Magnitude at Transformer (A) |
|---|---|---|---|---|---|
| 2nd | 0.05 | 0.04 | 1.60 | 0.27 | 0.16 |
| 3rd | 0.73 | 0.70 | 4.00 | 6.57 | 3.76 |
| 4th | 0.02 | 0.02 | 1.00 | 0.08 | 0.05 |
| 5th | 0.67 | 0.64 | 4.00 | 3.85 | 2.16 |
| 6th | 0.03 | 0.03 | 0.50 | 0.12 | 0.07 |
| 7th | 0.95 | 0.93 | 4.00 | 3.63 | 2.01 |
| 8th | 0.02 | 0.02 | 0.40 | 0.08 | 0.04 |
| 9th | 0.33 | 0.30 | 1.20 | 2.03 | 1.10 |
| 10th | 0.03 | 0.03 | 0.40 | 0.11 | 0.06 |
| 11th | 0.61 | 0.60 | 3.00 | 2.21 | 1.18 |
| 12th | 0.03 | 0.03 | 0.20 | 0.11 | 0.06 |
| 13th | 0.61 | 0.58 | 2.50 | 2.36 | 1.23 |
| 14th | 0.03 | 0.03 | 0.20 | 0.11 | 0.06 |
| 15th | 0.26 | 0.23 | 0.50 | 1.20 | 0.61 |
| 16th | 0.06 | 0.05 | 0.20 | 0.24 | 0.12 |
| 17th | 0.22 | 0.20 | 1.60 | 1.13 | 0.56 |
| 18th | 0.05 | 0.05 | 0.20 | 0.23 | 0.11 |
| 19th | 0.26 | 0.24 | 1.50 | 1.11 | 0.55 |
| 20th | 0.02 | 0.02 | 0.20 | 0.06 | 0.03 |
| 21st | 0.15 | 0.14 | 0.20 | 0.64 | 0.31 |
| 22nd | 0.02 | 0.02 | 0.20 | 0.06 | 0.03 |
| 23rd | 0.19 | 0.17 | 1.20 | 0.81 | 0.38 |
| 24th | 0.01 | 0.01 | 0.20 | 0.03 | 0.01 |
| 25th | 0.14 | 0.12 | 1.00 | 0.50 | 0.23 |
| 26th | 0.01 | 0.01 | 0.20 | 0.03 | 0.01 |
| 27th | 0.15 | 0.14 | 0.20 | 0.57 | 0.26 |
| 28th | 0.01 | 0.01 | 0.20 | 0.03 | 0.01 |
| 29th | 0.15 | 0.13 | 0.86 | 0.55 | 0.25 |
| 30th | 0.00 | 0.00 | 0.20 | 0.00 | 0.00 |
| 31st | 0.16 | 0.14 | 0.81 | 0.53 | 0.24 |
| 33rd | 0.13 | 0.12 | 0.20 | 0.43 | 0.19 |
| 35th | 0.14 | 0.12 | 0.71 | 0.41 | 0.18 |
| 37th | 0.11 | 0.10 | 0.68 | 0.32 | 0.14 |
| 39th | 0.12 | 0.10 | 0.20 | 0.31 | 0.13 |
| 41st | 0.08 | 0.07 | 0.61 | 0.22 | 0.09 |
| 43rd | 0.09 | 0.07 | 0.58 | 0.22 | 0.09 |
| 45th | 0.09 | 0.08 | 0.20 | 0.21 | 0.09 |
| 47th | 0.06 | 0.05 | 0.53 | 0.14 | 0.06 |
| 49th | 0.06 | 0.05 | 0.51 | 0.13 | 0.05 |
| Harmonics higher than the limits set by ER G5/5 | | | | | |
| Harmonics on the boundary of the limits set by ER G5/5 | | | | | |
| Harmonics higher than the result from 98.4% EVC penetration | | | | | |
| Number of PVs on Feeder 1: 18 Number of PVs on Feeder 2: 21 Voltage on Neutral: 1.741V | | | | | |

By introducing a two-phase fault between red and yellow phases, with red phase feeding the fault as seen in Figure 4.2.2.2, similar to Figure 4.2.1.2, it has been found that the THDv increases significantly along the length of feeder one on red phase, with the THDv also increasing slightly on yellow phase as the current travels from the pot end back towards the transformer. This leads to the THDv measured on the yellow phase supply terminal at the start of the network rising from 1.50% to 2.07%, an increase of 0.57%. There is no noticeable effect on the blue phase THDv which is excluded from the faulted phases. The THDv of yellow phase is 0.07% higher than the same scenario without the two-phase fault on feeder two, due to the additional current flow through red phase of the transformer, therefore increasing THDv at the transformer terminals.

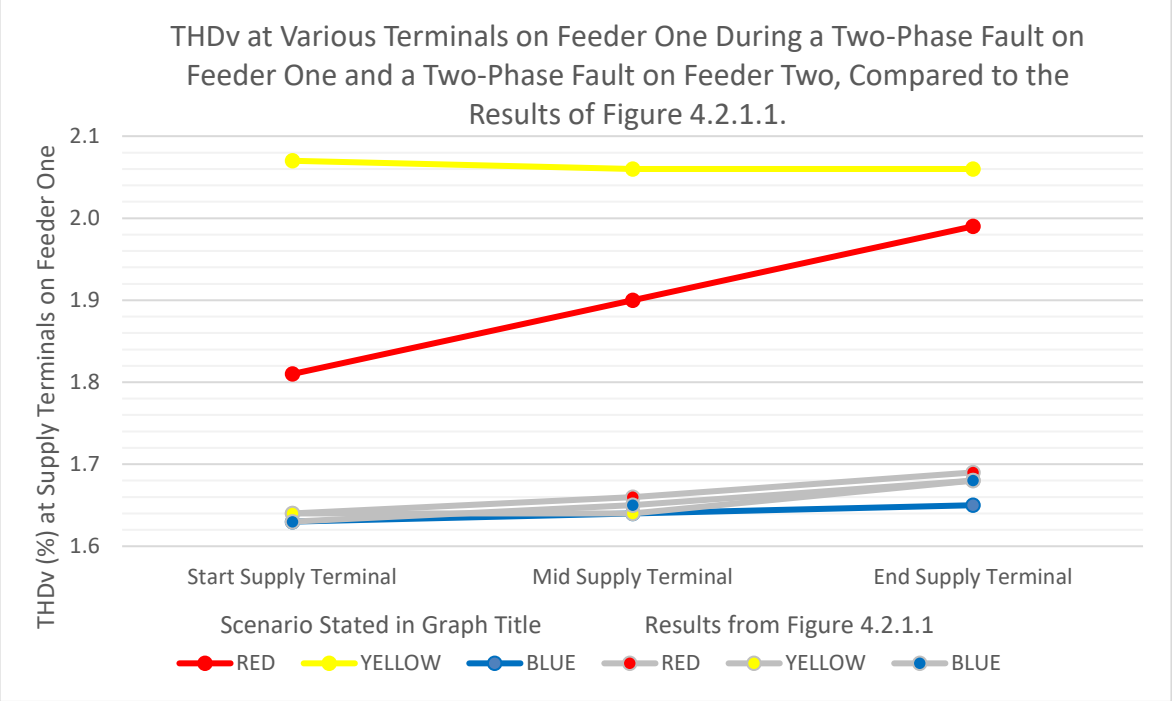


**Figure 4.2.2.2: Graphical representation of the THDv measured on each phase at supply terminals at the start, middle and end of feeder one during a two-phase fault at 31.2% EVC penetration whilst a two-phase fault is present on feeder two, compared to normal running arrangements on feeders one and two (Figure 4.2.1.1).**

The results of the worst-case harmonic distortion under a two-phase fault can be seen in Table 4.2.2.2. The worst-case harmonic distortion was measured between phase and neutral on the yellow phase supply terminal at the start of feeder one as shown in Figure 4.2.2.2. It can be seen that limits under ER G5/5 are exceeded on the 21$^{st}$ and 27$^{th}$ harmonics. This is an increase when compared to Table 4.2.1.2, where the 21$^{st}$ and 27$^{th}$ harmonics were on the boundary. Therefore, the two-phase fault on feeder two resulted in the harmonic limits being exceeded on feeder one. The neutral voltage in Table 4.2.2.2 is also higher than the comparable neutral voltage in Table 4.2.1.2 at 5.263V and 4.075V respectively, therefore presenting an increase of 1.188V. Similar to Table 4.2.1.2, the neutral voltage is high enough to cause shocks, but not high enough to cause ventricular fibrillation or respiratory tetanus.

The tipping point for this particular two-phase fault to remain compliant with ER G5/5 was identified. It was found that a penetration of 26.4% allowed the EDN to remain compliant. This penetration value represents an EVC number of thirty-three evenly distributed amongst the three phases, fifteen on feeder one and eighteen on feeder two. This level of penetration was required to reduce the 21$^{st}$ and 27$^{th}$ harmonics to or below the 0.2% harmonic limit. This is lower than Table 4.2.1.2, which was compliant at 31.2% penetration. Therefore, the two-phase fault on feeder two resulted in less EVCs which can be connected to the EDN before harmonic limits are exceeded.

During a three-phase fault, fed by red, as seen in Figure 4.2.2.3, the THDv increased further at the start, middle and end of feeder one on the red phase. Similar to Figure 4.2.1.3, yellow and blue phase THDv does not increase along the length of the cable, in fact blue phase THDv reduces. The maximum THDv on yellow phase increases to 2.24% as shown in Figure 4.2.2.3. This presents an increase of 0.07% when compared to Figure 4.2.1.3, therefore this is the additional effect of the two-phase fault on feeder two. Additionally, when compared to Figure 4.2.2.1, the yellow phase THDv increased by 0.74%.

**Table 4.2.2.2: Table of harmonics on feeder one for a two-phase fault with an EVC penetration of 31.2% whilst a two-phase fault is present on feeder two against the limits set out in ER G5/5 (Energy Networks Association, 2020).**

| Harmonic Number | Worst Case Voltage Harmonic Magnitude at Supply Terminals (%) | Worst Case Voltage Harmonic Magnitude at Transformer (%) | ER G5/5 Limits (%) | Worst Case Phase Current Harmonic Magnitude at Transformer (A) | Neutral Harmonic Current Magnitude at Transformer (A) |
|---|---|---|---|---|---|
| 2nd | 0.05 | 0.05 | 1.60 | 0.34 | 0.29 |
| 3rd | 0.86 | 0.73 | 4.00 | 8.35 | 6.88 |
| 4th | 0.02 | 0.02 | 1.00 | 0.10 | 0.09 |
| 5th | 0.77 | 0.67 | 4.00 | 4.87 | 3.88 |
| 6th | 0.03 | 0.03 | 0.50 | 0.14 | 0.12 |
| 7th | 1.01 | 0.94 | 4.00 | 4.53 | 3.51 |
| 8th | 0.02 | 0.02 | 0.40 | 0.09 | 0.07 |
| 9th | 0.42 | 0.33 | 1.20 | 2.52 | 1.90 |
| 10th | 0.03 | 0.03 | 0.40 | 0.14 | 0.10 |
| 11th | 0.66 | 0.60 | 3.00 | 2.70 | 1.98 |
| 12th | 0.03 | 0.03 | 0.20 | 0.13 | 0.10 |
| 13th | 0.71 | 0.59 | 2.50 | 2.85 | 2.03 |
| 14th | 0.03 | 0.03 | 0.20 | 0.13 | 0.09 |
| 15th | 0.33 | 0.25 | 0.50 | 1.43 | 0.99 |
| 16th | 0.07 | 0.06 | 0.20 | 0.29 | 0.20 |
| 17th | 0.31 | 0.22 | 1.60 | 1.33 | 0.90 |
| 18th | 0.07 | 0.05 | 0.20 | 0.27 | 0.18 |
| 19th | 0.35 | 0.25 | 1.50 | 1.30 | 0.86 |
| 20th | 0.01 | 0.02 | 0.20 | 0.07 | 0.05 |
| 21st | 0.21 | 0.15 | 0.20 | 0.74 | 0.48 |
| 22nd | 0.01 | 0.01 | 0.20 | 0.07 | 0.05 |
| 23rd | 0.27 | 0.19 | 1.20 | 0.92 | 0.60 |
| 24th | 0.01 | 0.01 | 0.20 | 0.03 | 0.02 |
| 25th | 0.18 | 0.13 | 1.00 | 0.56 | 0.35 |
| 26th | 0.01 | 0.01 | 0.20 | 0.03 | 0.02 |
| 27th | 0.21 | 0.15 | 0.20 | 0.63 | 0.40 |
| 28th | 0.01 | 0.01 | 0.20 | 0.03 | 0.02 |
| 29th | 0.21 | 0.14 | 0.86 | 0.60 | 0.38 |
| 30th | 0.00 | 0.00 | 0.20 | 0.00 | 0.00 |
| 31st | 0.22 | 0.15 | 0.81 | 0.58 | 0.36 |
| 33rd | 0.18 | 0.13 | 0.20 | 0.46 | 0.29 |
| 35th | 0.19 | 0.13 | 0.71 | 0.45 | 0.28 |
| 37th | 0.15 | 0.10 | 0.68 | 0.34 | 0.22 |
| 39th | 0.16 | 0.11 | 0.20 | 0.33 | 0.21 |
| 41st | 0.11 | 0.08 | 0.61 | 0.24 | 0.15 |
| 43rd | 0.12 | 0.08 | 0.58 | 0.23 | 0.15 |
| 45th | 0.12 | 0.08 | 0.20 | 0.22 | 0.14 |
| 47th | 0.08 | 0.05 | 0.53 | 0.14 | 0.09 |
| 49th | 0.08 | 0.05 | 0.51 | 0.14 | 0.09 |
| Harmonics higher than the limits set by ER G5/5 | | | | | |
| Harmonics on the boundary of the limits set by ER G5/5 | | | | | |
| Harmonics higher than the result from 98.4% EVC penetration | | | | | |
| Number of PVs on Feeder 1: 18 Number of PVs on Feeder 2: 21 Voltage on Neutral: 5.263V | | | | | |

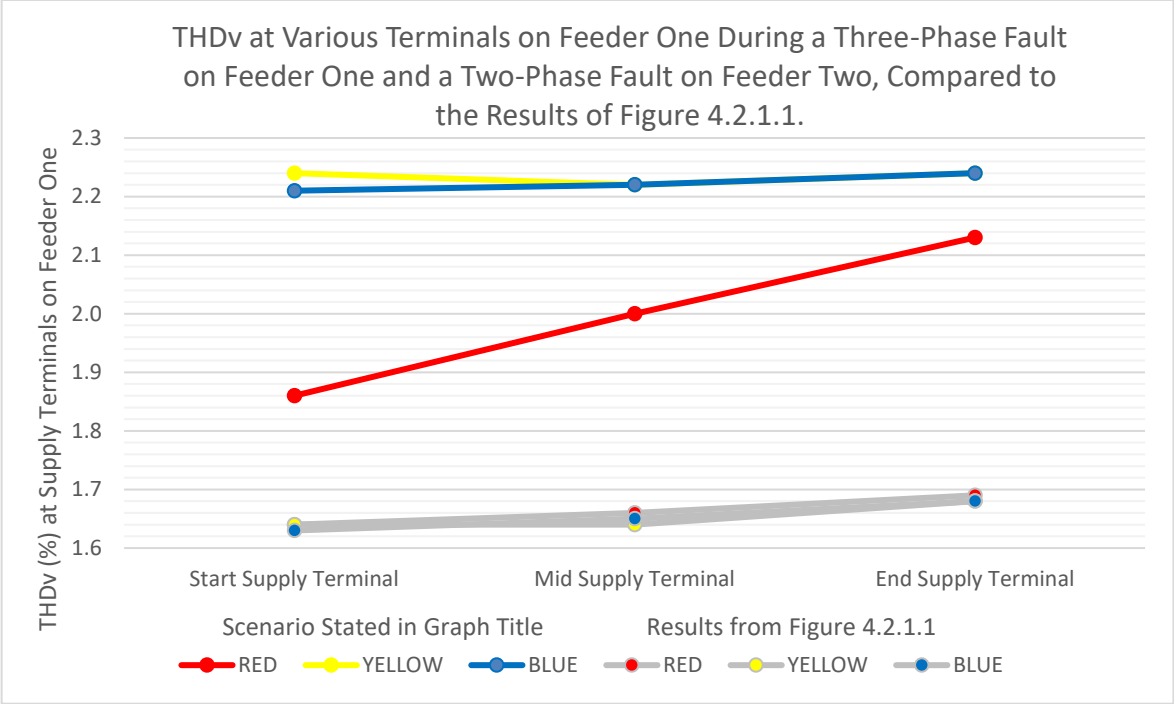


**Figure 4.2.2.3: Graphical representation of the THDv measured on each phase at supply terminals at the start, middle and end of feeder one during a three-phase fault at 31.2% EVC penetration whilst a two-phase fault is present on feeder two, compared to normal running arrangements on feeders one and two (Figure 4.2.1.1).**

Further to this, ER G5/5 limits have been exceeded on the 21$^{st}$ and 27$^{th}$ harmonic orders and met on the 33$^{rd}$ harmonic order. This is the same as Table 4.2.1.3, however, the effect of the two-phase fault on feeder two leads to an increase in harmonic distortion of 0.01% for the 21$^{st}$ harmonic. In addition, the tipping point for this particular three-phase fault to remain compliant with ER G5/5 was identified. It was found that a penetration of 21.6% allowed the EDN to remain compliant. This penetration value represents an EVC number of twenty-seven evenly distributed amongst the three phases, twelve on feeder one and fifteen on feeder two. This level of penetration was required to reduce the 21$^{st}$ and 27$^{th}$ harmonics to or below the 0.2% harmonic limit. This is a reduction from the 26.4% EVC penetration which remained compliant under ER G5/5 shown in Table 4.2.1.3.

The neutral voltage also increases to 7.968V in Table 4.2.2.3 from 6.971V in Table 4.2.1.3. Despite this increase, the neutral voltage is high enough to cause shocks, but not high enough to cause ventricular fibrillation or respiratory tetanus.

**Table 4.2.2.3: Table of harmonics on feeder one for a three-phase fault with an EVC penetration of 31.2% whilst a two-phase fault is present on feeder two against the limits set out in ER G5/5 (Energy Networks Association, 2020).**

| Harmonic Number | Worst Case Voltage Harmonic Magnitude at Supply Terminals (%) | Worst Case Voltage Harmonic Magnitude at Transformer (%) | ER G5/5 Limits (%) | Worst Case Phase Current Harmonic Magnitude at Transformer (A) | Neutral Harmonic Current Magnitude at Transformer (A) |
|---|---|---|---|---|---|
| 2nd | 0.05 | 0.05 | 1.60 | 0.41 | 0.36 |
| 3rd | 0.96 | 0.77 | 4.00 | 9.97 | 8.72 |
| 4th | 0.02 | 0.02 | 1.00 | 0.12 | 0.11 |
| 5th | 0.85 | 0.70 | 4.00 | 5.76 | 4.92 |
| 6th | 0.03 | 0.03 | 0.50 | 0.17 | 0.14 |
| 7th | 1.05 | 0.95 | 4.00 | 5.29 | 4.41 |
| 8th | 0.02 | 0.02 | 0.40 | 0.11 | 0.09 |
| 9th | 0.48 | 0.35 | 1.20 | 2.91 | 2.37 |
| 10th | 0.03 | 0.03 | 0.40 | 0.16 | 0.13 |
| 11th | 0.68 | 0.60 | 3.00 | 3.07 | 2.43 |
| 12th | 0.02 | 0.03 | 0.20 | 0.15 | 0.12 |
| 13th | 0.76 | 0.60 | 2.50 | 3.20 | 2.48 |
| 14th | 0.02 | 0.02 | 0.20 | 0.14 | 0.11 |
| 15th | 0.37 | 0.26 | 0.50 | 1.59 | 1.20 |
| 16th | 0.08 | 0.06 | 0.20 | 0.32 | 0.24 |
| 17th | 0.35 | 0.23 | 1.60 | 1.45 | 1.07 |
| 18th | 0.08 | 0.05 | 0.20 | 0.29 | 0.21 |
| 19th | 0.39 | 0.26 | 1.50 | 1.40 | 1.00 |
| 20th | 0.01 | 0.01 | 0.20 | 0.08 | 0.06 |
| 21st | 0.23 | 0.15 | 0.20 | 0.79 | 0.55 |
| 22nd | 0.01 | 0.01 | 0.20 | 0.08 | 0.05 |
| 23rd | 0.30 | 0.19 | 1.20 | 0.98 | 0.66 |
| 24th | 0.01 | 0.01 | 0.20 | 0.04 | 0.02 |
| 25th | 0.20 | 0.13 | 1.00 | 0.59 | 0.39 |
| 26th | 0.01 | 0.01 | 0.20 | 0.03 | 0.02 |
| 27th | 0.23 | 0.15 | 0.20 | 0.66 | 0.43 |
| 28th | 0.01 | 0.01 | 0.20 | 0.03 | 0.02 |
| 29th | 0.23 | 0.15 | 0.86 | 0.62 | 0.39 |
| 30th | 0.00 | 0.00 | 0.20 | 0.00 | 0.00 |
| 31st | 0.24 | 0.15 | 0.81 | 0.60 | 0.37 |
| 33rd | 0.20 | 0.13 | 0.20 | 0.47 | 0.28 |
| 35th | 0.20 | 0.13 | 0.71 | 0.45 | 0.27 |
| 37th | 0.16 | 0.11 | 0.68 | 0.35 | 0.20 |
| 39th | 0.17 | 0.11 | 0.20 | 0.33 | 0.19 |
| 41st | 0.12 | 0.08 | 0.61 | 0.24 | 0.13 |
| 43rd | 0.12 | 0.08 | 0.58 | 0.23 | 0.12 |
| 45th | 0.12 | 0.08 | 0.20 | 0.22 | 0.12 |
| 47th | 0.08 | 0.05 | 0.53 | 0.14 | 0.07 |
| 49th | 0.08 | 0.05 | 0.51 | 0.14 | 0.07 |
| Harmonics higher than the limits set by ER G5/5 | | | | | |
| Harmonics on the boundary of the limits set by ER G5/5 | | | | | |
| Harmonics higher than the result from 98.4% EVC penetration | | | | | |
| Number of PVs on Feeder 1: 18 Number of PVs on Feeder 2: 21 Voltage on Neutral: 7.968V | | | | | |

### 4.2.3 – Results of Phase-to-Phase Faults, with a Three-Phase Fault on Feeder Two

Further to Sections 4.2.1 and 4.2.2, the effect of faults on feeder one will be explored whilst a second three-phase fault on feeder two is present. Similar to Figure 4.2.2.1 it can be seen in Figure 4.2.3.1 that there is a marked drop in THDv on the yellow phase and marked increase in THDv on the red phase when compared to Figure 4.2.1.1. Additionally, there is also a drop in the THDv on the blue phase. This is due to load being removed from the yellow and blue phases and added to the red phase via a three-phase fault on feeder two. Considering the calculations for harmonic voltage drop explained in Section 1.2.1 explains the difference in THDv. Due to the current being drawn on feeder one remaining the same, the increase in THDv between the beginning and the end of feeder one remains at 0.03-0.04%, similar to Figure 4.2.1.1. The individual harmonic levels can be seen in Table 4.2.3.1 and it can be seen that there are no breaches of harmonic limits on feeder one under ER G5/5. Despite the three-phase fault on feeder two leading to the neutral voltage increasing from 0.540V to 2.403V, the voltage does not exceed 2.70V on feeder one and therefore, should not be high enough to cause perceived shocks to residents. However, based on the results of Table 4.2.1.2, it is likely that residents will receive shocks off of feeder two.

The tipping point for this scenario with normal running arrangements on feeder one to remain compliant with ER G5/5 was identified. It was found that a penetration of 31.2% allowed the EDN to remain compliant on feeder one. The THDv of this penetration level can be seen in Figure 4.2.3.1 and Table 4.2.3.1. This relates to an EVC number of thirty-nine evenly distributed amongst three phases, eighteen on feeder one and twenty-one on feeder two. This level of penetration was required to keep the 21$^{st}$ and 27$^{th}$ harmonics to or below the 0.2% harmonic limit on feeder one. This is lower than normal arrangements under Section 4.2.1 which allowed an EVC penetration of 60% and two-phase fault arrangements under Section 4.2.2 which allowed an EVC penetration of 50.4%. Therefore, the three-phase fault on feeder two reduced the number of EVCs which can be connected to the network by thirty-six or twenty-four for Sections 4.2.1 and 4.2.2 respectively.

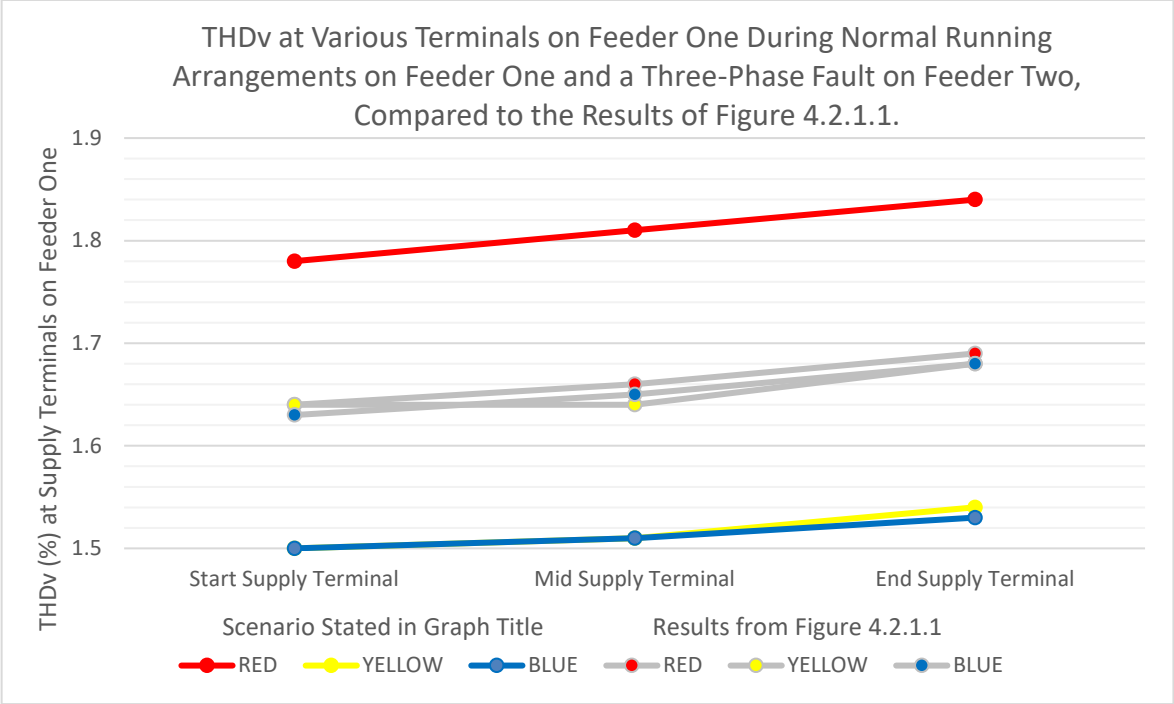


**Figure 4.2.3.1: Graphical representation of the THDv measured on each phase at supply terminals at the start, middle and end of feeder one under normal running arrangements at 31.2% EVC penetration whilst a three-phase fault is present on feeder two, compared to normal running arrangements on feeders one and two (Figure 4.2.1.1).**

By introducing a two-phase fault between red and yellow phases on feeder one, with red phase feeding the fault as seen in Figure 4.2.3.2, similar to Figures 4.2.1.2 and 4.2.2.2, it has been found that the THDv increases significantly along the length of feeder one on red phase, with the THDv also increasing slightly on yellow phase as the current travels from the pot end back towards the transformer. This leads to the THDv measured on the yellow phase supply terminal at the start of the network rising from 1.50% to 2.12%, an increase of 0.62%. There is no noticeable effect on the blue phase THDv when compared to Figure 4.2.3.1 which is excluded from the faulted phases. The THDv of yellow phase is 0.12% higher than the same scenario without the three-phase fault on feeder two, and 0.07% higher than the same scenario with a two-phase fault on feeder two.

**Table 4.2.3.1: Table of harmonics on feeder one for normal running arrangements with an EVC penetration of 31.2% whilst a three-phase fault is present on feeder two against the limits set out in ER G5/5 (Energy Networks Association, 2020).**

| Harmonic Number | Worst Case Voltage Harmonic Magnitude at Supply Terminals (%) | Worst Case Voltage Harmonic Magnitude at Transformer (%) | ER G5/5 Limits (%) | Worst Case Phase Current Harmonic Magnitude at Transformer (A) | Neutral Harmonic Current Magnitude at Transformer (A) |
|---|---|---|---|---|---|
| 2nd | 0.05 | 0.05 | 1.60 | 0.34 | 0.27 |
| 3rd | 0.77 | 0.74 | 4.00 | 8.47 | 6.41 |
| 4th | 0.02 | 0.02 | 1.00 | 0.10 | 0.08 |
| 5th | 0.70 | 0.68 | 4.00 | 4.93 | 3.73 |
| 6th | 0.03 | 0.03 | 0.50 | 0.15 | 0.11 |
| 7th | 0.96 | 0.94 | 4.00 | 4.58 | 3.49 |
| 8th | 0.02 | 0.02 | 0.40 | 0.10 | 0.07 |
| 9th | 0.35 | 0.33 | 1.20 | 2.53 | 1.91 |
| 10th | 0.03 | 0.03 | 0.40 | 0.14 | 0.10 |
| 11th | 0.61 | 0.60 | 3.00 | 2.71 | 2.05 |
| 12th | 0.03 | 0.03 | 0.20 | 0.13 | 0.10 |
| 13th | 0.62 | 0.59 | 2.50 | 2.84 | 2.14 |
| 14th | 0.03 | 0.03 | 0.20 | 0.13 | 0.09 |
| 15th | 0.27 | 0.25 | 0.50 | 1.42 | 1.06 |
| 16th | 0.06 | 0.06 | 0.20 | 0.29 | 0.21 |
| 17th | 0.24 | 0.22 | 1.60 | 1.31 | 0.97 |
| 18th | 0.05 | 0.05 | 0.20 | 0.26 | 0.20 |
| 19th | 0.27 | 0.25 | 1.50 | 1.27 | 0.94 |
| 20th | 0.02 | 0.02 | 0.20 | 0.07 | 0.05 |
| 21st | 0.16 | 0.15 | 0.20 | 0.72 | 0.53 |
| 22nd | 0.01 | 0.01 | 0.20 | 0.07 | 0.05 |
| 23rd | 0.20 | 0.18 | 1.20 | 0.90 | 0.66 |
| 24th | 0.01 | 0.01 | 0.20 | 0.03 | 0.02 |
| 25th | 0.14 | 0.13 | 1.00 | 0.55 | 0.40 |
| 26th | 0.01 | 0.01 | 0.20 | 0.03 | 0.02 |
| 27th | 0.16 | 0.14 | 0.20 | 0.61 | 0.45 |
| 28th | 0.01 | 0.01 | 0.20 | 0.03 | 0.02 |
| 29th | 0.16 | 0.14 | 0.86 | 0.58 | 0.42 |
| 30th | 0.00 | 0.00 | 0.20 | 0.00 | 0.00 |
| 31st | 0.16 | 0.15 | 0.81 | 0.56 | 0.40 |
| 33rd | 0.14 | 0.12 | 0.20 | 0.45 | 0.32 |
| 35th | 0.14 | 0.12 | 0.71 | 0.43 | 0.30 |
| 37th | 0.11 | 0.10 | 0.68 | 0.33 | 0.23 |
| 39th | 0.11 | 0.10 | 0.20 | 0.32 | 0.22 |
| 41st | 0.08 | 0.07 | 0.61 | 0.23 | 0.16 |
| 43rd | 0.08 | 0.08 | 0.58 | 0.22 | 0.15 |
| 45th | 0.09 | 0.08 | 0.20 | 0.21 | 0.14 |
| 47th | 0.06 | 0.05 | 0.53 | 0.14 | 0.09 |
| 49th | 0.06 | 0.05 | 0.51 | 0.13 | 0.09 |
| Harmonics higher than the limits set by ER G5/5 | | | | | |
| Harmonics on the boundary of the limits set by ER G5/5 | | | | | |
| Harmonics higher than the result from 98.4% EVC penetration | | | | | |
| Number of PVs on Feeder 1: 18 Number of PVs on Feeder 2: 21 Voltage on Neutral: 2.403V | | | | | |

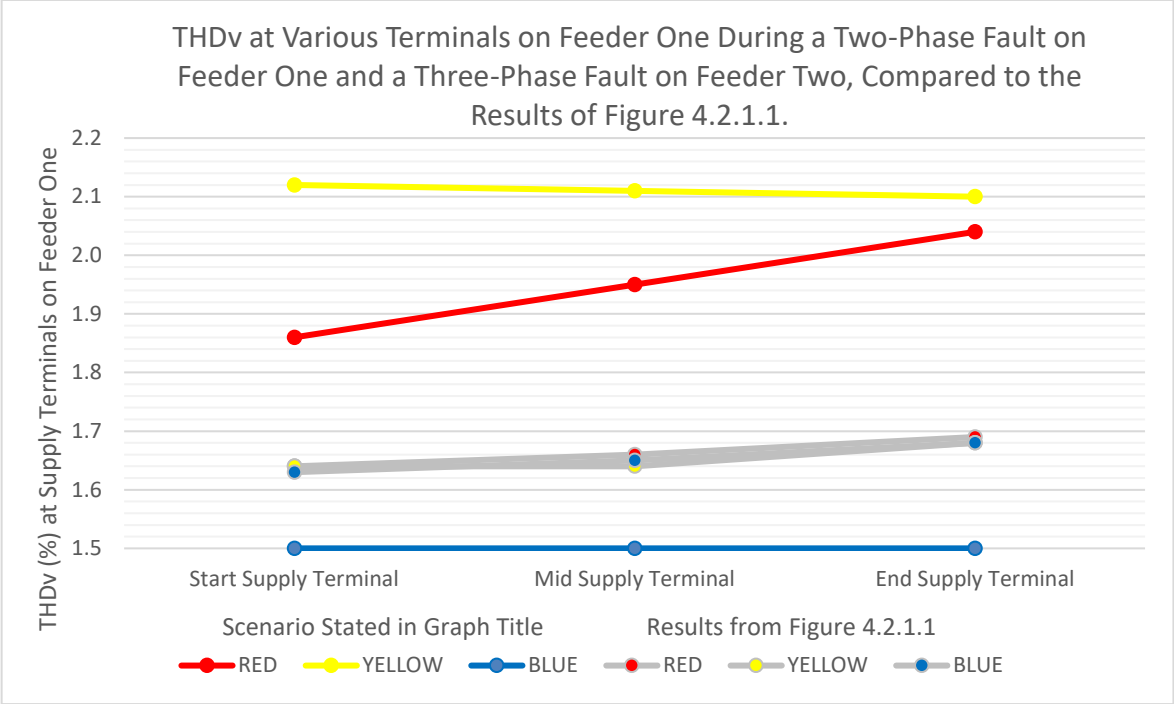


**Figure 4.2.3.2: Graphical representation of the THDv measured on each phase at supply terminals at the start, middle and end of feeder one during a two-phase fault at 31.2% EVC penetration whilst a three-phase fault is present on feeder two, compared to normal running arrangements on feeders one and two (Figure 4.2.1.1).**

The results of the worst-case harmonic distortion on feeder one under a two-phase fault can be seen in Table 4.2.3.2. The worst-case harmonic distortion was measured between phase and neutral on the yellow phase supply terminal at the start of feeder one as shown in Figure 4.2.3.2. It can be seen that limits under ER G5/5 are exceeded on the 21$^{st}$ and 27$^{th}$ harmonics. This matches the two-phase fault when compared to Table 4.2.2.2. The neutral voltage in Table 4.2.3.2 is also higher than the comparable neutral voltage in Table 4.2.2.2 at 5.787V and 5.263V respectively, therefore presenting an increase of 0.524V. Similar to Table 4.2.2.2, the neutral voltage is high enough to cause shocks, but not high enough to cause ventricular fibrillation or respiratory tetanus.

The tipping point for this particular two-phase fault EDN to remain compliant with ER G5/5 was identified. It was found that a penetration of 26.4% allowed the EDN to remain compliant. This penetration value is the same as the two-phase fault scenario presented in Figure 4.2.2.2.

**Table 4.2.3.2: Table of harmonics on feeder one for a two-phase fault with an EVC penetration of 31.2% whilst a three-phase fault is present on feeder two against the limits set out in ER G5/5 (Energy Networks Association, 2020).**

| Harmonic Number | Worst Case Voltage Harmonic Magnitude at Supply Terminals (%) | Worst Case Voltage Harmonic Magnitude at Transformer (%) | ER G5/5 Limits (%) | Worst Case Phase Current Harmonic Magnitude at Transformer (A) | Neutral Harmonic Current Magnitude at Transformer (A) |
|---|---|---|---|---|---|
| 2nd | 0.05 | 0.05 | 1.60 | 0.42 | 0.38 |
| 3rd | 0.91 | 0.77 | 4.00 | 10.22 | 9.08 |
| 4th | 0.02 | 0.02 | 1.00 | 0.12 | 0.11 |
| 5th | 0.81 | 0.70 | 4.00 | 5.90 | 5.14 |
| 6th | 0.03 | 0.03 | 0.50 | 0.17 | 0.15 |
| 7th | 1.02 | 0.95 | 4.00 | 5.43 | 4.64 |
| 8th | 0.02 | 0.02 | 0.40 | 0.11 | 0.10 |
| 9th | 0.45 | 0.35 | 1.20 | 2.98 | 2.49 |
| 10th | 0.03 | 0.03 | 0.40 | 0.16 | 0.13 |
| 11th | 0.66 | 0.60 | 3.00 | 3.14 | 2.58 |
| 12th | 0.02 | 0.03 | 0.20 | 0.15 | 0.12 |
| 13th | 0.72 | 0.60 | 2.50 | 3.27 | 2.62 |
| 14th | 0.02 | 0.02 | 0.20 | 0.14 | 0.11 |
| 15th | 0.35 | 0.26 | 0.50 | 1.62 | 1.27 |
| 16th | 0.07 | 0.06 | 0.20 | 0.33 | 0.25 |
| 17th | 0.32 | 0.24 | 1.60 | 1.48 | 1.13 |
| 18th | 0.07 | 0.05 | 0.20 | 0.29 | 0.22 |
| 19th | 0.36 | 0.26 | 1.50 | 1.42 | 1.07 |
| 20th | 0.01 | 0.01 | 0.20 | 0.08 | 0.06 |
| 21st | 0.21 | 0.19 | 0.20 | 0.80 | 0.58 |
| 22nd | 0.01 | 0.01 | 0.20 | 0.08 | 0.06 |
| 23rd | 0.27 | 0.19 | 1.20 | 0.99 | 0.71 |
| 24th | 0.01 | 0.01 | 0.20 | 0.04 | 0.03 |
| 25th | 0.18 | 0.13 | 1.00 | 0.60 | 0.42 |
| 26th | 0.01 | 0.01 | 0.20 | 0.03 | 0.02 |
| 27th | 0.21 | 0.15 | 0.20 | 0.67 | 0.46 |
| 28th | 0.01 | 0.01 | 0.20 | 0.03 | 0.02 |
| 29th | 0.21 | 0.15 | 0.86 | 0.63 | 0.42 |
| 30th | 0.00 | 0.00 | 0.20 | 0.00 | 0.00 |
| 31st | 0.22 | 0.15 | 0.81 | 0.61 | 0.39 |
| 33rd | 0.18 | 0.13 | 0.20 | 0.48 | 0.31 |
| 35th | 0.19 | 0.13 | 0.71 | 0.46 | 0.29 |
| 37th | 0.15 | 0.11 | 0.68 | 0.35 | 0.21 |
| 39th | 0.15 | 0.11 | 0.20 | 0.34 | 0.20 |
| 41st | 0.11 | 0.08 | 0.61 | 0.24 | 0.14 |
| 43rd | 0.11 | 0.08 | 0.58 | 0.23 | 0.13 |
| 45th | 0.11 | 0.08 | 0.20 | 0.22 | 0.12 |
| 47th | 0.08 | 0.05 | 0.53 | 0.14 | 0.08 |
| 49th | 0.08 | 0.05 | 0.51 | 0.14 | 0.07 |
| Harmonics higher than the limits set by ER G5/5 | | | | | |
| Harmonics on the boundary of the limits set by ER G5/5 | | | | | |
| Harmonics higher than the result from 98.4% EVC penetration | | | | | |
| Number of PVs on Feeder 1: 18 Number of PVs on Feeder 2: 21 Voltage on Neutral: 5.787V | | | | | |

During a three-phase fault, fed by red phase, as seen in Figure 4.2.3.3, the THDv increased further at the start, middle and end of the network on the red phase on feeder one. Similar to Figure 4.2.2.3, yellow and blue phase THDv does not increase along the length of the cable, in fact yellow and blue phase THDv reduces on feeder one. The maximum THDv on yellow phase increases to 2.29% as shown in Figure 4.2.2.3. This presents an increase of 0.12% when compared to Figure 4.2.1.3, and 0.05% when compared to Figure 4.2.2.3 and therefore is the additional effect of the three-phase fault on feeder two. Additionally, when compared to Figure 4.2.3.1, the yellow phase THDv at the start of feeder one increased by 0.78%.

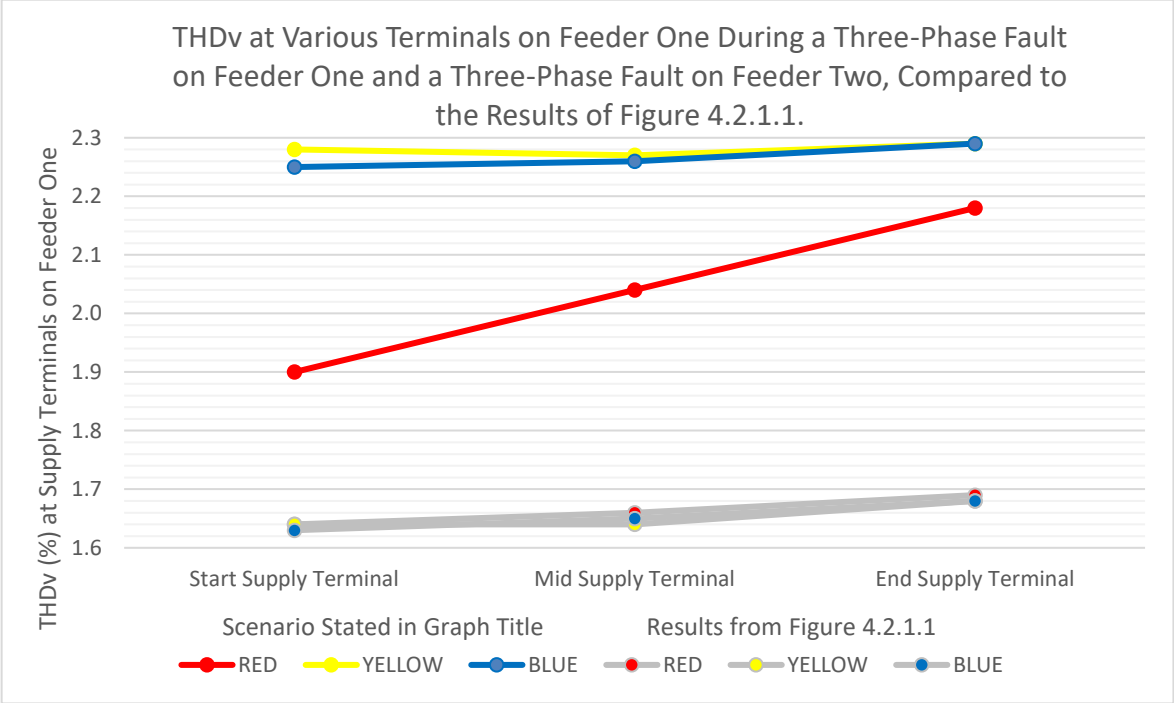


**Figure 4.2.3.3: Graphical representation of the THDv measured on each phase at supply terminals at the start, middle and end of feeder one during a three-phase fault at 31.2% EVC penetration whilst a three-phase fault is present on feeder two, compared to normal running arrangements on feeders one and two (Figure 4.2.1.1).**

Further to this, ER G5/5 limits on feeder one have been exceeded on the 21st and 27th harmonic orders and met on the 33rd harmonic order. This is the same as Tables 4.2.1.3 and 4.2.2.3, however, the effect of the three-phase fault on feeder two leads to an increase in harmonic distortion of 0.01% for the 21st harmonic over Table 4.2.1.3. In addition, the tipping point for this particular three-phase fault to remain compliant with ER G5/5 was identified. It was found that a penetration of 21.6% allowed feeder one to remain compliant. This penetration value represents an EVC number of twenty-seven evenly distributed amongst the three phases, twelve on feeder one and fifteen on feeder two. This level of penetration was required to reduce the 21st and 27th harmonics to or below the 0.2% harmonic limit. This is a reduction from the 26.4% EVC penetration which remained compliant under ER G5/5 shown in Table 4.2.1.3, however, is identical to the maximum compliant penetration for Table 4.2.2.3.

The neutral voltage also increases to 8.912V in Table 4.2.3.3 from 7.968V in Table 4.2.2.3. Despite this, the increase in the neutral voltage is high enough to cause shocks, but not high enough to cause ventricular fibrillation or respiratory tetanus.

**Table 4.2.3.3: Table of harmonics on feeder one for a three-phase fault with an EVC penetration of 31.2% whilst a three-phase fault is present on feeder two against the limits set out in ER G5/5 (Energy Networks Association, 2020)**

| Harmonic Number | Worst Case Voltage Harmonic Magnitude at Supply Terminals (%) | Worst Case Voltage Harmonic Magnitude at Transformer (%) | ER G5/5 Limits (%) | Worst Case Phase Current Harmonic Magnitude at Transformer (A) | Neutral Harmonic Current Magnitude at Transformer (A) |
|---|---|---|---|---|---|
| 2nd | 0.05 | 0.05 | 1.60 | 0.48 | 0.48 |
| 3rd | 1.02 | 0.81 | 4.00 | 11.80 | 11.80 |
| 4th | 0.02 | 0.02 | 1.00 | 0.14 | 0.14 |
| 5th | 0.88 | 0.73 | 4.00 | 6.75 | 6.75 |
| 6th | 0.03 | 0.03 | 0.50 | 0.20 | 0.20 |
| 7th | 1.06 | 0.96 | 4.00 | 6.13 | 6.13 |
| 8th | 0.02 | 0.02 | 0.40 | 0.13 | 0.13 |
| 9th | 0.50 | 0.37 | 1.20 | 3.33 | 3.33 |
| 10th | 0.03 | 0.03 | 0.40 | 0.18 | 0.18 |
| 11th | 0.68 | 0.59 | 3.00 | 3.47 | 3.47 |
| 12th | 0.02 | 0.02 | 0.20 | 0.17 | 0.17 |
| 13th | 0.77 | 0.61 | 2.50 | 3.57 | 3.57 |
| 14th | 0.02 | 0.02 | 0.20 | 0.15 | 0.15 |
| 15th | 0.38 | 0.27 | 0.50 | 1.74 | 1.74 |
| 16th | 0.08 | 0.06 | 0.20 | 0.35 | 0.35 |
| 17th | 0.36 | 0.24 | 1.60 | 1.58 | 1.58 |
| 18th | 0.08 | 0.05 | 0.20 | 0.31 | 0.31 |
| 19th | 0.39 | 0.27 | 1.50 | 1.51 | 1.51 |
| 20th | 0.01 | 0.01 | 0.20 | 0.09 | 0.09 |
| 21st | 0.23 | 0.16 | 0.20 | 0.84 | 0.84 |
| 22nd | 0.01 | 0.01 | 0.20 | 0.08 | 0.08 |
| 23rd | 0.30 | 0.20 | 1.20 | 1.04 | 1.04 |
| 24th | 0.01 | 0.01 | 0.20 | 0.04 | 0.04 |
| 25th | 0.20 | 0.13 | 1.00 | 0.62 | 0.62 |
| 26th | 0.01 | 0.01 | 0.20 | 0.04 | 0.04 |
| 27th | 0.23 | 0.15 | 0.20 | 0.69 | 0.69 |
| 28th | 0.00 | 0.01 | 0.20 | 0.03 | 0.03 |
| 29th | 0.23 | 0.15 | 0.86 | 0.65 | 0.65 |
| 30th | 0.00 | 0.00 | 0.20 | 0.00 | 0.00 |
| 31st | 0.24 | 0.16 | 0.81 | 0.62 | 0.62 |
| 33rd | 0.20 | 0.13 | 0.20 | 0.49 | 0.49 |
| 35th | 0.20 | 0.13 | 0.71 | 0.47 | 0.47 |
| 37th | 0.16 | 0.11 | 0.68 | 0.36 | 0.36 |
| 39th | 0.16 | 0.11 | 0.20 | 0.34 | 0.34 |
| 41st | 0.12 | 0.08 | 0.61 | 0.24 | 0.24 |
| 43rd | 0.12 | 0.08 | 0.58 | 0.23 | 0.23 |
| 45th | 0.12 | 0.08 | 0.20 | 0.22 | 0.22 |
| 47th | 0.08 | 0.05 | 0.53 | 0.14 | 0.14 |
| 49th | 0.08 | 0.05 | 0.51 | 0.14 | 0.14 |
| Harmonics higher than the limits set by ER G5/5 | | | | | |
| Harmonics on the boundary of the limits set by ER G5/5 | | | | | |
| Harmonics higher than the result from 98.4% EVC penetration | | | | | |
| Number of PVs on Feeder 1: 18 Number of PVs on Feeder 2: 21 Voltage on Neutral: 8.912V | | | | | |

## 4.2.4 – Maximum Penetration and Overall Results

To summarise the results from Sections 4.2.1-3, Figure 4.2.4.1 has been produced. The results of maximum THDv measured at customer terminals on feeder one with an EVC penetration of 31.2% and the maximum EVC penetration on feeder one to remain compliant with ER G5/5 under different running arrangements can be seen in Figure 4.2.4.1. The blue/grey lines and left-hand y-axis refers to the maximum THDv. The orange/yellow/green lines and right-hand y-axis refers to the maximum EVC penetration. It should be noted that although trends may be similar across all networks, these results are specific to the case study network and harmonic profiles used.

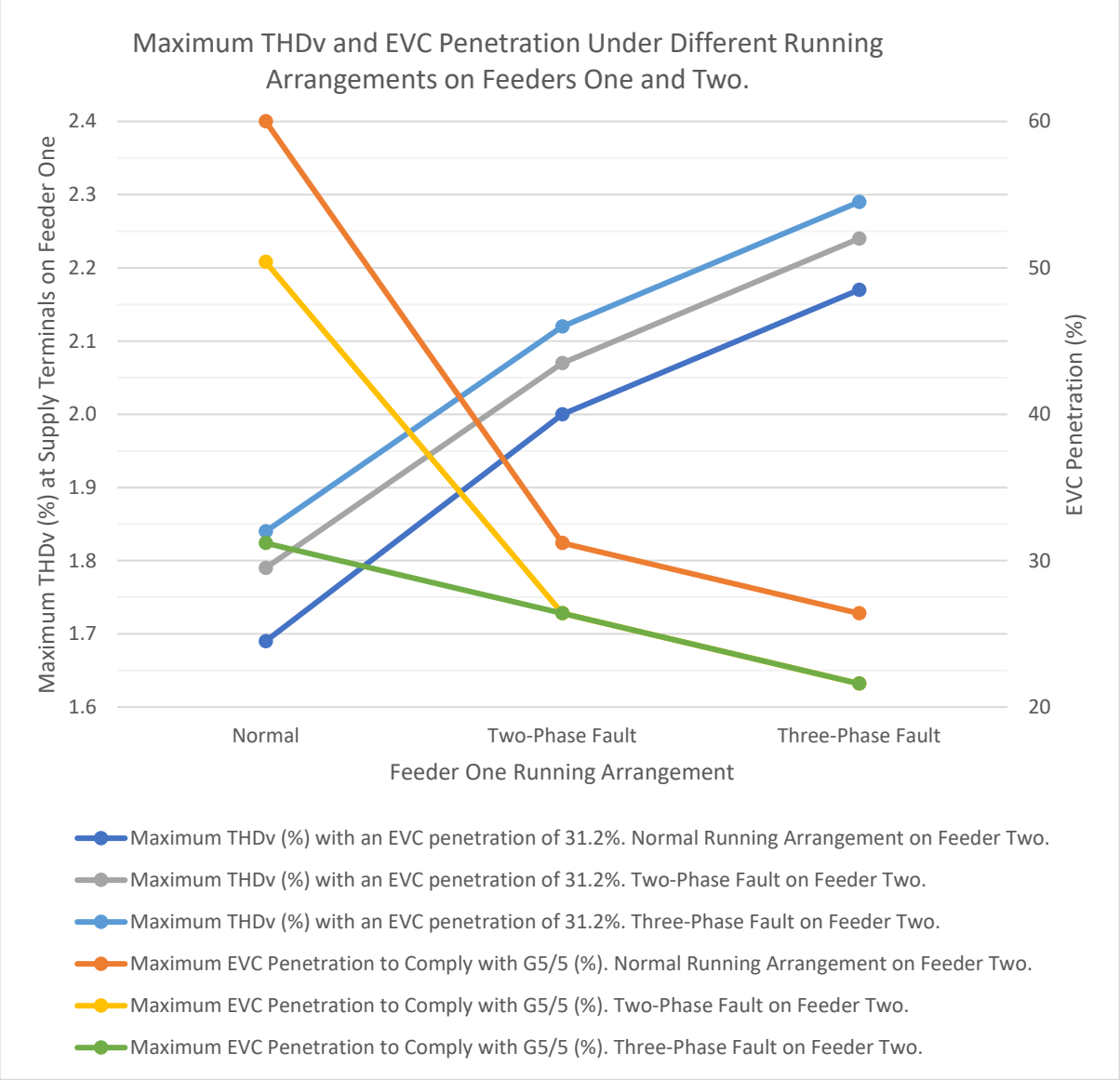


**Figure 4.2.4.1: Maximum THDv measured at customer terminals on feeder one with an EVC penetration of 31.2% and maximum EVC penetration to remain compliant with ER G5/5 under different running arrangements on feeders one and two.**

It can be seen from Figure 4.2.4.1 that for normal conditions on feeder two, the maximum THDv increases from 1.69% to 2.17% on feeder one (an increase of 0.48%) when comparing normal conditions and a three-phase fault on feeder one. For a three-phase fault on feeder two, the maximum THDv increases from 1.84% to 2.29% on feeder one (an increase of 0.45%) when comparing normal conditions and a three-phase fault on feeder one. For faults on feeder two, the increase in THDv stays consistent, but is stepped up.

More important is the maximum EVC penetration permissible to ensure compliance with ER G5/5. It can be seen in Figure 4.2.4.1 that for normal conditions on feeder two, the maximum EVC penetration decreases from 60% to 26.4% on feeder one (a decrease of 33.6%) when comparing normal conditions and a three-phase fault on feeder one. For a three-phase fault on feeder two, the maximum EVC penetration decreases from 31.2% to 21.6% on feeder one (a decrease of 9.6%) when comparing normal conditions and a three-phase fault on feeder one.

The reason for differences in maximum penetration is due to the limiting harmonics. These are the 21$^{st}$ and 27$^{th}$ harmonics as defined by ER G5/5 which are limited to 0.2%. These harmonics are met in the most part due to the number of EVCs effectively connected to the same phase. This is due to the harmonic contributions compounding when connected to the same phase.

Based on the results of Sections 4.2.1-3, the limiting harmonics, both the 21$^{st}$ and 27$^{th}$ increase during phase-to-phase conditions on both feeder one and feeder two. Tables 4.2.4.1-2 summarises the increases in these limiting harmonics under the conditions covered in Sections 4.2.1-3. It can be seen that generally, a fault on feeder one, has a much greater effect on the 21$^{st}$ and 27$^{th}$ voltage harmonic on feeder one, than a fault on feeder two, which would be expected. Additionally, as faults compound, for example, for a two-phase fault to a three-phase fault on feeder one, or a two-phase fault on feeder one, compounding with a two-phase fault on feeder two, the percentage increase in the voltage harmonic magnitude is not as significant as the first fault. Therefore, as faults compound, the impact of any one fault on the 21$^{st}$ and 27$^{th}$ voltage harmonic magnitude reduces. The first fault always produces the most the impact.

**Table 4.2.4.1: Increase in 21st and 27th voltage harmonic magnitude measured on feeder one between normal and phase-to-phase fault arrangements on feeder one for varying network arrangements on feeder two with an EVC penetration of 31.2%.**

| Increase in 21st and 27th voltage harmonic magnitude on feeder one under specified conditions measured at the point of highest THDv. | | Feeder One | |
|---|---|---|---|
| | | Normal Arrangements to Two-Phase Fault | Normal Arrangements to Three-Phase Fault |
| Feeder Two | Normal Arrangements | 43% | 57-64% |
| | Two-Phase Fault Arrangements | 40% | 53% |
| | Three-Phase Fault Arrangements | 31% | 44% |

**Table 4.2.4.2: Increase in 21st and 27th voltage harmonic magnitude measured on feeder one between normal and phase-to-phase fault arrangements on feeder two for varying network arrangements on feeder one with an EVC penetration of 31.2%.**

| Increase in 21st and 27th voltage harmonic magnitude on feeder one under specified conditions measured at the point of highest THDv. | | Feeder Two | |
|---|---|---|---|
| | | Normal Arrangements to Two-Phase Fault | Normal Arrangements to Three-Phase Fault |
| Feeder One | Normal Arrangements | 7% | 15% |
| | Two-Phase Fault Arrangements | 5% | 5% |
| | Three-Phase Fault Arrangements | 0-5% | 0-5% |

This data can be used by DNOs to indicate the maximum allowable numbers of EVCs which can be connected to an LV network under different conditions. Data showing this relationship has not been published previously. This provides niche and novel data which will aid with network planning and determine the actions taken by a DNO following a fault to remain compliant with ER G5/5.

Lastly, although the neutral voltage rose high enough to cause residents to perceive shocks off exposed bonded metalwork it was not high enough to cause ventricular fibrillation or respiratory tetanus. This, however, should not be ignored simply because the voltage does not pose a risk to life. Despite this not being the core focus of this thesis, the neutral voltages, and the potential risk of causing harm to residents should be taken seriously. Therefore, neutral voltages should be monitored by a DNO following a two-phase or three-phase fault on a PME EDN. Should the voltages exceed 2.70V, remedial action should be taken to reduce the voltage. This should be the repair of the fault to rebalance the network.

## 4.2.5 – Results of Open Circuit Faults

Figure 4.2.5.1 shows the effect that a backfed three-phase open circuit fault at the beginning of feeder one, has on the harmonic distortion of the supply terminals along the network. In this case, the link box outside number eighty-two is used to backfeed the network so that supplies are restored. Therefore, all the current for feeder one is diverted along feeder two. Although the THDv does increase along the feeder under this scenario, it does not increase significantly beyond the values of the end supply terminal on feeder one under normal running arrangements. Using Figure 4.2.1.1 it can be seen that at the end supply terminal on feeder one under normal running arrangements with an EVC penetration of 31.2% leads to the THDv sitting at 1.68-1.69%. It is assumed that under this open circuit scenario with the same EVC penetration, that a worst case THDv of 1.70-1.75% will not pose any additional issues. The harmonic boundary for a two-phase scenario seems to be around 2.00% THDv as per Figure 4.2.1.2. This is corroborated by Table 4.2.5.1 as no harmonic limits are exceeded. Additionally, due to the balanced nature of the network, neutral voltage of 0.533V does not present any safety concerns.

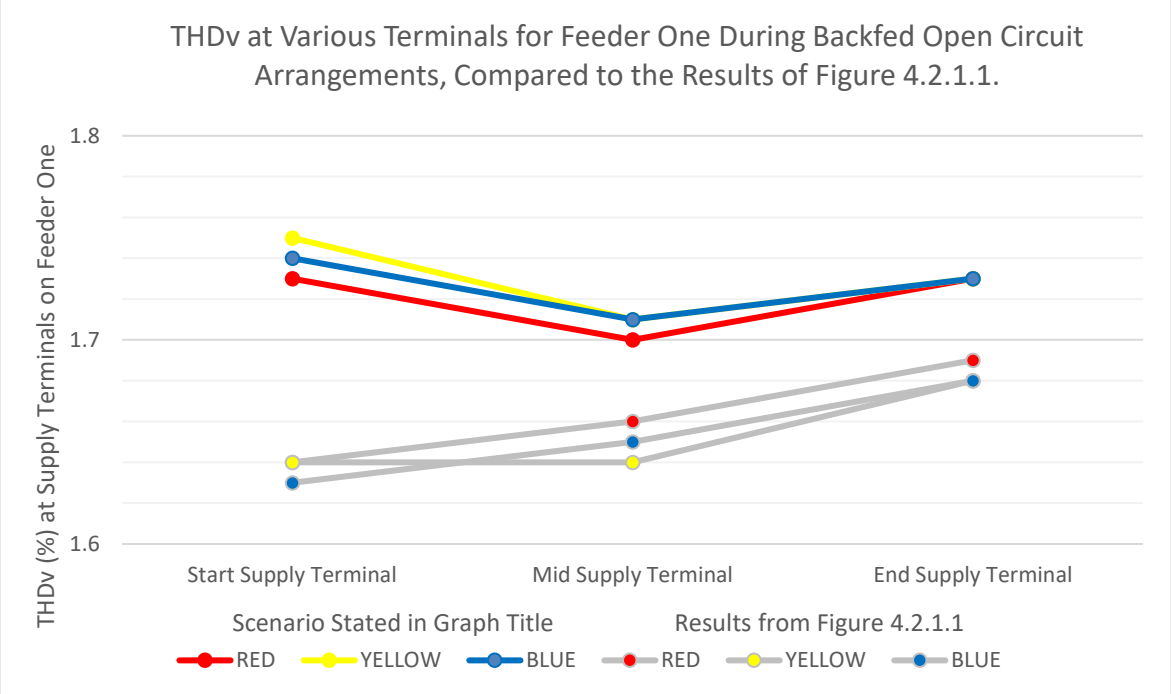


**Figure 4.2.5.1: Graphical representation of the THDv measured on each phase at supply terminals at the beginning, middle and end of the circuit during a backfed three-phase open circuit fault at 31.2% EVC penetration, compared to normal running arrangements on feeders one and two (Figure 4.2.1.1).**

**Table 4.2.5.1: Table of harmonics on feeder one during a backfed three-phase open circuit arrangement with an EVC penetration of 31.2% against the limits set out in ER G5/5 (Energy Networks Association, 2020).**

| Harmonic Number | Worst Case Voltage Harmonic Magnitude at Supply Terminals (%) | Worst Case Voltage Harmonic Magnitude at Transformer (%) | ER G5/5 Limits (%) | Worst Case Phase Current Harmonic Magnitude at Transformer (A) | Neutral Harmonic Current Magnitude at Transformer (A) |
|---|---|---|---|---|---|
| 2nd | 0.04 | 0.04 | 1.60 | 0.17 | 0.02 |
| 3rd | 0.70 | 0.65 | 4.00 | 4.37 | 0.01 |
| 4th | 0.02 | 0.02 | 1.00 | 0.05 | 0.01 |
| 5th | 0.65 | 0.61 | 4.00 | 2.57 | 0.01 |
| 6th | 0.03 | 0.03 | 0.50 | 0.07 | 0.01 |
| 7th | 0.94 | 0.91 | 4.00 | 2.43 | 0.01 |
| 8th | 0.02 | 0.02 | 0.40 | 0.05 | 0.00 |
| 9th | 0.31 | 0.27 | 1.20 | 1.38 | 0.00 |
| 10th | 0.03 | 0.03 | 0.40 | 0.07 | 0.00 |
| 11th | 0.61 | 0.58 | 3.00 | 1.51 | 0.00 |
| 12th | 0.03 | 0.03 | 0.20 | 0.07 | 0.00 |
| 13th | 0.60 | 0.54 | 2.50 | 1.64 | 0.00 |
| 14th | 0.03 | 0.03 | 0.20 | 0.07 | 0.00 |
| 15th | 0.24 | 0.20 | 0.50 | 0.85 | 0.00 |
| 16th | 0.06 | 0.05 | 0.20 | 0.17 | 0.00 |
| 17th | 0.21 | 0.17 | 1.60 | 0.81 | 0.00 |
| 18th | 0.05 | 0.04 | 0.20 | 0.16 | 0.00 |
| 19th | 0.25 | 0.20 | 1.50 | 0.81 | 0.00 |
| 20th | 0.02 | 0.02 | 0.20 | 0.05 | 0.00 |
| 21st | 0.15 | 0.12 | 0.20 | 0.47 | 0.00 |
| 22nd | 0.02 | 0.02 | 0.20 | 0.05 | 0.00 |
| 23rd | 0.18 | 0.14 | 1.20 | 0.61 | 0.00 |
| 24th | 0.01 | 0.01 | 0.20 | 0.02 | 0.00 |
| 25th | 0.13 | 0.10 | 1.00 | 0.38 | 0.00 |
| 26th | 0.01 | 0.01 | 0.20 | 0.02 | 0.00 |
| 27th | 0.15 | 0.11 | 0.20 | 0.44 | 0.00 |
| 28th | 0.01 | 0.01 | 0.20 | 0.02 | 0.00 |
| 29th | 0.15 | 0.11 | 0.86 | 0.43 | 0.00 |
| 30th | 0.00 | 0.00 | 0.20 | 0.00 | 0.00 |
| 31st | 0.16 | 0.12 | 0.81 | 0.42 | 0.00 |
| 33rd | 0.14 | 0.10 | 0.20 | 0.34 | 0.00 |
| 35th | 0.14 | 0.10 | 0.71 | 0.33 | 0.00 |
| 37th | 0.12 | 0.09 | 0.68 | 0.26 | 0.00 |
| 39th | 0.12 | 0.09 | 0.20 | 0.26 | 0.00 |
| 41st | 0.09 | 0.06 | 0.61 | 0.19 | 0.00 |
| 43rd | 0.09 | 0.07 | 0.58 | 0.18 | 0.00 |
| 45th | 0.09 | 0.07 | 0.20 | 0.18 | 0.00 |
| 47th | 0.06 | 0.05 | 0.53 | 0.12 | 0.00 |
| 49th | 0.07 | 0.05 | 0.51 | 0.11 | 0.00 |
| Harmonics higher than the limits set by ER G5/5 | | | | | |
| Harmonics on the boundary of the limits set by ER G5/5 | | | | | |
| Harmonics higher than the result from 98.4% EVC penetration | | | | | |
| Number of PVs on Feeder 1: 18 Number of PVs on Feeder 2: 21 Voltage on Neutral: 0.533V | | | | | |

Following in the footsteps of Sections 4.2.2-3 which consider two-phase and three-phase faults on feeder two, a two-phase fault was modelled on feeder two at the same location as Sections 4.2.2-3 whilst also backfeeding the open-circuit fault at the start of feeder one via the linkbox. However, this resulted in 488.0A being drawn through a 315A fuse on feeder two at the LV cabinet. This type of fuse is the same class of fuse used in Beama (2022). Therefore, based on data published within Beama (2022) the 315A fuse should blow in approximately 6,000-8,000 seconds or 100-133 minutes. Additionally, this resulted in 403.0A flowing through 95mm Wavecon and 95mm Consac cable which is rated at 237A summer sustained as per Baker (2019). Therefore, an engineer would not make a conscious decision to configure the network in this way.

Additionally, a three-phase fault was modelled on feeder two whilst also backfeeding the open-circuit fault at the start of feeder one via the linkbox. This also resulted in a higher current flow at the 315A fuse on feeder two at the LV cabinet of 678.8A. Using data published within Beama (2022), this would result in the 315A fuse blowing in around 250 seconds, or just over 4 minutes.

Because of these unfeasible current flows, the harmonic results for these two scenarios have been omitted from this study.

## 4.2.6 – Complex Faults

Power system faults are complex entities and are usually not as simple as the examples looked at in Sections 4.2.1-5. It is possible to have any combination of open-circuit, phase to phase and neutral faults in the same or multiple locations. For example, it is possible for one side of a faulty joint to be a three-phase and neutral open circuit and the other to be a three-phase fault. As long as the fault occurs as part of an open ring with a link box, supplies could be restored via the link box. This can be seen in Figure 4.2.6.1 below. It should be quickly noted at this point that open ring networks, as opposed to radial networks, can normally cope with one of each of these faults on a mains cable. It is when multiple faults start to occur that emergency fault repairs are required to restore supplies.

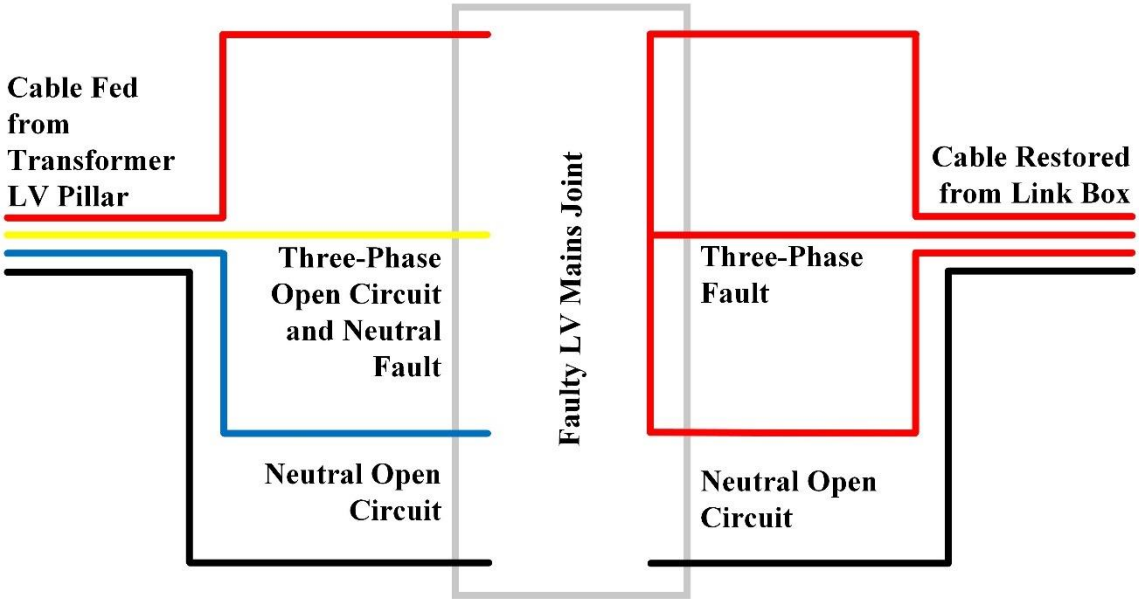


**Figure 4.2.6.1: Three-phase open circuit with an open circuit fault on the neutral fed from a transformer feeder pillar and a three-phase fault restored from a linkbox.**

To help visualise how these complex faults occur please see Figure 1.5.8. This shows how little clearance the cores have inside a joint. Therefore, with fault levels as high as 19.4 MVA as explained by Electricity North West (2019) it is understandable that these cores can melt, weld, or blow apart.

As explained in Section 4.2.5 a fault backfed via the linkbox on the Road A LV EDN will be via 200A fuses to grade with the 315A fuses in the LV cabinet. Therefore, this is the limiting factor for backfeeding the LV network. As an example, consider the arrangement shown in Figure 4.2.6.2 occurring just outside the LV cabinet on feeder one with an EVC penetration of 31.2%. In this case, as explained in Section 4.2, the current drawn by a three-phase fault on feeder one is 338.9A. To backfeed the network and restore supplies a 200A fuse is inserted into the red phase of the link box as shown in Figure 4.2.6.2 below.

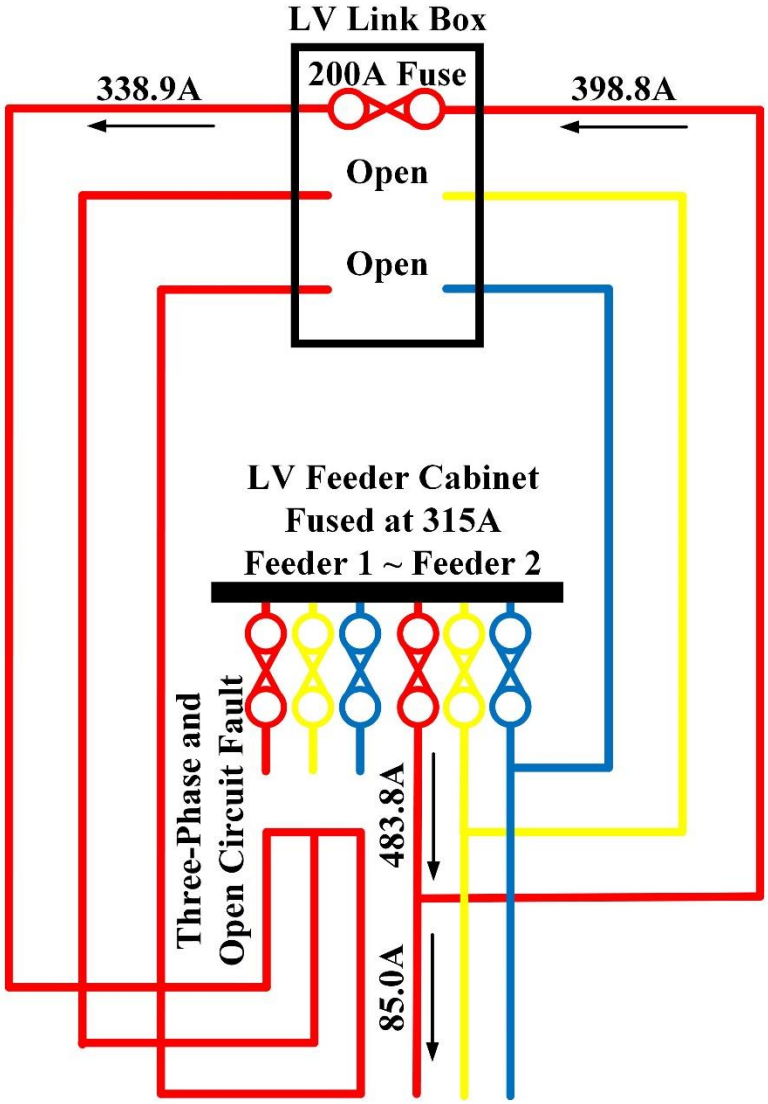


**Figure 4.2.6.2: Simplification of the LV EDN, showing the key components, current flow and fault arrangement shown in Figure 4.2.6.1 outside the LV cabinet on feeder one.**

A 200A fuse drawing 338.9A will not last particularly long. 338.9A is 1.69 times the fuse rating. Additionally, the 315A fuse draws 483.8A, 1.53 times the fuse rating. This type of fuse is the same class of fuse used in Beama (2022). Therefore, based on data published within Beama (2022) the 200A fuse will blow in approximately 2,000 seconds or 33 minutes or the 315A fuse will blow in approximately 6,000-8,000 seconds or 100-133 minutes. Therefore, this is not a viable solution. Additionally, it should be noted that the 95mm$^2$ Wavecon and 95mm$^2$ Consac is rated at 237A summer sustained as per Baker (2019), not 398.8A, which is the portion of the current from feeder two which flows towards the linkbox. Therefore, drawing this current for long periods could damage the cable. However, it is likely that the 200A fuse will operate well before any damage is done. Therefore, a three-phase fault on feeder one, fed from feeder two via the linkbox is not possible.

At this point it should be explained where 398.8A comes from. The red phase of feeder two at an EVC penetration of 31.2% draws 144.9A for the load on feeder two only. However, using Figure 3.1.1.2 it can be seen that the cable feeding numbers 'eighty-two,' 'ninety-four A' and the linkbox is diverted off from the rest of the feeder outside the substation via 95mm$^2$ Wavecon cable. 59.9A is the proportion of the current which flows along this cable. Simplistically, 338.9A, which was previously mentioned to be the current drawn by feeder one under this fault scenario plus 59.9A equals 398.8A.

As the three-phase fault shown in Figure 4.2.6.2, fed via the linkbox will lead to fuses operating, a two-phase fault at the same location shown in Figure 4.2.6.3 shall be investigated. The red phase of feeder two draws 143.9A for the load on feeder two, with only 58.7A being diverted towards the linkbox. A two-phase fault between red and yellow, fed by a 200A fuse in the linkbox draws 230.7A at the fuse. Therefore, at the LV cabinet, the 315A fuse feeding the red phase of feeder two draws 374.6A. in this situation, the current passing through the 315A fuse is 1.19 times the fuse rating and the current passing through the 200A fuse is 1.15 times the fuse rating. Therefore, one of these two fuses will operate, resulting in a loss of supplies.

However, for arguments sake, it will be assumed that the fuses do not operate. By running a simulation of the network at 31.2% EVC penetration with the fault scenario shown in Figure 4.2.6.3, the worst-case voltage harmonic profile on feeder one was found to be at the yellow phase supply terminal at the end of feeder one at 2.06% as shown in Table 4.2.6.1. This is 0.11% lower than the worst-case voltage harmonic profile on feeder one produced from a three-phase fault, at the end of feeder one and fed from feeder one, as seen in Figure 4.2.1.3. Under these simulations 0.11% is a significant percentage difference. In addition, under the three-phase fault, the current passing through the 315A fuse was only 1.08 times the fuse rating as opposed to 1.19 times in the linkbox fed two-phase fault. Additionally, the worst-case voltage harmonic profile measured on the terminals of feeder one is only 0.06% higher than the two-phase fault, at the end of feeder one, fed from feeder one shown in Figure 4.2.1.2. Therefore, the scenario presented in Figure 4.2.6.3 does not produce a significant THDv increase.

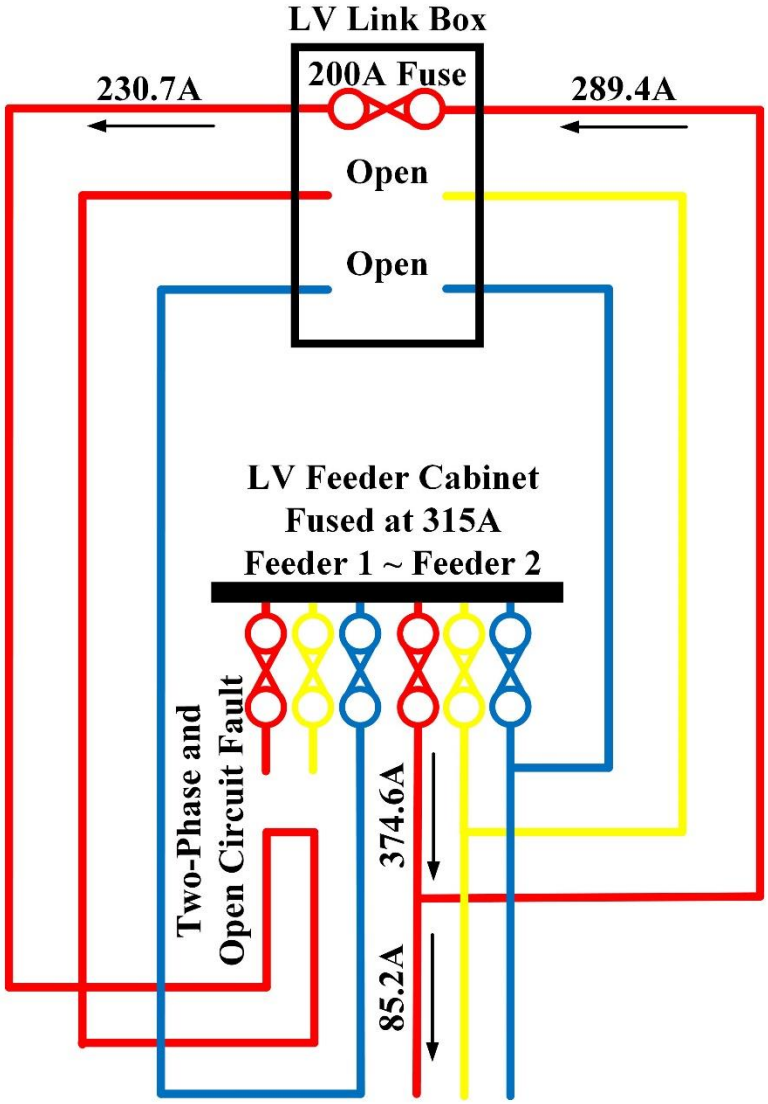


**Figure 4.2.6.3: Simplification of the LV EDN, showing the key components, current flow, and two-phase fault, similar to the fault arrangement shown in Figure 4.2.6.1 outside the LV cabinet on feeder one.**

The results of Figure 4.2.6.3 have been compared to the two-phase fault results in Table 4.2.1.2 within Table 4.2.6.1. Harmonic current is lower, but voltage harmonics are higher. The higher harmonic voltage levels are due to the harmonic current travelling over the greater impedance, the current travelling through both feeder one and two cables. Therefore, this is to be expected. The harmonic current is lower; however, this is likely due to additional harmonic cancellation since the current is no longer split down feeder one and feeder two cables as in Figure 4.2.1.2. The full current magnitude is forced through the feeder two cable before flowing through the feeder one cable. The lower harmonic current has also translated to lower voltage harmonic magnitude at the transformer which is to be expected.

**Table 4.2.6.1: Table of harmonics on feeder one for a two-phase fault outside the LV cabinet fed from feeder two with an EVC penetration of 31.2% against the limits set out in ER G5/5 (Energy Networks Association, 2020).**

| Harmonic Number | Worst Case Voltage Harmonic Magnitude at Supply Terminals (%) | Worst Case Voltage Harmonic Magnitude at Transformer (%) | ER G5/5 Limits (%) | Worst Case Phase Current Harmonic Magnitude at Transformer (A) | Neutral Harmonic Current Magnitude at Transformer (A) |
|---|---|---|---|---|---|
| 2nd | 0.05 | 0.04 | 1.60 | 0.25 | 0.14 |
| 3rd | 0.86 | 0.69 | 4.00 | 6.16 | 3.12 |
| 4th | 0.02 | 0.02 | 1.00 | 0.07 | 0.04 |
| 5th | 0.76 | 0.64 | 4.00 | 3.61 | 1.77 |
| 6th | 0.03 | 0.03 | 0.50 | 0.11 | 0.06 |
| 7th | 1.02 | 0.92 | 4.00 | 3.37 | 1.61 |
| 8th | 0.02 | 0.02 | 0.40 | 0.07 | 0.04 |
| 9th | 0.41 | 0.29 | 1.20 | 1.90 | 0.89 |
| 10th | 0.03 | 0.03 | 0.40 | 0.10 | 0.05 |
| 11th | 0.67 | 0.59 | 3.00 | 2.05 | 0.92 |
| 12th | 0.03 | 0.03 | 0.20 | 0.10 | 0.05 |
| 13th | 0.71 | 0.56 | 2.50 | 2.20 | 0.96 |
| 14th | 0.03 | 0.03 | 0.20 | 0.10 | 0.04 |
| 15th | 0.33 | 0.23 | 0.50 | 1.12 | 0.48 |
| 16th | 0.07 | 0.05 | 0.20 | 0.23 | 0.10 |
| 17th | 0.30 | 0.19 | 1.60 | 1.05 | 0.43 |
| 18th | 0.07 | 0.04 | 0.20 | 0.21 | 0.09 |
| 19th | 0.34 | 0.22 | 1.50 | 1.03 | 0.42 |
| 20th | 0.02 | 0.02 | 0.20 | 0.06 | 0.02 |
| 21st | 0.21 | 0.13 | 0.20 | 0.59 | 0.23 |
| 22nd | 0.02 | 0.02 | 0.20 | 0.06 | 0.02 |
| 23rd | 0.26 | 0.16 | 1.20 | 0.75 | 0.29 |
| 24th | 0.01 | 0.01 | 0.20 | 0.03 | 0.01 |
| 25th | 0.18 | 0.11 | 1.00 | 0.46 | 0.17 |
| 26th | 0.01 | 0.01 | 0.20 | 0.03 | 0.01 |
| 27th | 0.21 | 0.13 | 0.20 | 0.52 | 0.19 |
| 28th | 0.01 | 0.01 | 0.20 | 0.03 | 0.01 |
| 29th | 0.21 | 0.12 | 0.86 | 0.50 | 0.18 |
| 30th | 0.00 | 0.00 | 0.20 | 0.00 | 0.00 |
| 31st | 0.22 | 0.13 | 0.81 | 0.49 | 0.17 |
| 33rd | 0.19 | 0.11 | 0.20 | 0.39 | 0.13 |
| 35th | 0.19 | 0.11 | 0.71 | 0.38 | 0.12 |
| 37th | 0.16 | 0.09 | 0.68 | 0.29 | 0.09 |
| 39th | 0.16 | 0.09 | 0.20 | 0.28 | 0.09 |
| 41st | 0.12 | 0.07 | 0.61 | 0.20 | 0.06 |
| 43rd | 0.12 | 0.07 | 0.58 | 0.20 | 0.06 |
| 45th | 0.12 | 0.07 | 0.20 | 0.19 | 0.06 |
| 47th | 0.08 | 0.05 | 0.53 | 0.12 | 0.04 |
| 49th | 0.08 | 0.05 | 0.51 | 0.12 | 0.03 |
| Harmonics higher than the limits set by ER G5/5 | | | | | |
| Harmonics on the boundary of the limits set by ER G5/5 | | | | | |
| Harmonics higher than the result from Figure 4.2.1.2 | | | | | |
| Number of PVs on Feeder 1: 18 Number of PVs on Feeder 2: 21 Voltage on Neutral: 4.002V | | | | | |

The 21st and 27th voltage harmonic limits are exceeded within Table 4.2.6.1. They are both 0.01% higher than during the two-phase fault shown in Table 4.2.1.2, which is the percentage that the limit is exceeded. The 21st and 27th voltage harmonics within Table 4.2.6.1 are 0.01% and 0.02% lower than during the three-phase fault shown in Table 4.2.1.3.

Lastly, the highest neutral voltage measured at 4.002V was lower than both the two and three-phase fault scenarios shown in Tables 4.2.1.2-3. The neutral voltage is high enough to cause shocks, but not high enough for ventricular fibrillation or respiratory tetanus.

Based on these results, it can be concluded that the fault scenarios modelled in Sections 4.2.1-3 produce higher THDv, THDi and neutral voltage than the scenario modelled in this section without exceeding fuse or cable ratings significantly. Although more complex faults are possible, as discussed in this section, they will either exceed the limitations of the network or produce lower voltage harmonic profiles than the three-phase faults simulated in Sections 4.2.1-3.

## 4.2.7 – Discussion, Conclusions and Asset Lifespan

Based on the scenarios modelled and results from Sections 4.2.5-6, both open-circuit faults and complex faults do not have as high an impact as phase-to-phase faults, without first exceeding either fuse or cable ratings. Based on these findings, it would be more efficient for future fault models to exclude both open-circuit and complex faults, therefore, prioritising the modelling of phase-to-phase faults. This assumes that the impact of these faults does not differ considerably under different EVCs.

The impact of phase-to-phase faults is significant, both on THDv levels and maximum EVC penetration levels. Additionally, concurrent faults on both feeders one and two will lead to further increases in THDv and further reductions in maximum EVC penetration. This has been covered in Section 4.2.4. However, in Tables 4.2.4.1-2 it can be seen that for a three-phase fault on feeder one, an additional two-phase or three-phase fault on feeder two could have very little effect on the limiting 21st and 27th harmonics.

The effect of fundamental current on the expected service life of transformers and conductors is well understood by DNOs, however, similar to Section 3.2.8, it is important to ascertain whether the harmonic currents are sufficient in magnitude to lead to a noticeable loss of transformer or conductor life. The same assumptions and values such as reference hottest-spot temperature, ambient temperature and conductor impedance will be made as per Section 3.2.8 to carry out these calculations. Although unlikely in the event of a phase-to-phase fault, for fair comparison between scenarios, it will also be assumed that the transformer hot-spot temperature is 110ºC and cable temperature is currently 90ºC before considering heating from harmonics.

Additionally, in the case of phase-to-phase faults, it will be assumed that the heating effect of the phase with the highest harmonic content will produce the highest hot-spot temperature and lead to overall loss of asset life. Equations 3.2.8.1-10 assume a fully balanced load, which of course is not applicable. Equations 3.2.8.11-19 do consider the heat produced from individual phases, however, assumes uniform heating across the whole cable, rather than within the individual phase with the highest harmonic current. Therefore, using the phase with the highest harmonic content will produce a worst possible case heating effect.

Table 4.2.7.1 displays the increase in transformer hot-spot temperature and loss of transformer life. Table 4.2.7.2 displays the increase in cable temperature and loss of cable life. Values are calculated using Equations 3.2.8.1-19 and data from Tables 4.2.1.1-3, 4.2.2.1-3 and 4.2.3.1-3. Equations have been validated as per Section 3.2.8.

**Table 4.2.7.1: Transformer hot-spot temperature increase and loss of transformer life assuming an existing hot-spot temperature of 110ºC for various fault arrangements on feeders one and two with an EVC penetration of 31.2%.**

| Increase in transformer hot-spot temperature (ºC) and loss of transformer life under specified conditions (Years). | | Feeder One | | |
|---|---|---|---|---|
| | | Normal Arrangements | Two-Phase Fault Arrangements | Three-Phase Fault Arrangements |
| Feeder Two | Normal Arrangements | 0.2528ºC<br>1.020 Years | 0.2998ºC<br>1.207 Years | 0.3268ºC<br>1.314 Years |
| | Two-Phase Fault Arrangements | 0.3115ºC<br>1.253 Years | 0.3582ºC<br>1.437 Years | 0.3874ºC<br>1.552 Years |
| | Three-Phase Fault Arrangements | 0.3494ºC<br>1.403 Years | 0.3960ºC<br>1.586 Years | 0.4220ºC<br>1.687 Years |

**Table 4.2.7.2: Cable temperature increase and loss of cable life assuming an existing cable temperature of 90ºC for various fault arrangements on feeders one and two with an EVC penetration of 31.2%.**

| Increase in cable temperature (ºC) and loss of cable life under specified conditions (Years). | | Feeder One | | |
|---|---|---|---|---|
| | | Normal Arrangements | Two-Phase Fault Arrangements | Three-Phase Fault Arrangements |
| Feeder Two | Normal Arrangements | 0.0085ºC<br>0.0494 Years | 0.0223ºC<br>0.1297 Years | 0.0277ºC<br>0.1616 Years |
| | Two-Phase Fault Arrangements | 0.0192ºC<br>0.1121 Years | 0.0324ºC<br>0.1883 Years | 0.0449ºC<br>0.2614 Years |
| | Three-Phase Fault Arrangements | 0.0325ºC<br>0.1892 Years | 0.0475ºC<br>0.2765 Years | 0.0652ºC<br>0.3784 Years |

Comparing Tables 4.2.7.1-2, to the results of Section 3.2.8, 98.4% EVC penetration has a much greater effect on the hot-spot temperature and loss of life than 31.2% EVC penetration, even under three-phase fault conditions on both feeders one and two. 98.4% EVC penetration produced an increase in transformer hot-spot temperature of 0.6520ºC and loss of transformer life of 2.58 years. In comparison, the increase in cable temperature and loss of cable life at 98.4% EVC penetration is comparable to 31.2% EVC penetration under three-phase fault conditions on both feeders one and two. 98.4% EVC penetration produced an increase in cable temperature of 0.0610ºC and loss of cable life of 0.35 years.

Additionally, it can be seen under both Tables 4.2.7.1-2 that fault conditions increase the temperature and reduce the asset life as would be expected, since increases in current and voltage harmonics, which occur under phase-to-phase conditions will result in higher asset temperatures and lower asset life. A three-phase fault on feeder two has a greater effect on the transformer and cable temperature than a comparable two-phase fault on feeder one. Feeder two contains more services and EVCs and therefore a fault on feeder two will result in a greater harmonic current shift.

It should be noted that the increase in temperature for both transformers and cables is not substantial. Should the transformer hot-spot temperature be below 110ºC, and cable temperature be below 90ºC before considering heating from harmonics, the transformer and cable will not suffer the loss of life stated.

Further to the results of Tables 4.2.7.1-2, Tables 4.2.7.3-6 show the additional effect that different fault scenarios have on the temperature and loss of asset life as they compound. Tables 4.2.7.3-4 show that as faults compound, the effect of any one of those faults on the hot-spot temperature and asset life of transformers remains consistent. However, the effect of normal arrangements to a two-phase fault is much greater than a two-phase fault to a three-phase fault by a magnitude of 50-80%. This is to be expected looking at the results of Figure 4.2.4.1. Conversely, Tables 4.2.7.5-6 shows that the temperature gain and loss of asset life for cables increases as faults on feeders one and two compound. The difference in the way harmonics impact on transformers and cables is explained in Equations 3.2.8.1-19. Transformers are affected by both terminal voltage and phase current harmonics. Cables are affected by both phase and neutral current harmonics. However, the impact these harmonics have in each scenario differ according to these equations. The values within Tables 4.2.7.3-6 have been calculated by measuring the difference in temperature and asset life between network fault arrangements within the table stated within the table title. For example, for Table 4.2.7.3, the values stated within the top left box is calculated by subtracting the top left values from the top middle values within Table 4.2.7.1.

**Table 4.2.7.3: Increase in transformer hot-spot temperature and loss of transformer life between different fault scenarios on feeder one for data from Table 4.2.7.1.**

| Increase in transformer hot-spot temperature (ºC) and loss of transformer life (Years) for Table 4.2.7.1 under specified conditions. | | Feeder One | |
|---|---|---|---|
| | | Normal Arrangements to Two-Phase Fault | Two-Phase Fault to Three-Phase Fault |
| Feeder Two | Normal Arrangements | 0.0470ºC<br>0.187 Years | 0.0270ºC<br>0.107 Years |
| | Two-Phase Fault Arrangements | 0.0467ºC<br>0.184 Years | 0.0292ºC<br>0.115 Years |
| | Three-Phase Fault Arrangements | 0.0466ºC<br>0.183 Years | 0.0260ºC<br>0.101 Years |

**Table 4.2.7.4: Increase in transformer hot-spot temperature and loss of transformer life between different fault scenarios on feeder two for data from Table 4.2.7.1.**

| Increase in transformer hot-spot temperature (ºC) and loss of transformer life (Years) for Table 4.2.7.1 under specified conditions. | | Feeder Two | |
|---|---|---|---|
| | | Normal Arrangements to Two-Phase Fault | Two-Phase Fault to Three-Phase Fault |
| Feeder One | Normal Arrangements | 0.0587ºC<br>0.233 Years | 0.0379ºC<br>0.150 Years |
| | Two-Phase Fault Arrangements | 0.0584ºC<br>0.230 Years | 0.0378ºC<br>0.149 Years |
| | Three-Phase Fault Arrangements | 0.0606ºC<br>0.238 Years | 0.0346ºC<br>0.135 Years |

**Table 4.2.7.5: Increase in cable temperature and loss of cable life between different fault scenarios on feeder one for data from Table 4.2.7.2.**

| Increase in cable temperature (ºC) and loss of cable life (Years) for Table 4.2.7.2 under specified conditions. | | Feeder One | |
|---|---|---|---|
| | | Normal Arrangements to Two-Phase Fault | Two-Phase Fault to Three-Phase Fault |
| Feeder Two | Normal Arrangements | 0.0138ºC<br>0.0803 Years | 0.0054ºC<br>0.0319 Years |
| | Two-Phase Fault Arrangements | 0.0132ºC<br>0.0762 Years | 0.0125ºC<br>0.0731 Years |
| | Three-Phase Fault Arrangements | 0.0150ºC<br>0.0873 Years | 0.0177ºC<br>0.1019 Years |

**Table 4.2.7.6: Increase in cable temperature and loss of cable life between different fault scenarios on feeder two for data from Table 4.2.7.2.**

| Increase in cable temperature (ºC) and loss of cable life (Years) for Table 4.2.7.2 under specified conditions. | | Feeder Two | |
|---|---|---|---|
| | | Normal Arrangements to Two-Phase Fault | Two-Phase Fault to Three-Phase Fault |
| Feeder One | Normal Arrangements | 0.0107ºC<br>0.0627 Years | 0.0133ºC<br>0.0771 Years |
| | Two-Phase Fault Arrangements | 0.0101ºC<br>0.0586 Years | 0.0151ºC<br>0.0882 Years |
| | Three-Phase Fault Arrangements | 0.0172ºC<br>0.0998 Years | 0.0203ºC<br>0.1170 Years |

Based on the results of this section, it is recommended that the numbers of EVCs connected to LV EDNs should be restricted, or harmonic reducing technology implemented, to observe compliance with industrial standards or regulations during phase-to-phase faults. Increases in asset temperature under fault conditions are not substantial, however, do result in the loss of asset life. Therefore, this should be a consideration when putting a financial value to repairing or leaving a fault which still complies with the ESQCRs.

# 4.3 – PV Generation

To analyse the effect that faults, and PV generation have on the LV EDN, the PV generation penetration was set at 98.4% as per Section 3.3.4. This penetration value represents one-hundred and twenty-three single-phase 2kW PVs each connected to separate properties on the LV EDN and evenly distributed amongst the three phases, fifty-four on feeder one and sixty-nine on feeder two. This is the maximum load penetration which can be sustained in the event of a three-phase fault without blowing the LV fuse at the substation and allows for a whole number of PVs to be applied to the network. At this penetration, the current drawn by the phase feeding the fault under three-phase conditions is 319.6A which is 1.01 times the fuse rating of 315A at the LV cabinet.

## 4.3.1 – Results of Phase-to-Phase Faults

Like the EVC simulations, the supply terminals to be measured will be on all three phases at the start, middle and end of feeder one between phase and neutral as defined within Figure 3.1.1.2. The results for normal conditions for each of the PV generation harmonic profiles can be seen in Figures 4.3.1.1(A-C) and Table 4.3.1.1. It can be seen that THDv increases the further the supply terminal is from the 11kV:400V transformer, similar to the EVC simulation in Section 4.2.1 under normal running arrangements. The larger the network impedance, the higher the harmonic voltage drop measured as THDv as per Section 1.2.1. However, the increase in THDv between the beginning and end of the network varies depending on the PV harmonic profile used and varies between 0.03-0.13%. As stated in Section 3.3.5 there are breaches of the harmonic limits under ER G5/5 on the 21$^{st}$ harmonic.

The tipping points for this scenario with normal running arrangements on feeder one to remain compliant under the different PV generation profiles within ER G5/5 was identified. It was found that for the harmonic profile within Table 3.3.1.1, the maximum penetration was 60% (seventy-five PV generators), for the harmonic profile within Table 3.3.1.4 was 98.4% (one-hundred and twenty-three PV generators) and for the harmonic profile within Table 3.3.1.7 was 39% (forty-eight PV generators). These were evenly distributed across three phases on feeders one and two as close as is achievable to a 44-56% split between the PV generators on feeders one and two respectively.

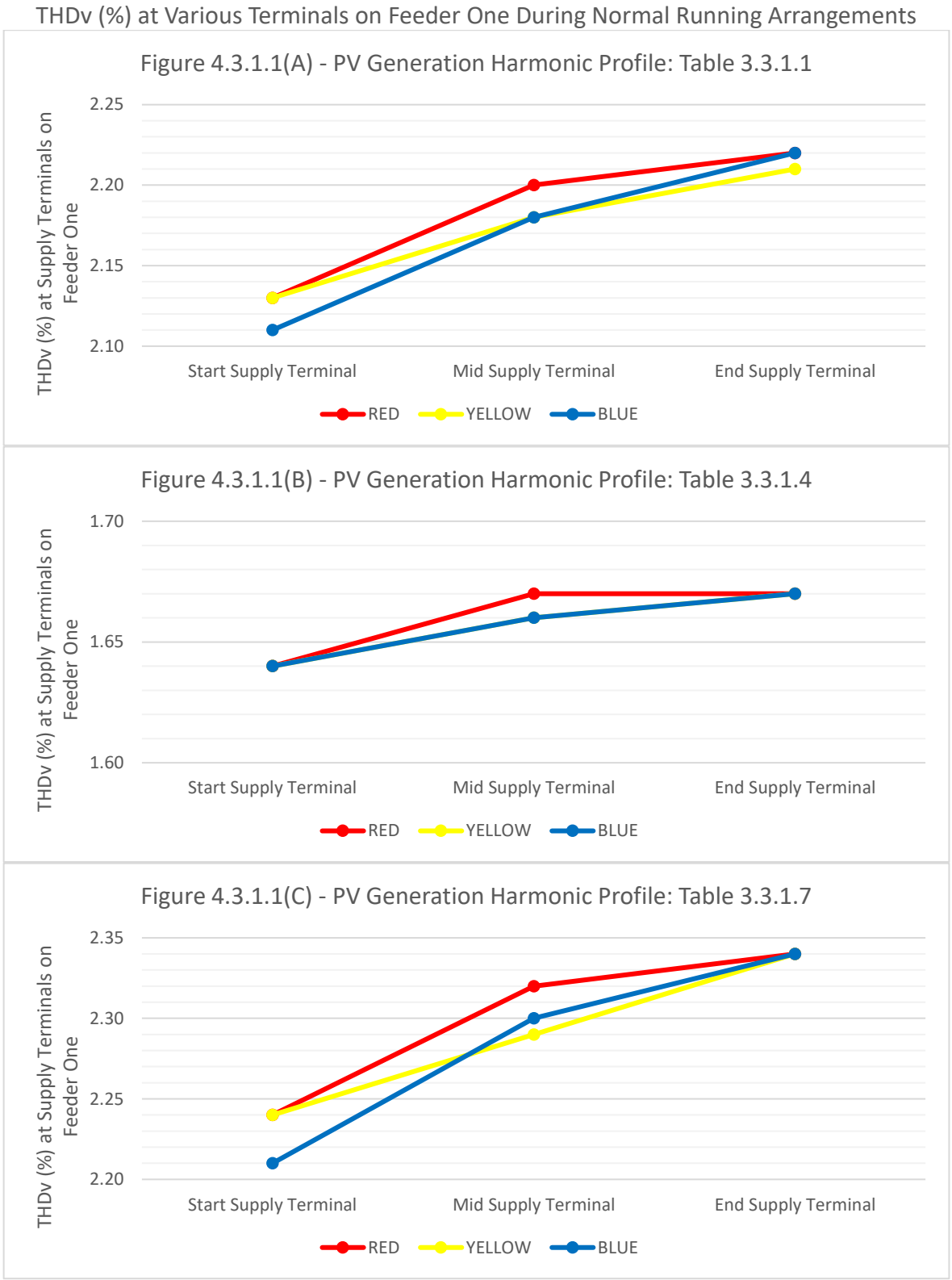


**Figure 4.3.1.1: Graphical representation of the THDv measured on each phase at supply terminals at the start, middle and end of feeder one under normal running arrangements at 98.4% PV generation penetration and the PV generation harmonic profile stated.**

**Table 4.3.1.1: Table of harmonics on feeder one for normal running arrangements at 98.4% PV generation penetration against the limits set out in ER G5/5 for the PV generation harmonic profile stated (Energy Networks Association, 2020).**

| Harmonic Number | Worst Case Voltage Harmonic Magnitude at Supply Terminals (%) | | | Worst Case Voltage Harmonic Magnitude at Transformer (%) | | | ER G5/5 Limits (%) | Worst Case Phase Current Harmonic Magnitude at Transformer (A) | | | Neutral Harmonic Current Magnitude at Transformer (A) | | |
|---|---|---|---|---|---|---|---|---|---|---|---|---|---|
| | PV Generation Harmonic Profile from Table 3.3.1.- | | | PV Generation Harmonic Profile from Table 3.3.1.- | | | | PV Generation Harmonic Profile from Table 3.3.1.- | | | PV Generation Harmonic Profile from Table 3.3.1.- | | |
| | .1 | .4 | .7 | .1 | .4 | .7 | | .1 | .4 | .7 | .1 | .4 | .7 |
| 2nd | 0.09 | 0.09 | 0.09 | 0.08 | 0.08 | 0.08 | 1.6 | 2.72 | 2.72 | 2.72 | 0.01 | 0.01 | 0.01 |
| 3rd | 0.80 | 0.62 | 0.94 | 0.76 | 0.61 | 0.88 | 4.0 | 9.81 | 3.04 | 15.24 | 0.03 | 0.00 | 0.06 |
| 4th | 0.07 | 0.02 | 0.03 | 0.06 | 0.02 | 0.03 | 1.0 | 1.36 | 0.02 | 0.34 | 0.00 | 0.00 | 0.00 |
| 5th | 0.87 | 0.59 | 0.74 | 0.83 | 0.59 | 0.71 | 4.0 | 8.47 | 2.06 | 5.42 | 0.02 | 0.00 | 0.01 |
| 6th | 0.05 | 0.05 | 0.05 | 0.04 | 0.04 | 0.05 | 0.5 | 0.34 | 0.34 | 0.34 | 0.00 | 0.00 | 0.00 |
| 7th | 1.13 | 0.91 | 1.11 | 1.10 | 0.91 | 1.09 | 4.0 | 5.11 | 1.53 | 4.77 | 0.00 | 0.01 | 0.01 |
| 8th | 0.04 | 0.04 | 0.04 | 0.04 | 0.04 | 0.04 | 0.4 | 0.34 | 0.34 | 0.34 | 0.00 | 0.00 | 0.00 |
| 9th | 0.46 | 0.25 | 0.49 | 0.42 | 0.24 | 0.45 | 1.2 | 3.73 | 1.03 | 4.07 | 0.01 | 0.01 | 0.01 |
| 10th | 0.06 | 0.06 | 0.06 | 0.05 | 0.05 | 0.05 | 0.4 | 0.34 | 0.34 | 0.34 | 0.00 | 0.00 | 0.00 |
| 11th | 0.77 | 0.61 | 0.83 | 0.74 | 0.61 | 0.80 | 3.0 | 2.74 | 1.11 | 3.41 | 0.01 | 0.01 | 0.01 |
| 12th | 0.06 | 0.06 | 0.06 | 0.06 | 0.06 | 0.06 | 0.2 | 0.34 | 0.34 | 0.34 | 0.00 | 0.00 | 0.00 |
| 13th | 0.76 | 0.46 | 0.76 | 0.72 | 0.46 | 0.72 | 2.5 | 3.06 | 0.51 | 3.06 | 0.00 | 0.01 | 0.01 |
| 14th | 0.03 | 0.03 | 0.03 | 0.03 | 0.03 | 0.03 | 0.2 | 0.03 | 0.03 | 0.03 | 0.00 | 0.00 | 0.00 |
| 15th | 0.37 | 0.20 | 0.46 | 0.34 | 0.19 | 0.42 | 0.5 | 2.03 | 0.68 | 2.70 | 0.00 | 0.00 | 0.00 |
| 16th | 0.08 | 0.08 | 0.08 | 0.07 | 0.07 | 0.07 | 0.2 | 0.34 | 0.34 | 0.34 | 0.00 | 0.00 | 0.00 |
| 17th | 0.31 | 0.21 | 0.36 | 0.28 | 0.19 | 0.32 | 1.6 | 1.68 | 1.01 | 2.02 | 0.00 | 0.00 | 0.00 |
| 18th | 0.07 | 0.07 | 0.07 | 0.06 | 0.06 | 0.06 | 0.2 | 0.34 | 0.34 | 0.34 | 0.00 | 0.00 | 0.00 |
| 19th | 0.26 | 0.15 | 0.42 | 0.24 | 0.14 | 0.38 | 1.5 | 1.01 | 0.35 | 2.02 | 0.00 | 0.00 | 0.00 |
| 20th | 0.08 | 0.08 | 0.08 | 0.07 | 0.07 | 0.07 | 0.2 | 0.34 | 0.34 | 0.34 | 0.00 | 0.00 | 0.00 |
| 21st | 0.29 | 0.11 | 0.41 | 0.26 | 0.10 | 0.36 | 0.2 | 1.34 | 0.34 | 2.02 | 0.00 | 0.00 | 0.00 |
| 22nd | 0.02 | 0.02 | 0.02 | 0.02 | 0.02 | 0.02 | 0.2 | 0.02 | 0.02 | 0.02 | 0.00 | 0.00 | 0.00 |
| 23rd | 0.17 | 0.24 | 0.37 | 0.15 | 0.20 | 0.32 | 1.2 | 0.67 | 1.00 | 1.67 | 0.00 | 0.00 | 0.00 |
| 24th | 0.08 | 0.08 | 0.08 | 0.07 | 0.07 | 0.07 | 0.2 | 0.33 | 0.33 | 0.33 | 0.00 | 0.00 | 0.00 |
| 25th | 0.25 | 0.18 | 0.32 | 0.22 | 0.16 | 0.28 | 1.0 | 1.00 | 0.67 | 1.34 | 0.00 | 0.00 | 0.00 |
| 26th | 0.01 | 0.01 | 0.01 | 0.01 | 0.01 | 0.01 | 0.2 | 0.01 | 0.01 | 0.01 | 0.00 | 0.00 | 0.00 |
| 27th | 0.18 | 0.18 | 0.18 | 0.16 | 0.16 | 0.16 | 0.2 | 0.66 | 0.66 | 0.66 | 0.00 | 0.00 | 0.00 |
| 28th | 0.09 | 0.09 | 0.09 | 0.08 | 0.08 | 0.08 | 0.2 | 0.33 | 0.33 | 0.33 | 0.00 | 0.00 | 0.00 |
| 29th | 0.26 | 0.26 | 0.26 | 0.23 | 0.23 | 0.23 | 0.86 | 1.00 | 1.00 | 1.00 | 0.00 | 0.00 | 0.00 |
| 30th | 0.08 | 0.08 | 0.08 | 0.07 | 0.07 | 0.07 | 0.2 | 0.33 | 0.33 | 0.33 | 0.00 | 0.00 | 0.00 |
| 31st | 0.29 | 0.29 | 0.29 | 0.25 | 0.25 | 0.25 | 0.81 | 1.00 | 1.00 | 1.00 | 0.00 | 0.00 | 0.00 |
| 32nd | 0.09 | 0.09 | 0.09 | 0.08 | 0.08 | 0.08 | 0.2 | 0.33 | 0.33 | 0.33 | 0.00 | 0.00 | 0.00 |
| 33rd | 0.20 | 0.20 | 0.20 | 0.18 | 0.18 | 0.18 | 0.2 | 0.66 | 0.66 | 0.66 | 0.00 | 0.00 | 0.00 |
| 34th | 0.09 | 0.10 | 0.09 | 0.08 | 0.08 | 0.08 | 0.2 | 0.33 | 0.33 | 0.33 | 0.00 | 0.00 | 0.00 |
| 35th | 0.12 | 0.12 | 0.12 | 0.10 | 0.10 | 0.10 | 0.71 | 0.33 | 0.33 | 0.33 | 0.00 | 0.00 | 0.00 |
| 36th | 0.10 | 0.10 | 0.10 | 0.09 | 0.08 | 0.09 | 0.2 | 0.33 | 0.33 | 0.33 | 0.00 | 0.00 | 0.00 |
| 37th | 0.12 | 0.12 | 0.12 | 0.11 | 0.11 | 0.11 | 0.68 | 0.33 | 0.33 | 0.33 | 0.00 | 0.00 | 0.00 |
| 38th | 0.00 | 0.00 | 0.00 | 0.00 | 0.00 | 0.00 | 0.2 | 0.00 | 0.00 | 0.00 | 0.00 | 0.00 | 0.00 |
| 39th | 0.13 | 0.13 | 0.13 | 0.11 | 0.11 | 0.11 | 0.2 | 0.33 | 0.33 | 0.33 | 0.00 | 0.00 | 0.00 |
| 40th | 0.11 | 0.11 | 0.11 | 0.10 | 0.09 | 0.10 | 0.2 | 0.33 | 0.33 | 0.33 | 0.00 | 0.00 | 0.00 |
| Harmonics higher than the limits set by ER G5/5 | | | | | | | | | | | | | |
| Harmonics on the boundary of the limits set by ER G5/5 | | | | | | | | | | | | | |
| Number of PVs on Feeder 1: 54 Number of PVs on Feeder 2: 69 Voltage on Neutral: 0.020V | | | | | | | | | | | | | |

The data stated in Table 4.3.1.1 and subsequent tables is as follows unless otherwise stated:

- The worst-case voltage harmonic magnitude at supply terminal data was measured at the end of feeder one on red phase between phase and neutral as per Figures 4.3.1.1 (A-C).
- The worst-case voltage harmonic magnitude at the transformer was measured on the red phase at the LV terminals at the 11kV:400V transformer.
- the worst-case phase current harmonic magnitude at the transformer was measured on the red phase at the LV terminals of the 11kV:400V transformer.
- The neutral harmonic current magnitude at the transformer was measured on the neutral at the LV terminals of the 11kV:400V transformer.

By introducing a two-phase fault, between red and yellow phases, with red phase feeding the fault as seen in Figures 4.3.1.2(A-C), it has been found that the THDv increases significantly along the length of feeder one on red phase, with the THDv also increasing slightly on yellow phase as the current travels from the pot end outside one-hundred and fifty-eight back towards the transformer. This leads to the THDv measured on the yellow phase supply terminal at the start of feeder one reaching the highest level. There is no noticeable effect on the blue phase THDv which is excluded from the faulted phases.

The results of the worst-case harmonic distortion under a two-phase fault can be seen in Table 4.3.1.2. The worst-case harmonic distortion was measured between phase and neutral on the yellow phase supply terminal at the start of feeder one as shown in Figures 4.3.1.2(A-C). The worst-case THDv varies between each of the harmonic profiles due to the harmonic current contribution seen in Table 4.3.1.2. ER G5/5 limits are exceeded across multiple harmonics including $15^{th}$, $21^{st}$, $27^{th}$ and $33^{rd}$, therefore, resulting in non-compliance. Additionally, ER G5/5 limits are met for the $39^{th}$ harmonic. Lastly, due to the network imbalance, the neutral voltage has increased to 3.449V, which is high enough to provide residents with potential shocks off of exposed metalwork.

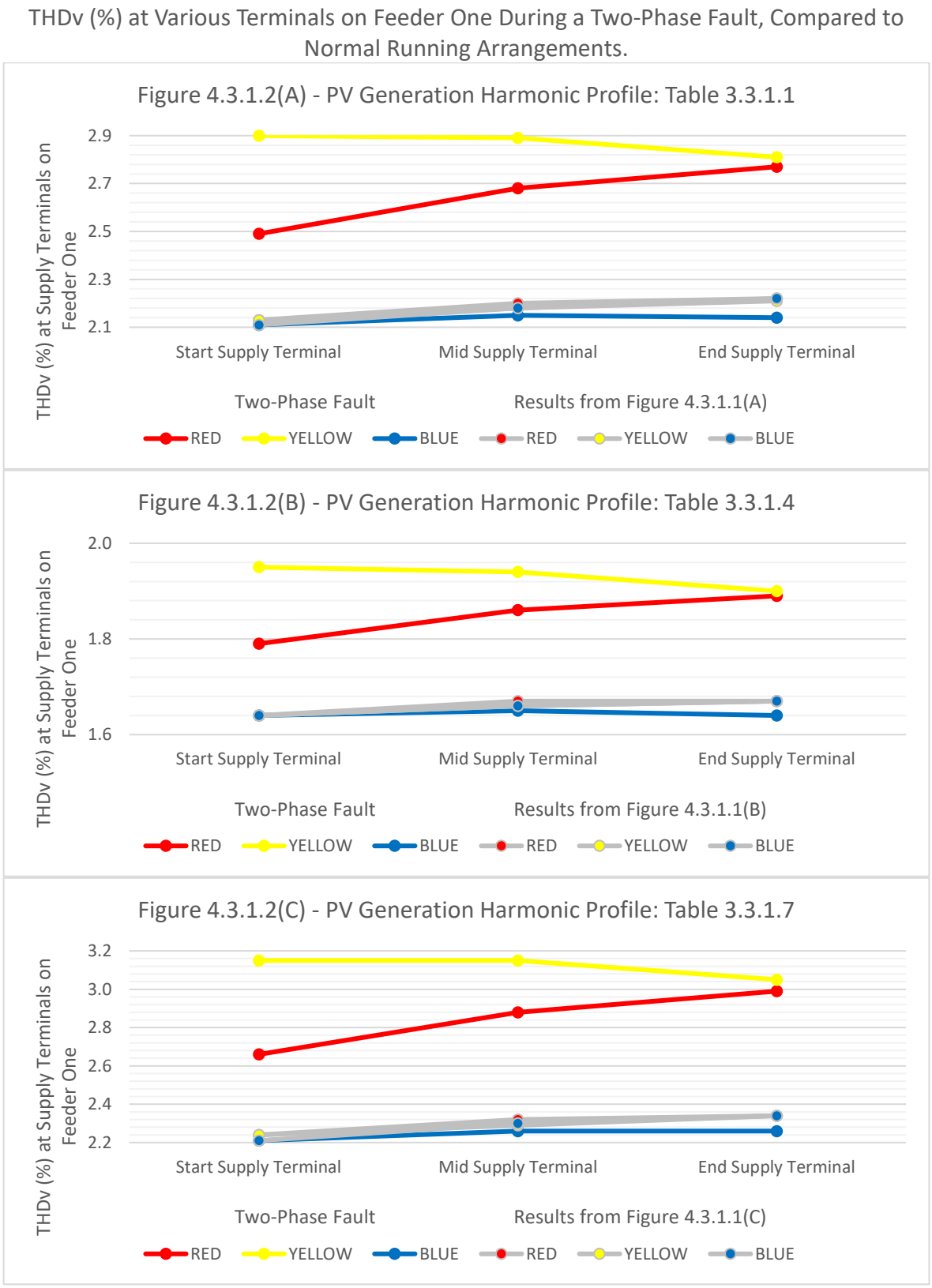


**Figure 4.3.1.2: Graphical representation of the THDv measured on each phase at supply terminals at the start, middle and end of feeder one during a two-phase fault at 98.4% PV generation penetration and the PV generation harmonic profile stated compared to normal running arrangements.**

**Table 4.3.1.2: Table of harmonics on feeder one during a two-phase fault at 98.4% PV generation penetration against the limits set out in ER G5/5 for the PV generation harmonic profile stated (Energy Networks Association, 2020).**

| Harmonic Number | Worst Case Voltage Harmonic Magnitude at Supply Terminals (%) | | | Worst Case Voltage Harmonic Magnitude at Transformer (%) | | | ER G5/5 Limits (%) | Worst Case Phase Current Harmonic Magnitude at Transformer (A) | | | Neutral Harmonic Current Magnitude at Transformer (A) | | |
|---|---|---|---|---|---|---|---|---|---|---|---|---|---|
| | PV Generation Harmonic Profile from Table 3.3.1.- | | | PV Generation Harmonic Profile from Table 3.3.1.- | | | | PV Generation Harmonic Profile from Table 3.3.1.- | | | PV Generation Harmonic Profile from Table 3.3.1.- | | |
| | .1 | .4 | .7 | .1 | .4 | .7 | | .1 | .4 | .7 | .1 | .4 | .7 |
| 2nd | 0.14 | 0.14 | 0.14 | 0.10 | 0.10 | 0.10 | 1.6 | 3.87 | 3.87 | 3.87 | 2.01 | 2.01 | 2.01 |
| 3rd | 0.99 | 0.65 | 1.27 | 0.85 | 0.64 | 1.02 | 4.0 | 13.98 | 4.33 | 21.73 | 7.25 | 2.25 | 11.26 |
| 4th | 0.11 | 0.02 | 0.04 | 0.08 | 0.03 | 0.03 | 1.0 | 1.94 | 0.03 | 0.48 | 1.00 | 0.01 | 0.01 |
| 5th | 1.14 | 0.63 | 0.90 | 0.95 | 0.62 | 0.79 | 4.0 | 12.07 | 2.93 | 7.73 | 6.22 | 1.52 | 1.52 |
| 6th | 0.06 | 0.06 | 0.06 | 0.05 | 0.05 | 0.05 | 0.5 | 0.48 | 0.48 | 0.48 | 0.25 | 0.25 | 0.25 |
| 7th | 1.32 | 0.92 | 1.28 | 1.20 | 0.93 | 1.18 | 4.0 | 7.27 | 2.17 | 6.80 | 3.73 | 1.12 | 1.12 |
| 8th | 0.06 | 0.06 | 0.06 | 0.05 | 0.05 | 0.05 | 0.4 | 0.48 | 0.48 | 0.48 | 0.25 | 0.25 | 0.25 |
| 9th | 0.67 | 0.30 | 0.72 | 0.52 | 0.27 | 0.55 | 1.2 | 5.30 | 1.46 | 5.78 | 2.69 | 0.74 | 0.74 |
| 10th | 0.08 | 0.08 | 0.08 | 0.06 | 0.06 | 0.06 | 0.4 | 0.48 | 0.48 | 0.48 | 0.24 | 0.24 | 0.24 |
| 11th | 0.93 | 0.65 | 1.04 | 0.83 | 0.63 | 0.90 | 3.0 | 3.88 | 1.58 | 4.83 | 1.97 | 0.80 | 0.80 |
| 12th | 0.09 | 0.09 | 0.09 | 0.07 | 0.07 | 0.07 | 0.2 | 0.48 | 0.48 | 0.48 | 0.24 | 0.24 | 0.24 |
| 13th | 0.98 | 0.45 | 0.98 | 0.83 | 0.47 | 0.83 | 2.5 | 4.33 | 0.72 | 4.33 | 2.18 | 0.37 | 0.37 |
| 14th | 0.03 | 0.03 | 0.03 | 0.03 | 0.03 | 0.03 | 0.2 | 0.04 | 0.04 | 0.04 | 0.02 | 0.02 | 0.02 |
| 15th | 0.56 | 0.26 | 0.71 | 0.43 | 0.22 | 0.53 | 0.5 | 2.86 | 0.96 | 3.82 | 1.43 | 0.48 | 0.48 |
| 16th | 0.11 | 0.11 | 0.11 | 0.08 | 0.08 | 0.08 | 0.2 | 0.48 | 0.48 | 0.48 | 0.24 | 0.24 | 0.24 |
| 17th | 0.49 | 0.32 | 0.57 | 0.36 | 0.24 | 0.42 | 1.6 | 2.38 | 1.43 | 2.85 | 1.18 | 0.71 | 0.71 |
| 18th | 0.11 | 0.11 | 0.11 | 0.08 | 0.08 | 0.08 | 0.2 | 0.47 | 0.47 | 0.47 | 0.23 | 0.23 | 0.23 |
| 19th | 0.37 | 0.18 | 0.66 | 0.29 | 0.16 | 0.49 | 1.5 | 1.42 | 0.49 | 2.84 | 0.70 | 0.24 | 0.24 |
| 20th | 0.12 | 0.12 | 0.12 | 0.09 | 0.09 | 0.09 | 0.2 | 0.47 | 0.47 | 0.47 | 0.23 | 0.23 | 0.23 |
| 21st | 0.46 | 0.15 | 0.67 | 0.33 | 0.12 | 0.48 | 0.2 | 1.88 | 0.47 | 2.82 | 0.92 | 0.23 | 0.23 |
| 22nd | 0.02 | 0.02 | 0.02 | 0.02 | 0.02 | 0.02 | 0.2 | 0.03 | 0.03 | 0.03 | 0.01 | 0.01 | 0.01 |
| 23rd | 0.26 | 0.37 | 0.60 | 0.19 | 0.27 | 0.43 | 1.2 | 0.94 | 1.40 | 2.34 | 0.45 | 0.68 | 0.68 |
| 24th | 0.13 | 0.13 | 0.13 | 0.09 | 0.09 | 0.09 | 0.2 | 0.47 | 0.47 | 0.47 | 0.22 | 0.22 | 0.22 |
| 25th | 0.40 | 0.28 | 0.52 | 0.29 | 0.21 | 0.37 | 1.0 | 1.39 | 0.93 | 1.86 | 0.67 | 0.45 | 0.45 |
| 26th | 0.01 | 0.01 | 0.01 | 0.01 | 0.01 | 0.01 | 0.2 | 0.01 | 0.01 | 0.01 | 0.01 | 0.01 | 0.01 |
| 27th | 0.29 | 0.29 | 0.29 | 0.21 | 0.21 | 0.21 | 0.2 | 0.92 | 0.92 | 0.92 | 0.44 | 0.44 | 0.44 |
| 28th | 0.14 | 0.14 | 0.14 | 0.10 | 0.10 | 0.10 | 0.2 | 0.46 | 0.46 | 0.46 | 0.22 | 0.22 | 0.22 |
| 29th | 0.44 | 0.44 | 0.44 | 0.31 | 0.31 | 0.31 | 0.86 | 1.37 | 1.37 | 1.37 | 0.65 | 0.65 | 0.65 |
| 30th | 0.14 | 0.14 | 0.14 | 0.10 | 0.10 | 0.10 | 0.2 | 0.46 | 0.46 | 0.46 | 0.22 | 0.22 | 0.22 |
| 31st | 0.47 | 0.47 | 0.47 | 0.33 | 0.31 | 0.31 | 0.81 | 1.36 | 1.36 | 1.36 | 0.64 | 0.64 | 0.64 |
| 32nd | 0.15 | 0.15 | 0.15 | 0.10 | 0.10 | 0.10 | 0.2 | 0.45 | 0.45 | 0.45 | 0.21 | 0.21 | 0.21 |
| 33rd | 0.33 | 0.33 | 0.33 | 0.23 | 0.23 | 0.23 | 0.2 | 0.90 | 0.90 | 0.90 | 0.42 | 0.42 | 0.42 |
| 34th | 0.16 | 0.16 | 0.16 | 0.11 | 0.11 | 0.11 | 0.2 | 0.45 | 0.45 | 0.45 | 0.21 | 0.21 | 0.21 |
| 35th | 0.18 | 0.18 | 0.18 | 0.13 | 0.13 | 0.13 | 0.71 | 0.45 | 0.45 | 0.45 | 0.21 | 0.21 | 0.21 |
| 36th | 0.17 | 0.17 | 0.17 | 0.12 | 0.12 | 0.12 | 0.2 | 0.45 | 0.45 | 0.45 | 0.21 | 0.21 | 0.21 |
| 37th | 0.19 | 0.19 | 0.19 | 0.14 | 0.14 | 0.14 | 0.68 | 0.44 | 0.44 | 0.44 | 0.20 | 0.20 | 0.20 |
| 38th | 0.00 | 0.00 | 0.00 | 0.00 | 0.00 | 0.00 | 0.2 | 0.00 | 0.00 | 0.00 | 0.00 | 0.00 | 0.00 |
| 39th | 0.20 | 0.20 | 0.20 | 0.14 | 0.14 | 0.14 | 0.2 | 0.44 | 0.44 | 0.44 | 0.20 | 0.20 | 0.20 |
| 40th | 0.18 | 0.18 | 0.18 | 0.13 | 0.13 | 0.13 | 0.2 | 0.44 | 0.44 | 0.44 | 0.20 | 0.20 | 0.20 |
| Harmonics higher than the limits set by ER G5/5 | | | | | | | | | | | | | |
| Harmonics on the boundary of the limits set by ER G5/5 | | | | | | | | | | | | | |
| Number of PVs on Feeder 1: 54 Number of PVs on Feeder 2: 69 Voltage on Neutral: 3.449V | | | | | | | | | | | | | |

The tipping points for this scenario with a two-phase fault on feeder one to remain compliant under the different PV generation profiles within ER G5/5 on feeder one was identified. It was found that for Table 3.3.1.1, the maximum penetration was 33.6% (forty-two PV generators), for Table 3.3.1.4 was 55.2% (sixty-nine PV generators) and for Table 3.3.1.7 was 21.6% (twenty-seven PV generators). These were evenly distributed across three phases on feeders one and two as close as is achievable to a 44-56% split between the PV generators on feeders one and two respectively.

During a three-phase fault, fed by red, as seen in Figures 4.3.1.3(A-C), the THDv increased further at the start, middle and end of the network on the red phase. Dissimilar to the EVC simulations, the THDv increases along the length of the network on the yellow and blue phases as the current travels from the pot end back towards the transformer. The maximum THDv recorded on feeder one is 3.37% for the harmonic profile from Table 3.3.1.1, 2.14% for the harmonic profile from Table 3.3.1.4 and 3.72% for the harmonic profile from Table 3.3.1.7. The highest THDv on feeder one was measured on the yellow phase supply terminal at the start of the EDN.

By comparing the results in Table 4.3.1.3 to the results seen in Tables 4.3.1.2, under the three-phase fault condition, the magnitude of individual voltage harmonics at the yellow phase supply terminal at the start of feeder one increase significantly. When analysing the increase in harmonic currents for a two-phase fault to a three-phase fault arrangement they increase significantly, however, similar to the phase voltage harmonics, not to the same magnitude seen from normal to two-phase fault arrangements. A three-phase fault results in the $15^{th}$, $21^{st}$, $27^{th}$, $33^{rd}$, $39^{th}$, and $40^{th}$ voltage harmonics on feeder one exceeding the boundary of limits set out by ER G5/5 for the harmonic profiles from Tables 3.3.1.1 and 3.3.1.7. For the harmonic profile from Table 3.3.1.4, the three-phase fault results in the $27^{th}$, $33^{rd}$, $39^{th}$, and $40^{th}$ voltage harmonic on feeder one exceeding the boundary of limits set out by ER G5/5. The $34^{th}$ and $36^{th}$ harmonics sit on the boundary of these limits for all PV harmonic profiles. Therefore, if this LV EDN was to be left with a three-phase fault, as would be compliant with the ESQCRs, this would result in a non-compliance with ER G5/5.

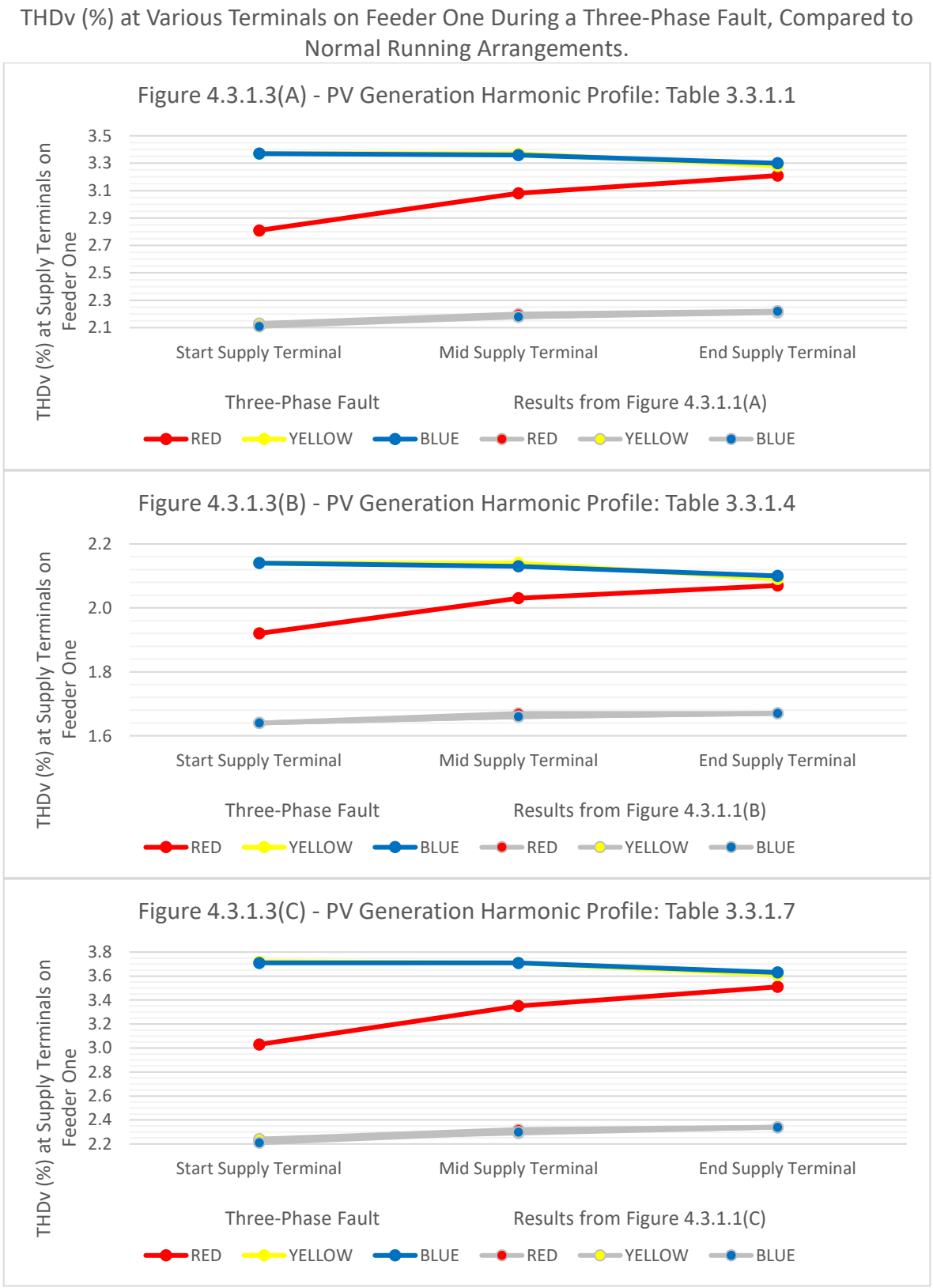


**Figure 4.3.1.3: Graphical representation of the THDv measured on each phase at supply terminals at the start, middle and end of feeder one during a three-phase fault at 98.4% PV generation penetration and the PV generation harmonic profile stated compared to normal running arrangements.**

**Table 4.3.1.3: Table of harmonics on feeder one during a three-phase fault at 98.4% PV generation penetration against the limits set out in ER G5/5 for the PV generation harmonic profile stated (Energy Networks Association, 2020).**

| Harmonic Number | Worst Case Voltage Harmonic Magnitude at Supply Terminals (%) | | | Worst Case Voltage Harmonic Magnitude at Transformer (%) | | | ER G5/5 Limits (%) | Worst Case Phase Current Harmonic Magnitude at Transformer (A) | | | Neutral Harmonic Current Magnitude at Transformer (A) | | |
|---|---|---|---|---|---|---|---|---|---|---|---|---|---|
| | PV Generation Harmonic Profile from Table 3.3.1.- | | | PV Generation Harmonic Profile from Table 3.3.1.- | | | | PV Generation Harmonic Profile from Table 3.3.1.- | | | PV Generation Harmonic Profile from Table 3.3.1.- | | |
| | .1 | .4 | .7 | .1 | .4 | .7 | | .1 | .4 | .7 | .1 | .4 | .7 |
| 2nd | 0.18 | 0.18 | 0.18 | 0.11 | 0.11 | 0.11 | 1.6 | 4.99 | 4.99 | 4.99 | 3.46 | 3.46 | 3.46 |
| 3rd | 1.14 | 0.68 | 1.51 | 0.93 | 0.66 | 1.15 | 4.0 | 18.04 | 5.59 | 28.04 | 12.52 | 3.89 | 19.45 |
| 4th | 0.13 | 0.02 | 0.05 | 0.09 | 0.02 | 0.04 | 1.0 | 2.50 | 0.03 | 0.64 | 1.73 | 0.02 | 0.43 |
| 5th | 1.33 | 0.66 | 1.01 | 1.07 | 0.64 | 0.87 | 4.0 | 15.56 | 3.78 | 9.95 | 10.79 | 2.63 | 6.91 |
| 6th | 0.07 | 0.07 | 0.07 | 0.06 | 0.06 | 0.06 | 0.5 | 0.62 | 0.62 | 0.62 | 0.43 | 0.43 | 0.43 |
| 7th | 1.45 | 0.93 | 1.40 | 1.30 | 0.96 | 1.27 | 4.0 | 9.36 | 2.79 | 8.74 | 6.50 | 1.95 | 6.08 |
| 8th | 0.07 | 0.07 | 0.07 | 0.06 | 0.06 | 0.06 | 0.4 | 0.62 | 0.62 | 0.62 | 0.43 | 0.43 | 0.43 |
| 9th | 0.82 | 0.34 | 0.88 | 0.61 | 0.30 | 0.65 | 1.2 | 6.80 | 1.87 | 7.42 | 4.72 | 1.30 | 5.15 |
| 10th | 0.09 | 0.09 | 0.09 | 0.07 | 0.07 | 0.07 | 0.4 | 0.62 | 0.62 | 0.62 | 0.43 | 0.43 | 0.43 |
| 11th | 1.04 | 0.68 | 1.19 | 0.90 | 0.66 | 1.00 | 3.0 | 4.97 | 2.02 | 6.19 | 3.45 | 1.40 | 4.29 |
| 12th | 0.11 | 0.11 | 0.11 | 0.08 | 0.08 | 0.08 | 0.2 | 0.61 | 0.61 | 0.61 | 0.43 | 0.43 | 0.43 |
| 13th | 1.14 | 0.45 | 1.14 | 0.93 | 0.47 | 0.93 | 2.5 | 5.53 | 0.92 | 5.53 | 3.83 | 0.64 | 3.83 |
| 14th | 0.03 | 0.03 | 0.03 | 0.03 | 0.03 | 0.03 | 0.2 | 0.05 | 0.05 | 0.05 | 0.03 | 0.03 | 0.03 |
| 15th | 0.69 | 0.30 | 0.88 | 0.51 | 0.25 | 0.64 | 0.5 | 3.64 | 1.22 | 4.85 | 2.52 | 0.85 | 3.36 |
| 16th | 0.13 | 0.13 | 0.13 | 0.10 | 0.10 | 0.10 | 0.2 | 0.60 | 0.60 | 0.60 | 0.42 | 0.42 | 0.42 |
| 17th | 0.61 | 0.39 | 0.72 | 0.43 | 0.29 | 0.51 | 1.6 | 3.01 | 1.81 | 3.61 | 2.08 | 1.25 | 2.50 |
| 18th | 0.13 | 0.13 | 0.13 | 0.10 | 0.10 | 0.10 | 0.2 | 0.60 | 0.60 | 0.60 | 0.41 | 0.41 | 0.41 |
| 19th | 0.45 | 0.20 | 0.81 | 0.34 | 0.18 | 0.58 | 1.5 | 1.79 | 0.61 | 3.58 | 1.24 | 0.43 | 2.47 |
| 20th | 0.14 | 0.14 | 0.14 | 0.10 | 0.10 | 0.10 | 0.2 | 0.59 | 0.59 | 0.59 | 0.41 | 0.41 | 0.41 |
| 21st | 0.57 | 0.17 | 0.84 | 0.40 | 0.14 | 0.58 | 0.2 | 2.36 | 0.59 | 3.54 | 1.63 | 0.41 | 2.44 |
| 22nd | 0.02 | 0.02 | 0.02 | 0.02 | 0.02 | 0.02 | 0.2 | 0.03 | 0.03 | 0.03 | 0.02 | 0.02 | 0.02 |
| 23rd | 0.32 | 0.46 | 0.75 | 0.23 | 0.33 | 0.52 | 1.2 | 1.17 | 1.75 | 2.92 | 0.81 | 1.21 | 2.01 |
| 24th | 0.16 | 0.16 | 0.16 | 0.11 | 0.11 | 0.11 | 0.2 | 0.58 | 0.58 | 0.58 | 0.40 | 0.40 | 0.40 |
| 25th | 0.49 | 0.34 | 0.65 | 0.35 | 0.24 | 0.45 | 1.0 | 1.73 | 1.15 | 2.30 | 1.19 | 0.79 | 1.59 |
| 26th | 0.01 | 0.01 | 0.01 | 0.01 | 0.01 | 0.01 | 0.2 | 0.02 | 0.02 | 0.02 | 0.01 | 0.01 | 0.01 |
| 27th | 0.35 | 0.35 | 0.35 | 0.25 | 0.25 | 0.25 | 0.2 | 1.14 | 1.14 | 1.14 | 0.78 | 0.78 | 0.78 |
| 28th | 0.18 | 0.18 | 0.18 | 0.12 | 0.12 | 0.12 | 0.2 | 0.57 | 0.57 | 0.57 | 0.39 | 0.39 | 0.39 |
| 29th | 0.54 | 0.54 | 0.54 | 0.37 | 0.37 | 0.37 | 0.86 | 1.68 | 1.68 | 1.68 | 1.16 | 1.16 | 1.16 |
| 30th | 0.18 | 0.18 | 0.18 | 0.12 | 0.12 | 0.12 | 0.2 | 0.56 | 0.56 | 0.56 | 0.38 | 0.38 | 0.38 |
| 31st | 0.57 | 0.57 | 0.57 | 0.40 | 0.40 | 0.40 | 0.81 | 1.66 | 1.66 | 1.66 | 1.14 | 1.14 | 1.14 |
| 32nd | 0.19 | 0.19 | 0.19 | 0.13 | 0.13 | 0.13 | 0.2 | 0.55 | 0.55 | 0.55 | 0.38 | 0.38 | 0.38 |
| 33rd | 0.40 | 0.40 | 0.40 | 0.28 | 0.28 | 0.28 | 0.2 | 1.09 | 1.09 | 1.09 | 0.75 | 0.75 | 0.75 |
| 34th | 0.20 | 0.20 | 0.20 | 0.13 | 0.13 | 0.13 | 0.2 | 0.54 | 0.54 | 0.54 | 0.37 | 0.37 | 0.37 |
| 35th | 0.22 | 0.22 | 0.22 | 0.15 | 0.15 | 0.15 | 0.71 | 0.54 | 0.54 | 0.54 | 0.37 | 0.37 | 0.37 |
| 36th | 0.20 | 0.20 | 0.20 | 0.14 | 0.14 | 0.14 | 0.2 | 0.53 | 0.53 | 0.53 | 0.36 | 0.36 | 0.36 |
| 37th | 0.22 | 0.22 | 0.22 | 0.16 | 0.16 | 0.16 | 0.68 | 0.53 | 0.53 | 0.53 | 0.36 | 0.36 | 0.36 |
| 38th | 0.00 | 0.00 | 0.00 | 0.00 | 0.00 | 0.00 | 0.2 | 0.00 | 0.00 | 0.00 | 0.00 | 0.00 | 0.00 |
| 39th | 0.23 | 0.23 | 0.23 | 0.16 | 0.16 | 0.16 | 0.2 | 0.52 | 0.52 | 0.52 | 0.36 | 0.36 | 0.36 |
| 40th | 0.22 | 0.22 | 0.22 | 0.15 | 0.15 | 0.15 | 0.2 | 0.52 | 0.52 | 0.52 | 0.35 | 0.35 | 0.35 |
| Harmonics higher than the limits set by ER G5/5 | | | | | | | | | | | | | |
| Harmonics on the boundary of the limits set by ER G5/5 | | | | | | | | | | | | | |
| Number of PVs on Feeder 1: 54 Number of PVs on Feeder 2: 69 Voltage on Neutral: 5.881V | | | | | | | | | | | | | |

The tipping points for this scenario with a three-phase fault on feeder one to remain compliant under the different PV generation harmonic profiles with ER G5/5 on feeder one was identified. It was found that for Table 3.3.1.1, the maximum penetration was 24% (thirty PV generators), for Table 3.3.1.4 was 45.6% (fifty-seven PV generators) and for Table 3.3.1.7 was 16.8% (twenty-one PV generators). These were evenly distributed across three phases on feeders one and two as close as is achievable to a 44-56% split between the PV generators on feeders one and two respectively.

In addition, it was found that the neutral voltage present at the end of feeder one increased to 5.881V under three-phase fault conditions shown in Table 4.3.1.3 from 3.449V under two-phase conditions in Table 4.3.1.2 and 0.020V under normal arrangements shown in Table 4.3.1.1. Based on Table 3.2.7.4, the voltages caused by a two or three-phase fault could lead to residents perceiving shocks off exposed bonded metal work, potentially leading to complaints. However, it does not seem high enough to cause ventricular fibrillation or respiratory tetanus.

## 4.3.2 – Results of Phase-to-Phase Faults, with a Two-Phase Fault on Feeder Two

Further to Section 4.3.1, the effect of faults on feeder one will be explored whilst a second two-phase fault on feeder two is present. Firstly, similar to Section 4.2.2, it can be seen that there is a marked drop in THDv on the yellow phase and a marked increase in THDv on the red phase on feeder one, when compared to Figures 4.3.1.1(A-C), as seen in Figures 4.3.2.1(A-C). This is due to load being removed from the yellow phase and added to the red phase via a two-phase fault on feeder two. Due to the current being drawn on feeder one remaining the same, the increase in THDv between the beginning and the end of feeder one remains low at 0.02-0.12%, similar to Figures 4.3.1.1(A-C). The individual harmonic levels can be seen in Table 4.3.2.1 and it can be seen that the fault on feeder two has led to additional breaches of ER G5/5 on feeder one such as the $15^{th}$ and $27^{th}$ harmonic when compared to Table 4.3.1.1. Despite the two-phase fault on feeder two leading to the neutral voltage increasing from 0.020V to 1.232V, the voltage does not exceed 2.70V on feeder one and therefore, should not be high enough to cause perceived shocks to residents. However, based on the results of Table 4.3.1.2, it is likely that residents will receive shocks off of feeder two.

THDv (%) at Various Terminals on Feeder One During Normal Running Arrangements on Feeder One and a Two-Phase Fault on Feeder Two, Compared to the Results of Figures 4.3.1.1 (A-C).

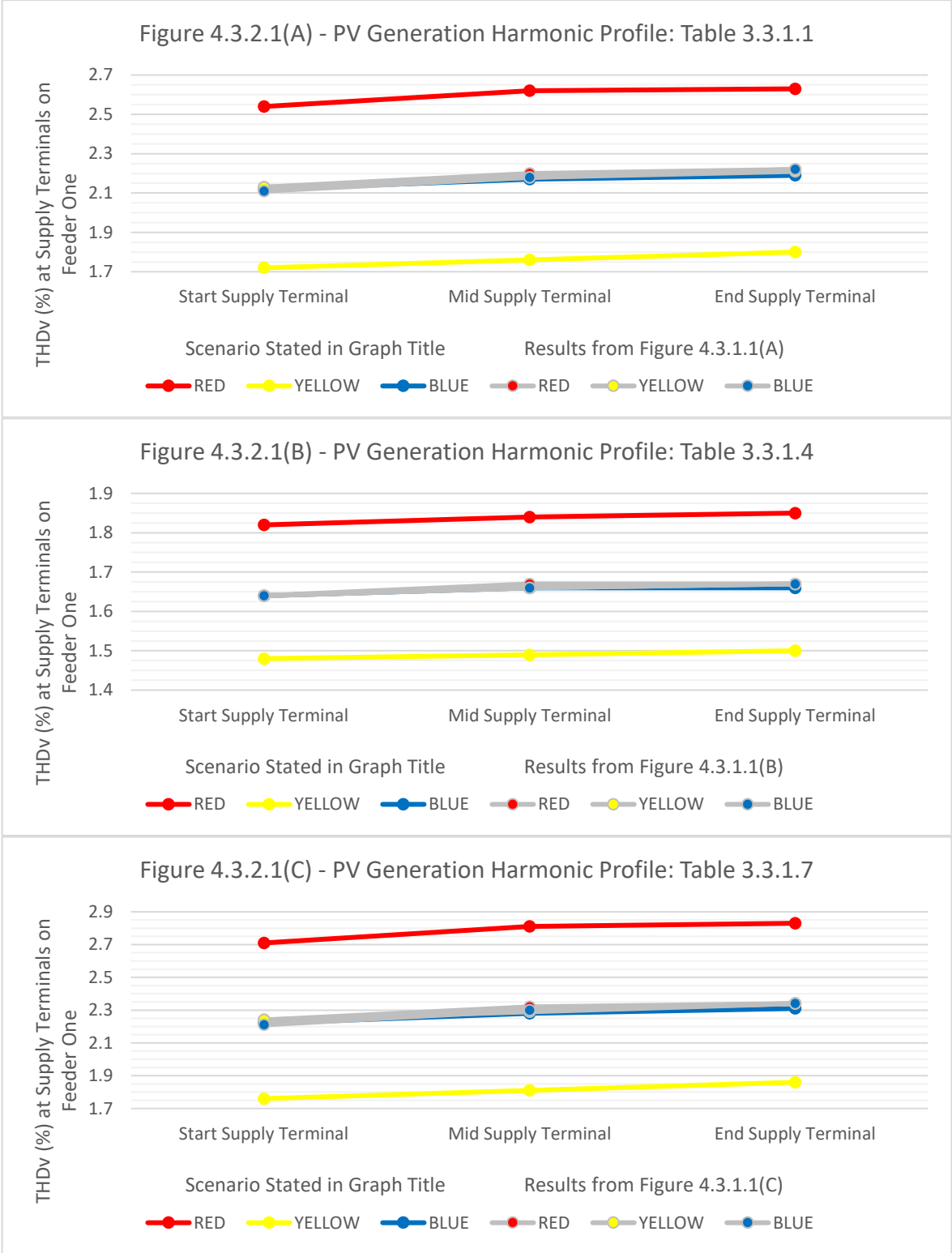


**Figure 4.3.2.1: Graphical representation of the THDv measured on each phase at supply terminals at the start, middle and end of feeder one under normal running arrangements at 98.4% PV generation penetration and the PV generation harmonic profile stated whilst a two-phase fault is present on feeder two, compared to normal running arrangements on feeders one and two (Figures 4.3.1.1 (A-C)).**

**Table 4.3.2.1: Table of harmonics on feeder one for normal running arrangements at 98.4% PV generation penetration against the limits set out in ER G5/5 for the PV generation harmonic profile stated whilst a two-phase fault is present on feeder two (Energy Networks Association, 2020).**

| Harmonic Number | Worst Case Voltage Harmonic Magnitude at Supply Terminals (%) | | | Worst Case Voltage Harmonic Magnitude at Transformer (%) | | | ER G5/5 Limits (%) | Worst Case Phase Current Harmonic Magnitude at Transformer (A) | | | Neutral Harmonic Current Magnitude at Transformer (A) | | |
|---|---|---|---|---|---|---|---|---|---|---|---|---|---|
| | PV Generation Harmonic Profile from Table 3.3.1.- | | | PV Generation Harmonic Profile from Table 3.3.1.- | | | | PV Generation Harmonic Profile from Table 3.3.1.- | | | PV Generation Harmonic Profile from Table 3.3.1.- | | |
| | .1 | .4 | .7 | .1 | .4 | .7 | | .1 | .4 | .7 | .1 | .4 | .7 |
| 2nd | 0.11 | 0.11 | 0.11 | 0.10 | 0.10 | 0.10 | 1.6 | 4.18 | 4.18 | 4.18 | 2.56 | 2.56 | 2.56 |
| 3rd | 0.91 | 0.65 | 1.12 | 0.87 | 0.64 | 1.05 | 4.0 | 15.12 | 4.68 | 23.50 | 9.23 | 2.86 | 14.35 |
| 4th | 0.09 | 0.02 | 0.04 | 0.08 | 0.02 | 0.03 | 1.0 | 2.09 | 0.03 | 0.52 | 1.27 | 0.02 | 0.32 |
| 5th | 1.04 | 0.63 | 0.84 | 0.98 | 0.62 | 0.81 | 4.0 | 13.05 | 3.17 | 8.35 | 7.91 | 1.93 | 5.07 |
| 6th | 0.05 | 0.05 | 0.05 | 0.05 | 0.05 | 0.05 | 0.5 | 0.52 | 0.52 | 0.52 | 0.32 | 0.32 | 0.32 |
| 7th | 1.26 | 0.94 | 1.23 | 1.23 | 0.94 | 1.20 | 4.0 | 7.86 | 2.35 | 7.35 | 4.74 | 1.42 | 4.43 |
| 8th | 0.05 | 0.05 | 0.05 | 0.05 | 0.05 | 0.05 | 0.4 | 0.52 | 0.52 | 0.52 | 0.31 | 0.31 | 0.31 |
| 9th | 0.59 | 0.29 | 0.63 | 0.55 | 0.28 | 0.58 | 1.2 | 5.73 | 1.57 | 6.25 | 3.42 | 0.94 | 3.73 |
| 10th | 0.07 | 0.07 | 0.07 | 0.07 | 0.07 | 0.07 | 0.4 | 0.52 | 0.52 | 0.52 | 0.31 | 0.31 | 0.31 |
| 11th | 0.88 | 0.65 | 0.97 | 0.85 | 0.64 | 0.93 | 3.0 | 4.20 | 1.70 | 5.22 | 2.50 | 1.02 | 3.10 |
| 12th | 0.08 | 0.08 | 0.08 | 0.07 | 0.07 | 0.07 | 0.2 | 0.52 | 0.52 | 0.52 | 0.31 | 0.31 | 0.31 |
| 13th | 0.90 | 0.47 | 0.90 | 0.85 | 0.47 | 0.85 | 2.5 | 4.68 | 0.78 | 4.68 | 2.76 | 0.46 | 2.76 |
| 14th | 0.03 | 0.03 | 0.03 | 0.03 | 0.03 | 0.03 | 0.2 | 0.04 | 0.04 | 0.04 | 0.02 | 0.02 | 0.02 |
| 15th | 0.49 | 0.24 | 0.61 | 0.45 | 0.23 | 0.56 | 0.5 | 3.09 | 1.04 | 4.12 | 1.81 | 0.61 | 2.41 |
| 16th | 0.09 | 0.09 | 0.09 | 0.09 | 0.09 | 0.09 | 0.2 | 0.51 | 0.51 | 0.51 | 0.30 | 0.30 | 0.30 |
| 17th | 0.42 | 0.28 | 0.49 | 0.38 | 0.26 | 0.44 | 1.6 | 2.56 | 1.54 | 3.08 | 1.49 | 0.89 | 1.79 |
| 18th | 0.09 | 0.09 | 0.09 | 0.09 | 0.09 | 0.09 | 0.2 | 0.51 | 0.51 | 0.51 | 0.30 | 0.30 | 0.30 |
| 19th | 0.33 | 0.17 | 0.56 | 0.31 | 0.17 | 0.51 | 1.5 | 1.53 | 0.53 | 3.06 | 0.88 | 0.30 | 1.76 |
| 20th | 0.10 | 0.10 | 0.10 | 0.09 | 0.09 | 0.09 | 0.2 | 0.51 | 0.51 | 0.51 | 0.29 | 0.29 | 0.29 |
| 21st | 0.39 | 0.13 | 0.56 | 0.35 | 0.12 | 0.51 | 0.2 | 2.03 | 0.51 | 3.04 | 1.16 | 0.29 | 1.74 |
| 22nd | 0.02 | 0.02 | 0.02 | 0.02 | 0.02 | 0.02 | 0.2 | 0.03 | 0.03 | 0.03 | 0.02 | 0.02 | 0.02 |
| 23rd | 0.22 | 0.32 | 0.50 | 0.20 | 0.29 | 0.45 | 1.2 | 1.01 | 1.51 | 2.52 | 0.57 | 0.86 | 1.43 |
| 24th | 0.11 | 0.11 | 0.11 | 0.10 | 0.10 | 0.10 | 0.2 | 0.50 | 0.50 | 0.50 | 0.28 | 0.28 | 0.28 |
| 25th | 0.34 | 0.24 | 0.44 | 0.31 | 0.22 | 0.40 | 1.0 | 1.50 | 1.00 | 2.00 | 0.85 | 0.56 | 1.13 |
| 26th | 0.01 | 0.01 | 0.01 | 0.01 | 0.01 | 0.01 | 0.2 | 0.01 | 0.01 | 0.01 | 0.01 | 0.01 | 0.01 |
| 27th | 0.24 | 0.24 | 0.24 | 0.22 | 0.22 | 0.22 | 0.2 | 0.99 | 0.99 | 0.99 | 0.56 | 0.56 | 0.56 |
| 28th | 0.12 | 0.12 | 0.12 | 0.11 | 0.11 | 0.11 | 0.2 | 0.49 | 0.49 | 0.49 | 0.28 | 0.28 | 0.28 |
| 29th | 0.36 | 0.36 | 0.36 | 0.33 | 0.33 | 0.33 | 0.86 | 1.48 | 1.48 | 1.48 | 0.82 | 0.82 | 0.82 |
| 30th | 0.12 | 0.12 | 0.12 | 0.11 | 0.11 | 0.11 | 0.2 | 0.49 | 0.49 | 0.49 | 0.27 | 0.27 | 0.27 |
| 31st | 0.39 | 0.39 | 0.39 | 0.35 | 0.35 | 0.35 | 0.81 | 1.46 | 1.46 | 1.46 | 0.81 | 0.81 | 0.81 |
| 32nd | 0.12 | 0.12 | 0.12 | 0.11 | 0.11 | 0.11 | 0.2 | 0.49 | 0.49 | 0.49 | 0.27 | 0.27 | 0.27 |
| 33rd | 0.27 | 0.27 | 0.27 | 0.25 | 0.25 | 0.25 | 0.2 | 0.97 | 0.97 | 0.97 | 0.53 | 0.53 | 0.53 |
| 34th | 0.13 | 0.13 | 0.13 | 0.12 | 0.12 | 0.12 | 0.2 | 0.48 | 0.48 | 0.48 | 0.26 | 0.26 | 0.26 |
| 35th | 0.15 | 0.15 | 0.15 | 0.14 | 0.14 | 0.14 | 0.71 | 0.48 | 0.48 | 0.48 | 0.26 | 0.26 | 0.26 |
| 36th | 0.14 | 0.14 | 0.14 | 0.12 | 0.12 | 0.12 | 0.2 | 0.48 | 0.48 | 0.48 | 0.26 | 0.26 | 0.26 |
| 37th | 0.16 | 0.16 | 0.16 | 0.14 | 0.14 | 0.14 | 0.68 | 0.47 | 0.47 | 0.47 | 0.26 | 0.26 | 0.26 |
| 38th | 0.00 | 0.00 | 0.00 | 0.00 | 0.00 | 0.00 | 0.2 | 0.00 | 0.00 | 0.00 | 0.00 | 0.00 | 0.00 |
| 39th | 0.16 | 0.16 | 0.16 | 0.15 | 0.15 | 0.15 | 0.2 | 0.47 | 0.47 | 0.47 | 0.25 | 0.25 | 0.25 |
| 40th | 0.15 | 0.15 | 0.15 | 0.13 | 0.13 | 0.13 | 0.2 | 0.47 | 0.47 | 0.47 | 0.25 | 0.25 | 0.25 |
| Harmonics higher than the limits set by ER G5/5 | | | | | | | | | | | | | |
| Harmonics on the boundary of the limits set by ER G5/5 | | | | | | | | | | | | | |
| Number of PVs on Feeder 1: 54 Number of PVs on Feeder 2: 69 Voltage on Neutral: 1.232V | | | | | | | | | | | | | |

The tipping points for this scenario with normal running arrangements on feeder one and a two-phase fault on feeder two to remain compliant under the different PV generation profiles with ER G5/5 was identified on feeder one. It was found that for Table 3.3.1.1, the maximum penetration was 43.2% (fifty-four PV generators), for Table 3.3.1.4 was 69.6% (eighty-seven PV generators) and for Table 3.3.1.7 was 26.4% (thirty-three PV generators). These were evenly distributed across three phases on feeders one and two as close as is achievable to a 44-56% split between PV generators on feeders one and two respectively.

By introducing a two-phase fault on feeder one, between red and yellow phases, with red phase feeding the fault as seen in Figures 4.3.2.2(A-C), it has been found that the THDv increases significantly along the length of feeder one on red phase, with the THDv also increasing slightly on yellow phase as the current travels back towards the transformer. This is alongside a two-phase fault on feeder two. This leads to the THDv measured on the yellow phase supply terminal at the start of feeder one reaching the highest level for the data from Tables 3.3.1.1 and 3.3.1.4. For the data from Table 3.3.1.7, the yellow phase supply terminal measured in the middle of feeder one reached the highest THDv level. Across feeder one there is no noticeable effect on the blue phase THDv, which is excluded from the faulted phases. The maximum THDv recorded on feeder one is 3.27% for the harmonic profile from Table 3.3.1.1, 2.12% for the harmonic profile from Table 3.3.1.4 and 3.59% for the harmonic profile from Table 3.3.1.7.

The results of the worst-case harmonic distortion on feeder one under a two-phase fault can be seen in Table 4.3.2.2. The worst-case harmonic distortion was measured between phase and neutral across the yellow phase supply terminals on feeder one in shown in Figures 4.3.1.2(A-C). The worst-case THDv varies between each of the harmonic profiles due to the harmonic current contribution seen in Table 4.3.2.2. ER G5/5 limits are exceeded across multiple harmonics including $15^{th}$, $21^{st}$, $27^{th}$, and $33^{rd}$, therefore resulting in non-compliance. Further to the two-phase fault analysed in Section 4.3.1, the two-phase fault on feeder two has led to the $39^{th}$ and $40^{th}$ harmonic limits under ER G5/5 being breached. ER G5/5 limits are met for the $36^{th}$ harmonic, for the harmonic profiles stated in Tables 3.3.1.1 and 3.3.1.4. Lastly, due to the network imbalance, the neutral voltage on feeder one has increased to 4.669V, which is high enough to provide residents with potential shocks off exposed metalwork.

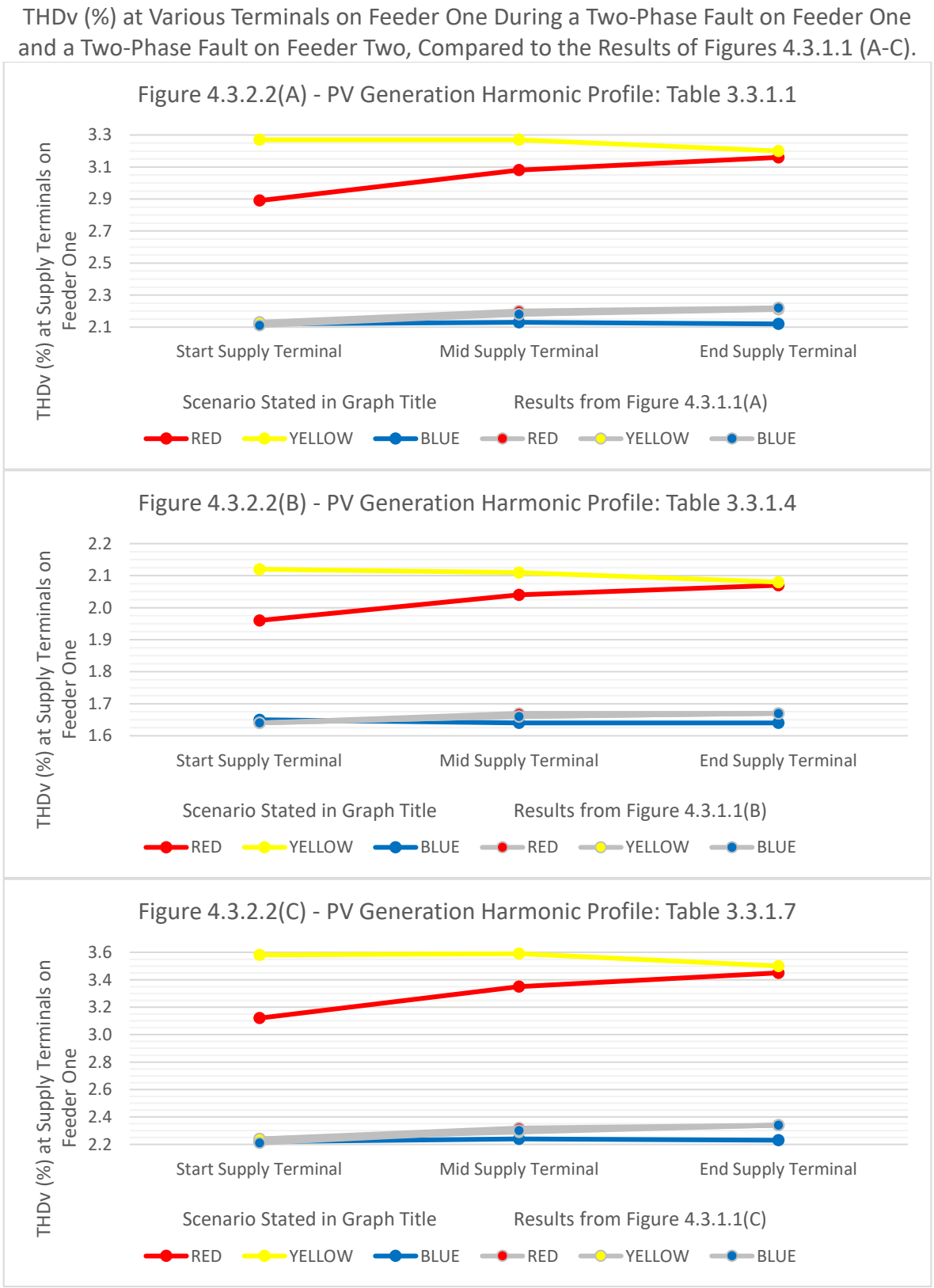


**Figure 4.3.2.2: Graphical representation of the THDv measured on each phase at supply terminals at the start, middle and end of feeder one during a two-phase fault at 98.4% PV generation penetration and PV generation harmonic profile stated whilst a two-phase fault is present on feeder two, compared to normal running arrangements on feeders one and two (Figures 4.3.1.1 (A-C)).**

**Table 4.3.2.2: Table of harmonics on feeder one for during a two-phase fault at 98.4% PV generation penetration against the limits set out in ER G5/5 for the PV generation harmonic profile stated whilst a two-phase fault is present on feeder two (Energy Networks Association, 2020).**

| Harmonic Number | Worst Case Voltage Harmonic Magnitude at Supply Terminals (%) | | | Worst Case Voltage Harmonic Magnitude at Transformer (%) | | | ER G5/5 Limits (%) | Worst Case Phase Current Harmonic Magnitude at Transformer (A) | | | Neutral Harmonic Current Magnitude at Transformer (A) | | |
|---|---|---|---|---|---|---|---|---|---|---|---|---|---|
| | PV Generation Harmonic Profile from Table 3.3.1.- | | | PV Generation Harmonic Profile from Table 3.3.1.- | | | | PV Generation Harmonic Profile from Table 3.3.1.- | | | PV Generation Harmonic Profile from Table 3.3.1.- | | |
| | .1 | .4 | .7 | .1 | .4 | .7 | | .1 | .4 | .7 | .1 | .4 | .7 |
| 2nd | 0.16 | 0.16 | 0.16 | 0.12 | 0.12 | 0.12 | 1.6 | 5.33 | 5.33 | 5.33 | 4.56 | 4.56 | 4.56 |
| 3rd | 1.10 | 0.68 | 1.45 | 0.95 | 0.67 | 1.18 | 4.0 | 19.28 | 5.97 | 29.96 | 16.40 | 5.08 | 25.48 |
| 4th | 0.13 | 0.02 | 0.04 | 0.10 | 0.02 | 0.04 | 1.0 | 2.67 | 0.04 | 0.67 | 2.26 | 0.03 | 0.56 |
| 5th | 1.28 | 0.66 | 0.99 | 1.10 | 0.65 | 0.89 | 4.0 | 16.62 | 4.04 | 10.64 | 13.99 | 3.40 | 8.96 |
| 6th | 0.07 | 0.07 | 0.07 | 0.06 | 0.06 | 0.06 | 0.5 | 0.66 | 0.66 | 0.66 | 0.56 | 0.56 | 0.56 |
| 7th | 1.43 | 0.94 | 1.39 | 1.33 | 0.95 | 1.29 | 4.0 | 10.00 | 2.99 | 9.35 | 8.34 | 2.49 | 7.79 |
| 8th | 0.07 | 0.07 | 0.07 | 0.06 | 0.06 | 0.06 | 0.4 | 0.66 | 0.66 | 0.66 | 0.55 | 0.55 | 0.55 |
| 9th | 0.79 | 0.33 | 0.84 | 0.64 | 0.30 | 0.68 | 1.2 | 7.27 | 2.00 | 7.94 | 6.00 | 1.65 | 6.54 |
| 10th | 0.09 | 0.09 | 0.09 | 0.08 | 0.08 | 0.08 | 0.4 | 0.66 | 0.66 | 0.66 | 0.54 | 0.54 | 0.54 |
| 11th | 1.02 | 0.68 | 1.16 | 0.93 | 0.67 | 1.03 | 3.0 | 5.32 | 2.16 | 6.62 | 4.34 | 1.76 | 5.40 |
| 12th | 0.10 | 0.10 | 0.10 | 0.09 | 0.09 | 0.09 | 0.2 | 0.66 | 0.66 | 0.66 | 0.53 | 0.53 | 0.53 |
| 13th | 1.11 | 0.46 | 1.11 | 0.96 | 0.48 | 0.96 | 2.5 | 5.92 | 0.98 | 5.92 | 4.78 | 0.80 | 4.78 |
| 14th | 0.03 | 0.03 | 0.03 | 0.03 | 0.03 | 0.03 | 0.2 | 0.05 | 0.05 | 0.05 | 0.04 | 0.04 | 0.04 |
| 15th | 0.66 | 0.29 | 0.84 | 0.53 | 0.25 | 0.67 | 0.5 | 3.90 | 1.31 | 5.20 | 3.11 | 1.05 | 4.15 |
| 16th | 0.12 | 0.12 | 0.12 | 0.10 | 0.10 | 0.10 | 0.2 | 0.65 | 0.65 | 0.65 | 0.52 | 0.52 | 0.52 |
| 17th | 0.58 | 0.37 | 0.68 | 0.46 | 0.30 | 0.54 | 1.6 | 3.22 | 1.94 | 3.87 | 2.55 | 1.53 | 3.06 |
| 18th | 0.13 | 0.13 | 0.13 | 0.10 | 0.10 | 0.10 | 0.2 | 0.64 | 0.64 | 0.64 | 0.50 | 0.50 | 0.50 |
| 19th | 0.43 | 0.20 | 0.77 | 0.35 | 0.18 | 0.61 | 1.5 | 1.92 | 0.66 | 3.84 | 1.50 | 0.52 | 3.00 |
| 20th | 0.14 | 0.14 | 0.14 | 0.11 | 0.11 | 0.11 | 0.2 | 0.64 | 0.64 | 0.64 | 0.49 | 0.49 | 0.49 |
| 21st | 0.54 | 0.17 | 0.79 | 0.43 | 0.14 | 0.62 | 0.2 | 2.53 | 0.64 | 3.80 | 1.96 | 0.49 | 2.94 |
| 22nd | 0.02 | 0.02 | 0.02 | 0.02 | 0.02 | 0.02 | 0.2 | 0.03 | 0.03 | 0.03 | 0.03 | 0.03 | 0.03 |
| 23rd | 0.31 | 0.44 | 0.71 | 0.24 | 0.35 | 0.55 | 1.2 | 1.25 | 1.88 | 3.13 | 0.96 | 1.44 | 2.40 |
| 24th | 0.15 | 0.15 | 0.15 | 0.12 | 0.12 | 0.12 | 0.2 | 0.62 | 0.62 | 0.62 | 0.47 | 0.47 | 0.47 |
| 25th | 0.47 | 0.33 | 0.62 | 0.37 | 0.26 | 0.48 | 1.0 | 1.86 | 1.24 | 2.48 | 1.41 | 0.94 | 1.88 |
| 26th | 0.01 | 0.01 | 0.01 | 0.01 | 0.01 | 0.01 | 0.2 | 0.02 | 0.02 | 0.02 | 0.01 | 0.01 | 0.01 |
| 27th | 0.34 | 0.34 | 0.34 | 0.26 | 0.26 | 0.26 | 0.2 | 1.23 | 1.23 | 1.23 | 0.92 | 0.92 | 0.92 |
| 28th | 0.17 | 0.17 | 0.17 | 0.13 | 0.13 | 0.13 | 0.2 | 0.61 | 0.61 | 0.61 | 0.45 | 0.45 | 0.45 |
| 29th | 0.51 | 0.51 | 0.51 | 0.39 | 0.39 | 0.39 | 0.86 | 1.82 | 1.82 | 1.82 | 1.35 | 1.35 | 1.35 |
| 30th | 0.17 | 0.17 | 0.17 | 0.13 | 0.13 | 0.13 | 0.2 | 0.60 | 0.60 | 0.60 | 0.44 | 0.44 | 0.44 |
| 31st | 0.55 | 0.55 | 0.55 | 0.42 | 0.42 | 0.42 | 0.81 | 1.79 | 1.79 | 1.79 | 1.32 | 1.32 | 1.32 |
| 32nd | 0.18 | 0.18 | 0.18 | 0.14 | 0.14 | 0.14 | 0.2 | 0.59 | 0.59 | 0.59 | 0.43 | 0.43 | 0.43 |
| 33rd | 0.38 | 0.38 | 0.38 | 0.30 | 0.30 | 0.30 | 0.2 | 1.18 | 1.18 | 1.18 | 0.86 | 0.86 | 0.86 |
| 34th | 0.19 | 0.19 | 0.19 | 0.14 | 0.14 | 0.14 | 0.2 | 0.59 | 0.59 | 0.59 | 0.42 | 0.42 | 0.42 |
| 35th | 0.21 | 0.21 | 0.21 | 0.16 | 0.16 | 0.16 | 0.71 | 0.58 | 0.58 | 0.58 | 0.42 | 0.42 | 0.42 |
| 36th | 0.20 | 0.20 | 0.19 | 0.15 | 0.15 | 0.15 | 0.2 | 0.58 | 0.58 | 0.58 | 0.41 | 0.41 | 0.41 |
| 37th | 0.22 | 0.22 | 0.21 | 0.17 | 0.17 | 0.17 | 0.68 | 0.57 | 0.57 | 0.57 | 0.41 | 0.41 | 0.41 |
| 38th | 0.00 | 0.00 | 0.00 | 0.00 | 0.00 | 0.00 | 0.2 | 0.00 | 0.00 | 0.00 | 0.00 | 0.00 | 0.00 |
| 39th | 0.22 | 0.22 | 0.22 | 0.17 | 0.17 | 0.17 | 0.2 | 0.57 | 0.57 | 0.57 | 0.40 | 0.40 | 0.40 |
| 40th | 0.21 | 0.21 | 0.21 | 0.16 | 0.16 | 0.16 | 0.2 | 0.56 | 0.56 | 0.56 | 0.39 | 0.39 | 0.39 |
| Harmonics higher than the limits set by ER G5/5 | | | | | | | | | | | | | |
| Harmonics on the boundary of the limits set by ER G5/5 | | | | | | | | | | | | | |
| Number of PVs on Feeder 1: 54 Number of PVs on Feeder 2: 69 Voltage on Neutral: 4.669V | | | | | | | | | | | | | |

The tipping points for this scenario with a two-phase fault on feeder one to remain compliant under the different PV generation profiles with ER G5/5 on feeder one was identified. It was found that for Table 3.3.1.1, the maximum penetration was 28.8% (thirty-six PV generators), for Table 3.3.1.4 was 45.6% (fifty-seven PV generators) and for Table 3.3.1.7 was 16.8% (twenty-one PV generators). This is a considerable drop when compared to the normal running arrangement limits stated earlier in this section and the two-phase fault limits stated in Section 4.3.1.

During a three-phase fault, fed by red, as seen in Figures 4.3.2.3(A-C), the THDv increased further at the start, middle and end of feeder one on the red phase. Like the three-phase fault in Section 4.3.1, the THDv increases along the length of feeder one on the yellow and blue phases as the current travels from the pot end back towards the transformer. The maximum THDv recorded on feeder one is 3.71% for the harmonic profile from Table 3.3.1.1, 2.30% for the harmonic profile from Table 3.3.1.4 and 4.11% for the harmonic profile from Table 3.3.1.7. The highest THDv was measured on the yellow phase supply terminal at the start of the EDN.

By comparing the results in Table 4.3.2.3 to the results seen in Table 4.3.2.2, under the three-phase fault condition, the magnitude of individual voltage harmonics at the yellow phase supply terminal at the start of feeder one increase further. A three-phase fault results in the $15^{th}$, $21^{st}$, $27^{th}$, $32^{nd}$ $33^{rd}$, $34^{th}$, $36^{th}$, $39^{th}$, and $40^{th}$ harmonics exceeding the boundary of limits set out by ER G5/5 for the harmonic profiles from Tables 3.3.1.1 and 3.3.1.7. For the harmonic profile from Table 3.3.1.4, the three-phase fault results in the $27^{th}$, $32^{nd}$, $33^{rd}$, $34^{th}$, $36^{th}$, $39^{th}$, and $40^{th}$ harmonics exceeding the boundary of limits set out by ER G5/5. The $28^{th}$ and $30^{th}$ harmonics sit on the boundary of these limits for all PV generation harmonic profiles. Therefore, if this LV EDN was to be left with a three-phase fault, as would be compliant with the ESQCRs, this would result in a non-compliance with ER G5/5.

THDv (%) at Various Terminals on Feeder One During a Three-Phase Fault on Feeder One and a Two-Phase Fault on Feeder Two, Compared to the Results of Figures 4.3.1.1 (A-C).

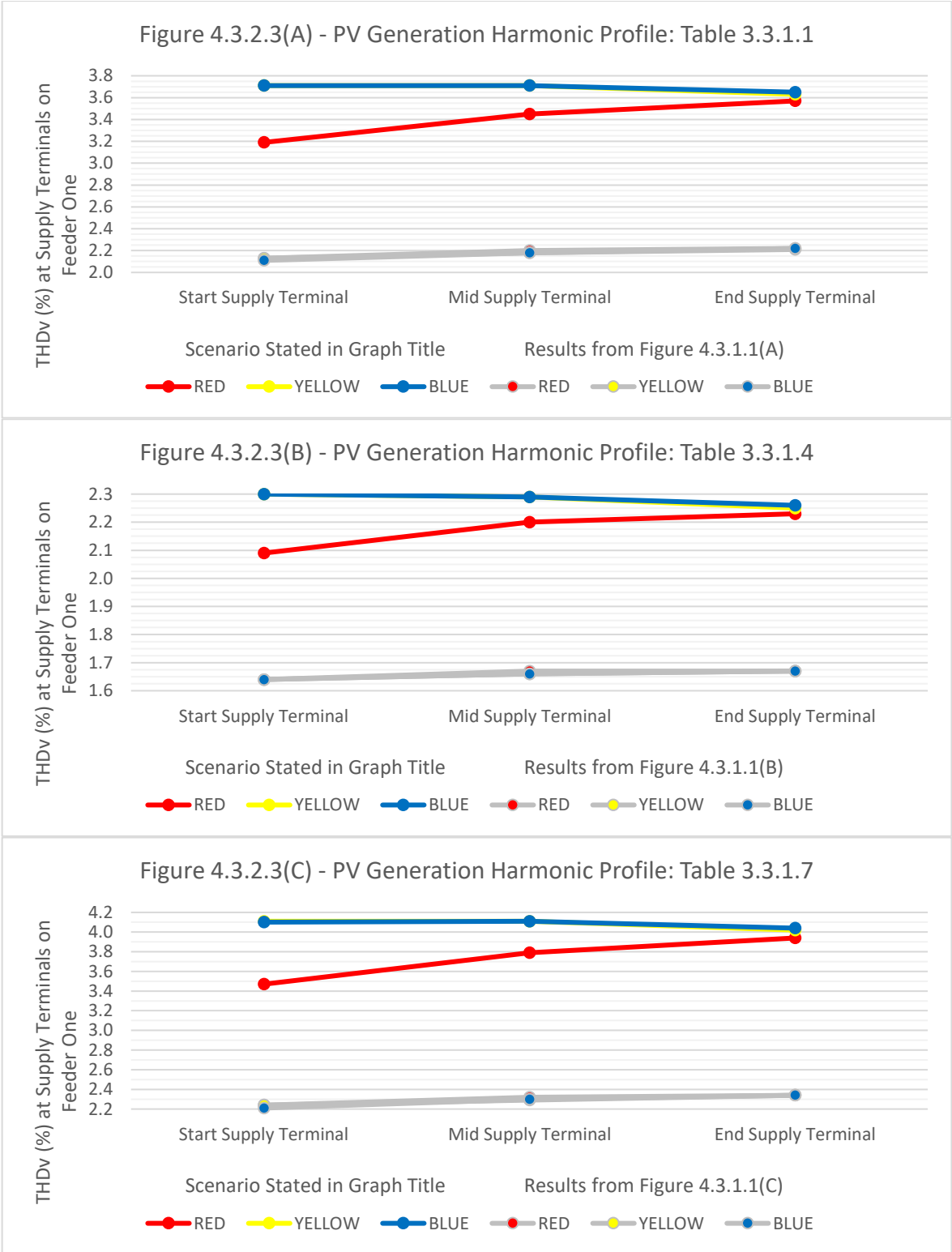


**Figure 4.3.2.3: Graphical representation of the THDv measured on each phase at supply terminals at the beginning, middle and end of feeder one during a three-phase fault at 98.4% PV generation penetration and PV generation harmonic profile stated whilst a two-phase fault is present on feeder two, compared to normal running arrangements on feeders one and two (Figures 4.3.1.1 (A-C)).**

**Table 4.3.2.3: Table of harmonics on feeder one during a three-phase fault at 98.4% PV generation penetration against the limits set out in ER G5/5 for the PV generation harmonic profile stated whilst a two-phase fault is present on feeder two (Energy Networks Association, 2020).**

| Harmonic Number | Worst Case Voltage Harmonic Magnitude at Supply Terminals (%) | | | Worst Case Voltage Harmonic Magnitude at Transformer (%) | | | ER G5/5 Limits (%) | Worst Case Phase Current Harmonic Magnitude at Transformer (A) | | | Neutral Harmonic Current Magnitude at Transformer (A) | | |
|---|---|---|---|---|---|---|---|---|---|---|---|---|---|
| | PV Generation Harmonic Profile from Table 3.3.1.- | | | PV Generation Harmonic Profile from Table 3.3.1.- | | | | PV Generation Harmonic Profile from Table 3.3.1.- | | | PV Generation Harmonic Profile from Table 3.3.1.- | | |
| | .1 | .4 | .7 | .1 | .4 | .7 | | .1 | .4 | .7 | .1 | .4 | .7 |
| 2nd | 0.19 | 0.19 | 0.19 | 0.13 | 0.13 | 0.13 | 1.6 | 6.45 | 6.45 | 6.45 | 5.79 | 5.79 | 5.79 |
| 3rd | 1.23 | 0.71 | 1.66 | 1.04 | 0.69 | 1.31 | 4.0 | 23.31 | 7.22 | 36.23 | 20.84 | 6.46 | 32.39 |
| 4th | 0.15 | 0.02 | 0.05 | 0.11 | 0.02 | 0.04 | 1.0 | 3.22 | 0.04 | 0.80 | 2.87 | 0.04 | 0.72 |
| 5th | 1.47 | 0.69 | 1.10 | 1.22 | 0.68 | 0.96 | 4.0 | 20.08 | 4.88 | 12.85 | 17.81 | 4.33 | 11.40 |
| 6th | 0.07 | 0.07 | 0.07 | 0.06 | 0.06 | 0.06 | 0.5 | 0.80 | 0.80 | 0.80 | 0.71 | 0.71 | 0.71 |
| 7th | 1.56 | 0.95 | 1.51 | 1.42 | 0.98 | 1.38 | 4.0 | 8.75 | 3.60 | 11.27 | 10.62 | 3.17 | 9.92 |
| 8th | 0.08 | 0.08 | 0.08 | 0.06 | 0.06 | 0.06 | 0.4 | 0.79 | 0.80 | 0.80 | 0.70 | 0.70 | 0.70 |
| 9th | 0.93 | 0.36 | 1.00 | 0.73 | 0.33 | 0.78 | 1.2 | 8.75 | 2.40 | 9.54 | 7.63 | 2.10 | 8.33 |
| 10th | 0.10 | 0.10 | 0.10 | 0.09 | 0.09 | 0.09 | 0.4 | 0.79 | 0.79 | 0.79 | 0.69 | 0.69 | 0.69 |
| 11th | 1.13 | 0.70 | 1.30 | 1.00 | 0.69 | 1.12 | 3.0 | 6.38 | 2.58 | 7.94 | 5.52 | 2.24 | 6.87 |
| 12th | 0.12 | 0.12 | 0.12 | 0.10 | 0.10 | 0.10 | 0.2 | 0.79 | 0.79 | 0.79 | 0.68 | 0.68 | 0.68 |
| 13th | 1.25 | 0.46 | 1.25 | 1.06 | 0.48 | 1.06 | 2.5 | 7.07 | 1.17 | 7.07 | 6.07 | 1.01 | 6.07 |
| 14th | 0.03 | 0.03 | 0.03 | 0.03 | 0.03 | 0.03 | 0.2 | 0.06 | 0.06 | 0.06 | 0.05 | 0.05 | 0.05 |
| 15th | 0.78 | 0.33 | 1.00 | 0.61 | 0.28 | 0.77 | 0.5 | 4.64 | 1.56 | 6.19 | 3.95 | 1.33 | 5.27 |
| 16th | 0.14 | 0.14 | 0.14 | 0.12 | 0.12 | 0.12 | 0.2 | 0.77 | 0.77 | 0.77 | 0.65 | 0.65 | 0.65 |
| 17th | 0.69 | 0.44 | 0.82 | 0.53 | 0.34 | 0.62 | 1.6 | 3.82 | 2.29 | 4.59 | 3.22 | 1.94 | 3.87 |
| 18th | 0.15 | 0.15 | 0.15 | 0.12 | 0.12 | 0.12 | 0.2 | 0.76 | 0.76 | 0.76 | 0.64 | 0.64 | 0.64 |
| 19th | 0.50 | 0.22 | 0.92 | 0.40 | 0.19 | 0.70 | 1.5 | 2.27 | 0.78 | 4.53 | 1.90 | 0.65 | 3.79 |
| 20th | 0.16 | 0.16 | 0.16 | 0.12 | 0.12 | 0.12 | 0.2 | 0.75 | 0.75 | 0.75 | 0.62 | 0.62 | 0.62 |
| 21st | 0.65 | 0.19 | 0.95 | 0.49 | 0.16 | 0.71 | 0.2 | 2.97 | 0.75 | 4.46 | 2.47 | 0.62 | 3.79 |
| 22nd | 0.02 | 0.02 | 0.02 | 0.02 | 0.02 | 0.02 | 0.2 | 0.04 | 0.04 | 0.04 | 0.03 | 0.03 | 0.03 |
| 23rd | 0.36 | 0.52 | 0.85 | 0.28 | 0.39 | 0.63 | 1.2 | 1.47 | 2.20 | 3.66 | 1.20 | 1.81 | 3.01 |
| 24th | 0.18 | 0.18 | 0.18 | 0.13 | 0.13 | 0.13 | 0.2 | 0.73 | 0.73 | 0.73 | 0.59 | 0.59 | 0.59 |
| 25th | 0.55 | 0.38 | 0.73 | 0.42 | 0.29 | 0.55 | 1.0 | 2.16 | 1.44 | 2.88 | 1.76 | 1.17 | 2.35 |
| 26th | 0.01 | 0.01 | 0.01 | 0.01 | 0.01 | 0.01 | 0.2 | 0.02 | 0.02 | 0.02 | 0.02 | 0.02 | 0.02 |
| 27th | 0.39 | 0.39 | 0.39 | 0.30 | 0.30 | 0.30 | 0.2 | 1.42 | 1.42 | 1.42 | 1.14 | 1.14 | 1.14 |
| 28th | 0.20 | 0.20 | 0.20 | 0.15 | 0.15 | 0.15 | 0.2 | 0.70 | 0.70 | 0.70 | 0.56 | 0.56 | 0.56 |
| 29th | 0.60 | 0.60 | 0.60 | 0.45 | 0.45 | 0.45 | 0.86 | 2.09 | 2.09 | 2.09 | 1.67 | 1.67 | 1.67 |
| 30th | 0.20 | 0.20 | 0.20 | 0.15 | 0.15 | 0.15 | 0.2 | 0.69 | 0.69 | 0.69 | 0.55 | 0.55 | 0.55 |
| 31st | 0.64 | 0.64 | 0.64 | 0.48 | 0.48 | 0.48 | 0.81 | 2.05 | 2.05 | 2.05 | 1.63 | 1.63 | 1.63 |
| 32nd | 0.21 | 0.21 | 0.21 | 0.15 | 0.15 | 0.15 | 0.2 | 0.68 | 0.68 | 0.68 | 0.53 | 0.53 | 0.53 |
| 33rd | 0.44 | 0.44 | 0.44 | 0.33 | 0.33 | 0.33 | 0.2 | 1.34 | 1.34 | 1.34 | 1.05 | 1.05 | 1.05 |
| 34th | 0.22 | 0.22 | 0.22 | 0.16 | 0.16 | 0.16 | 0.2 | 0.66 | 0.66 | 0.66 | 0.52 | 0.52 | 0.52 |
| 35th | 0.24 | 0.24 | 0.24 | 0.18 | 0.18 | 0.18 | 0.71 | 0.66 | 0.66 | 0.66 | 0.51 | 0.51 | 0.51 |
| 36th | 0.23 | 0.23 | 0.23 | 0.17 | 0.17 | 0.17 | 0.2 | 0.65 | 0.65 | 0.65 | 0.50 | 0.50 | 0.50 |
| 37th | 0.24 | 0.24 | 0.24 | 0.19 | 0.19 | 0.19 | 0.68 | 0.65 | 0.65 | 0.65 | 0.50 | 0.50 | 0.50 |
| 38th | 0.00 | 0.00 | 0.00 | 0.00 | 0.00 | 0.00 | 0.2 | 0.00 | 0.00 | 0.00 | 0.00 | 0.00 | 0.00 |
| 39th | 0.25 | 0.25 | 0.25 | 0.19 | 0.19 | 0.19 | 0.2 | 0.63 | 0.63 | 0.63 | 0.48 | 0.48 | 0.48 |
| 40th | 0.24 | 0.24 | 0.24 | 0.18 | 0.18 | 0.18 | 0.2 | 0.63 | 0.63 | 0.63 | 0.48 | 0.48 | 0.48 |
| Harmonics higher than the limits set by ER G5/5 | | | | | | | | | | | | | |
| Harmonics on the boundary of the limits set by ER G5/5 | | | | | | | | | | | | | |
| Number of PVs on Feeder 1: 54 Number of PVs on Feeder 2: 69 Voltage on Neutral: 6.953V | | | | | | | | | | | | | |

The tipping points for this scenario with a three-phase fault on feeder one to remain compliant under the different PV generation harmonic profiles with ER G5/5 was identified. It was found that for Table 3.3.1.1, the maximum penetration was 24% (thirty PV generators), for Table 3.3.1.4 was 40.8% (fifty-one PV generators) and for Table 3.3.1.7 was 12.0% (fifteen PV generators). These were evenly distributed across three phases on feeders one and two as close as is achievable to a 44-56% split between PV generators on feeders one and two respectively.

In addition, it was found that the neutral voltage present at the end of feeder one increased to 6.953V under three-phase fault conditions shown in Table 4.3.2.3, from 4.669V under two-phase conditions in Table 4.3.2.2 and 1.232V under normal arrangements shown in Table 4.3.2.1. Based on Table 3.2.7.4, the voltages caused by a two or three-phase fault could lead to residents perceiving shocks off exposed bonded metal work, potentially leading to complaints. This is in line with a two and three-phase faults mentioned in Section 4.3.1.

## 4.3.3 – Results of Phase-to-Phase Faults, with a Three-Phase Fault on Feeder Two

Further to Sections 4.3.1 and 4.3.2, the effect of faults on feeder one will be explored whilst a second three-phase fault on feeder two is present. It can be seen in Figures 4.3.3.1 (A-C) that the THDv measured on blue phase of feeder one has dropped when compared to Figure 4.3.2.1. This brings both yellow and blue THDv on feeder one to a similar level. This is due to the load on yellow and blue phases being shifted onto the red phase, caused by the three-phase fault on feeder two. This shift in load has also caused the THDv level of red phase on feeder one to rise by between 0.15-0.41% when compared to the similar scenario with a two-phase fault on feeder two shown in Figures 4.3.2.1 (A-C).

THDv (%) at Various Terminals on Feeder One During Normal Running Arrangements on Feeder One and a Three-Phase Fault on Feeder Two, Compared to the Results of Figures 4.3.1.1 (A-C).

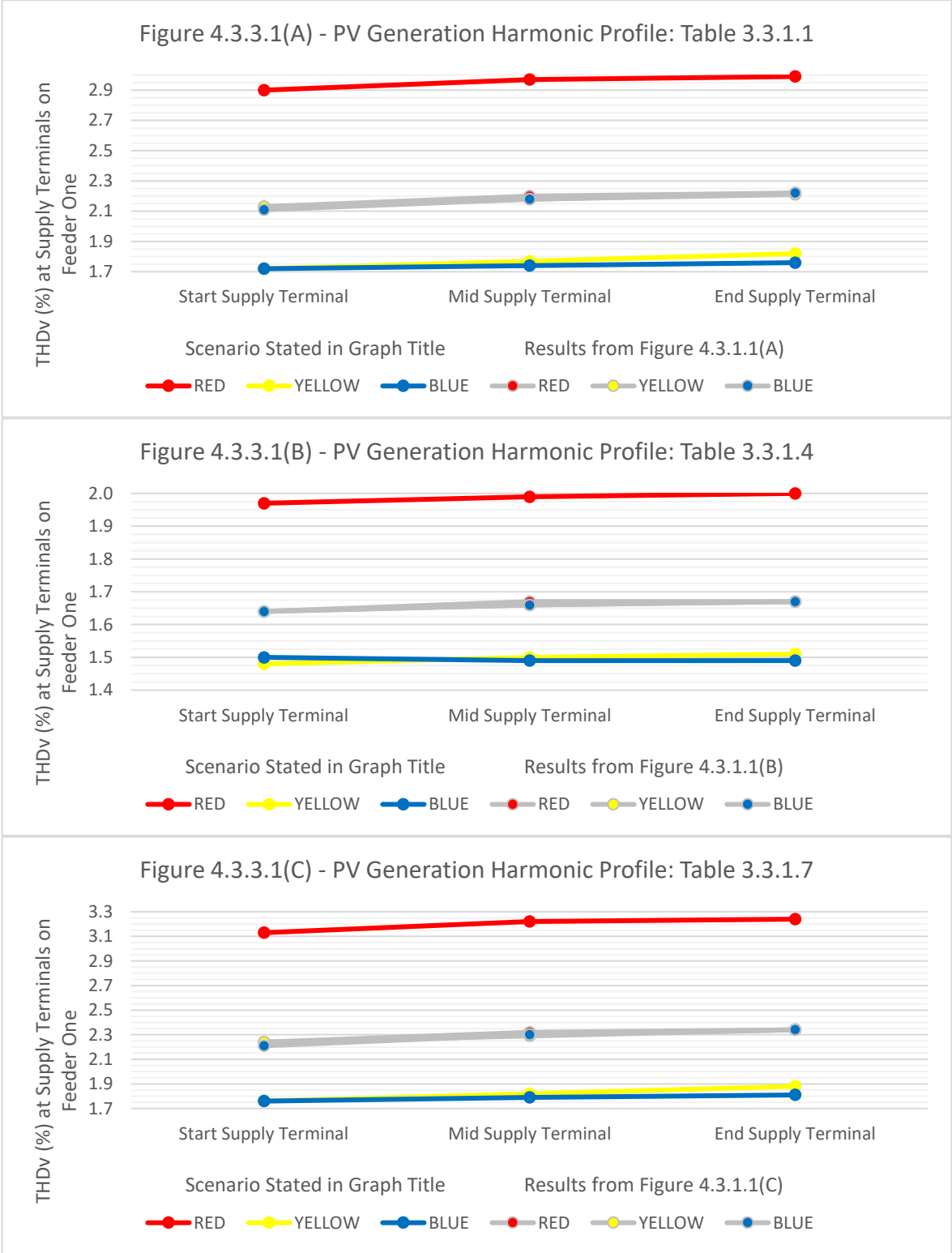


**Figure 4.3.3.1: Graphical representation of the THDv measured on each phase at supply terminals at the start, middle and end of feeder one under normal running arrangements at 98.4% PV generation penetration and PV generation harmonic profile stated whilst a three-phase fault is present on feeder two, compared to normal running arrangements on feeders one and two (Figures 4.3.1.1 (A-C)).**

**Table 4.3.3.1: Table of harmonics on feeder one for normal running arrangements at 98.4% PV generation penetration against the limits set out in ER G5/5 for the PV generation harmonic profile stated whilst a three-phase fault is present on feeder two (Energy Networks Association, 2020).**

| Harmonic Number | Worst Case Voltage Harmonic Magnitude at Supply Terminals (%) | | | Worst Case Voltage Harmonic Magnitude at Transformer (%) | | | ER G5/5 Limits (%) | Worst Case Phase Current Harmonic Magnitude at Transformer (A) | | | Neutral Harmonic Current Magnitude at Transformer (A) | | |
|---|---|---|---|---|---|---|---|---|---|---|---|---|---|
| | PV Generation Harmonic Profile from Table 3.3.1.- | | | PV Generation Harmonic Profile from Table 3.3.1.- | | | | PV Generation Harmonic Profile from Table 3.3.1.- | | | PV Generation Harmonic Profile from Table 3.3.1.- | | |
| | .1 | .4 | .7 | .1 | .4 | .7 | | .1 | .4 | .7 | .1 | .4 | .7 |
| 2nd | 0.13 | 0.13 | 0.13 | 0.12 | 0.12 | 0.12 | 1.6 | 5.60 | 5.60 | 5.60 | 4.40 | 4.40 | 4.40 |
| 3rd | 1.01 | 0.68 | 1.28 | 0.98 | 0.68 | 1.22 | 4.0 | 20.24 | 6.27 | 31.45 | 15.90 | 4.93 | 24.72 |
| 4th | 0.11 | 0.02 | 0.04 | 0.10 | 0.02 | 0.04 | 1.0 | 2.80 | 0.04 | 0.70 | 2.20 | 0.03 | 0.55 |
| 5th | 1.19 | 0.66 | 0.93 | 1.13 | 0.66 | 0.91 | 4.0 | 17.44 | 4.24 | 11.16 | 13.70 | 3.33 | 8.77 |
| 6th | 0.06 | 0.06 | 0.06 | 0.06 | 0.06 | 0.06 | 0.5 | 0.70 | 0.70 | 0.70 | 0.55 | 0.55 | 0.55 |
| 7th | 1.38 | 0.96 | 1.34 | 1.35 | 0.97 | 1.32 | 4.0 | 10.49 | 3.14 | 9.80 | 8.24 | 2.47 | 7.70 |
| 8th | 0.06 | 0.06 | 0.06 | 0.06 | 0.06 | 0.06 | 0.4 | 0.69 | 0.69 | 0.69 | 0.55 | 0.55 | 0.55 |
| 9th | 0.70 | 0.32 | 0.75 | 0.66 | 0.31 | 0.71 | 1.2 | 7.61 | 2.09 | 8.31 | 5.98 | 1.64 | 6.52 |
| 10th | 0.08 | 0.08 | 0.08 | 0.08 | 0.08 | 0.08 | 0.4 | 0.69 | 0.69 | 0.69 | 0.54 | 0.54 | 0.54 |
| 11th | 0.97 | 0.68 | 1.09 | 0.94 | 0.67 | 1.05 | 3.0 | 5.56 | 2.26 | 6.92 | 4.37 | 1.77 | 5.43 |
| 12th | 0.09 | 0.09 | 0.09 | 0.09 | 0.09 | 0.09 | 0.2 | 0.69 | 0.69 | 0.69 | 0.54 | 0.54 | 0.54 |
| 13th | 1.02 | 0.47 | 1.02 | 0.98 | 0.48 | 0.98 | 2.5 | 6.17 | 1.03 | 6.17 | 4.84 | 0.81 | 4.84 |
| 14th | 0.03 | 0.03 | 0.03 | 0.03 | 0.03 | 0.03 | 0.2 | 0.06 | 0.06 | 0.06 | 0.04 | 0.04 | 0.04 |
| 15th | 0.58 | 0.27 | 0.74 | 0.55 | 0.26 | 0.69 | 0.5 | 4.06 | 1.37 | 5.41 | 3.18 | 1.07 | 4.24 |
| 16th | 0.11 | 0.11 | 0.11 | 0.11 | 0.11 | 0.11 | 0.2 | 0.67 | 0.67 | 0.67 | 0.53 | 0.53 | 0.53 |
| 17th | 0.50 | 0.33 | 0.59 | 0.47 | 0.31 | 0.55 | 1.6 | 3.35 | 2.01 | 4.02 | 2.62 | 1.58 | 3.15 |
| 18th | 0.11 | 0.11 | 0.11 | 0.10 | 0.10 | 0.10 | 0.2 | 0.67 | 0.67 | 0.67 | 0.52 | 0.52 | 0.52 |
| 19th | 0.38 | 0.19 | 0.67 | 0.36 | 0.18 | 0.63 | 1.5 | 1.99 | 0.68 | 3.97 | 1.56 | 0.54 | 3.11 |
| 20th | 0.12 | 0.12 | 0.12 | 0.11 | 0.11 | 0.11 | 0.2 | 0.66 | 0.66 | 0.66 | 0.52 | 0.52 | 0.52 |
| 21st | 0.47 | 0.15 | 0.68 | 0.44 | 0.14 | 0.63 | 0.2 | 2.62 | 0.66 | 3.92 | 2.05 | 0.52 | 3.07 |
| 22nd | 0.02 | 0.02 | 0.02 | 0.02 | 0.02 | 0.02 | 0.2 | 0.04 | 0.04 | 0.04 | 0.03 | 0.03 | 0.03 |
| 23rd | 0.27 | 0.38 | 0.61 | 0.25 | 0.35 | 0.57 | 1.2 | 1.29 | 1.94 | 3.23 | 1.01 | 1.51 | 2.52 |
| 24th | 0.13 | 0.13 | 0.13 | 0.12 | 0.12 | 0.12 | 0.2 | 0.64 | 0.64 | 0.64 | 0.50 | 0.50 | 0.50 |
| 25th | 0.40 | 0.28 | 0.53 | 0.38 | 0.26 | 0.49 | 1.0 | 1.91 | 1.27 | 2.55 | 1.49 | 1.00 | 1.99 |
| 26th | 0.01 | 0.01 | 0.01 | 0.01 | 0.01 | 0.01 | 0.2 | 0.02 | 0.02 | 0.02 | 0.01 | 0.01 | 0.01 |
| 27th | 0.29 | 0.29 | 0.29 | 0.27 | 0.27 | 0.27 | 0.2 | 1.26 | 1.26 | 1.26 | 0.98 | 0.98 | 0.98 |
| 28th | 0.14 | 0.14 | 0.14 | 0.13 | 0.13 | 0.13 | 0.2 | 0.62 | 0.62 | 0.62 | 0.49 | 0.49 | 0.49 |
| 29th | 0.43 | 0.43 | 0.43 | 0.40 | 0.40 | 0.40 | 0.86 | 1.85 | 1.85 | 1.85 | 1.45 | 1.45 | 1.45 |
| 30th | 0.14 | 0.14 | 0.14 | 0.13 | 0.13 | 0.13 | 0.2 | 0.61 | 0.61 | 0.61 | 0.48 | 0.48 | 0.48 |
| 31st | 0.46 | 0.46 | 0.46 | 0.43 | 0.43 | 0.43 | 0.81 | 1.82 | 1.82 | 1.82 | 1.42 | 1.42 | 1.42 |
| 32nd | 0.15 | 0.15 | 0.15 | 0.14 | 0.14 | 0.14 | 0.2 | 0.60 | 0.60 | 0.60 | 0.47 | 0.47 | 0.47 |
| 33rd | 0.32 | 0.32 | 0.32 | 0.30 | 0.30 | 0.30 | 0.2 | 1.20 | 1.20 | 1.20 | 0.93 | 0.93 | 0.93 |
| 34th | 0.16 | 0.16 | 0.16 | 0.14 | 0.14 | 0.14 | 0.2 | 0.59 | 0.59 | 0.59 | 0.46 | 0.46 | 0.46 |
| 35th | 0.18 | 0.18 | 0.18 | 0.16 | 0.16 | 0.16 | 0.71 | 0.59 | 0.59 | 0.59 | 0.46 | 0.46 | 0.46 |
| 36th | 0.16 | 0.16 | 0.16 | 0.15 | 0.15 | 0.15 | 0.2 | 0.58 | 0.58 | 0.58 | 0.45 | 0.45 | 0.45 |
| 37th | 0.18 | 0.18 | 0.18 | 0.17 | 0.17 | 0.17 | 0.68 | 0.58 | 0.58 | 0.58 | 0.45 | 0.45 | 0.45 |
| 38th | 0.00 | 0.00 | 0.00 | 0.00 | 0.00 | 0.00 | 0.2 | 0.00 | 0.00 | 0.00 | 0.00 | 0.00 | 0.00 |
| 39th | 0.19 | 0.19 | 0.19 | 0.17 | 0.17 | 0.17 | 0.2 | 0.57 | 0.57 | 0.57 | 0.44 | 0.44 | 0.44 |
| 40th | 0.17 | 0.17 | 0.17 | 0.16 | 0.16 | 0.16 | 0.2 | 0.56 | 0.56 | 0.56 | 0.44 | 0.44 | 0.44 |
| Harmonics higher than the limits set by ER G5/5 | | | | | | | | | | | | | |
| Harmonics on the boundary of the limits set by ER G5/5 | | | | | | | | | | | | | |
| Number of PVs on Feeder 1: 54 Number of PVs on Feeder 2: 69 Voltage on Neutral: 2.129V | | | | | | | | | | | | | |

Due to the current being drawn on feeder one remaining the same, the increase in THDv between the beginning and the end of feeder one remains low at 0.03-0.12%, similar to Figures 4.3.1.1(A-C) and 4.3.2.1(A-C). The individual harmonic levels can be seen in Table 4.3.3.1 and it can be seen that the fault on feeder two has led to an additional breach of the 15$^{th}$ harmonic under ER G5/5 on feeder one when compared to Table 4.3.2.1. This breach of ER G5/5 is for the harmonic profile from Table 3.3.1.1. Despite the three-phase fault on feeder two leading to the neutral voltage increasing from 0.020V to 2.129V the voltage does not exceed 2.70V on feeder one and therefore should not be high enough to cause perceived shocks to residents. However, based on the results of Table 4.3.1.2, it is likely that residents will receive shocks off feeder two.

The tipping points for this scenario with normal running arrangements on feeder one and a three-phase fault on feeder two to remain compliant under the different PV generation profiles with ER G5/5 on feeder one was identified. It was found that for Table 3.3.1.1, the maximum penetration was 33.6% (forty-two PV generators), for Table 3.3.1.4 was 57.6% (seventy-two PV generators) and for Table 3.3.1.7 was 21.6% (twenty-seven PV generators). These were evenly distributed across three phases on feeders one and two as close as is achievable to a 44-56% split between PVs on feeders one and two respectively.

By introducing a two-phase fault between red and yellow phases on feeder one, with red phase feeding the fault as seen in Figures 4.3.3.2(A-C), the THDv increases when compared to Figures 4.3.3.1(A-C), similar to Figures 4.3.1.2(A-C) and 4.3.2.2(A-C). This is alongside a three-phase fault on feeder two and therefore the maximum THDv level is approximately 0.3-0.81% higher than Figures 4.3.1.2(A-C) and 0.13-0.38% higher than 4.3.2.2(A-C). The maximum THDv level was measured on the yellow phase supply terminal at the start of the feeder one. Similar to Figures 4.3.1.2(A-C) and 4.3.2.2(A-C), there is no noticeable increase in THDv for blue phase along the length of feeder one, however, the THDv level is lower than both of these figures due in part to the three-phase fault on feeder two removing harmonic load from this phase. The maximum THDv recorded on feeder one is 3.59% for the harmonic profile from Table 3.3.1.1, 2.25% for the harmonic profile from Table 3.3.1.4 and 3.96% for the harmonic profile from Table 3.3.1.7.

THDv (%) at Various Terminals on Feeder One During a Two-Phase Fault on Feeder One and a Three-Phase Fault on Feeder Two, Compared to the Results of Figures 4.3.1.1 (A-C).

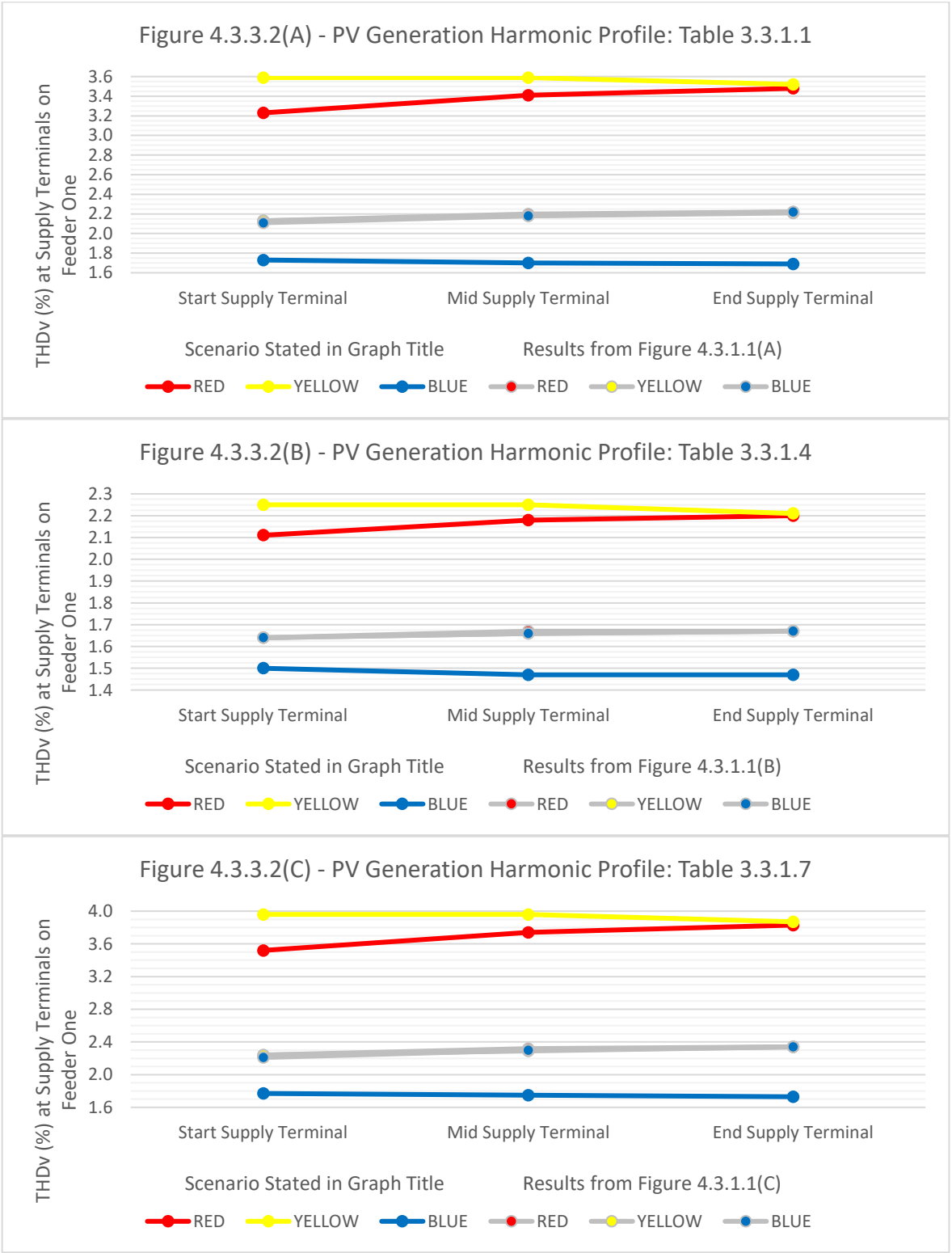


**Figure 4.3.3.2: Graphical representation of the THDv measured on each phase at supply terminals at the start, middle and end of feeder one during a two-phase fault at 98.4% PV generation penetration and PV generation harmonic profile stated whilst a three-phase fault is present on feeder two, compared to normal running arrangements on feeders one and two (Figures 4.3.1.1 (A-C)).**

The results of the worst-case harmonic distortion under a two-phase fault can be seen in Table 4.3.3.2. The worst-case harmonic distortion was measured between phase and neutral across yellow phase supply terminal at the start of feeder one shown in Figures 4.3.3.2(A-C). The worst-case THDv varies between each of the harmonic profiles due to the harmonic current contribution seen in Table 4.3.3.2. ER G5/5 limits are exceeded across multiple harmonics on feeder one including the 15$^{th}$, 21$^{st}$, 27$^{th}$, 33$^{rd}$, 34$^{th}$, 36$^{th}$, 39$^{th}$, and 40$^{th}$. This is a marked increase in breaches when compared to the two-phase faults in Sections 4.3.1-2 as would be expected since a three-phase fault is now present on feeder two. Additionally, the 32$^{nd}$ voltage harmonic on feeder one was on the boundary of the limits set out by ER G5/5. Lastly, due to the network imbalance, the neutral voltage on feeder one has increased to 5.368V, which is high enough to provide residents with potential shocks off exposed metalwork.

The tipping points for this scenario with a three-phase fault on feeder one to remain compliant under the different PV generation profiles with ER G5/5 on feeder one was identified. It was found that for Table 3.3.1.1, the maximum penetration was 24.0% (thirty PV generators), for Table 3.3.1.4 was 43.2% (fifty-four PV generators) and for Table 3.3.1.7 was 14.4% (eighteen PV generators). This is a considerable drop when compared to the normal running arrangement limits stated earlier in this section and the two-phase fault limits stated in Section 4.3.1. Further comparison will be provided in Section 4.3.4.

During a three-phase fault, fed by red phase, as seen in Figures 4.3.3.3(A-C), the THDv increased further at the start, middle and end of feeder one on the red phase. Like the three-phase faults in Sections 4.3.1-2, the THDv increases along the length of feeder one on the yellow and blue phases as the current travels from the pot end back towards the transformer. The maximum THDv recorded on feeder one is 4.01% for the harmonic profile from Table 3.3.1.1, 2.42% for the harmonic profile from Table 3.3.1.4 and 4.45% for the harmonic profile from Table 3.3.1.7. The highest THDv was measured on the yellow phase supply terminal at the start of feeder one.

**Table 4.3.3.2: Table of harmonics on feeder one during a two-phase fault at 98.4% PV generation penetration against the limits set out in ER G5/5 for the PV generation harmonic profile stated whilst a three-phase fault is present on feeder two (Energy Networks Association, 2020).**

| Harmonic Number | Worst Case Voltage Harmonic Magnitude at Supply Terminals (%) | | | Worst Case Voltage Harmonic Magnitude at Transformer (%) | | | ER G5/5 Limits (%) | Worst Case Phase Current Harmonic Magnitude at Transformer (A) | | | Neutral Harmonic Current Magnitude at Transformer (A) | | |
|---|---|---|---|---|---|---|---|---|---|---|---|---|---|
| | PV Generation Harmonic Profile from Table 3.3.1.- | | | PV Generation Harmonic Profile from Table 3.3.1.- | | | | PV Generation Harmonic Profile from Table 3.3.1.- | | | PV Generation Harmonic Profile from Table 3.3.1.- | | |
| | .1 | .4 | .7 | .1 | .4 | .7 | | .1 | .4 | .7 | .1 | .4 | .7 |
| 2nd | 0.18 | 0.18 | 0.18 | 0.14 | 0.14 | 0.14 | 1.6 | 6.75 | 6.75 | 6.75 | 6.19 | 6.19 | 6.19 |
| 3rd | 1.19 | 0.71 | 1.58 | 1.06 | 0.70 | 1.35 | 4.0 | 24.37 | 7.55 | 37.88 | 22.30 | 6.91 | 34.65 |
| 4th | 0.14 | 0.02 | 0.05 | 0.12 | 0.02 | 0.04 | 1.0 | 3.37 | 0.05 | 0.84 | 3.07 | 0.04 | 0.77 |
| 5th | 1.42 | 0.69 | 1.08 | 1.25 | 0.69 | 0.98 | 4.0 | 20.98 | 5.10 | 13.43 | 19.08 | 4.63 | 12.21 |
| 6th | 0.07 | 0.07 | 0.07 | 0.06 | 0.06 | 0.06 | 0.5 | 0.84 | 0.84 | 0.84 | 0.76 | 0.76 | 0.76 |
| 7th | 1.54 | 0.97 | 1.49 | 1.45 | 0.99 | 1.40 | 4.0 | 12.60 | 3.77 | 11.77 | 11.38 | 3.40 | 10.63 |
| 8th | 0.08 | 0.08 | 0.08 | 0.07 | 0.07 | 0.07 | 0.4 | 0.83 | 0.83 | 0.83 | 0.75 | 0.75 | 0.75 |
| 9th | 0.89 | 0.36 | 0.96 | 0.76 | 0.33 | 0.81 | 1.2 | 9.13 | 2.51 | 9.96 | 8.20 | 2.25 | 8.94 |
| 10th | 0.10 | 0.10 | 0.10 | 0.09 | 0.09 | 0.09 | 0.4 | 0.83 | 0.83 | 0.83 | 0.74 | 0.74 | 0.74 |
| 11th | 1.11 | 0.71 | 1.27 | 1.02 | 0.70 | 1.15 | 3.0 | 6.65 | 2.70 | 8.28 | 5.93 | 2.40 | 7.38 |
| 12th | 0.11 | 0.11 | 0.11 | 0.10 | 0.10 | 0.10 | 0.2 | 0.82 | 0.82 | 0.82 | 0.73 | 0.73 | 0.73 |
| 13th | 1.22 | 0.47 | 1.22 | 1.08 | 0.48 | 1.08 | 2.5 | 7.37 | 1.23 | 7.37 | 6.52 | 1.09 | 6.52 |
| 14th | 0.03 | 0.03 | 0.03 | 0.03 | 0.03 | 0.03 | 0.2 | 0.07 | 0.07 | 0.07 | 0.06 | 0.06 | 0.06 |
| 15th | 0.74 | 0.32 | 0.96 | 0.63 | 0.28 | 0.80 | 0.5 | 4.83 | 1.63 | 6.44 | 4.25 | 1.43 | 5.67 |
| 16th | 0.14 | 0.14 | 0.14 | 0.12 | 0.12 | 0.12 | 0.2 | 0.80 | 0.80 | 0.80 | 0.70 | 0.70 | 0.70 |
| 17th | 0.66 | 0.42 | 0.78 | 0.54 | 0.35 | 0.64 | 1.6 | 3.97 | 2.39 | 4.77 | 3.47 | 2.08 | 4.17 |
| 18th | 0.14 | 0.14 | 0.14 | 0.12 | 0.12 | 0.12 | 0.2 | 0.79 | 0.79 | 0.79 | 0.69 | 0.69 | 0.69 |
| 19th | 0.48 | 0.22 | 0.87 | 0.41 | 0.20 | 0.72 | 1.5 | 2.36 | 0.81 | 4.70 | 2.04 | 0.70 | 4.08 |
| 20th | 0.15 | 0.15 | 0.15 | 0.13 | 0.13 | 0.13 | 0.2 | 0.78 | 0.78 | 0.78 | 0.67 | 0.67 | 0.67 |
| 21st | 0.61 | 0.18 | 0.90 | 0.50 | 0.16 | 0.73 | 0.2 | 3.09 | 0.78 | 4.63 | 2.66 | 0.67 | 3.99 |
| 22nd | 0.02 | 0.02 | 0.02 | 0.02 | 0.02 | 0.02 | 0.2 | 0.04 | 0.04 | 0.04 | 0.04 | 0.04 | 0.04 |
| 23rd | 0.34 | 0.49 | 0.80 | 0.28 | 0.41 | 0.65 | 1.2 | 1.52 | 2.28 | 3.79 | 1.30 | 1.95 | 3.25 |
| 24th | 0.17 | 0.17 | 0.17 | 0.14 | 0.14 | 0.14 | 0.2 | 0.75 | 0.75 | 0.75 | 0.64 | 0.64 | 0.64 |
| 25th | 0.53 | 0.36 | 0.69 | 0.43 | 0.30 | 0.56 | 1.0 | 2.24 | 1.49 | 2.98 | 1.90 | 1.27 | 2.53 |
| 26th | 0.01 | 0.01 | 0.01 | 0.01 | 0.01 | 0.01 | 0.2 | 0.02 | 0.02 | 0.02 | 0.02 | 0.02 | 0.02 |
| 27th | 0.37 | 0.37 | 0.37 | 0.31 | 0.31 | 0.31 | 0.2 | 1.46 | 1.46 | 1.46 | 1.24 | 1.24 | 1.24 |
| 28th | 0.19 | 0.19 | 0.19 | 0.15 | 0.15 | 0.15 | 0.2 | 0.73 | 0.73 | 0.73 | 0.61 | 0.61 | 0.61 |
| 29th | 0.57 | 0.57 | 0.57 | 0.46 | 0.46 | 0.46 | 0.86 | 2.15 | 2.15 | 2.15 | 1.80 | 1.80 | 1.80 |
| 30th | 0.19 | 0.19 | 0.19 | 0.15 | 0.15 | 0.15 | 0.2 | 0.71 | 0.71 | 0.71 | 0.59 | 0.59 | 0.59 |
| 31st | 0.60 | 0.60 | 0.60 | 0.49 | 0.49 | 0.49 | 0.81 | 2.11 | 2.11 | 2.11 | 1.76 | 1.76 | 1.76 |
| 32nd | 0.20 | 0.20 | 0.20 | 0.16 | 0.16 | 0.16 | 0.2 | 0.70 | 0.70 | 0.70 | 0.58 | 0.58 | 0.58 |
| 33rd | 0.42 | 0.42 | 0.42 | 0.34 | 0.34 | 0.34 | 0.2 | 1.38 | 1.38 | 1.38 | 1.14 | 1.14 | 1.14 |
| 34th | 0.21 | 0.21 | 0.21 | 0.16 | 0.16 | 0.16 | 0.2 | 0.68 | 0.68 | 0.68 | 0.56 | 0.56 | 0.56 |
| 35th | 0.22 | 0.22 | 0.22 | 0.18 | 0.18 | 0.18 | 0.71 | 0.68 | 0.68 | 0.68 | 0.55 | 0.55 | 0.55 |
| 36th | 0.21 | 0.21 | 0.21 | 0.17 | 0.17 | 0.17 | 0.2 | 0.67 | 0.67 | 0.67 | 0.55 | 0.55 | 0.55 |
| 37th | 0.23 | 0.23 | 0.23 | 0.19 | 0.19 | 0.19 | 0.68 | 0.66 | 0.66 | 0.66 | 0.54 | 0.54 | 0.54 |
| 38th | 0.0 | 0.0 | 0.0 | 0.00 | 0.00 | 0.00 | 0.2 | 0.00 | 0.00 | 0.00 | 0.00 | 0.00 | 0.00 |
| 39th | 0.24 | 0.24 | 0.24 | 0.20 | 0.20 | 0.20 | 0.2 | 0.65 | 0.65 | 0.65 | 0.52 | 0.52 | 0.52 |
| 40th | 0.23 | 0.23 | 0.23 | 0.18 | 0.18 | 0.18 | 0.2 | 0.64 | 0.64 | 0.64 | 0.52 | 0.52 | 0.52 |
| Harmonics higher than the limits set by ER G5/5 | | | | | | | | | | | | | |
| Harmonics on the boundary of the limits set by ER G5/5 | | | | | | | | | | | | | |
| Number of PVs on Feeder 1: 54 Number of PVs on Feeder 2: 69 Voltage on Neutral: 5.368V | | | | | | | | | | | | | |

THDv (%) at Various Terminals on Feeder One During a Three-Phase Fault on Feeder One and a Three-Phase Fault on Feeder Two, Compared to the Results of Figures 4.3.1.1 (A-C).

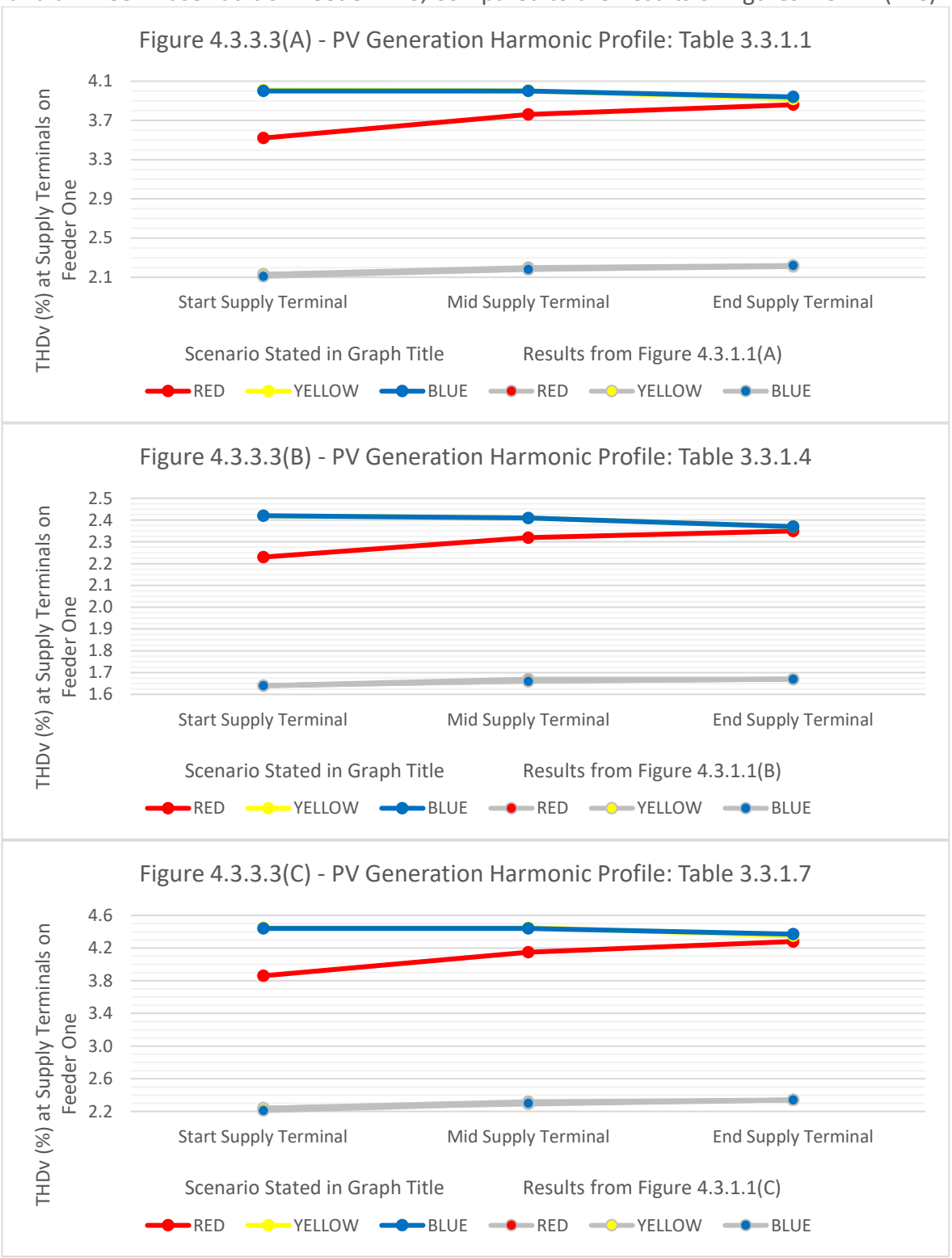


**Figure 4.3.3.3: Graphical representation of the THDv measured on each phase at supply terminals at the start, middle and end of feeder one during a three-phase fault at 98.4% PV generation penetration and PV generation harmonic profile stated whilst a three-phase fault is present on feeder two, compared to normal running arrangements on feeders one and two (Figures 4.3.1.1 (A-C)).**

By comparing the results in Table 4.3.3.3 to the results seen in Table 4.3.3.2, under the three-phase fault condition, the magnitude of individual voltage harmonics at the yellow phase supply terminal at the start of feeder one increase further. A three-phase fault results in the 15$^{th}$, 21$^{st}$, 27$^{th}$, 28$^{th}$, 30$^{th}$, 32$^{nd}$ 33$^{rd}$, 34$^{th}$, 36$^{th}$, 39$^{th}$, and 40$^{th}$ harmonics exceeding the boundary of limits set out by ER G5/5 on feeder one for the harmonic profiles from Tables 3.3.1.1 and 3.3.1.7. For the harmonic profile from Table 3.3.1.4, the three-phase fault results in the 21$^{st}$, 27$^{th}$, 28$^{th}$, 30$^{th}$, 32$^{nd}$, 33$^{rd}$, 34$^{th}$, 36$^{th}$, 39$^{th}$, and 40$^{th}$ harmonics exceeding the boundary of limits set out by ER G5/5 on feeder one. Therefore, if this network was to be left with a three-phase fault, as would be compliant with the ESQCRs, this would result in a non-compliance with ER G5/5.

The tipping points for this scenario with a three-phase fault on feeder one to remain compliant under the different PV generation harmonic profiles with ER G5/5 on feeder one was identified. It was found that for Table 3.3.1.1, the maximum penetration was 19.2% (twenty-four PV generators), for Table 3.3.1.4 was 36.0% (forty-five PV generators) and for Table 3.3.1.7 was 12.0% (fifteen PV generators). These were evenly distributed across three phases on feeders one and two as close as is achievable to a 44-56% split between PV generators on feeders one and two respectively.

In addition, it was found that the neutral voltage present at the end of feeder one increased to 7.987V under three-phase fault conditions shown in Table 4.3.3.3 from 5.368V under two-phase conditions in Table 4.3.3.2 and 2.129V under normal arrangements shown in Table 4.3.3.1. Based on Table 3.2.7.4, the voltages caused by a two or three-phase fault could lead to residents perceiving shocks from exposed bonded metal work, potentially leading to complaints. This is in line with two and three-phase faults mentioned in Sections 4.3.1-2.

**Table 4.3.3.3: Table of harmonics on feeder one during a three-phase fault at 98.4% PV generation penetration against the limits set out in ER G5/5 for the PV generation harmonic profile stated whilst a three-phase fault is present on feeder two (Energy Networks Association, 2020).**

| Harmonic Number | Worst Case Voltage Harmonic Magnitude at Supply Terminals (%) | | | Worst Case Voltage Harmonic Magnitude at Transformer (%) | | | ER G5/5 Limits (%) | Worst Case Phase Current Harmonic Magnitude at Transformer (A) | | | Neutral Harmonic Current Magnitude at Transformer (A) | | |
|---|---|---|---|---|---|---|---|---|---|---|---|---|---|
| | PV Generation Harmonic Profile from Table 3.3.1.- | | | PV Generation Harmonic Profile from Table 3.3.1.- | | | | PV Generation Harmonic Profile from Table 3.3.1.- | | | PV Generation Harmonic Profile from Table 3.3.1.- | | |
| | .1 | .4 | .7 | .1 | .4 | .7 | | .1 | .4 | .7 | .1 | .4 | .7 |
| 2nd | 0.21 | 0.21 | 0.21 | 0.15 | 0.15 | 0.15 | 1.6 | 7.86 | 7.86 | 7.86 | 7.86 | 7.86 | 7.86 |
| 3rd | 1.32 | 0.73 | 1.80 | 1.14 | 0.72 | 1.48 | 4.0 | 28.38 | 8.79 | 44.11 | 28.38 | 8.79 | 44.11 |
| 4th | 0.17 | 0.02 | 0.05 | 0.13 | 0.02 | 0.05 | 1.0 | 3.92 | 0.05 | 0.98 | 3.92 | 0.05 | 0.98 |
| 5th | 1.60 | 0.72 | 1.18 | 1.37 | 0.71 | 1.06 | 4.0 | 24.40 | 5.93 | 15.62 | 24.40 | 5.93 | 15.62 |
| 6th | 0.08 | 0.08 | 0.08 | 0.07 | 0.07 | 0.07 | 0.5 | 0.97 | 0.97 | 0.97 | 0.97 | 0.97 | 0.97 |
| 7th | 1.67 | 0.97 | 1.60 | 1.54 | 1.01 | 1.49 | 4.0 | 14.62 | 4.37 | 13.66 | 14.62 | 4.37 | 13.66 |
| 8th | 0.09 | 0.09 | 0.09 | 0.07 | 0.07 | 0.07 | 0.4 | 0.97 | 0.97 | 0.97 | 0.97 | 0.97 | 0.97 |
| 9th | 1.03 | 0.39 | 1.11 | 0.84 | 0.35 | 0.90 | 1.2 | 10.57 | 2.90 | 11.54 | 10.57 | 2.90 | 11.54 |
| 10th | 0.11 | 0.11 | 0.11 | 0.10 | 0.10 | 0.10 | 0.4 | 0.96 | 0.96 | 0.96 | 0.96 | 0.96 | 0.96 |
| 11th | 1.21 | 0.73 | 1.40 | 1.09 | 0.72 | 1.24 | 3.0 | 7.68 | 3.12 | 9.56 | 7.68 | 3.12 | 9.56 |
| 12th | 0.13 | 0.13 | 0.13 | 0.11 | 0.11 | 0.11 | 0.2 | 0.95 | 0.95 | 0.95 | 0.95 | 0.95 | 0.95 |
| 13th | 1.36 | 0.47 | 1.36 | 1.17 | 0.49 | 1.17 | 2.5 | 8.48 | 1.41 | 8.48 | 8.48 | 1.41 | 8.48 |
| 14th | 0.02 | 0.02 | 0.02 | 0.03 | 0.03 | 0.03 | 0.2 | 0.08 | 0.08 | 0.08 | 0.08 | 0.08 | 0.08 |
| 15th | 0.85 | 0.35 | 1.11 | 0.70 | 0.31 | 0.89 | 0.5 | 5.54 | 1.86 | 7.38 | 5.54 | 1.86 | 7.38 |
| 16th | 0.16 | 0.16 | 0.16 | 0.13 | 0.13 | 0.13 | 0.2 | 0.92 | 0.92 | 0.92 | 0.92 | 0.92 | 0.92 |
| 17th | 0.76 | 0.48 | 0.90 | 0.61 | 0.39 | 0.72 | 1.6 | 4.54 | 2.72 | 5.44 | 4.54 | 2.72 | 5.44 |
| 18th | 0.16 | 0.16 | 0.16 | 0.13 | 0.13 | 0.13 | 0.2 | 0.90 | 0.90 | 0.90 | 0.90 | 0.90 | 0.90 |
| 19th | 0.54 | 0.23 | 1.00 | 0.45 | 0.21 | 0.80 | 1.5 | 2.68 | 0.92 | 5.34 | 2.68 | 0.92 | 5.34 |
| 20th | 0.18 | 0.18 | 0.18 | 0.14 | 0.14 | 0.14 | 0.2 | 0.88 | 0.88 | 0.88 | 0.88 | 0.88 | 0.88 |
| 21st | 0.70 | 0.21 | 1.04 | 0.56 | 0.17 | 0.82 | 0.2 | 3.49 | 0.88 | 5.24 | 3.49 | 0.88 | 5.24 |
| 22nd | 0.02 | 0.02 | 0.02 | 0.02 | 0.02 | 0.02 | 0.2 | 0.05 | 0.05 | 0.05 | 0.05 | 0.05 | 0.05 |
| 23rd | 0.39 | 0.57 | 0.92 | 0.31 | 0.45 | 0.73 | 1.2 | 1.71 | 2.56 | 4.27 | 1.71 | 2.56 | 4.27 |
| 24th | 0.19 | 0.19 | 0.19 | 0.15 | 0.15 | 0.15 | 0.2 | 0.85 | 0.85 | 0.85 | 0.85 | 0.85 | 0.85 |
| 25th | 0.60 | 0.41 | 0.79 | 0.48 | 0.33 | 0.62 | 1.0 | 2.51 | 1.67 | 3.34 | 2.51 | 1.67 | 3.34 |
| 26th | 0.01 | 0.01 | 0.01 | 0.01 | 0.01 | 0.01 | 0.2 | 0.02 | 0.02 | 0.02 | 0.02 | 0.02 | 0.02 |
| 27th | 0.42 | 0.42 | 0.42 | 0.34 | 0.34 | 0.34 | 0.2 | 1.63 | 1.63 | 1.63 | 1.63 | 1.63 | 1.63 |
| 28th | 0.21 | 0.21 | 0.21 | 0.17 | 0.17 | 0.17 | 0.2 | 0.81 | 0.81 | 0.81 | 0.81 | 0.81 | 0.81 |
| 29th | 0.64 | 0.64 | 0.64 | 0.51 | 0.51 | 0.51 | 0.86 | 2.39 | 2.39 | 2.39 | 2.39 | 2.39 | 2.39 |
| 30th | 0.21 | 0.21 | 0.21 | 0.17 | 0.17 | 0.17 | 0.2 | 0.79 | 0.79 | 0.79 | 0.79 | 0.79 | 0.79 |
| 31st | 0.68 | 0.68 | 0.68 | 0.53 | 0.53 | 0.53 | 0.81 | 2.34 | 2.34 | 2.34 | 2.34 | 2.34 | 2.34 |
| 32nd | 0.22 | 0.22 | 0.22 | 0.17 | 0.17 | 0.17 | 0.2 | 0.77 | 0.77 | 0.77 | 0.77 | 0.77 | 0.77 |
| 33rd | 0.47 | 0.47 | 0.47 | 0.37 | 0.37 | 0.37 | 0.2 | 1.52 | 1.52 | 1.52 | 1.52 | 1.52 | 1.52 |
| 34th | 0.23 | 0.23 | 0.23 | 0.18 | 0.18 | 0.18 | 0.2 | 0.75 | 0.75 | 0.75 | 0.75 | 0.75 | 0.75 |
| 35th | 0.25 | 0.25 | 0.25 | 0.20 | 0.20 | 0.20 | 0.71 | 0.74 | 0.74 | 0.74 | 0.74 | 0.74 | 0.74 |
| 36th | 0.24 | 0.24 | 0.24 | 0.19 | 0.19 | 0.19 | 0.2 | 0.73 | 0.73 | 0.73 | 0.73 | 0.73 | 0.73 |
| 37th | 0.26 | 0.26 | 0.26 | 0.20 | 0.20 | 0.20 | 0.68 | 0.72 | 0.72 | 0.72 | 0.72 | 0.72 | 0.72 |
| 38th | 0.00 | 0.00 | 0.00 | 0.00 | 0.00 | 0.00 | 0.2 | 0.00 | 0.00 | 0.00 | 0.00 | 0.00 | 0.00 |
| 39th | 0.26 | 0.26 | 0.26 | 0.21 | 0.21 | 0.21 | 0.2 | 0.71 | 0.71 | 0.71 | 0.71 | 0.71 | 0.71 |
| 40th | 0.25 | 0.25 | 0.25 | 0.20 | 0.20 | 0.20 | 0.2 | 0.70 | 0.70 | 0.70 | 0.70 | 0.70 | 0.70 |
| Harmonics higher than the limits set by ER G5/5 | | | | | | | | | | | | | |
| Harmonics on the boundary of the limits set by ER G5/5 | | | | | | | | | | | | | |
| Number of PVs on Feeder 1: 54 Number of PVs on Feeder 2: 69 Voltage on Neutral: 7.987V | | | | | | | | | | | | | |

## 4.3.4 – Maximum Penetration and Overall Results

To summarise the results from Sections 4.3.1-3, Figures 4.3.4.1-3 have been produced. The results of maximum THDv measured at customer terminals on feeder one with a 2kW PV generation penetration of 98.4% and the maximum PV generation penetration to remain compliant with ER G5/5 on feeder one under different running arrangements, can be seen in Figures 4.3.4.1-3. The blue/grey lines and left-hand y-axis refers to the maximum THDv. The orange/yellow/green lines and right-hand y-axis refers to the maximum PV generation penetration. It should be noted that although trends may be similar across all networks, these results are specific to the case study network and harmonic profiles used.

For Figure 4.3.4.1, under normal conditions on feeder two, the maximum THDv increases from 2.22% to 3.37% on feeder one (an increase of 1.15%) when comparing normal conditions and a three-phase fault on feeder one. For a three-phase fault on feeder two, the maximum THDv increases from 2.99% to 4.01% on feeder one (an increase of 1.02%) when comparing normal conditions and a three-phase fault on feeder one. For faults on feeder two, the increase in THDv stays consistent, but is stepped up. This is very comparable to the results of the EVC penetration shown in Figure 4.2.4.1.

It can be seen from Figure 4.3.4.2 that for normal conditions on feeder two, the maximum THDv increases from 1.67% to 2.14% on feeder one (an increase of 0.47%) when comparing normal conditions and a three-phase fault on feeder one. For a three-phase fault on feeder two, the maximum THDv increases from 2.00% to 2.42% on feeder one (an increase of 0.42%) when comparing normal conditions and a three-phase fault on feeder one.

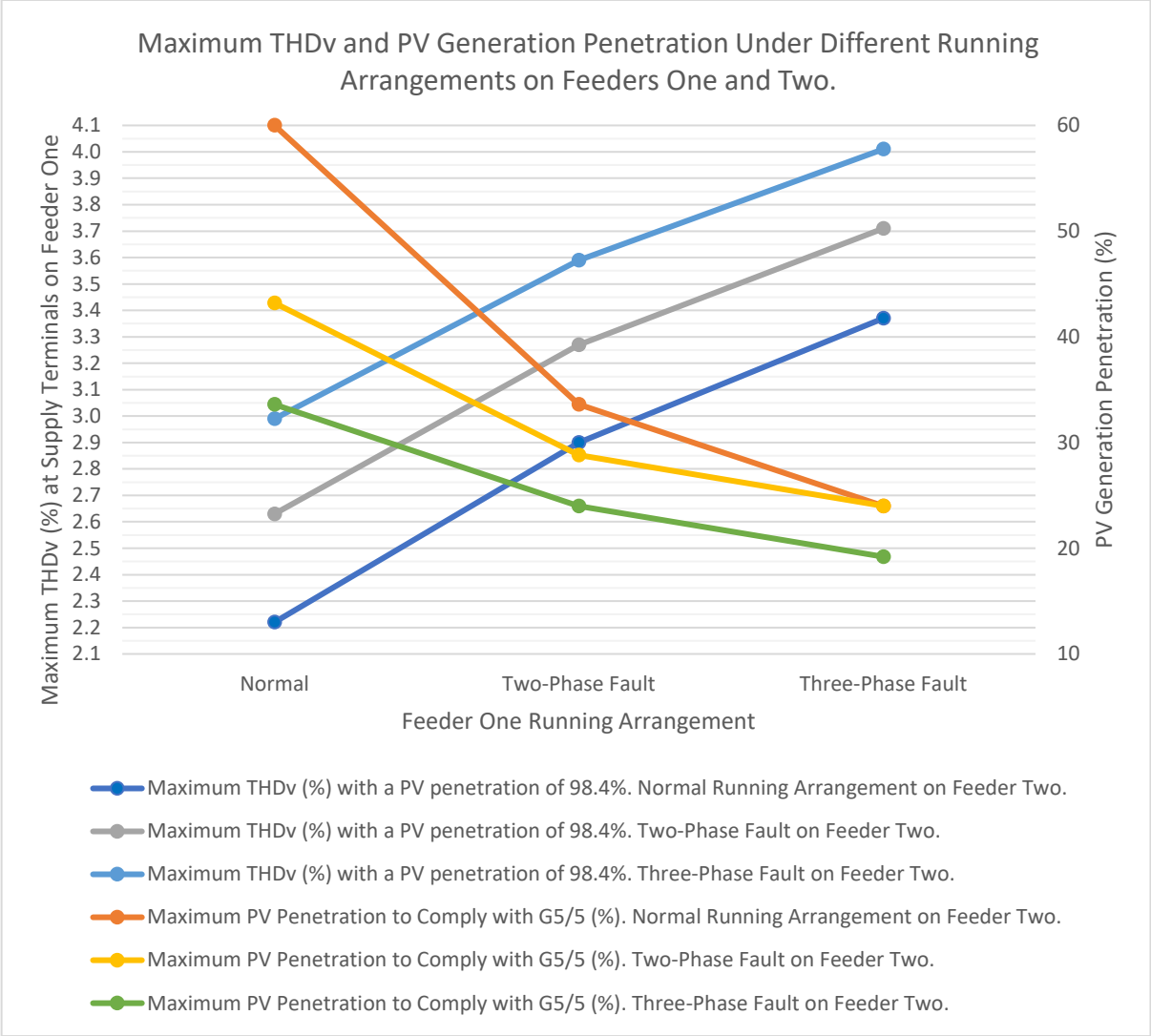


**Figure 4.3.4.1: Maximum THDv measured at customer terminals on feeder one with a PV generation penetration of 98.4% and maximum PV generation penetration to remain compliant with ER G5/5 under different running arrangements on feeders one and two using the PV generation harmonic profile from Table 3.3.1.1.**

For Figure 4.3.4.3, under normal conditions on feeder two, the maximum THDv increases from 2.34% to 3.72% on feeder one (an increase of 1.40%) when comparing normal conditions and a three-phase fault on feeder one. For a three-phase fault on feeder two, the maximum THDv increases from 3.24% to 4.45% on feeder one (an increase of 1.21%) when comparing normal conditions and a three-phase fault on feeder one.

From the results of Figures 4.3.4.1-3 it can be seen that the overall effect of faults on feeder one reduces when a fault is present on feeder two. This is due to increased levels of current harmonic cancellation.

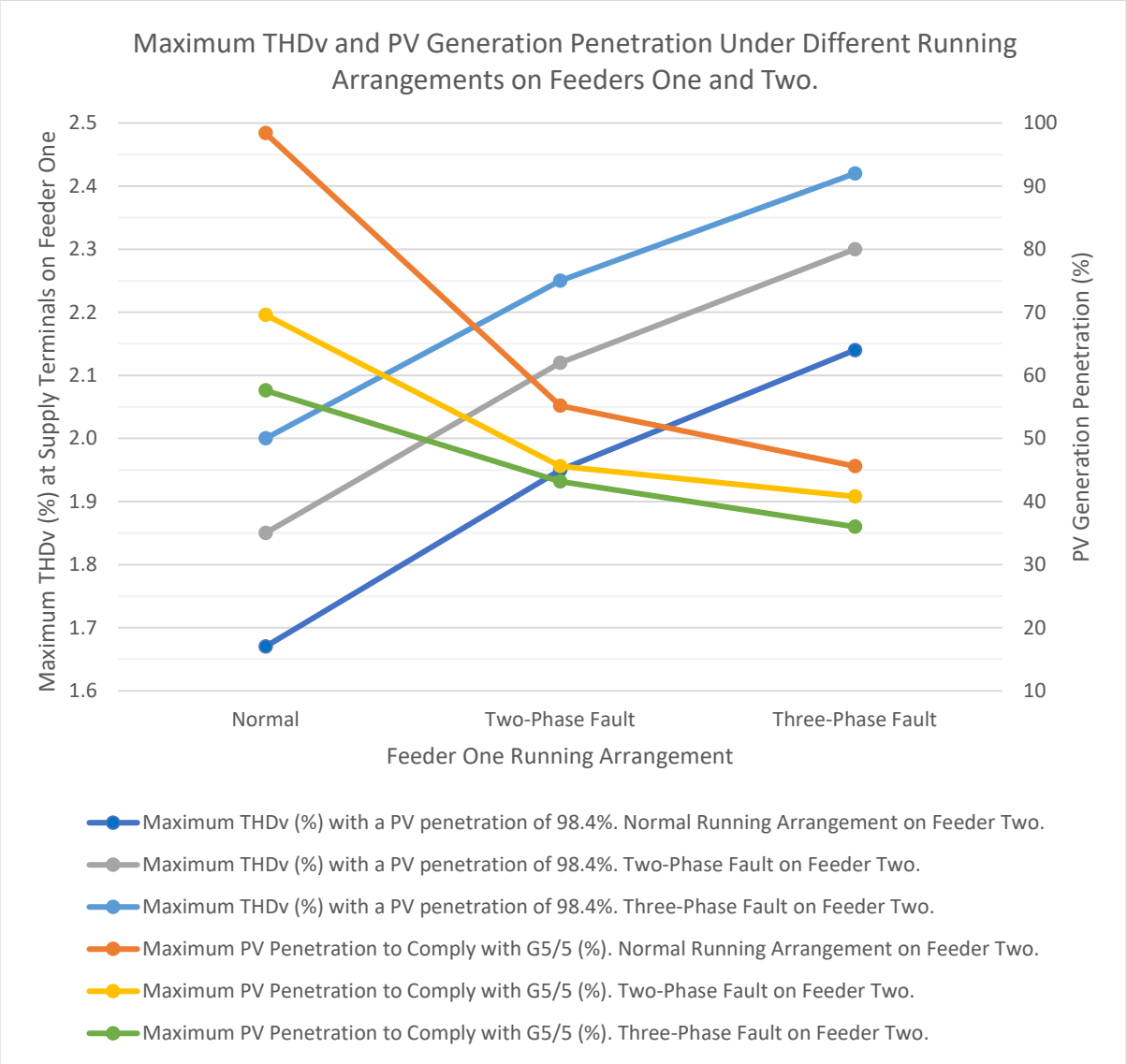


**Figure 4.3.4.2: Maximum THDv measured at customer terminals on feeder one with a PV generation penetration of 98.4% and maximum PV generation penetration to remain compliant with ER G5/5 under different running arrangements on feeders one and two using the PV generation harmonic profile from Table 3.3.1.4.**

More important is the maximum PV generation penetration permissible to ensure compliance with ER G5/5. It can be seen in Figure 4.3.4.1, that for normal conditions on feeder two, the maximum PV generation penetration decreases from 60% to 24.0% on feeder one (a decrease of 36.0%) when comparing normal conditions and a three-phase fault on feeder one. For a three-phase fault on feeder two, the maximum PV generation penetration decreases from 33.6% to 19.2% on feeder one (a decrease of 14.4%) when comparing normal conditions and a three-phase fault on feeder one. This is akin to the results of the EVC penetration shown in Figure 4.2.4.1.

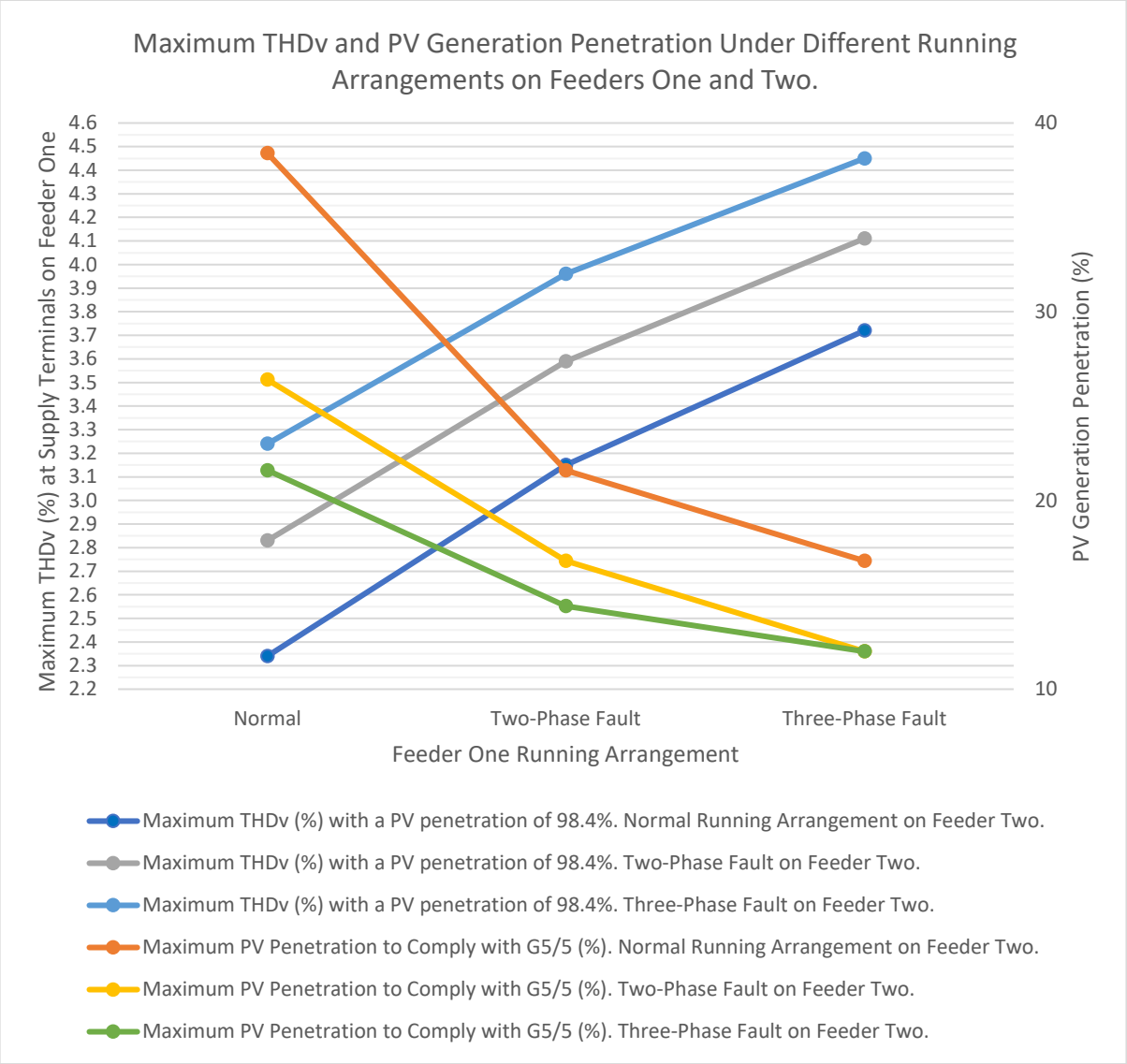


**Figure 4.3.4.3: Maximum THDv measured at customer terminals on feeder one with a PV generation penetration of 98.4% and maximum PV generation penetration to remain compliant with ER G5/5 under different running arrangements on feeders one and two using the PV generation harmonic profile from Table 3.3.1.7.**

The same applies to Figures 4.3.4.2-3. For normal conditions on feeder two, the maximum PV generation penetration decreases from 98.4% to 45.6% on feeder one (a decrease of 52.8%) for Figure 4.3.4.2, and 38.4% to 16.8% on feeder one (a decrease of 21.6%) for Figure 4.3.4.3 when comparing normal conditions and a three-phase fault on feeder one. For a three-phase fault on feeder two, the maximum PV generation penetration decreases from 57.6% to 36.0% on feeder one (a decrease of 21.6%) for Figure 4.3.4.2, and 21.6% to 12.0% on feeder one (a decrease of 9.6%) for Figure 4.3.4.3 when comparing normal conditions and a three-phase fault on feeder one.

The reason for differences in maximum penetration is due to the limiting harmonics. These are the 21st harmonic in the case of the harmonic profiles from Tables 3.3.1.1 and 3.3.1.7. and the 33rd harmonic in the case of the harmonic profile from Table 3.3.1.4. The 21st and 33rd harmonics are limited to 0.2% as defined by ER G5/5 (Energy Networks Association, 2020).

Based on the results of Sections 4.3.1-3, the limiting harmonics, both the 21st and 33rd increase during phase-to-phase conditions on both feeder one and feeder two. Tables 4.3.4.1-2 summarise the increase in these limiting harmonics under the conditions covered in Sections 4.3.1-3. It can be seen that generally, a fault on feeder one, has a much greater effect on the 21st and 33rd voltage harmonic on feeder one, than a fault on feeder two, which would be expected. Additionally, as faults compound, for example, a two-phase fault to a three-phase fault on feeder one, or a two-phase fault on feeder one, compounding with a two-phase fault on feeder two, the percentage increase in the voltage harmonic magnitude is not as significant. Therefore, as faults compound, the impact of any one fault on the 21st and 33rd voltage harmonic magnitude reduces. The first fault always produces the most the impact. This is in line with the results stated in Section 4.2.4.

**Table 4.3.4.1: Increase in 21st and 33rd voltage harmonic magnitude measured on feeder one between normal and phase-to-phase fault arrangements on feeder one for varying network arrangements on feeder two.**

| Increase in 21st and 33rd voltage harmonic magnitude on feeder one under specified conditions measured at the point of highest THDv. | | Feeder One | |
|---|---|---|---|
| | | Normal Arrangements to Two-Phase Fault | Normal Arrangements to Three-Phase Fault |
| Feeder Two | Normal Arrangements | 36-65% | 55-105% |
| | Two-Phase Fault Arrangements | 31-41% | 46-70% |
| | Three-Phase Fault Arrangements | 20-32% | 40-53% |

**Table 4.3.4.2: Increase in 21st and 33rd voltage harmonic magnitude measured on feeder one between normal and phase-to-phase fault arrangements on feeder two for varying network arrangements on feeder one.**

| Increase in 21st and 33rd voltage harmonic magnitude on feeder one under specified conditions measured at the point of highest THDv. | | Feeder Two | |
|---|---|---|---|
| | | Normal Arrangements to Two-Phase Fault | Normal Arrangements to Three-Phase Fault |
| Feeder One | Normal Arrangements | 18-37% | 36-66% |
| | Two-Phase Fault Arrangements | 13-18% | 20-34% |
| | Three-Phase Fault Arrangements | 10-14% | 18-24% |

This data can be used by DNOs to indicate the maximum allowable numbers of PV generators which can be connected to an LV EDN under different conditions. Data showing this relationship has not been published previously. This provides niche and novel data which will aid with network planning and determine the actions taken by a DNO following a fault to remain compliant with ER G5/5.

Similar to the results of Sections 4.2.1-4, neutral voltage rose as faults were added to the network, a three-phase fault having a higher impact than a two-phase fault. Despite this, the neutral voltage did not get high enough to cause ventricular fibrillation or respiratory tetanus as per Table 3.2.7.4. However, any fault on feeder one produced a voltage high enough for residents to perceive shocks. Neutral voltages should be monitored by a DNO following a two-phase or three-phase fault on a PME EDN. Should the voltages exceed 2.70V, remedial action should be taken to reduce the voltage. This should be the repair of the fault to rebalance the network.

## 4.3.5 – Discussion, Conclusions and Asset Lifespan

As mentioned in Section 4.2.7, both open-circuit faults and complex faults have not been included due to them not having as high an impact on voltage harmonics as phase-to-phase faults, without first exceeding either fuse or cable ratings.

The impact of phase-to-phase faults is significant, both on THDv levels and maximum EVC penetration levels. Additionally, concurrent faults on both feeders one and two will lead to further increases in THDv and further reductions in maximum EVC penetration. This has been covered in Section 4.3.4.

Similar to Section 3.3.8, it is important to ascertain whether the harmonic currents and voltages are sufficient in magnitude to lead to a noticeable loss of transformer or conductor life. The same assumptions and values such as reference hottest-spot temperature, ambient temperature and conductor impedance will be made as per Sections 3.2.8 and 4.2.7 to carry out these calculations.

Table 4.3.5.1 displays the increase in transformer hot-spot temperature and loss of transformer life. Table 4.3.5.2 displays the increase in cable temperature and loss of cable life. Values are calculated using Equations 3.2.8.1-19 and data from Tables 4.3.1.1-3, 4.3.2.1-3 and 4.3.3.1-3. Equations have been validated as per Section 3.2.8.

By comparing the data shown in Tables 4.3.1.1-3, 4.3.2.1-3, and 4.3.3.1-3 it can be clearly seen that, as the THDi of the PV harmonic profile increases, so does the impact on voltage and current harmonics. This impact can be seen to translate into Tables 4.3.5.1-2. The higher the THDi of the PV harmonic profile, the higher the impact on both transformer and cable temperature and the greater the asset life loss. This is to be expected.

**Table 4.3.5.1: Transformer hot-spot temperature increase and loss of transformer life assuming an existing hot-spot temperature of 110ºC for various fault arrangements on feeder one and two for the PV generation harmonic profile stated.**

| Increase in transformer hot-spot temperature (ºC) and loss of transformer life under specified conditions (Years). | | | Feeder One | | |
|---|---|---|---|---|---|
| | | | Normal Arrangements | Two-Phase Fault Arrangements | Three-Phase Fault Arrangements |
| PV Generation Harmonic Profile from Table 3.3.1.1 | Feeder Two | Normal Arrangements | 0.5356ºC<br>2.129 Years | 0.8521ºC<br>3.331 Years | 1.2005ºC<br>4.608 Years |
| | | Two-Phase Fault Arrangements | 0.9489ºC<br>3.690 Years | 1.3361ºC<br>5.091 Years | 1.7068ºC<br>6.380 Years |
| | | Three-Phase Fault Arrangements | 1.4043ºC<br>5.332 Years | 1.8382ºC<br>6.824 Years | 2.2672ºC<br>8.234 Years |
| PV Generation Harmonic Profile from Table 3.3.1.4 | Feeder Two | Normal Arrangements | 0.3313ºC<br>1.331 Years | 0.4941ºC<br>1.968 Years | 0.6698ºC<br>2.643 Years |
| | | Two-Phase Fault Arrangements | 0.5510ºC<br>2.188 Years | 0.7395ºC<br>2.908 Years | 0.9193ºC<br>3.5808 Years |
| | | Three-Phase Fault Arrangements | 0.7603ºC<br>2.986 Years | 0.9633ºC<br>3.743 Years | 1.1394ºC<br>4.387 Years |
| PV Generation Harmonic Profile from Table 3.3.1.7 | Feeder Two | Normal Arrangements | 0.6625ºC<br>2.616 Years | 1.0765ºC<br>4.159 Years | 1.5468ºC<br>5.830 Years |
| | | Two-Phase Fault Arrangements | 1.2080ºC<br>4.634 Years | 1.7270ºC<br>6.449 Years | 2.2620ºC<br>8.217 Years |
| | | Three-Phase Fault Arrangements | 1.8196ºC<br>6.762 Years | 2.3992ºC<br>8.654 Years | 2.9760ºC<br>10.426 Years |

Further considering the results of Tables 4.3.4.1-2, which show that as faults compound, the impact of any one fault on EDN harmonics reduces. The opposite can be seen in Tables 4.3.5.1-2. Taking the harmonic profile of Table 3.3.1.1 as an example, the difference between each step can be extrapolated, shown in Tables 4.3.5.3-6. Rather than the rate of temperature increase and loss of life decreasing as faults compound, they increase. This is contrary to Tables 4.2.7.1-2, where although these values increase, the rate of rise drops.

**Table 4.3.5.2: Cable temperature increase and loss of cable life assuming an existing cable temperature of 90ºC for various fault arrangements on feeder one and two for the PV generation harmonic profile stated.**

| Increase in cable temperature (ºC) and loss of cable life under specified conditions (Years). | | | Feeder One | | |
|---|---|---|---|---|---|
| | | | Normal Arrangements | Two-Phase Fault Arrangements | Three-Phase Fault Arrangements |
| PV Generation Harmonic Profile from Table 3.3.1.1 | Feeder Two | Normal Arrangements | 0.0458ºC 0.2663 Years | 0.1005ºC 0.5820 Years | 0.1768ºC 1.0181 Years |
| | | Two-Phase Fault Arrangements | 0.1210ºC 0.6997 Years | 0.2145ºC 1.2319 Years | 0.3031ºC 1.7290 Years |
| | | Three-Phase Fault Arrangements | 0.2302ºC 1.3205 Years | 0.3497ºC 1.9881 Years | 0.4924ºC 2.7695 Years |
| PV Generation Harmonic Profile from Table 3.3.1.4 | Feeder Two | Normal Arrangements | 0.0067ºC 0.0389 Years | 0.0144ºC 0.0837 Years | 0.0248ºC 0.1443 Years |
| | | Two-Phase Fault Arrangements | 0.0172ºC 0.1003 Years | 0.0299ºC 0.1744 Years | 0.0435ºC 0.2529 Years |
| | | Three-Phase Fault Arrangements | 0.0320ºC 0.1866 Years | 0.0478ºC 0.2779 Years | 0.0665ºC 0.3863 Years |
| PV Generation Harmonic Profile from Table 3.3.1.7 | Feeder Two | Normal Arrangements | 0.0625ºC 0.3633 Years | 0.1333ºC 0.7699 Years | 0.2414ºC 1.3834 Years |
| | | Two-Phase Fault Arrangements | 0.1653ºC 0.9530 Years | 0.2932ºC 1.6738 Years | 0.4335ºC 2.4491 Years |
| | | Three-Phase Fault Arrangements | 0.3143ºC 1.7916 Years | 0.4777ºC 2.6895 Years | 0.6722ºC 3.7304 Years |

The reason for the increase in rate of rise, as opposed to a rate of drop can be attributed to the increase in harmonics between fault conditions. Comparing Tables 4.2.4.1-2 and 4.3.4.1-2, it can be seen that the increase in the 21$^{st}$ and 33$^{rd}$ harmonic shown in Tables 4.3.4.1-2 is much higher than the increase in the 21$^{st}$ and 27$^{th}$ harmonic shown in Tables 4.2.4.1-2. The results from Table 4.3.4.1 is consistently at the top end or exceeding the results from Table 4.2.4.1. Additionally, the results from Table 4.3.4.2 far exceed Table 4.2.4.2. It should be mentioned that comparing these tables compares 127.92kVA of EVCs with 246kW of PV generation. Because of this, the THDv levels for comparable scenarios is considerably lower. This of course is due to PV generation removing base load, whereas EVCs add to it. Therefore, these values represent the maximum penetration to prevent overloading of fuses as previously mentioned. The values within Tables 4.3.5.3-6 have been calculated by measuring the difference in temperature and asset life between network fault arrangements within the table stated within the table title for the PV generation harmonic profile from Table 3.3.1.1. For example, for Table 4.3.5.3, the values stated within the top left box is calculated by subtracting the top left values from the top middle values within Table 4.3.5.1.

**Table 4.3.5.3: Increase in transformer hot-spot temperature and loss of transformer life between different fault scenarios on feeder one for data from Table 4.3.5.1 and PV generation harmonic profile from Table 3.3.1.1.**

| Increase in transformer hot-spot temperature (ºC) and loss of transformer life (Years) for Table 4.3.5.1 under specified conditions for the PV generation harmonic profile from Table 3.3.1.1. | | Feeder One | |
|---|---|---|---|
| | | Normal Arrangements to Two-Phase Fault | Two-Phase Fault to Three-Phase Fault |
| Feeder Two | Normal Arrangements | 0.3165ºC<br>1.202 Years | 0.3484ºC<br>1.277 Years |
| | Two-Phase Fault Arrangements | 0.3872ºC<br>1.401 Years | 0.3707ºC<br>1.289 Years |
| | Three-Phase Fault Arrangements | 0.4339ºC<br>1.492 Years | 0.4290ºC<br>1.410 Years |

**Table 4.3.5.4: Increase in transformer hot-spot temperature and loss of transformer life between different fault scenarios on feeder two for data from Table 4.3.5.1 and PV generation harmonic profile from Table 3.3.1.1.**

| Increase in transformer hot-spot temperature (ºC) and loss of transformer life (Years) for Table 4.3.5.1 under specified conditions for the PV generation harmonic profile from Table 3.3.1.1. | | Feeder Two | |
|---|---|---|---|
| | | Normal Arrangements to Two-Phase Fault | Two-Phase Fault to Three-Phase Fault |
| Feeder One | Normal Arrangements | 0.4133ºC<br>1.561 Years | 0.4554ºC<br>1.642 Years |
| | Two-Phase Fault Arrangements | 0.4840ºC<br>1.760 Years | 0.5021ºC<br>1.733 Years |
| | Three-Phase Fault Arrangements | 0.5063ºC<br>1.772 Years | 0.5604ºC<br>1.854 Years |

**Table 4.3.5.5: Increase in cable temperature and loss of cable life between different fault scenarios on feeder one for data from Table 4.3.5.2 and PV generation harmonic profile from Table 3.3.1.1.**

| Increase in cable temperature (ºC) and loss of cable life (Years) for Table 4.3.5.2 under specified conditions for the PV generation harmonic profile from Table 3.3.1.1. | | Feeder One | |
|---|---|---|---|
| | | Normal Arrangements to Two-Phase Fault | Two-Phase Fault to Three-Phase Fault |
| Feeder Two | Normal Arrangements | 0.0547ºC<br>0.3157 Years | 0.0763ºC<br>0.4361 Years |
| | Two-Phase Fault Arrangements | 0.0935ºC<br>0.5322 Years | 0.0886ºC<br>0.4971 Years |
| | Three-Phase Fault Arrangements | 0.1195ºC<br>0.6676 Years | 0.1427ºC<br>0.7814 Years |

**Table 4.3.5.6: Increase in cable temperature and loss of cable life between different fault scenarios on feeder two for data from Table 4.3.5.2 and PV generation harmonic profile from Table 3.3.1.1.**

| Increase in cable temperature (ºC) and loss of cable life (Years) for Table 4.3.5.2 under specified conditions for the PV generation harmonic profile from Table 3.3.1.1. | | Feeder Two | |
|---|---|---|---|
| | | Normal Arrangements to Two-Phase Fault | Two-Phase Fault to Three-Phase Fault |
| Feeder One | Normal Arrangements | 0.0752ºC<br>0.4334 Years | 0.1092ºC<br>0.6208 Years |
| | Two-Phase Fault Arrangements | 0.1140ºC<br>0.6499 Years | 0.1352ºC<br>0.7562 Years |
| | Three-Phase Fault Arrangements | 0.1263ºC<br>0.7109 Years | 0.1893ºC<br>1.0405 Years |

Furthermore, it should be noted that the loss of cable and transformer life starts to get substantial as faults compound. For example, under Table 4.3.5.1 and harmonic profile of Table 3.3.1.7, the transformer life during a three-phase fault on feeders one and two reduces by 10.426 years, representing a reduction of 26% of the transformers expected life. Additionally, for Table 4.3.5.2 under the same scenario the cable life reduces by 3.7304 years, representing a reduction of 9.3% of the cable's life. Of course, these are the worst examples and the reduction in life is not as pronounced for other PV harmonic profiles or fault scenarios. However, as mentioned in Section 4.2.7, should the transformer hot-spot temperature be below 110ºC, and cable temperature be below 90ºC before considering heating from harmonics, the transformer and cable will not suffer the loss of life stated.

Based on the results of this section it is recommended that the numbers of PV generators connected to LV EDNs should be restricted, or harmonic reducing technology implemented to observe compliance with industrial standards or regulations during phase-to-phase faults. To achieve this, network operators should actively monitor the voltage harmonic levels or PV generation penetration levels of LV EDNs. Once voltage harmonic levels or PV generation penetration reach the threshold levels identified earlier in this section, the network operator could determine that they can no longer accept any additional PV generators or require the installation of harmonic reducing technology. However, currently under ER G5/5, there are no restrictions on the connection of single-phase PV generation $\leqslant$16A, as long as they remain compliant with IEC 61000-3-2 (IEC, 2018b). Furthermore, the assessment for the connection of PV generation $\leqslant$75A is based on compliance with IEC 61000-3-12 (IEC, 2011) and short circuit calculations for harmonic contribution which assume that the background harmonic level is no higher than 75% of the planning level. Therefore, changes to ER G5/5 would need to be made to achieve this outcome.

# 4.4 – Interaction between PV Generation and EVCs

To analyse the effect that faults have on the LV EDN, with a combination of EVCs and PV generation, the penetration was set at 86.4% and 98.4% respectively. This penetration value represents one-hundred and eight single-phase 3.28kVA EVCs and one-hundred and twenty-three single-phase 2kW PVs each connected to separate properties on the LV EDN and evenly distributed amongst the three phases. There are forty-eight EVCs and fifty-four PVs on feeder one and sixty EVCs and sixty-nine PVs on feeder two. This is the maximum load penetration which can be sustained in the event of a three-phase fault without blowing the LV fuse at the substation and allows for a whole number of EVCs and PVs to be applied to the LV EDN. At this penetration, the current drawn by the phase feeding the fault under three-phase conditions is 317.2A which is 1.01 times the fuse rating of 315A at the LV cabinet.

## 4.4.1 – Results of Phase-to-Phase Faults

The supply terminals to be measured will be on all three phases at the start, middle and end of feeder one between phase and neutral as defined within Figure 3.1.1.2. The results for normal conditions for each of the PV generation harmonic profiles can be seen in Figures 4.4.1.1(A-C) and Table 4.4.1.1. It can be seen that THDv increases the further the supply terminal on feeder one is from the 11kV:400V transformer, as would be expected in line with the PV generation and EVC simulations in Sections 4.2.1 and 4.3.1 under normal running arrangements. The increase in THDv between the beginning and end of feeder one varies depending on the PV generation harmonic profile used and varies between 0.15-0.29%.

As mentioned in Section 3.4.2 by comparing these results with the standards in ER G5/5, shown in Table 3.4.2.1, it can be seen that the $15^{th}$, $21^{st}$, $27^{th}$, $33^{rd}$, and $39^{th}$ harmonics on feeder one exceeded or met limits. The only exception is the $15^{th}$ harmonic which was not exceeded for the PV generation harmonic profile from Table 3.3.1.4. The individual harmonic results, although covered in Section 3.4 have been summarised in Table 4.4.1.1

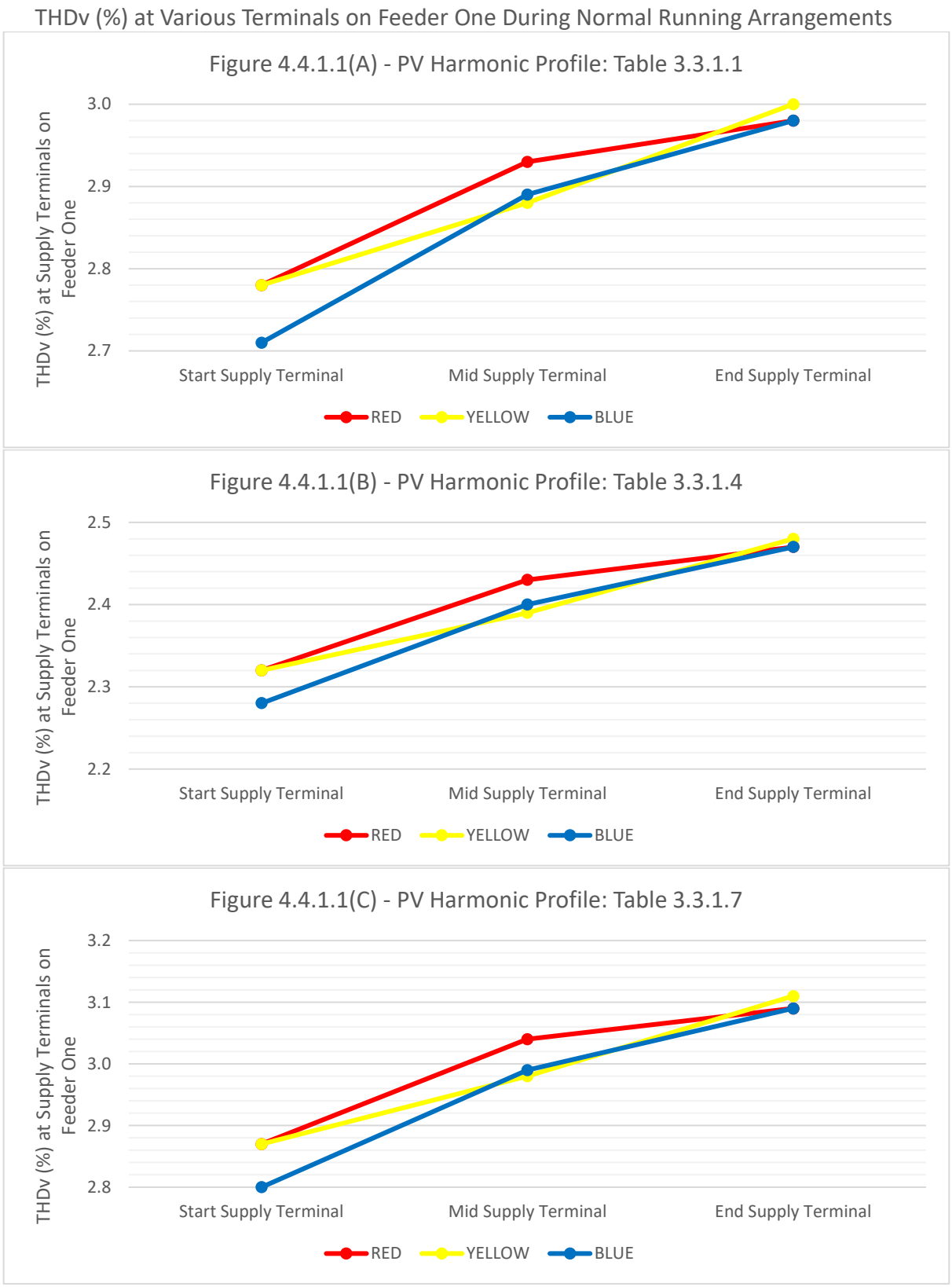


**Figure 4.4.1.1: Graphical representation of the THDv measured on each phase at supply terminals at the start, middle and end of feeder one under normal running arrangements at 86.4% EVC penetration, 98.4% PV generation penetration and PV generation harmonic profile stated.**

**Table 4.4.1.1: Table of harmonics on feeder one for normal running arrangements at 86.4% EVC penetration and 98.4% PV generation penetration against the limits set out in ER G5/5 for the PV generation harmonic profile stated (Energy Networks Association, 2020).**

| Harmonic Number | Worst Case Voltage Harmonic Magnitude at Supply Terminals (%) | | | Worst Case Voltage Harmonic Magnitude at Transformer (%) | | | ER G5/5 Limits (%) | Worst Case Phase Current Harmonic Magnitude at Transformer (A) | | | Neutral Harmonic Current Magnitude at Transformer (A) | | |
|---|---|---|---|---|---|---|---|---|---|---|---|---|---|
| | PV Generation Harmonic Profile from Table 3.3.1.- | | | PV Generation Harmonic Profile from Table 3.3.1.- | | | | PV Generation Harmonic Profile from Table 3.3.1.- | | | PV Generation Harmonic Profile from Table 3.3.1.- | | |
| | .1 | .4 | .7 | .1 | .4 | .7 | | .1 | .4 | .7 | .1 | .4 | .7 |
| 2nd | 0.10 | 0.10 | 0.10 | 0.09 | 0.09 | 0.09 | 1.6 | 3.05 | 3.05 | 3.05 | 0.22 | 0.22 | 0.22 |
| 3rd | 1.13 | 0.95 | 1.28 | 1.03 | 0.88 | 1.15 | 4.0 | 20.97 | 14.58 | 26.10 | 0.19 | 0.17 | 0.20 |
| 4th | 0.07 | 0.02 | 0.03 | 0.06 | 0.02 | 0.03 | 1.0 | 1.30 | 0.12 | 0.35 | 0.11 | 0.11 | 0.11 |
| 5th | 1.15 | 0.87 | 1.02 | 1.05 | 0.82 | 0.94 | 4.0 | 14.25 | 8.39 | 11.44 | 0.11 | 0.10 | 0.10 |
| 6th | 0.05 | 0.05 | 0.05 | 0.04 | 0.04 | 0.04 | 0.5 | 0.36 | 0.36 | 0.36 | 0.08 | 0.08 | 0.08 |
| 7th | 1.31 | 1.10 | 1.29 | 1.24 | 1.06 | 1.22 | 4.0 | 8.97 | 6.22 | 8.70 | 0.06 | 0.06 | 0.06 |
| 8th | 0.04 | 0.04 | 0.04 | 0.04 | 0.04 | 0.04 | 0.4 | 0.33 | 0.33 | 0.33 | 0.06 | 0.06 | 0.06 |
| 9th | 0.72 | 0.52 | 0.74 | 0.63 | 0.46 | 0.65 | 1.2 | 6.80 | 4.41 | 7.10 | 0.05 | 0.05 | 0.05 |
| 10th | 0.05 | 0.05 | 0.05 | 0.05 | 0.05 | 0.05 | 0.4 | 0.34 | 0.34 | 0.34 | 0.05 | 0.05 | 0.05 |
| 11th | 0.91 | 0.76 | 0.96 | 0.84 | 0.72 | 0.89 | 3.0 | 5.01 | 3.84 | 5.52 | 0.04 | 0.04 | 0.04 |
| 12th | 0.06 | 0.06 | 0.06 | 0.05 | 0.05 | 0.05 | 0.2 | 0.32 | 0.32 | 0.32 | 0.04 | 0.04 | 0.04 |
| 13th | 1.04 | 0.78 | 1.04 | 0.94 | 0.72 | 0.94 | 2.5 | 6.04 | 3.98 | 6.04 | 0.03 | 0.03 | 0.03 |
| 14th | 0.03 | 0.03 | 0.03 | 0.02 | 0.03 | 0.03 | 0.2 | 0.14 | 0.14 | 0.14 | 0.03 | 0.03 | 0.03 |
| 15th | 0.58 | 0.44 | 0.65 | 0.50 | 0.38 | 0.56 | 0.5 | 3.60 | 2.53 | 4.13 | 0.03 | 0.03 | 0.03 |
| 16th | 0.12 | 0.12 | 0.12 | 0.10 | 0.10 | 0.10 | 0.2 | 0.66 | 0.66 | 0.66 | 0.03 | 0.03 | 0.03 |
| 17th | 0.54 | 0.46 | 0.58 | 0.46 | 0.40 | 0.50 | 1.6 | 3.17 | 2.66 | 3.43 | 0.03 | 0.03 | 0.03 |
| 18th | 0.12 | 0.12 | 0.12 | 0.10 | 0.10 | 0.10 | 0.2 | 0.63 | 0.63 | 0.63 | 0.03 | 0.03 | 0.03 |
| 19th | 0.51 | 0.43 | 0.64 | 0.44 | 0.37 | 0.55 | 1.5 | 2.56 | 2.07 | 3.30 | 0.02 | 0.02 | 0.03 |
| 20th | 0.06 | 0.06 | 0.06 | 0.05 | 0.05 | 0.05 | 0.2 | 0.26 | 0.26 | 0.26 | 0.02 | 0.02 | 0.02 |
| 21st | 0.41 | 0.28 | 0.50 | 0.35 | 0.24 | 0.43 | 0.2 | 1.98 | 1.27 | 2.45 | 0.02 | 0.02 | 0.02 |
| 22nd | 0.01 | 0.01 | 0.01 | 0.02 | 0.01 | 0.01 | 0.2 | 0.08 | 0.08 | 0.08 | 0.02 | 0.02 | 0.02 |
| 23rd | 0.39 | 0.44 | 0.54 | 0.34 | 0.37 | 0.45 | 1.2 | 1.77 | 2.00 | 2.45 | 0.02 | 0.02 | 0.02 |
| 24th | 0.05 | 0.05 | 0.05 | 0.05 | 0.05 | 0.05 | 0.2 | 0.23 | 0.23 | 0.23 | 0.02 | 0.02 | 0.02 |
| 25th | 0.35 | 0.30 | 0.40 | 0.30 | 0.26 | 0.34 | 1.0 | 1.44 | 1.23 | 1.66 | 0.02 | 0.02 | 0.02 |
| 26th | 0.01 | 0.01 | 0.01 | 0.01 | 0.01 | 0.01 | 0.2 | 0.04 | 0.04 | 0.04 | 0.02 | 0.02 | 0.02 |
| 27th | 0.34 | 0.34 | 0.34 | 0.29 | 0.29 | 0.29 | 0.2 | 1.32 | 1.32 | 1.32 | 0.02 | 0.02 | 0.02 |
| 28th | 0.06 | 0.06 | 0.06 | 0.05 | 0.05 | 0.05 | 0.2 | 0.21 | 0.21 | 0.21 | 0.02 | 0.02 | 0.02 |
| 29th | 0.39 | 0.39 | 0.39 | 0.33 | 0.33 | 0.33 | 0.86 | 1.46 | 1.46 | 1.46 | 0.02 | 0.02 | 0.02 |
| 30th | 0.05 | 0.05 | 0.05 | 0.04 | 0.04 | 0.04 | 0.2 | 0.20 | 0.20 | 0.20 | 0.01 | 0.01 | 0.01 |
| 31st | 0.41 | 0.41 | 0.41 | 0.34 | 0.35 | 0.35 | 0.81 | 1.40 | 1.40 | 1.40 | 0.02 | 0.02 | 0.02 |
| 32nd | 0.05 | 0.05 | 0.05 | 0.04 | 0.05 | 0.05 | 0.2 | 0.19 | 0.19 | 0.19 | 0.01 | 0.01 | 0.01 |
| 33rd | 0.32 | 0.32 | 0.32 | 0.27 | 0.27 | 0.27 | 0.2 | 1.03 | 1.03 | 1.03 | 0.02 | 0.02 | 0.02 |
| 34th | 0.06 | 0.06 | 0.06 | 0.04 | 0.04 | 0.04 | 0.2 | 0.18 | 0.18 | 0.18 | 0.01 | 0.01 | 0.01 |
| 35th | 0.27 | 0.27 | 0.27 | 0.23 | 0.23 | 0.23 | 0.71 | 0.81 | 0.81 | 0.81 | 0.01 | 0.01 | 0.01 |
| 36th | 0.06 | 0.06 | 0.06 | 0.05 | 0.05 | 0.05 | 0.2 | 0.18 | 0.18 | 0.18 | 0.01 | 0.01 | 0.01 |
| 37th | 0.23 | 0.23 | 0.23 | 0.19 | 0.19 | 0.19 | 0.68 | 0.66 | 0.66 | 0.66 | 0.01 | 0.01 | 0.01 |
| 38th | 0.00 | 0.00 | 0.00 | 0.00 | 0.00 | 0.00 | 0.2 | 0.00 | 0.00 | 0.00 | 0.01 | 0.01 | 0.01 |
| 39th | 0.23 | 0.23 | 0.23 | 0.20 | 0.20 | 0.20 | 0.2 | 0.63 | 0.63 | 0.63 | 0.01 | 0.01 | 0.01 |
| 40th | 0.06 | 0.06 | 0.06 | 0.05 | 0.05 | 0.05 | 0.2 | 0.16 | 0.16 | 0.16 | 0.01 | 0.01 | 0.01 |
| 41st | 0.13 | 0.13 | 0.13 | 0.11 | 0.11 | 0.11 | 0.61 | 0.34 | 0.34 | 0.34 | 0.01 | 0.01 | 0.01 |
| 43rd | 0.13 | 0.13 | 0.13 | 0.11 | 0.11 | 0.11 | 0.58 | 0.33 | 0.33 | 0.33 | 0.01 | 0.01 | 0.01 |
| 45th | 0.13 | 0.13 | 0.13 | 0.11 | 0.11 | 0.11 | 0.20 | 0.31 | 0.31 | 0.31 | 0.01 | 0.01 | 0.01 |
| 47th | 0.09 | 0.09 | 0.09 | 0.08 | 0.08 | 0.08 | 0.53 | 0.20 | 0.20 | 0.20 | 0.01 | 0.01 | 0.01 |
| 49th | 0.09 | 0.09 | 0.09 | 0.08 | 0.08 | 0.08 | 0.51 | 0.20 | 0.20 | 0.20 | 0.01 | 0.01 | 0.01 |
| Harmonics higher than the limits set by ER G5/5 | | | | | | | Harmonics on the boundary of the limits set by ER G5/5 | | | | | | |
| Voltage on Neutral: 0.058V | | | | | | | | | | | | | |
| EVCs & PVs on Feeder 1: 48 & 54 respectively. EVCs & PVs on Feeder 2: 60 & 69 respectively. | | | | | | | | | | | | | |

The tipping points for this scenario with normal running arrangements on feeder one to remain compliant under the different PV generation profiles with ER G5/5 was identified. It was found that for Table 3.3.1.1, the maximum penetration of was 26.4% (thirty-three EVCs and PV generators), for Table 3.3.1.4 was 33.6% (forty-two EVCs and PV generators) and for Table 3.3.1.7 was 21.6% (twenty-seven EVCs and PV generators). These were evenly distributed across three phases on feeders one and two as close as is achievable to a 44-56% split between EVCs and PV generators on feeders one and two respectively.

The data stated in Table 4.4.1.1 and subsequent tables is as follows unless otherwise stated.

- The worst-case voltage harmonic magnitude at supply terminal data was measured at the end of feeder one on yellow phase between phase and neutral as per Figures 4.4.1.1 (A-C).
- The worst-case voltage harmonic magnitude at the transformer was measured on the red phase at the LV terminals of the 11kV:400V transformer.
- The worst-case phase current harmonic magnitude at the transformer was measured on the red phase at the LV terminals of the 11kV:400V transformer.
- The neutral harmonic current magnitude at the transformer was measured on the neutral at the LV terminals of the 11kV:400V transformer.

By introducing a two-phase fault, between red and yellow phases, with red phase feeding the fault as seen in Figures 4.4.1.2(A-C), it has been found that the THDv increases significantly along the length of feeder one on red phase, with the THDv also increasing on yellow phase as the current travels back towards the transformer. This leads to the THDv measured on the yellow phase supply terminal at the start of the LV EDN reaching the highest level. There is no noticeable effect on the blue phase THDv which is excluded from the faulted phases.

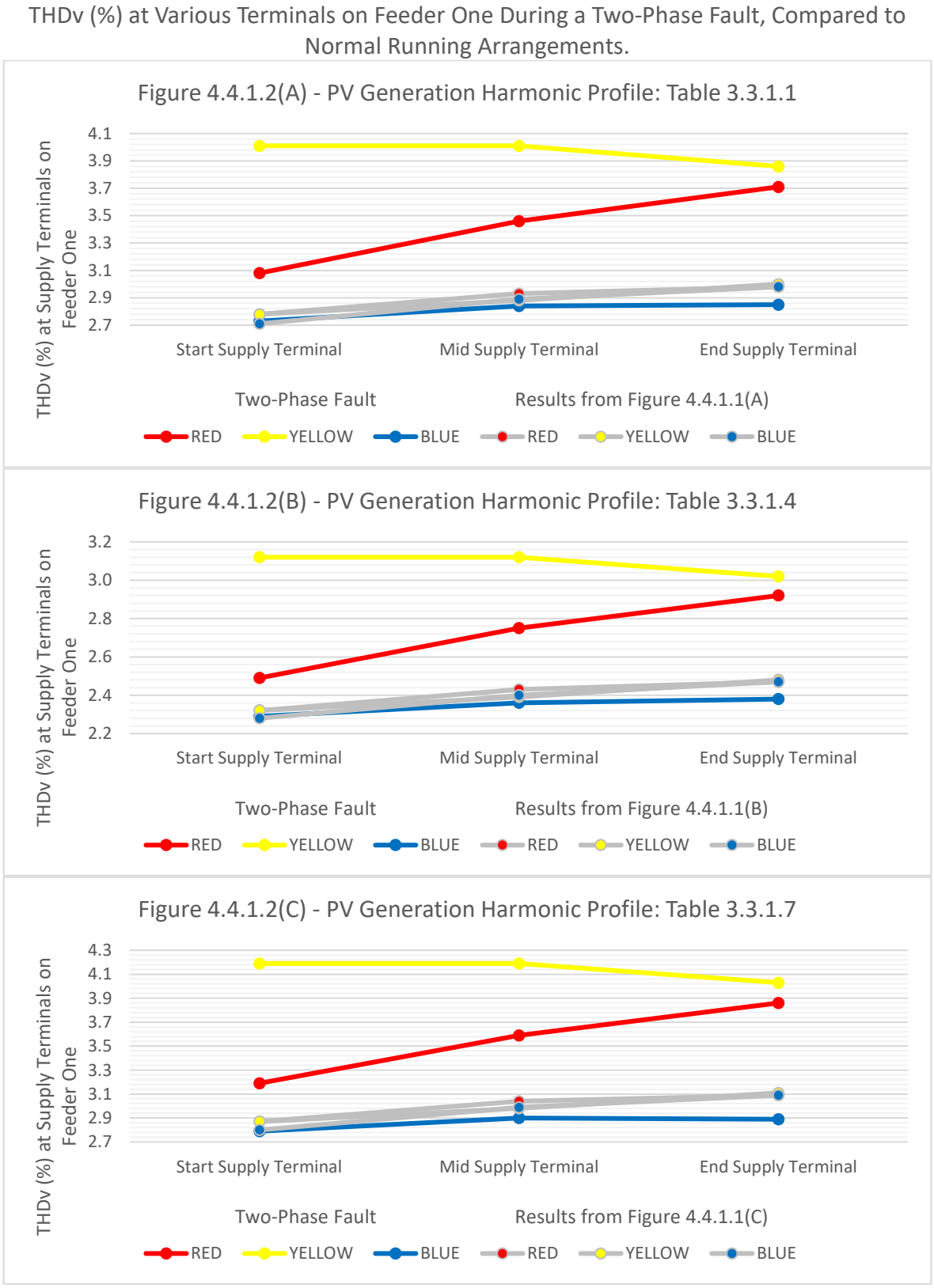


**Figure 4.4.1.2: Graphical representation of the THDv measured on each phase at supply terminals at the start, middle and end of feeder one during a two-phase fault on feeder one at 86.4% EVC penetration, 98.4% PV generation penetration and PV generation harmonic profile stated compared to normal running arrangements.**

The results of the worst-case harmonic distortion under a two-phase fault can be seen in Table 4.4.1.2. The worst-case harmonic distortion was measured between phase and neutral on the yellow phase supply terminal at the start of feeder one as shown in Figures 4.4.1.2(A-C). The worst-case THDv varies between each of the harmonic profiles due to the harmonic current contribution seen in Table 4.4.1.2. ER G5/5 limits are exceeded across multiple harmonics on feeder one including 15$^{th}$, 21$^{st}$, 27$^{th}$, 33$^{rd}$, and 39$^{th}$, therefore resulting in non-compliance. Lastly, due to the network imbalance, the neutral voltage has increased to 3.895V at the end of feeder one, which is high enough to provide residents with potential shocks off exposed metalwork.

The tipping point for this scenario with a two-phase fault on feeder one for feeder one to remain compliant under the different PV generation profiles with ER G5/5 was identified. It was found that for Tables 3.3.1.1 and 3.3.1.4, the maximum penetration was 16.8% (twenty-one EVCs and PV generators), and for Table 3.3.1.7 was 12.0% (fifteen EVCs and PV generators). These were evenly distributed across three phases on feeders one and two as close as is achievable to a 44-56% split between EVCs and PV generators on feeders one and two respectively.

One interesting point to note which differentiates these results from Sections 4.2 and 4.3 is the introduction of cancellation at higher harmonic orders on feeder one, to the point where the magnitude of those harmonics is lower. These have been highlighted with red text in Table 4.4.1.2. Harmonic current from the 33$^{rd}$ harmonic onwards and specific voltage harmonics from the 14$^{th}$ harmonic onwards are lower than those found in Table 4.4.1.1. This is not unexpected when combining different harmonic, generation, and load profiles. Sections 4.2 and 4.3 focussed on a worst-case scenario focussed solely on PV generation or EVCs. It can be seen in Figure 3.2.4.1 that this effect is present, just to a lesser effect.

During a three-phase fault, fed by red, as seen in Figures 4.4.1.3(A-C), the THDv increased further at the start, middle and end of feeder one on the red phase. Similar to the EVC simulations, the THDv stayed relatively constant along the length of feeder one on the yellow and blue phases as the current travels back towards the transformer. The maximum THDv recorded is 4.48% for the PV generation harmonic profile from Table 3.3.1.1, 3.38% for the PV generation harmonic profile from Table 3.3.1.4 and 4.70% for the PV generation harmonic profile from Table 3.3.1.7. The highest THDv was measured on either the yellow or blue phase supply terminal at the middle of feeder one.

**Table 4.4.1.2: Table of harmonics on feeder one during a two-phase fault on feeder one at 86.4% EVC penetration and 98.4% PV generation penetration against the limits set out in ER G5/5 for the PV generation harmonic profile stated (Energy Networks Association, 2020).**

| Harmonic Number | Worst Case Voltage Harmonic Magnitude at Supply Terminals (%) | | | Worst Case Voltage Harmonic Magnitude at Transformer (%) | | | ER G5/5 Limits (%) | Worst Case Phase Current Harmonic Magnitude at Transformer (A) | | | Neutral Harmonic Current Magnitude at Transformer (A) | | |
|---|---|---|---|---|---|---|---|---|---|---|---|---|---|
| | PV Generation Harmonic Profile from Table 3.3.1.- | | | PV Generation Harmonic Profile from Table 3.3.1.- | | | | PV Generation Harmonic Profile from Table 3.3.1.- | | | PV Generation Harmonic Profile from Table 3.3.1.- | | |
| | .1 | .4 | .7 | .1 | .4 | .7 | | .1 | .4 | .7 | .1 | .4 | .7 |
| 2nd | 0.16 | 0.16 | 0.16 | 0.10 | 0.10 | 0.10 | 1.6 | 4.12 | 4.12 | 4.12 | 2.05 | 2.05 | 2.05 |
| 3rd | 1.67 | 1.31 | 1.95 | 1.18 | 0.99 | 1.34 | 4.0 | 28.18 | 19.62 | 35.08 | 13.25 | 9.22 | 16.48 |
| 4th | 0.11 | 0.02 | 0.04 | 0.07 | 0.02 | 0.03 | 1.0 | 1.73 | 0.16 | 0.47 | 0.85 | 0.16 | 0.29 |
| 5th | 1.64 | 1.14 | 1.40 | 1.20 | 0.90 | 1.06 | 4.0 | 18.77 | 11.06 | 15.09 | 8.44 | 4.96 | 6.78 |
| 6th | 0.06 | 0.06 | 0.06 | 0.05 | 0.05 | 0.05 | 0.5 | 0.47 | 0.47 | 0.47 | 0.26 | 0.26 | 0.26 |
| 7th | 1.61 | 1.23 | 1.57 | 1.32 | 1.09 | 1.30 | 4.0 | 11.52 | 8.00 | 11.18 | 4.96 | 3.43 | 4.81 |
| 8th | 0.05 | 0.05 | 0.05 | 0.04 | 0.04 | 0.04 | 0.4 | 0.42 | 0.42 | 0.42 | 0.22 | 0.22 | 0.22 |
| 9th | 1.07 | 0.74 | 1.11 | 0.73 | 0.52 | 0.75 | 1.2 | 8.48 | 5.51 | 8.86 | 3.50 | 2.26 | 3.65 |
| 10th | 0.07 | 0.07 | 0.07 | 0.05 | 0.05 | 0.05 | 0.4 | 0.41 | 0.41 | 0.41 | 0.21 | 0.21 | 0.21 |
| 11th | 1.10 | 0.86 | 1.19 | 0.87 | 0.73 | 0.93 | 3.0 | 6.07 | 4.65 | 6.68 | 2.40 | 1.83 | 2.64 |
| 12th | 0.07 | 0.07 | 0.07 | 0.05 | 0.05 | 0.05 | 0.2 | 0.39 | 0.39 | 0.39 | 0.18 | 0.18 | 0.18 |
| 13th | 1.35 | 0.94 | 1.35 | 0.99 | 0.73 | 0.99 | 2.5 | 7.09 | 4.68 | 7.09 | 2.71 | 1.78 | 2.71 |
| 14th | 0.02 | 0.02 | 0.02 | 0.02 | 0.02 | 0.02 | 0.2 | 0.16 | 0.16 | 0.16 | 0.08 | 0.08 | 0.08 |
| 15th | 0.81 | 0.59 | 0.92 | 0.55 | 0.41 | 0.62 | 0.5 | 4.11 | 2.89 | 4.72 | 1.50 | 1.05 | 1.73 |
| 16th | 0.16 | 0.16 | 0.16 | 0.11 | 0.11 | 0.11 | 0.2 | 0.75 | 0.75 | 0.75 | 0.30 | 0.30 | 0.30 |
| 17th | 0.76 | 0.64 | 0.81 | 0.50 | 0.42 | 0.54 | 1.6 | 3.54 | 2.96 | 3.82 | 1.25 | 1.04 | 1.35 |
| 18th | 0.16 | 0.16 | 0.16 | 0.11 | 0.11 | 0.11 | 0.2 | 0.70 | 0.70 | 0.70 | 0.27 | 0.27 | 0.27 |
| 19th | 0.68 | 0.56 | 0.86 | 0.46 | 0.38 | 0.57 | 1.5 | 2.79 | 2.25 | 3.59 | 0.95 | 0.77 | 1.23 |
| 20th | 0.07 | 0.07 | 0.07 | 0.05 | 0.05 | 0.05 | 0.2 | 0.28 | 0.28 | 0.28 | 0.12 | 0.12 | 0.12 |
| 21st | 0.55 | 0.36 | 0.67 | 0.36 | 0.24 | 0.44 | 0.2 | 2.12 | 1.36 | 2.63 | 0.70 | 0.44 | 0.87 |
| 22nd | 0.01 | 0.01 | 0.01 | 0.01 | 0.01 | 0.01 | 0.2 | 0.08 | 0.08 | 0.08 | 0.04 | 0.04 | 0.04 |
| 23rd | 0.52 | 0.59 | 0.71 | 0.34 | 0.39 | 0.47 | 1.2 | 1.86 | 2.10 | 2.58 | 0.59 | 0.67 | 0.82 |
| 24th | 0.07 | 0.07 | 0.07 | 0.05 | 0.05 | 0.05 | 0.2 | 0.24 | 0.24 | 0.24 | 0.09 | 0.09 | 0.09 |
| 25th | 0.45 | 0.39 | 0.52 | 0.30 | 0.26 | 0.34 | 1.0 | 1.49 | 1.27 | 1.72 | 0.46 | 0.39 | 0.53 |
| 26th | 0.00 | 0.00 | 0.00 | 0.01 | 0.01 | 0.01 | 0.2 | 0.04 | 0.04 | 0.04 | 0.02 | 0.02 | 0.02 |
| 27th | 0.44 | 0.44 | 0.44 | 0.29 | 0.29 | 0.29 | 0.2 | 1.35 | 1.35 | 1.35 | 0.40 | 0.40 | 0.40 |
| 28th | 0.07 | 0.07 | 0.07 | 0.05 | 0.05 | 0.05 | 0.2 | 0.22 | 0.22 | 0.22 | 0.08 | 0.08 | 0.08 |
| 29th | 0.50 | 0.50 | 0.50 | 0.33 | 0.33 | 0.33 | 0.86 | 1.48 | 1.48 | 1.48 | 0.43 | 0.43 | 0.43 |
| 30th | 0.07 | 0.07 | 0.07 | 0.04 | 0.04 | 0.04 | 0.2 | 0.20 | 0.20 | 0.20 | 0.07 | 0.07 | 0.07 |
| 31st | 0.51 | 0.51 | 0.51 | 0.34 | 0.34 | 0.34 | 0.81 | 1.40 | 1.40 | 1.40 | 0.39 | 0.39 | 0.39 |
| 32nd | 0.07 | 0.07 | 0.07 | 0.04 | 0.05 | 0.04 | 0.2 | 0.19 | 0.19 | 0.19 | 0.07 | 0.07 | 0.07 |
| 33rd | 0.39 | 0.39 | 0.39 | 0.26 | 0.26 | 0.26 | 0.2 | 1.02 | 1.02 | 1.02 | 0.28 | 0.28 | 0.28 |
| 34th | 0.07 | 0.07 | 0.07 | 0.05 | 0.05 | 0.05 | 0.2 | 0.18 | 0.18 | 0.18 | 0.06 | 0.06 | 0.06 |
| 35th | 0.33 | 0.33 | 0.33 | 0.22 | 0.22 | 0.22 | 0.71 | 0.80 | 0.80 | 0.80 | 0.21 | 0.21 | 0.21 |
| 36th | 0.07 | 0.07 | 0.07 | 0.05 | 0.05 | 0.05 | 0.2 | 0.17 | 0.17 | 0.17 | 0.06 | 0.06 | 0.06 |
| 37th | 0.28 | 0.28 | 0.28 | 0.19 | 0.19 | 0.19 | 0.68 | 0.64 | 0.64 | 0.64 | 0.16 | 0.16 | 0.16 |
| 38th | 0.00 | 0.00 | 0.00 | 0.00 | 0.00 | 0.00 | 0.2 | 0.00 | 0.00 | 0.00 | 0.01 | 0.01 | 0.01 |
| 39th | 0.28 | 0.28 | 0.28 | 0.19 | 0.19 | 0.19 | 0.2 | 0.62 | 0.62 | 0.62 | 0.15 | 0.15 | 0.15 |
| 40th | 0.07 | 0.07 | 0.07 | 0.05 | 0.05 | 0.05 | 0.2 | 0.16 | 0.16 | 0.16 | 0.05 | 0.05 | 0.05 |
| 41st | 0.16 | 0.16 | 0.16 | 0.11 | 0.11 | 0.11 | 0.61 | 0.33 | 0.33 | 0.33 | 0.07 | 0.07 | 0.07 |
| 43rd | 0.16 | 0.16 | 0.16 | 0.11 | 0.11 | 0.11 | 0.58 | 0.31 | 0.31 | 0.31 | 0.07 | 0.07 | 0.07 |
| 45th | 0.16 | 0.16 | 0.16 | 0.11 | 0.11 | 0.11 | 0.20 | 0.30 | 0.30 | 0.30 | 0.06 | 0.06 | 0.06 |
| 47th | 0.10 | 0.10 | 0.10 | 0.07 | 0.07 | 0.07 | 0.53 | 0.19 | 0.19 | 0.19 | 0.04 | 0.04 | 0.04 |
| 49th | 0.10 | 0.10 | 0.10 | 0.07 | 0.07 | 0.07 | 0.51 | 0.19 | 0.19 | 0.19 | 0.04 | 0.03 | 0.04 |
| Harmonics higher than the limits set by ER G5/5 | | | | | | | Harmonics on the boundary of the limits set by ER G5/5 | | | | | | |
| Harmonics lower than the result from Table 4.4.1.1 | | | | | | | Voltage on Neutral: 3.895V | | | | | | |
| EVCs & PVs on Feeder 1: 48 & 54 respectively. EVCs & PVs on Feeder 2: 60 & 69 respectively. | | | | | | | | | | | | | |

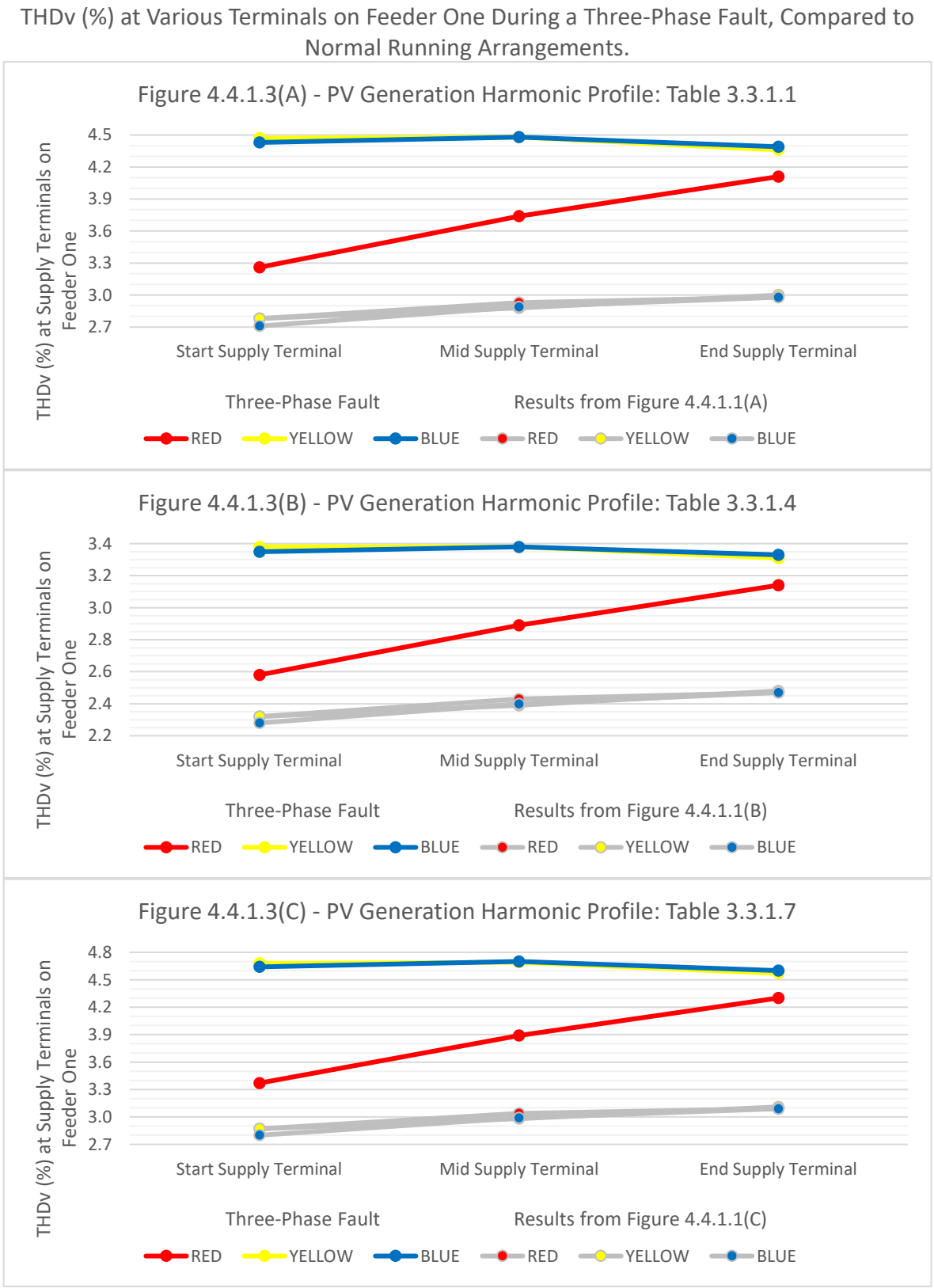


**Figure 4.4.1.3: Graphical representation of the THDv measured on each phase at supply terminals at the start, middle and end of feeder one during a three-phase fault on feeder one at 86.4% EVC penetration, 98.4% PV generation penetration and PV generation harmonic profile stated compared to normal running arrangements.**

By comparing the results in Table 4.4.1.3 to the results seen in Tables 4.4.1.1-2, under the three-phase fault condition, the voltage harmonic levels which have been exceeded under ER G5/5 have either increase or stayed constant. In addition, for the first time in a study within this thesis, the 9$^{th}$ harmonic limits have been exceeded on feeder one for the harmonic profiles in Tables 3.3.1.1 and 3.3.1.7. Therefore, if feeder one was to be left with a three-phase fault, as would be compliant with the ESQCRs, this would result in a non-compliance with ER G5/5.

Similar to the two-phase fault scenario, harmonic magnitudes on feeder one, which are lower than in Table 4.4.1.1, have been highlighted with red text in Table 4.4.1.3. Harmonic current from the 26$^{th}$ harmonic onwards and specific voltage harmonics from the 14$^{th}$ harmonic onwards are lower than those found in Table 4.4.1.1. Therefore, the degree of harmonic cancellation has increased when compared to Table 4.4.1.2. This is not unexpected since more harmonic current sources have been added to the same conductor.

The tipping points for this scenario with a three-phase fault on feeder one for feeder one to remain compliant under the different PV generation harmonic profiles with ER G5/5 was identified. It was found that for Table 3.3.1.1 and Table 3.3.1.4, the maximum penetration was 12.0% (fifteen EVCs and PV generators) and for Table 3.3.1.7 was 7.2% (nine EVCs and PV generators). These were evenly distributed across three phases on feeders one and two as close as is achievable to a 44-56% split between EVCs and PV generators on feeders one and two respectively.

In addition, it was found that the neutral voltage present at the end of feeder one increased to 6.283V under three-phase fault conditions shown in Table 4.4.1.3 from 3.895V under two-phase conditions in Table 4.4.1.2 and 0.058V under normal arrangements shown in Table 4.4.1.1. Based on Table 3.2.7.4, the voltages caused by a two or three-phase fault could lead to residents perceiving shocks off exposed bonded metal work, potentially leading to complaints. However, it does not seem high enough to cause ventricular fibrillation or respiratory tetanus.

**Table 4.4.1.3: Table of harmonics on feeder one during a three-phase fault on feeeder one at 86.4% EVC penetration and 98.4% PV generation penetration against the limits set out in ER G5/5 for the PV generation harmonic profile stated (Energy Networks Association, 2020).**

| Harmonic Number | Worst Case Voltage Harmonic Magnitude at Supply Terminals (%) | | | Worst Case Voltage Harmonic Magnitude at Transformer (%) | | | ER G5/5 Limits (%) | Worst Case Phase Current Harmonic Magnitude at Transformer (A) | | | Neutral Harmonic Current Magnitude at Transformer (A) | | |
|---|---|---|---|---|---|---|---|---|---|---|---|---|---|
| | PV Generation Harmonic Profile from Table 3.3.1.- | | | PV Generation Harmonic Profile from Table 3.3.1.- | | | | PV Generation Harmonic Profile from Table 3.3.1.- | | | PV Generation Harmonic Profile from Table 3.3.1.- | | |
| | .1 | .4 | .7 | .1 | .4 | .7 | | .1 | .4 | .7 | .1 | .4 | .7 |
| 2nd | 0.21 | 0.21 | 0.21 | 0.12 | 0.12 | 0.12 | 1.6 | 5.00 | 5.00 | 5.00 | 3.36 | 3.36 | 3.36 |
| 3rd | 2.02 | 1.54 | 2.41 | 1.32 | 1.08 | 1.51 | 4.0 | 34.05 | 23.72 | 42.37 | 22.19 | 15.46 | 27.60 |
| 4th | 0.13 | 0.02 | 0.04 | 0.08 | 0.02 | 0.03 | 1.0 | 2.06 | 0.19 | 0.55 | 1.39 | 0.15 | 0.41 |
| 5th | 1.93 | 1.29 | 1.63 | 1.31 | 0.96 | 1.15 | 4.0 | 22.16 | 13.06 | 17.81 | 14.32 | 8.45 | 11.52 |
| 6th | 0.06 | 0.06 | 0.06 | 0.05 | 0.05 | 0.05 | 0.5 | 0.54 | 0.54 | 0.54 | 0.38 | 0.38 | 0.38 |
| 7th | 1.75 | 1.28 | 1.70 | 1.37 | 1.10 | 1.34 | 4.0 | 13.22 | 9.19 | 12.83 | 8.47 | 5.88 | 8.21 |
| 8th | 0.06 | 0.06 | 0.06 | 0.04 | 0.04 | 0.04 | 0.4 | 0.47 | 0.47 | 0.47 | 0.33 | 0.33 | 0.33 |
| 9th | 1.23 | 0.84 | 1.28 | 0.78 | 0.56 | 0.81 | 1.2 | 9.47 | 6.15 | 9.89 | 5.96 | 3.87 | 6.23 |
| 10th | 0.07 | 0.07 | 0.07 | 0.05 | 0.05 | 0.05 | 0.4 | 0.46 | 0.45 | 0.45 | 0.30 | 0.30 | 0.30 |
| 11th | 1.15 | 0.88 | 1.26 | 0.88 | 0.72 | 0.94 | 3.0 | 6.60 | 5.06 | 7.27 | 4.09 | 3.14 | 4.51 |
| 12th | 0.07 | 0.07 | 0.07 | 0.05 | 0.05 | 0.05 | 0.2 | 0.42 | 0.42 | 0.42 | 0.27 | 0.27 | 0.27 |
| 13th | 1.44 | 0.98 | 1.44 | 1.00 | 0.73 | 1.00 | 2.5 | 7.55 | 4.99 | 7.55 | 4.59 | 3.03 | 4.59 |
| 14th | 0.02 | 0.02 | 0.02 | 0.02 | 0.02 | 0.02 | 0.2 | 0.17 | 0.17 | 0.17 | 0.09 | 0.09 | 0.09 |
| 15th | 0.88 | 0.63 | 1.00 | 0.56 | 0.41 | 0.63 | 0.5 | 4.29 | 3.02 | 4.93 | 2.54 | 1.79 | 2.92 |
| 16th | 0.17 | 0.17 | 0.17 | 0.11 | 0.11 | 0.11 | 0.2 | 0.78 | 0.78 | 0.78 | 0.47 | 0.47 | 0.47 |
| 17th | 0.81 | 0.69 | 0.88 | 0.51 | 0.43 | 0.55 | 1.6 | 3.64 | 3.04 | 3.93 | 2.10 | 1.76 | 2.27 |
| 18th | 0.17 | 0.17 | 0.17 | 0.11 | 0.11 | 0.11 | 0.2 | 0.71 | 0.71 | 0.71 | 0.41 | 0.41 | 0.41 |
| 19th | 0.71 | 0.58 | 0.91 | 0.46 | 0.38 | 0.58 | 1.5 | 2.83 | 2.29 | 3.65 | 1.59 | 1.29 | 2.05 |
| 20th | 0.07 | 0.07 | 0.07 | 0.05 | 0.05 | 0.05 | 0.2 | 0.28 | 0.28 | 0.28 | 0.16 | 0.16 | 0.16 |
| 21st | 0.58 | 0.38 | 0.71 | 0.36 | 0.24 | 0.44 | 0.2 | 2.13 | 1.37 | 2.64 | 1.16 | 0.75 | 1.44 |
| 22nd | 0.01 | 0.01 | 0.01 | 0.01 | 0.01 | 0.01 | 0.2 | 0.08 | 0.08 | 0.08 | 0.03 | 0.03 | 0.03 |
| 23rd | 0.54 | 0.61 | 0.75 | 0.34 | 0.38 | 0.47 | 1.2 | 1.86 | 2.10 | 2.57 | 0.98 | 1.11 | 1.36 |
| 24th | 0.07 | 0.07 | 0.07 | 0.05 | 0.05 | 0.05 | 0.2 | 0.24 | 0.24 | 0.24 | 0.13 | 0.13 | 0.13 |
| 25th | 0.47 | 0.40 | 0.54 | 0.30 | 0.26 | 0.34 | 1.0 | 1.48 | 1.26 | 1.70 | 0.76 | 0.64 | 0.87 |
| 26th | 0.00 | 0.00 | 0.00 | 0.01 | 0.01 | 0.01 | 0.2 | 0.04 | 0.04 | 0.04 | 0.01 | 0.01 | 0.01 |
| 27th | 0.45 | 0.45 | 0.45 | 0.29 | 0.29 | 0.29 | 0.2 | 1.33 | 1.33 | 1.33 | 0.66 | 0.66 | 0.66 |
| 28th | 0.07 | 0.07 | 0.07 | 0.05 | 0.05 | 0.05 | 0.2 | 0.21 | 0.21 | 0.21 | 0.11 | 0.11 | 0.11 |
| 29th | 0.52 | 0.52 | 0.52 | 0.33 | 0.33 | 0.33 | 0.86 | 1.45 | 1.45 | 1.45 | 0.69 | 0.69 | 0.69 |
| 30th | 0.07 | 0.07 | 0.07 | 0.04 | 0.04 | 0.04 | 0.2 | 0.20 | 0.20 | 0.20 | 0.10 | 0.10 | 0.10 |
| 31st | 0.52 | 0.52 | 0.52 | 0.34 | 0.34 | 0.34 | 0.81 | 1.38 | 1.38 | 1.38 | 0.64 | 0.64 | 0.64 |
| 32nd | 0.07 | 0.07 | 0.07 | 0.04 | 0.04 | 0.04 | 0.2 | 0.19 | 0.19 | 0.19 | 0.09 | 0.09 | 0.09 |
| 33rd | 0.40 | 0.40 | 0.40 | 0.26 | 0.26 | 0.26 | 0.2 | 1.00 | 1.00 | 1.00 | 0.45 | 0.45 | 0.45 |
| 34th | 0.07 | 0.07 | 0.07 | 0.04 | 0.04 | 0.04 | 0.2 | 0.18 | 0.18 | 0.18 | 0.08 | 0.08 | 0.08 |
| 35th | 0.33 | 0.33 | 0.33 | 0.22 | 0.22 | 0.22 | 0.71 | 0.78 | 0.78 | 0.78 | 0.34 | 0.34 | 0.34 |
| 36th | 0.07 | 0.07 | 0.07 | 0.05 | 0.05 | 0.05 | 0.2 | 0.17 | 0.17 | 0.17 | 0.07 | 0.07 | 0.07 |
| 37th | 0.28 | 0.28 | 0.28 | 0.19 | 0.19 | 0.19 | 0.68 | 0.63 | 0.63 | 0.63 | 0.26 | 0.26 | 0.26 |
| 38th | 0.00 | 0.00 | 0.00 | 0.00 | 0.00 | 0.00 | 0.2 | 0.00 | 0.00 | 0.00 | 0.01 | 0.01 | 0.01 |
| 39th | 0.28 | 0.28 | 0.28 | 0.19 | 0.19 | 0.19 | 0.2 | 0.60 | 0.60 | 0.60 | 0.24 | 0.24 | 0.24 |
| 40th | 0.07 | 0.07 | 0.07 | 0.05 | 0.05 | 0.05 | 0.2 | 0.16 | 0.16 | 0.16 | 0.06 | 0.06 | 0.06 |
| 41st | 0.16 | 0.16 | 0.16 | 0.10 | 0.10 | 0.10 | 0.61 | 0.32 | 0.32 | 0.32 | 0.12 | 0.12 | 0.12 |
| 43rd | 0.16 | 0.16 | 0.16 | 0.10 | 0.10 | 0.10 | 0.58 | 0.31 | 0.31 | 0.31 | 0.12 | 0.12 | 0.12 |
| 45th | 0.16 | 0.16 | 0.16 | 0.11 | 0.11 | 0.11 | 0.20 | 0.30 | 0.30 | 0.30 | 0.11 | 0.11 | 0.11 |
| 47th | 0.10 | 0.10 | 0.10 | 0.07 | 0.07 | 0.07 | 0.53 | 0.19 | 0.19 | 0.19 | 0.07 | 0.07 | 0.07 |
| 49th | 0.10 | 0.10 | 0.10 | 0.07 | 0.07 | 0.07 | 0.51 | 0.19 | 0.18 | 0.18 | 0.06 | 0.06 | 0.06 |
| Harmonics higher than the limits set by ER G5/5 | | | | | | | Harmonics on the boundary of the limits set by ER G5/5 | | | | | | |
| Harmonics lower than the result from Table 4.4.1.1 | | | | | | | Voltage on Neutral: 6.283V | | | | | | |
| EVCs & PVs on Feeder 1: 48 & 54 respectively. EVCs & PVs on Feeder 2: 60 & 69 respectively. | | | | | | | | | | | | | |

## 4.4.2 – Results of Phase-to-Phase Faults, with a Two-Phase Fault on Feeder Two

Further to Section 4.4.1, the effect of faults on feeder one will be explored whilst a second two-phase fault on feeder two is present. Firstly, similar to Sections 4.2.2 and 4.3.2, it can be seen that there is a marked drop in THDv on the yellow phase and marked increase in THDv on the red phase in Figures 4.4.2.1 (A-C) when compared to Figures 4.4.1.1(A-C). This is due to load being removed from the yellow phase and added to the red phase via a two-phase fault on feeder two. Due to the current drawn on feeder one remaining the same, the increase in THDv between the beginning and the end of feeder one remains low at 0.15-0.27%. Furthermore, individual harmonic levels can be seen in Table 4.4.2.1 and it can be seen that the fault on feeder two has led to an additional breach of ER G5/5 on feeder one on the 15$^{th}$ harmonic when compared to Table 4.4.1.1. Additionally, specific voltage harmonics from the 14$^{th}$ harmonic and specific current harmonics from the 41$^{st}$ harmonic on feeder one seem to either reduce or stay the same. This effect also increases in magnitude as the harmonic order increases. Harmonics which have reduced in magnitude have been highlighted in red text. As mentioned in Section 4.4.1 this is not unexpected when combining different harmonic, generation, and load profiles.

Despite the two-phase fault on feeder two leading to the neutral voltage on feeder one increasing from 0.058V to 1.214V, the voltage does not exceed 2.70V on feeder one and therefore should not be high enough to cause perceived shocks to residents. However, based on the results of Table 4.4.1.2, it is likely that residents will receive shocks off feeder two.

The tipping points for this scenario with normal running arrangements on feeder one and a two-phase fault on feeder two to remain compliant on feeder one under the different PV generation profiles with ER G5/5 was identified. It was found that for Table 3.3.1.1, the maximum penetration was 21.6% (twenty-seven EVCs and PV generators), for Table 3.3.1.4 was 28.8% (thirty-six EVCs and PV generators) and for Table 3.3.1.7 was 16.8% (twenty-one EVCs and PV generators). These were evenly distributed across three phases on feeders one and two as close as is achievable to a 44-56% split between PV generators on feeders one and two respectively.

THDv (%) at Various Terminals on Feeder One During Normal Running Arrangements on Feeder One and a Two-Phase Fault on Feeder Two, Compared to the Results of Figures 4.4.1.1 (A-C).

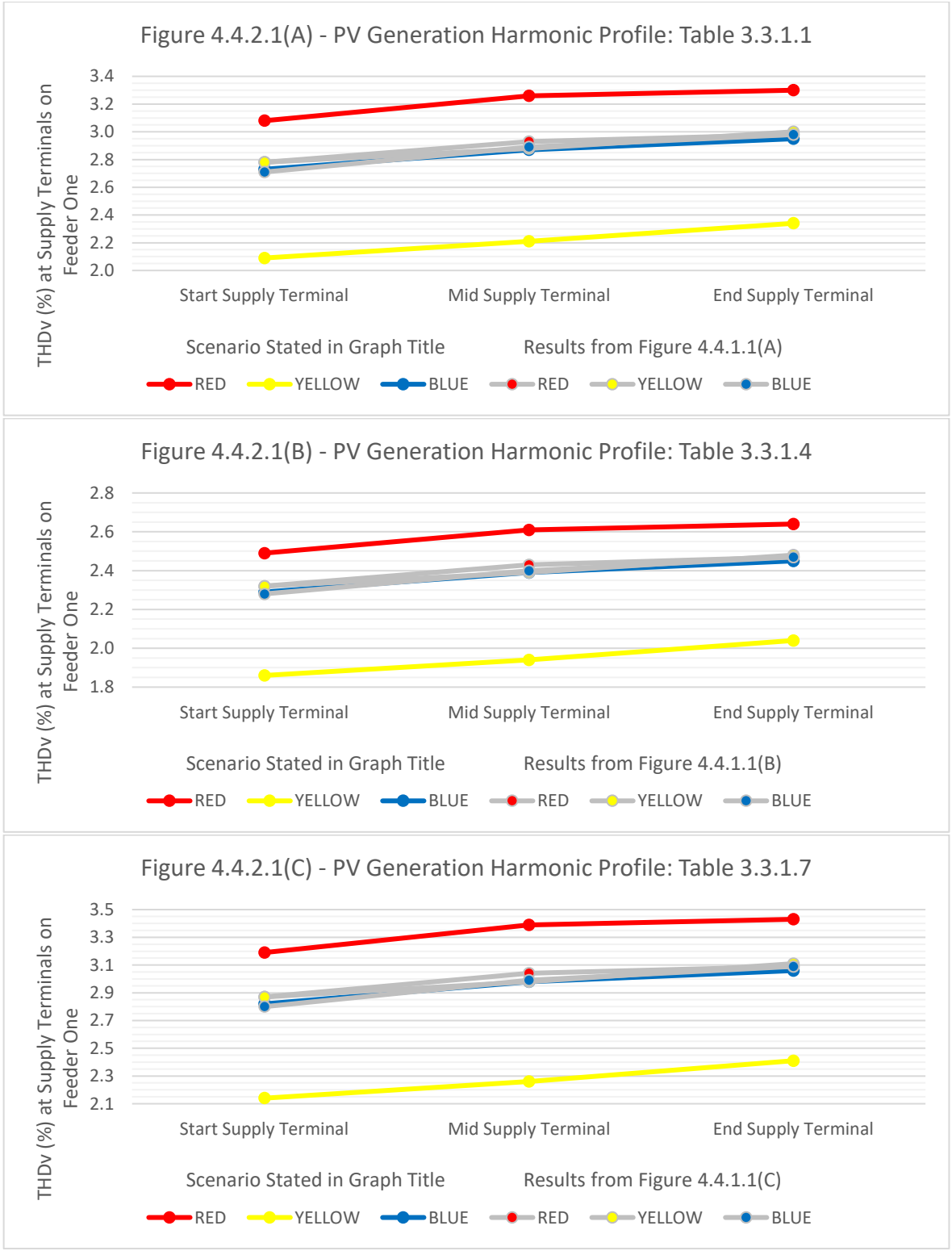


**Figure 4.4.2.1: Graphical representation of the THDv measured on each phase at supply terminals at the start, middle and end of feeder one under normal running arrangements on feeder one at 86.4% EVC penetration, 98.4% PV generation penetration and PV generation harmonic profile stated whilst a two-phase fault is present on feeder two, compared to normal running arrangements on feeders one and two (Figures 4.4.1.1 (A-C)).**

**Table 4.4.2.1: Table of harmonics on feeder one for normal running arrangements on feeder one at 86.4% EVC penetration and 98.4% PV generation penetration against the limits set out in ER G5/5 for the PV generation harmonic profile stated whilst a two-phase fault is present on feeder two (Energy Networks Association, 2020).**

| Harmonic Number | Worst Case Voltage Harmonic Magnitude at Supply Terminals (%) | | | Worst Case Voltage Harmonic Magnitude at Transformer (%) | | | ER G5/5 Limits (%) | Worst Case Phase Current Harmonic Magnitude at Transformer (A) | | | Neutral Harmonic Current Magnitude at Transformer (A) | | |
|---|---|---|---|---|---|---|---|---|---|---|---|---|---|
| | PV Generation Harmonic Profile from Table 3.3.1.- | | | PV Generation Harmonic Profile from Table 3.3.1.- | | | | PV Generation Harmonic Profile from Table 3.3.1.- | | | PV Generation Harmonic Profile from Table 3.3.1.- | | |
| | .1 | .4 | .7 | .1 | .4 | .7 | | .1 | .4 | .7 | .1 | .4 | .7 |
| 2nd | 0.12 | 0.12 | 0.12 | 0.11 | 0.11 | 0.11 | 1.6 | 4.38 | 4.38 | 4.38 | 2.55 | 2.55 | 2.55 |
| 3rd | 1.35 | 1.10 | 1.55 | 1.22 | 1.01 | 1.39 | 4.0 | 29.90 | 20.78 | 37.24 | 16.56 | 11.47 | 20.65 |
| 4th | 0.08 | 0.02 | 0.03 | 0.07 | 0.02 | 0.03 | 1.0 | 1.84 | 0.17 | 0.50 | 1.04 | 0.17 | 0.33 |
| 5th | 1.36 | 0.99 | 1.18 | 1.24 | 0.92 | 1.09 | 4.0 | 19.88 | 11.69 | 15.97 | 10.55 | 6.17 | 8.46 |
| 6th | 0.05 | 0.05 | 0.05 | 0.05 | 0.05 | 0.05 | 0.5 | 0.49 | 0.49 | 0.49 | 0.31 | 0.31 | 0.31 |
| 7th | 1.42 | 1.14 | 1.40 | 1.34 | 1.10 | 1.32 | 4.0 | 12.16 | 8.43 | 11.79 | 6.18 | 4.26 | 5.99 |
| 8th | 0.05 | 0.05 | 0.05 | 0.04 | 0.04 | 0.04 | 0.4 | 0.44 | 0.44 | 0.44 | 0.26 | 0.26 | 0.26 |
| 9th | 0.85 | 0.60 | 0.88 | 0.75 | 0.54 | 0.78 | 1.2 | 8.92 | 5.78 | 9.32 | 4.37 | 2.81 | 4.56 |
| 10th | 0.06 | 0.06 | 0.06 | 0.05 | 0.05 | 0.05 | 0.4 | 0.44 | 0.44 | 0.44 | 0.24 | 0.24 | 0.24 |
| 11th | 0.95 | 0.77 | 1.02 | 0.88 | 0.73 | 0.95 | 3.0 | 6.36 | 4.86 | 7.01 | 3.00 | 2.29 | 3.31 |
| 12th | 0.06 | 0.06 | 0.06 | 0.06 | 0.06 | 0.06 | 0.2 | 0.41 | 0.41 | 0.41 | 0.22 | 0.22 | 0.22 |
| 13th | 1.11 | 0.80 | 1.11 | 1.01 | 0.74 | 1.01 | 2.5 | 7.41 | 4.88 | 7.41 | 3.40 | 2.23 | 3.40 |
| 14th | 0.02 | 0.02 | 0.02 | 0.02 | 0.02 | 0.02 | 0.2 | 0.17 | 0.17 | 0.17 | 0.09 | 0.09 | 0.09 |
| 15th | 0.64 | 0.47 | 0.72 | 0.56 | 0.42 | 0.64 | 0.5 | 4.28 | 3.00 | 4.92 | 1.90 | 1.33 | 2.19 |
| 16th | 0.13 | 0.13 | 0.13 | 0.11 | 0.11 | 0.11 | 0.2 | 0.78 | 0.78 | 0.78 | 0.37 | 0.37 | 0.37 |
| 17th | 0.59 | 0.50 | 0.63 | 0.51 | 0.44 | 0.55 | 1.6 | 3.67 | 3.07 | 3.97 | 1.59 | 1.33 | 1.73 |
| 18th | 0.12 | 0.12 | 0.12 | 0.11 | 0.11 | 0.11 | 0.2 | 0.72 | 0.72 | 0.72 | 0.33 | 0.33 | 0.33 |
| 19th | 0.53 | 0.44 | 0.67 | 0.47 | 0.39 | 0.59 | 1.5 | 2.89 | 2.33 | 3.73 | 1.22 | 0.98 | 1.58 |
| 20th | 0.06 | 0.06 | 0.06 | 0.05 | 0.05 | 0.05 | 0.2 | 0.29 | 0.29 | 0.29 | 0.14 | 0.14 | 0.14 |
| 21st | 0.43 | 0.28 | 0.52 | 0.37 | 0.25 | 0.46 | 0.2 | 2.19 | 1.41 | 2.72 | 0.91 | 0.58 | 1.13 |
| 22nd | 0.01 | 0.01 | 0.01 | 0.01 | 0.01 | 0.01 | 0.2 | 0.09 | 0.09 | 0.09 | 0.04 | 0.04 | 0.04 |
| 23rd | 0.40 | 0.45 | 0.55 | 0.35 | 0.40 | 0.48 | 1.2 | 1.92 | 2.17 | 2.66 | 0.78 | 0.88 | 1.09 |
| 24th | 0.06 | 0.06 | 0.06 | 0.05 | 0.05 | 0.05 | 0.2 | 0.25 | 0.25 | 0.25 | 0.12 | 0.12 | 0.12 |
| 25th | 0.35 | 0.30 | 0.40 | 0.31 | 0.27 | 0.35 | 1.0 | 1.54 | 1.31 | 1.77 | 0.61 | 0.52 | 0.71 |
| 26th | 0.01 | 0.01 | 0.01 | 0.01 | 0.01 | 0.01 | 0.2 | 0.04 | 0.04 | 0.04 | 0.02 | 0.02 | 0.02 |
| 27th | 0.34 | 0.34 | 0.34 | 0.30 | 0.30 | 0.30 | 0.2 | 1.39 | 1.39 | 1.39 | 0.54 | 0.54 | 0.54 |
| 28th | 0.06 | 0.06 | 0.06 | 0.05 | 0.05 | 0.05 | 0.2 | 0.22 | 0.22 | 0.22 | 0.10 | 0.10 | 0.10 |
| 29th | 0.39 | 0.39 | 0.39 | 0.34 | 0.34 | 0.34 | 0.86 | 1.52 | 1.52 | 1.52 | 0.59 | 0.59 | 0.59 |
| 30th | 0.05 | 0.05 | 0.05 | 0.05 | 0.05 | 0.05 | 0.2 | 0.21 | 0.21 | 0.21 | 0.09 | 0.09 | 0.09 |
| 31st | 0.40 | 0.40 | 0.40 | 0.35 | 0.35 | 0.35 | 0.81 | 1.44 | 1.44 | 1.44 | 0.55 | 0.55 | 0.55 |
| 32nd | 0.05 | 0.05 | 0.05 | 0.05 | 0.05 | 0.05 | 0.2 | 0.20 | 0.20 | 0.20 | 0.09 | 0.09 | 0.09 |
| 33rd | 0.31 | 0.31 | 0.31 | 0.27 | 0.27 | 0.27 | 0.2 | 1.05 | 1.05 | 1.05 | 0.39 | 0.39 | 0.39 |
| 34th | 0.05 | 0.05 | 0.05 | 0.05 | 0.05 | 0.05 | 0.2 | 0.19 | 0.19 | 0.19 | 0.08 | 0.08 | 0.08 |
| 35th | 0.26 | 0.26 | 0.26 | 0.22 | 0.22 | 0.22 | 0.71 | 0.82 | 0.82 | 0.82 | 0.30 | 0.30 | 0.30 |
| 36th | 0.05 | 0.05 | 0.05 | 0.05 | 0.05 | 0.05 | 0.2 | 0.18 | 0.18 | 0.18 | 0.08 | 0.08 | 0.08 |
| 37th | 0.22 | 0.22 | 0.22 | 0.19 | 0.19 | 0.19 | 0.68 | 0.66 | 0.66 | 0.66 | 0.23 | 0.23 | 0.23 |
| 38th | 0.00 | 0.00 | 0.00 | 0.00 | 0.00 | 0.00 | 0.2 | 0.00 | 0.00 | 0.00 | 0.01 | 0.01 | 0.01 |
| 39th | 0.22 | 0.22 | 0.22 | 0.19 | 0.19 | 0.19 | 0.2 | 0.63 | 0.63 | 0.63 | 0.22 | 0.22 | 0.22 |
| 40th | 0.06 | 0.06 | 0.06 | 0.05 | 0.05 | 0.05 | 0.2 | 0.16 | 0.16 | 0.16 | 0.07 | 0.07 | 0.07 |
| 41st | 0.12 | 0.12 | 0.12 | 0.11 | 0.11 | 0.11 | 0.61 | 0.33 | 0.33 | 0.33 | 0.11 | 0.11 | 0.11 |
| 43rd | 0.13 | 0.13 | 0.13 | 0.11 | 0.11 | 0.11 | 0.58 | 0.32 | 0.32 | 0.32 | 0.10 | 0.10 | 0.10 |
| 45th | 0.13 | 0.13 | 0.13 | 0.11 | 0.11 | 0.11 | 0.20 | 0.31 | 0.31 | 0.31 | 0.10 | 0.10 | 0.10 |
| 47th | 0.09 | 0.09 | 0.09 | 0.07 | 0.07 | 0.07 | 0.53 | 0.20 | 0.20 | 0.20 | 0.06 | 0.06 | 0.06 |
| 49th | 0.09 | 0.09 | 0.09 | 0.07 | 0.07 | 0.07 | 0.51 | 0.19 | 0.19 | 0.19 | 0.06 | 0.06 | 0.06 |
| Harmonics higher than the limits set by ER G5/5 | | | | | | | Harmonics on the boundary of the limits set by ER G5/5 | | | | | | |
| Harmonics lower than the result from Table 4.4.1.1 | | | | | | | Voltage on Neutral: 1.214V | | | | | | |
| EVCs & PVs on Feeder 1: 48 & 54 respectively. EVCs & PVs on Feeder 2: 60 & 69 respectively. | | | | | | | | | | | | | |

By introducing a two-phase fault between red and yellow phases on feeder one, with red phase feeding the fault as seen in Figures 4.4.2.2(A-C), it has been found that the THDv increases significantly along the length of feeder one on red phase, with the THDv also increasing on yellow phase as the current travels back towards the transformer, similar to Section 4.4.1. However, unlike Section 4.4.1, the THDv level on the yellow phase is highest at the middle of feeder one, rather than start. There is no noticeable effect on the blue phase THDv which is excluded from the faulted phases.

The results of the worst-case harmonic distortion under a two-phase fault can be seen in Table 4.4.2.2. The worst-case harmonic distortion was measured between phase and neutral on the yellow phase supply terminal at the middle of feeder one as shown in Figures 4.4.2.2(A-C). The worst-case THDv varies between each of the harmonic profiles due to the harmonic current contributions seen in Table 4.4.1.2. ER G5/5 limits are exceeded across multiple harmonics on feeder one including $9^{th}$, $15^{th}$, $21^{st}$, $27^{th}$, $33^{rd}$, and $39^{th}$, therefore resulting in non-compliance. Lastly, due to the network imbalance, the neutral voltage has increased to 5.038V at the end of feeder one, which is high enough to provide residents with potential shocks off exposed metalwork.

The tipping points for this scenario with a two-phase fault on feeder one to remain compliant on feeder one under the different PV generation profiles with ER G5/5 was identified. It was found that for Table 3.3.1.1, the maximum penetration was 14.4% (eighteen EVCs and PV generators), for Table 3.3.1.4, the maximum penetration was 16.8% (twenty-one EVCs and PV generators), and for Table 3.3.1.7 was 9.6% (twelve EVCs and PV generators). These were evenly distributed across three phases on feeders one and two as close as is achievable to a 44-56% split between PV generators on feeders one and two respectively.

Furthermore, cancellation of harmonics at higher orders occurred, similar to Tables 4.4.1.2, 4.4.1.3 and 4.4.2.1 so that they are lower than comparable values in Table 4.4.1.1. These have been highlighted with red text in Table 4.4.2.2. Harmonic current from the $41^{st}$ harmonic onwards and specific voltage harmonics from the $14^{th}$ harmonic onwards are lower than those found in Table 4.4.1.1.

THDv (%) at Various Terminals on Feeder One During a Two-Phase Fault on Feeder One and a Two-Phase Fault on Feeder Two, Compared to the Results of Figures 4.4.1.1 (A-C).

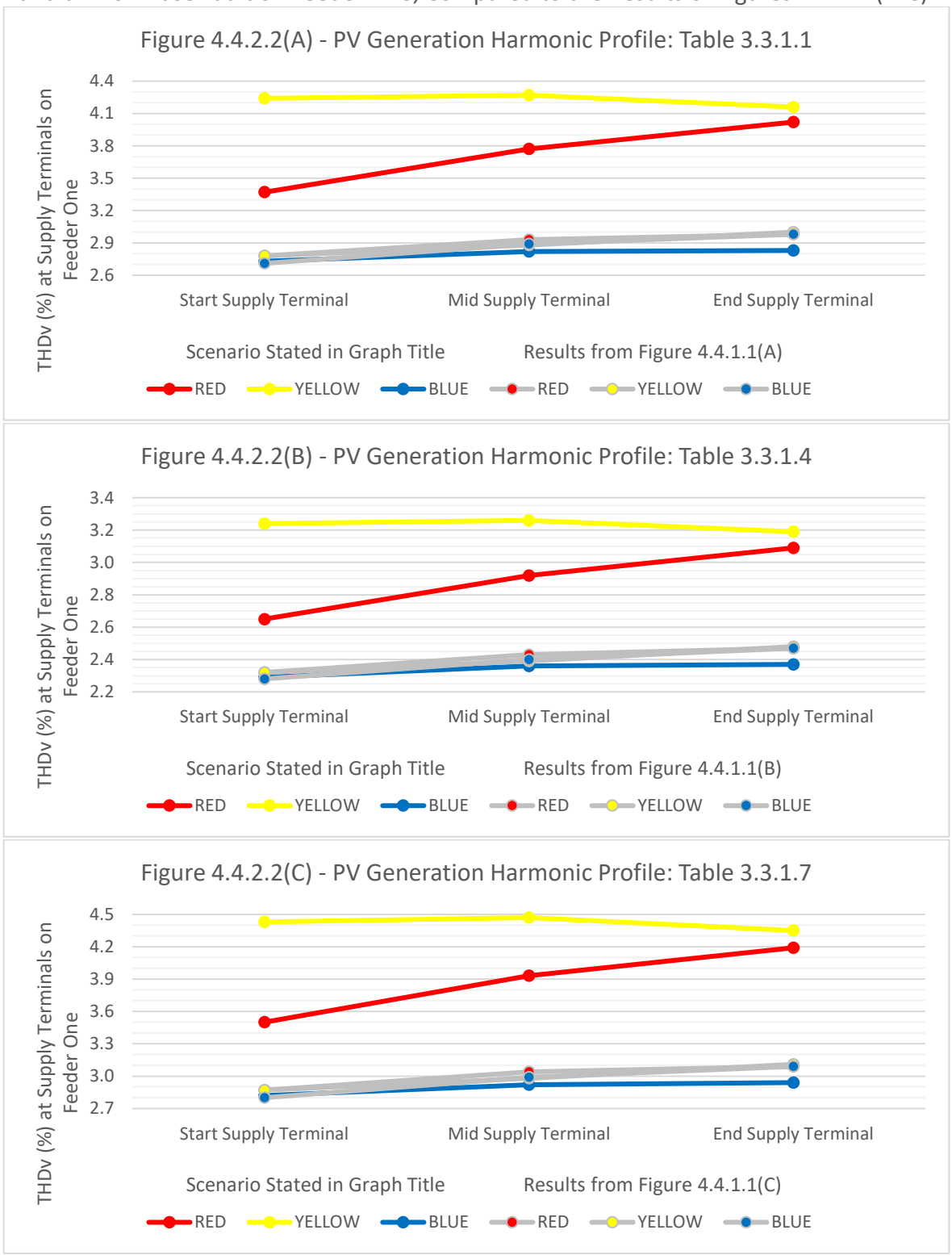


**Figure 4.4.2.2: Graphical representation of the THDv measured on each phase at supply terminals at the start, middle and end of feeder one during a two-phase fault on feeder one at 86.4% EVC penetration, 98.4% PV generation penetration and PV generation harmonic profile stated whilst a two-phase fault is present on feeder two, compared to normal running arrangements on feeders one and two (Figures 4.4.1.1 (A-C)).**

**Table 4.4.2.2: Table of harmonics on feeder one during a two-phase fault on feeder one at 86.4% EVC penetration and 98.4% PV generation penetration against the limits set out in ER G5/5 for the PV generation harmonic profile stated whilst a two-phase fault is present on feeder two (Energy Networks Association, 2020).**

| Harmonic Number | Worst Case Voltage Harmonic Magnitude at Supply Terminals (%) | | | Worst Case Voltage Harmonic Magnitude at Transformer (%) | | | ER G5/5 Limits (%) | Worst Case Phase Current Harmonic Magnitude at Transformer (A) | | | Neutral Harmonic Current Magnitude at Transformer (A) | | |
|---|---|---|---|---|---|---|---|---|---|---|---|---|---|
| | PV Generation Harmonic Profile from Table 3.3.1.- | | | PV Generation Harmonic Profile from Table 3.3.1.- | | | | PV Generation Harmonic Profile from Table 3.3.1.- | | | PV Generation Harmonic Profile from Table 3.3.1.- | | |
| | .1 | .4 | .7 | .1 | .4 | .7 | | .1 | .4 | .7 | .1 | .4 | .7 |
| 2nd | 0.19 | 0.19 | 0.19 | 0.12 | 0.12 | 0.12 | 1.6 | 5.41 | 5.41 | 5.41 | 4.40 | 4.40 | 4.40 |
| 3rd | 1.89 | 1.46 | 2.23 | 1.37 | 1.12 | 1.57 | 4.0 | 36.67 | 25.51 | 45.66 | 28.85 | 20.06 | 35.92 |
| 4th | 0.12 | 0.02 | 0.04 | 0.08 | 0.02 | 0.04 | 1.0 | 2.23 | 0.21 | 0.60 | 1.72 | 0.23 | 0.50 |
| 5th | 1.84 | 1.24 | 1.56 | 1.37 | 0.99 | 1.19 | 4.0 | 23.92 | 14.08 | 19.22 | 17.76 | 10.44 | 14.26 |
| 6th | 0.06 | 0.06 | 0.06 | 0.05 | 0.05 | 0.05 | 0.5 | 0.59 | 0.59 | 0.59 | 0.46 | 0.46 | 0.46 |
| 7th | 1.70 | 1.27 | 1.66 | 1.40 | 1.12 | 1.38 | 4.0 | 14.30 | 9.92 | 13.87 | 10.09 | 6.98 | 9.78 |
| 8th | 0.06 | 0.06 | 0.06 | 0.04 | 0.04 | 0.04 | 0.4 | 0.52 | 0.52 | 0.52 | 0.38 | 0.38 | 0.38 |
| 9th | 1.17 | 0.80 | 1.21 | 0.83 | 0.59 | 0.87 | 1.2 | 10.25 | 6.65 | 10.71 | 6.95 | 4.50 | 7.26 |
| 10th | 0.07 | 0.07 | 0.07 | 0.06 | 0.06 | 0.06 | 0.4 | 0.50 | 0.50 | 0.50 | 0.36 | 0.36 | 0.36 |
| 11th | 1.12 | 0.87 | 1.23 | 0.90 | 0.73 | 0.97 | 3.0 | 7.15 | 5.47 | 7.88 | 4.70 | 3.59 | 5.18 |
| 12th | 0.07 | 0.07 | 0.07 | 0.06 | 0.06 | 0.06 | 0.2 | 0.45 | 0.45 | 0.45 | 0.32 | 0.32 | 0.32 |
| 13th | 1.39 | 0.95 | 1.39 | 1.05 | 0.75 | 1.05 | 2.5 | 8.17 | 5.39 | 8.17 | 5.30 | 3.49 | 5.30 |
| 14th | 0.02 | 0.02 | 0.02 | 0.02 | 0.02 | 0.02 | 0.2 | 0.18 | 0.18 | 0.18 | 0.14 | 0.14 | 0.14 |
| 15th | 0.83 | 0.60 | 0.95 | 0.60 | 0.44 | 0.67 | 0.5 | 4.64 | 3.26 | 5.34 | 2.99 | 2.10 | 3.44 |
| 16th | 0.16 | 0.16 | 0.16 | 0.12 | 0.12 | 0.12 | 0.2 | 0.84 | 0.84 | 0.84 | 0.56 | 0.56 | 0.56 |
| 17th | 0.77 | 0.65 | 0.84 | 0.54 | 0.46 | 0.58 | 1.6 | 3.93 | 3.29 | 4.25 | 2.55 | 2.13 | 2.76 |
| 18th | 0.16 | 0.16 | 0.16 | 0.11 | 0.11 | 0.11 | 0.2 | 0.77 | 0.77 | 0.77 | 0.51 | 0.51 | 0.51 |
| 19th | 0.68 | 0.56 | 0.87 | 0.49 | 0.40 | 0.62 | 1.5 | 3.06 | 2.47 | 3.94 | 2.00 | 1.62 | 2.59 |
| 20th | 0.07 | 0.07 | 0.07 | 0.05 | 0.05 | 0.05 | 0.2 | 0.31 | 0.31 | 0.31 | 0.22 | 0.22 | 0.22 |
| 21st | 0.55 | 0.36 | 0.68 | 0.39 | 0.26 | 0.48 | 0.2 | 2.30 | 1.47 | 2.85 | 1.52 | 0.98 | 1.90 |
| 22nd | 0.01 | 0.01 | 0.01 | 0.01 | 0.01 | 0.01 | 0.2 | 0.09 | 0.09 | 0.09 | 0.07 | 0.07 | 0.07 |
| 23rd | 0.52 | 0.59 | 0.71 | 0.36 | 0.41 | 0.50 | 1.2 | 1.99 | 2.25 | 2.76 | 1.35 | 1.53 | 1.88 |
| 24th | 0.07 | 0.07 | 0.07 | 0.05 | 0.05 | 0.05 | 0.2 | 0.26 | 0.26 | 0.26 | 0.19 | 0.19 | 0.19 |
| 25th | 0.45 | 0.38 | 0.52 | 0.32 | 0.27 | 0.36 | 1.0 | 1.59 | 1.35 | 1.83 | 1.10 | 0.93 | 1.27 |
| 26th | 0.00 | 0.00 | 0.00 | 0.00 | 0.00 | 0.00 | 0.2 | 0.04 | 0.04 | 0.04 | 0.04 | 0.04 | 0.04 |
| 27th | 0.43 | 0.43 | 0.43 | 0.30 | 0.30 | 0.30 | 0.2 | 1.42 | 1.42 | 1.42 | 1.01 | 1.01 | 1.01 |
| 28th | 0.07 | 0.07 | 0.07 | 0.05 | 0.05 | 0.05 | 0.2 | 0.23 | 0.23 | 0.23 | 0.17 | 0.17 | 0.17 |
| 29th | 0.50 | 0.50 | 0.50 | 0.35 | 0.35 | 0.35 | 0.86 | 1.55 | 1.55 | 1.55 | 1.12 | 1.12 | 1.12 |
| 30th | 0.07 | 0.07 | 0.07 | 0.05 | 0.05 | 0.05 | 0.2 | 0.21 | 0.21 | 0.21 | 0.16 | 0.16 | 0.16 |
| 31st | 0.50 | 0.50 | 0.50 | 0.35 | 0.35 | 0.35 | 0.81 | 1.46 | 1.46 | 1.46 | 1.08 | 1.08 | 1.08 |
| 32nd | 0.07 | 0.07 | 0.07 | 0.05 | 0.05 | 0.05 | 0.2 | 0.20 | 0.20 | 0.20 | 0.16 | 0.16 | 0.16 |
| 33rd | 0.39 | 0.39 | 0.39 | 0.27 | 0.27 | 0.27 | 0.2 | 1.06 | 1.06 | 1.06 | 0.80 | 0.80 | 0.80 |
| 34th | 0.07 | 0.07 | 0.07 | 0.05 | 0.05 | 0.05 | 0.2 | 0.19 | 0.19 | 0.19 | 0.15 | 0.15 | 0.15 |
| 35th | 0.32 | 0.32 | 0.32 | 0.23 | 0.23 | 0.23 | 0.71 | 0.83 | 0.83 | 0.83 | 0.63 | 0.63 | 0.63 |
| 36th | 0.07 | 0.07 | 0.07 | 0.05 | 0.05 | 0.05 | 0.2 | 0.18 | 0.18 | 0.18 | 0.15 | 0.15 | 0.15 |
| 37th | 0.27 | 0.27 | 0.27 | 0.19 | 0.19 | 0.19 | 0.68 | 0.66 | 0.66 | 0.66 | 0.52 | 0.52 | 0.52 |
| 38th | 0.00 | 0.00 | 0.00 | 0.00 | 0.00 | 0.00 | 0.2 | 0.01 | 0.01 | 0.01 | 0.01 | 0.01 | 0.01 |
| 39th | 0.27 | 0.27 | 0.27 | 0.19 | 0.19 | 0.19 | 0.2 | 0.63 | 0.63 | 0.63 | 0.50 | 0.50 | 0.50 |
| 40th | 0.07 | 0.07 | 0.07 | 0.05 | 0.05 | 0.05 | 0.2 | 0.16 | 0.16 | 0.16 | 0.14 | 0.14 | 0.14 |
| 41st | 0.15 | 0.15 | 0.15 | 0.11 | 0.11 | 0.11 | 0.61 | 0.33 | 0.33 | 0.33 | 0.27 | 0.27 | 0.27 |
| 43rd | 0.15 | 0.15 | 0.15 | 0.11 | 0.11 | 0.11 | 0.58 | 0.32 | 0.32 | 0.32 | 0.26 | 0.26 | 0.26 |
| 45th | 0.15 | 0.15 | 0.15 | 0.11 | 0.11 | 0.11 | 0.20 | 0.31 | 0.31 | 0.31 | 0.25 | 0.25 | 0.25 |
| 47th | 0.10 | 0.10 | 0.10 | 0.07 | 0.07 | 0.07 | 0.53 | 0.20 | 0.20 | 0.20 | 0.16 | 0.16 | 0.16 |
| 49th | 0.10 | 0.10 | 0.10 | 0.07 | 0.07 | 0.07 | 0.51 | 0.19 | 0.19 | 0.19 | 0.16 | 0.16 | 0.16 |
| Harmonics higher than the limits set by ER G5/5 | | | | | | | Harmonics on the boundary of the limits set by G5/5 | | | | | | |
| Harmonics lower than the result from Table 4.4.1.1 | | | | | | | Voltage on Neutral: 5.038V | | | | | | |
| EVCs & PVs on Feeder 1: 48 & 54 respectively. EVCs & PVs on Feeder 2: 60 & 69 respectively. | | | | | | | | | | | | | |

During a three-phase fault, fed by red, as seen in Figures 4.4.2.3(A-C), the THDv increased further at the start, middle and end of feeder one on the red phase. Similar to the EVC simulations, the THDv stayed relatively constant along the length of feeder one on the yellow and blue phases as the current travels back towards the transformer. The maximum THDv recorded on feeder one is 4.73% for the harmonic profile from Table 3.3.1.1, 3.52% for the harmonic profile from Table 3.3.1.4 and 4.96% for the harmonic profile from Table 3.3.1.7. The highest THDv was measured on the blue phase supply terminal at the middle of feeder one.

By comparing the results in Table 4.4.2.3 to the results seen in Table 4.4.2.2, under the three-phase fault condition on feeder one, the voltage harmonic levels which have been exceeded on feeder one under ER G5/5 have either increased or stayed constant. In addition, the 45$^{th}$ and 47$^{th}$ harmonic current magnitudes have reduced when compared to Table 4.4.2.2. If this network was to be left with a three-phase fault, as would be compliant with the ESQCRs, this would result in a non-compliance with ER G5/5.

Similar to the two-phase fault scenario, harmonic magnitudes on feeder one which are lower than Table 4.4.1.1 have been highlighted with red text in Table 4.4.2.3. Harmonic current from the 41$^{st}$ harmonic onwards and specific voltage harmonics from the 14$^{th}$ harmonic onwards are lower than those found in Table 4.4.1.1. Therefore, the degree of harmonic cancellation has increased when compared to Table 4.4.2.2. This is not unexpected since more harmonic current sources have been added to the same conductor.

The tipping points for this scenario with a three-phase fault on feeder one to remain compliant under the different PV generation harmonic profiles on feeder one with ER G5/5 was identified. It was found that for Table 3.3.1.1 and Table 3.3.1.4, the maximum penetration was 12.0% (fifteen EVCs and PV generators) and for Table 3.3.1.7 was 7.2% (nine EVCs and PV generators). These were evenly distributed across three phases on feeders one and two as close as is achievable to a 44-56% split between PVs on feeders one and two respectively.

THDv (%) at Various Terminals on Feeder One During a Three-Phase Fault on Feeder One and a Two-Phase Fault on Feeder Two, Compared to the Results of Figures 4.4.1.1 (A-C).

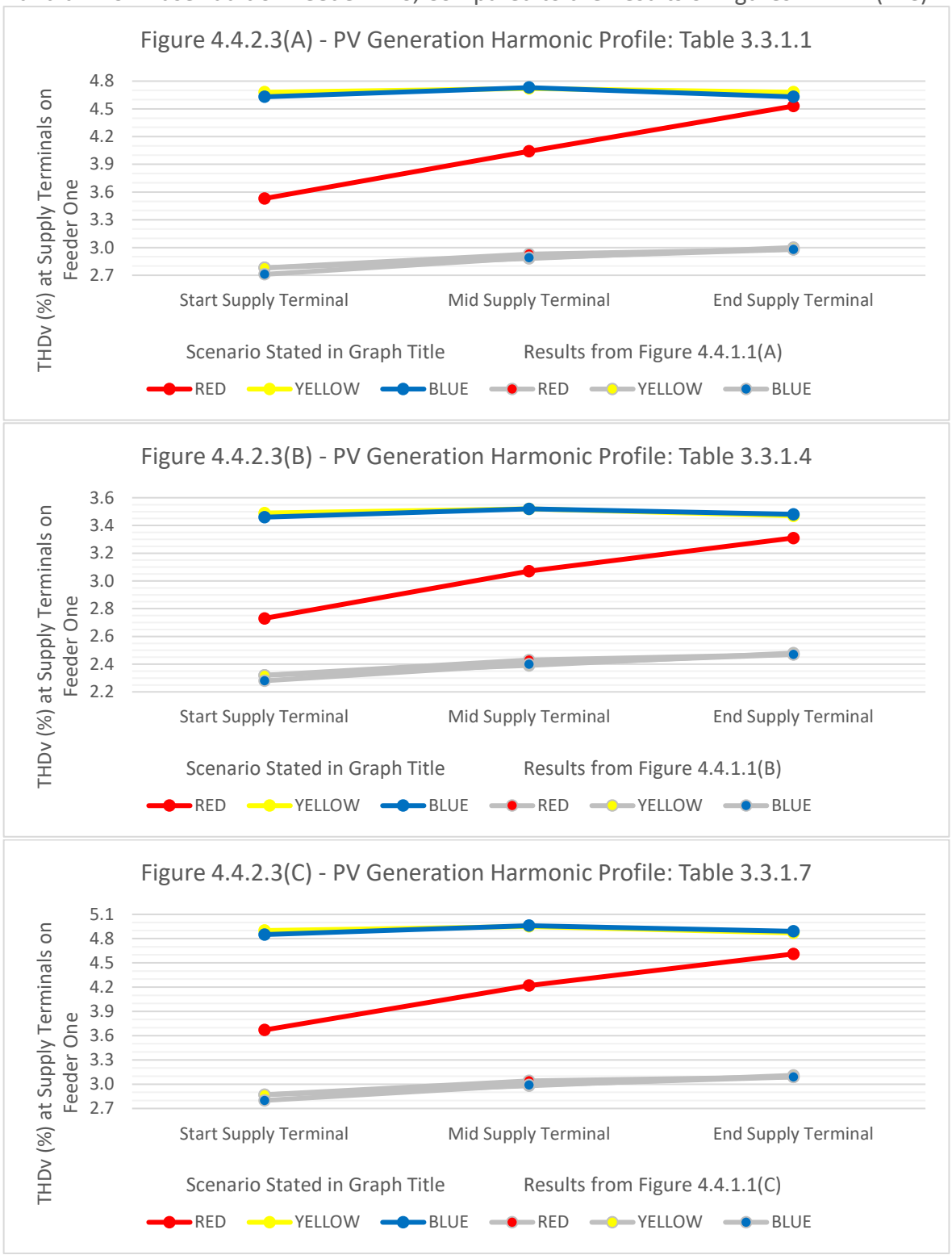


**Figure 4.4.2.3: Graphical representation of the THDv measured on each phase at supply terminals at the start, middle and end of feeder one during a three-phase fault on feeder one at 86.4% EVC penetration, 98.4% PV generation penetration and PV generation harmonic profile stated whilst a two-phase fault is present on feeder two, compared to normal running arrangements on feeders one and two (Figures 4.4.1.1 (A-C)).**

**Table 4.4.2.3: Table of harmonics on feeder one during a three-phase fault on feeder one at 86.4% EVC penetration and 98.4% PV generation penetration against the limits set out in ER G5/5 for the PV generation harmonic profile stated whilst a two-phase fault is present on feeder two (Energy Networks Association, 2020).**

| Harmonic Number | Worst Case Voltage Harmonic Magnitude at Supply Terminals (%) | | | Worst Case Voltage Harmonic Magnitude at Transformer (%) | | | ER G5/5 Limits (%) | Worst Case Phase Current Harmonic Magnitude at Transformer (A) | | | Neutral Harmonic Current Magnitude at Transformer (A) | | |
|---|---|---|---|---|---|---|---|---|---|---|---|---|---|
| | PV Generation Harmonic Profile from Table 3.3.1.- | | | PV Generation Harmonic Profile from Table 3.3.1.- | | | | PV Generation Harmonic Profile from Table 3.3.1.- | | | PV Generation Harmonic Profile from Table 3.3.1.- | | |
| | .1 | .4 | .7 | .1 | .4 | .7 | | .1 | .4 | .7 | .1 | .4 | .7 |
| 2nd | 0.23 | 0.23 | 0.23 | 0.13 | 0.13 | 0.13 | 1.6 | 6.24 | 6.24 | 6.24 | 5.35 | 5.35 | 5.35 |
| 3rd | 2.23 | 1.68 | 2.66 | 1.49 | 1.20 | 1.73 | 4.0 | 42.13 | 29.32 | 52.44 | 34.96 | 24.34 | 43.51 |
| 4th | 0.15 | 0.02 | 0.05 | 0.09 | 0.02 | 0.04 | 1.0 | 2.53 | 0.23 | 0.68 | 2.06 | 0.21 | 0.57 |
| 5th | 2.11 | 1.39 | 1.77 | 1.48 | 1.05 | 1.27 | 4.0 | 26.89 | 15.84 | 21.61 | 21.14 | 12.46 | 16.99 |
| 6th | 0.06 | 0.06 | 0.06 | 0.05 | 0.05 | 0.05 | 0.5 | 0.65 | 0.65 | 0.65 | 0.52 | 0.52 | 0.52 |
| 7th | 1.83 | 1.31 | 1.78 | 1.44 | 1.13 | 1.41 | 4.0 | 15.70 | 10.89 | 15.23 | 11.68 | 8.11 | 11.33 |
| 8th | 0.06 | 0.06 | 0.06 | 0.05 | 0.05 | 0.05 | 0.4 | 0.56 | 0.56 | 0.56 | 0.42 | 0.42 | 0.42 |
| 9th | 1.32 | 0.89 | 1.37 | 0.88 | 0.61 | 0.91 | 1.2 | 11.01 | 7.14 | 11.50 | 7.75 | 5.03 | 8.10 |
| 10th | 0.07 | 0.07 | 0.07 | 0.06 | 0.06 | 0.06 | 0.4 | 0.52 | 0.52 | 0.52 | 0.37 | 0.37 | 0.37 |
| 11th | 1.18 | 0.88 | 1.29 | 0.90 | 0.72 | 0.98 | 3.0 | 7.54 | 5.77 | 8.31 | 5.02 | 3.85 | 5.53 |
| 12th | 0.08 | 0.08 | 0.08 | 0.06 | 0.06 | 0.06 | 0.2 | 0.47 | 0.47 | 0.47 | 0.32 | 0.32 | 0.32 |
| 13th | 1.48 | 0.98 | 1.48 | 1.06 | 0.75 | 1.06 | 2.5 | 8.50 | 5.61 | 8.50 | 5.37 | 3.55 | 5.37 |
| 14th | 0.01 | 0.01 | 0.01 | 0.02 | 0.02 | 0.02 | 0.2 | 0.19 | 0.19 | 0.19 | 0.12 | 0.12 | 0.12 |
| 15th | 0.90 | 0.64 | 1.03 | 0.60 | 0.44 | 0.69 | 0.5 | 4.77 | 3.35 | 5.49 | 2.86 | 2.01 | 3.29 |
| 16th | 0.17 | 0.17 | 0.17 | 0.12 | 0.12 | 0.12 | 0.2 | 0.86 | 0.86 | 0.86 | 0.52 | 0.52 | 0.52 |
| 17th | 0.83 | 0.70 | 0.90 | 0.55 | 0.47 | 0.59 | 1.6 | 4.01 | 3.35 | 4.33 | 2.29 | 1.92 | 2.48 |
| 18th | 0.17 | 0.17 | 0.17 | 0.11 | 0.11 | 0.11 | 0.2 | 0.78 | 0.78 | 0.78 | 0.45 | 0.45 | 0.45 |
| 19th | 0.72 | 0.59 | 0.92 | 0.49 | 0.40 | 0.62 | 1.5 | 3.09 | 2.50 | 3.99 | 1.70 | 1.32 | 2.19 |
| 20th | 0.07 | 0.07 | 0.07 | 0.05 | 0.05 | 0.05 | 0.2 | 0.31 | 0.31 | 0.31 | 0.18 | 0.18 | 0.18 |
| 21st | 0.58 | 0.38 | 0.72 | 0.39 | 0.26 | 0.48 | 0.2 | 2.31 | 1.48 | 2.87 | 1.22 | 0.78 | 1.52 |
| 22nd | 0.01 | 0.01 | 0.01 | 0.01 | 0.01 | 0.01 | 0.2 | 0.09 | 0.09 | 0.09 | 0.05 | 0.05 | 0.05 |
| 23rd | 0.55 | 0.62 | 0.76 | 0.37 | 0.41 | 0.50 | 1.2 | 2.00 | 2.26 | 2.77 | 1.03 | 1.17 | 1.43 |
| 24th | 0.07 | 0.07 | 0.07 | 0.05 | 0.05 | 0.05 | 0.2 | 0.26 | 0.26 | 0.26 | 0.14 | 0.14 | 0.14 |
| 25th | 0.47 | 0.40 | 0.54 | 0.32 | 0.27 | 0.36 | 1.0 | 1.59 | 1.35 | 1.83 | 0.80 | 0.68 | 0.92 |
| 26th | 0.00 | 0.00 | 0.00 | 0.00 | 0.00 | 0.00 | 0.2 | 0.04 | 0.04 | 0.04 | 0.02 | 0.02 | 0.02 |
| 27th | 0.45 | 0.45 | 0.45 | 0.30 | 0.30 | 0.30 | 0.2 | 1.42 | 1.42 | 1.42 | 0.71 | 0.71 | 0.71 |
| 28th | 0.07 | 0.07 | 0.07 | 0.05 | 0.05 | 0.05 | 0.2 | 0.23 | 0.23 | 0.23 | 0.12 | 0.12 | 0.12 |
| 29th | 0.52 | 0.52 | 0.52 | 0.35 | 0.35 | 0.35 | 0.86 | 1.54 | 1.54 | 1.54 | 0.77 | 0.77 | 0.77 |
| 30th | 0.07 | 0.07 | 0.07 | 0.05 | 0.05 | 0.05 | 0.2 | 0.21 | 0.21 | 0.21 | 0.11 | 0.11 | 0.11 |
| 31st | 0.52 | 0.52 | 0.52 | 0.35 | 0.35 | 0.35 | 0.81 | 1.46 | 1.46 | 1.46 | 0.73 | 0.73 | 0.73 |
| 32nd | 0.07 | 0.07 | 0.07 | 0.05 | 0.05 | 0.05 | 0.2 | 0.20 | 0.20 | 0.20 | 0.11 | 0.11 | 0.11 |
| 33rd | 0.40 | 0.40 | 0.40 | 0.27 | 0.27 | 0.27 | 0.2 | 1.05 | 1.05 | 1.05 | 0.53 | 0.53 | 0.53 |
| 34th | 0.07 | 0.07 | 0.07 | 0.05 | 0.05 | 0.05 | 0.2 | 0.19 | 0.19 | 0.19 | 0.10 | 0.10 | 0.10 |
| 35th | 0.33 | 0.33 | 0.33 | 0.23 | 0.23 | 0.23 | 0.71 | 0.82 | 0.82 | 0.82 | 0.42 | 0.42 | 0.42 |
| 36th | 0.07 | 0.07 | 0.07 | 0.05 | 0.05 | 0.05 | 0.2 | 0.18 | 0.18 | 0.18 | 0.10 | 0.10 | 0.10 |
| 37th | 0.28 | 0.28 | 0.28 | 0.19 | 0.19 | 0.19 | 0.68 | 0.66 | 0.66 | 0.66 | 0.34 | 0.34 | 0.34 |
| 38th | 0.00 | 0.00 | 0.00 | 0.00 | 0.00 | 0.00 | 0.2 | 0.01 | 0.01 | 0.01 | 0.01 | 0.01 | 0.01 |
| 39th | 0.28 | 0.28 | 0.28 | 0.19 | 0.19 | 0.19 | 0.2 | 0.63 | 0.63 | 0.63 | 0.33 | 0.33 | 0.33 |
| 40th | 0.07 | 0.07 | 0.07 | 0.05 | 0.05 | 0.05 | 0.2 | 0.16 | 0.16 | 0.16 | 0.09 | 0.09 | 0.09 |
| 41st | 0.16 | 0.16 | 0.16 | 0.11 | 0.11 | 0.11 | 0.61 | 0.33 | 0.33 | 0.33 | 0.18 | 0.18 | 0.18 |
| 43rd | 0.16 | 0.15 | 0.16 | 0.11 | 0.11 | 0.11 | 0.58 | 0.32 | 0.32 | 0.32 | 0.17 | 0.17 | 0.17 |
| 45th | 0.16 | 0.16 | 0.16 | 0.11 | 0.11 | 0.11 | 0.20 | 0.30 | 0.30 | 0.30 | 0.17 | 0.17 | 0.17 |
| 47th | 0.10 | 0.10 | 0.10 | 0.07 | 0.07 | 0.07 | 0.53 | 0.19 | 0.19 | 0.19 | 0.11 | 0.11 | 0.11 |
| 49th | 0.10 | 0.10 | 0.10 | 0.07 | 0.07 | 0.07 | 0.51 | 0.19 | 0.19 | 0.19 | 0.11 | 0.11 | 0.11 |
| Harmonics higher than the limits set by ER G5/5 | | | | | | | Harmonics on the boundary of the limits set by ER G5/5 | | | | | | |
| Harmonics lower than the result from Table 4.4.1.1 | | | | | | | Voltage on Neutral: 7.243V | | | | | | |
| EVCs & PVs on Feeder 1: 48 & 54 respectively. EVCs & PVs on Feeder 2: 60 & 69 respectively. | | | | | | | | | | | | | |

In addition, it was found that the neutral voltage present at the end of feeder one increased to 7.243V under three-phase fault conditions on feeder one shown in Table 4.4.2.3 from 5.038V under two-phase conditions in Table 4.4.2.2 and 1.214V under normal arrangements shown in Table 4.4.2.1. Based on Table 3.2.7.4, the voltages caused by a two or three-phase fault could lead to residents perceiving shocks off exposed bonded metal work, potentially leading to complaints. However, it does not seem high enough to cause ventricular fibrillation or respiratory tetanus.

## 4.4.3 – Results of Phase-to-Phase Faults, with a Three-Phase Fault on Feeder Two

Further to Sections 4.4.1 and 4.4.2, the effect of faults on feeder one will be explored whilst a second three-phase fault on feeder two is present. It can be seen in Figures 4.4.3.1 (A-C) that the THDv measured on blue phase has dropped when compared to Section 4.4.2 under normal-running arrangements. This brings both yellow and blue THDv to a similar level. This is due to the load on yellow and blue phases being shifted onto the red phase, caused by the three-phase fault on feeder two. This shift in load has also caused the THDv level on red phase of feeder one to rise by between 0.17-0.35% when compared to the similar scenario with a two-phase fault on feeder two shown in Section 4.4.2.

Due to the current being drawn on feeder one remaining the same, the increase in THDv between the beginning and the end of feeder one remains low at 0.15-0.27%, similar to Figures 4.4.1.1(A-C) and 4.4.2.1(A-C). The individual harmonic levels on feeder one can be seen in Table 4.4.3.1. Similar to Table 4.4.2.1 when compared to Table 4.4.1.1, the increase in voltage harmonics is minimal and some cases reduces. For example, when comparing Tables 4.4.2.1 and 4.4.3.1, the $15^{th}$ harmonics increased by 0.00-0.02V, however, conversely the $33^{rd}$ harmonic reduced by 0.00-0.01V. However, there are still many breaches of the limits set by ER G5/5.

Despite the three-phase fault on feeder two leading to the neutral voltage on feeder one increasing from 0.058V to 1.960V the voltage does not exceed 2.70V on feeder one and therefore should not be high enough to cause perceived shocks to residents. However, based on the results of Tables 4.4.1.2-3, it is likely that residents will receive shocks off feeder two.

THDv (%) at Various Terminals on Feeder One During Normal Running Arrangements on Feeder One and a Three-Phase Fault on Feeder Two, Compared to the Results of Figures 4.4.1.1 (A-C).

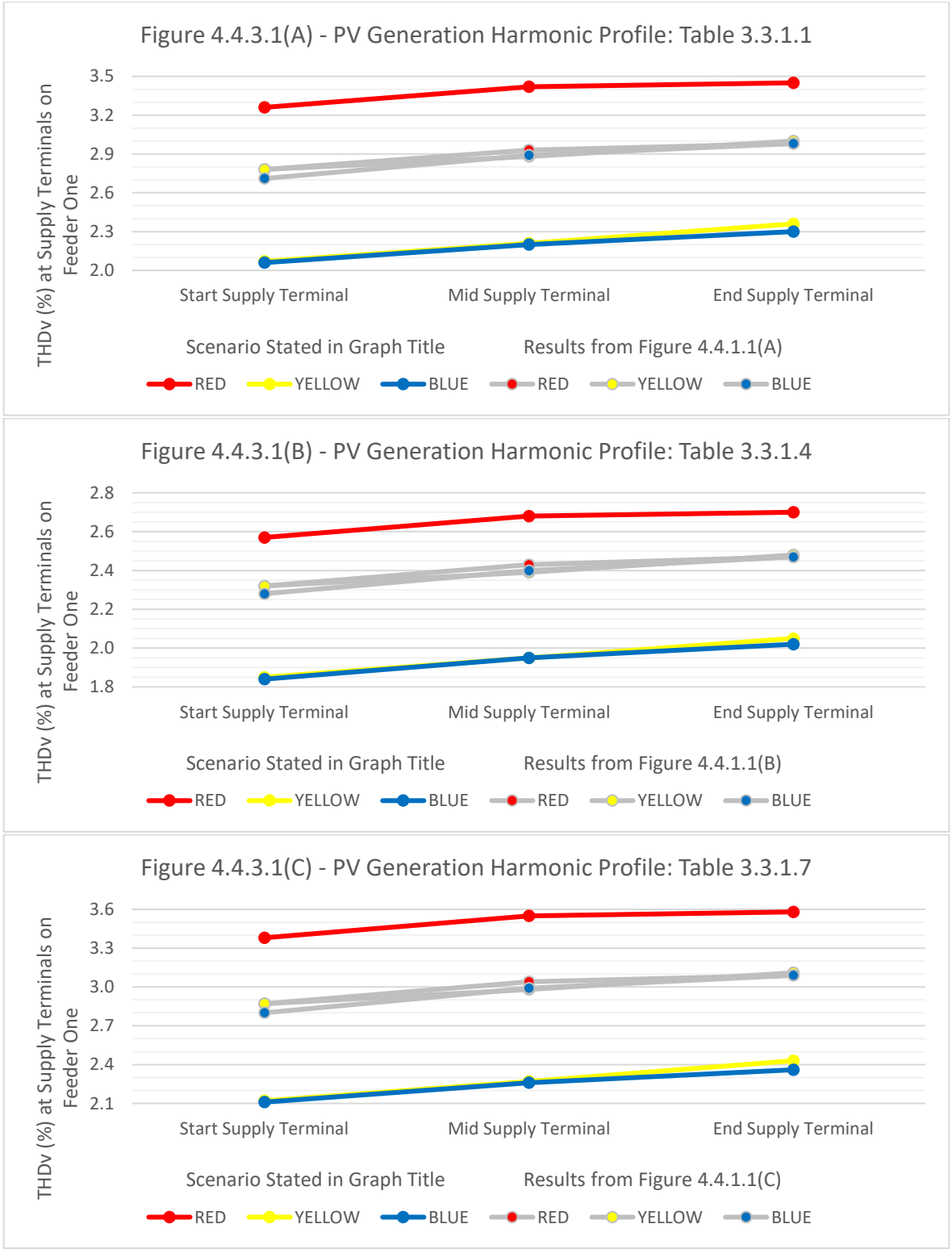


**Figure 4.4.3.1: Graphical representation of the THDv measured on each phase at supply terminals at the start, middle and end of feeder one under normal running arrangements on feeder one at 86.4% EVC penetration, 98.4% PV generation penetration and PV generation harmonic profile stated whilst a three-phase fault is present on feeder two, compared to normal running arrangements on feeders one and two (Figures 4.4.1.1 (A-C)).**

**Table 4.4.3.1: Table of harmonics on feeder one for normal running arrangements on feeder one at 86.4% EVC penetration and 98.4% PV generation penetration against the limits set out in ER G5/5 for the PV generation harmonic profile stated whilst a three-phase fault is present on feeder two (Energy Networks Association, 2020).**

| Harmonic Number | Worst Case Voltage Harmonic Magnitude at Supply Terminals (%) | | | Worst Case Voltage Harmonic Magnitude at Transformer (%) | | | ER G5/5 Limits (%) | Worst Case Phase Current Harmonic Magnitude at Transformer (A) | | | Neutral Harmonic Current Magnitude at Transformer (A) | | |
|---|---|---|---|---|---|---|---|---|---|---|---|---|---|
| | PV Generation Harmonic Profile from Table 3.3.1.- | | | PV Generation Harmonic Profile from Table 3.3.1.- | | | | PV Generation Harmonic Profile from Table 3.3.1.- | | | PV Generation Harmonic Profile from Table 3.3.1.- | | |
| | .1 | .4 | .7 | .1 | .4 | .7 | | .1 | .4 | .7 | .1 | .4 | .7 |
| 2nd | 0.14 | 0.14 | 0.14 | 0.12 | 0.12 | 0.12 | 1.6 | 5.44 | 5.44 | 5.44 | 4.14 | 4.14 | 4.14 |
| 3rd | 1.50 | 1.20 | 1.74 | 1.38 | 1.12 | 1.59 | 4.0 | 36.95 | 25.68 | 46.02 | 27.50 | 19.07 | 34.28 |
| 4th | 0.09 | 0.02 | 0.04 | 0.09 | 0.02 | 0.04 | 1.0 | 2.23 | 0.20 | 0.59 | 1.70 | 0.16 | 0.48 |
| 5th | 1.49 | 1.05 | 1.28 | 1.38 | 0.99 | 1.20 | 4.0 | 23.96 | 14.09 | 19.24 | 17.75 | 10.41 | 14.24 |
| 6th | 0.05 | 0.05 | 0.05 | 0.05 | 0.05 | 0.05 | 0.5 | 0.58 | 0.58 | 0.58 | 0.45 | 0.45 | 0.45 |
| 7th | 1.47 | 1.15 | 1.44 | 1.40 | 1.12 | 1.38 | 4.0 | 14.22 | 9.86 | 13.79 | 10.45 | 7.24 | 10.14 |
| 8th | 0.05 | 0.05 | 0.05 | 0.04 | 0.04 | 0.04 | 0.4 | 0.50 | 0.50 | 0.50 | 0.39 | 0.39 | 0.39 |
| 9th | 0.91 | 0.63 | 0.94 | 0.82 | 0.58 | 0.86 | 1.2 | 10.12 | 6.56 | 10.57 | 7.36 | 4.76 | 7.69 |
| 10th | 0.06 | 0.06 | 0.06 | 0.05 | 0.05 | 0.05 | 0.4 | 0.48 | 0.48 | 0.48 | 0.36 | 0.36 | 0.36 |
| 11th | 0.95 | 0.76 | 1.03 | 0.89 | 0.73 | 0.96 | 3.0 | 7.02 | 5.37 | 7.74 | 5.05 | 3.86 | 5.56 |
| 12th | 0.06 | 0.06 | 0.06 | 0.06 | 0.06 | 0.06 | 0.2 | 0.44 | 0.44 | 0.44 | 0.32 | 0.32 | 0.32 |
| 13th | 1.12 | 0.79 | 1.12 | 1.03 | 0.74 | 1.03 | 2.5 | 7.99 | 5.27 | 7.99 | 5.67 | 3.73 | 5.67 |
| 14th | 0.02 | 0.02 | 0.02 | 0.02 | 0.02 | 0.02 | 0.2 | 0.18 | 0.18 | 0.18 | 0.12 | 0.12 | 0.12 |
| 15th | 0.64 | 0.47 | 0.73 | 0.58 | 0.43 | 0.66 | 0.5 | 4.53 | 3.18 | 5.21 | 3.16 | 2.21 | 3.63 |
| 16th | 0.13 | 0.13 | 0.13 | 0.11 | 0.11 | 0.11 | 0.2 | 0.82 | 0.82 | 0.82 | 0.57 | 0.57 | 0.57 |
| 17th | 0.59 | 0.50 | 0.64 | 0.53 | 0.45 | 0.57 | 1.6 | 3.83 | 3.20 | 4.14 | 2.62 | 2.19 | 2.83 |
| 18th | 0.12 | 0.12 | 0.12 | 0.11 | 0.11 | 0.11 | 0.2 | 0.75 | 0.75 | 0.75 | 0.51 | 0.51 | 0.51 |
| 19th | 0.53 | 0.44 | 0.67 | 0.48 | 0.39 | 0.60 | 1.5 | 2.97 | 2.40 | 3.83 | 1.99 | 1.61 | 2.57 |
| 20th | 0.06 | 0.06 | 0.06 | 0.05 | 0.05 | 0.05 | 0.2 | 0.30 | 0.30 | 0.30 | 0.20 | 0.20 | 0.20 |
| 21st | 0.42 | 0.28 | 0.52 | 0.38 | 0.25 | 0.46 | 0.2 | 2.23 | 1.43 | 2.77 | 1.47 | 0.94 | 1.82 |
| 22nd | 0.01 | 0.01 | 0.01 | 0.01 | 0.01 | 0.01 | 0.2 | 0.09 | 0.09 | 0.09 | 0.05 | 0.05 | 0.05 |
| 23rd | 0.40 | 0.45 | 0.54 | 0.35 | 0.40 | 0.49 | 1.2 | 1.94 | 2.19 | 2.69 | 1.24 | 1.41 | 1.73 |
| 24th | 0.05 | 0.05 | 0.05 | 0.05 | 0.05 | 0.05 | 0.2 | 0.25 | 0.25 | 0.25 | 0.16 | 0.16 | 0.16 |
| 25th | 0.35 | 0.30 | 0.40 | 0.31 | 0.26 | 0.35 | 1.0 | 1.54 | 1.31 | 1.78 | 0.97 | 0.82 | 1.12 |
| 26th | 0.00 | 0.00 | 0.00 | 0.00 | 0.00 | 0.00 | 0.2 | 0.04 | 0.04 | 0.04 | 0.02 | 0.02 | 0.02 |
| 27th | 0.33 | 0.33 | 0.33 | 0.30 | 0.30 | 0.30 | 0.2 | 1.38 | 1.38 | 1.38 | 0.85 | 0.85 | 0.85 |
| 28th | 0.06 | 0.06 | 0.06 | 0.05 | 0.05 | 0.05 | 0.2 | 0.22 | 0.22 | 0.22 | 0.14 | 0.14 | 0.14 |
| 29th | 0.38 | 0.38 | 0.38 | 0.34 | 0.34 | 0.34 | 0.86 | 1.51 | 1.51 | 1.51 | 0.90 | 0.90 | 0.90 |
| 30th | 0.05 | 0.05 | 0.05 | 0.05 | 0.05 | 0.05 | 0.2 | 0.21 | 0.21 | 0.21 | 0.13 | 0.13 | 0.13 |
| 31st | 0.39 | 0.39 | 0.39 | 0.35 | 0.35 | 0.35 | 0.81 | 1.43 | 1.43 | 1.43 | 0.84 | 0.84 | 0.84 |
| 32nd | 0.05 | 0.05 | 0.05 | 0.05 | 0.05 | 0.05 | 0.2 | 0.20 | 0.20 | 0.20 | 0.12 | 0.12 | 0.12 |
| 33rd | 0.30 | 0.30 | 0.30 | 0.27 | 0.27 | 0.27 | 0.2 | 1.04 | 1.04 | 1.04 | 0.59 | 0.59 | 0.59 |
| 34th | 0.05 | 0.05 | 0.05 | 0.05 | 0.05 | 0.05 | 0.2 | 0.19 | 0.19 | 0.19 | 0.11 | 0.11 | 0.11 |
| 35th | 0.25 | 0.25 | 0.25 | 0.22 | 0.22 | 0.22 | 0.71 | 0.81 | 0.81 | 0.81 | 0.45 | 0.45 | 0.45 |
| 36th | 0.05 | 0.05 | 0.05 | 0.05 | 0.05 | 0.05 | 0.2 | 0.18 | 0.18 | 0.18 | 0.10 | 0.10 | 0.10 |
| 37th | 0.21 | 0.21 | 0.21 | 0.19 | 0.19 | 0.19 | 0.68 | 0.65 | 0.65 | 0.65 | 0.35 | 0.35 | 0.35 |
| 38th | 0.00 | 0.00 | 0.00 | 0.00 | 0.00 | 0.00 | 0.2 | 0.00 | 0.00 | 0.00 | 0.01 | 0.01 | 0.01 |
| 39th | 0.22 | 0.22 | 0.22 | 0.19 | 0.19 | 0.19 | 0.2 | 0.62 | 0.62 | 0.62 | 0.33 | 0.33 | 0.33 |
| 40th | 0.05 | 0.05 | 0.05 | 0.05 | 0.05 | 0.05 | 0.2 | 0.16 | 0.16 | 0.16 | 0.09 | 0.09 | 0.09 |
| 41st | 0.12 | 0.12 | 0.12 | 0.11 | 0.11 | 0.11 | 0.61 | 0.33 | 0.33 | 0.33 | 0.17 | 0.17 | 0.17 |
| 43rd | 0.12 | 0.12 | 0.12 | 0.11 | 0.11 | 0.11 | 0.58 | 0.32 | 0.32 | 0.32 | 0.16 | 0.16 | 0.16 |
| 45th | 0.12 | 0.12 | 0.12 | 0.11 | 0.11 | 0.11 | 0.20 | 0.30 | 0.30 | 0.30 | 0.15 | 0.15 | 0.15 |
| 47th | 0.08 | 0.08 | 0.08 | 0.07 | 0.07 | 0.07 | 0.53 | 0.19 | 0.19 | 0.19 | 0.09 | 0.09 | 0.09 |
| 49th | 0.08 | 0.08 | 0.08 | 0.07 | 0.07 | 0.07 | 0.51 | 0.19 | 0.19 | 0.19 | 0.09 | 0.09 | 0.09 |
| Harmonics higher than the limits set by ER G5/5 | | | | | | | Harmonics on the boundary of the limits set by ER G5/5 | | | | | | |
| Harmonics lower than the result from Table 4.4.1.1 | | | | | | | Voltage on Neutral: 1.960V | | | | | | |
| EVCs & PVs on Feeder 1: 48 & 54 respectively. EVCs & PVs on Feeder 2: 60 & 69 respectively. | | | | | | | | | | | | | |

The tipping points for this scenario with normal running arrangements on feeder one and a three-phase fault on feeder two to remain compliant on feeder one under the different PV generation profiles with ER G5/5 was identified. It was found that for Table 3.3.1.1, the maximum penetration was 21.6% (twenty-seven EVCs and PV generators), for Table 3.3.1.4 was 28.8% (thirty-six EVCs and PV generators) and for Table 3.3.1.7 was 16.8% (twenty-one EVCs and PV generators). These were evenly distributed across three phases on feeders one and two as close as is achievable to a 44-56% split between PV generators on feeders one and two respectively.

By introducing a two-phase fault, between red and yellow phases at the end of feeder one, with red phase feeding the fault as seen in Figures 4.4.3.2(A-C), it has been found that the THDv increases significantly along the length of feeder one on red phase, however, the THDv stays relatively level on the yellow phase as the current travels back towards the transformer varying between 0.07-0.13%. This leads to the THDv measured on the yellow phase supply terminal at the middle of feeder one reaching the highest level. There is no noticeable effect on the blue phase THDv which is excluded from the faulted phases on feeder one.

The results of the worst-case harmonic distortion under a two-phase fault on feeder one can be seen in Table 4.4.3.2. The worst-case harmonic distortion was measured between phase and neutral on the yellow phase supply terminal at the middle of feeder one as shown in Figures 4.4.3.2(A-C). The worst-case THDv varies between each of the harmonic profiles due to the harmonic current contribution seen in Table 4.4.3.2. ER G5/5 limits are exceeded across multiple harmonics on feeder one including the $9^{th}$, $15^{th}$, $21^{st}$, $27^{th}$, $33^{rd}$, and $39^{th}$, therefore resulting in non-compliance. Lastly, due to the network imbalance, the neutral voltage has increased to 5.467V on feeder one, which is high enough to provide residents with potential shocks off of exposed metalwork.

THDv (%) at Various Terminals on Feeder One During a Two-Phase Fault on Feeder One and a Three-Phase Fault on Feeder Two, Compared to the Results of Figures 4.4.1.1 (A-C).

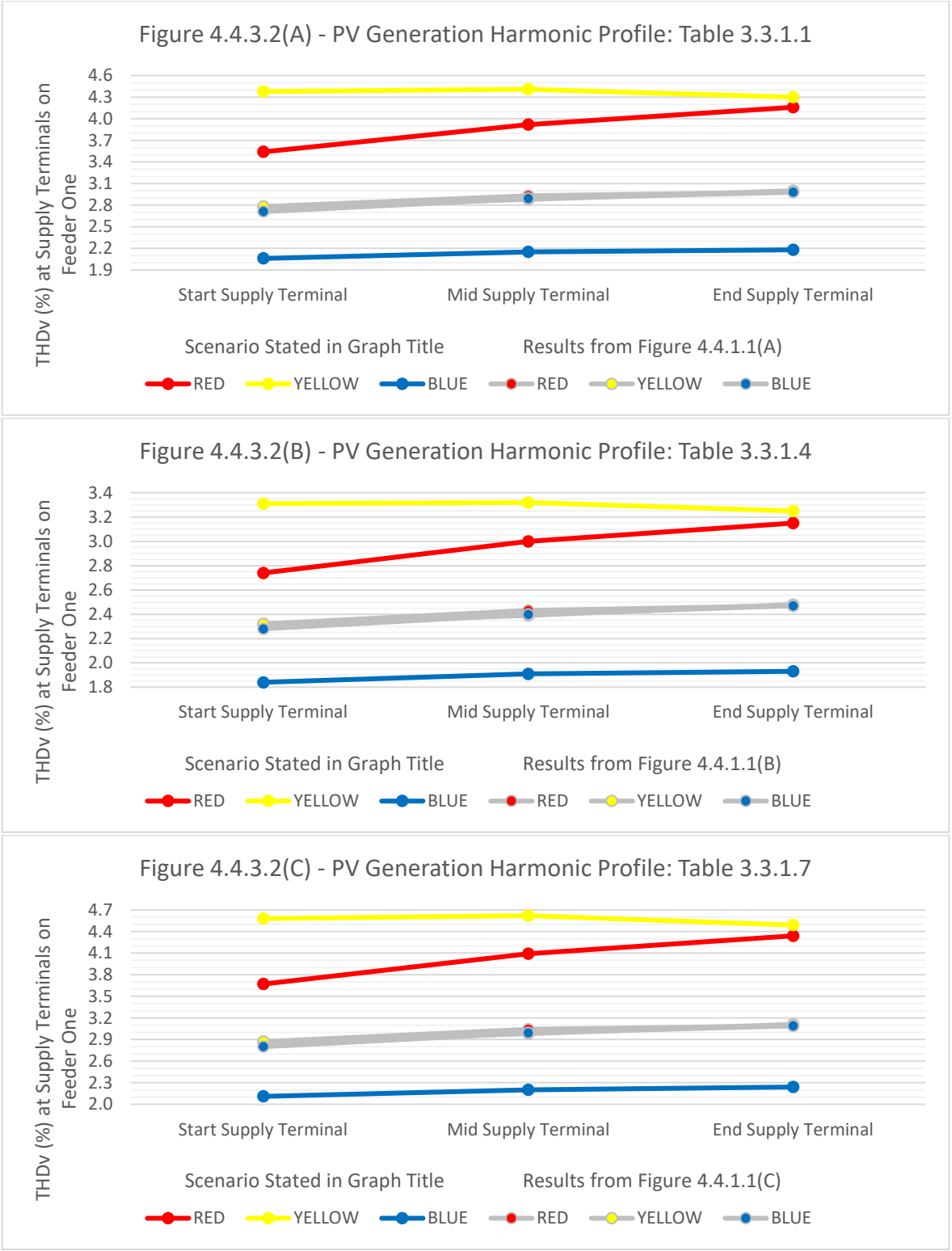


**Figure 4.4.3.2: Graphical representation of the THDv measured on each phase at supply terminals at the start, middle and end of feeder one during a two-phase fault on feeder one at 86.4% EVC penetration, 98.4% PV generation penetration and PV generation harmonic profile stated whilst a three-phase fault is present on feeder two, compared to normal running arrangements on feeders one and two (Figures 4.4.1.1 (A-C)).**

**Table 4.4.3.2: Table of harmonics on feeder one during a two-phase fault on feeder one at 86.4% EVC penetration and 98.4% PV generation penetration against the limits set out in ER G5/5 for the PV generation harmonic profile stated whilst a three-phase fault is present on feeder two (Energy Networks Association, 2020).**

| Harmonic Number | Worst Case Voltage Harmonic Magnitude at Supply Terminals (%) | | | Worst Case Voltage Harmonic Magnitude at Transformer (%) | | | ER G5/5 Limits (%) | Worst Case Phase Current Harmonic Magnitude at Transformer (A) | | | Neutral Harmonic Current Magnitude at Transformer (A) | | |
|---|---|---|---|---|---|---|---|---|---|---|---|---|---|
| | PV Generation Harmonic Profile from Table 3.3.1.- | | | PV Generation Harmonic Profile from Table 3.3.1.- | | | | PV Generation Harmonic Profile from Table 3.3.1.- | | | PV Generation Harmonic Profile from Table 3.3.1.- | | |
| | .1 | .4 | .7 | .1 | .4 | .7 | | .1 | .4 | .7 | .1 | .4 | .7 |
| 2nd | 0.20 | 0.20 | 0.20 | 0.14 | 0.14 | 0.14 | 1.6 | 6.43 | 6.43 | 6.43 | 5.67 | 5.68 | 5.67 |
| 3rd | 2.03 | 1.56 | 2.41 | 1.52 | 1.22 | 1.76 | 4.0 | 43.33 | 30.13 | 53.95 | 37.28 | 25.90 | 46.43 |
| 4th | 0.13 | 0.02 | 0.05 | 0.10 | 0.02 | 0.04 | 1.0 | 2.60 | 0.23 | 0.69 | 2.21 | 0.21 | 0.60 |
| 5th | 1.96 | 1.31 | 1.65 | 1.50 | 1.06 | 1.29 | 4.0 | 27.60 | 16.24 | 22.17 | 22.76 | 13.37 | 18.27 |
| 6th | 0.06 | 0.06 | 0.06 | 0.05 | 0.05 | 0.05 | 0.5 | 0.66 | 0.66 | 0.66 | 0.55 | 0.55 | 0.55 |
| 7th | 1.74 | 1.27 | 1.70 | 1.45 | 1.13 | 1.42 | 4.0 | 16.07 | 11.15 | 15.59 | 12.69 | 8.79 | 12.31 |
| 8th | 0.06 | 0.06 | 0.06 | 0.05 | 0.05 | 0.05 | 0.4 | 0.57 | 0.57 | 0.57 | 0.45 | 0.45 | 0.45 |
| 9th | 1.21 | 0.82 | 1.26 | 0.89 | 0.62 | 0.93 | 1.2 | 11.24 | 7.29 | 11.74 | 8.49 | 5.49 | 8.86 |
| 10th | 0.07 | 0.07 | 0.07 | 0.06 | 0.06 | 0.06 | 0.4 | 0.53 | 0.53 | 0.53 | 0.41 | 0.41 | 0.41 |
| 11th | 1.12 | 0.85 | 1.23 | 0.91 | 0.72 | 0.98 | 3.0 | 7.68 | 5.88 | 8.46 | 5.54 | 4.24 | 6.11 |
| 12th | 0.07 | 0.07 | 0.07 | 0.06 | 0.06 | 0.06 | 0.2 | 0.48 | 0.48 | 0.48 | 0.35 | 0.35 | 0.35 |
| 13th | 1.39 | 0.94 | 1.39 | 1.07 | 0.75 | 1.07 | 2.5 | 8.64 | 5.70 | 8.64 | 5.96 | 3.92 | 5.96 |
| 14th | 0.02 | 0.02 | 0.02 | 0.02 | 0.02 | 0.02 | 0.2 | 0.19 | 0.19 | 0.19 | 0.13 | 0.13 | 0.13 |
| 15th | 0.84 | 0.60 | 0.95 | 0.61 | 0.45 | 0.69 | 0.5 | 4.84 | 3.40 | 5.57 | 3.19 | 2.24 | 3.67 |
| 16th | 0.16 | 0.16 | 0.16 | 0.12 | 0.12 | 0.12 | 0.2 | 0.87 | 0.87 | 0.87 | 0.57 | 0.57 | 0.57 |
| 17th | 0.77 | 0.65 | 0.83 | 0.56 | 0.47 | 0.60 | 1.6 | 4.06 | 3.40 | 4.39 | 2.56 | 2.14 | 2.77 |
| 18th | 0.16 | 0.16 | 0.16 | 0.12 | 0.12 | 0.12 | 0.2 | 0.79 | 0.79 | 0.79 | 0.50 | 0.50 | 0.50 |
| 19th | 0.68 | 0.55 | 0.86 | 0.49 | 0.41 | 0.62 | 1.5 | 3.13 | 2.53 | 4.04 | 1.89 | 1.52 | 2.45 |
| 20th | 0.07 | 0.07 | 0.07 | 0.05 | 0.05 | 0.05 | 0.2 | 0.31 | 0.31 | 0.31 | 0.19 | 0.20 | 0.19 |
| 21st | 0.55 | 0.36 | 0.67 | 0.39 | 0.26 | 0.48 | 0.2 | 2.34 | 1.50 | 2.90 | 1.36 | 0.87 | 1.69 |
| 22nd | 0.01 | 0.01 | 0.01 | 0.01 | 0.01 | 0.01 | 0.2 | 0.09 | 0.09 | 0.09 | 0.05 | 0.05 | 0.05 |
| 23rd | 0.51 | 0.58 | 0.71 | 0.37 | 0.41 | 0.50 | 1.2 | 2.02 | 2.28 | 2.80 | 1.13 | 1.28 | 1.58 |
| 24th | 0.07 | 0.07 | 0.07 | 0.05 | 0.05 | 0.05 | 0.2 | 0.26 | 0.26 | 0.26 | 0.15 | 0.15 | 0.15 |
| 25th | 0.44 | 0.38 | 0.51 | 0.32 | 0.27 | 0.36 | 1.0 | 1.60 | 1.36 | 1.84 | 0.87 | 0.74 | 1.00 |
| 26th | 0.00 | 0.00 | 0.00 | 0.00 | 0.00 | 0.00 | 0.2 | 0.04 | 0.04 | 0.04 | 0.02 | 0.02 | 0.02 |
| 27th | 0.43 | 0.43 | 0.43 | 0.30 | 0.30 | 0.30 | 0.2 | 1.43 | 1.43 | 1.43 | 0.76 | 0.76 | 0.76 |
| 28th | 0.07 | 0.07 | 0.07 | 0.05 | 0.05 | 0.05 | 0.2 | 0.23 | 0.23 | 0.23 | 0.13 | 0.13 | 0.13 |
| 29th | 0.49 | 0.49 | 0.49 | 0.35 | 0.35 | 0.35 | 0.86 | 1.55 | 1.55 | 1.55 | 0.81 | 0.81 | 0.81 |
| 30th | 0.07 | 0.07 | 0.07 | 0.05 | 0.05 | 0.05 | 0.2 | 0.21 | 0.21 | 0.21 | 0.12 | 0.12 | 0.12 |
| 31st | 0.50 | 0.50 | 0.50 | 0.36 | 0.36 | 0.36 | 0.81 | 1.47 | 1.47 | 1.47 | 0.75 | 0.75 | 0.75 |
| 32nd | 0.07 | 0.07 | 0.07 | 0.05 | 0.05 | 0.05 | 0.2 | 0.20 | 0.20 | 0.20 | 0.11 | 0.11 | 0.11 |
| 33rd | 0.38 | 0.38 | 0.38 | 0.27 | 0.27 | 0.27 | 0.2 | 1.06 | 1.06 | 1.06 | 0.53 | 0.53 | 0.53 |
| 34th | 0.07 | 0.07 | 0.07 | 0.05 | 0.05 | 0.05 | 0.2 | 0.19 | 0.19 | 0.19 | 0.10 | 0.10 | 0.10 |
| 35th | 0.32 | 0.32 | 0.32 | 0.23 | 0.23 | 0.23 | 0.71 | 0.83 | 0.83 | 0.83 | 0.41 | 0.41 | 0.41 |
| 36th | 0.07 | 0.07 | 0.07 | 0.05 | 0.05 | 0.05 | 0.2 | 0.18 | 0.18 | 0.18 | 0.10 | 0.10 | 0.10 |
| 37th | 0.27 | 0.27 | 0.27 | 0.19 | 0.19 | 0.19 | 0.68 | 0.66 | 0.66 | 0.66 | 0.33 | 0.33 | 0.33 |
| 38th | 0.00 | 0.00 | 0.00 | 0.00 | 0.00 | 0.00 | 0.2 | 0.01 | 0.01 | 0.01 | 0.01 | 0.01 | 0.01 |
| 39th | 0.27 | 0.27 | 0.27 | 0.19 | 0.19 | 0.19 | 0.2 | 0.63 | 0.63 | 0.63 | 0.31 | 0.31 | 0.31 |
| 40th | 0.07 | 0.07 | 0.07 | 0.05 | 0.05 | 0.05 | 0.2 | 0.16 | 0.16 | 0.16 | 0.09 | 0.09 | 0.09 |
| 41st | 0.15 | 0.15 | 0.15 | 0.11 | 0.11 | 0.11 | 0.61 | 0.33 | 0.33 | 0.33 | 0.16 | 0.16 | 0.16 |
| 43rd | 0.15 | 0.15 | 0.15 | 0.11 | 0.11 | 0.11 | 0.58 | 0.32 | 0.32 | 0.32 | 0.16 | 0.16 | 0.16 |
| 45th | 0.15 | 0.15 | 0.15 | 0.11 | 0.11 | 0.11 | 0.20 | 0.31 | 0.31 | 0.31 | 0.15 | 0.15 | 0.15 |
| 47th | 0.10 | 0.10 | 0.10 | 0.07 | 0.07 | 0.07 | 0.53 | 0.19 | 0.19 | 0.19 | 0.10 | 0.10 | 0.10 |
| 49th | 0.10 | 0.10 | 0.10 | 0.07 | 0.07 | 0.07 | 0.51 | 0.19 | 0.19 | 0.19 | 0.10 | 0.10 | 0.10 |
| Harmonics higher than the limits set by ER G5/5 | | | | | | | Harmonics on the boundary of the limits set by ER G5/5 | | | | | | |
| Harmonics lower than the result from Table 4.4.1.1 | | | | | | | Voltage on Neutral: 5.467V | | | | | | |
| EVCs & PVs on Feeder 1: 48 & 54 respectively. EVCs & PVs on Feeder 2: 60 & 69 respectively. | | | | | | | | | | | | | |

The tipping points for this scenario with a two-phase fault on feeder one for feeder one to remain compliant under the different PV generation profiles with ER G5/5 was identified. It was found that for Tables 3.3.1.1 the maximum penetration was 12.0% (fifteen EVCs and PV generators), for Table 3.3.1.4 was 16.8% (twenty-one EVCs and PV generators), and for Table 3.3.1.7 was 9.6% (twelve EVCs and PV generators). These were evenly distributed across three phases on feeders one and two as close as is achievable to a 44-56% split between PV generators on feeders one and two respectively.

Similar to previous tables, it was found that due to harmonic cancellation, higher harmonic orders on feeder one can be found to be at a lower magnitude than Table 4.4.1.1. Some harmonic currents from the 41$^{st}$ harmonic onwards and specific voltage harmonics from the 14$^{th}$ harmonic onwards are lower than those found in Table 4.4.1.1. However, lower harmonic orders on feeder one such as the 3$^{rd}$, 5$^{th}$ and 7$^{th}$ were found to be significantly higher under these conditions. This is not unexpected, since phase shift between harmonic sources will be more significant at higher harmonic orders and less significant at lower harmonic orders.

During a three-phase fault, fed by red, as seen in Figures 4.4.3.3(A-C), the THDv increased further at the start, middle and end of feeder one on the red phase. Similar to Figures 4.4.1.3(A-C) and 4.4.2.3(A-C), the THDv stayed relatively constant along the length of feeder one on the yellow and blue phases as the current travels back towards the transformer. The maximum THDv recorded on feeder one is 4.87% for the harmonic profile from Table 3.3.1.1, 3.59% for the harmonic profile from Table 3.3.1.4 and 5.11% for the harmonic profile from Table 3.3.1.7. The highest THDv was measured on the blue phase supply terminal at the middle of the EDN.

By comparing the results in Table 4.4.3.3 to the results seen in Tables 4.4.3.2, under the three-phase fault condition, the voltage harmonic levels which have been exceeded under ER G5/5 on feeder one have either increase or stayed constant.

THDv (%) at Various Terminals on Feeder One During a Three-Phase Fault on Feeder One and a Three-Phase Fault on Feeder Two, Compared to the Results of Figures 4.4.1.1 (A-C).

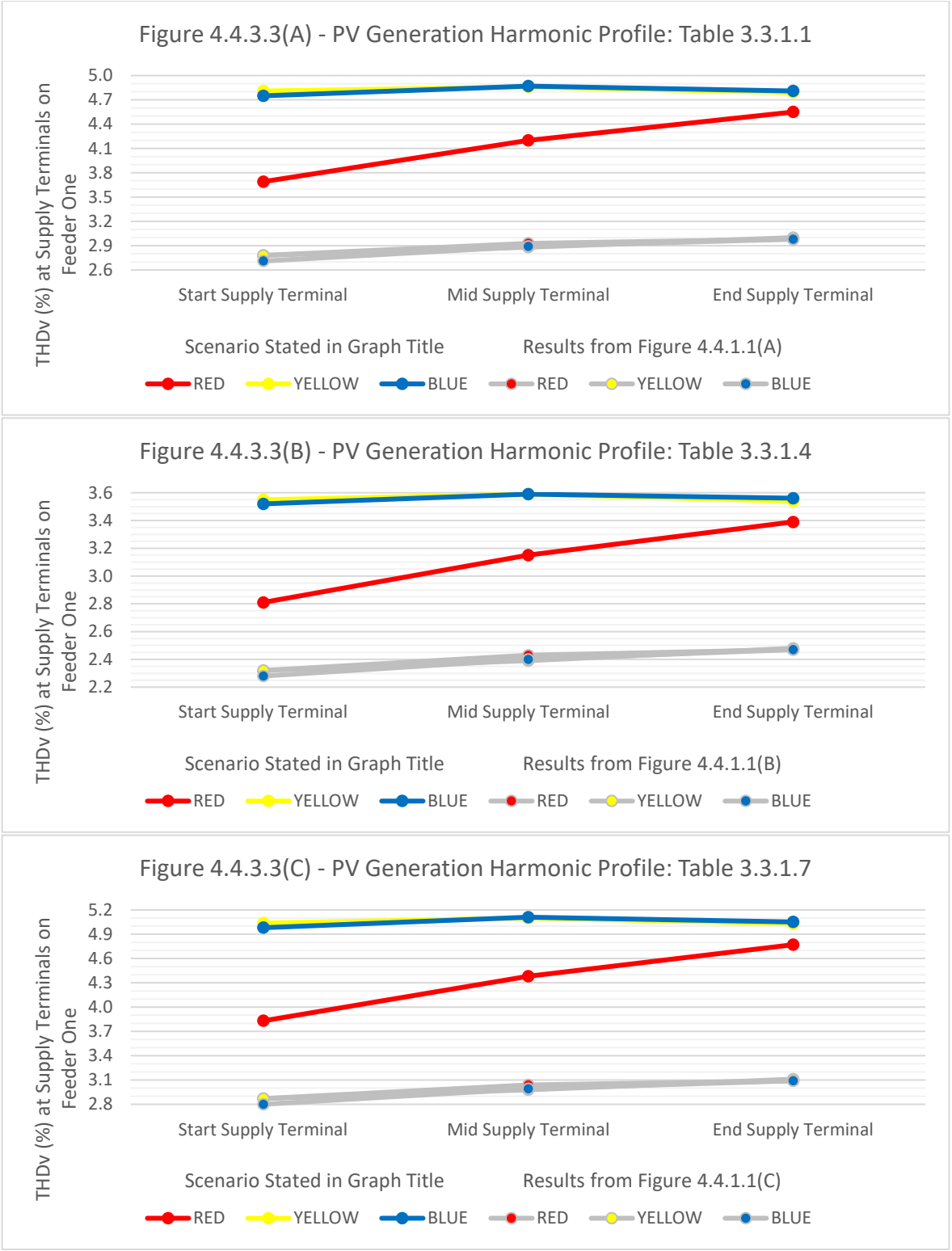


**Figure 4.4.3.3: Graphical representation of the THDv measured on each phase at supply terminals at the start, middle and end of feeder one during a three-phase fault on feeder one at 86.4% EVC penetration, 98.4% PV generation penetration and PV generation harmonic profile stated whilst a three-phase fault is present on feeder two, compared to normal running arrangements on feeders one and two (Figures 4.4.1.1 (A-C)).**

**Table 4.4.3.3: Table of harmonics on feeder one during a three-phase fault on feeder one at 86.4% EVC penetration and 98.4% PV generation penetration against the limits set out in ER G5/5 for the PV generation harmonic profile stated whilst a three-phase fault is present on feeder two (Energy Networks Association, 2020).**

| Harmonic Number | Worst Case Voltage Harmonic Magnitude at Supply Terminals (%) | | | Worst Case Voltage Harmonic Magnitude at Transformer (%) | | | ER G5/5 Limits (%) | Worst Case Phase Current Harmonic Magnitude at Transformer (A) | | | Neutral Harmonic Current Magnitude at Transformer (A) | | |
|---|---|---|---|---|---|---|---|---|---|---|---|---|---|
| | PV Generation Harmonic Profile from Table 3.3.1.- | | | PV Generation Harmonic Profile from Table 3.3.1.- | | | | PV Generation Harmonic Profile from Table 3.3.1.- | | | PV Generation Harmonic Profile from Table 3.3.1.- | | |
| | .1 | .4 | .7 | .1 | .4 | .7 | | .1 | .4 | .7 | .1 | .4 | .7 |
| 2nd | 0.25 | 0.25 | 0.25 | 0.15 | 0.15 | 0.15 | 1.6 | 7.22 | 7.22 | 7.22 | 7.22 | 7.22 | 7.22 |
| 3rd | 2.37 | 1.78 | 2.83 | 1.64 | 1.30 | 1.91 | 4.0 | 48.43 | 33.70 | 60.28 | 48.43 | 33.70 | 60.28 |
| 4th | 0.16 | 0.02 | 0.05 | 0.10 | 0.02 | 0.04 | 1.0 | 2.87 | 0.25 | 0.76 | 2.87 | 0.25 | 0.76 |
| 5th | 2.22 | 1.44 | 1.85 | 1.59 | 1.11 | 1.36 | 4.0 | 30.22 | 17.80 | 24.28 | 30.22 | 17.80 | 24.28 |
| 6th | 0.07 | 0.07 | 0.07 | 0.05 | 0.05 | 0.05 | 0.5 | 0.71 | 0.71 | 0.71 | 0.71 | 0.71 | 0.71 |
| 7th | 1.86 | 1.31 | 1.81 | 1.48 | 1.14 | 1.45 | 4.0 | 17.25 | 11.97 | 16.73 | 17.25 | 11.97 | 16.73 |
| 8th | 0.06 | 0.06 | 0.06 | 0.04 | 0.05 | 0.05 | 0.4 | 0.60 | 0.60 | 0.60 | 0.60 | 0.60 | 0.60 |
| 9th | 1.35 | 0.91 | 1.41 | 0.93 | 0.64 | 0.96 | 1.2 | 11.86 | 7.69 | 12.39 | 11.86 | 7.69 | 12.39 |
| 10th | 0.07 | 0.07 | 0.07 | 0.06 | 0.06 | 0.06 | 0.4 | 0.56 | 0.56 | 0.56 | 0.56 | 0.56 | 0.56 |
| 11th | 1.17 | 0.87 | 1.29 | 0.91 | 0.72 | 0.99 | 3.0 | 8.00 | 6.12 | 8.81 | 8.00 | 6.12 | 8.81 |
| 12th | 0.08 | 0.08 | 0.08 | 0.06 | 0.06 | 0.06 | 0.2 | 0.50 | 0.50 | 0.50 | 0.50 | 0.50 | 0.50 |
| 13th | 1.48 | 0.98 | 1.48 | 1.07 | 0.75 | 1.07 | 2.5 | 8.90 | 5.87 | 8.90 | 8.90 | 5.87 | 8.90 |
| 14th | 0.01 | 0.01 | 0.01 | 0.02 | 0.02 | 0.02 | 0.2 | 0.20 | 0.20 | 0.20 | 0.20 | 0.20 | 0.20 |
| 15th | 0.90 | 0.64 | 1.03 | 0.62 | 0.45 | 0.70 | 0.5 | 4.95 | 3.48 | 5.69 | 4.95 | 3.48 | 5.69 |
| 16th | 0.17 | 0.17 | 0.17 | 0.12 | 0.12 | 0.12 | 0.2 | 0.89 | 0.89 | 0.89 | 0.89 | 0.89 | 0.89 |
| 17th | 0.83 | 0.70 | 0.90 | 0.56 | 0.47 | 0.60 | 1.6 | 4.13 | 3.45 | 4.46 | 4.13 | 3.45 | 4.46 |
| 18th | 0.17 | 0.17 | 0.17 | 0.12 | 0.12 | 0.12 | 0.2 | 0.80 | 0.80 | 0.80 | 0.80 | 0.80 | 0.80 |
| 19th | 0.72 | 0.58 | 0.92 | 0.49 | 0.40 | 0.63 | 1.5 | 3.17 | 2.56 | 4.08 | 3.17 | 2.56 | 4.08 |
| 20th | 0.07 | 0.07 | 0.07 | 0.05 | 0.05 | 0.05 | 0.2 | 0.32 | 0.32 | 0.32 | 0.32 | 0.32 | 0.32 |
| 21st | 0.58 | 0.38 | 0.72 | 0.39 | 0.26 | 0.48 | 0.2 | 2.36 | 1.51 | 2.92 | 2.36 | 1.51 | 2.92 |
| 22nd | 0.01 | 0.01 | 0.01 | 0.01 | 0.01 | 0.01 | 0.2 | 0.09 | 0.09 | 0.09 | 0.09 | 0.09 | 0.09 |
| 23rd | 0.55 | 0.61 | 0.75 | 0.37 | 0.41 | 0.50 | 1.2 | 2.03 | 2.29 | 2.81 | 2.03 | 2.29 | 2.81 |
| 24th | 0.07 | 0.07 | 0.07 | 0.05 | 0.05 | 0.05 | 0.2 | 0.26 | 0.26 | 0.26 | 0.26 | 0.26 | 0.26 |
| 25th | 0.47 | 0.40 | 0.54 | 0.32 | 0.27 | 0.36 | 1.0 | 1.60 | 1.36 | 1.85 | 1.60 | 1.36 | 1.85 |
| 26th | 0.00 | 0.00 | 0.00 | 0.01 | 0.01 | 0.00 | 0.2 | 0.04 | 0.04 | 0.04 | 0.04 | 0.04 | 0.04 |
| 27th | 0.45 | 0.45 | 0.45 | 0.30 | 0.30 | 0.30 | 0.2 | 1.43 | 1.43 | 1.43 | 1.43 | 1.43 | 1.43 |
| 28th | 0.07 | 0.07 | 0.07 | 0.05 | 0.05 | 0.05 | 0.2 | 0.23 | 0.23 | 0.23 | 0.23 | 0.23 | 0.23 |
| 29th | 0.52 | 0.52 | 0.52 | 0.35 | 0.35 | 0.35 | 0.86 | 1.55 | 1.55 | 1.55 | 1.55 | 1.55 | 1.55 |
| 30th | 0.07 | 0.07 | 0.07 | 0.05 | 0.05 | 0.05 | 0.2 | 0.21 | 0.21 | 0.21 | 0.21 | 0.21 | 0.21 |
| 31st | 0.52 | 0.52 | 0.52 | 0.35 | 0.35 | 0.35 | 0.81 | 1.46 | 1.46 | 1.46 | 1.46 | 1.46 | 1.46 |
| 32nd | 0.07 | 0.07 | 0.07 | 0.05 | 0.05 | 0.05 | 0.2 | 0.20 | 0.20 | 0.20 | 0.20 | 0.20 | 0.20 |
| 33rd | 0.40 | 0.40 | 0.40 | 0.27 | 0.27 | 0.27 | 0.2 | 1.06 | 1.06 | 1.06 | 1.06 | 1.06 | 1.06 |
| 34th | 0.07 | 0.07 | 0.07 | 0.05 | 0.05 | 0.05 | 0.2 | 0.19 | 0.19 | 0.19 | 0.19 | 0.19 | 0.19 |
| 35th | 0.33 | 0.33 | 0.33 | 0.22 | 0.22 | 0.22 | 0.71 | 0.82 | 0.82 | 0.82 | 0.82 | 0.82 | 0.82 |
| 36th | 0.07 | 0.07 | 0.07 | 0.05 | 0.05 | 0.05 | 0.2 | 0.18 | 0.18 | 0.18 | 0.18 | 0.18 | 0.18 |
| 37th | 0.28 | 0.28 | 0.28 | 0.19 | 0.19 | 0.19 | 0.68 | 0.66 | 0.66 | 0.66 | 0.66 | 0.66 | 0.66 |
| 38th | 0.00 | 0.00 | 0.00 | 0.00 | 0.00 | 0.00 | 0.2 | 0.00 | 0.00 | 0.00 | 0.00 | 0.01 | 0.00 |
| 39th | 0.28 | 0.28 | 0.28 | 0.19 | 0.19 | 0.19 | 0.2 | 0.63 | 0.63 | 0.63 | 0.63 | 0.63 | 0.63 |
| 40th | 0.07 | 0.07 | 0.07 | 0.05 | 0.05 | 0.05 | 0.2 | 0.16 | 0.16 | 0.16 | 0.16 | 0.16 | 0.16 |
| 41st | 0.15 | 0.15 | 0.15 | 0.11 | 0.11 | 0.11 | 0.61 | 0.33 | 0.33 | 0.33 | 0.33 | 0.33 | 0.33 |
| 43rd | 0.15 | 0.15 | 0.15 | 0.11 | 0.11 | 0.11 | 0.58 | 0.32 | 0.32 | 0.32 | 0.32 | 0.32 | 0.32 |
| 45th | 0.16 | 0.15 | 0.16 | 0.11 | 0.11 | 0.11 | 0.20 | 0.30 | 0.30 | 0.30 | 0.30 | 0.30 | 0.30 |
| 47th | 0.10 | 0.10 | 0.10 | 0.07 | 0.07 | 0.07 | 0.53 | 0.19 | 0.19 | 0.19 | 0.19 | 0.19 | 0.19 |
| 49th | 0.10 | 0.10 | 0.10 | 0.07 | 0.07 | 0.07 | 0.51 | 0.19 | 0.19 | 0.19 | 0.19 | 0.19 | 0.19 |
| Harmonics higher than the limits set by ER G5/5 | | | | | | | Harmonics on the boundary of the limits set by ER G5/5 | | | | | | |
| Harmonics lower than the result from Table 4.4.1.1 | | | | | | | Voltage on Neutral: 8.125V | | | | | | |
| EVCs & PVs on Feeder 1: 48 & 54 respectively. EVCs & PVs on Feeder 2: 60 & 69 respectively. | | | | | | | | | | | | | |

Similar to the two-phase fault scenario, harmonic magnitudes which are lower on feeder one than Table 4.4.1.1 have been highlighted with red text in Table 4.4.3.3. Harmonic current from the 38$^{th}$ harmonic onwards and specific voltage harmonics from the 14$^{th}$ harmonic onwards are lower than those found in Table 4.4.1.1. Therefore, the degree of harmonic cancellation at higher harmonic magnitudes has increased when compared to Table 4.4.1.1.

The tipping points for this scenario with a three-phase fault on feeder one to remain compliant under the different PV generation harmonic profiles with ER G5/5 on feeder one was identified. It was found that for Table 3.3.1.1 the maximum penetration was 9.6% (twelve EVCs and PV generators), for Table 3.3.1.4 the maximum penetration was 12.0% (fifteen EVCs and PV generators) and for Table 3.3.1.7 was 7.2% (nine EVCs and PV generators). These were evenly distributed across three phases on feeders one and two as close as is achievable to a 44-56% split between PV generators on feeders one and two respectively.

In addition, it was found that the neutral voltage present at the end of feeder one increased to 8.125V under three-phase fault conditions on feeder one shown in Table 4.4.3.3 from 5.467V under two-phase conditions on feeder one in Table 4.4.3.2 and 1.960V under normal arrangements on feeder one shown in Table 4.4.3.1. Based on Table 3.2.7.4, the voltages caused by a two or three-phase fault could lead to residents perceiving shocks off exposed bonded metal work, potentially leading to complaints. However, it does not seem high enough to cause ventricular fibrillation or respiratory tetanus.

## 4.4.4 – Maximum Penetration and Overall Results

To summarise the results from Sections 4.4.1-3, Figures 4.4.4.1-3 have been produced. The results of maximum THDv measured at customer terminals on feeder one with a 3.28kVA EVC penetration of 86.4% and a 2kW PV generation penetration of 98.4%, in addition to the maximum EVC and PV generation penetration to remain compliant with ER G5/5 under different running arrangements can be seen in Figures 4.4.4.1-3. The blue/grey lines and left-hand y-axis refers to the maximum THDv. The orange/yellow/green lines and right-hand y-axis refers to the maximum EVC and PV generation penetration. It should be noted that although trends may be similar across all networks, these results are specific to the case study network and harmonic profiles used.

For Figure 4.4.4.1, under normal conditions on feeder two, the maximum THDv increases from 3.00% to 4.48% on feeder one (an increase of 1.48%) when comparing normal conditions and a three-phase fault on feeder one. For a three-phase fault on feeder two, the maximum THDv increases from 3.45% to 4.87% on feeder one (an increase of 1.42%) when comparing normal conditions and a three-phase fault on feeder one. For faults on feeder two, the increase in THDv stays consistent, but is stepped up. This is very comparable to the results of the EVC and PV generation penetrations shown in Figures 4.2.4.1-3 and 4.3.4.1-3.

It can be seen from Figure 4.4.4.2 that for normal conditions on feeder two, the maximum THDv increases from 2.48% to 3.38% on feeder one (an increase of 0.90%) when comparing normal conditions and a three-phase fault on feeder one. For a three-phase fault on feeder two, the maximum THDv increases from 2.70% to 3.59% on feeder one (an increase of 0.89%) when comparing normal conditions and a three-phase fault on feeder one.

For Figure 4.4.4.3, under normal conditions on feeder two, the maximum THDv increases from 3.11% to 4.70% on feeder one (an increase of 1.59%) when comparing normal conditions and a three-phase fault on feeder one. For a three-phase fault on feeder two, the maximum THDv increases from 3.58% to 5.11% on feeder one (an increase of 1.53%) when comparing normal conditions and a three-phase fault on feeder one.

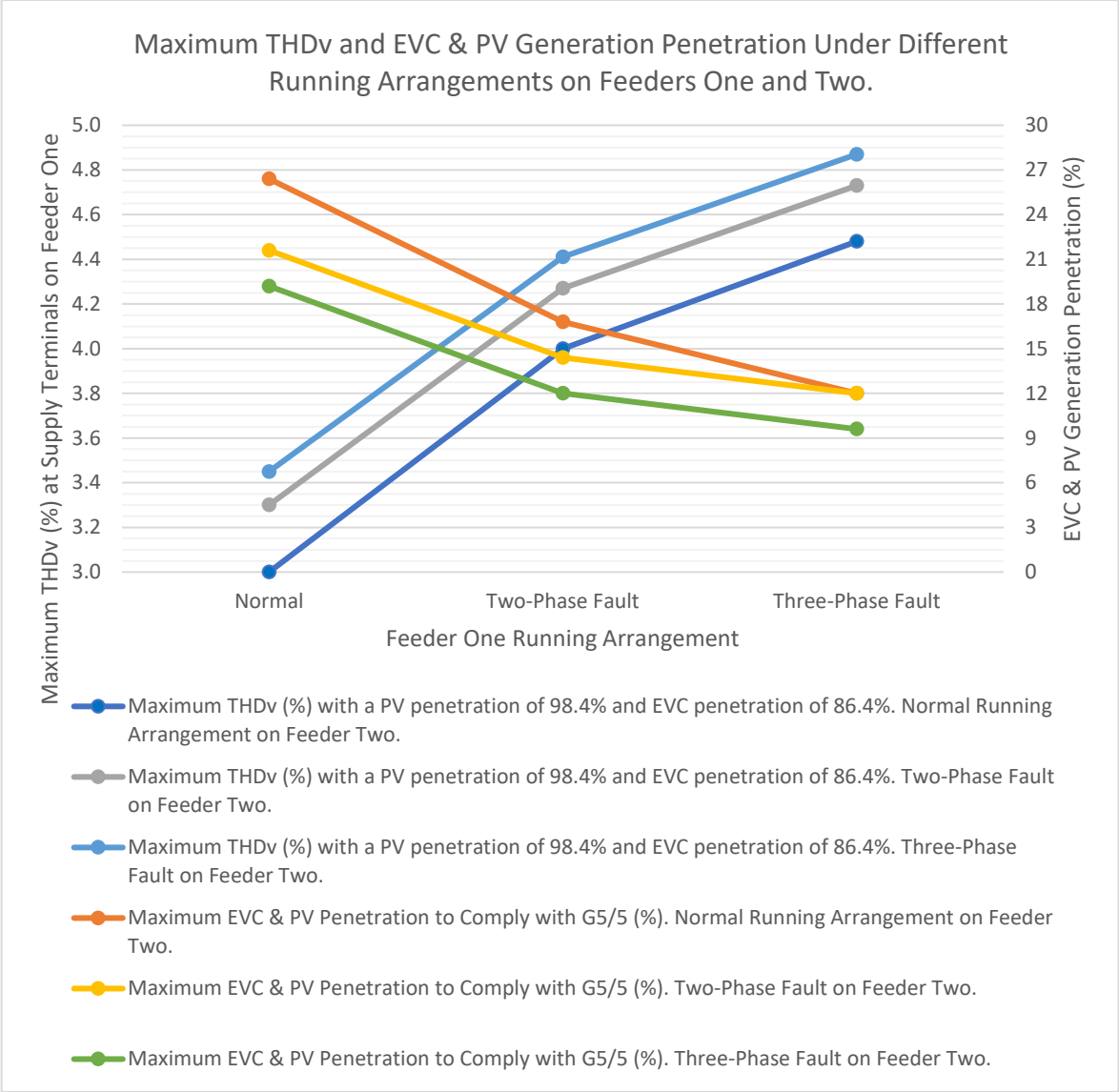


**Figure 4.4.4.1: Maximum THDv measured at customer terminals on feeder one with an EVC and PV generation penetration of 86.4% and 98.4% respectively and maximum EVC and PV generation penetration to remain compliant with ER G5/5 under different running arrangements on feeders one and two using the PV generation harmonic profile from Table 3.3.1.1.**

From the results of Figures 4.4.4.1-3, it can be seen that the overall effect of faults on feeder one reduces when a fault is present on feeder two. This is due to increased levels of current harmonic cancellation. As the THDv level increases, unless the voltage harmonics generated by the current harmonics is perfectly in phase with the existing voltage harmonics, the impact of each subsequent additional current harmonic on the voltage harmonics will be reduced.

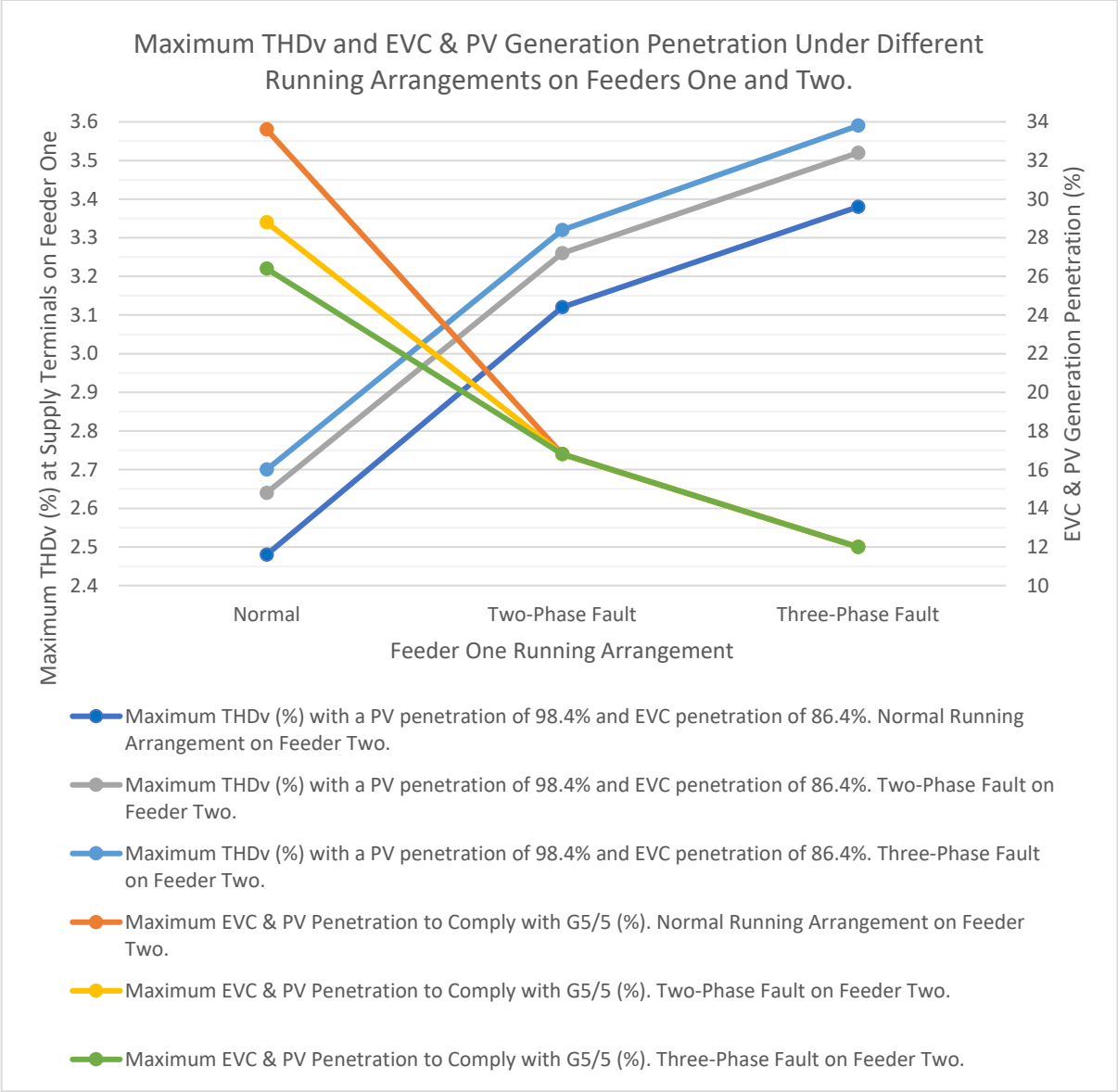


**Figure 4.4.4.2: Maximum THDv measured at customer terminals on feeder one with an EVC and PV generation penetration of 86.4% and 98.4% respectively and maximum EVC and PV generation penetration to remain compliant with ER G5/5 under different running arrangements on feeders one and two using the PV generation harmonic profile from Table 3.3.1.4.**

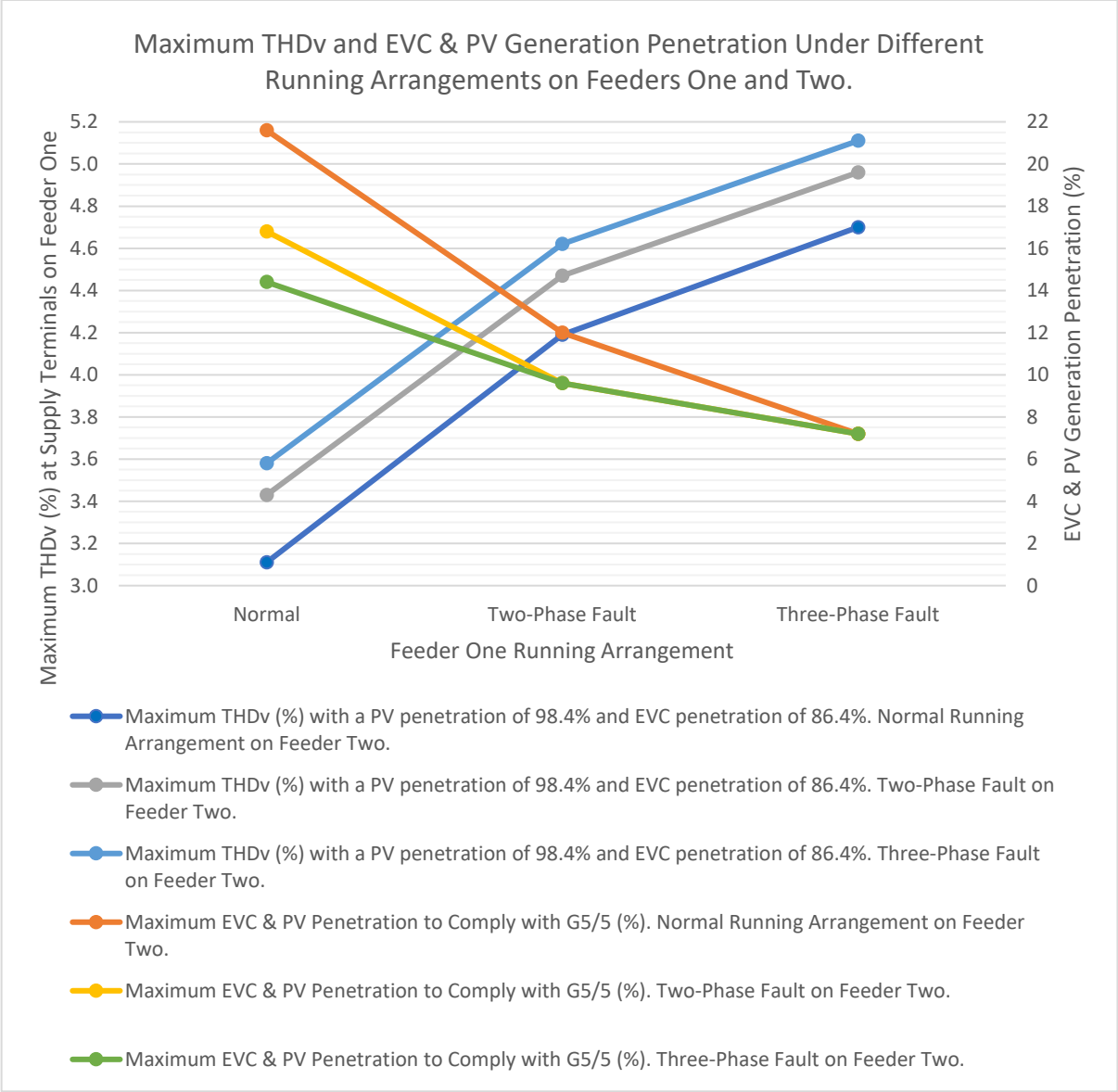


**Figure 4.4.4.3: Maximum THDv measured at customer terminals on feeder one with an EVC and PV generation penetration of 86.4% and 98.4% respectively and maximum EVC and PV generation penetration to remain compliant with ER G5/5 under different running arrangements on feeders one and two using the PV generation harmonic profile from Table 3.3.1.7.**

More important is the maximum EVC and PV generation penetration permissible to ensure compliance with ER G5/5 on feeder one. Figure 4.4.4.1 shows that for normal conditions on feeder two, the maximum EVC and PV generation penetration decreases from 26.4% to 12.0% on feeder one (a decrease of 14.4%) when comparing normal conditions and a three-phase fault on feeder one. For a three-phase fault on feeder two, the maximum PV generation penetration decreases from 19.2% to 9.6% on feeder one (a decrease of 9.6%) when comparing normal conditions and a three-phase fault on feeder one. This is much lower than the results of the EVC and PV generation penetrations shown in Figure 4.2.4.1 and 4.3.4.1. This is to be expected since this study contains both EVC and PV generation, which contribute to increasing voltage harmonics, therefore lowering the maximum numbers of EVCs and PV generators which can be connected to the circuit.

The same applies to Figures 4.4.4.2-3. For normal conditions on feeder two, the maximum EVC and PV generation penetration decreases from 33.6% to 12.0% on feeder one (a decrease of 21.6%) for Figure 4.4.4.2, and 21.6% to 7.2% on feeder one (a decrease of 14.4%) for Figure 4.4.4.3 when comparing normal conditions and a three-phase fault on feeder one. For a three-phase fault on feeder two, the maximum PV generation penetration decreases from 26.4% to 12.0% on feeder one (a decrease of 14.4%) for Figure 4.4.4.2, and 14.4% to 7.2% on feeder one (a decrease of 7.2%) for Figure 4.4.4.3 when comparing normal conditions and a three-phase fault on feeder one.

The reason for differences in maximum penetration is due to the limiting harmonics. These are the 21$^{st}$ harmonic in the case of the harmonic profiles from Tables 3.3.1.1 and 3.3.1.7 and the 27$^{th}$ harmonic in the case of the harmonic profile from Table 3.3.1.4. The 21$^{st}$ and 27$^{th}$ harmonics are limited to 0.2% as defined by ER G5/5. Table 4.4.4.1 (below) shows the maximum measured voltage harmonic profile for the penetration boundary for normal conditions on feeder one and a three-phase fault on feeder two. This shows that the limiting harmonics are reached as mentioned.

**Table 4.4.4.1: Maximum measured voltage harmonics on feeder one for normal running arrangements on feeder one at the EVC and PV generation penetration boundary against the limits set out in ER G5/5 for the PV generation harmonic profile stated and EVC and PV generation penetration stated whilst a three-phase fault is present on feeder two (Energy Networks Association, 2020).**

| Harmonic Number | Harmonic Magnitude (%) | Harmonic Magnitude (%) | Harmonic Magnitude (%) | G5/5 Limits (%) |
|---|---|---|---|---|
| PV Generation Harmonic Profile from: | Table 3.3.1.1 | Table 3.3.1.4 | Table 3.3.1.7 | |
| EVC and PV Generation Penetration: | 19.2% | 26.4% | 14.4% | |
| 2nd | 0.06 | 0.07 | 0.06 | 1.6 |
| 3rd | 0.78 | 0.78 | 0.77 | 4.0 |
| 4th | 0.04 | 0.02 | 0.02 | 1.0 |
| 5th | 0.76 | 0.72 | 0.67 | 4.0 |
| 6th | 0.04 | 0.04 | 0.03 | 0.5 |
| 7th | 1.02 | 0.98 | 0.98 | 4.0 |
| 8th | 0.03 | 0.03 | 0.03 | 0.4 |
| 9th | 0.39 | 0.37 | 0.35 | 1.2 |
| 10th | 0.04 | 0.04 | 0.04 | 0.4 |
| 11th | 0.67 | 0.64 | 0.66 | 3.0 |
| 12th | 0.04 | 0.04 | 0.04 | 0.2 |
| 13th | 0.67 | 0.61 | 0.62 | 2.5 |
| 14th | 0.03 | 0.03 | 0.03 | 0.2 |
| 15th | 0.31 | 0.29 | 0.29 | 0.5 |
| 16th | 0.07 | 0.08 | 0.06 | 0.2 |
| 17th | 0.27 | 0.29 | 0.24 | 1.6 |
| 18th | 0.06 | 0.07 | 0.05 | 0.2 |
| 19th | 0.27 | 0.28 | 0.28 | 1.5 |
| 20th | 0.03 | 0.04 | 0.03 | 0.2 |
| 21st | 0.20 | 0.18 | 0.20 | 0.2 |
| 22nd | 0.02 | 0.01 | 0.02 | 0.2 |
| 23rd | 0.19 | 0.26 | 0.21 | 1.2 |
| 24th | 0.03 | 0.03 | 0.02 | 0.2 |
| 25th | 0.17 | 0.18 | 0.16 | 1.0 |
| 26th | 0.01 | 0.01 | 0.01 | 0.2 |
| 27th | 0.17 | 0.20 | 0.14 | 0.2 |
| 28th | 0.03 | 0.03 | 0.03 | 0.2 |
| 29th | 0.19 | 0.23 | 0.16 | 0.86 |
| 30th | 0.02 | 0.03 | 0.02 | 0.2 |
| 31st | 0.20 | 0.24 | 0.17 | 0.81 |
| 32nd | 0.02 | 0.03 | 0.02 | 0.2 |
| 33rd | 0.15 | 0.19 | 0.13 | 0.2 |
| 34th | 0.02 | 0.03 | 0.02 | 0.2 |
| 35th | 0.13 | 0.16 | 0.11 | 0.71 |
| 36th | 0.02 | 0.03 | 0.02 | 0.2 |
| 37th | 0.12 | 0.14 | 0.10 | 0.68 |
| 38th | 0.00 | 0.00 | 0.00 | 0.2 |
| 39th | 0.12 | 0.14 | 0.10 | 0.2 |
| 40th | 0.02 | 0.03 | 0.02 | 0.2 |
| 41st | 0.07 | 0.08 | 0.06 | 0.61 |
| 43rd | 0.07 | 0.08 | 0.06 | 0.58 |
| 45th | 0.07 | 0.08 | 0.06 | 0.2 |
| 47th | 0.05 | 0.06 | 0.04 | 0.53 |
| 49th | 0.05 | 0.06 | 0.04 | 0.51 |
| Harmonics on the boundary of the limits set by ER G5/5 | | | | |

Based on the results of Sections 4.4.1-3, the limiting voltage harmonics, (21st and 27th), increase during phase-to-phase conditions on both feeder one and feeder two with the exception of Table 4.4.3.1. Tables 4.4.4.2-3 summarise the change in these limiting harmonics under the conditions covered in Sections 4.4.1-3. It can clearly be seen that a fault on feeder one has a much greater effect on the 21st and 27th voltage harmonic on feeder one, than a fault on feeder two, which would be expected. Additionally, as faults compound, for example, a two-phase fault to a three-phase fault on feeder one, the percentage increase in the voltage harmonic magnitude is not as significant. Further to this, Sections 4.2.4 and 4.3.4, show that as a two-phase fault on feeder one, compounds with a two-phase fault on feeder two, the percentage increase in the 21st and 27th voltage harmonic magnitude drops. There is not significant correlation to show this in Tables 4.4.4.2-3. Further to this, unlike Sections 4.2.4 and 4.3.4, there is negligible change in the 21st and 27th harmonic when a two-phase or three-phase fault occurs on feeder two. It is likely this occurs for the same reason that harmonic magnitudes can reduce, since different harmonic, generation, and load profiles have been combined. This could be considered to be closer to an average LV EDN, which contains a range, rather than either just EVCs or just PV generation as seen in Sections 4.2 or 4.3.

**Table 4.4.4.2: Increase in 21st and 27th voltage harmonic magnitude measured on feeder one between normal and phase-to-phase fault arrangements on feeder one for varying network arrangements on feeder two.**

| Increase in 21st and 27th voltage harmonic magnitude on feeder one under specified conditions measured at the point of highest THDv. | | Feeder One | |
|---|---|---|---|
| | | Normal Arrangements to Two-Phase Fault | Normal Arrangements to Three-Phase Fault |
| Feeder Two | Normal Arrangements | 29-34% | 32-42% |
| | Two-Phase Fault Arrangements | 26-31% | 32-38% |
| | Three-Phase Fault Arrangements | 29-31% | 36-38% |

**Table 4.4.4.3: Increase in 21st and 27th voltage harmonic magnitude measured on feeder one between normal and phase-to-phase fault arrangements on feeder two for varying network arrangements on feeder one.**

| Increase in 21st and 27th voltage harmonic magnitude on feeder one under specified conditions measured at the point of highest THDv. | | Feeder Two | |
|---|---|---|---|
| | | Normal Arrangements to Two-Phase Fault | Normal Arrangements to Three-Phase Fault |
| Feeder One | Normal Arrangements | 0-5% | -3%-4% |
| | Two-Phase Fault Arrangements | -2%-1% | -2%-0% |
| | Three-Phase Fault Arrangements | 0-1% | 0%-1% |

This data could be used by DNOs to indicate the maximum allowable numbers of combined EVCs and PV generation of equal magnitudes which can be connected to an LV EDN under different conditions. Data showing this relationship has not been published previously. This provides niche and novel data which will aid with network planning and determine the actions taken by a DNO following a fault in order to remain compliant with ER G5/5.

Similar to the results of Sections 4.2-3, neutral voltage on feeder one rose as faults were added to the network, a three-phase fault having a higher impact than a two-phase fault. Despite this, the neutral voltage did not get high enough to cause ventricular fibrillation or respiratory tetanus as per Table 3.2.7.4. However, any fault on feeder one produced a voltage high enough for residents to perceive shocks at the end terminals of feeder one. Neutral voltages should be monitored by a DNO following a two-phase or three-phase fault. Should the voltages exceed 2.70V, remedial action should be taken to reduce the voltage. This should be the repair of the fault to rebalance the network.

## 4.4.5 – Discussion, Conclusions and Asset Lifespan

As mentioned in Section 4.2.7, both open-circuit faults and complex faults have not been included due to them not having as high an impact on voltage harmonics as phase-to-phase faults, without first exceeding either fuse or cable ratings.

Similar to the previous two sections, the impact of phase-to-phase faults is significant, both on THDv levels and maximum combined EVC and PV generation penetration levels. However, a differentiating factor between this scenario and Sections 4.2.4 and 4.3.4, shown in Tables 4.4.4.1-2 is that a two-phase or three-phase fault on feeder two, at least at an EVC and PV generation penetration of 86.4% and 98.4% respectively, has little positive or negative impact on the limiting harmonic magnitudes ($21^{st}$ and $27^{th}$) measured on feeder one. A similar scenario was being seen within Section 4.2.4, when combining a phase-to-phase fault on feeder two with an existing phase-to-phase fault on feeder one.

Therefore, this situation may be due to several factors or a combination of them. Firstly, this could be due to harmonic saturation, due to the number of harmonic sources connected to the LV EDN, where additional harmonic load does not increase voltage harmonics significantly. This effect can be seen in Figure 3.2.4.1, where the relationship between THDv and EVC penetration loses its linearity at higher penetration levels.

Secondly, the overall impact of faults across both Tables 4.4.4.1-2, is lower than Sections 4.2.4 and 4.3.4. Additionally, it can be seen in Tables 4.4.1.2-3, 4.4.2.1-3, 4.4.3.1-3 that a number of specific harmonics, generally at higher harmonic orders, are lower than Table 4.4.1.1 which shows the harmonic levels on feeder one for normal running arrangements on both feeders. Therefore, the combination of EVCs and PV generation on the LV EDN results in additional cancellation at higher harmonic orders when compared to Sections 4.2 and 4.3. The harmonic source models, both the EVCs and PV generation assume that the harmonics are in phase to determine the maximum harmonic order magnitudes. Despite this, higher order harmonics, and therefore higher frequency waveforms are affected more by network reactance, therefore leading to higher levels of phase shift and cancellation.

Similar to Section 3.4.5, it is important to ascertain whether the harmonic currents are sufficient in magnitude to lead to a noticeable loss of transformer or conductor life. The same assumptions and values such as reference hottest-spot temperature, ambient temperature and conductor impedance will be made as per Sections 3.2.8, 4.2.7 and 4.3.5 to carry out these calculations.

Table 4.4.5.1 displays the increase in transformer hot-spot temperature and loss of transformer life. Table 4.4.5.2 displays the increase in cable temperature and loss of cable life. Values are calculated using Equations 3.2.8.1-19 and data from Tables 4.4.1.1-3, 4.4.2.1-3 and 4.4.3.1-3. Equations have been validated as per Section 3.2.8. By comparing the data shown in Tables 4.4.1.1-3, 4.4.2.1-3, and 4.4.3.1-3 it can be clearly seen that, as the THDi of the PV harmonic profile increases, so does the impact on lower order voltage and current harmonics. As mentioned, reductions in higher order harmonics could be due to cancellation. This impact can be seen to translate into Tables 4.4.5.1-2. The higher the THDi of the PV harmonic profile, the higher the impact on both transformer and cable temperature and the greater the asset life loss. This is to be expected.

Considering Tables 4.4.5.1-2, the difference between each step can be extrapolated, shown in Tables 4.4.5.3-6. Tables 4.4.5.3-4 show that the effect of a fault both on feeders one and two are pretty much stable; for example, a three-phase fault on feeder two results in a temperature increase of 0.2077-0.2199ºC when compared to a two-phase fault on feeder two, regardless of the EDN arrangement on feeder one. This is contrary to Tables 4.4.5.5-6 which shows that the temperature gain increases as faults on feeders one and two compound, similar to Tables 4.3.5.3-6. Tables 4.4.5.3-6 seem to follow the same pattern as Tables 4.2.7.3-6, where the transformer temperature increases and asset life lost is constant, whereas cable temperature and asset life lost increases as faults compound. This is caused by the harmonic interactions between the harmonic sources and the harmonic profiles of those sources and how they interact with the asset life calculations shown in Equations 3.2.8.1-19.

**Table 4.4.5.1: Transformer hot-spot temperature increase and loss of transformer life assuming an existing hot-spot temperature of 110ºC for various fault arrangements on feeder one and two for the PV generation harmonic profile stated.**

| Increase in transformer hot-spot temperature (ºC) and loss of transformer life under specified conditions (Years). | | | Feeder One | | |
|---|---|---|---|---|---|
| | | | Normal Arrangements | Two-Phase Fault Arrangements | Three-Phase Fault Arrangements |
| PV Generation Harmonic Profile from Table 3.3.1.1 | Feeder Two | Normal Arrangements | 1.2074ºC<br>4.6323 Years | 1.4270ºC<br>5.4122 Years | 1.5790ºC<br>5.9416 Years |
| | | Two-Phase Fault Arrangements | 1.5186ºC<br>5.7321 Years | 1.7702ºC<br>6.5953 Years | 1.9343ºC<br>7.1459 Years |
| | | Three-Phase Fault Arrangements | 1.7313ºC<br>6.4633 Years | 1.9901ºC<br>7.3310 Years | 2.1420ºC<br>7.8292 Years |
| PV Generation Harmonic Profile from Table 3.3.1.4 | Feeder Two | Normal Arrangements | 0.9087ºC<br>3.5412 Years | 1.0013ºC<br>3.8833 Years | 1.0610ºC<br>4.1020 Years |
| | | Two-Phase Fault Arrangements | 1.0567ºC<br>4.0862 Years | 1.1737ºC<br>4.5108 Years | 1.2439ºC<br>4.7632 Years |
| | | Three-Phase Fault Arrangements | 1.1455ºC<br>4.4090 Years | 1.2717ºC<br>4.8624 Years | 1.3340ºC<br>5.0842 Years |
| PV Generation Harmonic Profile from Table 3.3.1.7 | Feeder Two | Normal Arrangements | 1.3535ºC<br>5.1532 Years | 1.1767ºC<br>6.0075 Years | 1.7655ºC<br>6.5793 Years |
| | | Two-Phase Fault Arrangements | 1.7065ºC<br>6.3788 Years | 1.9859ºC<br>7.3171 Years | 2.1665ºC<br>7.9087 Years |
| | | Three-Phase Fault Arrangements | 1.9400ºC<br>7.1647 Years | 2.2253ºC<br>8.0990 Years | 2.3973ºC<br>8.6485 Years |

**Table 4.4.5.2: Cable temperature increase and loss of cable life assuming an existing cable temperature of 90ºC for various fault arrangements on feeder one and two for the PV generation harmonic profile stated.**

| Increase in cable temperature (ºC) and loss of cable life under specified conditions (Years). | | | Feeder One | | |
|---|---|---|---|---|---|
| | | | Normal Arrangements | Two-Phase Fault Arrangements | Three-Phase Fault Arrangements |
| PV Generation Harmonic Profile from Table 3.3.1.1 | Feeder Two | Normal Arrangements | 0.1595ºC 0.9195 Years | 0.2817ºC 1.6094 Years | 0.4090ºC 2.3150 Years |
| | | Two-Phase Fault Arrangements | 0.3222ºC 1.8353 Years | 0.4967ºC 2.7926 Years | 0.6326ºC 3.5211 Years |
| | | Three-Phase Fault Arrangements | 0.4943ºC 2.7795 Years | 0.6766ºC 3.7535 Years | 0.8837ºC 4.8281 Years |
| PV Generation Harmonic Profile from Table 3.3.1.4 | Feeder Two | Normal Arrangements | 0.0758ºC 0.4399 Years | 0.1316ºC 0.7606 Years | 0.1897ºC 1.0914 Years |
| | | Two-Phase Fault Arrangements | 0.1497ºC 0.8640 Years | 0.2298ºC 1.3181 Years | 0.2914ºC 1.6638 Years |
| | | Three-Phase Fault Arrangements | 0.2277ºC 1.3066 Years | 0.3109ºC 1.7725 Years | 0.4065ºC 2.3008 Years |
| PV Generation Harmonic Profile from Table 3.3.1.7 | Feeder Two | Normal Arrangements | 0.1874ºC 1.0784 Years | 0.3332ºC 1.8964 Years | 0.4869ºC 2.7399 Years |
| | | Two-Phase Fault Arrangements | 0.3817ºC 2.1646 Years | 0.5929ºC 3.3099 Years | 0.7606ºC 4.1936 Years |
| | | Three-Phase Fault Arrangements | 0.5897ºC 3.2930 Years | 0.8139ºC 4.4697 Years | 1.0672ºC 5.7522 Years |

The values within Tables 4.4.5.3-6 have been calculated by measuring the difference in temperature and asset life between network fault arrangements within the table stated within the table title for the PV generation harmonic profile from Table 3.3.1.1. For example, for Table 4.4.5.3, the values stated within the top left box is calculated by subtracting the top left values from the top middle values within Table 4.4.5.1.

**Table 4.4.5.3: Increase in transformer hot-spot temperature and loss of transformer life between different fault scenarios on feeder one for data from Table 4.4.5.1 and PV generation harmonic profile from Table 3.3.1.1.**

| Increase in transformer hot-spot temperature (ºC) and loss of transformer life (Years) for Table 4.4.5.1 under specified conditions for the PV generation harmonic profile from Table 3.3.1.1. | | Feeder One | |
|---|---|---|---|
| | | Normal Arrangements to Two-Phase Fault | Two-Phase Fault to Three-Phase Fault |
| Feeder Two | Normal Arrangements | 0.2196ºC 0.7799 Years | 0.1520ºC 0.5294 Years |
| | Two-Phase Fault Arrangements | 0.2516ºC 0.8632 Years | 0.1641ºC 0.5506 Years |
| | Three-Phase Fault Arrangements | 0.2588ºC 0.8677 Years | 0.1519ºC 0.4982 Years |

**Table 4.4.5.4: Increase in transformer hot-spot temperature and loss of transformer life between different fault scenarios on feeder two for data from Table 4.4.5.1 and PV generation harmonic profile from Table 3.3.1.1.**

| Increase in transformer hot-spot temperature (ºC) and loss of transformer life (Years) for Table 4.4.5.1 under specified conditions for the PV generation harmonic profile from Table 3.3.1.1. | | Feeder Two | |
|---|---|---|---|
| | | Normal Arrangements to Two-Phase Fault | Two-Phase Fault to Three-Phase Fault |
| Feeder One | Normal Arrangements | 0.3112ºC<br>1.0998 Years | 0.2127ºC<br>0.7312 Years |
| | Two-Phase Fault Arrangements | 0.3432ºC<br>1.1831 Years | 0.2199ºC<br>0.7357 Years |
| | Three-Phase Fault Arrangements | 0.3553ºC<br>1.21043 Years | 0.2077ºC<br>0.6833 Years |

**Table 4.4.5.5: Increase in cable temperature and loss of cable life between different fault scenarios on feeder two for data from Table 4.4.5.2 and PV generation harmonic profile from Table 3.3.1.1.**

| Increase in cable temperature (ºC) and loss of cable life (Years) for Table 4.4.5.2 under specified conditions for the PV generation harmonic profile from Table 3.3.1.1. | | Feeder One | |
|---|---|---|---|
| | | Normal Arrangements to Two-Phase Fault | Two-Phase Fault to Three-Phase Fault |
| Feeder Two | Normal Arrangements | 0.1222ºC<br>0.6899 Years | 0.1273ºC<br>0.7056 Years |
| | Two-Phase Fault Arrangements | 0.1745ºC<br>0.9573 Years | 0.1359ºC<br>0.7285 Years |
| | Three-Phase Fault Arrangements | 0.1823ºC<br>0.9740 Years | 0.2071ºC<br>1.0746 Years |

**Table 4.4.5.6: Increase in cable temperature and loss of cable life between different fault scenarios on feeder two for data from Table 4.4.5.2 and PV generation harmonic profile from Table 3.3.1.1.**

| Increase in cable temperature (ºC) and loss of cable life (Years) for Table 4.4.5.2 under specified conditions for the PV generation harmonic profile from Table 3.3.1.1. | | Feeder Two | |
|---|---|---|---|
| | | Normal Arrangements to Two-Phase Fault | Two-Phase Fault to Three-Phase Fault |
| Feeder One | Normal Arrangements | 0.1627ºC<br>0.9158 Years | 0.1721ºC<br>0.9442 Years |
| | Two-Phase Fault Arrangements | 0.2150ºC<br>1.1832 Years | 0.1799ºC<br>0.9609 Years |
| | Three-Phase Fault Arrangements | 0.2236ºC<br>1.2061 Years | 0.2511ºC<br>1.3070 Years |

Furthermore, it should be noted that loss of transformer life is substantial across all scenarios in Table 4.4.5.1, and, for cable life when faults compound in Table 4.4.5.2. Interestingly, the maximum transformer life loss shown in Table 4.3.5.1 for the harmonic profile from Table 3.3.1.7 is 10.426 years, whereas the maximum transformer life loss from Table 4.4.5.1 is 8.6485 years. The opposite can be seen in Tables 4.3.5.2 and 4.4.5.2 which result in a maximum cable life loss of 3.7304 and 5.7522 years respectively. The reason for comparing these values is because they present the worst-case scenario, both with a three-phase fault on both feeders one and two. The reason for the difference in increase and subsequent decrease in asset life loss is due to the way in which asset life loss is calculated in Equations 3.2.8.1-19 and the harmonic profiles shown in Tables 4.3.3.3 and 4.4.3.3. The differences that can be seen between Tables 4.3.3.3 and 4.4.3.3 is that higher order harmonics are of a lower magnitude and lower order harmonics are of a higher magnitude in Table 4.4.3.3. This suggests that the differences in asset lifespan is caused by the combined number of EVCs and PV generators. These contribute to a higher magnitude of lower order harmonics and additional harmonic cancellation leading to a lower magnitude of higher order harmonics in Table 4.4.3.3. Therefore, the additional harmonic cancellation seen in Table 4.4.3.3 can be seen to reduce the transformer life loss, even though an additional 86.4% EVC penetration was connected to the LV EDN and the maximum THDv increases from 4.45% to 5.11%. This is because within Equations 3.2.8.1-10, higher order harmonics have a much more significant effect on temperature increase. In contrast Equations 3.2.8.11-19, which are used to calculate the energy loss of cables with harmonic currents, do not increase the impact of the harmonic current as harmonic orders increase. Therefore, the significantly larger magnitude lower order harmonics shown in Table 4.4.3.3 lead to the higher cable temperature and asset life loss.

Based on the results of this section, it is recommended that the numbers of EVCs or PV generation connected to LV EDNs should be restricted, or harmonic reducing technology implemented to observe compliance with industrial standards and regulations during phase-to-phase faults.

# Chapter 5 – Advanced Learning Method Enabled Optimisation for THDv Minimisation

It is in a DNOs interest to minimise harmonics on the EDN as explained in ER G5/5. To aid them with their LV network planning, it is proposed that the optimum location of EVCs, PV generation and V2Gs on LV EDNs is investigated, and patterns determined. To do this, the optimum location of EVCs, PV generation and V2Gs under a range of network parameters, conditions, and harmonic phase-shifts are considered. The optimised quantity for this section will be the highest THDv value between phase and neutral measured at all of the customers supply terminals. Optimum conditions will be achieved when the highest THDv mentioned previously is at its lowest reading. The results will be analysed to identify the optimum POC for each device and determine what parameters or conditions influence the optimum POC. This information can be used by network planning engineers when planning new connections of these devices to minimise THDv levels. To carry this out manually would present an unrealistic timescale. Therefore, two algorithms were created to find the optimum POC for each scenario presented.

## 5.1– Optimisation Algorithms

### 5.1.1 – Research Question of THD Minimisation

Sections 2.1.4, 2.2.4 and 2.4.2 detail a range of existing research papers which cover the optimisation of EVCs, PV generation and V2Gs. The research gaps are stated in Sections 2.1.5, 2.2.5 and 2.4.3. Based on the findings of these sections, the optimisation of EVC, PV generation and V2G location on an LV EDN with respect to THDv under a range of different network conditions and harmonic phase angles is novel, advancing academic research.

In order to fulfil these research gaps, the following methodology should be deployed for EVCs, PV generation and V2G:

- The location of these EVCs, PV generation and V2G should be optimised on an LV EDN to minimise maximum THDv at all supply terminals.
- Different network parameters such as transformer size, cable/grid impedance, number of LV EDN feeders and connection of different loads should be considered.
- Network faults explained in Section 1.5 should be considered.
- Harmonic phase angle should be varied to account for real world variations in harmonic phase angle between different harmonic sources and background harmonics.
- For V2G, the optimum V2G location should be determined by converting an existing or proposed EVC, rather than implementing a V2G solely for the purposes of optimising the grid. Therefore, EVCs, should be applied at all busses, giving the most possible options for V2G location.

## 5.1.2 – Optimisation Algorithms

The objective of this model and optimisation algorithm is to determine the EVC, PV or V2G POC which results in the lowest THDv at any point of supply within the model. As mentioned in the previous section, there are a number of variables which must be considered. These variables are listed below:

$X_1$ = X/R ratio and impedance magnitude of the source.
$X_2$ = EVC/PV/V2G harmonic magnitude and phase angle up to the $50^{th}$ harmonic.
$X_3$ = Mains and service cable impedance.
$X_4$ = Background harmonic magnitude and phase angle up to the $50^{th}$ harmonic.
$X_5$ = Base load.
$X_6$ = Network configuration and load flow.
$X_7$ = Number of LV feeders.

In addition, as background harmonics increase, so does the harmonic output of the harmonic loads, this increases complexity.

Convex optimisation via a mathematical representation was considered to solve this optimisation problem. However, from manual testing, it was found that these functions were not convex in nature. Trehan (2020) explains that a convex function should have a single global minimum solution. The function was found to be non-convex, for example, depending on the scenario selected, the THDv value at busses one and eleven are quite often lower than busses within the middle of the network. Therefore, the non-convex function has multiple local optimal solutions. If trying to solve via convex methods, the solution may converge to local or sub-optimal solutions.

For this reason, and by following papers which have tried to solve similar optimisation problems with EVCs, PV generation and V2Gs on the electricity grid such as Ahmad, et al. (2022), Jamatia, Bhattacharjee and Sharma (2022) and Sharew, Kefale and Werkie (2021), it was determined that optimisation algorithms via a Simulink simulation should be used.

Based on the papers reviewed in Sections 2.1.4, 2.2.4 and 2.4.2, the following algorithms should be mentioned as potential choices for solving the proposed problem:

There are three main algorithm types covered. These are:

- Genetic Algorithms such as Genetic Algorithm (GA), Adaptive Genetic Algorithm (AGA), Discrete-Continuous Chu & Beasley Genetic Algorithm (DCCBGA), and Stud Genetic Algorithm (SGA).
- Lightning Search Algorithms (LSA) such as Binary Lightning Search Algorithm (BLSA), Modified Lightning Search Algorithm (MLSA), and Quantum Binary Lightning Search Algorithm (QBLSA)
- Swarm intelligence algorithms (SI) including but not limited to Artificial Bee Colony (ABC), Ant Colony Optimisation (ACO), Adaptive Cuckoo Search Algorithm (ACSA), Ant-Lion Optimisation Algorithm (ALOA), Bacterial Foraging Optimisation Algorithm (BFOA), Binary Particle Swarm Algorithm (BPSO), Coyote Optimisation Algorithm (COA), Discrete–Continuous Crow Search Algorithm (DCCSA), Discrete-Continuous Particle Swarm Optimisation (DCPSO), Differential Evolution (DE), Grey Wolf Optimisation (GWO), Harris Hawks Optimisation (HHO), Invasive Weed Optimisation Algorithm (IWO), Particle Swarm Optimisation (PSO), Symbiotic Organism Search (SOS), Salp Swarm Algorithm (SSA), and Whale Optimisation Algorithm (WOA).

Additionally, several other algorithms were covered. These are:

- Basic Open-source Nonlinear Mixed Integer programming (BONMIN)
- Biogeography-Based Optimisation Algorithm (BBO)
- Decoupled Harmonic Power Flow (DHPF)
- Discrete-Continuous Generalized Normal Distribution Optimizer (DCGNDO)
- Evolutionary Programming (EP)
- Fireworks Algorithm (FWA)
- Greedy Based Optimisation (GBO)
- Harmony Search Algorithm (HSA)
- Harmony Search Algorithm and Particle Artificial Bee Colony hybrid algorithm (HSA-PABC)
- Hamiltonian Optimisation (HOP)
- Improved Chimp Optimisation Algorithm (ICOA)
- Multi-paramedic Global Sensitivity Analysis (MPGSA)
- Optimal Harmonic Power Flow (OHPF)
- Optimized Location Scheme for electric charging stations (oLoC)
- Pareto-Fuzzy Technique (PFT)
- Quadratic Optimisation Technique (QOT)
- Multi-Objective Quasi-Oppositional Teaching Learning based Optimisation (QOTLBO)
- Simulated Annealing (SA)
- Teaching-Learning Based Optimisation (TLBO)
- Uniform Voltage Distribution Based Constructive Algorithm (UVDA)
- Vortex Search Algorithm (VSA)

This is a huge number of algorithms to consider. Therefore, research into algorithm comparisons within the papers reviewed in Sections 2.1.4, 2.2.4 and 2.4.2 was carried out.

Firstly, Tahir (2017) calculates the total losses in MW of a thirty bus and fifty-seven bus system with V2G. Within this paper it was found that the best solutions were obtained from algorithms in the following order, HOP, PSO, EP and finally GA. HOP also required less iterations when compared to the other algorithms.

Secondly, Awasthi, et al. (2017) identified the optimum connection location of EVCs with respect to power losses and voltage drop. In terms of convergence, it found that PSO converged in thirty iterations compared to thirty-four with GA and produced much less voltage variation. The study then produces a PSO variant, GAIPSO, which converged in twenty iterations with similar voltage variation to PSO, therefore providing the same accuracy whilst converging much faster. Similarly, Tran-The, Nguyen-Quoc and Vo-Ngoc (2020) identified the optimum DG to minimise power losses. Within this study, SOS performed the best, followed by UVDA, ACSA, FWA, MPGSA and HGWOPSO in that order. This was measured across thirty-three and sixty-nine bus networks under seven various scenarios. Interestingly, although an SI algorithm produced the best outcome, it also produced the third and worst outcomes. Therefore, there is large variability between the effectiveness of different SI algorithms.

Following this, Ahmad, et al. (2022) compared GA to GWO to identify the optimum connection location of V2G with respect of voltage, power loss, installation cost and power loss cost. It was found that GWO obtained a more optimum solution. However, in contrast, Fu, et al. (2023) identifies the optimum connection location of DG with regards to power losses and compares GA, PSO and ALOA. GA shows better optimisation results in bus loss, line loss rate, voltage deviation, and THDv.

Further to the above, Nguyen-Phuoc, Vo-Ngoc and Tran-The (2017) identified the optimum size, location, and number of DG on an EDN. SOS produced the best solution for the thirty-three bus system followed by PSO, GA, TLBO and HSA. For a sixty-nine bus system this was SOS followed by TLBO, PSO, HSA and GA. For a one-hundred and eighteen bus system with seven DGs, the best solution was obtained by SOS. It compared HSA, GA, TLBO, SOS and PSO. The optimum losses calculated by HSA and TLBO were far greater than GA, SOS and PSO, (126.695-135.69kW Vs 104.26-106.3) therefore not finding the optimum solution for the 33-bus system. Out of the remaining algorithms, SOS produced the best solution, followed by PSO and GA, however, there was not much difference in the losses produced by these algorithms. For the 69-bus system, similar results were seen with HSA and GA producing losses between 86.66-89kW. PSO, TLBO and SOS produced solutions with losses between 82.07-83.2kW. The best solution was produced by SOS, followed by TLBO and PSO. For the 118-bus system with up to 7 DGs it was found that SOS produced a far better solution than HSA-PABC and HSA, except for when a single DG was implemented.

Aljanad, et al. (2018) compared QBLSA, BLSA and BPSO to identify the optimum connection location of V2G capable charging stations during discharge mode with respect of line loading, voltage deviation, and circuit power loss. It was found that QBLSA, BLSA and BPSO converge in that order of speed, number of iterations and best solutions.

Doan, Duong and Mussetta (2021) identifies the optimum connection location of PV generation to reduce network losses. The optimal solutions were obtained by algorithms in the following order, ICOA, COA, SSA, AGA, QOTLBO, IWO, HSA, BFOA, SA and GA/PSO. However, the number of iterations required to reach its optimum solution were reversed with GA/PSO requiring the minimum number of iterations. The same could be seen within Cortés-Caicedo, et al. (2022) which was used to identify the optimum connection location of PV generation to reduce cost of purchase, investment in PV generation and operation/maintenance costs. The optimal solutions were obtained by algorithms in the following order, DCCSA, DCGNDO, DCPSO and BONMIN. However, the processing time was the opposite in the following order of speed, BONMIN, DCCBGA, DCPSO and DCCSA.

Quan-Duong, et al. (2019) identifies the optimum connection location and size of PV generation with regards to power losses. It found that BBO converges the quickest. Followed by GA, ABC and PSO. Although converging the slowest, PSO produces the second-best fitness which arguably is more important. It should also be noted that it can be observed that GA results in more voltage deviation across the busses when compared to the other algorithms. In contrast Islam, Shareef and Mohamed (2018) compares BLSA, another different technique to BPSO and GA. Its objective was to identify the optimum connection location of EVCs with respect of EV transportation energy loss, station build-up cost and sub-station energy loss. BLSA was found to converge quicker and produce better fitness values. Between BPSO and GA, GA converged faster and with a better value in three cases, whereas BPSO converged faster and with a better value in only one case.

However, generally from reading the twenty-four different papers covered in Sections 2.1.4, 2.2.4 and 2.4.2 a general conclusion is that many algorithms do perform better in general than others, however, much of the performance is due to optimising the parameters to work with the chosen algorithm and problem. Therefore, although many of the papers mentioned have drawn specific conclusions about certain algorithms, it is very likely that the gap between those algorithms could have been closed by optimising the parameters used.

Algorithms mentioned in a single paper reviewed, listed within the other algorithms, will not be considered for this thesis for the reason mentioned above. Without peer review of the same algorithm, it is likely that the parameters could have been manipulated to reach the conclusion the author was looking to achieve rather than how it might perform to future users of the algorithms. Therefore, the three main types of algorithms listed at the beginning of this section will be compared since, there are several papers peer reviewing these types of algorithms. Table 5.1.2.1 was constructed to compare these algorithms.

Taking the results of Table 5.1.2.1 into account, GA, LSA and SI algorithms are all suitable to solve the research gap proposed in Section 5.1.1. Overall, LSA seems to be the best performing algorithm, however, a limitation of this algorithm is that there are not many comparisons between LSA, SI and GA. As an example, some of the better performing SI algorithms such as COA, GWO and SOS were not compared to LSA, making it hard to draw the conclusion that LSA generally performs better than SI. The same is true of Gas and the only conclusion that can be drawn is that SI performs better than the basic GA only. SI algorithms were compared to a much broader range of other algorithms. For this reason, SI algorithms shall be chosen to solve the research gap stated in Section 5.1.1. Additionally, although speed of the algorithms is a factor to consider and SI was found to be slower than LSA, the algorithm does not need to be fast, it needs to produce the correct solution.

Further to the above, the specific SI algorithms for this thesis should be selected and should be easy to implement for the specific problem.

Taking these findings forward, Elephant Herding Optimisation (EHO), an SI algorithm was reviewed. Wang, Deb and Coelho (2015) compares the performance of EHO to BBO, DE and GA in their ability to solve fifteen complex functions. It was found that EHO produced the best solution 55% of the time and second-best solution a further 33% of the time. The remaining algorithms, BBO, DE and GA produced the best solution 33%, 13% and 13% of the time respectively. Further to this, EHO was compared in detail using the Alpine Function and Brown Function. For these functions, it was found that EHO was able to converge much faster than BBO, DE or GA. Additionally, for both functions, EHO achieved a much better optimum solution than BBO, DE and GA. Furthermore, Quan-Duong, et al. (2019) found that BBO achieved the best fitness and converged the quickest when compared to GA, ABC and PSO. Since EHO outperforms BBO, this suggests that this is also a significant improvement over DE, GA, and SI algorithms ABC and PSO.

**Table 5.1.2.1: Comparison of the three main algorithm types considered for this thesis.**

| Algorithm Type | Accuracy/Best Optimal Value | Speed/Number of Iterations | Type of Problem Solved | Limitations of Conclusions |
|---|---|---|---|---|
| Genetic Algorithm (GA) | Generally, GA produced the least optimal solutions. However, in some cases GA produced more optimal solutions than SI. | Generally, GA converged the slowest, However, in some cases GA converged quicker than SI. | Optimum connection location of PV generation, EVCs or V2G and the optimum connection location, size, and number of DG. | Most studies compare their algorithm to GA, the most basic GA. AGA and DCCBGA were not widely compared. |
| Lightning Search Algorithm (LSA) | Found to Produce a more optimum solution than SI or GA for the algorithms selected for comparison. | Found to converge quicker and require fewer iterations than SI or GA. | Optimum connection location of EVCs or V2G with respect of line loading, voltage deviation, energy loss, station build-up cost and sub-station energy loss. | Only BPSO and GA compared to LSA. Without further comparisons with other SI and GA algorithms, it is hard to determine if LSA is better than all, or just better than those specific SI and GA algorithms. |
| Swarm Intelligence (SI) | Does not produce as optimum a solution as LSA, however, generally produces a more optimal solution than GA. | Found to converge slower and with more iterations than LSA, however, generally converges faster and with less iterations than GA. | Optimum connection location of PV generation, EVCs or V2G and the optimum connection location, size, and number of DG. | Not a limitation, SI being the most abundant algorithm type. SI has been compared to in almost all papers considered. Many different types of SI algorithms have been considered. |

Lastly, further to the performance of EHO, the algorithm itself from Wang, Deb and Coelho (2015) was found to be easier to implement to the specific problem mentioned in Section 5.1.1 than many of the other SI algorithms covered previously.

Since EHO achieved the best solution 55% of the time when compared to fifteen functions as per Wang, Deb and Coelho (2015), a second algorithm was reviewed to check the results of EHO. The second SI algorithm is based on a technique created by Wang, Deb and Cui (2019) called Monarch Butterfly Optimisation (MBO). Wang, Deb and Cui (2019) compares the performance of MBO to ABC, ACO, BBO, DE and SGA in its ability to solve thirty-eight complex functions. MBO performed better than or equal to ABC, ACO, BBO, DE and SGA 68%, 71%, 50%, 66%, and 47% of the time for the thirty-eight functions respectively. Further to this, MBO was compared in detail using the Ackley, Alpine, Pathological, Rastrigin, Rosenbrock, and Schwefel Functions. In each of these functions, it was found that MBO would converge quicker than the other algorithms. Additionally, MBO also achieved the best solution for all of the aforementioned functions except for the Rastrigin Function, which was matched by BBO, although BBO did not converge as quickly. Summarising the results of MBO, Wang, Deb and Cui (2019) found that it was able to solve thirty-four out of thirty-eight benchmark functions, and similarly to EHO, is able to converge much quicker than the other algorithms. For high-dimensional functions, MBO performs much stronger than the comparison algorithms, however, for low-dimensional functions MBO performs similar to the comparison algorithms ABC, ACO, BBO, DE and SGA. Similarly to EHO, it was found that MBO was easier to implement to the specific problem mentioned in Section 5.1.1 than many of the other SI algorithms covered previously.

It is also important that a clear difference in methodology is present between the proposed algorithms, since similarities could lead to the incorrect or less optimal solutions being achieved by both algorithms for the same reason. The difference in methodology between the two algorithms can be seen in Figure 5.1.2.1. Both algorithms can be seen to produce a new iteration, followed by an evaluation of the solution against the previous best solution. This is common across multiple algorithm types. However, following this, the methodology diverges. This deviation of methodology will be covered in further detail in Sections 5.1.3-4. On completion of the divergent methodology, the algorithm is then either re-run if the maximum number of iterations has not been reached, or the best solution output if the maximum number of iterations are reached.

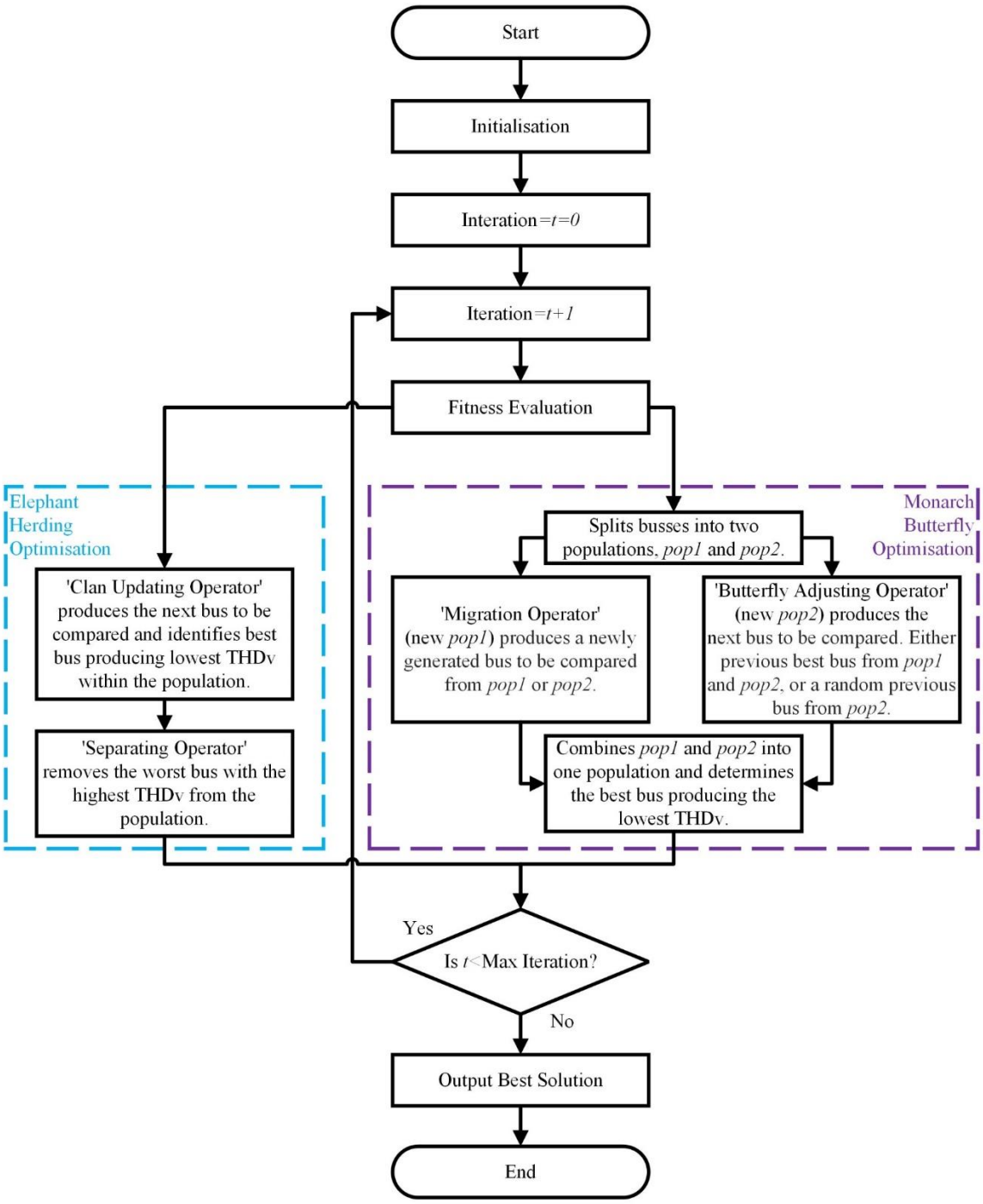


**Figure 5.1.2.1: Differences and similarities in method between EHO and MBO.**

Applying both EHO and MBO together ensures a strong pair of main and comparison algorithms are used with a clear difference in methodology to solve the same optimisation problem, therefore reducing the risk of algorithm methodology leading to inaccurate results.

## 5.1.3 – Elephant Herding Optimisation

Alterations have been made to the EHO script from Wang, Deb and Coelho (2015) to allow it to solve the optimisation of PV generation, EVC and V2G POC with respect of THDv levels. Table 5.1.3.1 show variables in MATLAB which can be altered to change the scenario which requires optimising. This includes the number of busses, number of busses which can have additional PV generation, EVCs or V2Gs on at any one time and the maximum/minimum number of additional PV generation, EVCs or V2Gs which can be connected to those busses. For this algorithm, 'No_of_EV_Sites', 'Max_EV_No', 'Min_EV_No', 'No_of_PV_Sites', 'Max_PV_No' and 'Min_PV_No' shall be set to one and 'N_Bus' shall be set to eleven. This results in an eleven-bus system which tests one PV generation, EVC or V2G per phase at a single bus per test.

**Table 5.1.3.1: Algorithm variables for specific network conditions that require optimising.**

| | |
|---|---|
| N_Bus | Number of busses in the system. |
| No_of_EV_Sites | Number of EVC sites/locations to be searched. |
| Max_EV_No | Maximum number of EVCs to be allowed to deploy at a single bus. |
| Min_EV_No | Minimum number of EVCs to be allowed to deploy at a single bus. |
| No_of_PV_Sites | Number of PV sites/locations to be searched. |
| Max_PV_No | Maximum number of PV generators to be allowed to deploy at a single bus. |
| Min_PV_No | Minimum number of PV generators to be allowed to deploy at a single bus. |

To aid optimisation computation, there are five additional parameters within MATLAB which can be varied as seen in Table 5.1.3.2. These are $\alpha$, $\beta$, N, $nc$ and $G_{Max}$. These are explained in Table 5.1.3.2 below.

**Table 5.1.3.2: Additional parameters which can be varied within the EHO algorithm.**

| | |
|---|---|
| $nc$ | Number of elephant clans. |
| $N$ | Number of elephants in each clan/parameter which effects parameter $j$. |
| $\alpha$ | Scaling factor alpha determining influence of $x_{best,ci}$ and $x_{ci,j}$. |
| $\beta$ | Scaling factor beta determining influence of $x_{center,ci}$. |
| $G_{Max}$ | Maximum number of generations/iterations. |

As shown in Figure 5.1.2.1, EHO uses a 'Clan Updating Operator' which evaluates the clan of elephants, identifying the fittest elephant which is the matriarch and generating a new individual. This is the first portion of the algorithm and can be represented by three main equations, which can be seen in Equations 5.1.3.1-3 from Wang, Deb and Coelho (2015). Equation 5.1.3.1 is the equation for the next iteration step. This is composed of $x_{ci,j}$ which is the last iteration, $\alpha$, which is a scale factor set in Table 5.1.3.2, $x_{best,ci}$ which is the individual of best fitness within clan $ci$ and $r$ which is a random number between zero and one. Equation 5.1.3.2 is the equation for a new iteration step where the last iteration is the best solution. In that case Equation 5.1.3.1 is not applicable. Additional symbols in Equation 5.1.3.2 are $\beta$ which is a scale factor set in Table 5.1.3.2 and $x_{center,ci}$ which is the centre of clan $ci$. Lastly, Equation 5.1.3.3 is $x_{center,ci,d}$ used within Equation 5.1.3.2. The additional symbols in Equation 5.1.3.3 are $n_{ci}$ which is the number of elephants in each clan and $x_{ci,j,d}$ which is the $d^{th}$ of the individual of last iteration. Equations 5.1.3.1-3 have been converted into MATLAB code for use within the algorithm, Equation 5.1.3.1 to Equation 5.1.3.4, Equation 5.1.3.2 to Equation 5.1.3.5 and Equation 5.1.3.3 to Equation 5.1.3.6.

Equation 5.1.3.1
$$x_{new,ci,j} = x_{ci,j} + \alpha\left(x_{best,ci} - x_{ci,j}\right) \times r$$

Equation 5.1.3.2
$$x_{new,ci,j} = \beta \times x_{center,ci}$$

Equation 5.1.3.3
$$x_{center,ci,d} = \frac{1}{n_{ci}} \times \sum_{j=1}^{n_{ci}} x_{ci,j,d}$$

Equation 5.1.3.4
$$pp_{new}(j,c) = round\left(pp(j,c) + alpha\left(pbest(c) - pp(j,c)\right) \times rand\right)$$

Equation 5.1.3.5
$$pp_{new}(j,c) = round(beta \times pp_{center})$$

Equation 5.1.3.6
$$pp_{center} = mean(pp(:,c))$$

Where:

$\alpha$ is a scale factor set in Table 5.1.3.2 (alpha within EHO Algorithm).

$\beta$ is the scale factor set in Table 5.1.3.2 (beta within EHO Algorithm).

*ci* is an elephant clan (*c* within EHO Algorithm).

$d$ is the $d^{th}$ element.

$j$ is an elephant individual within each clan.

$mean$ is a command within EHO Algorithm for mean average value.

$n_{ci}$ are the number of busses in the system set in Table 5.1.3.2 (*nc* within EHO Algorithm).

*r* is a random number between zero and one (*rand* within EHO Algorithm).

$round$ is a command within EHO Algorithm for rounding a value to the nearest integer.

$x_{best,ci}$ is the bus producing lowest THDv (*pbest(c)* within EHO Algorithm).

$x_{center,ci}$ is the centre bus (*pp_center* within EHO Algorithm).

$x_{ci,j}$ is the bus of the last iteration (*pp(j,c)* within EHO Algorithm).

$x_{ci,j,d}$ is the $d^{th}$ of bus of last iteration (*pp(:,c)* within EHO Algorithm).

$x_{new,ci,j}$ is the bus of the next iteration (*pp_new(j,c)* within EHO Algorithm).

The second portion of the algorithm shown in Figure 5.1.2.1 is the 'Separating Operator.' This removes the elephant with the worst fitness from the population, effectively replacing them with the new individual created within the 'Clan Updating Operator.' This is represented by Equation 5.1.3.7. $x_{worst,ci}$ represents the individual of worst fitness within clan $ci$. $x_{max}$ and $x_{min}$ represent the upper and lower bounds of elephant position with respect to the matriarch. $x_{worst,ci}$ is then replaced for the next iteration. Equation 5.1.3.7 has been converted to Equation 5.1.3.8 for use within the algorithm. This simplifies the expression by looking for the iteration which produced the highest THDv measured at all customers' supply terminals across the whole LV EDN.

Equation 5.1.3.7 $$x_{worst,ci} = x_{min} + (x_{max} - x_{min} + 1) \times r$$

Equation 5.1.3.8 $$fworst = \max(Fitness)$$

Where:

$Fitness$ is the THDv magnitude (elephant fitness).

$max$ is a command within EHO Algorithm for returning he maximum value from an array.

$x_{max}$ is the upper bound of bus position (upper bound of 'elephant position').

$x_{min}$ is the lower bound of bus position (lower bound of 'elephant position').

$x_{worst,ci}$ is the bus producing highest THDv (*fworst* within EHO Algorithm).

Figure 5.1.2.1 explains how EHO applies to this thesis. Furthermore, the variables previously mentioned can be explained within the context of this optimisation problem. $x_{best,ci}$ represents the best bus producing the lowest THDv, $x_{worst,ci}$ represents the worst bus producing the highest THDv, $x_{new,ci,j}$ represents the bus of the next iteration, $x_{ci,j}$ represents the bus of the last iteration and $x_{center,ci,d}$ represents the center bus. $x_{max}$ and $x_{min}$ represent the upper and lower bound of bus position with respect to the best bus.

## 5.1.4 – Monarch Butterfly Optimisation

Alterations have been made to the Monarch Butterfly Optimisation (MBO) script from Wang, Deb and Cui (2019) to allow it to solve the optimisation of PV generation, EVCs and V2G POCs with respect of THDv levels. Similar to EHO, Table 5.1.3.1 shows variables in MATLAB which can be altered to change the scenario which requires optimising. The same values were applied to the variables to produce the same scenario as EHO. Table 5.1.4.1 shows several additional parameters which can be used to vary the MBO algorithm.

There are two main portions of the algorithm. These are the 'Migration Operator' represented in Equations 5.1.4.1-9 and the 'Butterfly Adjusting Operator' represented in Equations 5.1.4.10-21 from Wang, Deb and Cui (2019). A diagram of how these operators fit within the overall algorithm structure can be seen in Figure 5.1.2.1. Firstly, the population of monarch butterflies is split into two subpopulations, *pop1* and *pop2*. this is to represent the migration of butterflies between regions at different times of year. The 'Migration Operator' updates the positions of monarch butterflies by generating a new subpopulation for *pop1* where a newly generated child butterfly replaces a parent butterfly if it has better fitness than its parent. In this case the parent butterfly is deemed to have passed away. The 'Butterfly Adjusting Operator' also updates the positions of monarch butterflies by generating a new subpopulation, *pop2*.

**Table 5.1.4.1: Additional parameters which can be varied within the MBO algorithm.**

| | |
|---|---|
| *iter* | Iteration. |
| *Levy* | Lévy flight performed by butterflies when migrating or moving. |
| *Lnd*1 | Flutter in region one. |
| *Lnd*2 | Flutter in region two. |
| *Max_iter* | Maximum number of iterations. |
| *nFlutr* | Flutter length. |
| *nBF1* | Butterflies in region one. |
| *nBF2* | Butterflies in region two. |
| *peri* | Migration period. |
| *Pn* | Population size. |
| *pop1* | Population one. |
| *pop2* | Population two. |
| *rand* | Random number drawn from uniform distribution. |
| *scale* ($\alpha$) | Weighting Factor. |
| *stepmax* ($S_{Max}$) | Maximum step size per iteration. |
| *stepsize* | Walk step size per iteration. |

To explain the 'Migration Operator' in more detail, the main equations used have been expressed below. Equations 5.1.4.1-2 and $x_{i,k}^{t+1}$are the equations for the next iteration step of $pop1$. $t+1$ represents the next generation or iteration and $i$ represents the monarch butterfly in $pop1$. $r_1$ or $r_2$ represent the monarch butterfly randomly selected from either *pop1* or *pop2* respectively. Equation 5.1.4.1 applies when $r \leq p$ where $p$ is the ratio of butterflies in *pop1* compared to *pop2*. Equation 5.1.4.2 applies when $r > p$. $r$ is calculated using Equation 5.1.4.3 where $rand$ is a random number drawn from uniform distribution and $peri$ is the migration period set to 1.2. Equations 5.1.4.1-3 have been converted into MATLAB code for use within the simulation; Equation 5.1.4.1 to Equations 5.1.4.4-6, Equation 5.1.4.2 to Equations 5.1.4.7-8 and Equation 5.1.4.3 to Equations 5.1.4.9.

Equation 5.1.4.1 $$x_{i,k}^{t+1} = x_{r1,k}^{t}$$

Equation 5.1.4.2 $$x_{i,k}^{t+1} = x_{r2,k}^{t}$$

Equation 5.1.4.3 $$r = rand \times peri$$

Equation 5.1.4.4 $$ci = 1{:}\,nFlutr$$

Equation 5.1.4.5 $$rr2 = round(nBF1 \times rand + 0.5)$$

Equation 5.1.4.6 $$Lnd1(j, ci) = pop1(rr2, ci)$$

Equation 5.1.4.7 $$rr3 = round(nBF2 \times rand + 0.5)$$

Equation 5.1.4.8 $$Lnd1(j, ci) = pop2(rr3, ci)$$

Equation 5.1.4.9 $$rr1 = rand \times 1.2$$

Where:

$i$ is the monarch butterfly in *pop1*.

$k$ is the k[th] element ($ci$ within the MBO Algorithm).

$Lnd1$ is the flutter in region one.

$nBF1$ are the butterflies in region one.

$nBF2$ are the butterflies in region two.

*nFlutr* is the flutter length.

$peri$ is the migration period (set to 1.2 within the MBO Algorithm).

$r$ is the position of the monarch butterfly ($rr1$ within the MBO Algorithm).

$r_1$ is the position of the monarch butterfly selected from *pop1* ($rr2$ within the MBO Algorithm).

$r_2$ is the position of the monarch butterfly selected from *pop2* ($rr3$ within the MBO Algorithm).

*rand* is a random number drawn from uniform distribution.

$round$ is a command within the MBO Algorithm for rounding to the nearest integer.

$x_{i,k}^{t+1}$is the next iteration step of *pop1*. ($Lnd1(j, ci)$ within the MBO Algorithm).

$x_{r1,k}^{t}$is the iteration step of *pop1*, newly generated position of the monarch butterfly $r_1$ ($pop1(rr2, ci)$ within the MBO Algorithm).

$x_{r2,k}^{t}$ is the iteration step of *pop2*, newly generated position of the monarch butterfly $r_2$ ($pop2(rr3, ci)$ within the MBO Algorithm).

$t$ is the current generation or iteration (*iter* within the MBO Algorithm).

$t + 1$ is the next generation or iteration.

The 'Butterfly Adjusting Operator' previously mentioned is shown in Equations 5.1.4.10-21. Equation 5.1.4.10 and $x_{j,k}^{t+1}$ is the equation for the next iteration step of *pop2* when $rand \leq p$ where $x_{best}$ is the best iteration in *pop1* or *pop2.* Additionally, $j$ represents the monarch butterfly in *pop2*. Equation 5.1.4.11 and $x_{j,k}^{t+1}$is the equation for the next iteration step of *pop2* when $rand > p$ unless $rand > BAR$ where $BAR$ indicates butterfly adjusting rate. In this case $x_{j,k}^{t+1}$ is changed to Equation 5.1.4.12. $x_{r3,k}^{t}$ is a randomly selected previous solution from *pop2*, $dx$ is the walk step of the monarch butterfly defined by Equation 5.1.4.13 and $\propto$ is a weighting factor defined by Equation 5.1.4.14. In these equations $Levy$ is the Lévy flight performed by butterflies when migrating or moving, $x_j^t$ is the last iteration, $S_{Max}$ is the maximum step size per iteration, and $t$ is the current iteration or generation. Equations 5.1.4.10-14 have been converted into MATLAB code for use within the simulation; Equation 5.1.4.10 to Equation 5.1.4.15, Equation 5.1.4.11 to Equations 5.1.4.16-17, Equation 5.1.4.12 to Equation 5.1.4.18, Equation 5.1.4.13 to Equations 5.1.4.19-20 and Equation 5.1.4.14 to Equation 5.1.4.21.

Equation 5.1.4.10 $$x_{j,k}^{t+1} = x_{best,k}^{t}$$

Equation 5.1.4.11 $$x_{j,k}^{t+1} = x_{r3,k}^{t}$$

Equation 5.1.4.12 $$x_{j,k}^{t+1} = x_{j,k}^{t+1} + \propto \times (dx_k - 0.5)$$

Equation 5.1.4.13 $$dx = Levy\ (x_j^t)$$

Equation 5.1.4.14 $$\alpha = \frac{S_{Max}}{t^2}$$

Equation 5.1.4.15 $$Lnd2(j, ci) = x_{best}(1,1)$$

Equation 5.1.4.16 $$rr4 = round(nBF2 \times rand + 0.5)$$

Equation 5.1.4.17 $$Lnd2(j, ci) = pop2(rr4, ci)$$

Equation 5.1.4.18 $$Lnd2(j, ci) = Lnd2(j, ci) + scale \times (deltaX(ci) - 0.5)$$

Equation 5.1.4.19 $$deltaX = LevyFlight(stepsize, nFlutr)$$

Equation 5.1.4.20 $$stepsize = ceil(exprnd(2 + Max\ iter, 1,1))$$

Equation 5.1.4.21 $$scale = Stepmax/(iter)^2$$

Where:

$\alpha$ is the weighting Factor (*scale* within the MBO Algorithm).

$ceil$ is a command within the MBO Algorithm for rounding to nearest integer.

$dx$ is the walk step of the monarch butterfly ($deltaX$ within the MBO Algorithm).

$exprnd(a, b, c)$ is a command within the MBO Algorithm to generate a random number or numbers from the exponential distribution with mean 'a' and matrix of 'b×c'.

$j$ is the monarch butterfly in *pop2*.

$Levy$ is the Lévy flight performed by butterflies when migrating or moving (*LevyFlight* within the MBO Algorithm).

$Lnd2$ is the flutter in region two.

*Max_iter* is the maximum number of iterations.

*pop1* is population one.

*pop2* is population two.

$S_{Max}$ is the maximum step size per iteration (*stepmax* within the MBO Algorithm).

*Stepsize* is the walk step size per iteration.

$x_{best,k}^{t}$ is the best iteration with respect to THDv in *pop1* or *pop2*.

$x_{j}^{t}$ is the current iteration step of *pop2*.

$x_{j,k}^{t+1}$ is the next iteration step of *pop2* ($Lnd2(j, ci)$ within MBO Algorithm).

$x_{r3,k}^{t}$ is the randomly selected solution from *pop2* ($pop2(rr4, ci)$ within MBO Algorithm).

Further to the above, *exprnd* shall be explained. This represents a random number or numbers from an exponential distribution with mean *a*. The calculation for a single random number can be seen within Equation 5.1.4.22 obtained from Ramachandran and Tsokos (2015). *Y* has been substituted for *exprnd* to represent a single random number from the exponential distribution. The inverse of mean *a* must also be calculated for use within Equation 5.1.4.22. This is $\lambda$ as shown within Equation 5.1.4.23 from The Pennsylvania State University (2023).

Equation 5.1.4.22 $$Y = -\frac{ln\,(1-rand)}{\lambda}$$

Equation 5.1.4.23 $$\lambda = \frac{1}{a}$$

Where:

$a$ is the mean of the exponential distribution.

$Y$ is a single random number from the exponential distribution.

$\lambda$ is the inverse of the mean of the exponential distribution.

$ln$ is the natural logarithm.

$rand$ is a random value between zero and one.

Figure 5.1.2.1 explains how MBO applies to this particular study. Additionally, the parameters mentioned earlier can be explained within the context of this optimization problem. $x_{best,k}^{t}$ represents the previous best bus producing the lowest THDv across *pop1* and *pop2*, $x_{i,k}^{t+1}$ and $x_{j,k}^{t+1}$ represent the next busses to be compared, representing *pop1* and *pop2* respectively. $x_{r1,k}^{t}$ represents the newly generated bus to be compared from *pop1*, $x_{r2,k}^{t}$ represents the newly generated bus to be compared from *pop*2, and $x_{r3,k}^{t}$ is a randomly selected previous solution and bus from *pop2*. $p$ represents the ratio of busses in *pop1* compared to *pop2*, whilst $BAR$, $Levy$ and $S_{Max}$ are parameters which can be set to optimise the algorithm.

## 5.1.5 – Case Study

To satisfy the first requirement of the methodology mentioned in Section 5.1.1 and to produce an optimisation solution with easily understood results, the layout of the LV EDN produced in Section 3.1 was modified to produce a single, radial LV distribution feeder shown in Figure 5.1.5.1. The radial LV EDN was divided into eleven sections (busses), with equal impedances between each bus. Three service cables are connected to each bus, one on each phase of a three-phase system with equal impedance service cable. The first and eleventh busses represent the first and last 5% of the LV EDN length. The remaining busses each represent 10% portions of the LV EDN length. The transformer, 11kV EDN, background THDv and base load per service were left unchanged from the case study simulation. Unless otherwise mentioned, the modified LV EDN corresponds to a network with the following characteristics:

- 230m long radial LV network using 185mm$^2$ Al Wavecon cable with 23m between busses. The impedance data was obtained from Baker (2017).
- A 500kVA 11kV:400V Dyn11 transformer of 4.74% impedance feeds the LV EDN.
- A fixed X/R ratio and 11kV bus impedance from Scottish and Southern Electricity Networks (2019) stated in Section 3.1.4.
- A background load of 500W per single-phase service derived from Elexon Ltd (1997).
- 15m long services using 25mm$^2$ Cu concentric cable. The impedance data was obtained from Baker (2017).
- No existing PV generation or EVCs are connected to the network.
- One LV feeder connected to bus one.

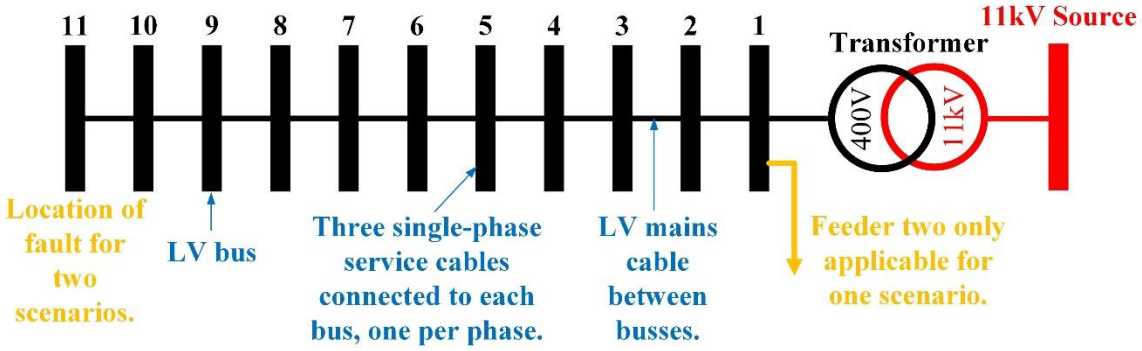


**Figure 5.1.5.1: Electrical layout of the optimisation LV EDN.**

Another difference between this LV EDN and the LV EDN used in Chapter 4 is that the voltage harmonics between phase and neutral at all supply terminals are measured, therefore a total of thirty-three supply terminals are measured. The purpose of this investigation is to minimise the maximum THDv at all supply terminals. Therefore, it was essential that all supply terminals were monitored. Connection of an EVC, PV generator or V2G at one location may have a greater impact relatively speaking at a different location on the LV EDN.

To satisfy the second and third requirement of the method it was important to consider a range of network parameters. Since every EDN is unique, carrying out a single simulation would not be adequate to draw a conclusion on the best placement of EVCs, PV generation or V2G as mentioned in Section 5.1.1. Therefore, seven parameters are varied within the simulation, and the algorithm run for each of them. This results in nineteen scenarios, including the base scenario. The eighteen additional scenarios can be seen in Table 5.1.5.1.

**Table 5.1.5.1: Additional scenarios tested within this optimisation problem.**

| 500kVA transformer changed to a: | | |
|---|---|---|
| 50kVA transformer | 200kVA transformer | |
| 1000kVA transformer | 2000kVA transformer | |
| 185mm$^2$ Al Wavecon cable changed to: | | |
| 35mm$^2$ mains plastic cable from Baker (2017). | 300mm$^2$ Al Wavecon cable from Baker (2017). | |
| Service length was changed from 15m to: | | |
| 30m | | |
| 11kV bus impedance changed to match: | | |
| Galileo Primary substation (GALI) from Scottish and Southern Electricity Networks (2019) given as R: 0.0086 p.u. and X: 0.2626 p.u. on a 100 MVA base. | Chickerell Primary substation (CERA) from Scottish and Southern Electricity Networks (2019) given as R: 0.7399 p.u. and X: 3.8974 p.u. on a 100 MVA base. | |
| One EVC connected to each phase of: | | |
| The first bus | The eleventh bus | All busses |
| One PV generator connected to each phase of: | | |
| The first bus | The eleventh bus | All busses |
| LV EDN alterations: | | |
| A red-yellow (two-phase) fault at the remote end of the LV feeder. | A red-yellow-blue (three-phase) fault at the remote end of the LV feeder. | Two LV feeders connected to bus one. The second feeder is from the LV EDN simulation used in Chapter 4. |

The network parameters mentioned above shall be explained to ensure that the values used are fully explained. In order to change the transformer size as mentioned from 500kVA to 50, 200, 1000 or 2000kVA, the type and impedance of the transformer shall remain constant. Therefore, they shall remain to be an 11kV:400V Dyn11 transformer of 4.74% impedance feeding the LV EDN, with either a lower or higher capacity. The X/R ratio of the transformer shall remain the same as Section 3.1.6. However, using the transformer size as a base, the 4.74% shall result in a higher or lower real transformer impedance measured in Ohms depending on the size of the transformer.

As mentioned, an algorithm shall be implemented to find the optimum EVC, PV generation and V2G location on the LV EDN. The algorithm will vary where the additional EVCs, PV generation or V2Gs are connected to the LV EDN and identify where the optimum POC is. This is repeated with the harmonic phase angle of EVCs, PV generation or V2Gs varied through $360^{o}$ at intervals of $45^{o}$ phase-shift with respect to the background harmonics and any EVCs or PV generation not under investigation. Therefore, there are eight tests per scenario mentioned above, one for $\pi$, $+0.75\pi$, $+0.5\pi$, $+0.25\pi$, $0\pi$, $-0.25\pi$, $-0.5\pi$ and $-0.75\pi$ radians phase-shift. In reality, within a power system there are multiple harmonic sources connected each producing harmonics at an infinite range of phase angles. However, conducting a study using randomised harmonic phase angles is not replicable, since every operation of the algorithm would result in differing phase angles, potentially leading to different results. Therefore, the use of a second algorithm could not be used to verify results. The aim of the study was to cover a range of harmonic interactions to produce a range of potential scenarios, however, there may be other scenarios resulting in different outcomes. These scenarios may change the way harmonics interact, and therefore influence the outcome of the results section.

### 5.1.6 – Effect of Harmonic Phase Shift Within the Simulation

As mentioned in Section 5.1.5, the algorithm will vary the phase shift of the EVCs, PV generation or V2Gs under investigation with respect to background harmonics and any EVCs and PV generation not under investigation. Increasing the phase shift between the EVCs, PV generation or V2Gs under investigation, the background harmonics and any EVCs and PV generation not under investigation will lead to increased harmonic cancellation. Decreasing the phase shift will lead to decreased harmonic cancellation or increased harmonic summation. This relationship can be seen in Figure 3.4.1.1. Therefore, although this method is required to ensure replicability of the tests, the method may also lead to harmonic cancellation or summation at specific points on the network. Therefore, this may lead to results which are an indication of the best POC for the specific phase shift. By looking at all eight phase shifts together, this will provide a much better indication of the best POC, rather than looking at each of the results in isolation.

# 5.2 – Optimisation of EVC POC

This section shall identify the optimal POC of EVCs across the eleven bus LV EDN for the scenarios explained in Section 5.1.5.

## 5.2.1 – EVC Model and Prediction

The EVC model used within this section shall be the same EVC model used within Sections 3.2, 3.4 and 4.2. Details of this EVC model can be seen in Figure 3.2.2.1. The EDN model consists of three EVCs at every bus, one per phase, thirty-three in total. However, an alteration to this model has been made to allow the algorithm to switch the EVC on or off via a CB as shown in Figure 3.2.2.1. Therefore, if the algorithm calls for EVCs to be connected to a particular bus, the CBs are closed. The remaining CBs are left open preventing current from flowing and the EVC contributing to the harmonics of the LV EDN.

Based on the mathematics behind harmonic voltage distortion, using Ohms law as explained in Section 1.2.1, generally speaking, it would be expected that as the EVCs are connected closer to the source, therefore reducing network impedance, the THDv would be reduced. Therefore, for most scenarios the optimum POC for EVCs would be expected to be the first bus. However, in the case of a phase-to-phase fault, the best location may not be the first bus, since this would no longer be the lowest impedance bus.

## 5.2.2 – EVC Effect

For each of the nineteen scenarios detailed in Section 5.1.5, eight phase-shift scenarios were produced. This totalled one-hundred and fifty-two individual tests, each of which would be repeated, once by EHO and once by MBO, resulting in three-hundred and four tests. By carrying out each of the tests with both algorithms, on the rare occasion that an incorrect bus was selected as producing the lowest THDv, this could be identified.

Overall, the optimum POC for EVCs is the first bus for 95% of scenarios and phase-shifts shown in Table 5.2.2.1. The first bus represents the first 5% of the LV EDN. This result is as expected for most scenarios. Considering Figure 1.2.1.1, voltage harmonics increase according to Ohms law stated in Equation 1.2.1.1. Current harmonics ($I_h$) travelling down an impedance (Z) will generate a harmonic voltage drop ($V_h$). Placement of the EVCs do not change the magnitude of $I_h$ significantly. The value that changes is Z. Therefore, by reducing Z, $V_h$ is reduced. $V_h$ relates to voltage harmonics. Identifying the lowest THDv POC is the objective of this algorithm. However, for the remaining 5% of scenarios and phase-shifts, the first bus is not the optimum POC for an EVC, these are shown in Figure 5.2.2.1, and this shall be discussed below.

For the '50kVA transformer' scenario, the results deviated from the first bus for some phase angles. These are the seventh bus for an EVC harmonic phase angle of $+0.75\pi$ radians, and the eleventh bus for an EVC harmonic phase angle of $-0.5\pi$ and $-0.75\pi$ radians. Although 63% of phase angles resulted in the first bus being the optimum POC for EVCs in this scenario, the reasons for this result shall be discussed.

**Table 5.2.2.1: Optimum EVC POC for various scenarios and phase-shifts mentioned in Section 5.1.5.**

| Bus Number | 1 | 2 | 3 | 4 | 5 | 6 | 7 | 8 | 9 | 10 | 11 |
|---|---|---|---|---|---|---|---|---|---|---|---|
| 50kVA TX | 5 | - | - | - | - | - | 1 | - | - | - | 2 |
| 200kVA TX | 8 | - | - | - | - | - | - | - | - | - | - |
| 500kVA TX | 8 | - | - | - | - | - | - | - | - | - | - |
| 1MVA TX | 8 | - | - | - | - | - | - | - | - | - | - |
| 2MVA TX | 8 | - | - | - | - | - | - | - | - | - | - |
| 35mm$^2$ Main | 8 | - | - | - | - | - | - | - | - | - | - |
| 300mm$^2$ Main | 8 | - | - | - | - | - | - | - | - | - | - |
| 30m services | 8 | - | - | - | - | - | - | - | - | - | - |
| GALI X/R | 8 | - | - | - | - | - | - | - | - | - | - |
| CERA X/R | 8 | - | - | - | - | - | - | - | - | - | - |
| PV 1$^{st}$ Bus | 8 | - | - | - | - | - | - | - | - | - | - |
| PV 11$^{th}$ Bus | 8 | - | - | - | - | - | - | - | - | - | - |
| PV All Bus | 4 | - | - | - | - | - | - | - | - | - | 4 |
| EV 1$^{st}$ Bus | 8 | - | - | - | - | - | - | - | - | - | - |
| EV 11$^{th}$ Bus | 8 | - | - | - | - | - | - | - | - | - | - |
| EV All Bus | 8 | - | - | - | - | - | - | - | - | - | - |
| 2 Ph Fault | 8 | - | - | - | - | - | - | - | - | - | - |
| 3 Ph Fault | 8 | - | - | - | - | - | - | - | - | - | - |
| 2$^{nd}$ Feeder | 8 | - | - | - | - | - | - | - | - | - | - |
| Total | 145 | - | - | - | - | - | 1 | - | - | - | 6 |
| Total (%) | 95% | 0% | 0% | 0% | 0% | 0% | 1% | 0% | 0% | 0% | 4% |

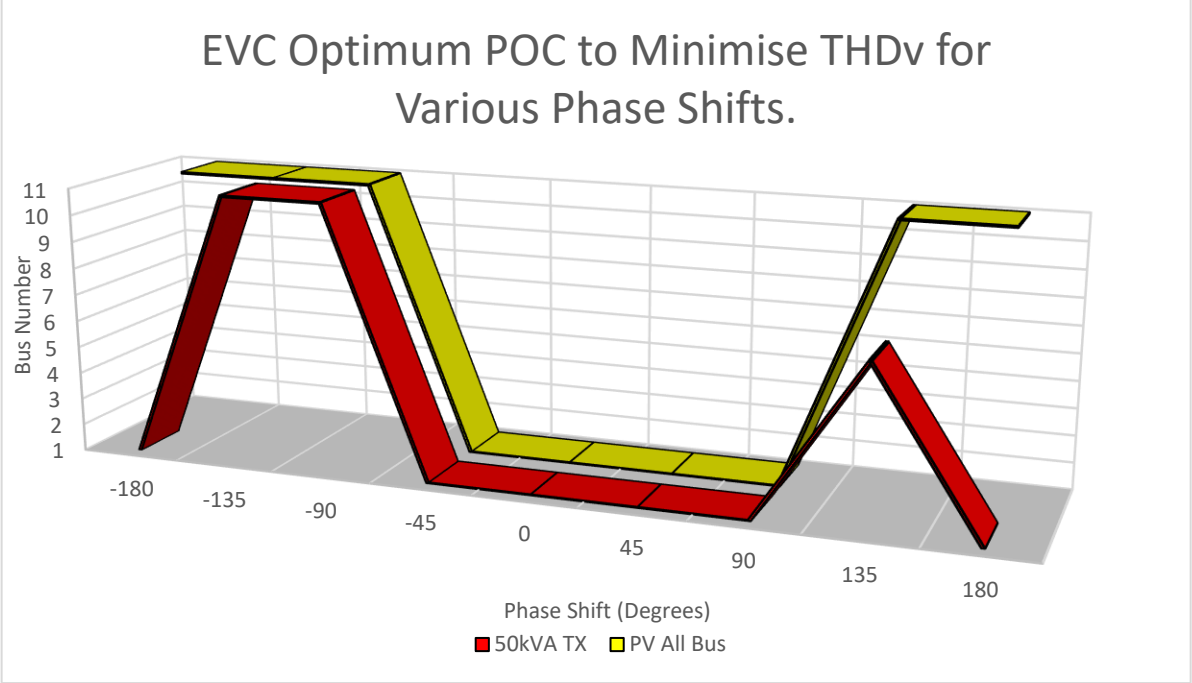


**Figure 5.2.2.1: Optimum EVC POC for eight phase-shifts, '50kVA transformer' and 'PV all bus' scenarios.**

For larger transformers, 200kVA, 500kVA, 1MVA and 2MVA, therefore having a lower impedance, the best bus was the first bus for all phase-shifts. Since the only difference between the scenarios is the size of the transformer, it must therefore be assumed that this is the reason for the deviation of results from bus one. Within the '50kVA transformer' scenario there are no additional EVCs connected to the LV EDN other than the EVC under investigation. Background harmonics have been modelled by injecting harmonic current with a $0\pi$ radians phase shift at the LV terminals of the transformer. The angle of the current harmonics injected by the EVC are relative to these current harmonics used to generate the background voltage harmonics. The phase-shift of harmonic current injected will not alter. However, the harmonic current injected will produce a proportional harmonic voltage drop across impedances in accordance with Ohms law and Section 1.2.1. Additionally, the phase angle and magnitude of the voltage harmonics produced by these current harmonics will influence the loads connected to the circuit, including the EVC. This scenario becomes incredibly complicated and almost impossible to solve via hand-calculation, with each harmonic order requiring a separate calculation, multiple load branches and the current harmonics across all three-phases and neutral interacting. Hence the reason for using simulation software to solve this problem.

However, by simplifying the problem, an overall explanation can be given. Voltage harmonics generated at the LV bus of the transformer via harmonic current injection from the EVC and background harmonic generator will produce a harmonic voltage drop as these harmonic currents flow through the transformer, along the 11kV cable and finally through the source impedance. These voltage harmonics will have both an angle and magnitude. There are eleven loads per phase on the LV EDN, each simulated as a 500W resistor at rated 240V. These resistors will draw current proportional to the voltage magnitude and angle of the LV EDN, this includes fundamental and harmonic voltages. The current drawn by these resistors will be relative to the magnitude and phase angle of the harmonic voltage at the supply terminals and will flow in the opposite direction to the currents which generated the harmonic voltage drop. It is this load harmonic current, interacting with the EVC harmonic current which will either lead to a cancellation or summation of the harmonic currents. The POC of the EVC influences the level of cancellation or summation of harmonic currents between the EVC and the loads. Furthermore, this starts a feedback loop since the resultant magnitude and phase angle of the harmonic currents will further change the voltage harmonics at different points on the EDN, influencing the harmonic currents drawn by the loads.

The reason that this applies to the ‘50kVA transformer’ scenario, not other transformer sizes is due to the small size of the transformer and therefore higher impedance. Therefore, the EVC current harmonics injected have a much greater impact on the LV EDN voltage harmonics and therefore influence harmonic current flows to a much greater extent. When the transformer size is increased, the ability of the single EVC to significantly influence the voltage harmonics at the LV bus of the transformer and therefore current harmonics drawn by the loads is reduced, therefore meaning that the first bus remains the optimum POC.

Although all of the same factors mentioned above are still at play, the 'PV all bus' scenario is much easier to explain. For phase angles of $+0.5\pi$, $+0.25\pi$, $0\pi$ and $-0.25\pi$ radians, the optimum POC was the first bus, for phase angles of $-0.5\pi$, $-0.75\pi$, $\pi$ and $+0.75\pi$ radians the optimum POC was the eleventh bus. In this scenario, both the PV generation current harmonics and background current harmonics are in phase with each other. Therefore, when the EVC current harmonics are in-phase with the PV generation and background current harmonics, the optimum POC is the first bus since this is the lowest impedance path for the current to flow. Therefore, this generates the lowest harmonic voltage drop in accordance with Ohms law stated in Section 1.2.1. When the EVC current harmonics are out-of-phase with the PV generation and background current harmonics, the optimum POC is the eleventh bus since this is the highest impedance path for current to flow. Therefore, leading to a higher amount of cancellation, lowering the overall voltage harmonic magnitude across multiple busses.

What was not expected is that the optimum EVC POC is the first bus when a two or three-phase fault is applied at the eleventh bus. In the case of a three-phase fault, EVC current destined for the yellow and blue phases must travel from the first bus to the eleventh bus along the red-phase and then from the eleventh bus to the first bus along the yellow and blue phases. Therefore, the distance the harmonic current must travel along the live conductors is increased, which is contrary to the theory using Ohms law discussed previously. However, since the neutral is not broken in these fault scenarios, the distance that harmonic current must travel along and therefore impedance must be taken into account. The first bus would result in the shortest distance for neutral current to travel back to the source.

Despite these results, it should be stated that the THDv differences between EVCs being connected to different busses was not significant. For example, in the case of the '500kVA transformer' scenario with a $0\pi$ radians phase-shift, the increase in the maximum measured THDv at all supply terminals across the LV EDN is 0.0133% for EVCs being connected at busses one and two, and 0.0127% for EVCs being connected at busses two and three. In the example of the '50kVA transformer' scenario with a $-0.5\pi$ radians phase-shift, the decrease in the maximum measured THDv at all supply terminals across the LV EDN is 0.0011% for EVCs being connected at busses one and eleven. These magnitudes of increase or decrease will have little effect on the LV EDN for small numbers of EVCs. However, the effect could become significant when EVCs start to become more numerous, leading to harmonics compounding.

### 5.2.3 – Conclusions

In conclusion, for the LV EDN studied, the optimum EVC POC with respect to harmonics is the first 5% of the network represented by the first bus for most scenarios shown in Table 5.2.2.1. This applies if balanced across all three phases as per most scenarios, or unbalanced, covered by the two and three-phase fault scenarios. This validates the prediction made in Section 5.2.1. There were however, some phase-shift scenarios, which resulted in the '50kVA transformer' and 'PV all bus' scenarios not resulting in the first bus being the optimum POC for EVCs.

The '50kVA transformer' scenario showed that for +0.75$\pi$, -0.5$\pi$ and -0.75$\pi$ radians phase angles the optimum POC was not the first bus as shown in Figure 5.2.2.1. However, by analysing the research of Dale (2018), Deilami, et al. (2010), Moses, et al. (2010), Staats, et al. (1998), Watson and Watson (2017a) and Xu, et al. (2014), it can be determined that EVCs lead to an increase in THDv on the LV system under steady state conditions assuming no other DERs are present. Therefore, $\pi$, +0.75$\pi$ and -0.75$\pi$ radians phase-shift can be ignored from the results as they would result in the harmonic current on the LV EDN reducing in magnitude. By considering the remaining phase angles, -0.5$\pi$, -0.25$\pi$, 0$\pi$, +0.25$\pi$ and +0.5$\pi$, only -0.5$\pi$ results in the optimum POC not being the first bus. Therefore, 80% of results lead to the first bus being the optimum POC for an additional EVC. Therefore, for the majority of harmonic interactions, the first bus should be considered the optimum POC for an EVC under the '50kVA transformer' scenario.

Unfortunately, the ‘PV all bus’ scenario is more complicated to analyse. Existing research is divided on how EVCs and PV generation current harmonics should combine, covered in Section 2.3. For example, results from Müller, et al. (2014) shows that some current harmonic orders summed arithmetically, whereas Watson and Watson (2017a) showed that current harmonics cancelled by up to 75%. There are also examples of variations in between these values given by Busatto, Rönnberg and Bollen (2020), Evans and MacLeman (2013), Foyer and Maruszak (2020) and Tovilović and Rajaković (2015). Therefore, the only phase angle which can be ignored is π radians as this would result in the current harmonics cancelling by 100%. Therefore in this case, four phase angles, -0.25π, 0π, +0.25π and +0.5π radians result in the first bus being the optimum POC, and, three phase angles, -0.75π, -0.5π and +0.75π radians result in the eleventh bus being the optimum POC. By analysing these results, 57% of phase angles lead to the first bus being the optimum POC. However this division, bearing in mind seven data points, is not enough of a distinction to state that the first bus will the majority of times be the optimum POC for an EVC where the LV EDN has eleven PV generation per phase, evenly distributed across the eleven busses.

Therefore, it is this thesis’ recommendation for planning purposes, that EVCs are connected as close as possible to the LV bus of the distribution transformer. The exception to this rule is in the case of the network having PV generation connected across all busses as per the ‘PV all bus’ scenario. The results of this scenario illudes to the first bus potentially being the optimum POC, however, there are not enough data points or enough of a correlation to state that this should be this thesis’ recommendation. Lastly, in the case of the ‘500kVA transformer’ scenario with a 0π radians phase-shift, the difference in the highest measured THDv at all supply terminals across the LV EDN, for an EVC being connected to the first, second or third bus was not significant. Therefore, for the connection of small numbers of EVCs, it is unlikely that connecting to other busses will have a significant impact on the overall THDv of the LV EDN.

Despite this, it should be mentioned, that there are limitations of the simulation that may have influenced the results. It was found in Section 5.2.2, that the EVC current harmonics within the '50kVA transformer' scenario had a significant impact on the harmonic voltage magnitude and phase angle at the LV bus of the transformer. Due to the base load being simulated as resistors, the harmonic voltage and phase angle directly influences the magnitude and phase angle of the harmonic currents drawn by these loads. This will in turn cause a feedback loop which will further influence the harmonic voltage and phase angle of the LV EDN. In reality, Yamini, et al. (2019) shows that although harmonic voltage of the system is a component, base load largely draws harmonic current based on the type of load rather than the harmonic voltage of the system. Despite this, it was decided within Section 3.1.8 that due to the impact that the additional complexity would have on the computation times and the reduction of control over the background voltage harmonic level, that this simplification was justified. Background voltage harmonic levels must be controlled to ensure consistency between tests. This limitation must be considered when drawing the conclusions above.

The cable model should also be mentioned. As covered in Section 3.1.5, it was decided that to simplify the simulation, the cable was modelled as several resistors and inductors in series, whereas in reality, the cable should be modelled as an infinite number of capacitors, inductors, and resistors. Since inductive impedance is proportional to frequency and capacitive impedance is inversely proportional to frequency, higher order harmonics may have been affected to a greater degree by taking this complex model into account, therefore impacting on the results. Additionally, the earthing resistance at the transformer was assumed to be 0.1Ω in Section 3.1.6. Varying this value may have impacted on the results drawn. Lastly, the algorithm determines the optimum POC based on overall THDv, not individual harmonic orders. Although THDv will be an indication of the magnitude of individual harmonic orders, it may be that a scenario with a lower THDv, but higher specific harmonic orders would have a more detrimental impact on consumers and connected equipment. This is the reason that Chapter 4 considered specific harmonic orders and compared them to limits stated within ER G5/5, however, it would be much harder to identify the optimum POC when considering individual harmonics. To do this, a weighting would need to be applied to each harmonic order, the magnitude of each order individually measured, and an overall score produced for each harmonic profile. To ensure that these scores are not subjective this would need to be based on the individual harmonic magnitudes and their magnitude compared to the limits set within ER G5/5.

# 5.3 – Optimisation of PV Generation POC

This section shall identify the optimal POC of PV generation across the eleven bus LV EDN for the scenarios explained in Section 5.1.5.

## 5.3.1 – PV Model and Prediction

The PV generation model used within this section shall be the same PV generation model used within Sections 3.3, 3.4 and 4.3. The current harmonic profile used shall be from Table 3.3.1.1. Details of this PV generation model can be seen in Figure 3.3.2.1. The LV EDN model consists of three PV generation at every bus, one per phase, thirty-three in total. However, similar to the EVC optimisation model, an alteration to this model seen in Figure 3.3.2.1 has been made to allow the algorithm to switch the PV generation on or off. Therefore, if the algorithm calls for PV generation to be connected a particular bus, the current source is switched on. The remaining current sources are switched off preventing current from flowing and the PV generation contributing to the harmonics of the LV EDN.

Based on the theory behind harmonic voltage distortion, explained in Section 1.2.1, generally speaking, it would be expected that as the PV generation is connected closer to the source, therefore reducing network impedance, the THDv would be reduced. Therefore, the optimum location for the connection of PV generation would be the first bus. However, in the case of a phase-to-phase fault, the optimum location may not be the first bus since this would no longer be the lowest impedance bus.

## 5.3.2 – PV Effect

For each of the nineteen scenarios detailed in Section 5.1.5, eight phase-shift scenarios were produced as previously covered. This totalled one-hundred and fifty-two individual tests, each of which would be repeated, once by EHO and once by MBO, resulting in three-hundred and four tests. By carrying out each of the tests with both algorithms, on the rare occasion that an incorrect bus was selected as producing the lowest THDv, this could be identified.

Overall, the optimum POC for PV generation is the first bus for 51% of scenarios or the first and second bus for 66% of scenarios and phase-shifts shown in Table 5.3.2.1. The first bus represents the first 5% of the LV EDN and the second bus represents the subsequent 10% of the LV EDN. This result is as expected for most scenarios. Considering Figure 1.2.1.1 and the explanation given at the beginning of Section 5.2.2 this would follow the prediction made in Section 5.3.1. What was not expected is that the eleventh bus was the optimum POC for 21% of the scenarios and phase-shifts. This was a considerable amount; therefore, investigation must take place.

**Table 5.3.2.1: Optimum PV generation POC for various scenarios and phase-shifts mentioned in Section 5.1.5.**

| Bus Number | 1 | 2 | 3 | 4 | 5 | 6 | 7 | 8 | 9 | 10 | 11 |
|---|---|---|---|---|---|---|---|---|---|---|---|
| 50kVA TX | 5 | - | - | - | - | - | - | 1 | - | - | 2 |
| 200kVA TX | 3 | 2 | - | 2 | - | - | - | 1 | - | - | - |
| 500kVA TX | 5 | 1 | - | - | - | - | - | - | - | - | 2 |
| 1MVA TX | 4 | 1 | - | - | 1 | - | - | - | - | - | 2 |
| 2MVA TX | 4 | 1 | - | - | - | - | - | 1 | - | - | 2 |
| 35mm$^2$ Main | 4 | 1 | - | 1 | - | - | - | - | - | - | 2 |
| 300mm$^2$ Main | 3 | 2 | - | 1 | - | - | - | - | - | - | 2 |
| 30m services | 3 | 2 | 1 | - | - | - | - | - | - | - | 2 |
| GALI X/R | 4 | 1 | - | 1 | - | - | - | - | - | - | 2 |
| CERA X/R | 3 | 2 | 1 | - | - | - | - | - | - | - | 2 |
| PV 1$^{st}$ Bus | 4 | 1 | - | - | - | - | - | - | - | - | 3 |
| PV 11$^{th}$ Bus | 4 | 1 | 1 | - | - | - | - | - | - | 1 | 1 |
| PV All Bus | 8 | - | - | - | - | - | - | - | - | - | - |
| EVC 1$^{st}$ Bus | 4 | 1 | 2 | - | 1 | - | - | - | - | - | - |
| EVC 11$^{th}$ Bus | 4 | 2 | - | - | - | - | - | - | - | 1 | 1 |
| EVC All Bus | 4 | - | - | - | - | - | - | - | - | - | 4 |
| 2 Ph Fault | 4 | 2 | - | - | - | - | - | - | - | - | 2 |
| 3 Ph Fault | 4 | 2 | - | - | - | - | 1 | - | - | - | 1 |
| 2$^{nd}$ Feeder | 4 | 1 | - | - | - | 1 | - | - | - | - | 2 |
| Total | 78 | 23 | 5 | 5 | 2 | 1 | 1 | 3 | - | 2 | 32 |
| Total (%) | 51% | 15% | 3% | 3% | 1% | 1% | 1% | 2% | 0% | 1% | 21% |

The results of Figure 5.3.2.1 shall now be investigated. Figure 5.3.2.1 varies the size of the transformer connected to the EDN. In contrast to the EVC results of Section 5.2.2 it can be seen that 200-2000kVA transformers do not result in the optimum POC always being the first bus. However, the results of the '50kVA transformer' scenario closely matches the results of the EVC scenario shown in Figure 5.2.2.1. Interestingly, as the transformer size increases and EDN impedance decreases, the results seem to flip with +0.25π and 0π phase angle changing from the first bus to the eleventh bus producing the lowest THDv. The same flipping of results applies to +0.75π, -0.5π and -0.75π phase-shift, with the optimum POC changing from the eleventh and eighth bus to the first or second bus.

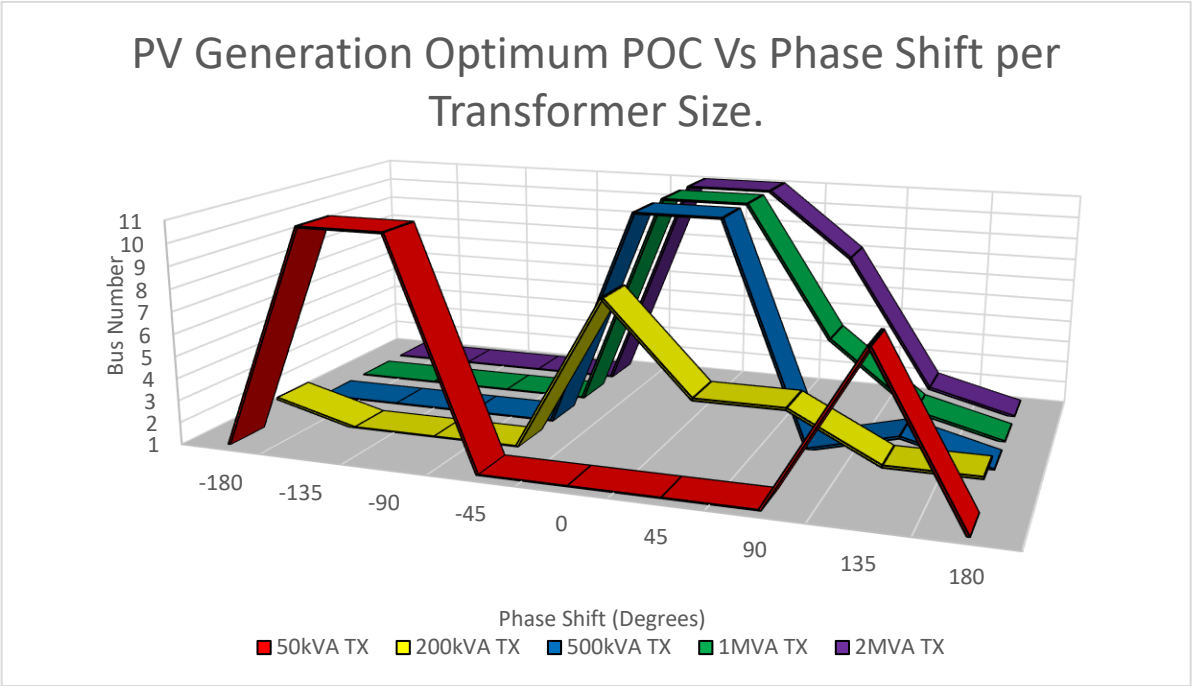


**Figure 5.3.2.1: Optimum PV generation POC for eight phase-shifts and different transformer size scenarios mentioned in Section 5.1.5.**

The explanation for the results of the '50kVA transformer' scenario can be attributed to the same reasoning stated in Section 5.2.2 and the results closely match. However, the results of the 200-2,000kVA transformers deviates from the results of Section 5.2.2. Similar to the '50kVA transformer' scenario mentioned in Section 5.2.2, the '200-2,000kVA transformer' scenarios have no additional EVCs or PV generators connected to the LV EDN other than the PV generation under investigation. Background harmonics have been modelled by injecting harmonic current with a 0π radians phase shift at the LV terminals of the transformer, similar to Section 5.2.2. The angle of the current harmonics injected by the PV generators are relative to these background current harmonics. Unlike the '50kVA transformer' scenario, the transformers in question are of a larger size and therefore, lower impedance.

Voltage harmonics generated at the LV bus of the transformer via harmonic current injection from the PV generation and the background harmonic generator will produce a harmonic voltage drop as these harmonic currents flow through the LV mains cable and transformer, along the 11kV cable and finally through the source impedance. These voltage harmonics will have both an angle and magnitude. There are eleven loads per phase on the LV EDN, each simulated as a 500W resistor at rated 240V. These resistors will draw current proportional to the voltage magnitude and phase angle of the EDN, this includes fundamental and harmonic voltages. The current drawn by these resistors will be determined by the voltage at the custormers LV supply terminals and will be at 0π radians to those voltages.

Because the '500-2,000kVA transformer' scenarios have larger transformers and therefore, a lower impedance, the PV generation current harmonics injected have a much lesser impact on the EDN voltage harmonics and as a result, influence harmonic current flows to a much lower extent. Therefore, the background harmonics are the major influence on the EDN voltage harmonics and as a result, the magnitude and phase angle of the base load current harmonics. Because of this, the optimum location of the PV generation is determined by the phase angle of the PV generation current harmonics allocated within the simulation.

The '500-2,000kVA transformer' characteristics produced in Figure 5.3.2.1 have been investigated. It has been identified that the optimum POC when the PV generator current harmonics are at 0π or +0.25π radians with reference to the current harmonics used to create the background harmonics is bus eleven. This is because additional phase shift is caused by the impedance of the mains cable between the PV generator at bus eleven and the transformer. When the transformer impedance is low, this additional impedance makes a difference in the optimum POC. Outside of those phase angles, the optimum POC is the first bus since significant phase-shift exists between the PV generators and the current harmonics used to create the background harmonics. Therefore, both of these scenarios leads to additional harmonic cancellation.

The ‘200kVA transformer’ scenario produces a result which is halfway between the results of the ‘50kVA transformer’ scenario and the ‘500-2,000kVA transformer’ scenarios. The reason quite logically is because this transformer has a higher impedance than a 500-2,000kVA transformer and a lower impedance than the 50kVA transformer. Therefore, this means that this scenario is influenced by both factors mentioned in the previous paragraphs and in Section 5.2.2 for the ‘50kVA transformer’ scenario.

However, similarly to Section 5.2.2 for the EVC scenario, the differences in THDv between the PV generation being connected to different busses was not significant. In the case of the ‘2,000kVA transformer’ scenario with 0π radians phase-shift, the difference in the maximum measured THDv at all supply terminals across the LV EDN is 0.0012% for PV generation being connected at busses one and two, 0.0004% for PV generation being connected at busses two and three, 0.0009% for PV generation being connected at busses three and six, and 0.0002% for PV generation being connected at busses six and eleven. Therefore, for a single bus to have PV generation connected, it does not make a significant difference to the THDv level for which bus the PV generation is connected to.

Following this, the results of Figure 5.3.2.2 shows the effect of cable size and service length on the bus producing the lowest THDv. The cable size and therefore cable impedance does not seem to have a significant effect on the optimum POC producing the lowest THDv. The results seem to be in line with the base scenario with 15m long services using 25mm$^2$ Cu concentric cable and 185mm$^2$ Al Wavecon mains cable. The same applies to Figure 5.3.2.3, which shows the effect of 11kV bus impedance on the busses which produce the lowest THDv. It can be seen here that variance in the 11kV bus impedance has little effect on the best POC producing the lowest THDv. However, similar to Figure 5.3.2.1 it can be noted that for +0.25π and 0π phase angle, the eleventh bus produces the lowest THDv and for the remaining phase angles the first four busses, usually the first produces the lowest THDv.

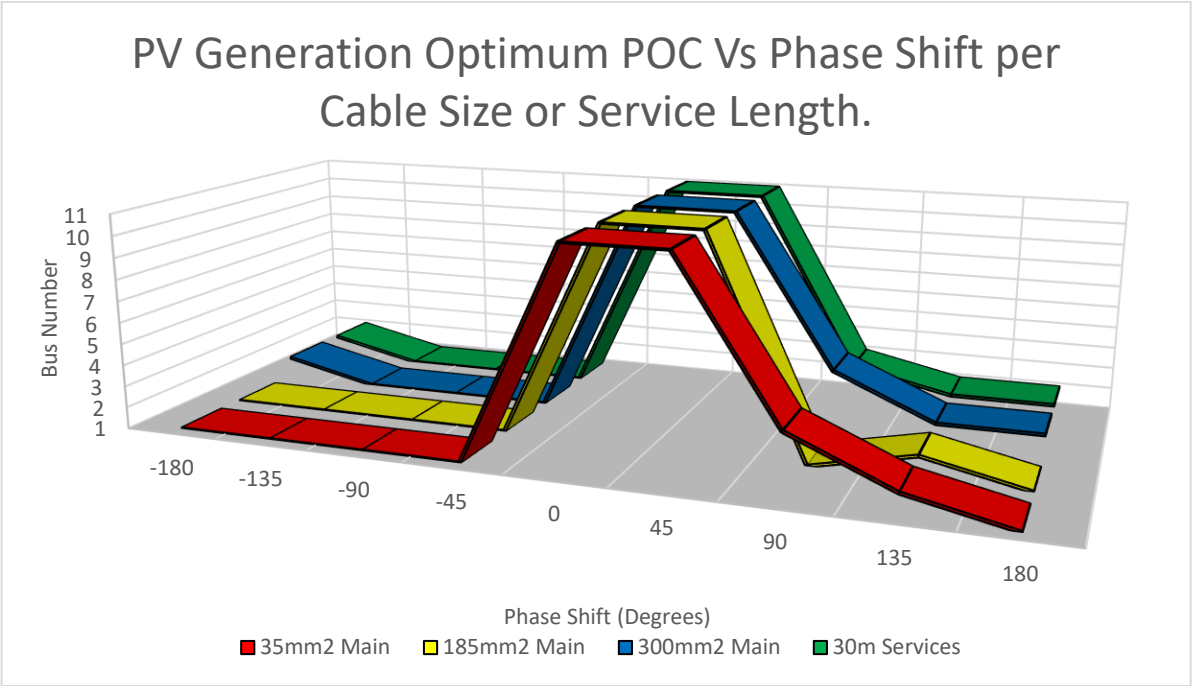


**Figure 5.3.2.2: Optimum PV generation POC for eight phase-shifts, different mains cable size and different service length scenarios mentioned in Section 5.1.5.**

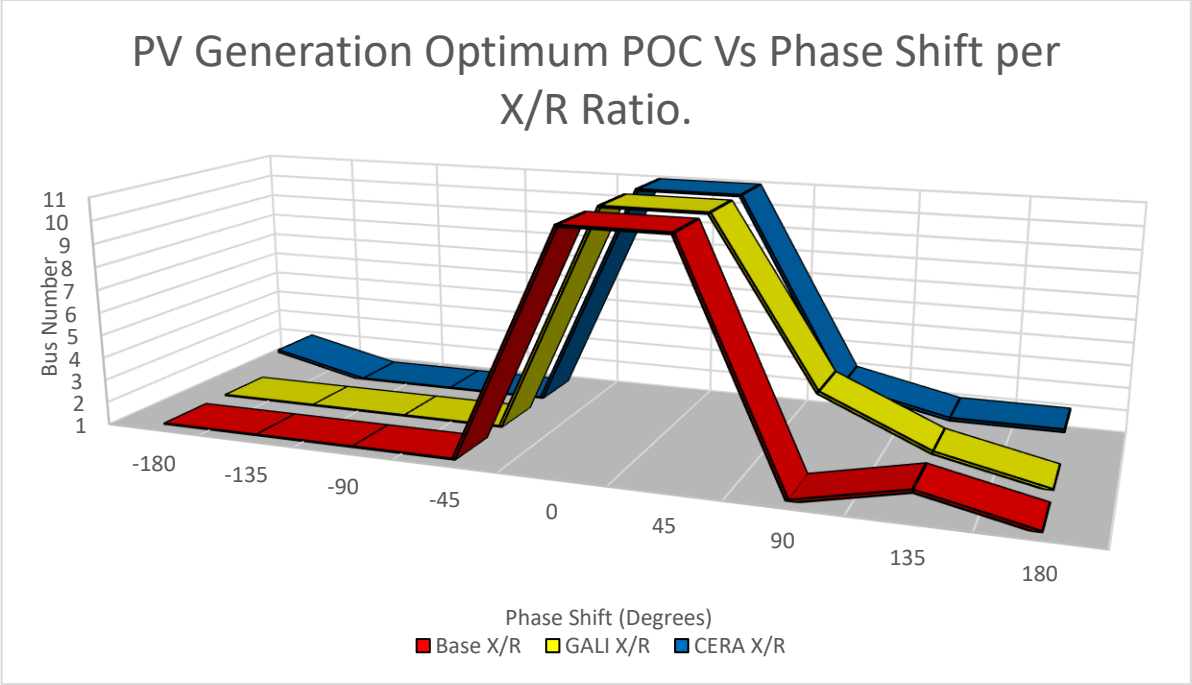


**Figure 5.3.2.3: Optimum PV generation POC for eight phase-shifts and different 11kV bus impedance scenarios mentioned in Section 5.1.5.**

The next scenarios to be discussed are the PV generation scenarios shown in Figure 5.3.2.4. When PV generation is already connected to the eleventh bus, this does not have much effect on the optimum POC for additional PV generation. However, for +0.25π phase angle, the optimum PV generation POC shifts from the eleventh bus, which is already occupied by PV generation to the tenth bus. The same can be seen for the scenario with PV generation connected to the first bus. For +0.5π phase angle the optimum PV generation POC shifts from bus one to bus eleven. Where there are PV generators connected at all busses, one through eleven. The optimum POC for additional PV generation is always the first bus, regardless of the phase angle. This is a significant shift from the base scenario but is in line with the results achieved during Section 5.2.2 for the 'EVC all bus' scenario. The reasoning for this is that the dominant current harmonics on the LV EDN are from the PV generators. Since there are thirty-six PV generators all in phase with each other, this negates any benefit created from the additional phase-shift produced by connecting the additional PV generators to bus eleven when PV generator current harmonics are at 0π or +0.25π radians with reference to the current harmonics used to create the background harmonics. In this case, placing the additional PV generation at the first bus results in the lowest impedance path and therefore, lowest voltage harmonic levels.

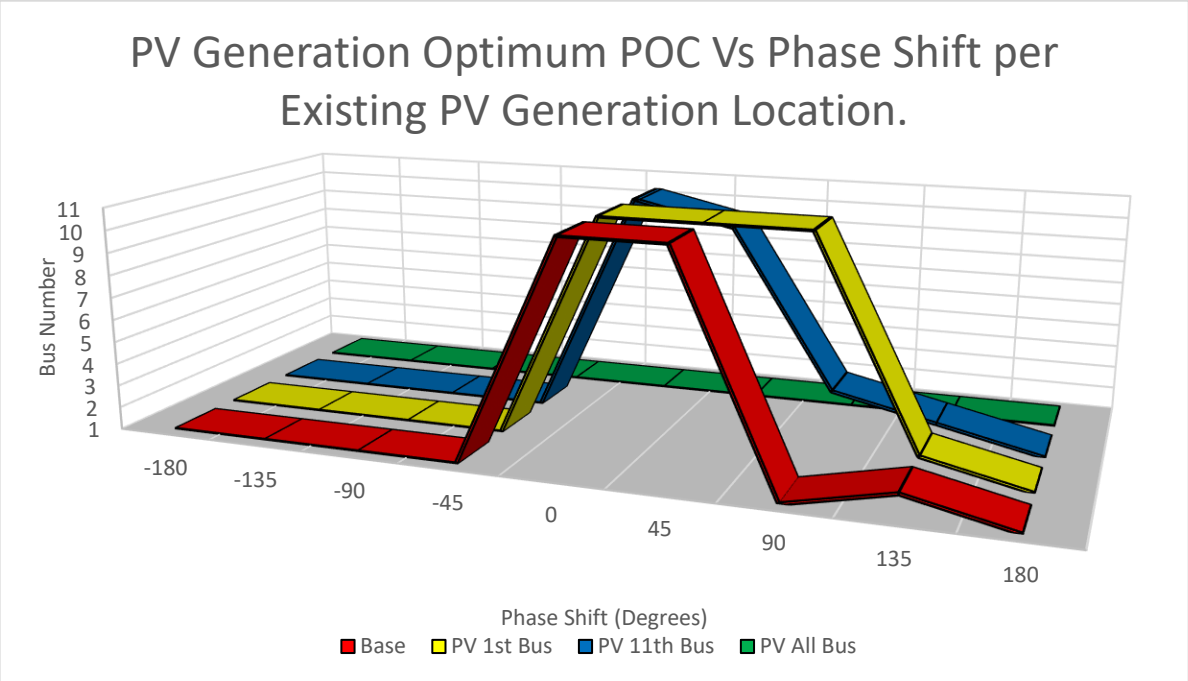


**Figure 5.3.2.4: Optimum PV generation POC for eight phase-shifts and different PV generation scenarios mentioned in Section 5.1.5.**

Similar to the last scenario, the next scenario covers the optimum POC for PV generation when EVCs are already connected to the LV EDN as shown in Figure 5.3.2.5. When EVCs are connected to the eleventh bus, this does not have much effect on the optimum POC for additional PV generation. However, for +0.25π radians phase angle the optimum PV generation POC shifts from the eleventh bus, which is already occupied by EVCs to the tenth bus. This is very similar to Figure 5.3.2.4. What is not similar to Figure 5.3.2.4 is the optimum POC to connect PV generation when an EVC is connected to the first bus. The optimum POC can be seen to be the first bus for half of the phase angles and no higher than the fifth bus. Lastly, for the scenario when EVCs are connected to all busses, the results appear to invert except for +0.5π and -0.25π radians phase angle scenarios.

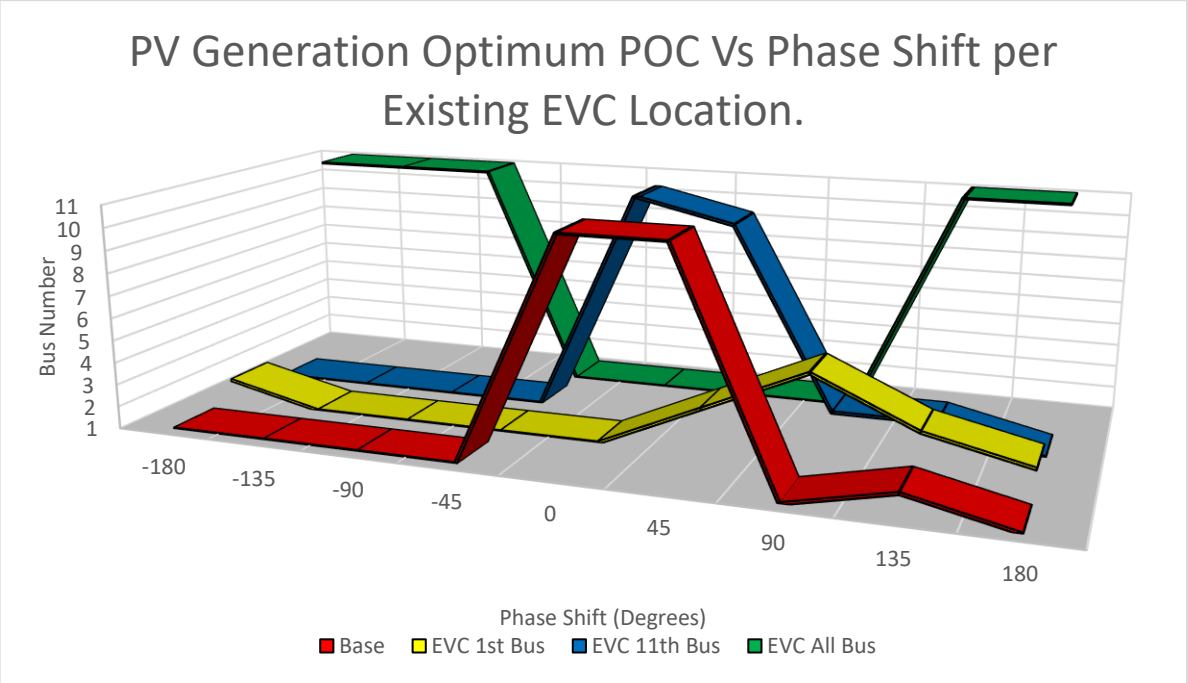


**Figure 5.3.2.5: Optimum PV generation POC for eight phase-shifts and different EVC scenarios mentioned in Section 5.1.5.**

The reasons for the difference between the base scenario and the 'EVC first bus' scenario is caused by minor interactions between harmonics. For the 'EVC first bus' scenario, the maximum difference in THDv measured when the phase angle of the PV generators are set at 0π radians is 0.00001% both between the first and second bus, and the first and eleventh bus. Due to the minor differences in maximum THDv between busses, this shall not be investigated further.

The reason for the difference between the base scenario and the 'EVC all bus' scenario is due to the phase angle of the harmonics drawn by the EVCs. The EVC current harmonics and their phase angle are the dominant harmonic currents within the LV EDN. Therefore, in line with the 'PV all bus' scenario within Section 5.2.2, when the PV generation current harmonics are out of phase with the EVC current harmonics for phase angles of -0.5$\pi$, -0.75$\pi$, $\pi$ and +0.75$\pi$ radians, the optimum PV generation POC is bus eleven since this provides the highest impedance path for the currents to flow. When the PV generation current harmonics are in phase with the EVC current harmonics for phase angles of +0.5$\pi$, +0.25$\pi$, 0$\pi$ and -0.25$\pi$ radians, the optimum PV generation POC is the first bus since this provides the lowest impedance path for the current harmonics to flow.

The last scenarios to be considered covers the optimum POC for PV generation during different network arrangements seen in Figure 5.3.2.6. Comparing the second feeder, two-phase and three-phase fault scenarios to the normal network arrangements, it can be seen that these scenarios have very little effect on the optimum placement of PV generation on the network. However, a three-phase fault does result in the optimum POC diverging from the eleventh bus for +0.25π radians phase angle. A similar result applies to the second feeder scenario where the optimum POC diverges from the first bus for +0.5π radians phase angle.

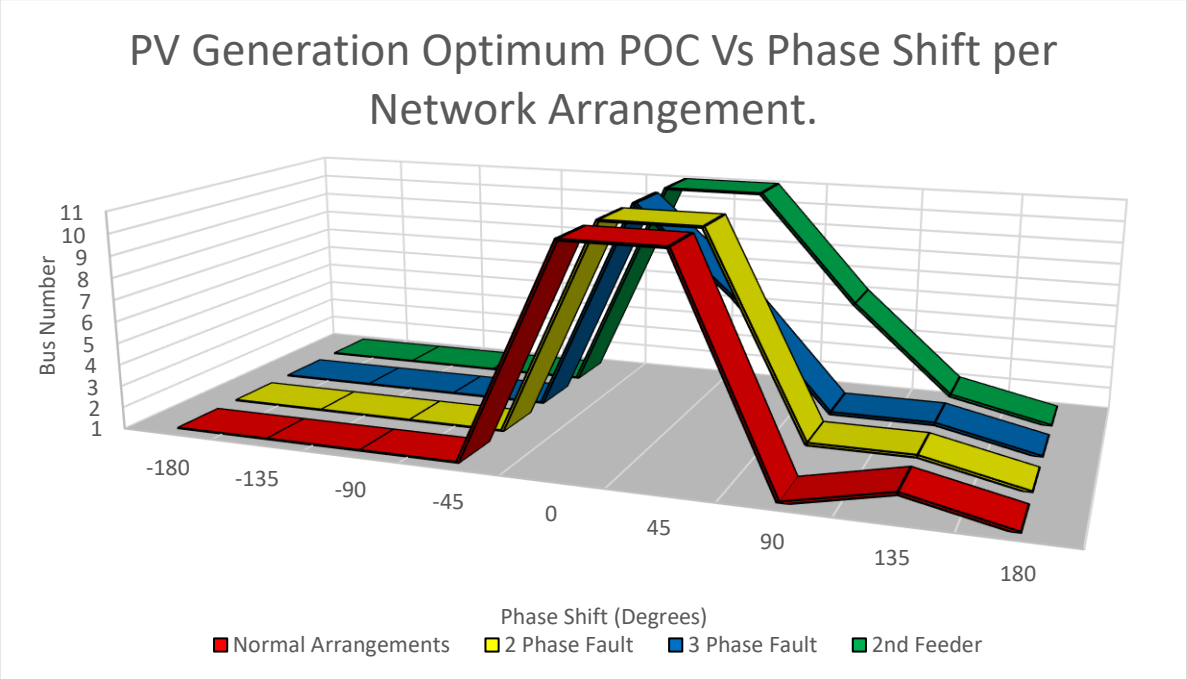


**Figure 5.3.2.6: Optimum PV generation POC for eight phase-shifts and different network arrangement scenarios mentioned in Section 5.1.5.**

For the three-phase fault scenario, the optimum POC for +0.25π radians phase angle deviates from the base scenario and is closer to the first bus than the base scenario at the seventh bus. This is in opposition to the prediction in Section 5.3.1. Additionally, it was expected for the two-phase fault scenarios best POC to deviate from the first bus when compared to the base scenario. The same situation was found for EVCs within Section 5.2.2.

From analysing the results of the three-phase fault scenario for +0.25π radians, it was found that connecting the PV generation to the eleventh bus rather than the first bus resulted in a higher fundamental current magnitude at the transformer increasing by 0.06A from 56.79A to 56.85A rms, but a lower third harmonic magnitude of 0.47A compared to 0.48A rms. Both of these busses resulted in a higher THDv of 1.3943% and 1.3945% for the first and eleventh busses. However, the seventh bus was a sweet spot producing a current magnitude of 56.84A rms and third harmonic magnitude of 0.47A rms. This resulted in a THDv of 1.3890%. Despite this, it can be seen that neither of these busses make a huge difference to the THDv of the network, just 0.0053-0.0055%.

Secondly, the ‘second feeder’ scenario results in additional fundamental current travelling to the second feeder. At +0.5π radians phase-shift, the sixth bus was identified as the best POC. When comparing the first, sixth and eleventh busses, the maximum difference in measured THDv at all supply terminals across the LV EDN is 0.00557% for PV generation being connected at busses one and six, and 0.00002% for PV generation being connected at busses six and eleven. Therefore, there is very little difference between connecting the PV generation to the sixth or eleventh bus, however, other scenarios in Figure 5.2.3.6 identified the first or second bus as being the optimum POC at +0.5π radians phase-shift which is not the case for the ‘second feeder’ scenario. It should be noted however, that in order to keep the methodology the same, only feeder one THDv levels are monitored. Therefore, although this may be the best point of coupling with respect to minimising THDv on feeder one, it may not be with respect to the overall THDv across both feeders one and two.

### 5.3.3 – Conclusions

For the LV EDN studied, generally for all phase-shifts, the optimum PV generation POC with respect to THDv is the first bus for 51% of scenarios or the first and second bus for 66% of scenarios and phase-shifts shown in Table 5.3.2.1. This applies if balanced across all three phases as per most scenarios, or unbalanced, covered by the two and three-phase fault scenarios. This validates the prediction made in Section 5.3.1. However, for 21% of the scenarios and phase-shifts, the eleventh bus was the optimum POC. Additionally, there were a number of further results placing the optimum POC in between these values.

Firstly, the scenarios which varied the transformer size will be covered as shown in Figure 5.3.2.1. Similar to Section 5.2.3, existing research such as Busatto, Bollen and Rönnberg (2018) and De Silva, Jayamaha and Lidula (2019) show that PV generation leads to an increase in THDv on the LV system under steady state conditions, assuming no other DERs are present. Therefore, π, +0.75π and -0.75π radians phase-shift can be ignored from the results as they would result in the harmonic voltage on the LV EDN reducing in magnitude. By considering the remaining phase angles, -0.5$\pi$, -0.25$\pi$, 0$\pi$, +0.25$\pi$ and +0.5$\pi$ radians, only -0.5$\pi$ radians results in the optimum POC for the '50kVA transformer' scenario not being the first bus. Conversely, for 500-2000kVA transformers, 0$\pi$ and +0.25$\pi$ radians results in the eleventh bus being the optimum POC, -0.5π and -0.25π radians results in the first bus being the optimum POC, and, +0.5$\pi$ radians results in a mixture of the first, fifth and eighth busses being the optimum POC. For the '200kVA transformer' scenario, -0.5π and -0.25π radians results in the first bus being the optimum POC; 0$\pi$, +0.25$\pi$ and +0.5$\pi$ radians results in a mixture of the fourth and eighth busses being the optimum POC.

Based on the results obtained, it would appear that for a small transformer size of 50kVA, the optimum POC for PV generation would generally, when considering multiple phase-shifts, be the first bus. However, for 200-2000kVA transformers, conclusions are much more difficult to draw. Therefore, Table 5.3.3.1 has been produced to try and determine patterns and investigate the characteristics shown in Figures 5.3.2.1 and 5.3.2.3. The scenarios shown in Table 5.3.3.1 were selected as Figure 5.3.2.1 showed a clear change in characteristics as transformer capacity increased and therefore EDN impedance decreased.

**Table 5.3.3.1: ΔTHDv for PV generation POC between busses one and eleven for selected scenarios and phase-shifts from Section 5.1.5.**

| Phase-Shift | | Scenario | | | | |
|---|---|---|---|---|---|---|
| | | 200kVA | 500kVA | 1000kVA | 2000kVA | GALI X/R |
| $\pi$ | Better Bus 1/11 | 1 | 1 | 1 | 1 | 1 |
| | ΔTHDv | 0.0004% | 0.0000% | 0.0056% | 0.0061% | 0.0010% |
| $+0.75\pi$ | Better Bus 1/11 | 11 | 1 | 11 | 11 | 11 |
| | ΔTHDv | 0.0037% | 0.0002% | 0.0023% | 0.0016% | 0.0032% |
| $+0.5\pi$ | Better Bus 1/11 | 11 | 1 | 11 | 11 | 11 |
| | ΔTHDv | 0.0034% | 0.0000% | 0.0033% | 0.0029% | 0.0059% |
| $+0.25\pi$ | Better Bus 1/11 | 1 | 11 | 11 | 11 | 11 |
| | ΔTHDv | 0.0029% | 0.0042% | 0.0046% | 0.0046% | 0.0047% |
| $0\pi$ | Better Bus 1/11 | 1 | 11 | 11 | 11 | 11 |
| | ΔTHDv | 0.0022% | 0.0000% | 0.0022% | 0.0027% | 0.0013% |
| $-0.25\pi$ | Better Bus 1/11 | 1 | 1 | 1 | 1 | 1 |
| | ΔTHDv | 0.0030% | 0.0031% | 0.0019% | 0.0013% | 0.0027% |
| $-0.5\pi$ | Better Bus 1/11 | 1 | 1 | 1 | 1 | 1 |
| | ΔTHDv | 0.0039% | 0.0069% | 0.0066% | 0.0062% | 0.0051% |
| $-0.75\pi$ | Better Bus 1/11 | 1 | 1 | 1 | 1 | 1 |
| | ΔTHDv | 0.0040% | 0.0000% | 0.0049% | 0.0080% | 0.0044% |

Table 5.3.3.1 shows that within the range of phase angles considered, $-0.5\pi$, $-0.25\pi$, $0\pi$, $+0.25\pi$ and $+0.5\pi$ radians, and when only considering busses one and eleven, generally the better POC is bus eleven for a transformer capacity of 1000kVA or higher. The 500kVA transformer scenario is unclear, due to two phase-shifts within the considered range having 0.0000% THDv difference between the first and eleventh bus. Therefore, the optimum POC can easily be influenced by other factors. This can be seen within many phase angle data points given in Figures 5.3.2.1-6.

The 200kVA transformer scenario is the only one within Table 5.3.3.1 that has clear results. Of the phase angles considered, only one of the better POCs is bus eleven, leaving four which are bus one. Additionally, within the phase angle range considered there are clear differences in THDv between bus one and bus eleven.

Without knowing the exact phase angle of all harmonics on the EDN, and the phase angle of the devices to be connected, it will be very hard to determine a conclusion which applies to all EDNs. However, based on the data presented in Figure 5.3.2.1 and Table 5.3.3.1, it can be determined that if applied to the National Grid as a whole, generally, the first bus is the optimal POC for the '50kVA transformer' scenario. Additionally, if applied to the National Grid as a whole, generally, the first bus, or first few busses should minimise overall LV EDN THDv levels and should be treated as the optimum POCs for the '200kVA transformer' scenario. Due to the variability and lack of THDv differential between the first and eleventh bus, a general recommendation should not be stated for the '500kVA transformer' scenario. Furthermore, due to the variability of optimum POC and THDv between the first and eleventh bus, a general conclusion should not be provided for the 1000kVA and 2000kVA transformer scenarios.

A similar conclusion can be drawn for the scenarios which vary cable size, service length and X/R ratio as per Figures 5.3.2.2-3 which are based on the '500kVA transformer' scenario. Again, by excluding π, +0.75π and -0.75π radians phase-shift, the remaining phase angles, -0.5$\pi$, -0.25$\pi$, 0$\pi$, +0.25$\pi$ and +0.5$\pi$ radians do not provide consistent enough answers to determine a definitive conclusion. Furthermore, by considering the 'GALI X/R' scenario within Table 5.3.3.1, a similar pattern to the 1000kVA and 2000kVA transformer scenarios can be seen. Therefore, similar to the '500kVA transformer' scenario, a general conclusion on optimal POC should not be provided.

For the 'PV all bus' scenario shown in Figure 5.3.2.4, it can clearly be seen that the first bus is the optimum POC when PV penetration levels are high. The same result does not appear to be valid when one PV generation is connected per phase at a single bus. In the case of PV generation on the first and eleventh bus scenarios, and by excluding π, +0.75π and -0.75π radians phase-shift, the optimum POC is not clear. Results vary between the first, third, tenth and eleventh busses as per Table 5.3.2.1. However, it can be seen that the additional PV generation tries to avoid connecting to the same bus for specific phase angles. This can be seen at +0.25π radians and +0.5π radians when PV generation is connected to the eleventh and first bus respectively. The 'PV first bus' and 'PV eleventh bus' scenarios generally mirror and are based on the '500kVA transformer' scenario. Therefore, similar to the '500kVA transformer' scenario, a general recommendation on optimal POC for the 'PV first bus' and 'PV eleventh bus' scenarios should not be provided.

When considering the interaction of PV generation and EVCs shown in Figure 5.3.2.5, only π radians phase-shift can be excluded as per Müller, et al. (2014) and Watson and Watson (2017a) which was previously mentioned in Section 5.2.3. The 'EVC all bus' scenario shows that 50% of phase angles result in the first bus being the optimum POC, and the reverse stating that the eleventh bus is the optimum POC. If harmonic currents are assumed to sum as per Müller, et al. (2014), all data points except for -0.5π radians result in the first bus being the optimum POC. If the harmonic currents are assumed to cancel as per Watson and Watson (2017a), the eleventh bus would be the optimum POC. In the case of an EVC being connected to the first bus, the results deviate from the base scenario by fluctuating between the first, second, third and fifth busses. Therefore, the first half of the network contains all of the optimum POCs. However, as stated within Section 5.3.2, the maximum difference in THDv measured when the phase angle of the PV generators are set at 0π radians is 0.00001% both between the first and second bus, and the first and eleventh bus. Therefore, there is not enough of a THDv differential between busses to draw a clear conclusion. This is likely attributed to the lack of THDv differential between busses for the '500kVA transformer' scenario with which the 'EVC first bus' and 'EVC eleventh bus' scenarios share many of the same characteristics. Therefore, for the reasons mentioned, a general conclusion regarding the optimal POC for these two scenarios cannot be drawn.

When considering the different network arrangements shown in Figure 5.3.2.6, the scenarios are based on, and the results generally mirror the '500kVA transformer' scenario. Therefore, for the reasons mentioned for the '500kVA transformer' scenario, a general recommendation regarding the optimal POC cannot be drawn.

Therefore, it is this thesis' general recommendation that for planning purposes, when considering the spectrum of possible phase-shifts, that PV generation is connected to the first bus, or first few busses of the distribution transformer for the '50kVA transformer,' '200kVA transformer' and 'PV all bus' scenarios. If applied to the National Grid as a whole, generally, the first bus, or first few busses should minimise overall LV EDN THDv levels. The reason for stating this is that, as seen in Figure 5.3.2.1, there may be specific phase-shift scenarios which lead to other busses being the optimum POC. A general recommendation regarding optimum POC outside of the scenarios stated cannot be given. Further simulation of the scenarios covered in Figures 5.3.2.2-6 should be undertaken for 50kVA, 200kVA, 1000kVA and 2000kVA transformers to expand the validity of recommendations previously mentioned outside of the specific scenarios stated.

The same limitations mentioned in Section 5.2.3 are valid. These include base load current harmonics, cable model and THDv comparison measurements, rather than individual harmonic levels.

Lastly, due to the small changes in THDv identified between different POCs such as those mentioned earlier in this conclusion, it may be more beneficial for a DNO to consider THDv levels, but ultimately make decisions on the chosen POC based on voltage and loading constraints. This particularly applies to scenarios sharing the majority of characteristics with the '500kVA transformer' scenario. Voltage and loading issues would lead to costly infrastructure upgrades requiring excavation and disruption, whilst THDv levels might be resolved by implementing filters, which could be connected above ground, requiring much lower initial outlay and disturbances.

## 5.4 – Optimisation of V2G POC

Based on the research gaps referenced in Section 2.4.3, the best location for an EVC to be capable of operating as a V2G for reducing THDv levels on the EDN will be established within this section. As mentioned in Section 2.4.3, this assessment should be carried out whilst there are significant penetrations of EVCs on the network. Therefore, it was decided that the EDN model previously used in Sections 5.2-3 shall consist of three V2G capable EVCs at every bus, one per phase, thirty-three in total. The changes to the LV EDN for the optimisation of V2G when compared to Figure 5.1.5.1 can be seen below in Figure 5.4.1. Section 2.4.3 also states that changes in network parameters and different network arrangements must also be considered.

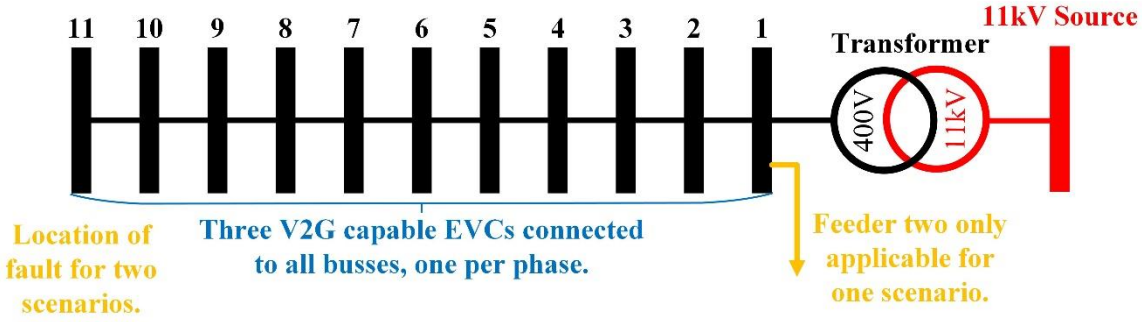


**Figure 5.4.1: Electrical layout of the LV EDN for V2G POC optimisation.**

## 5.4.1 – V2G Model and Prediction

The V2G model used within this section shall be based on the PV generation model used within sections 3.3, 3.4, 4.3 and 4.4. Details of this PV generation model can be seen in Figure 3.3.2.1. Casalerio, et al. (2021) states that models used to represent the power quality of PV generation are suitable to represent the behaviour of V2G systems. However, the current harmonic profile of the model needed to be changed. The EVC model with V2G capability can be seen in Figure 5.4.1.1.

Based on the research carried out in Section 2.4.1, it was felt that a THDi level of 7.82% from Tan, Chen, Zhou and Zhang (2019) was appropriate to represent a V2G. This value is in line with the research carried out by Casaleiro, et al. (2021), Ekström and Leijon (2014) and Grasel, Baptista and Tragner (2022) at an output of between 50-75%. However, the value is slightly higher than Pinto, et al. (2017), Magnum Cap (2018) and Monteiro, Pinto and Alfonso (2019) without the iV4G algorithm implemented. As mentioned, the values stated by Magnum Cap (2018) should not be taken at face value since the value given on manufacturer specification sheets are generally not achievable outside of lab conditions. Additionally, at rated power, Monteiro, Pinto and Alfonso (2019) state that V2G will produce a higher THDi magnitude than G2V. Tan, Chen, Zhou and Zhang (2019) used measured values obtained from a single-phase 220V, 10kW four-leg inverter. Based on this value being measured rather than simulated, and being in line with with similar papers mentioned above, this source can be treated as reliable. The current harmonic profile generated by Tan, Chen, Zhou and Zhang (2019) can be seen in Table 5.4.1.1.

In order to ensure consistency throughout the simulations and to ensure the optimum location of V2G was not determined based on power output alone, the power output of the EVC and V2G were matched. The difference was within the phase angle of the current produced. The EVC drew a current of 3.05kW and 3.28kVA as per Pinto, et al. (2017) and Section 3.2.2. In contrast, the V2G was set to generate 3.28kW and 0kVA. This was determined based on measured data from Casaleiro, et al. (2021), Grasel, Baptista and Tragner (2022) and Monteiro, Pinto and Alfonso (2019). Casaleiro, et al. (2021) shows that between 50-100% of maximum output, the power factor of the V2G is 1.00. This is supported by Grasel, Baptista and Tragner (2022), quoting the same figure of between 50-100%. Lastly, Monteiro, Pinto and Alfonso (2019) published a measured power factor value of 0.99.

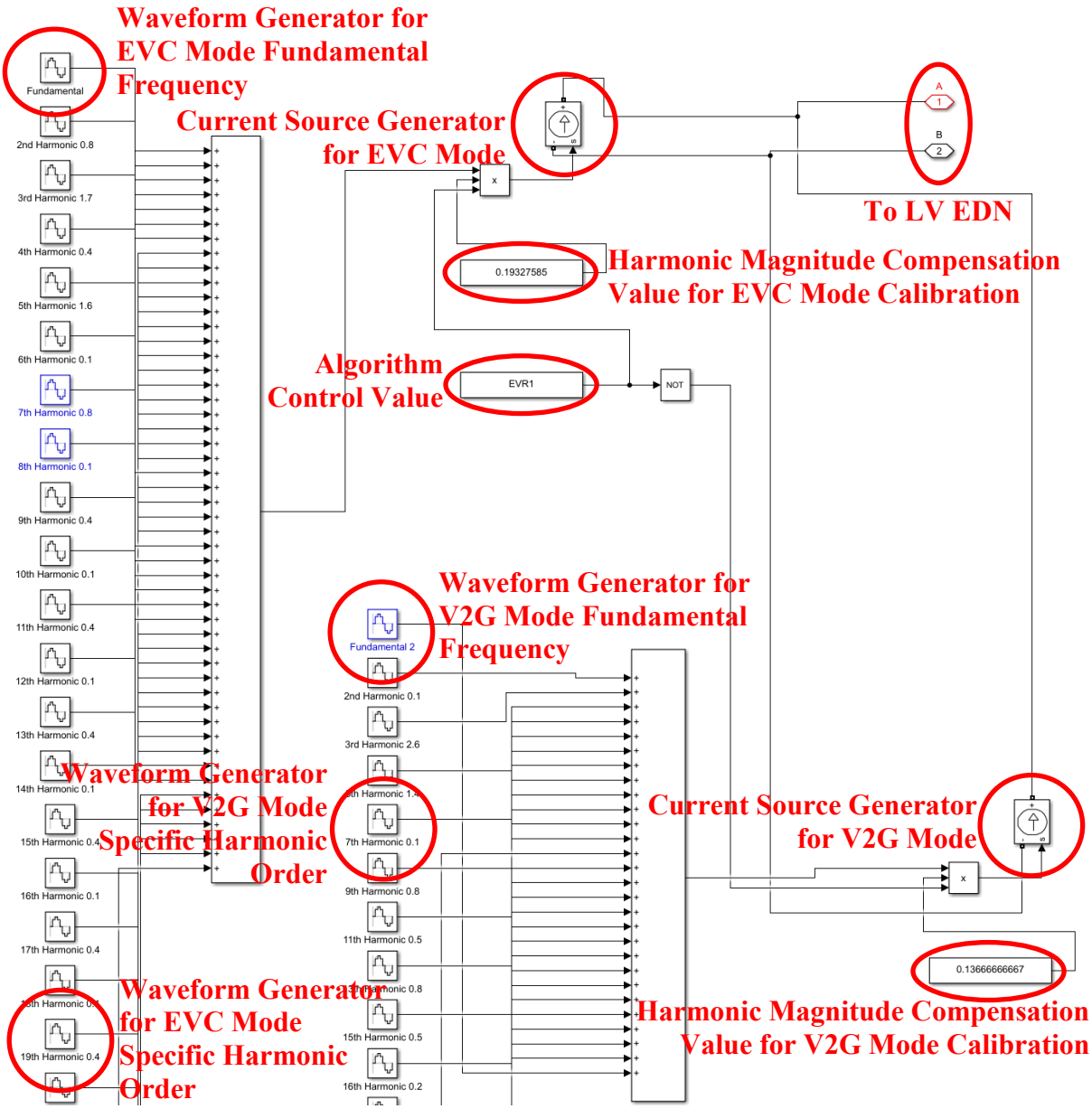


**Figure 5.4.1.1: Overview of the simulated single-phase V2G capable EVC using Simulink (The Mathworks, Inc., 2021).**

**Table 5.4.1.1: Table of the current harmonic profile of a V2G measured by Tan, Chen, Zhou and Zhang (2019).**

| Harmonic Order | THDi | 2 | 3 | 4 | 5 | 6 | 7 | 8 | 9 | 10 |
|---|---|---|---|---|---|---|---|---|---|---|
| Percentage of Fundamental (%) | 7.82 | 0.52 | 3.19 | 0.84 | 5.28 | 0.52 | 2.05 | 0.69 | 1.50 | 0.42 |
| Harmonic Order | 11 | 12 | 13 | 14 | 15 | 16 | 17 | 18 | 19 | 20 |
| Percentage of Fundamental (%) | 0.41 | 0.38 | 0.80 | 0.08 | 0.65 | 0.49 | 1.65 | 0.17 | 0.91 | 0.91 |
| Harmonic Order | 21 | 22 | 23 | 24 | 25 | 26 | 27 | 28 | 29 | 30 |
| Percentage of Fundamental (%) | 0.83 | 0.33 | 0.74 | 0.27 | 0.22 | 0.19 | 0.32 | 0.03 | 0.11 | 0.11 |
| Harmonic Order | 31 | 32 | 33 | 34 | 35 | 36 | 37 | 38 | 39 | 40 |
| Percentage of Fundamental (%) | 0.01 | 0.03 | 0.09 | 0.02 | 0.06 | 0.08 | 0.02 | 0.06 | 0.14 | 0.01 |
| Harmonic Order | 41 | 42 | 43 | 44 | 45 | 46 | 47 | 48 | 49 | 50 |
| Percentage of Fundamental (%) | 0.01 | 0.06 | 0.05 | 0.00 | 0.02 | 0.01 | 0.03 | 0.00 | 0.01 | 0.00 |

Additionally, as mentioned, the best location for a V2G capable EVC should be obtained for an LV EDN with EVCs connected to all busses. Therefore, for this study, the EVC and V2G model shall be merged together into a single model with a separate current source for the EVC component and V2G components. The current sources shall then control whether the EVC or V2G is connected to the network. The current sources shall be controlled by the algorithm. Therefore, if the algorithm calls for V2G to be connected at a particular bus, the current source controlling the V2G shall be on and the current source controlling the EVC shall be off. If the algorithm does not call for V2G to be connected at the remaining busses, the current source controlling the V2G shall be off and the current source controlling the EVC shall be on. Unfortunately, for the algorithm to work as expected, the EVC model needed to be simplified and the resistor and inductor combination used in Sections 5.2 and 5.3 needed to be updated to a fundamental current source with a phase angle matching that of the resistor and inductor combination.

Since the THDi of V2G is over double the magnitude of the THDi of EVCs shown in Section 3.2.2, it would be expected that when V2G and EVC current harmonics are in phase, the optimum location for V2G to be active would be the first bus. When V2G and EVC harmonics are out of phase, the optimum location for V2G to be active would be the eleventh bus since harmonic cancellation across a greater impedance would reduce the overall THDi level, therefore, reducing the harmonic voltage drop. This is in line with the results of the ‘PV all bus’ and ‘EVC all bus’ scenarios within Sections 5.2.2 and 5.3.2 respectively. However, in the case of a phase-to-phase fault, the best location may not be the first bus, since this would no longer be the lowest impedance bus.

## 5.4.2 – V2G Effect

Due to the methodology of this section which places three V2G capable EVCs at all busses, one per phase, the scenarios which include additional EVCs at busses have been excluded, therefore reducing the number of scenarios from nineteen within Section 5.1.5 to sixteen. For each of the sixteen scenarios, eight phase-shift scenarios were produced as previously covered. This totalled one-hundred and twenty-eight individual tests, each of which would be repeated, once by EHO and once by MBO, resulting in two-hundred and fifty-six tests. By carrying out each of the tests with both algorithms, on the rare occasion that an incorrect bus was selected as producing the lowest THDv, this could be identified.

Overall, the optimum POC for V2G is the eleventh bus for 73% of scenarios and phase-shifts shown in Table 5.4.2.1. The eleventh bus represents the last 5% of the LV EDN. This result was expected when the V2G and EVC harmonics were out of phase, or there is a significant amount harmonic phase-shift as seen in Table 5.4.2.1. However, there are a number of results which did not fit this prediction, including but not limited to, the 50kVA, 200kVA, 1000kVA and 2000kVA transformer scenarios. Therefore, investigation must take place to determine the reasoning for this.

**Table 5.4.2.1: Optimum V2G POC for various scenarios and phase-shifts mentioned in Section 5.1.5.**

| Bus Number | 1 | 2 | 3 | 4 | 5 | 6 | 7 | 8 | 9 | 10 | 11 |
|---|---|---|---|---|---|---|---|---|---|---|---|
| 50kVA TX | - | - | - | - | - | - | - | - | - | - | 8 |
| 200kVA TX | - | - | - | - | - | - | - | - | - | - | 8 |
| 500kVA TX | 2 | - | - | - | - | - | - | - | - | - | 6 |
| 1MVA TX | 2 | - | - | - | - | - | 3 | - | 2 | - | 1 |
| 2MVA TX | 6 | 2 | - | - | - | - | - | - | - | - | - |
| 35mm$^2$ Main | 1 | - | - | - | - | - | - | - | - | 1 | 6 |
| 300mm$^2$ Main | 1 | - | - | - | - | - | - | - | - | 1 | 6 |
| 30m services | 2 | - | - | - | - | - | - | - | 1 | - | 5 |
| GALI X/R | 1 | - | - | - | - | - | - | - | - | 1 | 6 |
| CERA X/R | - | - | - | - | - | - | - | - | - | 1 | 7 |
| PV 1$^{st}$ Bus | 1 | - | - | - | - | - | - | - | - | - | 7 |
| PV 11$^{th}$ Bus | 1 | - | - | - | - | - | - | - | - | 1 | 6 |
| PV All Bus | 1 | - | - | - | - | - | - | - | - | - | 7 |
| 2 Ph Fault | - | - | - | - | - | - | - | - | - | 1 | 7 |
| 3 Ph Fault | 1 | - | - | - | - | - | - | - | - | - | 7 |
| 2$^{nd}$ Feeder | 1 | - | - | - | - | - | - | - | 1 | - | 6 |
| Total | 20 | 2 | - | - | - | - | 3 | - | 4 | 6 | 93 |
| Total (%) | 16% | 1% | 0% | 0% | 0% | 0% | 2% | 0% | 3% | 5% | 73% |

The results of Figure 5.4.2.1 shall now be investigated. Figure 5.4.2.1 varies the size of the transformer connected to the EDN. In contrast to the EVC and PV generation results from Sections 5.2.2 and 5.3.2 it can be seen that there is a flip in the optimum POC between 200-2000kVA. The results for the '500kVA transformer scenario' match the prediction stated in Section 5.4.1, however, the results for the 50kVA, 200kVA, 1000kVA and 2000kVA transformers are contrary to the predictions stated within Section 5.4.1.

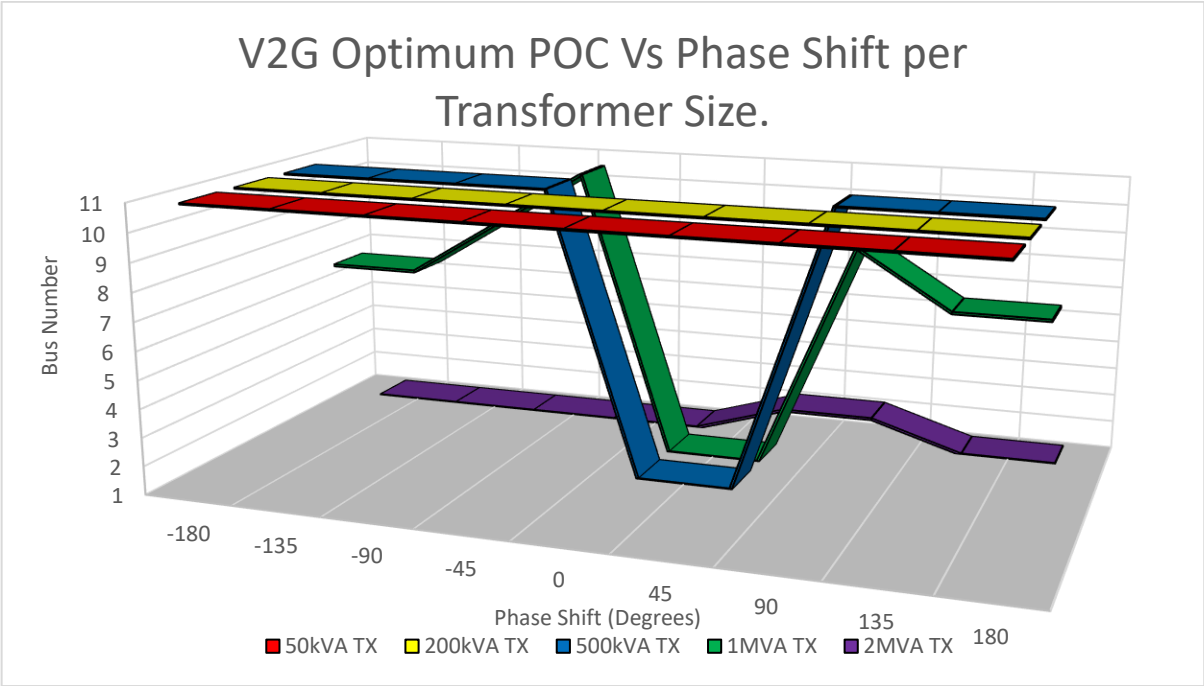


**Figure 5.4.2.1: Optimum V2G POC for eight phase-shifts and different transformer size scenarios mentioned in Section 5.1.5.**

When analysing the results for the '2000kVA transformer' scenario at 0π radians phase-shift it was identified that the choice to enable the V2G at the first or eleventh bus made no difference to the harmonic current drawn through the transformer. However, it did make a small difference to the THDv which increased from 1.3803% to 1.3829% when the V2G was enabled at the first and eleventh bus respectively. Comparatively, the '50kVA transformer' and '500kVA transformer' scenarios changed the harmonic current drawn through the transformer and the THDv depending on whether the first or eleventh bus was selected to enable V2G. The '50kVA transformer' scenario resulted in the phase angle of the currents altering by up to 2.1% when the V2G was enabled at the eleventh bus, resulting in the THDv to drop from 5.0439% to 5.0276% when the V2G was enabled at the first and eleventh bus respectively at 0π radians phase-shift. The same occurred for the '500kVA transformer' scenario which resulted in the phase angle of the harmonic currents altering depending on which bus the V2G was enabled, resulting in the THDv to drop from 1.7449% to 1.7448% when the V2G was enabled at the eleventh and first bus respectively at 0π radians phase-shift. In each case the difference between V2G being enabled on either the first or eleventh bus is minimal. Therefore, the reason for the difference between these results is due to the different impedances of the transformers and difference in impedance between the first and eleventh bus. As the impedance increases, the phase angle of the harmonic currents drawn change. Depending on the EDN parameters, this might lead to further cancellation or summation of harmonic currents, influencing the optimum POC.

In conclusion, for the scenarios shown in Figure 5.4.2.1, 100% of phase-shifts for the '50kVA transformer' and '200kVA transformer' scenarios and 75% of phase-shifts for the '500kVA transformer' scenario, it can be determined that the optimum POC to enable V2G is the eleventh bus. However, for larger transformer sizes such as the '1000kVA transformer' scenario and '2000kVA transformer' scenario, the eleventh bus was the optimum POC to enable V2G for 12.5% and 0% of phase shifts respectively. The results of the '1000kVA transformer' scenario are spread out over several busses, making drawing a definitive conclusion irresponsible. However, for the '2000kVA transformer' scenario, the optimum POC to enable V2G is the first bus for 75% of phase-shifts. Therefore, it can be determined that transformer impedance has an impact on which bus V2G should be enabled on. For higher impedance transformers such as 50, 200 and 500kVA, the best bus is the eleventh, however, for lower impedance EDNs such as a 2000kVA transformer, the optimum POC is the first bus.

Following this, the results of Figure 5.4.2.2 show the effect cable size and service length have on the POC producing the lowest THDv. The cable size and therefore cable impedance, when compared to the '185mm$^2$ main' scenario does not seem to have a significant effect on the optimum POC producing the lowest THDv. Similar to the '185mm$^2$ main' scenario, for 62.5% of phase-shifts within the '30m Services' scenario and 75% of phase-shifts within the '35mm$^2$ main' and '300mm$^2$ main' scenarios within Figure 5.4.2.2, it can be determined that the optimum POC to enable V2G is the eleventh bus.

In contrast to Figure 5.4.2.2 and Sections 5.2-3, it can be seen in Figure 5.4.2.3 that the 11kV bus impedance has an impact on the best bus for the V2G to be enabled. The results of the base scenario, named 'Base X/R' will be compared with 'CERA X/R.' 'Base X/R' scenario resulted in the phase angle of the harmonic currents altering depending on which bus the V2G was enabled, resulting in the THDv to drop from 1.7449% to 1.7448% when the V2G was enabled at the eleventh and first busses respectively at 0π radians phase-shift. Similarly, 'CERA X/R' scenario also resulted in the phase angle of the harmonic currents altering depending on which bus the V2G was enabled, resulting in the THDv to drop from 1.9656% to 1.9646% when the V2G was enabled at the first and eleventh busses respectively at 0π radians phase-shift. Similar to Figure 5.4.2.1, the impact of the bus in which the V2G is enabled under these two scenarios has minimal impact on the THDv of the EDN.

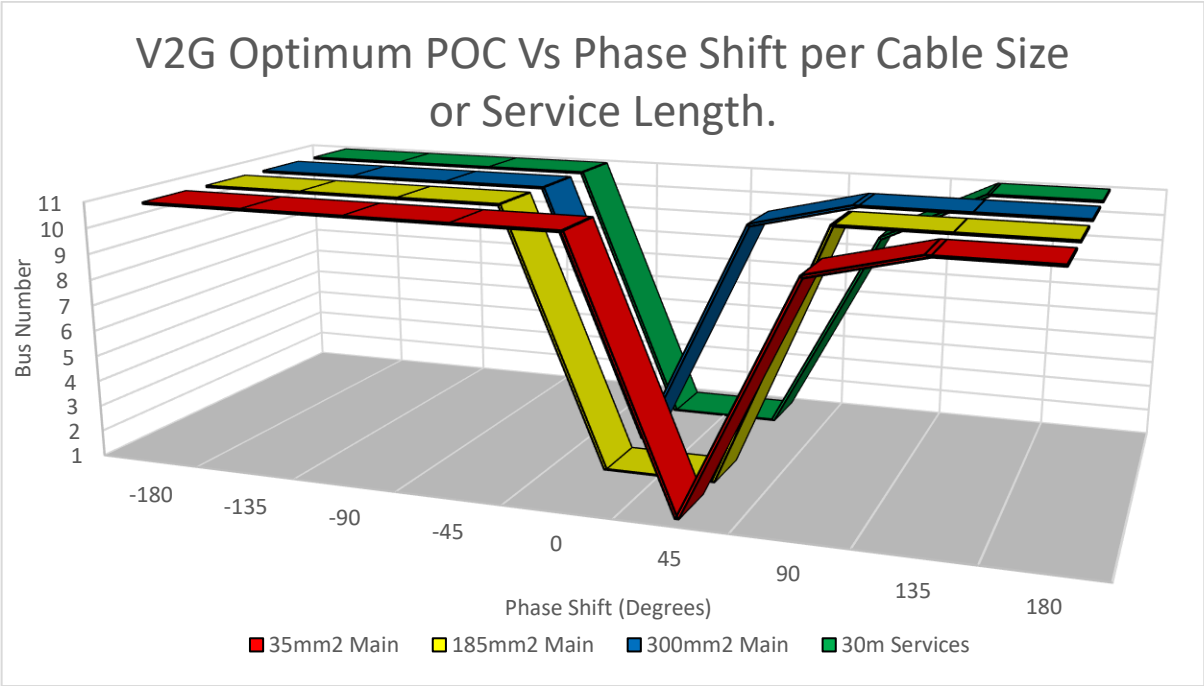


**Figure 5.4.2.2: Optimum V2G POC for eight phase-shifts, different mains cable size and different service length scenarios mentioned in Section 5.1.5.**

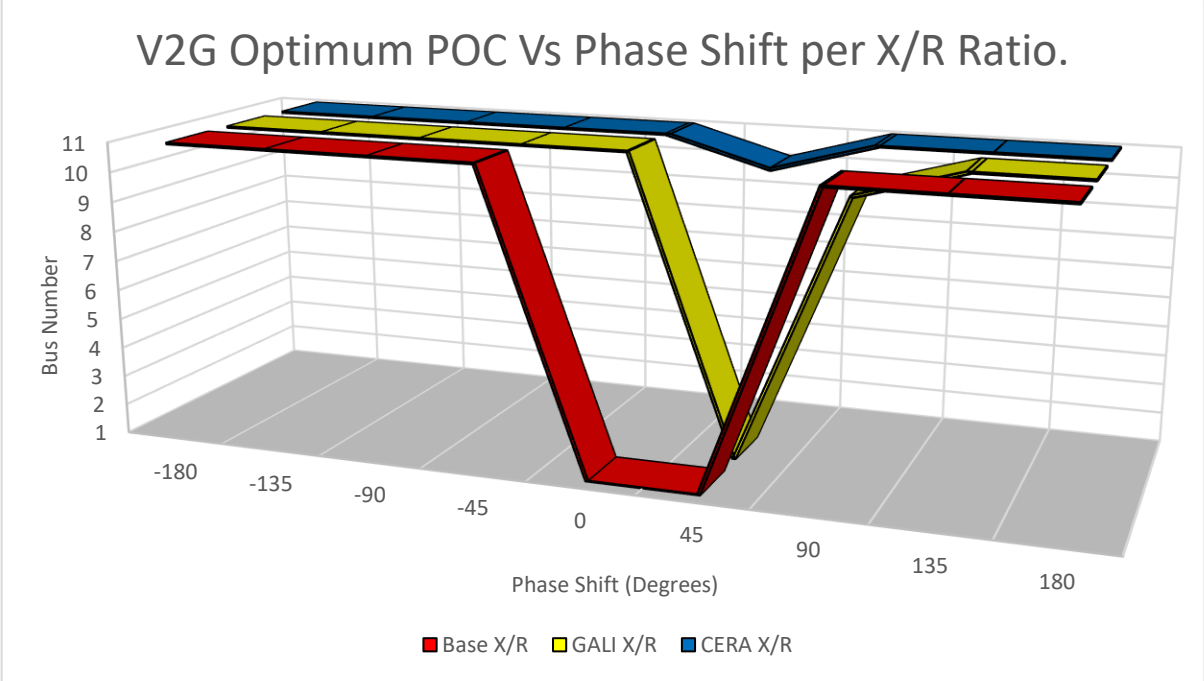


**Figure 5.4.2.3: Optimum V2G POC for eight phase-shifts and different 11kV bus impedance scenarios mentioned in Section 5.1.5.**

In conclusion, for 75% of phase-shifts for the 'GALI X/R' scenario and 87.5% of phase-shifts for the 'CERA X/R' scenario within Figure 5.4.2.3, it can be determined that the optimum POC to enable V2G is the eleventh bus. This follows the narrative identified in Figure 5.4.2.1 that higher impedance EDNs will result in the eleventh bus being the optimum POC to enable V2G, since the impedance of CERA is 9.47 times larger than the 'Base' as shown in Sections 3.1.4 and 5.1.5.

The next scenario to be discussed is the PV generation scenario shown in Figure 5.4.2.4. Here it can be seen for all scenarios that there is little effect on the optimum POC for an EVC to operate as a V2G and it follows the prediction stated in Section 5.4.1. However, similar to Figures 5.3.2.4-5, it can be seen that for the 'PV eleventh bus' scenario that with a phase-shift of +0.5π, the eleventh bus is avoided, changing the optimum POC to the tenth bus. It should be noted however that the V2G phase angle is set in relation to the harmonic current used to produce the background voltage harmonics, the PV generation and the EVCs. The same applies for the 'PV first bus' scenario at a phase shift of 0π radians. In this case the first bus is avoided, changing the optimum POC to the eleventh bus.

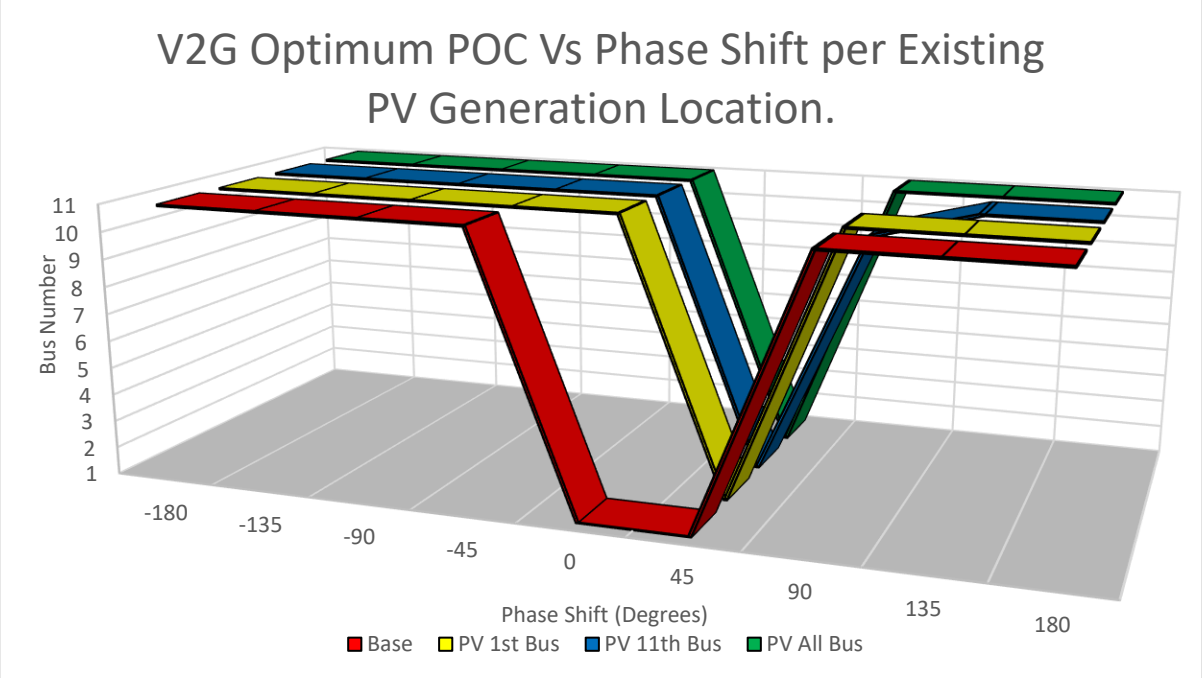


**Figure 5.4.2.4: Optimum V2G POC for eight phase-shifts and different PV generation scenarios mentioned in Section 5.1.5.**

Lastly, for 75% of phase-shifts for the 'PV eleventh bus' scenario and 87.5% of phase-shifts for the 'PV first bus' and 'PV all bus' scenarios within Figure 5.4.2.4, it can be determined that the optimum POC to enable V2G is the eleventh bus.

The last scenarios to be considered covers the optimum bus for the V2G to be enabled during different network arrangements seen in Figure 5.4.2.5. By comparing the second feeder, two-phase and three-phase fault scenarios to the normal network arrangements, it can be seen that only the 'two-phase fault' scenario produces a clear difference in outcome and therefore will be investigated. As per the previously identified differences between scenarios at 0π radians phase-shift, the harmonic current magnitudes between the first and eleventh bus did not alter, however, the phase angle of those harmonic currents did. The 'normal arrangements' scenario resulted in the THDv to drop from 1.7449% to 1.7448% when the V2G was enabled at the eleventh and first busses respectively. In comparison the 'two-phase fault' scenario resulted in the THDv to drop from 2.5558% to 2.5536% when the V2G was enabled at the first and eleventh busses respectively. Similar to previous examples, the difference in THDv is minimal.

Despite this, for 75% of phase-shifts for the 'second feeder' scenario and 87.5% of phase-shifts for the 'two-phase fault' and 'three-phase fault' scenarios within Figure 5.4.2.5, it can be determined that the optimum POC to enable V2G is the eleventh bus.

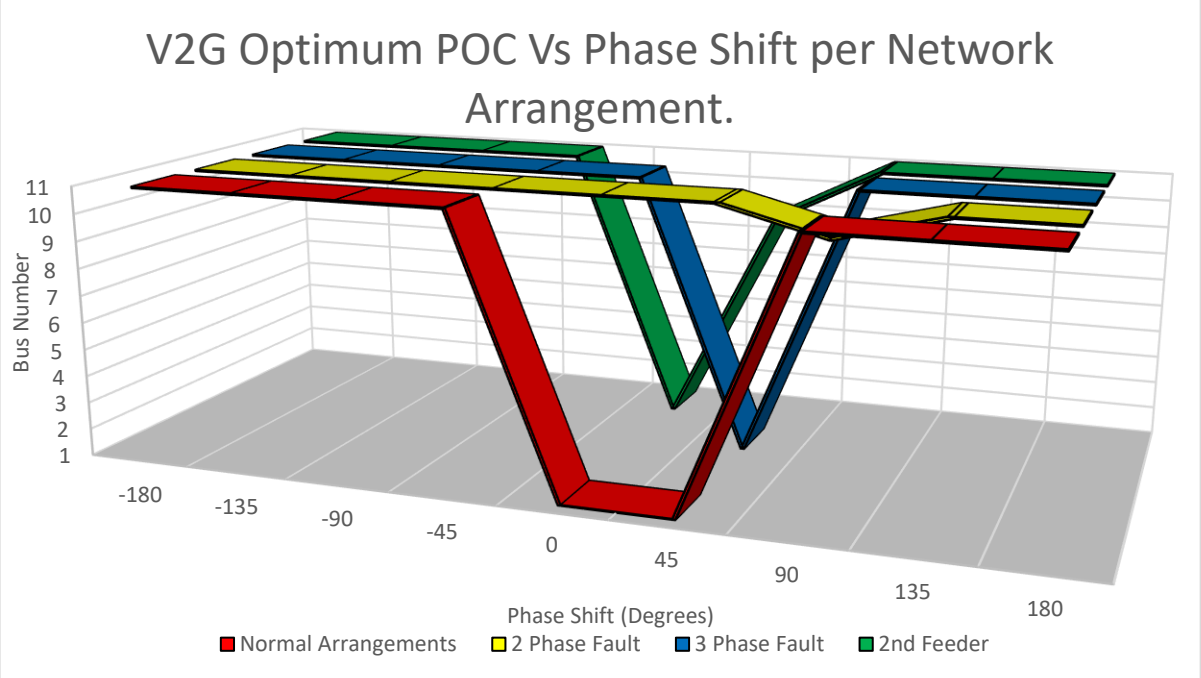


**Figure 5.4.2.5: Optimum V2G POC for eight phase-shifts and different network arrangement scenarios mentioned in Section 5.1.5.**

## 5.4.3 – Conclusions

For the LV EDN studied, generally, for all phase-shifts, the optimum POC to enable V2G with respect to harmonics is the eleventh bus for 73% of scenarios and phase-shifts shown in Table 5.4.2.1. The eleventh bus represents the last 5% of the LV EDN. This result was expected when the V2G and EVC harmonics were out of phase, or there is a significant amount of harmonic phase angle as seen in Table 5.4.2.1. However, the 1000kVA and 2000kVA transformer scenarios do not follow this conclusion. By analysing Figure 5.4.2.1, it shows that as transformer size increases and therefore impedance decreases, the likelihood increases that the first bus is the optimum bus to enable V2G. Conversely, by analysing Figures 5.4.2.1 and 5.4.2.3, as EDN impedance increases, the likelihood increases that the eleventh bus is the optimum bus to enable V2G. The reasoning for this was due to the harmonic phase-shift created across the impedance as covered in Section 5.4.2. Following this, a two-phase fault had a significant impact on the optimum POC to enable V2G, as seen in Figure 5.4.2.5.

Considering that transformer size was found to have the largest impact on the optimum POC to enable V2G within Figure 5.4.2.1, it should be considered that Figures 5.4.2.2-5 all used a 500kVA transformer within their simulations. Therefore, these figures generally mirrored the results of the '500kVA transformer' scenario shown within Figure 5.4.2.1. This is a limitation of the study. Carrying out these scenarios for multiple transformer sizes may have been prudent, however, it would have taken a huge amount of additional time to complete. In total, nine-hundred and sixty simulation runs would have needed to be carried out, therefore, taking almost four times as long as the simulations carried out for this section of the thesis.

When considering the interaction of V2Gs, PV generation and EVCs, there is limited data available on the harmonic interactions between these power electronic devices. However, Casalerio, et al. (2021) states that models used to represent the power quality of PV generation are suitable to represent the behaviour of V2G systems. Taking this into account, as per Müller, et al. (2014) and Watson and Watson (2017a) only $\pi$ radians can be ignored as previously mentioned in Section 5.2.3. Therefore, all the phase-shifts, except for $\pi$ radians shown in Figures 5.4.2.1-5 must be considered.

Additionally, another factor to consider within this study is that in order to simplify the simulation, all current harmonics including, EVCs, PV generation and those used to generate the background harmonics were considered to be in phase with each other. As previously mentioned by Müller, et al. (2014) and Watson and Watson (2017a), this is unlikely to be the case. Therefore, it is possible that the optimum POC to enable V2G is based on the harmonic phase-shift of the V2G with respect to other current harmonic sources. This is further reinforced since for many scenarios, 0π and +0.25π radians phase-shift resulted in the optimum POC being the first bus. If the EVC harmonics, PV generation and background harmonics were varied with regards to each other, the result could be different.

Therefore, to explore this research gap, Figure 5.4.3.1 and Table 5.4.3.1 was produced which compares the 'PV all bus' scenario and alters the phase-shift of the PV generation and EVCs as stated within the figure. The reasons for the EVC and PV generation phase-shifts chosen are that as per Watson and Watson (2017a), current harmonics from PV generation and EVCs can cancel by up to 75%. Therefore, the maximum phase angle scenario simulated was 0.75π radians. π radians phase-shift would result in a 100% harmonic current cancellation between the PV generation and EVCs which is contrary to existing research. Additionally, as per sources such as Busatto, Bollen and Rönnberg (2018), De Silva, Jayamaha and Lidula (2019), Moses, et al. (2010) and Watson and Watson (2017), EVCs and PV generation when connected separately should lead to an increase in harmonics with regard to the background harmonics. Therefore, the EVC and PV generation phase-shift needed to be in the range of +0.5π, +0.25π, 0π, -0.25π or -0.5π with respect to background harmonics.

**Table 5.4.3.1: Optimum V2G POC for various scenarios and phase-shifts shown in Figure 5.4.3.1.**

| Bus Number | 1 | 2 | 3 | 4 | 5 | 6 | 7 | 8 | 9 | 10 | 11 |
|---|---|---|---|---|---|---|---|---|---|---|---|
| PV All Bus | 1 | - | - | - | - | - | - | - | - | - | 7 |
| PV +0.25π & EVC -0.25π radians | 2 | - | - | - | - | - | - | - | 1 | - | 5 |
| PV +0.25π & EVC -0.5π radians | 4 | - | - | - | - | - | 1 | - | - | - | 3 |

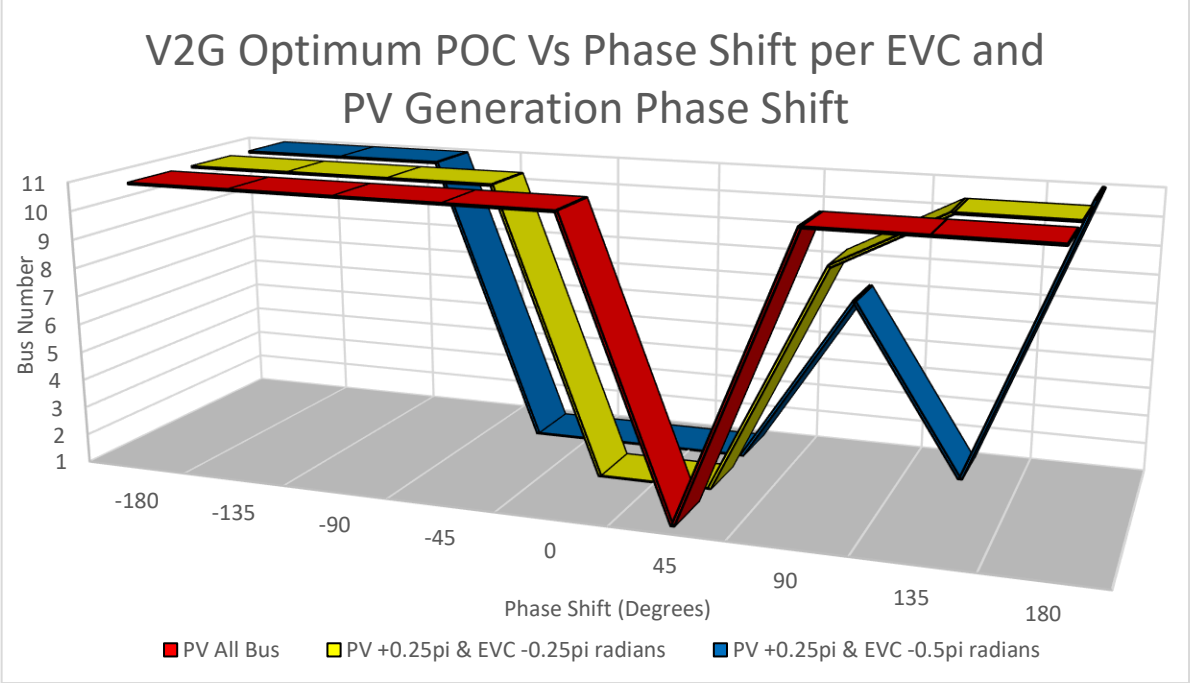


**Figure 5.4.3.1: Optimum V2G POC for eight phase-shifts, different EVC and PV generation phase shifts for the 'PV all bus' scenario.**

Within Figure 5.4.3.1 and Table 5.4.3.1 it can be seen that the broadening of harmonic phase-shifts across PV generation and EVCs leads to the broadening of the optimum POC being the first bus. Due to the broadening of PV generation and EVC phase-shift, π radians phase-shift for the V2G can no longer be excluded from the results. By analysing the results of Table 5.4.3.1, it can be seen that under the 'PV all bus' scenario, the optimum POC is the first bus for 14% of results and the eleventh bus for 86% of results by excluding the result for π radians. By considering the 'PV +0.25π & EVC -0.25π radians' scenario, the optimum POC is the first bus for 25% of results and the eleventh bus for 63% of results by not excluding the result for π radians. For the 'PV +0.25π & EVC -0.5π radians' scenario, the optimum POC is the first bus for 50% of results and the eleventh bus for 38% of results by not excluding the result for π radians. Therefore, it would appear that as the EDN becomes more complex with regards to harmonic phase angle between harmonic sources, it is more likely that the first bus may become the optimal POC. This can be explained as the first bus is the lowest impedance bus. Therefore, the new V2G can no longer be π radians out of phase with all harmonic sources. Therefore, the optimum POC becomes the first bus since cancelling with one harmonic source results in summing with another. In each of these cases, the current harmonics used to generate the background harmonics is set at 0π radians. By taking these results into account, it could be interpreted that varying the phase-shift between particular devices could lead to the first bus becoming the optimum POC more frequently for more scenarios. This would need to be explored further in future research.

Within Section 5.4.2, for comparison, the phase-shift of the V2G was with respect to the EVCs, PV generation and current harmonics used to generate the background harmonics which was 0π radians. However, this results in small differences in the THDv between the first and last bus being the POC. In reality, harmonics generated could be at an infinite number of phase angles with regards to the background harmonics and other harmonic sources. For illustrative purposes the difference in THDv of the '50kVA transformer' scenario was compared between the first and eleventh bus for a phase angle of +0.75π. It was found that the maximum THDv levels were 4.2928% and 4.2236% for the first and eleventh bus respectively. This phase angle represents a possible scenario suggested by Watson and Watson (2017a) and although the difference is 0.0692%, this represents a difference in connection bus for a single V2G per phase. This percentage change is much larger than identified within section 5.4.2 and for every additional V2G, this number could multiply, meaning that this could have a significant effect for a larger network with multiple V2Gs.

Although not covered within this section, V2G technology can be used for the purposes of active filtering as per Asghar, et al. (2022), Mojumder, et al. (2022) and Tirunagari, Gu and Meegahapola (2022). This would change the use of V2G from a power source, not designed to assist with reducing harmonic levels to being specifically used to carry out that task. It is very likely that this use of V2G would change the optimum POC. In this case, the optimal POC of active filters should be identified based on the research of Hashemian, Latify and Yousefi (2020), Ying-Yi and Ying-Kwun (1996) and Schwanz, et al. (2016). Depending on whether V2G will solely operate as an active filter, or, with the capability to act as a power source and an active filter, will determine whether this thesis' conclusion should be disregarded or whether the conclusions of this thesis and the active filter research mentioned should be jointly considered.

In conclusion, the results stated regarding the optimum POC to enable V2G should be taken as a guide rather than a definitive conclusion. Therefore, the prediction made in Section 5.4.1 cannot be validated. One limitation of this research is the consideration of harmonic interaction and phase-shift between different devices such as V2G, EVCs, PV generation and background voltage harmonic distortion. Using the results from Figure 5.4.3.1, it can be seen that the effect of this phase-shift on results is substantial. However, without conclusive data stating how V2G, PV generation and EVC harmonics should interact, it is hard to produce a definitive conclusion, since variations in the harmonic phase-shifts would likely lead to differing results being produced. The consensus on harmonic interaction between these devices is currently split as per Müller, et al. (2014) and Watson and Watson (2017a). Additionally, due to the differences in results between different transformer sizes, unless specifically a scenario altering transformer size, the scenario should be considered specific to a 500kVA transformer. Furthermore, changes in the use of V2G from a power source to a filter will likely change the results. Similar to the conclusions stated in 5.3.3 and due to the small changes in THDv identified between enabling V2G at different busses, it may be more beneficial for a DNO to consider THDv levels, but ultimately make decisions on the V2G POC based on voltage and loading constraints. Voltage and loading issues could lead to costly infrastructure upgrades requiring excavation and disruption, however, THDv levels might be resolved by installing filters, which could be connected above ground, requiring much lower initial outlay and disturbances.

# Chapter 6 – Conclusions and Future Work

The following chapter concludes this thesis. It contains the primary research findings and contributions of the thesis, as well as the conclusions and recommendations for future research.

## 6.1 – Research Findings

The research findings of this thesis are summarised as follows:

The type of LV EDN cable fault which has the greatest impact on LV EDN harmonic levels was identified. It was found within Chapter 4 that a three-phase fault has the greatest impact on harmonic levels and therefore, can be used by network planning engineers to identify the worst possible harmonic outcome. As expected, two-phase and open-circuit faults did not have as great an impact on harmonic levels. Furthermore, due to LV EDN fusing constraints, it was found that complex faults explained in Section 4.2.6 do not impact on harmonic levels as high as three-phase faults. THDv was measured at multiple points of supply to overcome a limitation of ER G5/5 which only calculates the THDv at the POC.

The maximum voltage and current harmonic levels under different fault conditions have been identified. As expected, when considering worst case harmonic interaction, a combination of PV generation and EVCs has a much greater impact on harmonic levels than when PV generation or EVCs are considered separately. Under three-phase fault conditions on feeder one of the case-study network, with no faults on feeder two, THDv increased, from 1.69% to 2.17% for EVCs at 31.2% penetration, 1.67-2.34% to 2.42-3.72% for PV generation at 98.4% penetration and 2.48-3.11% to 3.38-4.70% for combined EVCs and PV generation at 86.4% and 98.4% penetration. This shows the considerable impact of faults on harmonic levels. The THDv levels increased further if a fault sharing the same phase was present on both feeders one and two, or, decreased if a single two-phase fault was present on feeder one. This can be seen in more detail within Sections 4.2.4, 4.3.4 and 4.4.4.

The THDv can give an indication, however, it is more important to consider the individual voltage harmonic orders exceeded or met under planning limits within ER G5/5. For a three-phase fault on feeders one and two, these were the 21st, 27th and 33rd harmonics for EVCs, the 15th, 21st, 27th, 28th, 30th, 32nd, 33rd, 34th, 36th, 39th and 40th for PV generation and the 9th, 15th, 21st, 27th, 33rd and 39th for combined EVCs and PV generation. It was found within this thesis that the individual harmonic planning limits of the orders mentioned, stated within ER G5/5 were met earlier than the overall THDv planning level of 5%.

More importantly, the maximum penetrations of different devices permissible to remain compliant with ER G5/5 were identified for different network conditions. Under three-phase fault conditions on feeder one of the case-study network with no faults on feeder two, maximum penetration decreases from 60% to 26.4% for EVCs, decreases from between 38.4-98.4% to 16.8-45.6% for PV generation and decreases from between 21.6-33.6% to 7.2-12.0% for combined EVCs and PV generation when compared to normal running arrangements. This shows that these faults will potentially limit the maximum penetration of devices considerably. It is this thesis' recommendation that the numbers of EVCs or PV generation connected to LV EDNs should be restricted, or harmonic reducing technology implemented to observe compliance with industrial standards and regulations during phase-to-phase faults.

Using the current and voltage harmonics identified under various normal and fault conditions for EVCs, PV generation and combined EVCs and PV generation within Sections 4.2-4, the impact on the temperature and lifespan of transformers and cables were determined. This information is published in Tables 4.2.7.1-2, 4.3.5.1-6, and 4.4.5.1-6. Furthermore, the additional impact on temperature and lifespan of each successive fault across both feeders is tabulated within Tables 4.2.7.3-6, 4.3.5.7-10, and 4.4.5.7-10. Due to harmonic cancellation at higher harmonic orders, the impact of some combinations of faults on feeders one and two led to PV generation when connected in isolation having a more detrimental effect on transformer life than the combined impact of PV generation and EVCs when connected together.

Additionally, although not the core focus of this thesis, an observation was made that the neutral voltage of the LV PME EDN increased significantly under fault conditions. It was found that, for the case-study network under all fault conditions, the neutral voltage did not increase enough to cause ventricular fibrillation or respiratory tetanus. However, it was found, on multiple occasions, that the neutral voltage was high enough to startle members of the public if touching bonded metalwork. Although this is not an imminent risk to life, remedial action should be taken to reduce the neutral voltage. This should be the repair of the fault to rebalance the network. Furthermore, these voltages only apply to this LV EDN. If the conductor impedance or the earthing resistance at the transformer were to increase as would be expected within less interconnected networks as per Butter, Batten and Paalman (2020), it is likely that the neutral voltages would be higher, therefore, potentially reaching the respiratory tetanus threshold of 18.38V.

Lastly, the optimum POC for EVCs, V2G and PV generation was determined using a modified version of the case-study EDN which comprised of a single, radial LV distribution feeder with eleven busses. To determine the optimum POCs, two algorithms, EHO and MBO, were implemented. Each scenario was run eight times to account for various phase-shifts which is a limitation of ER G5/5. For EVCs, the optimum POC is the first bus in line with the prediction in Section 5.2.1 except for the 'PV all bus' scenario as stated in Section 5.2.3. Furthermore, for the majority of harmonic interactions, the first bus should be considered the optimum POC for the '50kVA transformer' scenario. For PV generation, the general recommendation for planning purposes, when considering the spectrum of possible phase-shifts, is that PV generation is connected to the first bus, or first few busses of the LV EDN for the '50kVA transformer,' '200kVA transformer' and 'PV all bus' scenarios. A general recommendation regarding optimum POC outside of these scenarios cannot be given. For V2G, the optimum POCs stated in Figures 5.4.2.1-5 should be taken as a guide rather than a definitive conclusion since these conclusions are only valid for the harmonic interactions assumed. Outside of these scenarios and their specific harmonic interactions, Figure 5.4.3.1 explains that varying the phase-shift of EVCs, PV generation, V2G and background harmonics with respect to each other will likely lead to changes in the optimal POCs. Furthermore, if V2G was to be used to facilitate active filtering of the network, the findings made would not be applicable. Lastly, it was found for several scenarios across V2Gs and PV generation that when identifying the optimum POC, if a device is already connected to a bus, the connection of a further device to the same bus may not be optimum, but only for specific phase angles.

## 6.2 – Contributions

The contributions of this thesis are summarised as follows:

As mentioned in Section 6.1, for the purposes of network planning and design, this thesis has determined that three-phase faults should be used by network planning engineers to determine the worst possible harmonic outcome. This can be used to ascertain the possible violations of ER G5/5. This information is critical considering the predicted increases in EVCs and PV generation on the National Grid as stated within Chapter 1.

As covered in Section 6.1, the maximum penetration of different devices permissible to remain compliant with ER G5/5 was identified for different fault conditions. Using these results, it was essential to provide data which could be applied by network planning engineers. To fulfil this, the first harmonic limits to be met for each of the devices studied were determined. These were the 21$^{st}$ and 27$^{th}$ for EVCs, 21$^{st}$ and 33$^{rd}$ for PV generation and 21$^{st}$ and 27$^{th}$ for combined EVCs and PV generation. Using these specific harmonic magnitudes, the range of percentage increases in these harmonic magnitudes for the LV EDN were calculated under different fault scenarios. These can be seen in Figures 4.2.4.1-2, 4.3.4.1-2, and 4.4.4.2-3. Network planning engineers can use these values as a worst-case guide to determine potential breaches of ER G5/5 under different fault scenarios.

Further to Section 6.1, the impact of devices and each successive fault across both feeders studied on the lifespan of transformers and cables was identified. This additional information can be used by network planning engineers to provide a financial value to leaving network faults unrepaired, either by requiring asset replacement earlier or due to the increased likelihood of failure, which will have costs associated with the asset replacement and power disruption. Unfortunately, it is not possible to calculate financial costs within this thesis since this would also need to account for the cable or transformer size and physical location.

Neutral voltage data obtained within this thesis can be used by network planning engineers as a guide to determine the worst-case possible increase in neutral voltage under phase faults based on measured values during normal running arrangements. This only applies to PME EDNs due to combining the neutral and earth conductors. This contribution could significantly reduce the risk of injury to members of the public.

Lastly, a general recommendation regarding the optimum POC for EVCs except for the 'PV all bus' scenario, and PV generators for the '50kVA transformer,' '200kVA transformer' and 'PV all bus' scenarios was determined. Network planning engineers can use this contribution to ensure that THDv levels on LV EDNs are minimised where practicable. Therefore, this will reduce the impact of harmonics on equipment and consumers as highlighted within Section 1.4. POC recommendations for V2G and PV generation outside of the scenarios stated could not be determined based on the data obtained in Sections 5.3.2 and 5.4.2. However, the methodology produced within this thesis can be used by network planning engineers to determine the optimum POC for their specific LV EDN. Once harmonic interactions between different harmonic sources are confirmed by future research and further simulation of the scenarios covered in Figures 5.3.2.2-6 are undertaken for 50kVA, 200kVA, 1000kVA and 2000kVA transformers, accurate conclusions can be drawn.

## 6.3 – Future Work

Potential future work is proposed and listed as follows:

To draw more accurate conclusions when the harmonics from different devices including EVCs, PV generation and V2G interact, further research into these harmonic interactions needs to be carried out. Existing research has produced conflicting data showing that current harmonics between EVCs and PV generation may sum arithmetically as stated by Müller, et al. (2014), or cancel by up to 75% as stated by Watson and Watson (2017a). Once a consensus of outcome for harmonic interactions between devices is obtained, the optimisation algorithms can be re-run to identify the optimal POCs. Furthermore, it would be beneficial to research the optimum POC(s) for multiple EVCs, PV generation or V2Gs which would increase complexity substantially due to the number of potential combinations.

As identified within Section 5.3.3, further simulation of the scenarios covered in Figures 5.3.2.2-6 should be undertaken for 50kVA, 200kVA, 1000kVA and 2000kVA transformers to expand the validity of recommendations stated within Section 5.3.3 outside of the specific scenarios stated.

Although the simulation model produced by this thesis is sufficient to achieve the aims identified in Section 2.5.2, further modifications should be made to improve the model in order to be able to draw conclusions where identified limitations have prevented conclusions being drawn, particularly within Chapter 5. A look-up table should be produced, containing power input or output levels for each of the individual devices, harmonic magnitudes and phase angles for the background harmonics and each of the individual devices simulated within this thesis. This means that every device, not group of devices would select their own harmonics, phase angles and input or output levels. The look-up tables should allow for variations in background harmonics and different models of device. Based on research, selection of devices or background harmonics within the look-up table should be based on probability distribution using random number generation from exponential distribution as shown in Equation 5.1.4.22. Additionally, it is important to ensure that every distribution table for each device and background harmonics interact correctly with each other. Therefore, the values selected as part of the probability distribution may need to change depending on the scenario selected. To protect against results which may be closer to the upper or lower expected limits, each simulation or scenario would need to be repeated multiple times and the data from each of these simulation runs analysed to produce a probability distribution curve. Furthermore, the selection of individual devices and background harmonics must be logged, including their placement to ensure any results can be replicated.

This thesis focusses on single-phase devices, since the LV EDN which was the case study for this thesis will have a greater proportion of single-phase devices connected. The way three and single-phase devices present themselves with respect to harmonics can be quite different, producing different outcomes. Therefore, the conclusions of this thesis are only applicable to single-phase devices. Future studies should consider three-phase devices with respect to optimum POC, voltage harmonic levels, maximum penetration and asset life.

As mentioned in Sections 3.1.8 and 5.2.3, the base load is modelled using resistors. Therefore, the harmonic voltage and phase angle directly influences the magnitude and phase angle of the harmonic currents drawn by the base load. This will in turn cause a feedback loop which will further influence the harmonic voltage and phase angle of the EDN. In reality, Yamini, et al. (2019) shows that although harmonic voltage of the system is a component, base load largely draws harmonic current based on the type of load rather than the harmonic voltage of the system. Therefore, in the future, the base load model shown in Figure 3.1.8.2 should be used. However, it is likely that this will add considerable computation time to the simulation.

Furthermore, as stated in Sections 3.1.5 and 5.2.3, the cable model was simplified to several resistors and inductors in series. Although usually not applied to LV cable, the correct model should be an infinite number of resistors and inductors being modelled in series, with an infinite number of capacitors and resistors being modelled in parallel between all cable conductors and earth as shown in Turan and Kalenderli (2009). However, as previously mentioned, the parallel capacitive and resistive components of the cable are not easily available. Secondly, transformer resistance increases with temperature as stated within Najar, et al. (2015). These additions would complicate the EDN model, slowing down the simulation for very little gain. A few simulation scenarios should be repeated with this complex cable and transformer model implemented to confirm whether this influences the results.

One limitation of the <16A median EVC harmonic profile is that the profile provides median values for multiple EVCs, rather than the measured profile of individual chargers. Therefore, the simulation may not capture the impact of low numbers of EVCs. When reliable harmonic profile data for multiple individual EVCs with a base background harmonic profile is available, future simulations should include multiple harmonic charger profiles and charging rates from a range of different EVCs representative of the most popular UK BEVs and PHEVs shown in Table 2.1.1.1. The same comment is applicable for V2G. Due to limited measured data being available for V2G, a single V2G harmonic profile was used. Only one V2G was simulated at a time. Therefore, the simulation results are only applicable for the V2G profile used.

As mentioned within Section 5.2.3, the algorithms mentioned in Sections 5.1.3-4 determine the optimum POC based on overall THDv, not individual harmonic orders. Although THDv will be an indication of the magnitude of individual harmonic orders, it may be that a scenario with a lower THDv, but higher specific harmonic orders would have a more detrimental impact on consumers and connected equipment. Therefore, future algorithm operations should apply a weighting to each harmonic order, the magnitude of each order individually measured, and an overall score produced for each harmonic profile. To ensure that these scores are not subjective this would need to be based on the individual harmonic magnitudes and how the magnitude sits with relation to the limits set within ER G5/5.
The improvements suggested, especially the use of look-up tables which would require multiple runs of the simulation, would not be feasible with the existing simulation model due to the length of time required per simulation run with the hardware available for the PhD. Therefore, for the purposes of efficiency, a less resource intensive computation software should be sought or streamlining of the simulation model should be carried out.

Where impact to asset life is identified, it may be more cost effective to connect active filters or operate a V2G as an active filter. The optimal location of active filters can be identified based on the research of Hashemian, Latify and Yousefi (2020), Ying-Yi and Ying-Kwun (1996) and Schwanz, et al. (2016). Additionally, as mentioned in Section 2.1, load related issues relating to EVCs on the LV EDN with existing infrastructure has largely been solved using demand side load control using smart meters. However, there has been little research into using the same technology to limit harmonics. Therefore, as an extension of the two solutions mentioned above, the improvement in asset life and therefore cost saving to DNOs should be researched.

Lastly, following on from the statements made in Section 2.5.1 and results produced in Figure 5.4.3.1, it is important that the results of this thesis are verified using live networks or physical EDN models where possible due to the lack of pre-existing research on the topic.

# Bibliography

Abdullah, M.F., Hamid, N.H., Baharudin, Z. and Khamis, M.F.I., 2011. Triplen harmonics currents propagation through medium voltage distribution network. In: Institute of Electrical and Electronics Engineers, *2011 Fourth International Conference on Modeling, Simulation and Applied Optimization.* Kuala Lumpur, Malaysia, 19-21 April 2011. United States of America: Institute of Electrical and Electronics Engineers.

Acker, C.R., 1976. Transformer Insulation and Transformer Life Expectancy—A More Comprehensive Concept. In: Institute of Electrical and Electronics Engineers, *IEEE PES Winter Meeting and Tesla Symposium.* New York, United Stated of America, 25-30 January 1976. United States of America: Institute of Electrical and Electronics Engineers.

Ahmad, F., Iqbal, A., Ashraf, I., Marzband, M. and Khan, I., 2022. Placement of Electric Vehicle Fast Charging Stations using Grey Wolf Optimization in Electrical Distribution Network. In: Institute of Electrical and Electronics Engineers, *2022 International Conference on Power Electronics, Smart Grid, and Renewable Energy.* Trivandrum, India, 02-05 January 2022. United States of America: Institute of Electrical and Electronics Engineers.

Alame, D., Azzouz, M. and Kar, N., 2020. Assessing and Mitigating Impacts of Electric Vehicle Harmonic Currents on Distribution Systems. *Energies,* 13(12), 3257.

Aljanad, A., Mohamed, A., Shareef, H. and Khatib, T., 2018. A novel method for optimal placement of vehicle-to-grid charging stations in distribution power system using a quantum binary lightning search algorithm. *Sustainable Cities and Society,* 38, pp.174-183.

Alkahtani, A.A., Alfalahi, S.T.Y., Athamneh, A.A., Al-Shetwi, A.Q., Mansor, M.B., Hannan, M.A. and Agelidis, V.G., 2020. Power Quality in Microgrids Including Supraharmonics: Issues, Standards, and Mitigations. *IEEE Access,* 8, pp.127104-127122.

Aprilia, E.C., 2012. *Modelling of Photovoltaic (PV) Inverter for Power Quality Studies.* MEng. Eindhoven, Netherlands: Technische Universiteit Eindhoven. Available at: <http://energynautics.com/content/uploads/2019/02/App19_TUE_Master_Thesis_Modelling_of_Photovoltaic_PV_Inverter_for_Power_Quality_Studies.pdf> [Accessed 23rd March 2021].

Anurangi, R.O., Rodrigo, A.S. and Jayatunga, U., 2017. Effects of High Levels of Harmonic Penetration in Distribution Networks with Photovoltaic Inverters. In: Institute of Electrical and Electronics Engineers, *2017 International Conference on Industrial and Information Systems.* Peradeniya, Sri Lanka, 15-16 December 2017. United States of America: Institute of Electrical and Electronics Engineers.

Armstrong, M., Atkinson, D.J., Johnson, C.M. and Abeyasekera T.D., 2005. Low order harmonic cancellation in a grid connected multiple inverter system via current control parameter randomization. *IEEE Transactions on Power Electronics.* 20 (4), pp. 885-892.

Asghar, R., Sulaiman, M.H., Mustaffa, Z., Ali, Z. and Ullah, Z., 2022. Integration of electric vehicles in smart grids: A review of the advantages and challenges of vehicle-to-grid technology. In: Institute of Electrical and Electronics Engineers, *2022 International Conference on IT and Industrial Technologies.* Chiniot, Pakistan, 03-04 October 2022. United States of America: Institute of Electrical and Electronics Engineers.

Awasthi, A., Venkitusamy, K., Padmanaban, S., Selvamuthukumaran, R., Blaabjerg, F. and Singh, A.K., 2017. Optimal planning of electric vehicle charging station at the distribution system using hybrid optimization algorithm. *Energy,* 133, pp.70-78.

Baker, J., 2015. *TG-PS-123: Technical Guide for Load Ratings of Underground Cables (Rev 2.02).* [Internal Document] Reading, United Kingdom: Scottish and Southern Energy Power Distribution Ltd.

Baker, J., 2017. *TG-NET-CAB-010: Electrical Constants for LV to 33kV Underground Electricity Cables – Data Sheets.* [Internal Document] Reading, United Kingdom: Scottish and Southern Electricity Networks.

Baker, J., 2019. *TG-NET-CAB-009: Load Ratings of LV to 33kV Underground Cables – Design Data.* [Internal Document] Reading, United Kingdom: Scottish and Southern Electricity Networks.

Baker, K., Stoker, G. and Simpson, J., 2012. Assessing the prospects for a revival of nuclear power in Britain. *Journal of Power and Energy,* 226(3), pp.339-350.

Balda, J.C., Barnes, T.M., Emannuel, A.E., Ferraro, R.J., Griffith, D.C., Hartmann, D.P., Horton, W.F., Jewell, W.T., McEachern, A., Phileggi, D.J., Reid, W.E. and Wagner, V.E., 1993. Effects of Harmonics on Equipment. *IEEE Transactions on Power Delivery.* 8 (2), pp.672 – 680.

Ball, W.C., and Poarch, C.K., 1961. Telephone Influence Factor (TIF) and Its Measurement. *Transactions of the American Institute of Electrical Engineers, Part I: Communication and Electronics.* 79 (6), pp.659-664.

Banks, N., 2021. *Vehicle to Grid (V2G) Barriers and Opportunities: a capability approach.* [.pdf] Oxford, United Kingdom: University of Oxford. Available at: <https://project-leo.co.uk/wp-content/uploads/2022/01/V2G-barriers-and-opportunities-211221-covered.pdf> [Accessed 28th August 2023].

Bayerische Motoren Werke, 2020. O*wners Handbook. The BMW 3 Series Touring Plug-In-Hybrid.* [.pdf] Bayerische Motoren Werke. Available at: <https://g20.bimmerpost.com/forums/attachment.php?attachmentid=2505187&d=1610657012> [Accessed 2nd January 2024].

Beama, 2022. *Guide to low-voltage switch and fusegear devices.* [.pdf] London, United Kingdom: Beama. Available at: <https://www.beama.org.uk/static/71238b5e-cce6-4a1b-b74b91530e056f94/BEAMA-Guide-Low-Voltage-Switch-and-Fusegear-Devices.pdf> [Accessed 4th January 2024].

Bentley, E.C., Suwanapingkarl, P., Weerasinghe, S., Jiang, T., Putrus, G. A., Johnston, D., 2010. The Interactive Effects of Multiple EV Chargers within a Distribution Network. In: Institute of Electrical and Electronics Engineers, *2010 Vehicle Power and Propulsion Conference.* Lille, France, 01-03 September 2010. United States of America: Institute of Electrical and Electronics Engineers.

Biegelmeier, G., 1985. New experiments with regard to basic safety measures for electric equipment and installations. *Electrical Shock Safety Criteria,* 1985, pp.161-172.

Bilal, M., Rizwan, M., Alsaidan, I. and Almasoudi, F.M., 2021. AI-Based Approach for Optimal Placement of EVCS and DG With Reliability Analysis. *IEEE Access,* 9, pp.154204-154224.

Bosman, A.J.A., 2006. *Harmonic Modelling of Solar Inverters and Their Interaction with the Distribution Grid.* MEng. Eindhoven, Netherlands: Technische Universiteit Eindhoven. Available at: Library Search <https://tue.on.worldcat.org/discovery> [Accessed 20th March 2021].

Bouchakour, S., Chouder, A., Cherfa, F., Abdeladim, K. and Kerkouche, K., 2012. The First Grid-Connected Photovoltaic System in Algeria: Power Quality Observation, *Second International Days on Renewable Energies and Sustainable Development.* Laghouat, Algeria, 3-4 June 2012. Amar Telidji University of Laghouat.

Busatto, T., Bollen, M., and Rönnberg, S., 2018. *Photovoltaics and Harmonics in Low Voltage Networks.* [.pdf] Stockholm, Sweden: Energiforsk. Available at: Energiforsk Report Search <https://energiforsk.se/rapportsok/> [Accessed 19th March 2021]

Busatto, T., Rönnberg, S.K., and Bollen, M.H.J., 2020. Harmonic Analysis of Electric Vehicle Charging on the Distribution System Network with Distributed Solar Generation. *Renewable Energy and Power Quality Journal,* 18, pp.103-108.

Butter, K., Batten, S. and Paalman, E., 2020. *EART-03-003: Technical specification for earthing and bonding at secondary substations. Issue 1.* [.pdf] Glasgow, Scotland: SP Energy Networks. Available at: <https://www.spenergynetworks.co.uk/userfiles/file/EART-03-003.pdf> [Accessed 23rd December 2023].

Cai, H., Jiang, Z., Huang, R., Xu, H., Liu, S. and Xu, J., 2022. Harmonic Analysis of V2G System Based on Integrated Filter Inductor. In: Institute of Electrical and Electronics Engineers, *5th International Electrical and Energy Conference*. Nangjing, China, 27-29 May 2022. United States of America: Institute of Electrical and Electronics Engineers.

Calais, M., Myrzik, J., Spooner, T. and Agelidis, V.G., 2002. Inverters for single-phase grid connected photovoltaic systems-an overview. In: Institute of Electrical and Electronics Engineers, 3rd Annual IEEE Power Electronics Specialists Conference. Cairns, Queensland, Australia, 23-27 June 2002. United States of America: Institute of Electrical and Electronics Engineers.

Capper, I., 2013. *Ludlow Primary Substation.* [image online] Available at: <https://www.geograph.org.uk/photo/3623457> [Accessed 30th March 2020]

Casalerio, Â., e Silva, R.A., Teixeira, B. and Serra, J.M., 2021. Experimental assessment and model validation of power quality parameters for vehicle-to-grid systems. *Electric Power Systems Research,* 191, pp.1-15.

Ceylan, O., Paudyal, S., Dahal, S. and Karki, N.R., 2017. Assessment of Harmonic Distortion on Distribution Feeders with Electric Vehicles and Residential PVs. In: International Conference on Power Systems, *7th International Conference on Power Systems.* Pune, India, 21-23 December 2017. United States of America: Institute of Electrical and Electronics Engineers.

Cherian, E., Bindu, G.R. and Chandramohanan Nair, P.S., 2016. Pollution Impact of Residential Loads on Distribution System and Prospects of DC Distribution. *Engineering Science and Technology, an International Journal,* 19(2016) pp.1655-1660.

Chicco, G., Schlabbach, J., and Spertino, F., 2008. Characterisation and Assessment of the Harmonic Emission of Grid-Connected Photovoltaic Systems. In: Institute of Electrical and Electronics Engineers, *2005 Russia Power Tech.* St. Petersburg, Russia, 27-30 June 2005. United States of America: Institute of Electrical and Electronics Engineers.

Chidurala, A., Saha, T., and Mithulananthan, N., 2015. Harmonic Characterization of Grid Connected PV Systems & Validation with Field Measurements. In: Institute of Electrical and Electronics Engineers, *2015 Power & Energy Society General Meeting.* Denver, Colorado, United States of America, 26-30 July 2015. United States of America: Institute of Electrical and Electronics Engineers.

Chou, C. and Liu, C., 1994. Harmonic compensation of induction watthour meter performance. *Electric Power Systems Research,* 32 (2), pp. 89-99.

CIGRE, 2014. *Benchmark systems for network integration of renewable and distributed energy resources.* [.pdf] Paris, France: Conseil International des Grands Réseaux Electriques (CIGRE). Available at: <https://www.e-cigre.org/publications/detail/575-benchmark-systems-for-network-integration-of-renewable-and-distributed-energy-resources.html/> [Accessed 4th January 2024].

Collin, A.J., Djokic, S.Z., Thomas, H.F. and Meyer, J., 2012. Modelling of electric vehicle chargers for power system analysis. In: Institute of Electrical and Electronics Engineers, *11th International Conference on Electrical Power Quality and Utilisation.* Lisbon, Portugal, 17-19 October 2011. United States of America: Institute of Electrical and Electronics Engineers.

Collombet, C., Lupin, J. and Schonek, J., 1999. *Harmonic disturbances in networks, and their treatment.* [.pdf] Claix, France: Schneider Electric. Available at: <https://www.studiecd.dk/cahiers_techniques/Harmonic_disturbances_in_networks.pdf> [Accessed 13th July 2023].

Comfort, R., Gonzalez, M., Mansoor, A., Barker, P., Short, T. and Sundaram, A., 2001. Power Quality Impact of Distributed Generation: Effect on Steady State Voltage Regulation. *Electrical Power Quality and Utilisation Journal,* 7(2), pp. 35-42.

Cortés-Caicedo, B., Grisales-Noreña, L.F., Montoya, O.D., Perea-Moreno, M. and Perea-Moreno, A., 2022. Optimal Location and Sizing of PV Generation Units in Electrical Networks to Reduce the Total Annual Operating Costs: An Application of the Crow Search Algorithm. *Mathematics,* 10, pp.1-22.

Cyganski, D., Orr, J.A., Chakravorti, A.K., Emanuel, A.E., Gulachenski, E.M., Root, C.E., and Bellemare, R.C., 1989. Current and voltage harmonic measurements and modeling at the Gardner photovoltaic project. *IEEE Transactions on Power Delivery,* 4(1), pp.800-809.

Dale, M., 2018. *Electric Vehicle Emissions Testing Closedown Report.* [.pdf] UK: Western Power Distribution - Innovation Available at: National Grid ESO Website <https://www.nationalgrid.co.uk/downloads/1916> [Accessed 8th April 2023]

Dalziel, C. F. and Lee W. R., 1969. Lethal electric currents. *IEEE Spectrum,* 6(2), pp.44-50.

Deilami, S., Masoum, A.S., Moses, P.S. and Masoum, M.A.S., 2010. Voltage profile and THD distortion of residential network with high penetration of plug-in electrical vehicles. In: Institute of Electrical and Electronics Engineers, *2010 Power and Energy Society Innovative Smart Grid Technologies Conference Europe,* Gothenberg, Sweden,11-13 October 2010. United States of America: Institute of Electrical and Electronics Engineers.

Demoulias, C., Labridis, D.P., Dokopoulos, P.S. and Gouramanis, K., 2007. Ampacity of Low-Voltage Power Cables Under Nonsinusoidal Currents. *IEEE Transactions on Power Delivery,* 22(1), pp.584-594.

Department of the Army U.S. Army Corps of Engineers, 1995. *Design of Coastal Revetments, Seawalls, and Bulkheads.* [.pdf] United States of America: Department of the Army U.S. Army Corps of Engineers. Available at: <https://www.publications.usace.army.mil/Portals/76/Publications/EngineerManuals/EM_1110-2-1614.pdf> [Accessed 10th February 2020].

Dermot, H., 2018. *Development of the UK Public Chargepoint Network.* [.pdf] London, United Kingdom: The Royal Automobile Club Foundation for Motoring Ltd. Available at: <https://www.racfoundation.org/wp-content/uploads/Development_of_the_UK_CPN_Harold_Dermott_December_2018.pdf> [Accessed 5th January 2024].

De Boer, F., Woods, D., Forsyth, C., Antosik, M., Newton, C., Fischer, S., Johnson, M., and Bruton, T., 2020. *Economic and policy advice to support the design and implementation of the new microgeneration support scheme in Ireland: Report for Department of the Environment, Climate and Communications (DECC).* [.pdf] Glasgow, United Kingdom: Ricardo. Available at: Government of Ireland Publications Search <https://www.gov.ie/en/publications/#> [Accessed 17th January 2024]

De Silva, H.H.H., Jayamaha, D.K.J.S., and Lidula, N.W.A., 2019. Power Quality Issues Due to High Penetration of Rooftop Solar PV in Low Voltage Distribution Networks: A Case Study. In: Institute of Electrical and Electronics Engineers, *14th International Conference on Industrial and Information Systems.* Peradeniya, Sri Lanka, 18-20 December 2019. United States of America: Institute of Electrical and Electronics Engineers.

DESNZ, 2023. *Solar Photovoltaics Deployment in the UK November 2023.* [.xls]. London, United Kingdom: Department for Energy Security and Net Zero. Available at: <https://www.gov.uk/government/statistics/solar-photovoltaics-deployment> [Accessed 3rd January 2024].

DfT and DVLA, 2023a. *Licensed plug-in vehicles (PiVs) at the end of the quarter by body type and fuel type, including breakdown of generic models June 2023.* [.xls] London, United Kingdom: Department for Transport and Driver and Vehicle Licensing Agency. Available at: <https://www.gov.uk/government/statistical-data-sets/vehicle-licensing-statistics-data-tables> [Accessed 3rd January 2024].

DfT and DVLA, 2023b. *Licensed ultra low emission vehicles (ULEVs) at the end of the quarter by fuel type, keepership (private and company) and upper and lower tier local authority.* [.xls] London, United Kingdom: Department for Transport and Driver and Vehicle Licensing Agency. Available at: <https://www.gov.uk/government/statistical-data-sets/vehicle-licensing-statistics-data-tables> [Accessed 14th January 2024].

Diahovchenko, I., Volokhin, V., Kurochkina, V., Špes, M. and Kosterec, M., 2019. Effect of harmonic distortion on electric energy meters of different metrological principles. *Frontiers in Energy,* 13 (2), pp. 377-385.

Doan, A.T., Duong, M.Q. and Mussetta, M., 2021. Optimally Placing Photovoltaic Systems in Distribution Networks Considering the Influence of Harmonics on Power Losses. *International Journal on Electrical Engineering and Informatics,* 13(2), pp.252-270.

Domeki, H., Ishihara, Y., Kaido, C., Kawase, Y., Kitamura, S., Shimomura, T., Takahashi, N., Yamada, T., and Yamazaki, K., 2004. Investigation of Benchmark Model for Estimating Iron Loss in Rotating Machine. *IEEE Transactions on Magnetics,* 40 (2), pp.794-797.

Du, Y., Dah-Chuan Lu, D., Geoffrey, J., and Cornforth D.J., 2013. Modeling and analysis of current harmonic distortion from grid connected PV inverters under different operating conditions. *Solar Energy,* 94, pp.182-194.

Dyer, P., 2023. *ETS 04-6020: Ground Mounted Unit Distribution Transformers 11kV and 6.6kV – Tier 2 Losses Specification (V6.0).* [Internal Document] London, United Kingdom: UK Power Networks.

Eirgrid, 2013. *An Information Note on Harmonic Issues and their impact on Customer connections.* [.pdf] Dublin, Ireland: Eirgrid. Available at: <https://www.eirgridgroup.com/site-files/library/EirGrid/AnInformationNoteOnHarmonicIssuesv1.0.pdf> [Accessed 20th July 2023].

Ekström, R. and Leijon, M., 2014. Lower order grid current harmonics for a voltage-source inverter connected to a distorted grid. *Electric Power Systems Research,* 106, pp.226-231.

*Electric Lighting Act, 1882. (45 & 46 Vict. c. 56).* London, United Kingdom: UK Parliament.

Electricity North West, 2019. *System Earthing and Fault Levels.* [online] Available at: <https://www.enwl.co.uk/get-connected/network-information/long-term-development-statement/policies-and-technical-references/system-earthing-and-fault-levels/> [Accessed 29th March 2019].

*Electricity (Supply) Act, 1926. (16 & 17 Geo. 5. c. 51).* London, United Kingdom: UK Parliament.

Elexon Ltd., 1997. *Electricity user load profiles by profile class.* [.pdf] London, United Kingdom: Elexon Ltd. Available at: <http://data.ukedc.rl.ac.uk/browse/edc/Electricity/LoadProfile/doc/Load_Profiles.pdf> [Accessed 25th March 2015].

Elisabeta, S., Piroi, I. and Piroi, F., 2020. Technical performance analysis of a 40kW photovoltaic installation. *Studia Universitatis Babes-Bolyai Engineering,* 65(1), pp.171

Elphick, S., Smith, V., Gosbell, V. and Barr. R., 2010. The Australian Long Term Power Quality Survey project update. In: Institute of Electrical and Electronics Engineers, *14th International Conference on Harmonics and Quality of Power.* Bergamo, Italy, 26-29 September 2010. United States of America: Institute of Electrical and Electronics Engineers.

Energy Networks Association, 2018. *Engineering Recommendation P23/2: Guidance on Earth Fault Loop Impedance at Customers' Intake Supply Terminals.* London, United Kingdom: Energy Networks Association.

Energy Networks Association, 2020. *Engineering Recommendation G5/5: Harmonic voltage distortion and the connection of harmonic sources and/or resonant plant to transmission systems and distribution networks in the United Kingdom.* London, United Kingdom: Energy Networks Association.

Electric Power Research Institute, 1982a. *EL-2443 Basic Transformer Life Characteristics.* Palo Alto, California, United States of America: Electric Power Research Institute.

Electric Power Research Institute, 1982b. *2622 Basic Research on Transformer Life Characteristics.* Palo Alto, California, United States of America: Electric Power Research Institute.

Estrada, T., Briggs, S.J. and Khosla, N., 1995. *A Test of Circuit Breakers Under Harmonic Loading Conditions. USACERL Technical Report 96/13* [.pdf] US Army Corps of Engineers. Available at: <https://apps.dtic.mil/sti/pdfs/ADA303103.pdf> [Accessed 13th July 2023].

Evans, G. and MacLeman, D., 2013. *LCNF Tier 1 Close-Down Report Demonstrating the Benefits of Monitoring LV Networks with embedded PV Panels and EV Charging Point.* [.pdf] Reading, United Kingdom: Scottish and Southern Power Distribution. Available at: Ofgem Publications Library <https://www.ofgem.gov.uk/ofgem-publications> [Accessed 19th March 2021].

Fekete, K., Klaic, Z. and Majdandzic, L., 2011. Expansion of the residential photovoltaic systems and its harmonic impact on the distribution grid. *Renewable Energy,* 43, pp.140-148.

Foskolos, G., 2021. *Current Harmonic Modeling of Aggregated Electric Vehicle Loads in the Low Voltage Grid.* MEng. Mälardalen University. Available at: <https://www.diva-portal.org/smash/get/diva2:1521978/FULLTEXT02.pdf> [Accessed 13th August 2023].

Foyer, J.W. and Maruszak, M., 2020. *Power Quality Assessment of Electric Distribution Grids Integrated with Distributed Energy Sources.* MEng. Aalborg Universitet. Available at: Aalborg Universitet Project Library <https://projekter.aau.dk/projekter/> [Accessed 19th March 2021].

Fu, J., Han, Y., Li, W., Feng, Y., Zalhaf, A. S., Zhou, S., Yang, P. and Wang, C., 2023. A novel optimization strategy for line loss reduction in distribution networks with large penetration of distributed generation. *Electrical Power and Energy Systems,* 150, pp.1-16.

Gandolfi, M., 2016. *Retail Energy Markets in 2016.* [.pdf] London, United Kingdom: Ofgem. Available at: Ofgem Search < https://www.ofgem.gov.uk/search> [Accessed 2nd April 2021].

Ghijselen, J.A., Ryckaert, W.A. and Melkebeek, J.A., 2003. Influence of electric power distribution system design on harmonic propagation. *Electrical Energy,* 86, pp.181-190.

Ghorbani, M.J. and Mokhtari, H., 2015. Impact of Harmonics on Power Quality and Losses in Power Distribution Systems. *International Journal of Electrical and Computer Engineering,* 5(1). pp.166-174.

Golla, N. K., Sudabattula, S. K. and Suresh, V., 2022. Optimal Placement of Electric Vehicle Charging Station in Distribution System Using Meta-Heuristic Techniques. *Mathematical Modelling of Engineering Problems,* 9(1), pp.60-66.

Gomatom, K., Dorr, D. and Sutherland, P.E., 2005. Human current sensitivities and resistance values in the presence of electrically energized objects. In: Institute of Electrical and Electronics Engineers, *IEEE Systems Technical Conference on Industrial and Commercial Power 2005.* Saratoga Springs, United States of America, 08-12 May 2005. United States of America: Institute of Electrical and Electronics Engineers.

Gomez, J.C. and Morcos, M. M., 2003. Impact of EV battery chargers on the power quality of distribution systems. *IEEE Transactions on Power Delivery,* 18, pp.975-981.

Google, 2020. *Google Maps.* [online] Available at: <https://www.google.com/maps/> [Accessed 28th March 2020].

Grasel, B., Baptista, J. and Tragner, M., 2022. Supraharmonic and Harmonic Emissions of a Bi-Directional V2G Electric Vehicle Charging Station and Their Impact to the Grid Impedance. *Energies,* 15(8), 2920.

Grasel, B., Baptisa, J., Tragner, M, Leonhartsberger, K. and Igel, S., 2021. Harmonic emissions of a bidirectional electric vehicle charging station - a research methodology based on tests at a reconstructed smart grid. In: Institute of Electrical and Electronics Engineers, *2021 International Conference on Environment and Electrical Engineering and 2021 Industrial and Commercial Power Systems Europe.* Bari, Italy, 07-10 September 2021. United States of America: Institute of Electrical and Electronics Engineers.

Haeberlin, H., Kaeser, F., Liebi, Ch. and Beutler, Ch., 1995. Results of Recent Performance and Reliability Tests of the Most Popular Inverters for Grid Connected PV Systems in Switzerland. In: Europäische Kommission, 13th EU PV Conference on Photovoltaic Solar Energy Conversion. Nice, France, 23-27 October 1995. Switzerland, Berner Fachhochschule.

Haeberlin, H., Liebi, Ch., and Beutler, Ch., 1997. Inverters for Grid Connected PV Systems: Test Results of some New Inverters and Latest Reliability Data of the Most Popular Inverters in Switzerland. In: Europäische Kommission, 14th European Photovoltaic Solar Energy Conference. Barcelona, Spain, 30 June-4 July 1997. Switzerland, Berner Fachhochschule.

Hall, G., 2015. *Asset Management Plan Underground System – Distribution.* [.pdf] Lenah Valley, Australia: TasNetworks. Available at: <https://www.aer.gov.au/system/files/TasNetworks%20-%20TN046%20-%20Underground%20System%20-%20January%202016.pdf> [Accessed 11th February 2020].

Harrington, N. 2023. *Heat Pumps and Domestic Heat Decarbonisation in the UK: A Systems Thinking Analysis of Barriers to Adoption.* Glasgow, United Kingdom: UK Collaborative Centre for Housing Evidence.

Hashemian, S.N., Latify, M.A. and Yousefi, G.R., 2020. PEV Fast-Charging Station Sizing and Placement in Coupled Transportation-Distribution Networks Considering Power Line Conditioning Capability. *IEEE Transactions on Smart Grid,* 11(6), pp.4773-4783.

Hickory Mitsubishi., 2018. *Mitsubishi PHEV Technology.* [image online] Available at: <http://www.hickorymitsubishi.com/blog/2018-mitsubishi-outlander-phev-fuel-economy/2018-mitsubishi-phev-technology-charging-fast-charge-d_o/> [Accessed 25th September 2018]

Hongkun, L., Tianhao, L., Lingqi, X., Xianggao, Z., Yuyan, H., Mingliang, Y., Jiecong, C. and Zhuo, L., 2020. Assessment of thermally aged XLPE insulation material under extreme operating temperatures. *Polymer Testing,* 88 (2020), pp.1-7.

Hu, Z., Han, Y., Zalhaf, A.S., Zhou, E. and Yang, P., 2023. Harmonic Sources Modeling and Characterization in Modern Power Systems: A Comprehensive Overview. *Electric Power Systems Research,* 218, pp.1-25.

Iglesias, J. G., Bartak, G., Baumier, N., Defait, B., Dussart, M., Farrell, F., Graser, C., Sinclair, J., Start, D. and Mazzoni, M., 2002. *Power Quality in European Electricity Supply Networks - 1st edition.* [.pdf] Brussels, Belgium: Eurelectric. Available at: <http://patricioconcha.ubb.cl/eureka/pq_in_europe.pdf> [Accessed 7th September 2023].

IEEE, 1993. *IEEE Std 519-1992 - IEEE Recommended Practices and Requirements for Harmonic Control in Electrical Power Systems.* United States of America: Institute of Electrical and Electronics Engineers.

IEEE, 2012a. *IEEE Std 367-2012 - IEEE Recommended Practice for Determining the Electric Power Station Ground Potential Rise and Induced Voltage from a Power Fault.* United States of America: Institute of Electrical and Electronics Engineers.

IEEE, 2012b. *IEEE Std C57.91-2011 - IEEE Guide for Loading Mineral-Oil-Immersed Transformers and Step-Voltage Regulators Standard.* United States of America: Institute of Electrical and Electronics Engineers.

IEEE, 2014. *IEEE Std 519-2014 - IEEE Recommended Practice and Requirements for Harmonic Control in Electric Power Systems.* United States of America: Institute of Electrical and Electronics Engineers.

IEEE, 2018. *IEEE Std C57.110-2018 - IEEE Recommended Practice for Establishing Liquid Immersed and Dry-Type Power and Distribution Transformer Capability when Supplying Nonsinusoidal Load Currents.* United States of America: Institute of Electrical and Electronics Engineers.

IEC, 1994. *IEC TS 60479-1:1994 - Effects of current on human beings and livestock - Part 1: General aspects.* Geneva, Switzerland: International Electrotechnical Commission.

IEC, 2006. *IEC 60287-1-1:2006 - Electric cables - Calculation of the current rating - Part 1: Current rating equations (100% load factor) and calculation of losses – Section 1: General.* Geneva, Switzerland: International Electrotechnical Commission.

IEC, 2008. *IEC 61000-4-7:2002+AMD1:2008 - Electromagnetic compatibility (EMC) - Part 4-7: Testing and measurement techniques - General guide on harmonics and interharmonics measurements and instrumentation, for power supply systems and equipment connected thereto.* Geneva, Switzerland: International Electrotechnical Commission.

IEC, 2011. *IEC 61000-3-12:2011 - Electromagnetic compatibility (EMC) - Part 3-12: Limits - Limits for harmonic currents produced by equipment connected to public low-voltage systems with input current >16 A and ⩽ 75 A per phase.* Geneva, Switzerland: International Electrotechnical Commission.

IEC, 2018a. *IEC 61000-2-2:2002+AMD1:2017+AMD2:2018 - Electromagnetic compatibility (EMC) - Environment - Compatibility levels for low-frequency conducted disturbances and signalling in public low-voltage power supply systems.* Geneva, Switzerland: International Electrotechnical Commission.

IEC, 2018b. *IEC 61000-3-2:2018 - Electromagnetic compatibility (EMC) - Part 3-2: Limits - Limits for harmonic current emissions (equipment input current ⩽16 A per phase).* Geneva, Switzerland: International Electrotechnical Commission.

Illing, L., 2008. *Fourier Analysis.* [.pdf] Portland, Oregon, United States of America: Reed College. Available at: <https://www.reed.edu/physics/courses/Physics331.f08/pdf/Fourier.pdf> [Accessed 9th January 2024].

Islam, M., Shareef, H. and Mohamed, A., 2018. Optimal location and sizing of fast charging stations for electric vehicles by incorporating traffic and power networks. *IET Intelligent Transport Systems,* 12(8), pp.1-12.

Issouribehere, P., Barbero, J., Barbera, G. and Issouribehere, F., 2010. Assessment of Power Quality indices over a decade of control in Argentinian distribution system. In: Institute of Electrical and Electronics Engineers, *2010 IEEE PES General Meeting.* Minneapolis,

Minnesota, United States of America, 25-29 July 2010. United States of America: Institute of Electrical and Electronics Engineers.

Jacobson, K., 2005. *Power Influence on Telecom System.* [.pdf] Alberta, Canada: University of Alberta. Available at: <http://www.jacobsonengineering.ca/documents/power_infl_UofA_2005_1.pdf> [Accessed 20th July 2023].

Jamatia, P., Bhattacharjee, S. and Sharma, S., 2022. Optimal allocation of EV charging station in Distribution Network. In: Institute of Electrical and Electronics Engineers, *4th International Conference on Energy, Power and Environment.* Shillong, India, 29 April 2022 - 01 May 2022. United States of America: Institute of Electrical and Electronics Engineers.

Kalair, A., Abas, N., Kalair, A.R., Saleem, Z. and Khan, N., 2017. Review of harmonic analysis, modeling and mitigation techniques. *Renewable and Sustainable Energy Reviews,* 78, pp.1152-1187.

Kontogiannis, K.P., Vokas, G.A., Nanou, S., and Papathanassiou, S., 2013. Power Quality Field Measurements on PV Inverters. *International Journal of Advanced Research in Electrical, Electronics and Instrumentation Engineering,* 2(11), pp.5301-5314.

Lachaume, J., Deflandre, T. and Meunier, M., 2002. Harmonics in MV and LV distribution systems: present and future levels. In: The International Conference of Electricity Distribution, *12th International Conference and Exhibition on Electricity Distribution.* Birmingham, United Kingdom, 17-21 May 1993. United Kingdom: Institute of Engineering and Technology.

Langella, R., Testa, T., Meyer, J., Möller, F., Stiegler, R., and Djokic S.Z., 2016. Experimental-Based Evaluation of PV Inverter Harmonic and Interharmonic Distortion Due to Different Operating Conditions. *IEEE Transactions on Instrumentation and Measurement,* 65(10), pp.2221-2233.

Latheef, A.A., 2006. *Harmonic Impact of Photovoltaic Inverter Systems on Low and Medium Voltage Distribution Systems.* MEng. Wollongong, Australia: University of Wollongong. Available at: University of Wollongong Thesis Collection 1954-2016 <https://ro.uow.edu.au/theses/> [Accessed 20th March 2021].

Li, J., Yu, H., Shumei, C. and Xu, B., 2014. Research on Simulation and Harmonics of EV Charging Stations for V2G Application. *Intelligent Computing in Smart Grid and Electrical Vehicles,* 463, pp.496-504.

Li, L., Wang, B. and Deng Y., 2018. Model establishment and harmonic analysis of electric vehicle charger. In: Institute of Electrical and Electronics Engineers, *13th Conference on Industrial Electronics and Applications.* Wuhan, China, 31 May 2018 - 02 June 2018. United States of America: Institute of Electrical and Electronics Engineers.

Liang, Z., Li, Y., Zhao, L., Tao, S. and Fan, Y., 2020. Study on Influence of Voltage Deviation on Loss of Low Voltage Distribution Network. *IOP Conference Series: Earth and Environmental Science,* 440 032030, pp.1-9.

Liao, H., Milanović, J.V. and Hashempour, M.M., 2021. Optimization Framework for Harmonic Mitigation in Transmission Networks with Renewable Generation. In: Institute of Engineering and Technology, *12th Mediterranean Conference on Power Generation, Transmission, Distribution and Energy Conversion.* Online Conference, 09-12 November 2020. United Kingdom: Institute of Engineering and Technology.

*Liverpool (Corporation) Electric Lighting Act, 1879. (42 & 43 Vict. c. ccxiii).* London, United Kingdom: UK Parliament.

Lucas, A., Bonavitacola, F., Kotsakis, E. and Fulli, G., 2015. Grid harmonic impact of multiple electric vehicle fast charging. *Electric Power Systems Research,* 127, pp.13-21.

L&T Electrical & Automation, 2018. *Understanding Current & Voltage Harmonics.* [.pdf] Maharashtra, India: L&T Electrical & Automation. Available at: <https://corpwebstorage.blob.core.windows.net/media/36814/understanding-current-voltage-harmonics.pdf> [Accessed 3rd September 2023].

Macedo, J.R., Resende, J.W. and Samesima, M.I., 2003. Low voltage customers modeling for harmonic penetration studies. In: Institute of Electrical and Electronics Engineers, *10th International Conference on Harmonics and Quality of Power.* Rio de Janeiro, Brazil, 06-09 October 2002. United States of America: Institute of Electrical and Electronics Engineers.

Magnum Cap, 2018. *MC V2G Outdoor V1.5 User and Installation Manual.* [.pdf] Aveiro, Portugal: Magnum Cap. Available at: <https://procurement-notices.undp.org/view_file.cfm?doc_id=157275> [Accessed 13th August 2023].

Mak, A., 2014. *Corrosion of Steel, Aluminum and Copper in Electrical Applications.* [.pdf] Atlanta, United States of America: General Cable. Available at: <http://www.stabiloy.com/NR/rdonlyres/E5F38E54-48BF-43C1-9415-865B903605EE/0/CorrosioninElecApplications.pdf> [Accessed 11th February 2020].

McNutt, W.J. and Kaufmann, G.H., 1983. Evaluation of a Functional Life Test Model for Power Transformers. *IEEE Transactions on Power Apparatus and Systems,* PAS-102(5), pp.1151-1162.

Mehar, S. and Senouci, S.M., 2013. An optimization location scheme for electric charging stations. In: Institute of Electrical and Electronics Engineers, *2013 International Conference on Smart Communications in Network Technologies.* Paris, France, 17-19 June 2013. United States of America: Institute of Electrical and Electronics Engineers.

Meliopoulos, A.P.S. and Martin, M.A., 1992. Calculation of secondary cable losses and ampacity in the presence of harmonics. *IEEE Transactions on Power Delivery,* 7(2), pp.451-459.

Mexis, I. and Todeschini, G., 2020. Battery Energy Storage Systems in the United Kingdom: A Review of Current State-of-the-Art and Future Applications. *Energies,* 13, pp.1-30.

Michalowski, A., 2006. *Replacement of LV Consac Cable - This is Only the Beginning.* [.pdf] London, United Kingdom: Institute of Engineering and Technology. Available at: <https://ieeexplore.ieee.org/stamp/stamp.jsp?tp=&arnumber=1632411> [Accessed 10th February 2020].

Mitsubishi Motors Europe B.V., 2017. *Outlander PHEV Owner's Manual.* [.pdf] Mitsubishi Motors Europe B.V. Available at: <https://mitsubishi-motors.co.uk/wp-content/uploads/2021/06/18MY-Outlander-PHEV-Owners-Manual.pdf> [Accessed 5th August 2023]

Mojumder, M.R.H., Antara, F.A., Hasanuzzaman, M., Alamri, B. and Alsharef, M., 2022. Electric Vehicle-to-Grid (V2G) Technologies: Impact on the Power Grid and Battery. *Sustainability 2022,* 14(21), pp.1-53.

Monteiro, V., Pinto, J.G. and Afonso, J.L., 2019. Improved vehicle-for-grid (iV4G) mode: Novel operation mode for EVs battery chargers in smart grids. *International Journal of Electrical Power & Energy Systems,* 110, pp.579-587.

Morva, G., Volokhin, V., Diahovchenko, I. and Čonka, Z., 2017. Analysis of the impact of nonlinear distortion in voltage and current curves on the errors of electric energy metering devices. In: Institute of Electrical and Electronics Engineers, *First Ukraine Conference on Electrical and Computer Engineering.* Kyiv, Ukraine, 29 May 2017 - 02 June 2017. United States of America: Institute of Electrical and Electronics Engineers.

Moses, P.S., Deilami, S., Masoum, A.S. and Masoum, M.A.S., 2010. Power quality of smart grids with plug-in electric vehicles considering battery charging profile. In: Institute of Electrical and Electronics Engineers, *2010 Power and Energy Society Innovative Smart Grid Technologies Conference Europe,* Gothenberg, Sweden,11-13 October 2010. United States of America: Institute of Electrical and Electronics Engineers.

Moupuri, S. and Kamakshy, S., 2020. Optimal placement of electric vehicle charging station for unbalanced radial distribution systems. Energy Sources, Part A: Recovery, Utilization, and Environmental Effects, 2020, pp.1-15.

Müller, S., Möller, F., Meyer, J., Collin, A.J., and Djokic, S.Z., 2014. Characterisation of Harmonic Interactions Between Electric Vehicle Battery Chargers and PV Inverters. In: Institute of Electrical and Electronics Engineers, *16th International Conference on Harmonics and Quality of Power.* Bucharest, Romania, 25-28 May 2014. United States of America: Institute of Electrical and Electronics Engineers.

Najar, S., Tissier, J.F., Caulet, S. and Etien, E., 2015. A Coupled Thermal and Electrical Soft Sensor for ONAN Distribution Transformers. In: Institute of Electrical and Electronics Engineers, *2015 International Conference on Industrial Technology.* Seville, Spain, 17-19 March 2015. United States of America: Institute of Electrical and Electronics Engineers.

Nasir, S.N.S., Jamian, J.J. and Mustafa, M.W., 2018. Minimizing Harmonic Distortion Impact at Distribution System with Considering Large-Scale EV Load Behaviour Using Modified Lightning Search Algorithm and Pareto-Fuzzy Approach. *Complex Optimization and Simulation in Power Systems,* 2018, pp.1-14.

National Grid, 201?. *Generator Self Build Enduring Regime Harmonic Assessment Process Flow.* London, United Kingdom: National Grid.

National Grid ESO, 2022. *July 2022 Future energy scenarios.* [online]. London, United Kingdom: National Grid ESO. Available at: <https://www.nationalgrideso.com/document/263951/download> [Accessed 3rd January 2024].

National Grid ESO, 2023. *July 2023 Future energy scenarios.* [online]. London, United Kingdom: National Grid ESO. Available at: <https://www.nationalgrideso.com/document/283101/download> [Accessed 29th March 2024].

National Institute of Standards and Technology, 2023. *Boltzmann constant in eV/K.* [.pdf] National Institute of Standards and Technology. Available at: <https://physics.nist.gov/cgi-bin/cuu/Value?kev> [Accessed 4th October 2023].

Nduka, O.S. and Pal, B.C., 2017. Harmonic domain modelling of PV system for the assessment of grid integration impact. *IEEE Transactions on Sustainable Energy,* 8(3), pp.1154-1165.

Nguyen-Phuoc, T., Vo-Ngoc, D. and Tran-The, T., 2017. Optimal Number, Location, and Size of Distributed Generators in Distribution Systems by Symbiotic Organism Search Based Method. *Power Engineering and Electrical Engineering,* 15(5), pp.724-735

Nissan, 2023. *Charging your LEAF at home.* [online] Available at: <https://www.nissan.co.uk/owners/nissan-ownership/resources/leaf-how-to-guides/leaf-charging-guide.html> [Accessed 5th August 2023].

Niitsoo, J., Taklaja, P., Palu, I., and Klüss, J., 2015. Power Quality Issues Concerning Photovoltaic Generation and Electrical Vehicle Loads in Distribution Grids. *Smart Grid and Renewable Energy,* 6, pp.164-177.

Ofgem, 2015. *Knowing your rights: power cuts.* [.pdf] London, UK: Office of Gas and Electricity Markets. Available at: <https://www.ofgem.gov.uk/ofgem-publications/108669> [Accessed 21st April 2019]

Ofgem, 2021. *Case study (UK): Electric vehicle-to-grid (V2G) charging.* [online] Available at: <https://www.ofgem.gov.uk/publications/case-study-uk-electric-vehicle-grid-v2g-charging> [Accessed 28th August 2023].

ONS, 2021. *Mid-Year Population Estimates, UK, June 2021.* [.xls] London, United Kingdom: Office for National Statistics. Available at: <https://www.ons.gov.uk/peoplepopulationandcommunity/populationandmigration/populationestimates/datasets/populationestimatesforukenglandandwalesscotlandandnorthernireland> [Accessed 14th January 2024].

Orr, J.A., Emanuel, A.E. and Pileggi, D.J., 1984. Current Harmonics, Voltage Distortion, and Powers Associated with Electric Vehicle Battery Chargers Distributed on the Residential Power System. *IEEE Transactions on Industry Applications,* IA-20(4), pp.727-734.

Ostheimer, M., 2013. *NJUG Guidelines on the Positioning and Colour Coding of Underground Utilities' Apparatus Issue 8.* [.pdf] The National Joint Utilities Group. Available at: <http://streetworks.org.uk/wp-content/uploads/V1-Positioning-Colour-Coding-Issue-8.pdf> [Accessed 22nd July 2023].

Outram Research Ltd, 2012. *Ranger Power Master 7000 (PM7000) Power Quality Analyzer Operation Manual.* [.pdf] Bosham, United Kingdom: Outram Research Ltd. Available at: <http://www.rangerpq.com/uploads/3/9/6/2/39627747/pm7000_manual_usa_09.03.12.pdf> [Accessed 11th February 2020].

Pal, A., Bhattacharya, A. and Chakraborty, A. K., 2020. Allocation of EV Fast Charging Station with V2G Facility in Distribution Network. In: Institute of Electrical and Electronics Engineers, *8th International Conference on Power Systems.* Jaipur, India, 20-22 December 2019. United States of America: Institute of Electrical and Electronics Engineers.

Paolo, M.D., 2017. Analysis of Harmonic Impact of Electric Vehicle Charging on the Electric Power Grid Based on Smart Grid Regional Demonstration Project – Los Angeles. In: Institute of Electrical and Electronics Engineers, *2017 Green Energy and Smart Systems Conference.* Long Beach, California, United States of America, 06-07 November 2017. United States of America: Institute of Electrical and Electronics Engineers.

Papaioannou, I.T., Alexiadis, M.C., Demoulias, C.S., Labridis, D.P., and Dokopoulos, P.S., 2011. Modeling and Field Measurements of Photovoltaic Units Connected to LV Grid. Study of Penetration Scenarios. *IEEE Transactions on Power Delivery,* 26(2), pp.979-987.

Parihar, S.S. and Malik, N., 2022. Analysing the impact of optimally allocated solar PV-based DG in harmonics polluted distribution network. *Sustainable Energy Technologies and Assessments,* 49, pp.1-13.

Patil, K.D., and Gandhare, W.Z., 2012. Effects of harmonics in distribution systems on temperature rise and life of XLPE power cables. In: Institute of Electrical and Electronics Engineers, *2011 International Conference on Power and Energy Systems.* Chennai, India, 22-24 December 2011. United States of America: Institute of Electrical and Electronics Engineers.

Phannil, N., Jettanasen, C., Ngaopitakkul, A., 2017. Power quality analysis of grid connected solar power inverter. In: Institute of Electrical and Electronics Engineers, *3rd International Future Energy Electronics Conference and ECCE Asia.* Kaohsiung, Taiwan, 03-07 June 2017. United States of America: Institute of Electrical and Electronics Engineers.

Pinto, D.R., Arioli, V.T., Hax, G.R.T., Borges, R.T. and Teixeira, W.W., 2017. Analysis of the Impact on Power Quality During the Recharge of Electric Vehicles and Vehicle-to-Grid Functionality. In: Institute of Electrical and Electronics Engineers, *2017 Power and Energy Society Innovative Smart Grid Technologies Conference Europe.* Turin, Italy, 26-29 September 2017. United States of America: Institute of Electrical and Electronics Engineers.

Pinyol, R., 2015. *Harmonics: Causes, effects and minimization. Salicru white papers.* [.pdf] Salicru. Available at: <https://www.salicru.com/files/pagina/72/278/jn004a01_whitepaper-armonics_(1).pdf> [Accessed 13th July 2023].

Quan-Duong, M., Dinh-Pham, T., Trung-Nguyen, T., Tuan-Doan, A. and Van-Tran, H., 2019. Determination of Optimal Location and Sizing of Solar Photovoltaic Distribution Generation Units in Radial Distribution Systems. *Energies,* 12(1), pp.1-24.

Ramachandran, K. M. and Tsokos, C. P., 2015. *Mathematical Statistics with Applications in R.* 2nd ed. Oxford, United Kingdom: Academic Press.

Reddy, M.S.K. and Selvajyothi, K., 2020. Optimal placement of electric vehicle charging station for unbalanced radial distribution systems. *Energy Sources, Part A: Recovery, Utilization, and Environmental Effects,* 2020, pp.1-15.

Riba, J. R., 2015. Analysis of formulas to calculate the AC resistance of different conductors' configurations. *Electric Power Systems Research,* 127 (2015), pp.93-100.

Reilly, J.P., 1998. *Applied Bioelectricity: From Electrical Stimulation to Electropathology.* 1st ed. New York, United States of America: Springer-Verlag New York Inc.

Ruwaida, Y., Holmberg, D. and Bollen, M.H.J., 2015. Mapping of Harmonic Levels in the Low-Voltage Network. In: The International Conference on Electricity Distribution, *23rd International Conference on Electricity Distribution.* Lyon, France, 15-18 June 2015. Belgium: The International Conference on Electricity Distribution.

Schlabbach, J., 2008. Harmonic Current Emission of Photovoltaic Installations under System Conditions. In: Institute of Electrical and Electronics Engineers, *2008 5th International Conference on the European Electricity Market.* Lisboa, Portugal, 28-30 May 2008. United States of America: Institute of Electrical and Electronics Engineers.

Schlabbach, J., and Gross, A., 2007. Harmonic Current Emission of Photovoltaic Inverters. In: The International Conference on Electricity Distribution, *19th International Conference on Electricity Distribution.* Vienna, Austria, 21-24 May 2007. Belgium: The International Conference on Electricity Distribution.

Schwanz, D., Bollen, M., Larsson, A. and Kocewiak, Ł.H., 2016. Harmonic mitigation in wind power plants: Active filter solutions. In: Institute of Electrical and Electronics Engineers, *17th International Conference on Harmonics and Quality of Power.* Belo Horizonte, Brazil, 16-19 October 2016. United States of America: Institute of Electrical and Electronics Engineers.

Scottish and Southern Electricity Networks, 2019. *Long Term Development Statement for Southern Electric Power Distribution plc's Electricity Distribution System.* Reading, United Kingdom: Scottish and Southern Energy Power Distribution Ltd.

Scottish and Southern Energy Power Distribution Ltd, 2020. *Electric Office Web.* [online] Available at: <https://eoweb-op.ssen.co.uk/login> [Accessed 10th February 2020].

Sharew, E.A., Kefale, H.A. and Werkie, Y.G., 2021. Power Quality and Performance Analysis of Grid-Connected Solar PV System Based on Recent Grid Integration Requirements. *International Journal of Photoenergy,* 2021, pp.1-14.

Shklyarskiy, Y., Hanzelka, Z., and Skamyin, A., 2020. *Experimental Study of Harmonic Influence on Electrical Energy Metering.* Energies, 13(21), 5536.

Silva, F.D., and Mohammed, O., 2013. Demand side load control with smart meters. In: Institute of Electrical and Electronics Engineers, *2013 Power & Energy Society General Meeting.* Vancouver, BC, Canada. 21-25 July 2013. United States of America, Institute of Electrical and Electronics Engineers.

Sivaraman, P. and Sharmeela, C., 2021. *Power Quality in Modern Power Systems.* London, United Kingdom: Academic Press.

Staats, P.T., Grady, W.M., Arapostathis, A., and Thallam, R.S., 1998. A statistical analysis of the effect of electric vehicle battery charging on distribution system harmonic voltages, *IEEE Transactions on Power Delivery,* 13, pp.640-646.

Stevens, W. G. S., 1963. The current-voltage relationship in human skin, *Medical electronics and biological engineering,* 1, pp.389-399.

Tahir, M., 2017. *Electric vehicles and vehicle-to-grid technology How utilities can play a role.* MEng. Norway: The Arctic University of Norway. Available at: <https://munin.uit.no/bitstream/handle/10037/11358/thesis.pdf?sequence=1> [Accessed 25th August 2023].

Tan, C., Chen, Q., Zhou, K. and Zhang, L., 2019. A Simple High-Performance Current Control Strategy for V2G Three-Phase Four-Leg Inverter with LCL Filter. *IEEE Transactions on Transportation Electrification,* 5(3), pp.695-701.

Tesla, 2023. *Support - Vehicle Charging Speeds.* [online] Available at: <https://www.tesla.com/support/home-charging-installation/wall-connector#:~:text=%E2%80%A0Maximum%20charge%20rate%20for,miles%20of%20range%20per%20hour> [Accessed 5th August 2023].

The Electricity Council, 1987. *Electricity Supply in the UK: A chronology.* London, United Kingdom: The Electricity Council.

*The Electromagnetic Compatibility Regulations 2016.* SI 2016/1091. London: His Majesty's Stationery Office.

*The Electricity Safety, Quality and Continuity Regulations 2002 (ESQCRs).* SI 2002/2665. London, United Kingdom: The National Archives.

The Mathworks, Inc., 2021. MATLAB R2021a. [software]

The Pennsylvania State University, 2023. *15.1 - Exponential Distributions.* [online] Available at: <https://online.stat.psu.edu/stat414/lesson/15/15.1> [Accessed 17th March 2024]

Thorne & Derrick International, 2020. *Consac Cable Joints.* [online] Available at: <https://www.powerandcables.com/tag/consac-cable-joints/> [Accessed 4th April 2020].

Thorne & Derrick International, 2023. *Waveform Cables 3 Core & 4 Core BS7870-3.40:2011.* [online] Available at: <https://www.powerandcables.com/product/product-category/waveform-cables-3-core-4-core-bs7870-3-402011/> [Accessed 7th October 2023].

Tirunagari, S., Gu, M. and Meegahapola, L., 2022. Reaping the Benefits of Smart Electric Vehicle Charging and Vehicle-to-Grid Technologies: Regulatory, Policy and Technical Aspects. *IEEE Access,* 10, pp.114657-114672.

Tovilović, D.M. and Rajaković, N.L.J., 2015. The simultaneous impact of photovoltaic systems and plug-in electric vehicles on the daily load and voltage profiles and the harmonic voltage distortions in urban distribution systems. *Renewable Energy,* 76, pp.454-464.

Tran-The, T., Nguyen-Quoc, S. and Vo-Ngoc, D., 2020. Symbiotic Organism Search Algorithm for Power Loss Minimization in Radial Distribution Systems by Network Reconfiguration and Distributed Generation Placement. *Mathematical Problems in Engineering,* 2020, pp.1-22.

Transport for London, 2023. *ULEZ Expansion 2023.* [online] Available at: <https://tfl.gov.uk/modes/driving/ultra-low-emission-zone/ulez-expansion-2023> [Accessed 2nd September 2023].

Trehan, D., 2020. Non-Convex Optimization: A Review. In: Institute of Electrical and Electronics Engineers, *4th International Conference on Intelligent Computing and Control Systems.* Madurai, India, 13-15 May 2020. United States of America: Institute of Electrical and Electronics Engineers.

Tucker, S., 2023. *EDS 06-0014: Secondary Substation Earthing Design (V5.0).* [Internal Document] London, United Kingdom: UK Power Networks.

Turan, S. and Kalenderli, Ö., 2009. A novel reflectometer for cable fault analysis with pulse reflection method. In: Institute of Electrical and Electronics Engineers, *2009 International Conference on Electrical and Electronics Engineering.* Bursa, Turkey, 05-08 November 2009. United States of America: Institute of Electrical and Electronics Engineers.

Vasanasong, E., and Spooner, E.D., 2000. The Effect of Net Harmonic Currents Produced by Numbers of the Sydney Olympic Village's PV Systems on the Power Quality of Local Electrical Network. In: Institute of Electrical and Electronics Engineers, *2000 International Conference on Power System Technology.* Perth, Western Australia, Australia, 04-07 December 2000. United States of America: Institute of Electrical and Electronics Engineers.

Wakileh, G.J., 2003. Harmonics in rotating machines. *Electric Power Systems Research,* 66 (1), pp.31-37.

Wan, D., Zhao, M., Duan, X., Zhou, H., Mao, L., and You, K., 2020. Life Assessment Study on Distribution Electric Power Transmission Equipment Based on Harmonic Modified Hot Spot Temperature Calculating Model. In: Institute of Electrical and Electronics Engineers, *2019 3rd Conference on Energy Internet and Energy System Integration.* Changsha, China, 08-10 November 2019. United States of America: Institute of Electrical and Electronics Engineers.

Wang, G., Deb, S. and Coelho, L.S., 2015. Elephant Herding Optimization. In: Institute of Electrical and Electronics Engineers, *3rd International Symposium on Computational and Business Intelligence.* Bali, Indonesia, 07-09 December 2015. United States of America: IEEE Computer Society's Conference Publishing Services.

Wang, G., Deb, S. and Cui, Z., 2019. Monarch Butterfly Optimization. *Neural Computing and Applications,* 31, pp.1995-2014.

Waters, L., 2023. *Chapter 6: Renewable sources of energy.* [.pdf] London, United Kingdom: Department for Energy Security and Net Zero and Department for Business, Energy & Industrial Strategy. Available at: Digest of UK Energy Statistics <https://www.gov.uk/government/collections/digest-of-uk-energy-statistics-dukes> [Accessed 29th December 2023].

Watson, J.D., and Watson, N.R., 2017a. Impact of electric vehicle chargers on harmonic levels in New Zealand. In: Institute of Electrical and Electronics Engineers, *2017 Innovative Smart Grid Technologies - Asia.* Auckland, New Zealand, 04-07 December 2017. United States of America: Institute of Electrical and Electronics Engineers.

Watson, J.D., and Watson, N.R., 2017b. Impact of Residential PV on Harmonic Levels in New Zealand. In: Institute of Electrical and Electronics Engineers, *2017 Power and Energy Society Innovative Smart Grid Technologies Conference Europe.* Turin, Italy, 26-29 September 2017. United States of America: Institute of Electrical and Electronics Engineers.

Watson, N.R., Watson, J.D., Watson, R.M., Sharma, K. and Miller, A., 2015. Impact of Electric Vehicle Chargers on a Low Voltage Distribution System. In: Electricity Engineers' Association, *EEA Conference & Exhibition 2015.* Wellington, New Zealand, 24-26 June 2015. Wellington, New Zealand: Electricity Engineers' Association.

Western Power Distribution, 2013. *Connecting Microgeneration and Other New Technology.* [.pdf] Bristol, United Kingdom: Western Power Distribution. Available at: < https://www.nationalgrid.co.uk/downloads/2807> [Accessed 3rd March 2024].

Western Power Distribution, 2016. *SoLa Bristol SDRC 9.8 Final Report.* [.pdf] Bristol, United Kingdom: Western Power Distribution. Available at: <https://www.nationalgrid.co.uk/downloads-view-reciteme/2527> [Accessed 3rd March 2024].

Woodman, N., Bass, R.B. and Donnelly, M., 2018. Modeling Harmonic Impacts of Electric Vehicle Chargers on Distribution Networks. In: Institute of Electrical and Electronics Engineers, *2018 IEEE Energy Conversion Congress and Exposition.* Portland, Oregon, United States of America, 23-27 September 2018. United States of America: Institute of Electrical and Electronics Engineers.

Wu, B., Chen, H., Guan, G, Ding, T. and Yin, L., 2018. Simulation model of three-phase PWM rectifier charging station and harmonic analysis on grid. In: Institute of Electrical and Electronics Engineers, *2017 Innovative Smart Grid Technologies – Asia.* Auckland, New Zealand, 04-07 December 2017. United States of America: Institute of Electrical and Electronics Engineers.

Xu, H. and Huang, X., 2020. A Multi-Objective Coordinated Charging and Discharging Strategy for Electric Vehicles Based on Stackelberg Game. *Energy and Power Engineering,* 12, pp.63-72.

Xu, Y., Xu, Y., Chen, Z., Peng, F., and Beshir, M., 2014. Harmonic analysis of electric vehicle loadings on distribution system. In: Institute of Electrical and Electronics Engineers, *2014 International Conference on Control Science and Systems Engineering.* Yantai, China, 29-30 December 2014. United States of America: Institute of Electrical and Electronics Engineers.

Yamini, N.G., Sanjan, P.S. and Gowtham, N., 2019. Analysis of Current Harmonics in Various Domestic Loads: A Case Study. In: Institute of Electrical and Electronics Engineers, *2019 International Conference on Power, Energy and Innovations.* Pattaya, Thailand, 16-18 October 2019. United States of America: Institute of Electrical and Electronics Engineers.

Yang, Q., Li, J., Cao, W., Li, S., Lin, J., Huo, D. and He, H., 2020. An improved vehicle to the grid method with battery longevity management in a microgrid application. *Energy,* 198, pp.1-9.

Ying-Yi, H. and Ying-Kwun, C., 1996. Determination of locations and sizes for active power line conditioners to reduce harmonics in power systems. *IEEE Transactions on Power Delivery,* 11(3), pp.1610-1617.

Yuan, K., Song, Y., Sun, C., Xue, Z., Wu, Z., Li, J. and Yuan, B., 2017. Harmonic characteristics of distributed generation and electric vehicle integrating to the grid. In: Institute of Electrical and Electronics Engineers, *2017 Conference on Energy Internet and Energy System Integration.* Beijing, China, 26-28 November 2017. United States of America: Institute of Electrical and Electronics Engineers.

Yukihira, K., 2009. Statistical analyses of the distribution and the annual trend of harmonic voltage in Japan. In: The International Conference of Electricity Distribution, *20th International Conference and Exhibition on Electricity Distribution - Part 1.* Prague, Czech Republic, 08-11 June 2009. United Kingdom: Institute of Engineering and Technology.

Zhao, G. and Yue, Y., 2017. Harmonic Analysis and Suppression of Electric Vehicle Charging Station. In: Institute of Electrical and Electronics Engineers, *2017 International Conference on Mechatronics and Automation.* Takamatsu, Japan, 06-09 August 2017. United States of America: Institute of Electrical and Electronics Engineers.

Zubi, H. and Khalifa, S., 2017. Power quality investigation of a typical Telecom data centre electrical network. In: International Conference on Control, Engineering and Information Technology, *4th International Conference on Control Engineering & Information Technology.* Hammamet, Tunisia, 16-18 December 2016. United States of America: Institute of Electrical and Electronics Engineers.

# Publications

## Under Submission

[1] Gissing, G., Yang, J. and Meena, N., 2024. Location Optimization of Electric Vehicle Chargers, Photovoltaic Generation and Vehicle to Grid Point of Connection for Minimizing Voltage Harmonic Levels on Low Voltage Power Distribution Networks. *International Journal of Green Energy, TBC*, pp.TBC.

## Published Articles in Conference Proceedings

[2] Gissing, G., Yang, J. and Meena, N., 2023. Location Optimisation of EVC Point of Coupling for Minimising Voltage Harmonic Levels of a UK Based LV Power Distribution Network. In: Springer Proceedings in Energy, *15th International Green Energy Conference.* Glasgow, Scotland, 10-13 July 2023. Berlin, Germany: Springer Nature.

[3] Gissing, G., Yang, J. and Fahmi, N., 2020. Effect of Electric Vehicle Chargers on the Harmonic Levels of a UK LV Electricity Distribution Network under Steady-State Cable Faults. In: International Conference on Renewable Energy Research and Application, *9th International Conference on Renewable Energy Research and Application.* Glasgow, Scotland, 27-30 September 2020. United States of America: Institute of Electrical and Electronics Engineers.

[4] Ivry, P., Yang, J., Scott, J., Lin, Z., Serrano, C. and Gissing, G., 2019. An evaluation of V2G for distribution network harmonic suppression. In: International Conference on Electricity Distribution, *25th International Conference on Electricity Distribution.* Madrid, Spain, 3-6 June 2019. Liège, Belgium: International Conference on Electricity Distribution.